CFIRE

Cone Penetrometer Comparison Testing

CFIRE 04-21
December 2011

National Center for Freight & Infrastructure Research & Education
Department of Civil and Environmental Engineering
College of Engineering
University of Wisconsin–Madison

Authors:
James Schneider Jonathan Hotstream
University of Wisconsin–Madison

Principal Investigator:
James Schneider
University of Wisconsin–Madison

Technical Report Documentation Page

1. Report No. CFIRE 04-21	2. Government Accession No.	3. Recipient's Catalog No. **CFDA 20.701**
4. Title and Subtitle **Cone Penetrometer Comparison Testing**		5. Report Date **December 2011** 6. Performing Organization Code
7. Author/s James Schneider and Jonathan Hotstream, UW-Madison		8. Performing Organization Report No.
9. Performing Organization Name and Address National Center for Freight and Infrastructure Research and Education (CFIRE) University of Wisconsin-Madison 1415 Engineering Drive, 2205 EH Madison, WI 53706		10. Work Unit No. (TRAIS) 11. Contract or Grant No. **0092-10-10**
12. Sponsoring Organization Name and Address Wisconsin Department of Transportation 4802 Sheboygan Ave. Madison, WI 53707		13. Type of Report and Period Covered **Final Report [11/20/09 – 9/30/11]** 14. Sponsoring Agency Code
15. Supplementary Notes **Project completed for the Wisconsin Department of Transportation with assistance from CFIRE.**		

16. Abstract

The study proposed in this research will first work with Mn/DOT and other regional DOTs to build upon their experiences in implementation of cone penetration testing for transportation projects, and then address additional issues specific to the needs of the Wisconsin Department of Transportation. Data will be collected in Wisconsin and discussed in light of conventional geotechnical soil properties so that practitioners are familiar with factors controlling the behavior of CPT measurements, minimizing the reliance on blind application of 'black box' data processing and interpretation programs.

The work plan and experimental design are developed around aiding engineers and geologists in within the Wisconsin Department of Transportation to understand the mechanisms controlling cone penetration test readings so that they can decide when the testing method is appropriate for use, know how to design an appropriate exploration program, and rapidly interpret the results of the tests for more efficient and reliable engineering.

17. Key Words CPT, Penetration, Wisconsin	18. Distribution Statement **No restrictions. This report is available through the Transportation Research Information Services of the National Transportation Library.**		
19. Security Classification (of this report) **Unclassified**	20. Security Classification (of this page) **Unclassified**	21. No. Of Pages 298	22. Price **-0-**

Form DOT F 1700.7 (8-72) **Reproduction of form and completed page is authorized.**

DISCLAIMER

This research was funded by the Wisconsin Department of Transportation through the National Center for Freight and Infrastructure Research and Education at the University of Wisconsin-Madison. The contents of this report reflect the views of the authors, who are responsible for the facts and the accuracy of the information presented herein. This document is disseminated under the sponsorship of the Department of Transportation, University Transportation Centers Program, in the interest of information exchange. The U.S. Government assumes no liability for the contents or use thereof. The contents do not necessarily reflect the official views of the National Center for Freight and Infrastructure Research and Education, the University of Wisconsin, the Wisconsin Department of Transportation, or the USDOT's RITA at the time of publication.

Wisconsin Highway Research Program

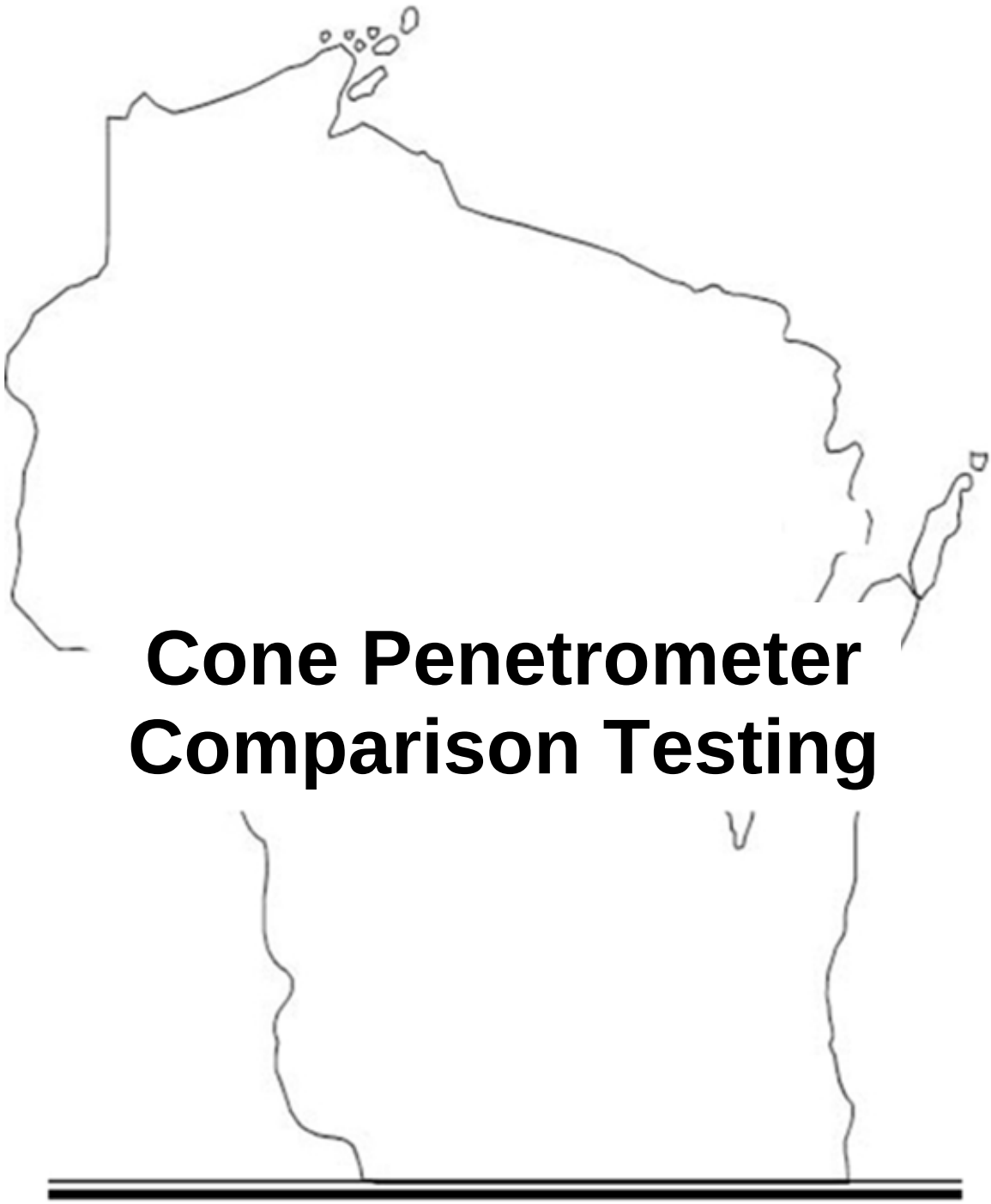

Cone Penetrometer Comparison Testing

James A. Schneider & Jonathan N. Hotstream
University of Wisconsin – Madison
Department of Civil and Environmental Engineering

WHRP 0092-10-10

DISCLAIMER

This research was funded through the Wisconsin Highway Research Program by the Wisconsin Department of Transportation and the Federal Highway Administration under Project 0092-10-10. The contents of this report reflect the views of the authors who are responsible for the facts and accuracy of the data presented herein. The contents do not necessarily reflect the official views of the Wisconsin Department of Transportation or the Federal Highway Administration at the time of publication.

This document is disseminated under the sponsorship of the Department of Transportation in the interest of information exchange. The United States Government assumes no liability for its contents or use thereof. This report does not constitute a standard, specification or regulation.

The United States Government does not endorse products or manufacturers. Trade and manufacturers' names appear in this report only because they are considered essential to the object of the document.

EXECUTIVE SUMMARY

A total of 61 cone penetration tests were performed at 14 sites in the state of Wisconsin. Data reinforced conclusions from practice in Minnesota and previously performed test programs related to the Marquette Interchange and Mitchell interchange project that use of the CPT can be successful in glacial geologies. Within in this study CPTs were performed to depths in excess of 75 feet in alluvial deposits, outwash, and lacustrine soils. Difficulties were encountered in clay tills and fill placed for highway structures. However, previous experience in Milwaukee by commercial CPT operators had success in clayey tills of eastern Wisconsin.

CPT data are discussed in relation to:

- soil classification
- assessment of water flow characteristics of soils
- assessment of compressibility of clayey soils
- assessment of shear stiffness of clays and sands
- assessment of undrained strength of clay soils
- assessment of drained strength of sandy soils
- design applications for shallow foundations, axially loaded piles, and embankments

It is recommended to continue to perform CPTs on transportation projects in Wisconsin as a complement to drilling operations. Boreholes should be performed adjacent to a number of CPTs for each project and targeted sampling of critical and representative layers should be performed. Sampling and laboratory testing procedures for WisDOT projects needs to be improved such that consistency is observed between in-situ and laboratory test results.

TABLE OF CONTENTS

LIST OF FIGURES

LIST OF TABLES

ACKNOWLEDGEMENTS

The authors would like to acknowledge The U.S. Bureau of Reclamation for donating a 24 ton CPT rig and accessories to the University of Wisconsin. This project could not have been performed without that generous gift. Additionally, support from Vertek when updating the CPT equipment and rig controls is gratefully acknowledged. Professor Rodrigo Salgado of Purdue University is thanked for allowing use of the Purdue CPT rig, and Seth Scheilz is thanked for donating his time during testing in Summer 2011.

Jeff Horsfall and Bob Arndorfer of WisDOT are thanked for assistance in site selection and liaising with local maintenance crews in testing areas. Derrick Dasenbrock at Mn/DOT is thanked for sharing their CPT experiences as well as vast quantities of electronic CPT data and boring logs. Elliott Mergen is thanked for assistance with field work and initial review of Mn/DOT CPT data. Professor Dave Bohnoff and Andy Holstein from the Agricultural Engineering Department are thanked for donated time and a skid steer to perform soil borings in Middleton and Sheboygan Falls. Tom Wright of the West Madison Agricultural Research Station is thanked for providing a site for rig storage and initial testing.

Rory Holland and staff at the UW-Madison Physical Sciences Lab (PSL) are acknowledged for developing creative and cost effective solutions to repair a 1982 vintage CPT rig.

Professor Paul Mayne of Georgia Tech is thanked for providing electronic copies of CPT correlation databases.

Additional funding for this project was provided through CFIRE (National Center for Freight and Infrastructure Research and Education), as well as the UW-Madison College of Engineering and Wisconsin Alumni Research Foundation (WARF). This support is gratefully acknowledged.

1 Project Overview

1.1 Introduction

The cone penetration test (CPT) has a long history of use in geotechnical engineering. The mechanical version of the tool was developed in the Netherlands over 75 years ago primarily for efficient evaluation of the length needed for driven piles bearing in deep sand layers underlying thick compressible clays (Delft 1936). Due to the similarity in geometry and full displacement method of installation it is logical to estimate the end bearing of closed ended piles with the device (when accounting for differences in diameter). Further extension of the CPT to estimate pile shaft friction in sands was proposed by Meyerhof (1956), and shaft friction of piles in clay was, and is, often related to CPT cone tip resistance indirectly through undrained shear strength (e.g., Schmertmann 1975, Almeida et al. 1996). Major advances in speed of use, repeatability, and reliability in CPT measurement came with the development of the Fugro electric friction cone penetrometer which was in use by 1966 (Fugro 2002). The flexibility and applicability of cone penetration testing for geotechnical engineering has been aided by the incorporation of additional sensors into the device, such as pore pressure measurements during penetration (piezocone, CPTU, e.g., Wissa et al. 1975, Torstensson 1975), and downhole seismic measurements (seismic piezocone, SCPTU, e.g., Campanella et al. 1986). Figure 1.1 illustrates equipment, setup and procedures for piezocone penetration testing.

In current geotechnical engineering practice, results of the electric cone and piezocone penetration tests are applied in a variety of applications, including (i) bridges; (ii) embankments; (iii) deep foundations; (iv) slopes; (v) retaining wall design (including foundations); (vi) soft soil delineation; (vii) earthquake site amplification and soil liquefaction; (viii) degree of soil improvement; (ix) excavations; and (x) subgrades (e.g., Mayne 2007). Additionally, results of the cone penetration test can be used to estimate a number of different soil characteristics and properties, including: (i) soil type and stratigraphy; (ii) effective stress friction angle of ‘sands’; (iii) relative density of ‘sands’; (iv) undrained shear strength of ‘clays’; (v) preconsolidation stress of ‘clays’; (vi) water flow characteristics (coefficient of consolidation and hydraulic

conductivity) of 'clays'; as well as (vii) shear, elastic, and constrained modulus, to name a few (e.g., Lunne et al. 1997, Mayne 2007).

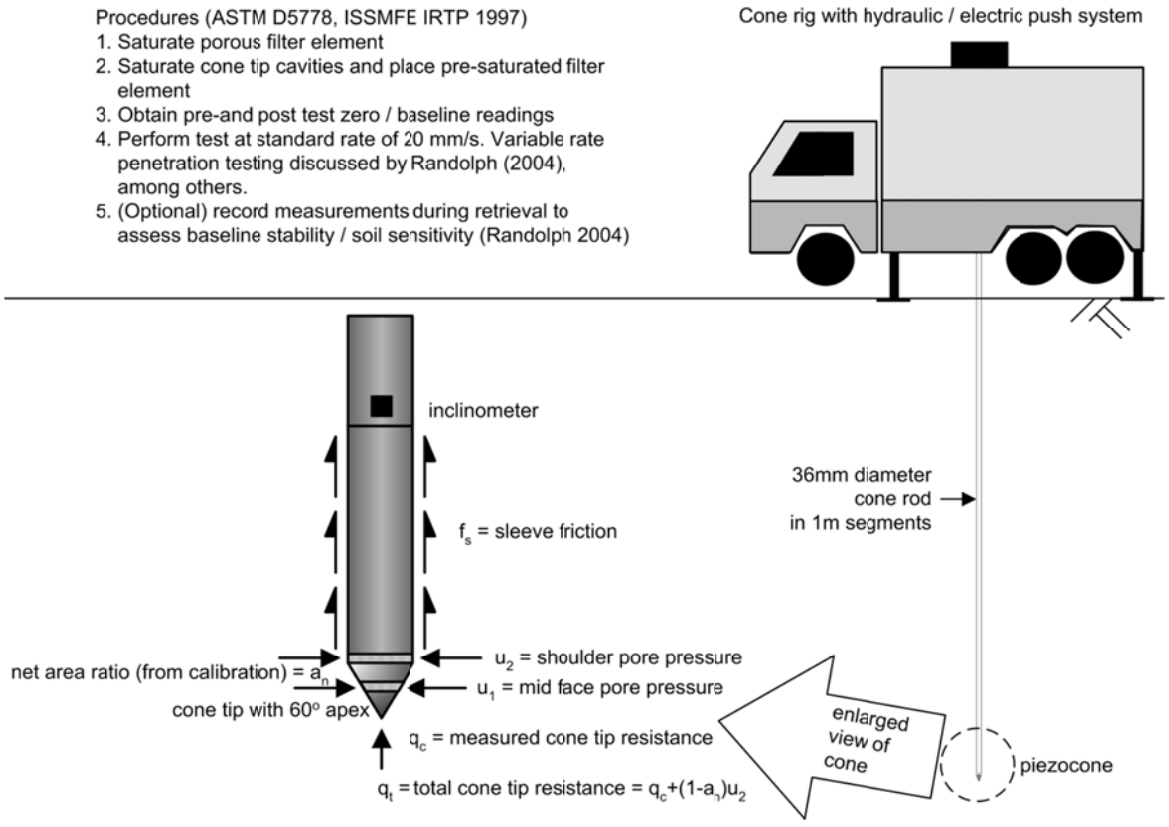

Figure 1.1. Equipment, setup and procedures for piezocone testing (after Mayne 2007)

The first major use of CPT equipment in the U.S. was by the waterways experiment station in the 1950's (Hvorslev 1953, Shockley et al. 1961), but the technology did not start to rapidly grow in U.S. practice until the adoption and promotion started at the University of Florida (Schmertmann 1995). A survey of State Departments of Transportation (DOT) by Mayne (2007) indicates the current level of CPT use for transportation projects. Over 40% of DOTs in the U.S. do not use the CPT at all, with reasons for the lack of use ranging from hard and gravelly ground conditions to lack of expertise in the equipment and interpretation of results. It may be fortunate for this study that the only State DOT with use of CPT on over 50% of their projects is Wisconsin's neighbor to the west, Minnesota (the response of Nebraska in the Mayne 2007 survey was in error). The Minnesota DOT (Mn/DOT) uses the CPT on approximately 75% of their 'foundation

engineering' projects, and has performed over 7500 cone tests since 2001 (personal communication Glenn Engstrom and Derrick Dasenbrock, Mn/DOT).

The glacial geological conditions of Minnesota are similar to those of the northern and eastern half to ⅔ of Wisconsin, suggesting that the use of CPT may be viable for a majority of areas in the state. However, the underlying bedrock conditions in the two states are different in that much of Minnesota is underlain by shale, while Wisconsin is primarily underlain by dolomite / limestone. This would cause a different type of sediment / clast entrained in the till and could lead to differences in potential for CPT refusal if the cone encountered these clasts during penetration. The study proposed in this research will first work with Mn/DOT and other regional DOTs to build upon their experiences in implementation of cone penetration testing for transportation projects, and address additional issues specific to the needs of the Wisconsin Department of Transportation. Data collected in Wisconsin will be analyzed and discussed using conventional soil parameters so that practitioners are familiar with factors controlling the behavior of the measurements of the device, minimizing the reliance on 'black box' data processing and interpretation programs.

1.2 Problem Statement

WisDOT is considering the use of CPT investigations on transportation projects. The Department needs to learn more about the technology, its advantages and limitations, and feel comfortable that CPT data correlates with Wisconsin soil boring methods/information/geology and leads to design assumptions that are comparable to WisDOT's current methods.

1.3 Objectives

It is the objective of this research project to evaluate the potential use of CPT technology for Wisconsin DOT projects through performance of tests around the state and comparing CPT results to available data. Specific objectives include:

- Departmental subsurface investigative methods (generally soil borings) and cone penetrometer findings will be compared at a number of sites with differing soils and geology.
- Evaluation of design parameters will be compared.
- Discuss advantages and limitations of CPT equipment, operations and interpretation.
- Detailed suggestions for the application of this technology on WisDOT projects will be presented.

2 Additional Background and Previous Regional Experience

The cone penetration test (CPT) and variants [piezocone penetration test (CPTU), seismic piezocone penetration test (SCPTU), resistivity cone penetration test (RCPT), etc.] have had successful application in geotechnical engineering for over 75 years. At present there is still a relatively limited application of CPT data by DOTs to design and construction of transportation projects in the United States. Some of the reasons / perceptions for this lack of use include (e.g., Mayne 2007):

- ground conditions are too hard;
- soil contains gravel and stones;
- CPTs are more expensive than borings;
- data analysis requires too much expertise;
- practice is acceptable using SPT;
- equipment too expensive / not available in the area.

Many of these same obstacles exist for the glacial soil conditions of Wisconsin and need to be assessed. However, similar geological conditions exist in the neighboring state of Minnesota and their continued experience with CPTs since 2001 allows for use of CPT on more than 75% of Minnesota DOT (Mn/DOT) "foundations" projects. These projects include (i) bridge and culvert foundations; (ii) large embankment fills; (iii) buildings, towers, and other structures; (iv) slopes; (v) retaining wall foundations; (vi) roadway alignment and soft soil delineation; (vii) excavations; and (viii) sinkholes. A review of previous use of the CPT for Minnesota DOT and Wisconsin DOT projects is presented in this chapter. Preliminary discussion of assessed profiles is contained herein, with data included for supplemental analysis in later chapters. Attempts to obtain data from other Midwestern state DOTs (i.e., Ohio) was unsuccessful. Discussion of Minnesota data is largely taken from the conference paper Dasenbrock, Schneider & Mergen (2010).

2.1 Additional Background

2.1.1 Wisconsin geology and soils

The CPT is a method used to determine the layering and engineering properties of unconsolidated sediment overlying the local bedrock. This report addresses CPT testing at various locations across the state of Wisconsin. A brief discussion of Wisconsin geologic history is provided for a more thorough understanding of the regional soil conditions.

In the Quaternary period, or the past 2.6 million years (International Commission on Stratigraphy 2010), the planet has experienced fluctuations in the continental ice sheets. The amount of ice on the surface of the earth has varied with climatic conditions throughout time as observed in the oxygen isotope records in the skeletons of sea organisms and the variation in sea-level (Lambeck & Chappell 2001, Lisiecki & Raymo 2005). Currently, the planet is in an interglacial period where large continental ice sheets have regressed to Greenland and Antarctica. The last glacial maximum occurred during the late Wisconsinan period from approximately 23,000 to 15,000 radiocarbon years before present (Clark et al. 2009). The extent of glacial ice coverage in Wisconsin is provided in Figure 2.1 (Clayton et al. 2006). Approximately 60% of Wisconsin's land surface was covered by ice at some time in the past, either during the last glacial maximum or during a previous glacial episode. The south west corner of the state is known as the driftless area, Figure 2.1. This name is derived from the lack of glacial deposits historically grouped into the all-encompassing term "drift". Figure 2.2 illustrates the expected thickness of soil over bedrock. Soil thickness is also thinner in the driftless area.

The areas covered by glaciers in the past bear distinct landforms associated with the prior glaciations including till plains, drumlins, moraines, eskers, outwash plains, kettle and kame landscapes, glacial lake plains, and ice-walled lake plains. Areas not directly glaciated do have some glacially derived sediment typically in the form of loess, wind-blown silt, deposits.

Geologists have described the different drift deposits and divided them into different groups to determine the chronology and extent of the fluctuations concerning the advance and retreat of continental glaciers in the region (Clayton and Moran 1982, Attig et al. 1985, Acomb et al.

1982). Although engineering properties between different glacial deposits have been observed to vary for this region (Mickelson et al. 1978, Edil & Mickelson 1995), identification of depositional setting is more relevant to understanding the engineering behavior of the soil, specifically stress history and drainage conditions.

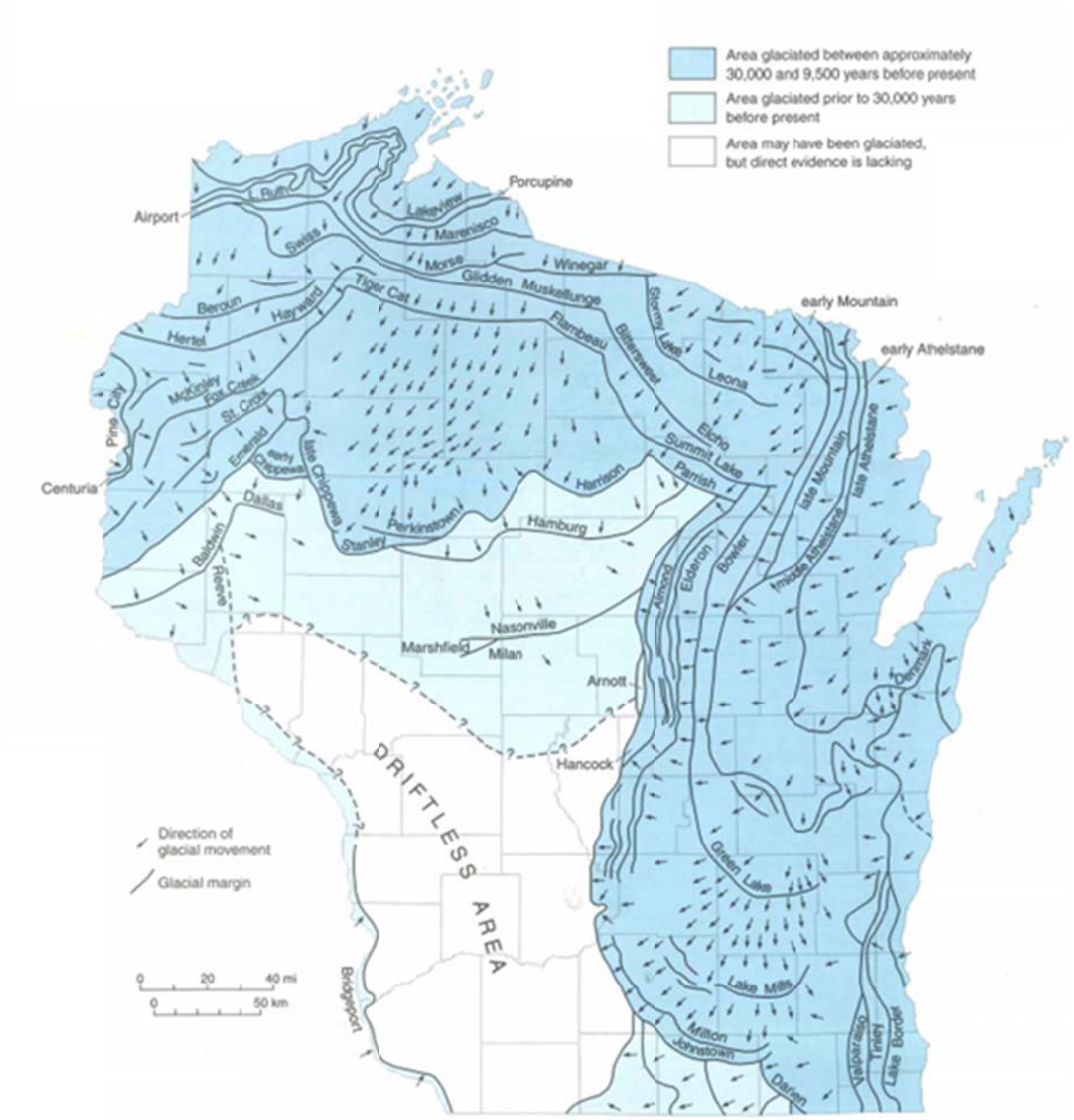

Figure 2.1: Extent of the glaciated areas in Wisconsin during the last glacial maximum from Clayton et al. (2006)

Glaciers are an extremely effective agent for erosion and deposition across a landscape. Sediment can be entrained in two mediums within a glacial system: glacial ice or meltwater. These two mediums can be further classified by location within the system above the glacier, supraglacial, within the glacier, englacial, or below the glacier, subglacial. Water may be present in all of these locations, for example, meltwater flowing on top of a glacier due to surface melt may become englacial if it encounters a crevasse, or crack in the glacier, whereby it flows down to a subglacial stream or lake.

Sediment may be entrained by falling on top of a glacier by debris flows in areas of high relief or be frozen into the ice at the base of a glacier, and moved in the direction of glacier movement. The weight of the overlying ice produces a large shear stress on the subglacial bed allowing for significant erosion and deformation to occur in the underlying material where glaciers are not frozen to the bed.

The glacial ice releases entrained sediment when it melts, where the sediment may be reworked and transported by the glaciofluvial system or be deposited in place. In this document till refers to sediment directly deposited by the ice and typically is not sorted. Till is broadly classified into two groups. Basal till is deposited at the base of a glacier and can be associated with frictional forces lodging the sediment in place and in cases melting and refreezing of basal ice. These deposits are also referred to as lodgement tills. The second group of till is deposited at the margin ice and typically does not have any overburden when deposited and is referred to as meltout till. Meltout till is composed of supra-, en-, and subglacial sediment.

Glacial sediment transported and deposited by water within the system is typically sorted, poorly graded, and bedded. These deposits may occur supra-, en-, and subglacially, but typically only the subglacial deposits and landforms are preserved. Subglacial deposits are typically in the form of melt water channels where rivers of meltwater flowing at the base of a glacier have deposited beds of stream deposits or scoured out channels into the basal sediment. Most of the lasting deposition of glacial meltwater is observed in the proglacial area, in front of the glacier terminus, where large glacial lakes and outwash plains form.

The map shown in Figure 2.3 depicts the spatial distribution of the different depositional environments of the surficial soils across WI. The map was generated by simplifying a series of regional Quaternary Geologic maps produced by the United States Geological Survey (USGS, Lineback et al. 1983, Geoebal et al. 1983, Farrand et al. 1984, Hallberg et al. 1991). These maps were generated at a scale of 1:1,000,000 using a mixture of aerial mapping and geologic boring logs. The units identified by the map authors were regrouped based on the depositional environment and the expected engineering properties of the soils. The maps were broken into eight different divisions as explained below.

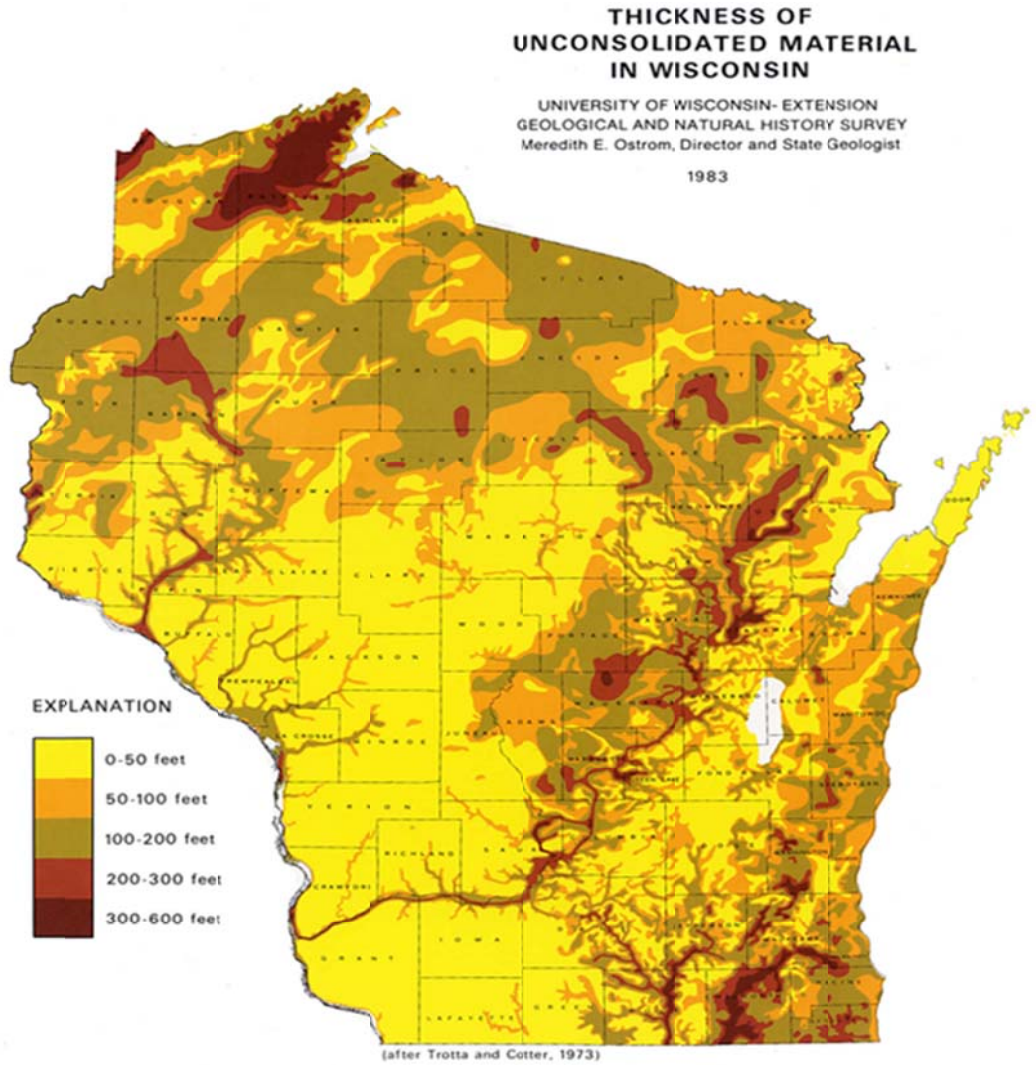

Figure 2.2: Thickness of soil overlying bedrock in Wisconsin from WGNHS (1983)

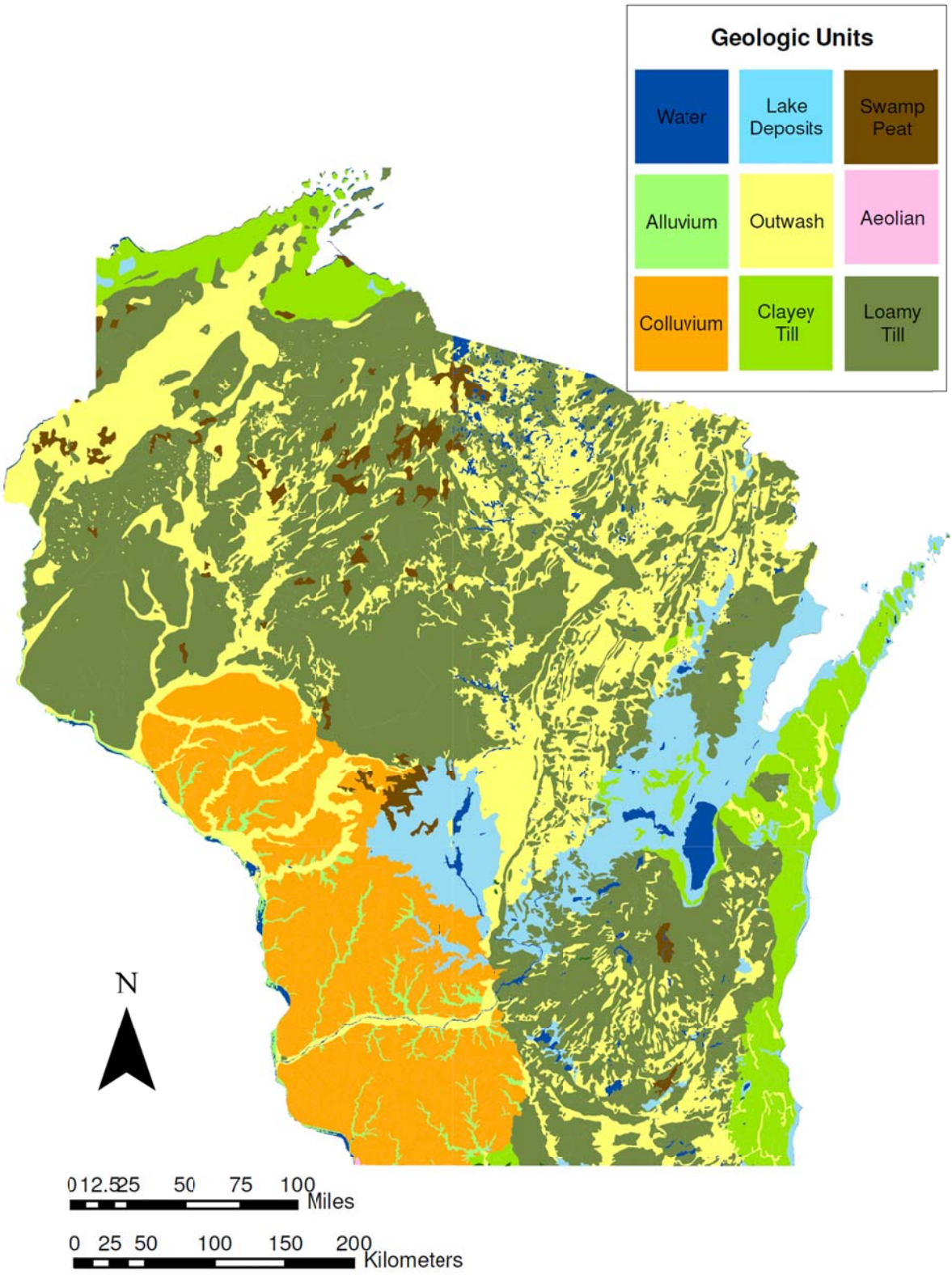

Figure 2.3: Depositional units of the surficial unconsolidated material. Map compiled from data of previously published maps (Lineback et al. 1983, Geoebal et al. 1983, Farrand et al. 1984, Hallberg et al. 1991)

The first division is non-glacial residual soils or colluvium. The colluvium group represents residual soils that developed in place by weathering of the underlying bedrock. This unit occurs primarily in the driftless area. These soils typically overly a shallow bedrock and are composed of clay to boulder sized material. The landscape of the driftless area is characterized by hill and steep valleys where streams have incised into the bedrock surface. Many of the soil deposits are the result of debris flows and rock falls from the slopes.

Included in the non glacial soils are the alluvial deposits which represent recent stream deposits placed after glaciers retreated from the region. These deposits are mostly found along the major streams and rivers in the driftless area. The soils in the alluvial deposits are composed of clays to gravel deposits representing overbank deposits, point bars, and abandoned channels. Typically the soils in this category are primarily classified as sands from an engineering standpoint.

Outwash deposits form proglacially where meltwater streams transport and deposit glacial sediment. These deposits occur well dispersed throughout the state as a result of deposition in front of the retreating glacial front. The soils in outwash deposits are silt to gravel sized particles typically deposited in sorted, bedded, braided stream networks. Also included in this group are the ice contact sands and gravels which are a form of meltout till. Although the original map classification indicates transport solely by ice, the engineering behavior should be similar and therefore was grouped with the outwash deposits.

Aeolian deposits representing loess and sand dunes that formed from wind re-working glacial deposits. Local aeolian deposits occur throughout the mapped area in thin coverings, but they were not separated out when the regional maps were created. Thick sequences, >5m thick, were not mapped within the state and therefore this unit is not observed in Figure 2.3.

Till was mapped in the USGS sources as basal till, moraines, or undifferentiated and was typically grouped as loamy, sandy, or clayey. From an engineering standpoint, interest in the behavior of the till matrix will govern the behavior of the soil. The maps generated in this study divided the tills into two groups: loamy and clayey. Sandy tills were incorporated with the

loamy tills. These till descriptions are very generalized and it must be understood that the grain size distributions and descriptions are generated using the United States Department of Agriculture (USDA) soil classification system percent silt, clay, and sand are compared. It is also important to note that the tills were typically described with two grain sizes identified, for example a loamy clayey till. It was assumed that there are no single modal grain size tills. This assumption was taken further as an indication of water flow characteristics. Specifically, that any clayey till would for the most part have a low hydraulic conductivity and display undrained behavior and loamy-sandy tills would possess medium to high hydraulic conductivities and behave partially drained to drained.

The distributions of the two till units indicate that the loamy tills cover much more area of the state than clayey tills. The low occurrence of clayey tills relates back to the concept that a glacier cannot produce clay because no significant chemical weathering occurs when particles are entrained in ice. These clayey tills also occur above previously deposited tills, and therefore reflect further transport and reworking of entrained sediment from the pre-existing tills. The clayey tills occur mainly along the eastern shore of Lake Michigan and correlate with an interstadial period where the glaciers receded northward out of the Great Lake basins prior to re-advancing. When the glaciers receded northward, clayey sediment was deposited in Lake Michigan. During the re-advance, this clay was entrained in the glacial ice and deposited in the till associated with that advance.

The lake deposits represent depositional facies related to glacial lakes. These deposits are well distributed in the central and eastern-central portions of the state where glacial lakes Wisconsin (Attig and Knox 2008) and Oshkosh (Hooyer 2007) have been identified. The large extent of these lakes is indicative of how large the impact of ice sheet loading is on crustal deformation. Note that these deposits show the extents over time and are not meant to suggest that both lakes were that size concurrently. Typical soils associated with the lake deposits are clays, silts and sands representing subaqueous stream fans and deltas, and fine grained deposits related to release of suspended sediment load in low energy environments. Occasional drop stones of gravel to boulder size can be found which represent deposition of sediment from melting ice blocks that calved and floated from the ice margin. These deposits are primarily composed of silts and clays

The swamp and peat deposits are closely associated with the lake deposits from a formation standpoint. The deposits can be associated with the glacial lake deposits or occur as standalone features where either large stagnant ice blocks formed a low area for water to collect or meltwater collected in a natural topographic low. These deposits are composed of fine grained silts and clays with high organic contents with anticipated low strengths and high compressibilities. These soils make up a small portion of the mapped areas; however, this may be a function of the scale of the mapping.

2.1.2 Fundamentals of soil behavior

Soil behavior is typically analyzed as a continuum, and interpretation and application revolves around 5 primary characteristics:

- Water flow characteristics – rate at which water moves through a soil matrix as a function of a hydraulic gradient and/or change in volume
- Compressibility – change in volume due to a change in *effective* stress (i.e., change in size of a soil element)
- Shear Stiffness – resistance to shear distortions that result from shear stresses (i.e., change is shape of a soil element)
- Strength – ultimate resistance to shear stresses
- Dilation – change in volume due to shear deformations (i.e., change in size due to change in shape)

Interpretation of soil behavior is largely influenced by the rate of loading as compared to the rate of water flow through the soil. If a soil is loaded slowly as compared to how fast water flows through the soil (e.g., loading of saturated sand), no excess water pressure builds up and changes in total stress are equal to changes in effective stress. This is referred to as drained loading. Increases in effective stress lead to increases in strength of the soil, and dilation of soil particles affect the geometry of a failure surface and changes in effective stress during loading. If a soil is loaded rapidly compared to how fast water can flow through the pores (e.g., loading of saturated clays), strength is generally controlled by short term loading prior to increases in effective stress, while a majority of deformations are time dependent, provided that a shear failure does not

occur. This situation is referred to as undrained loading. Figure 2.4 illustrates rate effects on soil response.

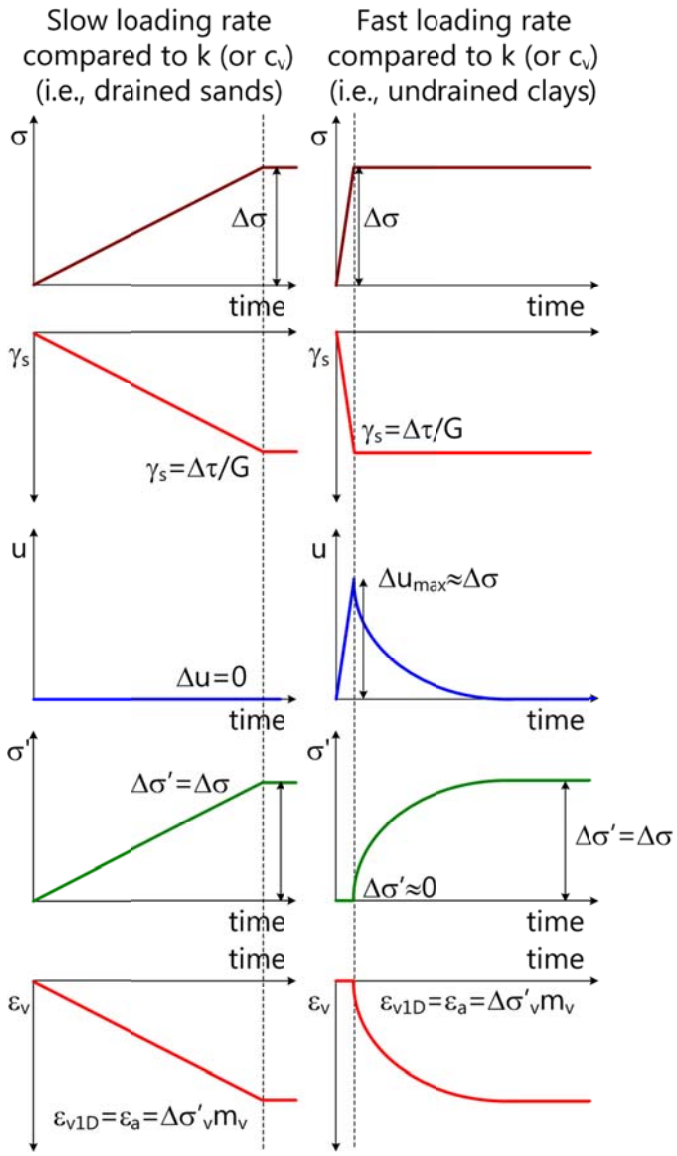

Figure 2.4. Influence of loading rate on changes in effective stress and volume during loading (after Atkinson 2007)
σ = total stress, γ_s = shear strain, u = pore water pressure, σ' = effective stress, ε_v = volumetric strain

Water flow characteristics are quantified by the hydraulic conductivity (k_v or k_h) and the coefficient of consolidation (c_v or c_h). The subscripts account for vertical (v) or horizontal (h) flow paths. The relationship between the hydraulic conductivity, in this case for a horizontal flow path which is more applicable to cone penetration testing, and the coefficient of consolidation is:

$$c_h = \frac{k_h \cdot D}{\gamma_w} = \frac{k_h}{m_h \cdot \gamma_w} \approx \frac{k_h \cdot (1 + e_0) \cdot \sigma'_{h,avg}}{0.435 \cdot \sqrt{C_C \cdot C_R} \cdot \gamma_w} \quad (2.1)$$

Where D is the constrained modulus, γ_w is the unit weight of water, m_h is the *horizontal* 1D coefficient of volume change, C_c and C_r are the 1D compression and recompression indices, respectively, $\sigma'_{h,avg}$ is the average horizontal effective stress during the loading increment, and e_0 is the initial in-situ void ratio. A relationship between water flow characteristics and soil type is shown in Figure 2.5.

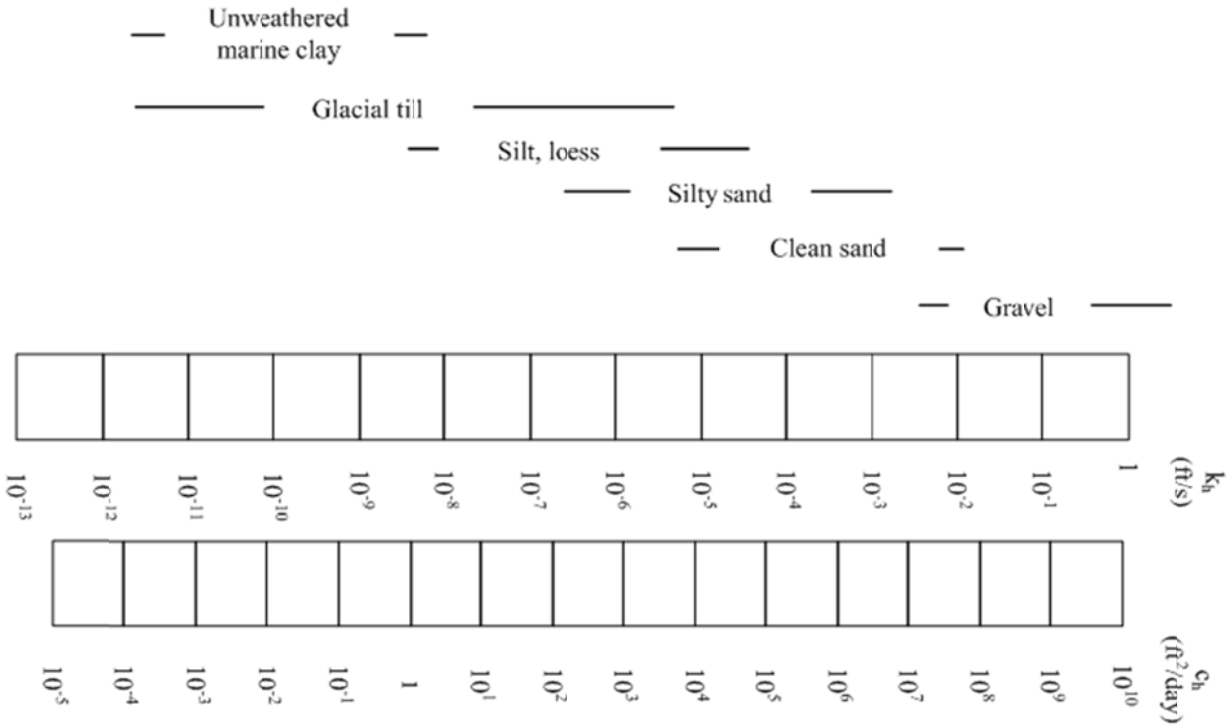

Figure 2.5. Relationship between soil type and water flow characteristics (after Salgado 2008)

Compression of soils is typically defined based on the one dimensional (1D) case where lateral strains are equal to zero and axial strain equals volumetric strain. Figure 2.6 illustrates typical laboratory compression curves for two unstructured clays. For soils which have not been previously compressed, the 1D soil compressibility is defined using the compression index (C_c):

$$C_c = \frac{\Delta e}{\log\left(\frac{\sigma'_{v,f}}{\sigma'_{v,i}}\right)} \tag{2.2}$$

Where $\sigma'_{v,f}$ is the final vertical effective stress and $\sigma'_{v,i}$ is the initial vertical effective stress, and Δe is the change in void ratio for that change in effective stress. Likewise, below the maximum previous effective stress that a soil has been loaded to, or a vertical effective yield stress that has resulted from ageing or cementation, the recompression index (C_r) is defined as:

$$C_r = \frac{\Delta e}{\log\left(\frac{\sigma'_{v,f}}{\sigma'_{v,i}}\right)} \tag{2.3}$$

Use of C_c and C_r indicate that as effective stress increases, compressibility decreases. The 1D coefficient of volume change, $m_v = \Delta\varepsilon_a/\Delta\sigma'_v$, is the inverse of the 1D constrained modulus, $D = 1/m_v = \Delta\sigma'_v/\Delta\varepsilon_a$. The relationship between constrain modulus and coefficient of compression for normally consolidated soil is:

$$D = \frac{1}{m_v} = \frac{(1+e_0)\cdot\sigma'_{v,avg}}{0.435\cdot C_c} \tag{2.4}$$

Constrained modulus, the inverse of compressibility, tends to increase with effective stress. For overconsolidated soils, constrained modulus is related to the recompression index.

$$D = \frac{1}{m_v} = \frac{(1+e_0)\cdot\sigma'_{v,avg}}{0.435\cdot C_r} \tag{2.5}$$

This equation would also result in the constrained modulus in the overconsolidated region increasing (essentially linearly) with increasing effective stress. However, it is common to assume that constrained modulus is constant within the overconsolidated region (e.g., Janbu

1985). This assumption is partially influenced by laboratory testing procedures and sample disturbance, but is a reasonable assumption due to the small changes in modulus with effective stress in the overconsolidated region (small C_r) as well as the limited stress range over which that modulus may apply (for a relatively low p'_c or $\Delta\sigma'$ during loading).

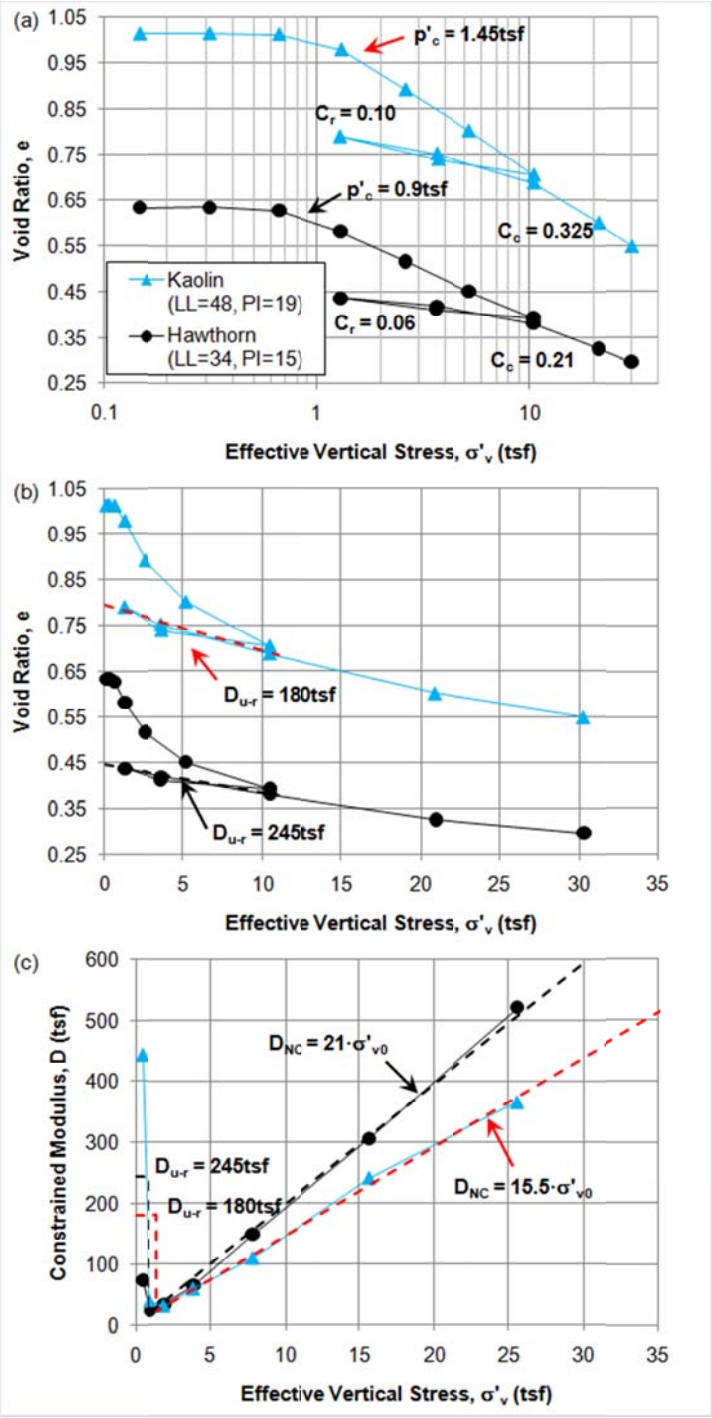

Figure 2.6. Compression/recompression indices and constrained modulus in two unstructured clays

While compressibility is the 'change in size' of a soil element due to increases in effective stress, shear stiffness is the resistance to distortion from a resulting shear stress. Differences between shear stiffness and compressibility (and its relationship to dilation angle) are illustrated in Figure 2.7.

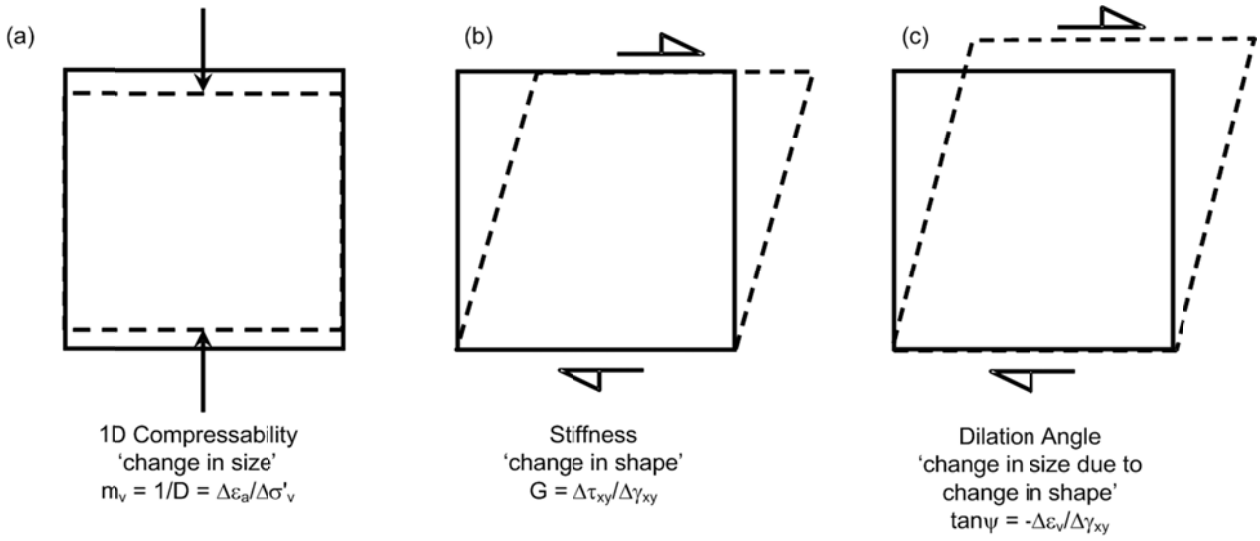

Figure 2.7. Comparison of (a) compression, (b) distortion, and (c) dilation for an element of soil

When using elastic theory, stiffness is related to compressibility through the Poisson ratio (ν):

$$D = \frac{(1-\nu)E}{(1+\nu)(1-2\nu)} = \frac{(1-\nu)2G}{(1-2\nu)} \tag{2.6}$$

Where E (=$\Delta\sigma_y/\Delta\varepsilon_y$, for plane stress conditions) is the elastic (Young's) modulus and G is the shear modulus ($\Delta\tau_{xz}/\Delta\gamma_{xy}$). Shear stiffness of soil is characterized by shear modulus, G. Simple relationships for shear modulus for soils can be expressed as (e.g., after Santamarina et al. 2001):

$$G = G_{ref}\left(\frac{s'}{p_{ref}}\right)^n \tag{2.7}$$

where G_{ref} is the shear modulus for a certain soil at a reference stress (p_{ref}) of 100 kPa and s' is the mean effective stress in the shear plane [$s'=(\sigma'_1+ \sigma'_3)/2$]. The exponent *n* varies between 0 (for cemented soils, e.g., Santamarina et al. 2001, Coop 2005) to 1.0 (for normally consolidated clays at large strains, e.g., Viggiani & Atkinson 1995). The exponent *n* (i.e., rate of change of stiffness with changes in effective stress) is soil type, stress history, and strain level dependent, and tends to increase with strain level (e.g., Viggiani & Atkinson 1995, Coop 2005). Additionally, as G_{ref} increases, the exponent *n* tends to decrease for the case of small strain stiffness (Santamarina et al. 2001). The exponent *n* may be greater than unity if large reductions in void ratio occur due to increases in effective stress (i.e., compressibility).

A main difficulty in evaluating shear modulus is the dependence of G on (shear) strain. Figure 2.8 illustrates the influence of strain on shear stiffness. Operational shear stiffness for a retaining wall or foundation are often ½ to ¼ of the value of stiffness measured from geophysical tests, and equal to stiffness measured in a pressuremeter unload-reload loop ranging to approximately ½ that value. For aged and cemented soils, the ratio of G/G_0 tends to be lower for a given strain level when compared to uncemented soils (e.g., Fahey 2005).

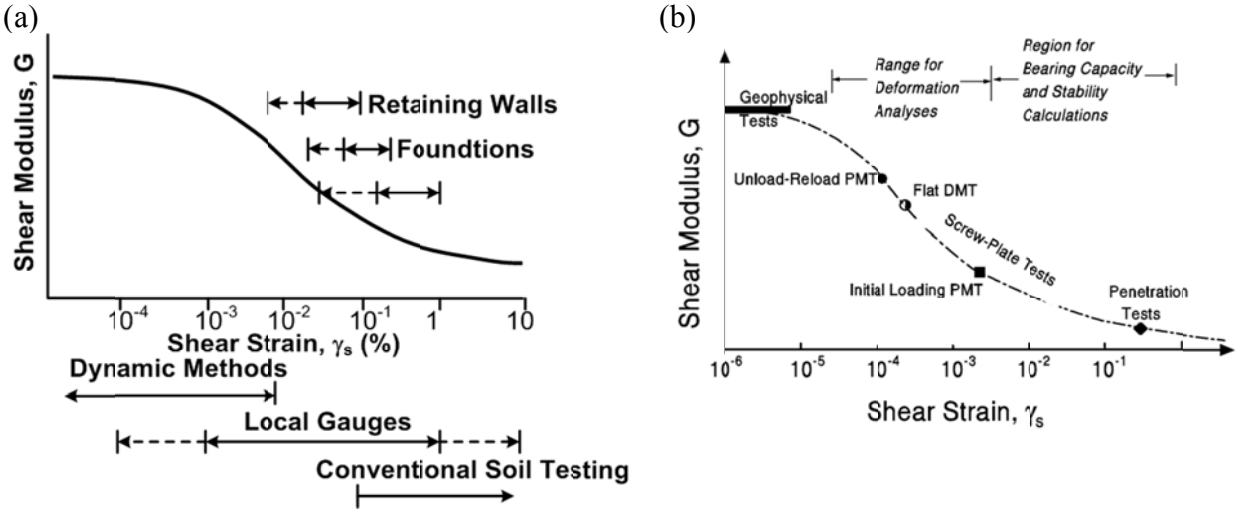

Figure 2.8. Influence of strain level on soil stiffness for (a) laboratory tests and design applications (after Atkinson 2000) (b) in-situ tests and design applications (Mayne 2001)

Much of geotechnical design is based on ultimate states, where soil strength is the paramount design parameter of interest. Uncemented soils are a frictional material, and strength (maximum

shear stress the soil can resist) is a function of the friction angle (ϕ) and the effective normal stress on the failure plane (σ'_n, Figure 2.9a):

$$\tau_f = \sigma'_n \tan\phi \tag{2.8}$$

When the major (σ'_1) and minor (σ'_3) principal effective stresses, or the mean effective stress [$s' = (\sigma_1' + \sigma_3') / 2$], is known, the shear stress at failure is:

$$\tau_f = \frac{(\sigma'_1+\sigma'_3)}{2}\sin\phi = s'\cdot\sin\phi \tag{2.9}$$

For cases of rapid loading in soils with a low coefficient of consolidation (i.e., clays, typ.), the changes in total stress are essentially equal to changes in pore pressure. The mean octahedral effective stress does not significantly change and soil strength is more reliably evaluated using the undrained shear strength (s_u, Figure 2.9b):

$$\tau_f = s_u \tag{2.10}$$

The undrained shear strength is sometimes referred to as the undrained cohesion, c_u, however, this terminology does not reflect the mechanical behavior and will not be used further in this report. The undrained shear strength in Figure 2.9b is shown to be independent of total stress. This is not because the friction angle is zero, but it is that the mean octahedral effective stress does not change during shearing ($\Delta\sigma \approx \Delta u_{oct}$), and therefore the strength (or state / OCR) does not immediately change due to application of a load.

Shearing of the soil induces changes in pore pressures and effective stress, resulting from the potential for a soil to contract or dilate. The normalized undrained shear strength (s_u/σ'_{v0}) must be modified to account for the soil state. The soil state is most commonly assessed using the overconcolidation ratio (OCR = p'_c/σ'_{v0}, where p'_c is the preconsolidation stress). The

relationship between s_u/σ'_{v0} and OCR can be approximated as (e.g., Schofield & Wroth 1968, Mayne 1980, Wroth & Houlsby 1985, Ladd 1991):

$$\frac{s_u}{\sigma'_{v0}} \approx \frac{\sin\phi}{2} OCR^{(1-C_r/C_c)} \approx 0.23 \cdot OCR^{0.8} \qquad (2.11)$$

The parameter $\sin\phi/2$ (assumed to be approximately 0.23) is often termed the normally consolidated undrained strength ratio $[(s_u/\sigma'_{v0})_{NC}]$.

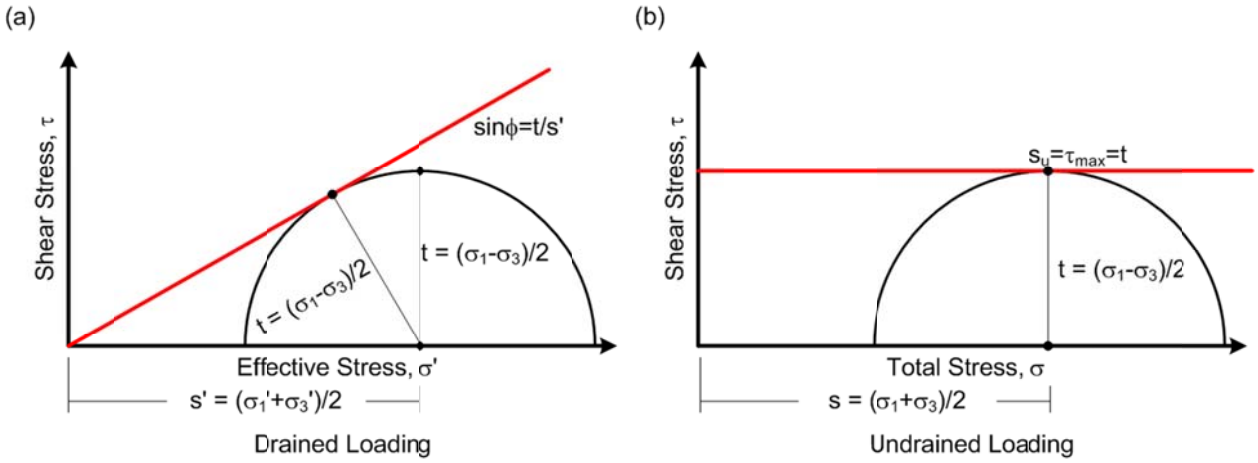

Figure 2.9. Drained and undrained strength parameters

Undrained strength ratios, such as that described by Equation 2.11, vary by direction of loading. This strength anisotropy can be observed in laboratory tests, with different normally consolidated normalized undrained strength ratios being observed for (i) K_0 anisotropically consolidated triaxial undrained compression tests (CK_0UC); (ii) direct simple shear (DSS); (iii) K_0 anisotropically consolidated triaxial undrained extension tests (CK_0UE); and (iv) the vane shear test (VST), among others. Table 2.1 summarizes typical normally consolidated undrained strength ratios for clays and varved clays.

Table 2.1. Comparison of normally consolidated undrained shear strength ratio for typical and varved clays (after Ladd & DeGroot 2003).

Test	Typical $(s_u/\sigma'_{vo})_{NC}$	Varved Clay $(s_u/\sigma'_{vo})_{NC}$ DeGroot & Lutenegger (2003)
CK_0UC	0.33	0.25
DSS	0.20	0.18
CKoUE	0.16	0.21
VST	0.21	0.21

The dilation angle quantifies the change in volume due to shearing of a soil specimen. These volume changes, or the tendency for volume change to occur, results in peak friction angles for sands and the influence of overconsolidation ratio of undrained strength for clays (e.g., Eq. 2.11). Since dilation decreases as mean effective stress at failure increases (e.g., Bolton 1986), understanding dilation is of paramount importance for estimating operational friction angle in sandy soils.

Peak friction angle (ϕ'_{pk}) under drained conditions results from friction (ϕ'_{cv}) and dilation (ψ) (Bolton 1986):

$$\phi_{pk} = \phi_{cv} + \Delta\phi \approx \phi_{cv} + 0.8\psi \tag{2.12}$$

For conditions of triaxial compression (Bolton 1986):

$$\Delta\phi = 3I_{RD} \tag{2.13}$$

For conditions of plane strain (Bolton 1986):

$$\Delta\phi = 5I_{RD} \tag{2.14}$$

The parameter I_{RD} is a relative density index that is a function of relative density (D_R) and mean effective stress at failure [$p'_f = (\sigma'_1+\sigma'_2+\sigma'_3)/3$]. I_{RD} increases with relative density and decreases with mean effective stress at failure (Bolton 1986):

$$I_{RD} = D_r \left[Q - \ln\left(100 \cdot p'_f / p_{ref}\right) \right] - R \qquad (2.15)$$

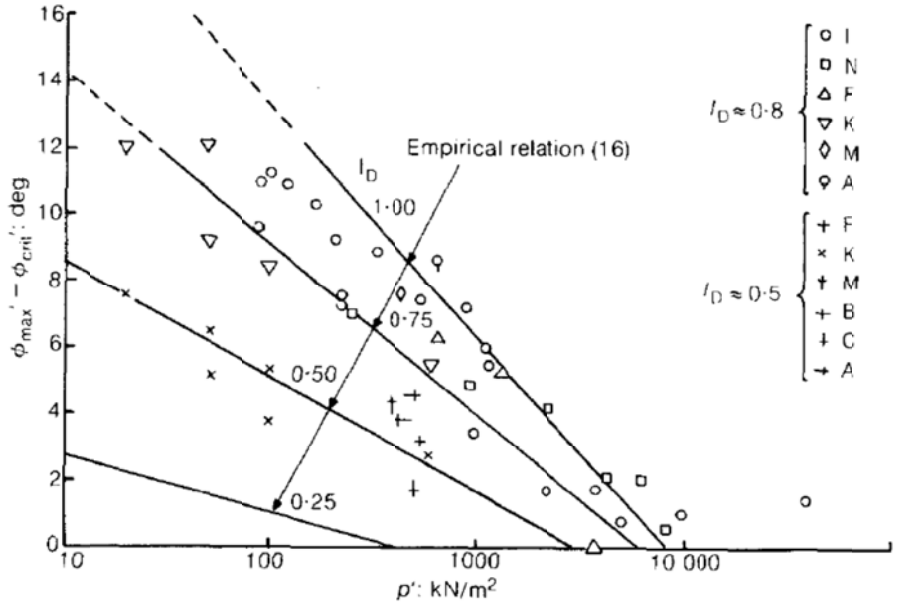

Figure 2.10. Influence of mean stress at failure on the peak friction angle due to dilation (Bolton 1986)

The parameter Q (which is <u>not</u> the normalized cone tip resistance in this case) is a function of soil mineralogy, and is typically taken as 10 in quartz sands and 8 in calcareous sands. The parameter R is typically taken as unity. Constant volume friction angles tend to vary between 27° and 40°, increasing with angularity, and values of $\Delta\phi'$ in excess of 12° should be used with caution (Bolton 1986). The influence of stress level on dilation and peak friction angle is shown in Figure 2.10, and is particularly important for evaluating ϕ from CPT data, as well as for applications such as bearing capacity of shallow foundations on sand.

2.1.3 CPT Parameters and Normalization

As highlighted in Figure 1.1, three parameters are measured during a standard piezocone penetration test:

- cone tip resistance, q_c
- sleeve friction, f_s

- penetration pore pressure measured at the cone shoulder, u_2

Cone tip resistance is influenced by the geometry of a specific cone penetrometer. The corrected cone tip resistance needs to be used for all analyses such that uncertainty in comparison to previous studies and theoretical analysis is minimized. The corrected cone tip resistance is expressed as:

- cone tip resistance corrected for pore pressure effects, $q_t = q_c + (1-a_n)u_2$

where a_n is the net area ratio of the penetrometer that typically varies between 0.5 and 0.95 (Lunne et al. 1986, Lunne et al. 1997). To account for initial in-situ conditions on CPT measurements, the following derived parameters are often used:

- net cone tip resistance, $q_{cnet} = q_t - \sigma_{v0}$
- excess penetration pore pressure, $\Delta u_2 = u_2 - u_0$
- effective cone tip resistance, $q_E = q_t - u_2$

For the above derived parameters σ_{v0} is the total stress at a given depth prior to penetration, and u_0 is the in-situ pore pressure at a given depth prior to penetration.

Since soil mechanical properties are controlled by initial effective stress and changes in effective stress during loading, rational interpretation of CPT measurements requires normalization by some measure of effective stress (e.g., Wroth 1984, 1988). For soil classification based on normalized piezocone parameters, a combination of two of the seven following parameters is typically used (e.g., Douglas & Olsen 1981,Wroth 1984, Wroth 1988, Robertson 1990, Olsen & Mitchell 1995, Robertson & Wride 1998, Jefferies & Been 2006, Schneider et al. 2008, Robertson 2010):

- normalized cone tip resistance, $Q = q_{cnet}/\sigma'_{v0}$
- modified normalized cone tip resistance, $Q_{tn} = (q_{cnet}/p_{ref})/(\sigma'_{v0}/p_{ref})^n$
- normalized effective cone tip resistance, $Q_E = (q_t-u_2)/\sigma'_{v0}$

- friction ratio, F (%) = $f_s/q_{cnet} \cdot 100$
- normalized sleeve friction, f_s/σ'_{v0}
- pore pressure parameter, $B_q = \Delta u_2/q_{cnet}$
- normalized excess penetration pore pressure, $\Delta u_2/\sigma'_{v0}$

While the initial horizontal effective stress or preconsolidation stress may be more appropriate for normalization (e.g., Mayne 1986, Houlsby 1988, Houlsby & Hitchman 1988, Been & Jefferies 2006), the in-situ vertical effective stress is used for the above mentioned normalized parameters as it can be calculated without significant additional analyses. For initial classification purposes, it is preferred to use Q rather than Q_{tn}. Q is equal to Q_{tn} for a stress exponent (n) equal to unity, and therefore does not require iteration in its interpretation (i.e., is easier to use). Additionally, no significant advantages have been observed when using Q_{tn} over Q for classification purposes (e.g., Schneider et al. 2008), and use of Q allows for plotting data in a variety of different frameworks to highlight different responses. Plotting Q vs. B_q or Q vs. $\Delta u_2/\sigma'_{v0}$ are analogous since $Q \cdot B_q = \Delta u_2/\sigma'_{v0}$. Likewise, plotting Q vs. F or Q vs. f_s/σ'_{v0} are analogous since $Q \cdot F = f_s/\sigma'_{v0}$. Each plotting format has advantages and disadvantages for highlighting aspects of soil behavior.

As mentioned in the previous section, soil strength and stiffness generally increase with effective stress, but this relationship is also influenced by the effective stress loading history of a soil element and/or crushable nature of the soil grains, herein discusses as 'state.' Undrained behavior in clay soils is used as an example to illustrate the influence of state on normalized response. If we assume that soil undrained strength (s_u) is the primary factor controlling cone tip resistance, q_t, a direct relationship between the two properties would exist (through a 'bearing capacity', or cone, factor, N_{kt}):

$$q_{cnet} = s_u \cdot N_{kt} \tag{2.16}$$

For a constant N_{kt}, the normalized cone tip resistance would therefore be equal to:

$$Q = \frac{s_u}{\sigma'_{v0}} \cdot N_{kt} \tag{2.17}$$

For normally consolidated clays that have not been previously loaded (or aged), s_u/σ'_{v0} is typically taken as a constant [i.e., $(s_u/\sigma'_{v0})_{NC}$], and therefore Q is a constant value (generally around 3 to 5). Q is essentially constant in normally consolidated clays and as the overconsolidation ratio (OCR) increases Q will also increase:

$$Q = \left(\frac{s_u}{\sigma'_{v0}} \right)_{NC} \cdot OCR^{\Lambda} \cdot N_{kt} \tag{2.18}$$

Figure 2.11 shows normalized cone tip resistance in normally consolidated and an overconsolidated clay.

When evaluating specific engineering behavior, such as friction angle, relative density, liquefaction resistance, Q may not be the most appropriate normalizing parameter, and Q_{tn} is often used. Observations of stress exponents less than unity are largely influenced by stress dependency on dilation angle and crushability of sands at high stresses (e.g., Bolton 1986, Salgado et al. 1997, Olsen & Mitchell 1995, Moss et al. 2006). Figure 2.12 illustrates normalized cone tip resistance in loose and dense sands. At shallow depths Q in both drained sands and undrained clays may exceed 20 and approach 1000.

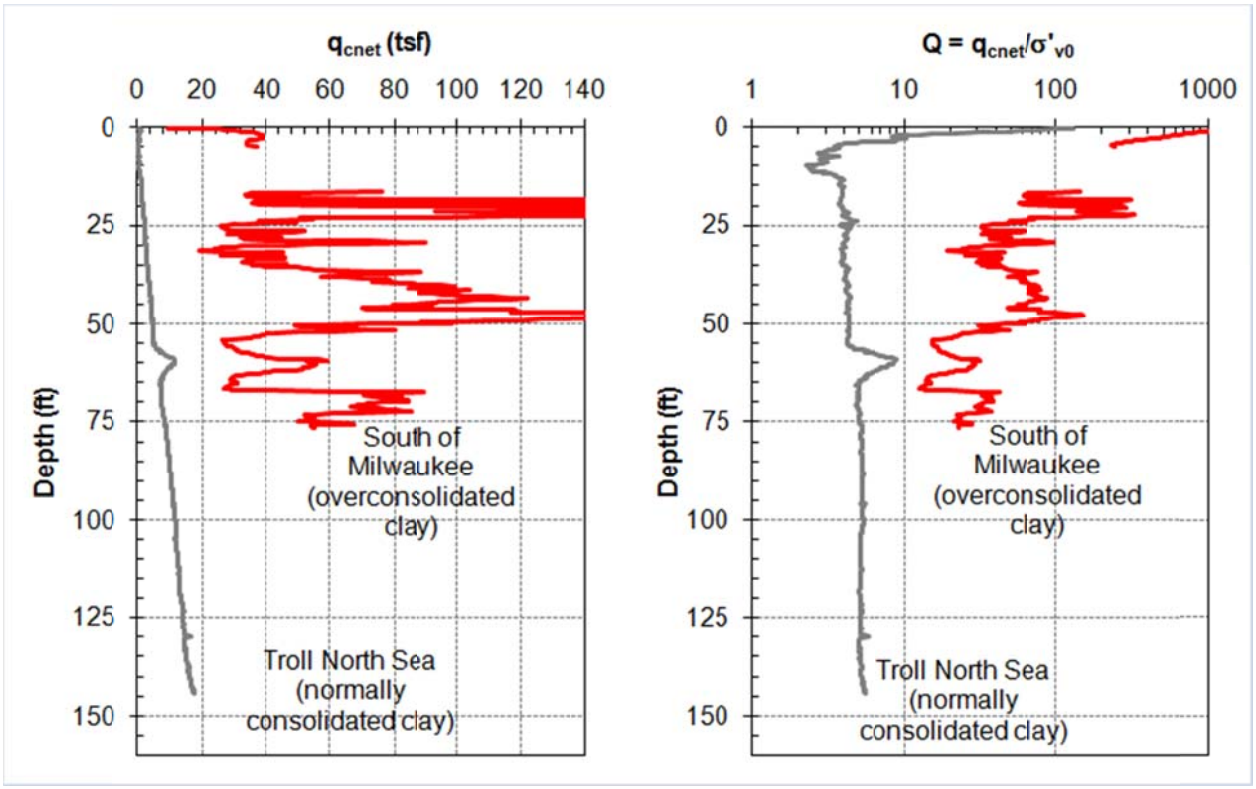

Figure 2.11. Normalized cone tip resistance in normally consolidated and overconsolidated clays (data from Amundsen et al. 1985, Liao et al. 2010)

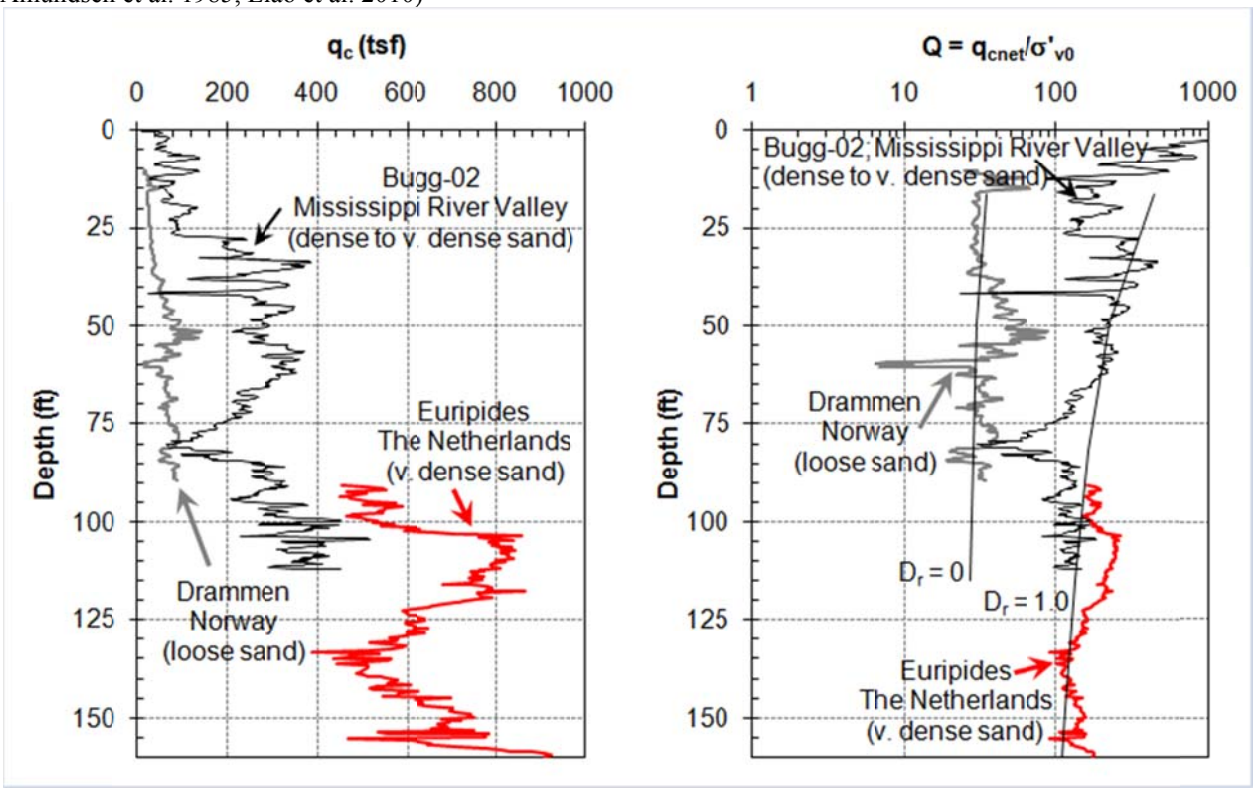

Figure 2.12. Normalized cone tip resistance in loose and very dense sands (after Schneider et al. 2008)

2.2 Minnesota DOT (after Dasenbrock, Schneider & Mergen 2010)

Since 2001 the Minnesota DOT (Mn/DOT) has performed over 7500 CPTs in glacial geological conditions. Despite these conditions often being considered as difficult ground for this technique, Mn/DOT uses the CPT on more than 75% of their "foundations" projects. Over 400 of those CPTs from 21 sites are assessed herein.

Boring logs and electronic CPT data have been made available through Mn/DOT are included as electronic files on the ArcGIS database complied for this project. Additional site information can be found through the Mn/DOT Geotechnical Investigation Information Interchange Internet Interface (GI^5) (e.g., Dasenbrock 2008):

http://www.mrr.dot.state.mn.us/geotechnical/foundations/Gis/gi5_splash.html

2.2.1 Procedures and cone performance

To minimize the potential for cone damage and ensure collection of high quality data, Mn/DOT has adopted standard procedures for test preparation, performance, and data recording (e.g., Lunne et al. 1997). Mn/DOT has 3 CPT rigs in year round operation; a 11 ton tracked rig, a 13 ton 4x4 truck, and a 30 ton 6x6 truck. Many projects require only shallow exploration, and investigations are performed to depths of 30 ft to 50 ft. For bridges, explorations in excess of 100 ft are often required. Hole sealing procedures for depths in excess of 50 ft require grouting from the bottom of the hole during cone extraction. For these projects Mn/DOT utilizes a standard setup for grouting during cone extraction, which is semi-automated on the 30 ton truck.

Both 10 cm^2 (1.44 inch diameter) and 15 cm^2 (1.72 inch diameter) cones are used; the two truck rigs typically use the larger diameter cones. Mn/DOT keeps approximately 15 'service ready cones' on hand (distributed among the 3 rigs and the lab) at any given time. Calibrations are performed by the penetrometer manufacturer and occur annually or at the time of a cone repair. The net area ratio (a_n) used for correction of the tip resistance for pore pressure effects is 0.8, as provided by the cone manufacturer. Due to hard ground conditions or obstructions, approximately one cone is broken per year. Additionally, approximately every 1.5 months, an in-

service cone will need to be repaired. These repairs are usually for a bad channel (e.g. pore pressure), bending or crushing of the sleeve or probe housing, or water damage due to an issue with one of the seals. To minimize cone damage, methods suggested by Lunne et al. (1997) have been adopted, namely, (i) keeping the inclination less than 10^o, particularly for shallow holes; (ii) minimizing total force applied to dense soils underlying thick zones of very soft material, such as peat; and (iii) having a presence of mind to realize that there may be boulders or cobbles in certain geological conditions, and that sharp spikes in tip resistance associated with rapid changes in inclination (> 1^o/m push) should result in termination of a sounding.

On projects where clay soils are present and consolidation characteristics are of interest, or where materials are not well defined, pore pressure dissipation test data have proved valuable on many Mn/DOT projects. An effort is made to ensure reliable pore pressure data; Mn/DOT purchases filter element from the CPT manufacturer that are pre-saturated with silicone oil. While the oil viscosity may result in sluggish response, it also helps reduce the likelihood that the system will become unsaturated. In some cases it is difficult to maintain proper saturation and record high quality pore pressure data through an entire layer, particularly in deposits above the water table, very stiff soils, or layered clays and silty sands. More detailed review of data quality is required when evaluating design parameters from q_t and or u_2 data in these situations.

2.2.2 Geology and typical soil profiles

The geology of Minnesota has primarily been shaped by glacial action. As a result, the state has highly variable deposits consisting of (i) alluvium; (ii) colluvium; (iii) glacial lake deposits; (iv) outwash; (v) peat; (vi) weathered bedrock; and (vii) glacial till. Initial review of single CPTs from 6 sites was performed for this section. The six locations include geologic conditions consisting of (i) till soils; (ii) lake deposits; (iii) peat; (iv) outwash; and (v) alluvium. Details on the project types and soil conditions are included in Figure 2.13 and Table 2.2.

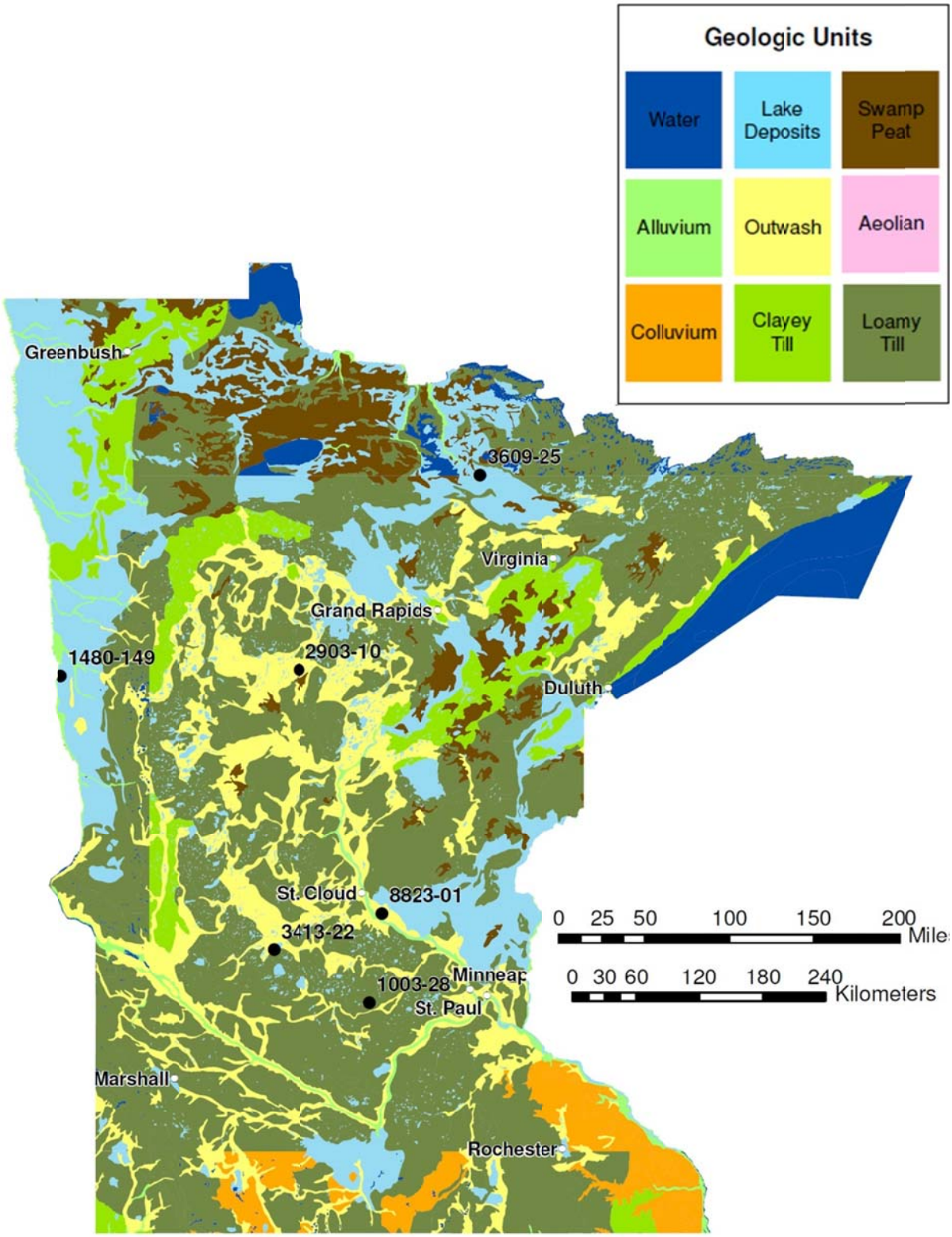

Figure 2.13. Location of initial Mn/DOT CPT sites on a map of Minnesota Quaternary geology. Map adapted from data on previously published maps (Goebal et al. 1983, Farrand et al. 1984, Hallberg et al. 1991, Sado et al. 1994, Swinehart et al. 1994, Fullerton et al. 1995, Sado et al. 1995, Fullerton et al. 2000)

Table 2.2. Description of initial Mn/DOT CPT sites

UW Site No.	Depth Range Analyzed (ft)	Site Project ID: Design Issues	Regional Geology	Number of CPTs
-	10-36	1003-28: Roadway / settlement	Loamy Till	40
8	5-50	3609-25: Roadway / bridge / geofoam	Lake Clays	60
-	5-80	1480-149: Landslide	Lake Clays	13
13	6-25	3413-22: Roadway failure / Retaining Wall	Peat	149
-	0-35	2903-10: Roadway Alignment	Outwash (Sand)	20
-	0-33	8823-01: Groundwater monitoring	Alluvium (Silty Sand)	3

Upon completion of a site investigation, CPT (and boring) data are processed, entered into project databases, and exported for use in a web enabled Geographic Information System (GIS) (Dasenbrock 2008). Individual vertical profiles are analyzed, and cross sections are developed for larger projects. Profiles of net tip resistance and friction ratio from the 6 sites are shown in Figure 2.14, and profiles of net tip resistance ($q_{cnet}=q_t-\sigma_{v0}$) and excess pore pressure ($\Delta u_2=u_2-u_0$) are shown in Figure 2.15. Normalized soil behavior type is used by Mn/DOT for preliminary evaluation of layering. Both the Robertson (1990, 1991) Q-F and Q-B_q charts have been used by Mn/DOT, depending upon soil layering. In sandy soils, Q-F charts are typically used, while in clayey soils, Q-B_q charts are typically used. Use of these charts requires selection of appropriate normalized parameters and requires judgment that is dependent upon data quality and design application.

Since soil behavior is controlled by 'soil state' as well as rate of drainage (particle size), among other factors, Figures 2.14 and 2.15 include a trend line reflecting inferred soil state. In glacial deposits where the soil can often be considered preconsolidated by a vertical load (i.e., a glacier), the preconsolidation difference ($\Delta p'_c$) allows for assessment of reduction in OCR (state) with depth in clayey soils. Assuming a constant N_k value of 15 and a normally consolidated undrained strength ratio [$(s_u/\sigma'_{v0})_{NC}$] of 0.27 for preliminary analyses, the net cone tip resistance ($q_{cnet} = q_t-\sigma_{v0}$) can be estimated as a function $\Delta p'_c$ and σ'_{v0}.

$$q_{cnet} = N_k \left(\frac{s_u}{\sigma'_{v0}} \right)_{NC} \cdot \sigma'_{v0} \cdot OCR^{\Lambda} \approx 4 \cdot \sigma'_{v0} \left(1 + \frac{\Delta p'_c}{\sigma'_{v0}} \right)^{0.75} \tag{2.19}$$

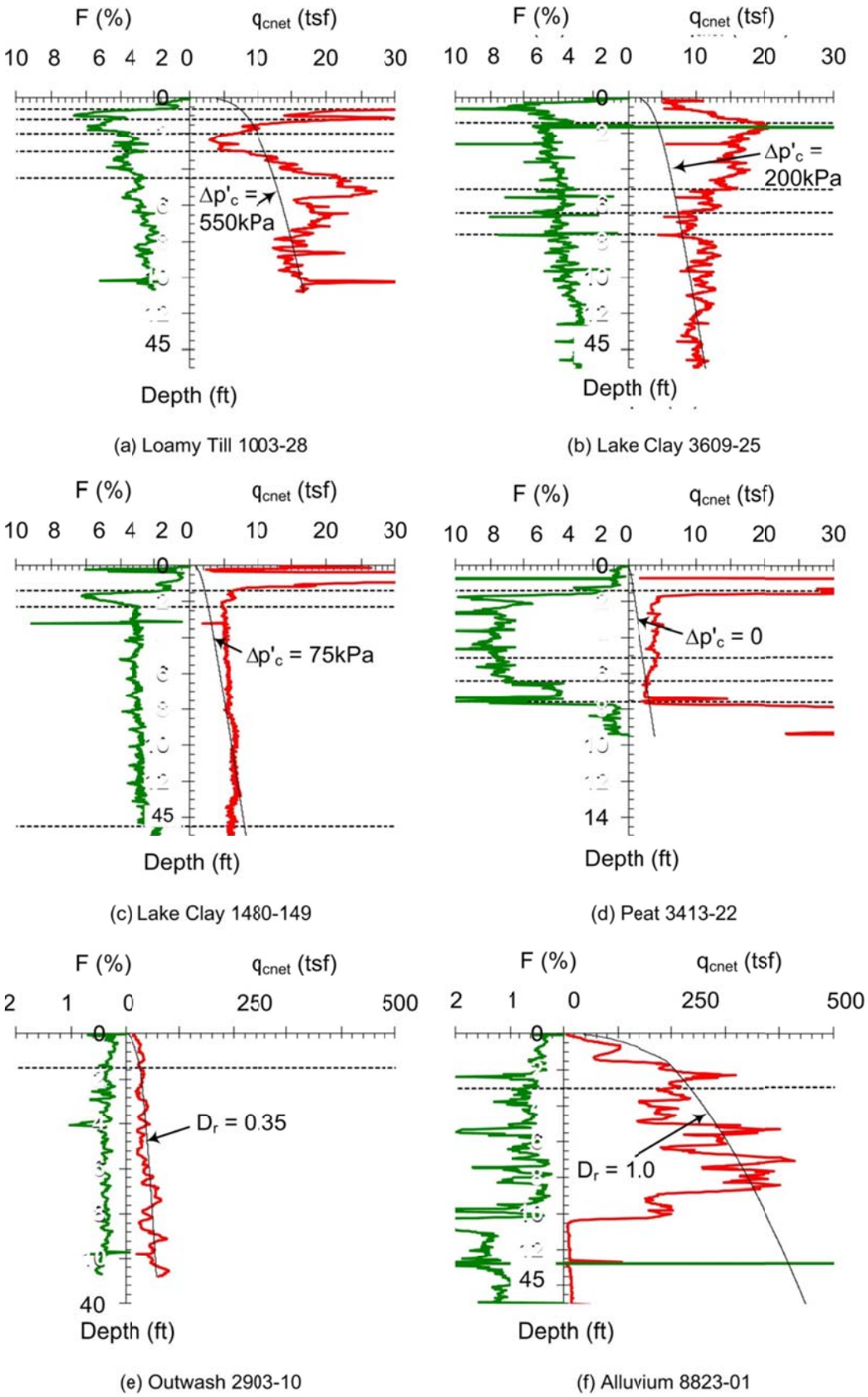

Figure 2.14. Profiles of q_{cnet} and F for selected sites in Minnesota

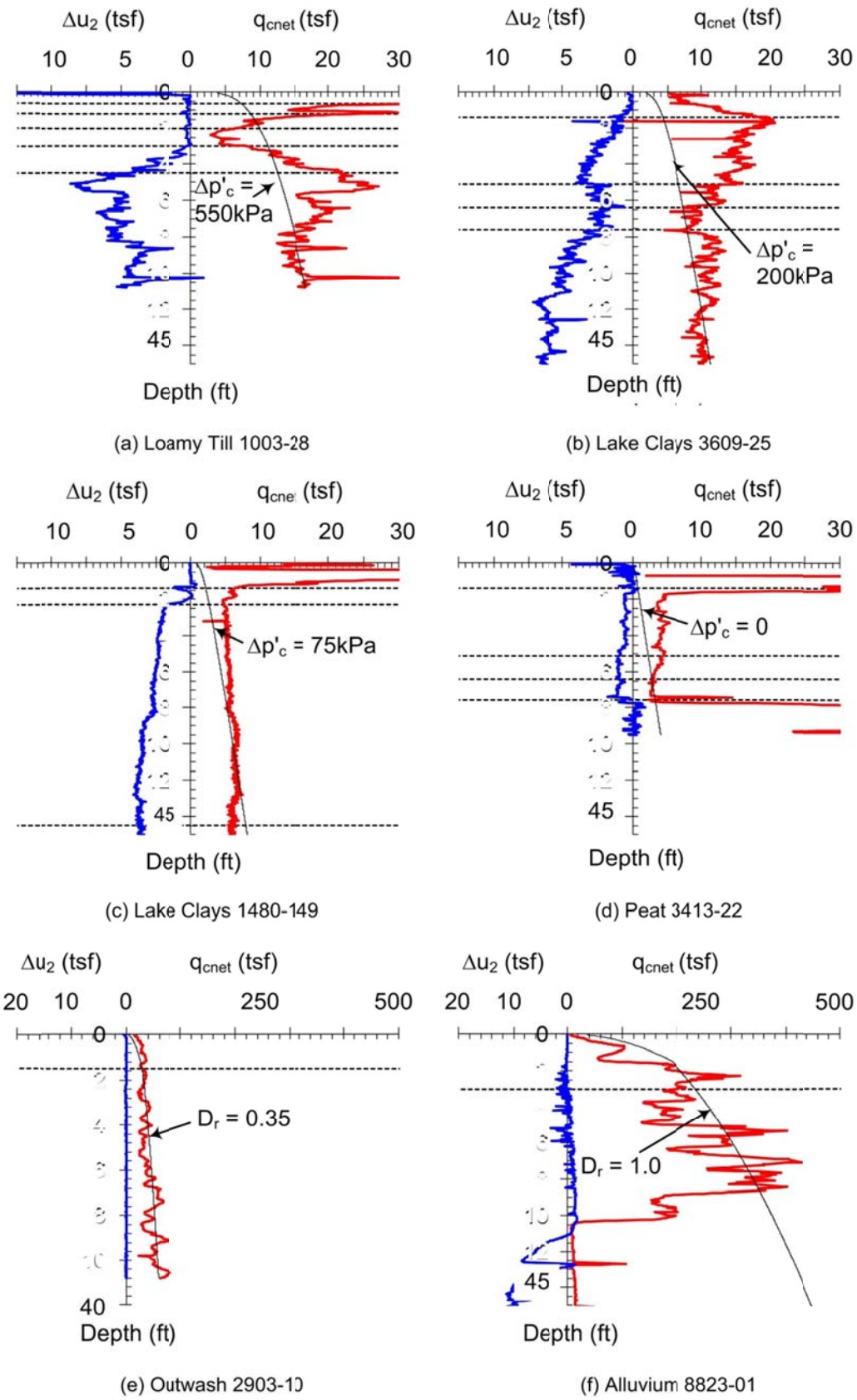

Figure 2.15. Profiles of q_{cnet} and Δu_2 for selected sites in Minnesota

Estimated values of $\Delta p'_c$ vary from 75kPa to 200 kPa for the lake deposits, and 550kPa for the loamy till soil shown. The peat soils have very low tip resistance, and are modeled fairly well as a normally consolidated deposit ($\Delta p'_c$=0), particularly at depth. While use of $\Delta p'_c$ does not satisfactorily match the entire depth of each profile, it does provide an indication of soil state such that design issues can be addressed in a more rational framework.

Relative density (D_r) is a useful parameter for evaluation of the anticipated behavior of sandy soils, and is related to soil state when combined with effective stress at failure (e.g., Figure 2.10). Profiles of net cone tip resistance are estimated from an inferred relative density in Figures 2.14 and 2.15 using the following equation (e.g. updated based on Jamiolkowski et al. 2003):

$$q_{cnet} \approx p_{ref}\, 20e^{(2.86 \cdot D_r)} \left(\frac{\sigma'_{v0}}{p_{ref}} \right)^{0.5} \tag{2.20}$$

Two extremes of sand density can be seen, with these outwash soils having a relative density on the order of 0.35 and these alluvial soils have a relative density near 1.0.

2.2.3 Performance at additional sites

Detailed evaluation of 21 sites and over 400 CPTUs was performed (Figure 2.16), as summarized in Tables 2.3 and 2.4, and Appendix 1 and 3. The main purpose of this exercise was to assess the typical geological conditions, penetration depths, and soil types in which Mn/DOT has had successful use of the CPT. Lateral spatial variability of cone tip resistance and friction ratio were quantified to see if variability had an influence of likelihood of meeting premature refusal when testing in a given soil environment. Borings were compared to a given CPT at 20/21 sites. Table 2.2 summarizes typical geological environments where CPTs were performed:

- Alluvium – 8 sites
- Clay Till – 2 sites
- Lake deposits – 5 sites
- Loamy Till – 5 sites

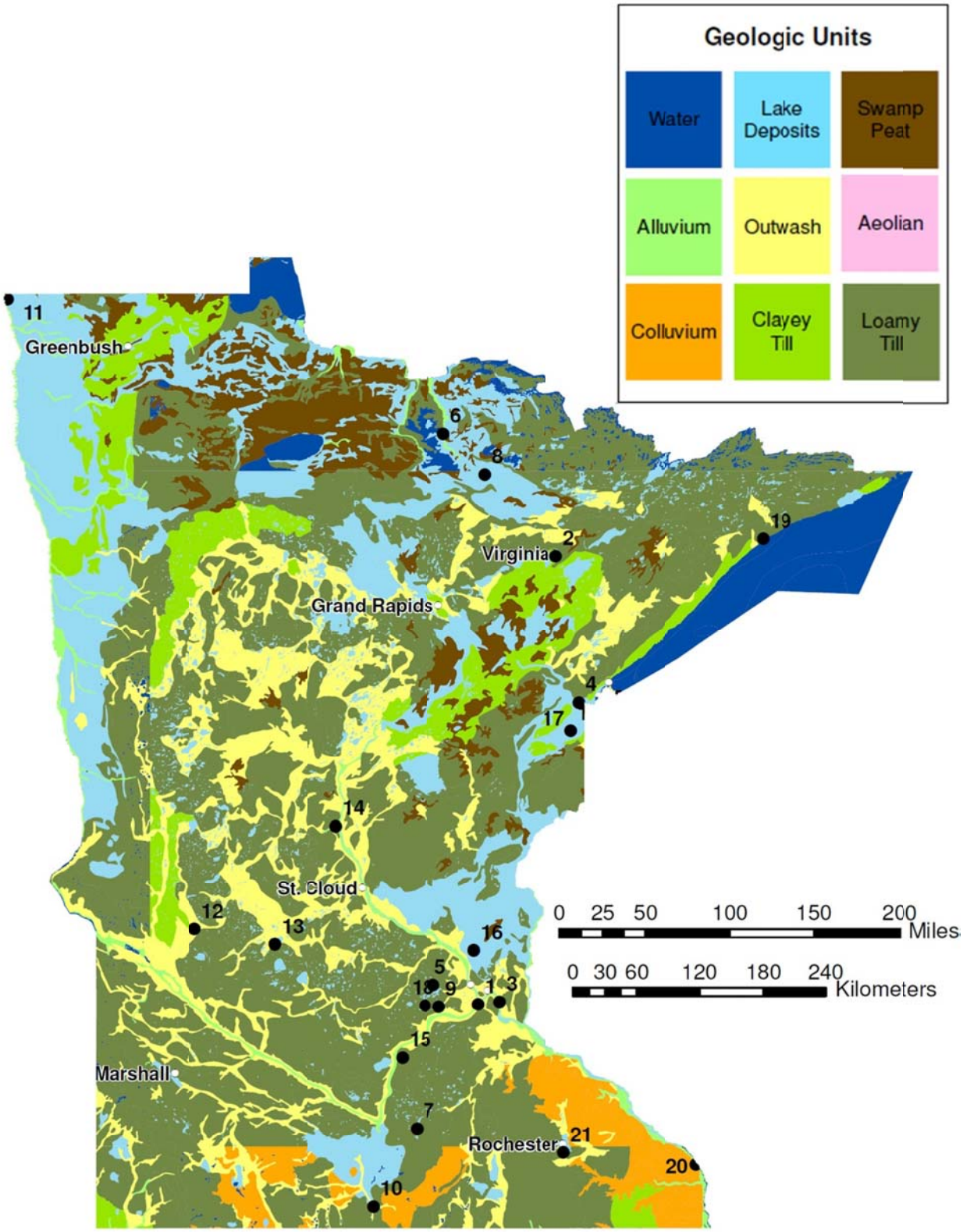

Figure 2.16. Location of Mn/DOT CPT sites with detailed analysis on a map of Minnesota Quaternary geology. Map adapted from data on previously published maps (Goebal et al. 1983, Farrand et al. 1984, Hallberg et al. 1991, Sado et al. 1994, Swinehart et al. 1994, Fullerton et al. 1995, Sado et al. 1995, Fullerton et al. 2000)

Table 2.3. Summary of regional geology for Mn/DOT sites analyzed

UW Site No.	Mn/DOT Proj. No.	County	Regional Geology
1	MAC	Hennepin	**Alluvial** valley of Minnesota river within outwash deposits
2	6918-69	St. Louis	**Clayey till**
3	8285-80	Washington	**Alluvial** valley of Mississippi river within outwash deposits
4	0916-16	Carlton	**Alluvial** valley of St. Louis river between Lake and Loamy till deposits
5	2713-75	Hennepin	**Loamy till**
6	3609-30	Koochiching	**Alluvial** valley of Little Fork river adjacent to Loamy till, Lake clays, and **Peat**
7	8103-47	Waseca	**Loamy till**
8	3609-25	Koochiching	**Lake** clay & silt adjacent to Sandy till, crossing Little Fork river
9	1009-16	Carver	**Clayey till**
10	2207-32	Faribault	**Loamy till** adjacent to Lake clays / silt (no borings)
11	3507-12	Kittson	**Lake deposits** adjacent to Alluvial valley of Red river
12	7602-16	Swift	**Alluvial** valley of the Chippewa river adjacent to Clayey and Loamy till
13	3413-22	Kandiyohi	**Lake** deposits within Outwash (Peat)
14	4913-21	Morrison	**Alluvial** valley of the Mississippi river within Outwash deposits adjacent to Sandy till
15	4013-43	LeSueur	**Loamy till**
16	0208-123	Anoka	**Lake** deposits within Outwash
17	0901-74	Carlton	**Lake** clay & silt within Outwash adjacent to Clayey till
18	1002-79	Carver	**Loamy till**
19	1601-48	Cook	**Alluvium** over Sandy / Clayey Till, Onion river at Lake Superior
20	8580-149	Winona	**Alluvial** valley of Mississippi river w/in Outwash adjacent to Colluvium
21	5509-63	Olmsted	Sandy **Loamy till**

Table 2.4. Summary of CPT performance for Mn/DOT sites analyzed

UW Site No.	Mn/DOT Proj. No.	County	# CPTs	Depth (ft)			Median CPTU values			lateral variability[1]
				min	median	max	q_t (tsf)	F (%)	u_2 (tsf)	
1	MAC	Hennepin	14	5.6	20.5	30	155	1.0	0.2	moderate
2	6918-69	St. Louis	14	4.4	37	48	18.3	3.4	0.1	high
3	8285-80	Washington	14	48	77	119	52.1	0.6	1.2	moderate
4	0916-16	Carlton	2	32.6	34.5	36.4	13.5	3.9	0.2	moderate
5	2713-75	Hennepin	7	24.8	41.3	41.2	12.2	2.0	2.3	low-mod
6	3609-30	Koochiching	7	19.5	93.2	103.5	11.2	4.2	6.0	low
7	8103-47	Waseca	41	11	24	44	13.7	2.6	0.4	mod-high
8	3609-25	Koochiching	60	40	50	98	13.4	3.3	4.6	low-mod
9	1009-16	Carver	9	9	49	50	24.1	2.6	2.3	low-mod
10	2207-32	Faribault	33	27	48.4	49	10	4.1	1.3	high
11	3507-12	Kittson	24	40	115	163	11.5	3.3	4.4	low
12	7602-16	Swift	3	43	44	46	7.5	4.6	1.4	moderate
13	3413-22	Kandiyohi	25	18	33	50	16.1	2.3	0.7	high
14	4913-21	Morrison	6	13	23	29	91.4	0.9	0.1	low-mod
15	4013-43	LeSueur	54	44	71.5	80	13.6	3.7	0.6	high
16	0208-123	Anoka	13	40	49.5	50	85.0	0.7	0.3	low
17	0901-74	Carlton	12	49	53.5	54	11.8	2.1	4.5	low
18	1002-79	Carver	11	14	37	49	14.2	2.5	0.3	moderate
19	1601-48	Cook	34	1.5	12	32	14.2	1.7	0	high
20	8580-149	Winona	4	4	5	6.5	45.9	1.2	0.1	moderate
21	5509-63	Olmsted	30	5	20	42	30.4	1.6	0.1	mod-high

[1] for lateral variability, high = a majority of depths with q_t COV > 1, low = a majority of depths with q_t COV ≤ 0.3, moderate = a majority of depths with $0.3 \leq q_t$ COV ≤ 1, dual symbols used for profiles with mixed variability

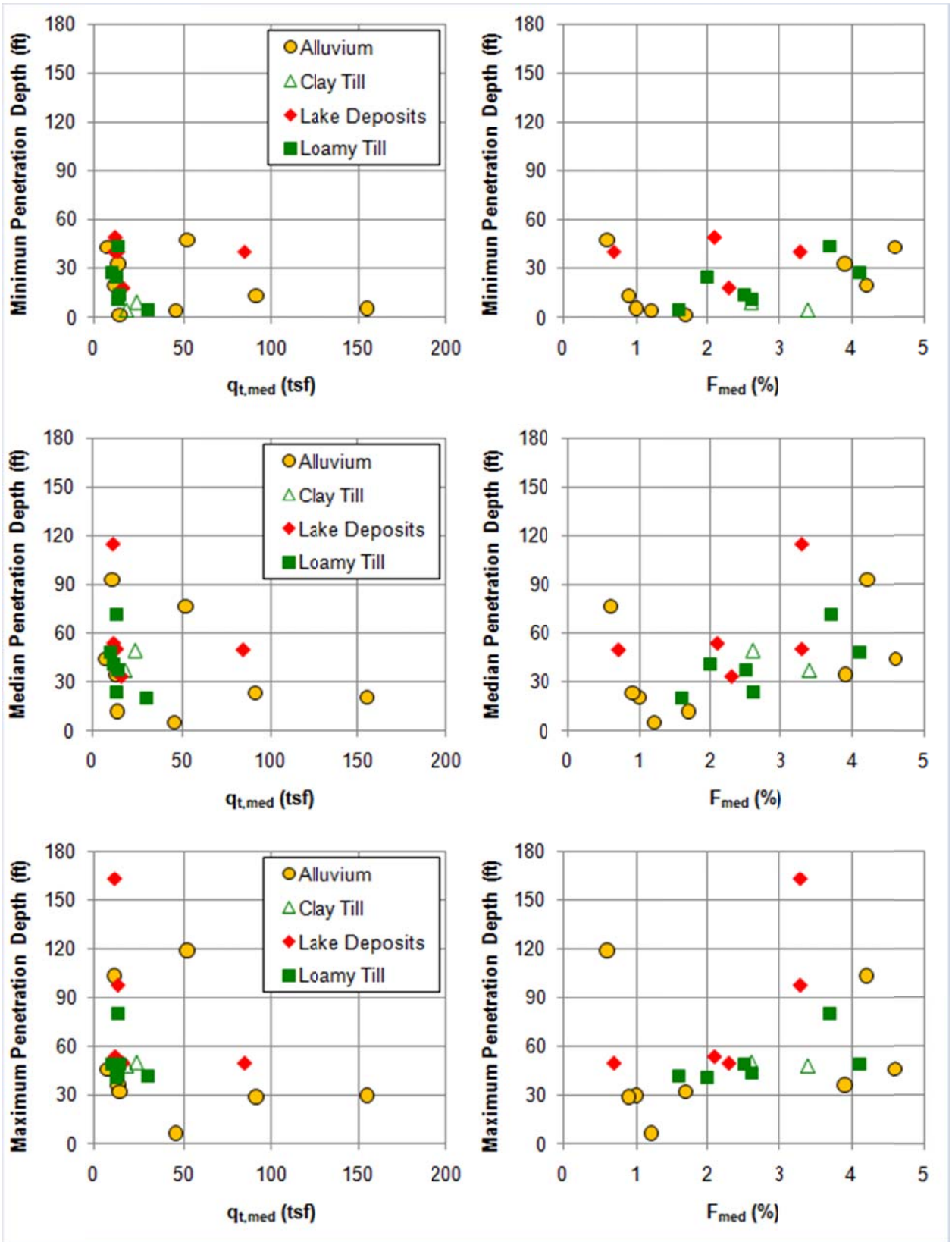

Figure 2.17. Comparison between penetration depth and CPT parameters for a range of geologic conditions in MN

A majority of sites (16/21) had low median cone tip resistance less than 40 tsf, and moderate to high median friction ratios greater than 2%. This indicates predominantly clayey soils. Of the 5 sites with sands and silty sands, 4 of them were from alluvial environments and 1 was lacustrine.

There was little correlation between formation environment or CPT parameters and depth of penetration, as illustrated in Figure 2.17. This tends to occur because of the layered nature of soils, refusal for onshore projects is typically met when a hard layer is reached rather than an accumulation of frictional resistance along the cone rods. Additionally, the median depth of soundings for many sites was on the order of 50 ft. This is often the depth required for investigation, so soundings were terminated because project objectives were met rather than soil response. Shallower soundings with a maximum depth of 30ft were observed in some high tip resistance low friction ratio sandy sites, however it is possible that the soundings were also terminated due to project requirements rather than soil response.

2.2.4 Summary and conclusions related to Mn/DOT data

Mn/DOT has enjoyed successful use of CPT for projects in glacial soil conditions. Cone damage occurs, but breakage and complete loss of cones is relatively infrequent. Depth ranges of interest are typically less than 50 ft for most projects (100 ft for bridges). Within these depth ranges, normalized Q-F and Q-B_q soil classification charts can be used, provided engineering judgment is applied.

Significantly, use of CPT on Mn/DOT projects provides the ability to collect much larger amounts of high quality data to develop detailed profiles of soil strength and stiffness, and detailed cross sections highlighting thin continuous layers, which ultimately impact design decisions. When designing based on limited SPT data, the stratigraphic detail (particularly the horizontal variation across a site) was comparatively crude and imprecise. While site investigations, performed now with the addition of CPT techniques, typically cost about the same as SPT-only based investigations, they are faster, provide significantly more data for assessment of variability, and the data quality is higher such that correlations to lab data can be relied upon with greater certainty. Two compelling observations are that (i) critical time sensitive investigations would have been otherwise impossible to perform without use of the CPT; and (ii)

on many occasions the justification for very expensive or time consuming soil improvement procedures, or use of additional structural systems, was made more compelling by the large amount of high quality soil strength data and stratigraphy inferred from the CPT.

2.3 Wisconsin DOT

CPT data from 2 major projects in the Milwaukee area have been evaluated:

- Marquette Interchange
- Mitchell Interchange

The Marquette Interchange project included a number of CPTs in Lake clays and silts, as well as Clayey Tills. The soils for the Mitchell Interchange were predominantly Clayey Tills. This section will focus on typical characteristics of CPTs at each project, and analyses related to engineering parameters will be included in Chapter 5. Figure 2.18 shows locations of soundings for both sites on a geological map of Milwaukee county. Locations at each site are enlarged in Figures 2.19 and 2.20.

Table 2.5. Summary of regional geology for previous WisDOT sites analyzed

UW Site No.	WisDOT Project	County	Regional Geology
W1a	Marquette	Milwaukee	Clayey Till and Fill
W1b	Marquette	Milwaukee	Lake Clays and Silts
W2	Mitchell	Milwaukee	Clayey Till

Table 2.6. Summary of CPT performance for previous WisDOT sites analyzed

UW Site No.	WisDOT Project	County	# CPTs	Depth (ft)			Median CPTU values			lateral variability[1]
				min	median	max	q_t (tsf)	F (%)	u_2 (tsf)	
W1a	Marquette	Milwaukee	23	13	41	92	38.6	2.9	0.2	high
W1b	Marquette	Milwaukee	4	43	65	70	12.2	3.6	1.8	low-mod
W2	Mitchell	Milwaukee	8	18	55	61	40.2	2.8	0.1	moderate

[1] for lateral variability, high = a majority of depths with q_t COV > 1, low = a majority of depths with q_t COV ≤ 0.3, moderate = a majority of depths with 0.3 ≤ q_t COV ≤ 1, dual symbols used for profiles with mixed variability

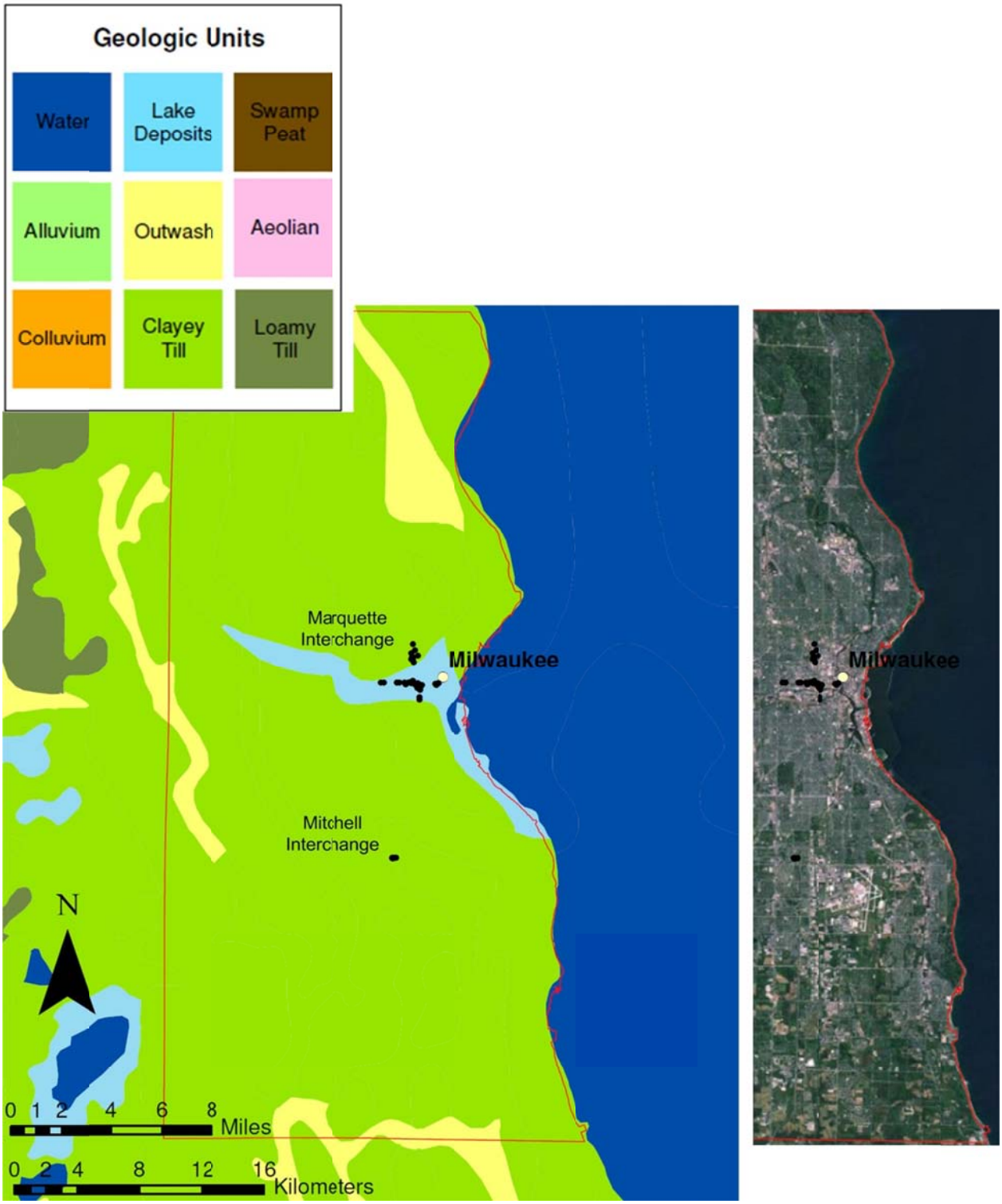

Figure 2.18. Location of WisDOT CPT sites from previous projects. Wisconsin Quaternary geology adapted from data on previously published maps (Linebeck et al. 1983) Aerial photo from ESRI ArcGIS Online, World Imagery.

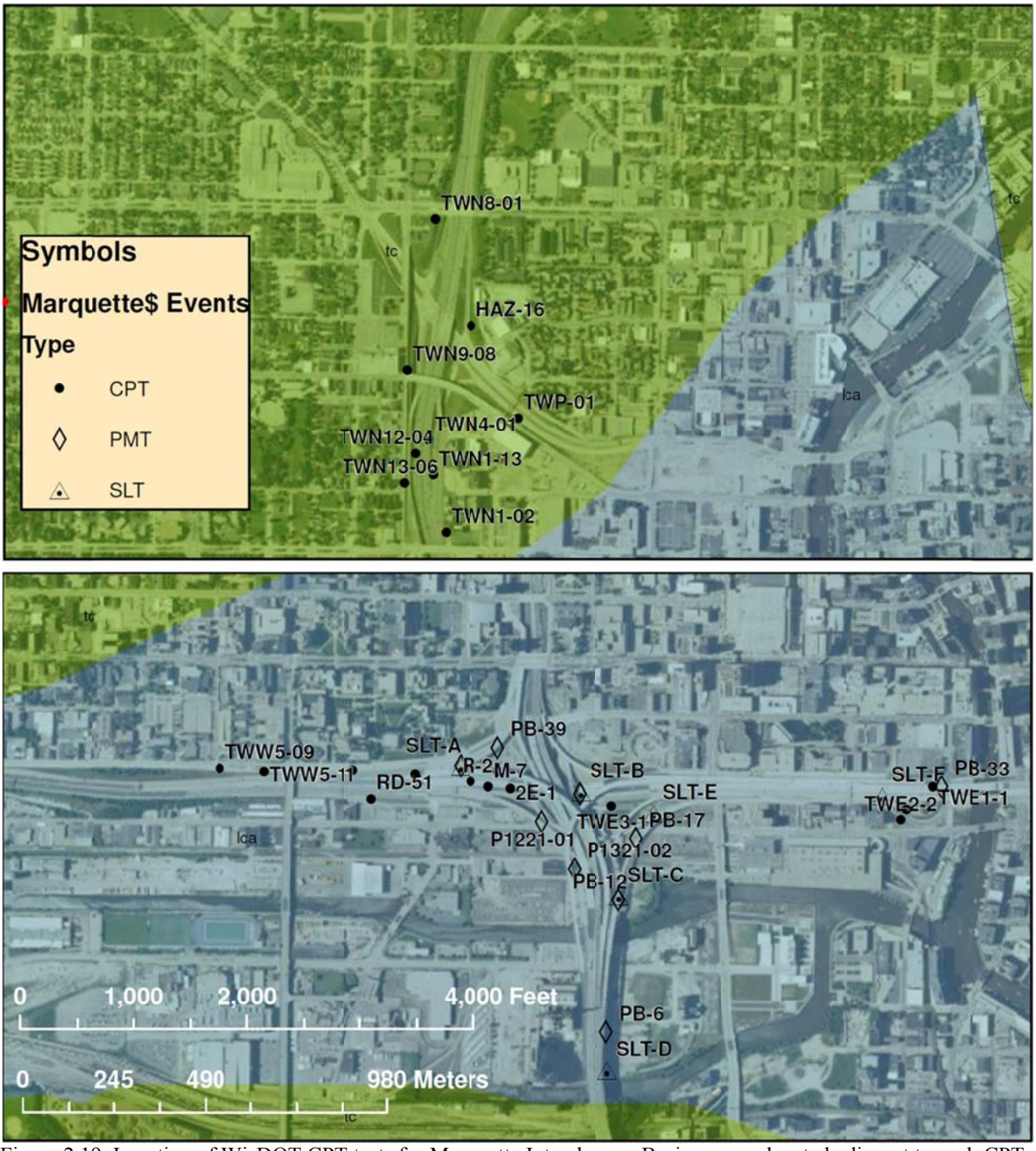

Figure 2.19. Location of WisDOT CPT tests for Marquette Interchange. Borings were located adjacent to each CPT. Borings with pressuremeter testing (PMT) and static load tests (SLT) shown on map. Wisconsin Quaternary geology adapted from data on previously published maps (Linebeck et al. 1983) Aerial photo from ESRI ArcGIS Online, World Imagery.

Figure 2.20. Location of WisDOT CPT tests and adjacent borings for Mitchell Interchange. Pressuremeter data available for Boring 178 and 210A. Wisconsin Quaternary geology adapted from data on previously published maps (Linebeck et al. 1983) Aerial photo from ESRI ArcGIS Online, World Imagery.

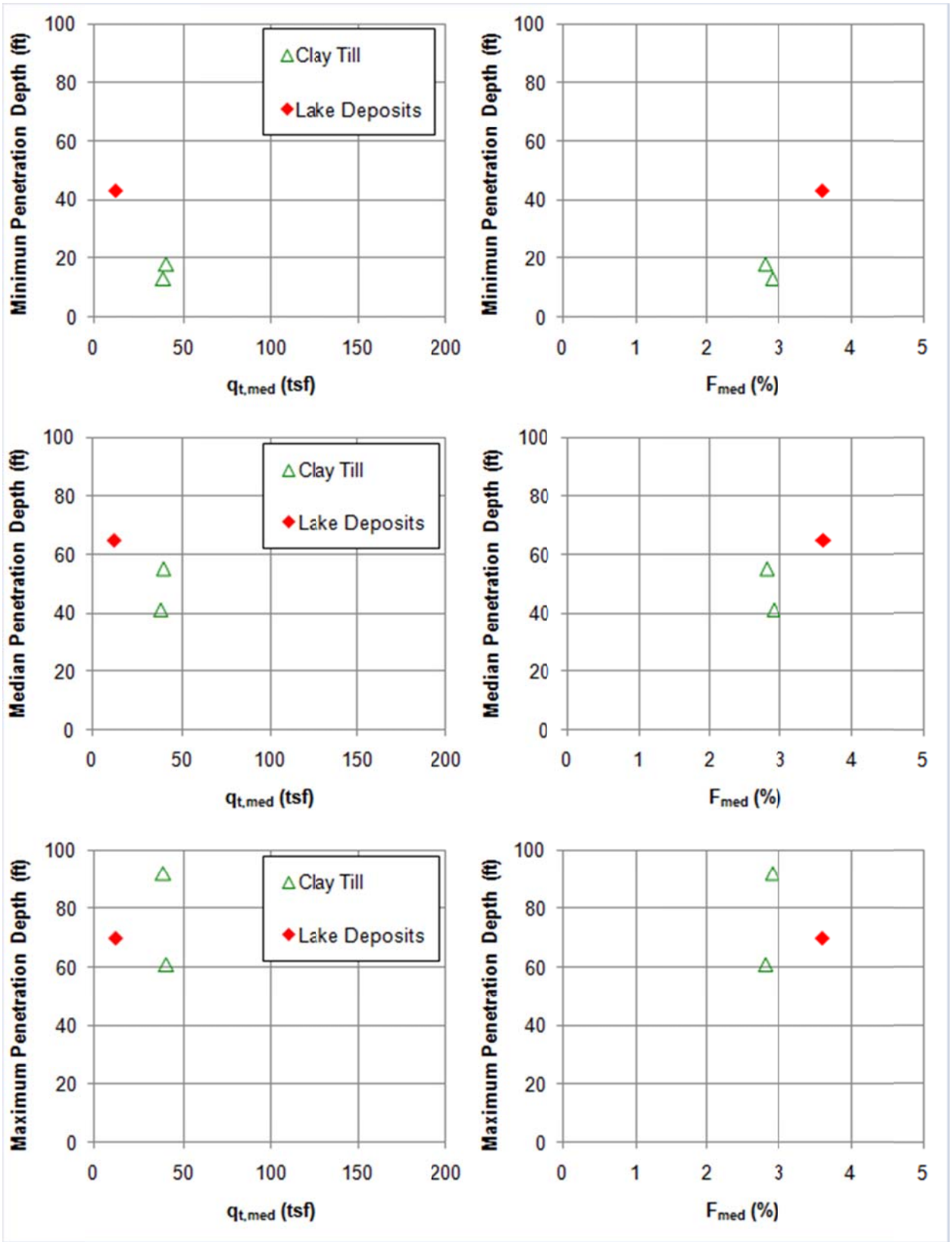

Figure 2.21. Comparison between penetration depth and CPT parameters for geologic conditions near Milwaukee, WI

Cone penetration testing for the Marquette Interchange and Mitchell Interchange can be considered moderately successful. Median values of penetration depth were 40 to 65 ft, with penetrations in general being deeper in the Lake Deposits. The deepest penetration of 92 feet was achieved in a clayey till. Dense sands underlying the Lake Deposits resulted in a maximum penetration of 70 ft. Early refusal in the dense layers underlying the Lake deposits may be somewhat problematic from a foundation design standpoint. Cone tip resistance must be averaged over 8 diameters above a proposed pile tip depth and to up to 4 diameters below a proposed pile tip depth to account for differences in response of small diameter cones and large diameter piles (see section 6.2).

It is noted that 4/27 CPTs for the Marquette interchange were identified as soft Lake deposits based on the results of CPT tests. Geologic maps indicated 18/27 CPTs may contain significant thicknesses of near surface soft Lake sediment.

CPTs in Clayey Tills at the Marquette Interchange and Mitchell Interchange produced similar results, with median tip resistance values on the order of 40 tsf and median friction ratios just under 3. Only one CPTU collected high quality measurements of pore pressure for the Mitchell Interchange project (CPTU-03), and the combination of testing above the water table as well as interlayer sands and clays resulted in low mean pore pressures observed in the Marquette data.

3 Equipment and testing procedures

3.1 Field Equipment

CPTs were primarily performed using the University of Wisconsin-Madison's 24 ton CPT truck, Figure 3.1. The truck is a 1982 Mack RM series Hogentogler modified truck that transports the equipment and powers the hydraulic system. The hydraulic system in turn powers the jacks mounted at the front, center, and rear of the truck. These jacks elevate the truck to maximize the reaction force and to provide a level surface to advance the cone. The two exterior jacks at the center of the truck, closest to the cone, are connected by a beam that provides additional stability where the cone is pushed into the ground. The hydraulic system also operates the ram system used to advance the CPT probe, Figure 3.2. The hydraulic ram is capable of 25 ton capacity and is setup with a rate control allowing advance rates from 0.004 in/sec to 4 in/sec. The hydraulic pump, rams, and control equipment are located within the box compartment aft of the truck cab.

Due to a hydraulic pump failure, an additional CPT truck was used for a portion of this study. The Purdue University's CPT truck is a lighter 7-ton Hogentogler open bed truck, Figure 3.3. This is a smaller truck had a similar hydraulic system and control panel. Because the dead weight of the vehicle is much lighter, the truck is equipped with a helical anchoring system to develop additional reaction force to advance the cone.

The CPT data acquisition equipment was obtained through Vertek in the spring of 2010. The data acquisition equipment is hard-wired to the CPT probe during sounding and converts the voltage output from the cone sensors to a digital signal which is transmitted to a conversion box in the cone truck. The conversion box transforms the digital signal to engineering units based on a calibration factor that the field laptop can record and display real-time measurements during the push. The proprietary Vertek software package displays real-time plots of cone measured data and records measurements for later analysis.

The cone penetrometer probe used for testing is a Hogentogler subtraction type digital seismic piezocone with a 1.44 in diameter, a 1.55 in^2 (10 cm^2) projected tip end area, and a friction

sleeve surface area that is 15 times greater than the projected tip area. The peizocone is a subtraction type cone where one load cell measures both tip and sleeve friction at different locations and the individual values are determined by subtracting the two measurements along the load cell. The piezocone load cell is rated to 1000 tsf for the tip resistance and was calibrated by the manufacturer, Vertek Inc., in April 2010. Calibration documents are included in Appendix 5.

Depth during cone advance was measured by a mounted wheel that rolled when the hydraulic rams moved. The depth wheel has indicators mounted for every 2 inches of ram movement with a proximity switch that is connected to the data acquisition system. With this setup cone measurements were recorded for every 2 inches of penetration. An alternative depth measuring setup was used for a portion of the testing where an encoder measures extension of a cable. This setup allowed for much finer depth increments, but was not used for the majority of the testing.

Figure 3.1. University of Wisconsin-Madison's 24-ton CPT truck setup at site DOT-3R. Note front and rear wheels are not in contact with the ground, so that all of the truck weight is suspended.

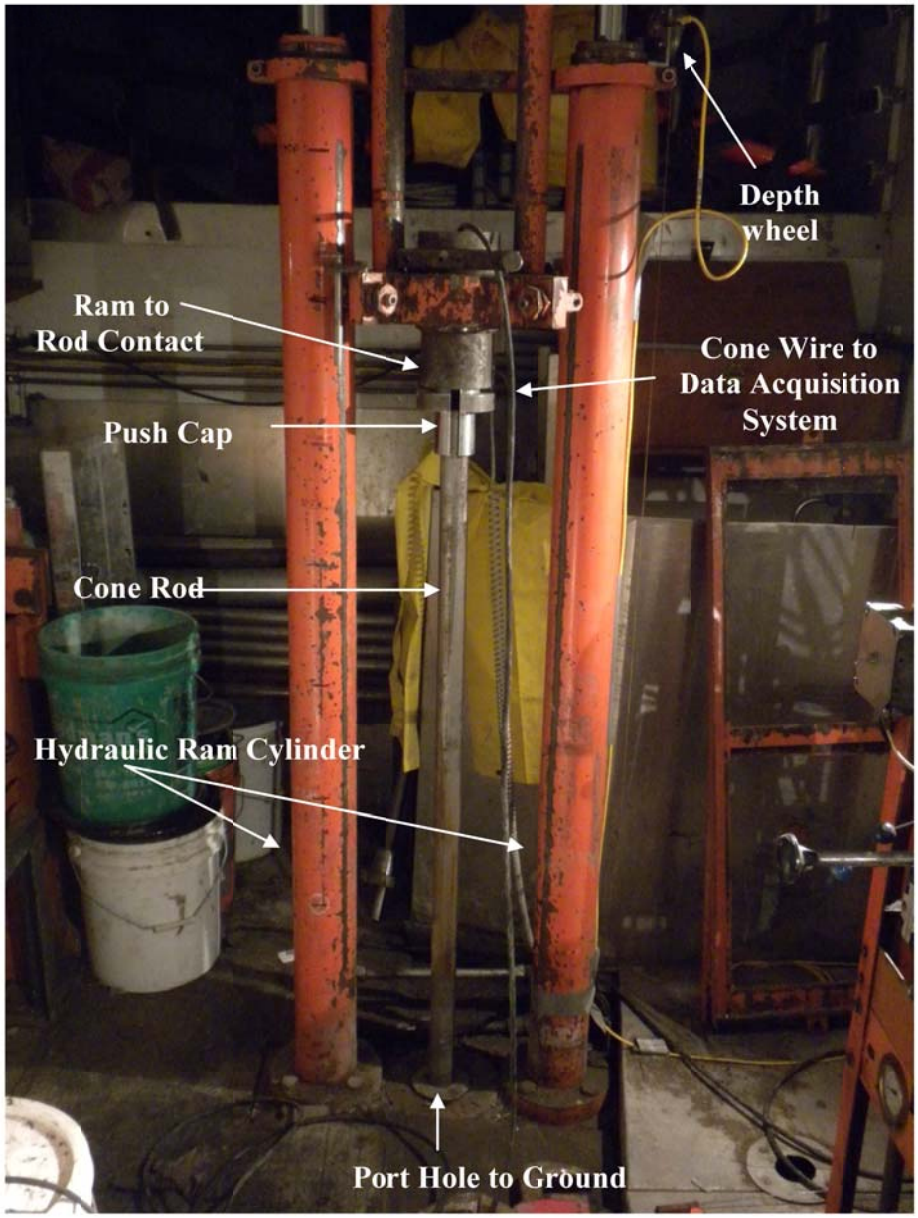

Figure 3.2. Hydraulic ram that advances the cone. Picture is taken mid test with the rams fully extended, top of frame, and a new rod with push cap in place.

Figure 3.3. Purdue University's CPT truck setup on site at Long-10. Jacks for lifting truck and helical anchors are called out.

The cone is capable of measuring tip resistance, sleeve friction, and pore-water pressure continuously during penetration. Pore-water pressure measurements were typically made with the porous filter located just above the cone tip at the u_2 position. At rod breaks dissipation testing was conducted where the change in pore water pressures was measured with respect to time after cone arrest. Times allowed for dissipation tests varied. CPT soundings were conducted following the procedures outlined in ASTM D 5778. CPT sounding holes were abandoned according to Wisconsin Department of Natural Resources guidelines NR 141 and NR 812.

The probe also has a geophone installed 6 inches above the friction sleeve, allowing shear wave arrival times to be measured during pauses in penetration. To measure the shear wave velocity a shear wave was generated at the surface by striking the center beam of the truck with a sledge hammer, Figure 3.4. When the truck is jacked, the center beam is coupled with the ground surface which allows the shear wave to propagate into the subsurface. The sledge hammer is wired into a circuit with the center beam such that when contact is made the computer can begin measuring time and particle velocity from the geophone.

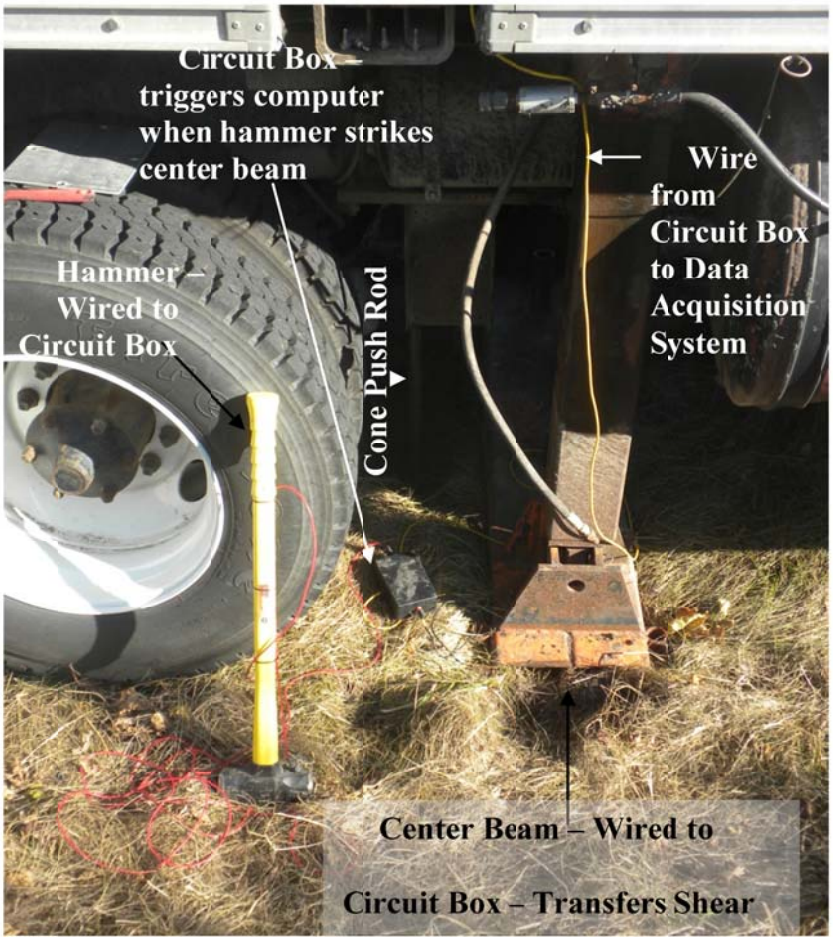

Figure 3.4. Setup for seismic shear wave testing for SCPTU2-01 at DOT-1.

3.2 Site Setup

When arriving at the site and prior to CPT work proper safety precautions were taken to protect equipment and staff. All testing occurred on or near roadways so temporary, reflective road signage was set up to alert motorists of workers in the area as outlined by the Transportation Research Center (1999), Figure 3.5. Lighting was also a key safety feature especially while working at night. Use of emergency flashers and exterior flood lighting indicated the presence of workers to drivers. Safety vests were worn at all times while working outside of the cone truck to increase visibility. When available, locations with barriers between the road and test location were selected.

Figure 3.5. Site setup at DOT-10c with traffic control devices in the form of signage and cones.

Because the test sites are located on previously developed land additional site preparation was performed prior to sounding. Typically, some form of an exploratory pit was performed at each site. These pits were small 0.3 m by 0.3 m and 0.5m deep and excavated with hand tools to determine the nature of the near surface fill, Figure 3.5. A sounding would then be performed in this exploration trench or pilot hole. For subsequent soundings at the same site, the dummy rod would be advanced through the fill with gravel prior to advancing the CPT probe. This procedure was performed for two reasons. First it protected the cone from damage and shallow refusal. Secondly, it reduced the amount of near surface inclination change associated with initially advancing the cone into the ground.

Figure 3.6. Exploration trench performed for CPTU2-05 at Long-13. Frame a. shows exploration trench and frame b. is the material excavated from the trench. Note the gravel size fill found at the near surface.

Prior to each sounding the truck was also jacked and leveled over the desired location. The cone equipment was prepared by saturating the cone, attaching the friction reducer, obtaining the zero readings at the beginning of the test and lowering the cone into the port hole in the truck decking to the ground surface. Centralizers are used to reduce the amount of bending in the cone rods above the ground surface and keep the push rod in a vertical position during push.

After termination of a sounding and retrieval of push rods, a final baseline zero reading was obtained at the surface to check for baseline zero drift during the cone sounding.

3.3 Pressure Transducer Saturation

Measurement of penetration pore pressures is a great advantage during cone testing; however, proper saturation of the measurement system is needed. The pore water pressure transducer is housed within a cavity inside of the cone body just above where the cone tip threads into the assembly. For accurate and precise measurements of the pore water pressure this cavity must be completely filled with a non-compressible fluid. Glycerin was used to fill the cavity prior to advancing the cone into the ground. Disposable plastic filter elements pre-saturated in silicone

oil were used during the testing program. To saturate the pressure transducer the following procedure was performed:

- Unthread cone tip and invert cone clamping to vise so that pressure transducer cavity is facing upward
- Fill entire cavity with glycerin such that meniscus forms above cone body
- Inspect cavity for small air bubbles. If bubbles are present gently tap cone body to agitate bubbles to the surface
- Using syringe fill the channel in the cone tip with glycerin allowing a bead of glycerin to form around the seat for the pore water pressure filter
- Remove saturated filter from the silicone oil container and fit onto tip
- Make sure that there is a meniscus above the cone tip and cone body prior to placing the tip onto the cone
- Quickly invert the tip onto the cone to minimize the chance of air bubbles entering the tip and thread the tip into place. Threading of the tip will displace the excess glycerin out of the cone body cavity.
- Place a thin latex membrane filled with additional glycerin around the saturated cone pressure transducer and filter to reduce chance of losing saturation prior to initializing the sounding.

3.4 Test Naming Convention

Tip, friction sleeve, and pore water pressures were measured continuously for all soundings. The test naming system provides insight into the configuration and data collected for each cone test. Most soundings are designated CPTU#-##. The U indicates that a piezocone test was performed and the number directly following, for instance U2, identifies the position of the pore water filter element. With the CPT probe used for this study u_1 and u_2 positions are possible, although u_2 is the primary configuration used Figure 1.2. In addition seismic piezocone tests are identified as SCPTU2-##. The numbers following the cone configuration represent the test number performed for that study area. In some cases a letter is designated after the cone number indicating that the sounding was stopped, CPT probe removed from the ground, and a new

sounding was started in the same location. This process was typically performed if initial readings indicated poor saturation of the pore water pressure transducer or some equipment error was indicated.

3.5 Supplemental Testing

3.5.1 Drilling Operations

Four independent borings were conducted to obtain samples for laboratory testing. These borings are outlined in Table 3.1. Nominally undisturbed tube samples were obtained at sites UW-1, DOT-7 and DOT-10c. Disturbed auger samples were obtained at all locations. Samples were field identified according to the procedures outlined by ASTM D 2488 by an engineer in the field and preserved for review and subsequent laboratory testing. Logs for borings are included with site descriptions in Appendix 4.

Table 3.1: Summary of soil borings conducted

Site	Drill Rig	Depth of Sampling	Sample Type
UW-1	CME- D 120	98 ft	Tube and Split Spoon
Long-10	Hand Auger	13 ft	Auger (Disturbed)
DOT-7	Gehl Skid Steer	10 ft	Tube and Auger
DOT-10c	Gehl Skid Steer	10 ft	Tube and Auger

3.5.2 Laboratory Testing

At multiple study areas laboratory data was available for CPT comparison. These data included DOT-1 with data provided by WisDOT, UW-1, DOT-7, and DOT-10c with laboratory testing conducted in the University of Wisconsin-Madison's geotechnical laboratory. Laboratory tests conducted include moisture content determination (ASTM D 2216), Atterberg limits (ASTM D 4318), fall cone testing, grain size analysis using mechanical sieves and hydrometer (ASTM D 422 and D 6913), oedometer tests (ASTM D 2435), unconsolidated undrained triaxial tests (ASTM D 2850) and consolidated undrained triaxial tests with pore water pressure measurements (ASTM D 4767). Available lab data is provided in Appendix 4.

3.6 CPT Study Areas

CPT testing was performed at multiple locations across the state of Wisconsin in order to investigate the different soil types that are typically encountered in engineering design. Specific locations were coordinated with WisDOT engineers to focus on locations with specific interest. Coordination with WisDOT was key because use of previous soil boring data was considered for subsurface interpretation. These locations were typically close to large population centers in the state and are therefore representative of soil conditions for many foundation design projects.

Site selection was chiefly determined by accessibility for the CPT truck, location proximal to existing boring data, and site geology. Accessibility was a top priority because most testing occurred on the side of the road near highway structures. Soundings typically took at least one day for advance and closure operations. When conducting dissipation testing, individual soundings required up to 3 days to conduct. For these reasons finding a safe location was a paramount concern. In addition to safety, slopes and ground hazards were also considered in evaluating accessibility. Most testing occurred near existing highway structures so that the subsurface explorations for the highway structure could be used for comparison to CPT results. Finally, the site geology and depth to bedrock played a role in the site selection.

The cone was advanced until one of multiple refusal criterion were met. The term refusal is used to indicate a point during a sounding where it is not possible or impractical to continue advancing the cone deeper. The most apparent case of refusal occurs when the resistance to pushing is larger than the reaction load of the vehicle. In this case the CPT truck is lifted off of the ground when attempting to advance deeper and the sounding is stopped for safety reasons. More commonly, soundings are determined to be at refusal when large changes in inclination occur over short depth intervals. A high degree of inclination over a short distance stresses the cone and push rods that may potentially cause damage. This condition was achieved for an increase of inclination over 1 degree over a depth of 1 m.

4 Data presentation and results

4.1 Data presentation

4.1.1 Graphs and Figures

It is most common to show plots of cone tip resistance (q_t), friction ratio ($F=f_s/q_{cnet}$ %), and penetration pore pressure (u_2) with depth for a CPT sounding (Figure 4.1, Figure 4.2). The estimated in-situ pore pressure, u_0, is plotted on the pore pressure figure, and is typically equal to u_2 in drained sandy soils. Scales are adjusted to encompass the most important aspects of the data; the sandy soils at the Mn/DOT Wakota Bridge site have a maximum tip resistance scale of 450 tsf, while the soft lake clays at the Mn/DOT St. Vincent's site have a maximum tip resistance scale that is an order of magnitude lower, at 40 tsf.

Typical layering can be selected based on major changes in tip resistance, friction ratio, and/or pore pressure response. These layers can be subgrouped based on estimated formation environment and/or anticipated engineering response. Five major layers with up to three occurrences (at different vertical locations) are identified (on the pore pressure plot) in Figure 4.1. It is evident that Layer I generally has a higher tip resistance and lower friction ratio than Layer II. From bearing capacity theory it is conceptually known that drained sandy soils have higher bearing capacity factors (N_q) than undrained clayey soils (N_c) [additionally noting that undrained strength is on the order of 0.25 to 1.0 times σ'_{v0}, after Ladd 1991] which is reflected in Figure 4.1 by higher q_t values for the Layer I 'drained' sands than the Layer II 'undrained' clayey soils. Layer II is split into two sub layers due to variation in friction ratio as well as tip resistance (which is difficult to see on this linear scale). Layer III is broadly similar to Layer I in that it has a high cone tip resistance. Additionally, for Layer III the measured penetration pore pressure (u_2) is increasing along the (dashed) hydrostatic (u_0) line. Hydrostatic penetration pore pressures below the water table are also indicative of drained penetration in sandy soils. Sharp drops in q_t are observed in Layer IV at about 55ft and 72ft, which are clear indications of changes in material behavior. The low tip resistance is coupled with high u_2 values, indicating undrained behavior in a clayey soil. Two thin silty layers are observed in Layer V between 80 and 90 ft, which are characterized by tip resistance that is slightly higher than the undrained case

and penetration pore pressures which are lower than the undrained case. As materials transition from clays to silts to sands, the cone penetration behavior shifts from undrained to partially drained to drained, and tip resistance increases while penetration pore pressures decrease.

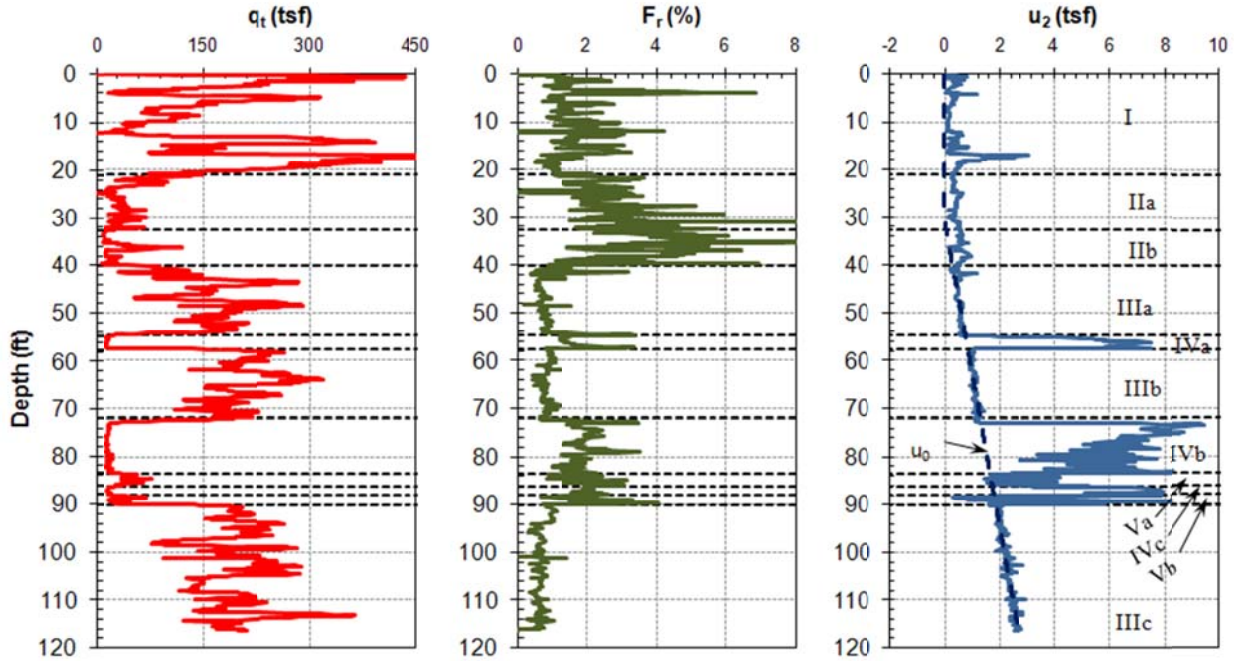

Figure 4.1. Vertical profile of CPT parameters at the sandy Wakota Bridge site, MN

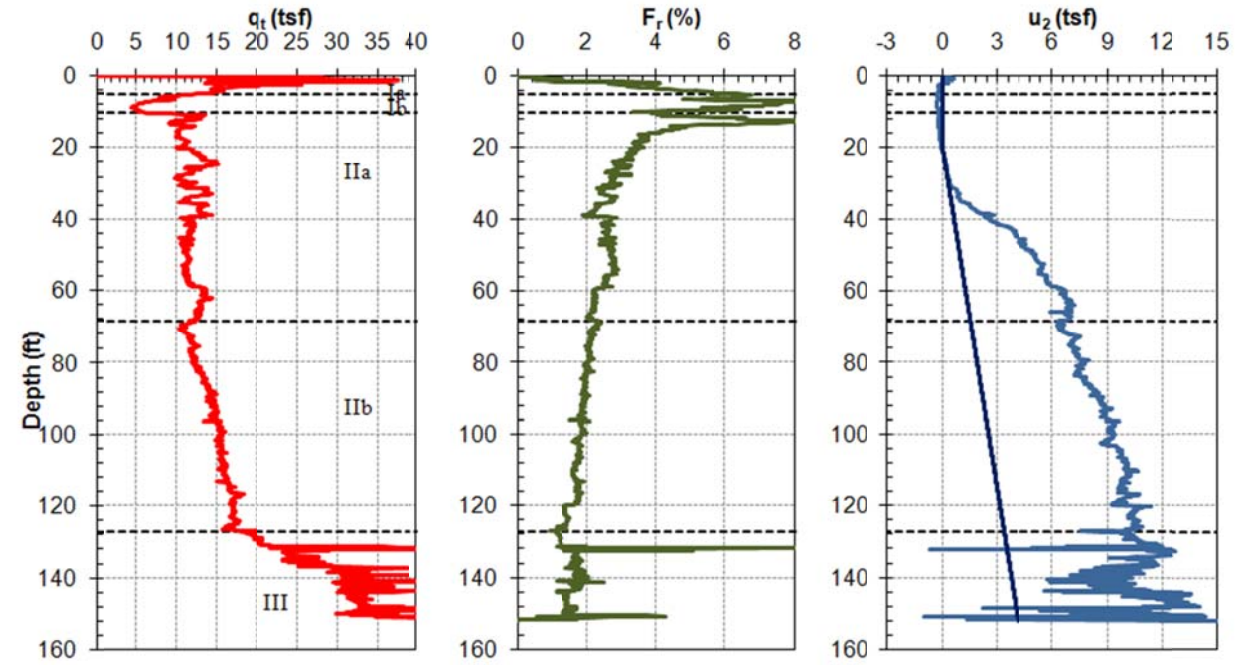

Figure 4.2. Vertical profile of CPT parameters at the clayey St. Vincent site, MN

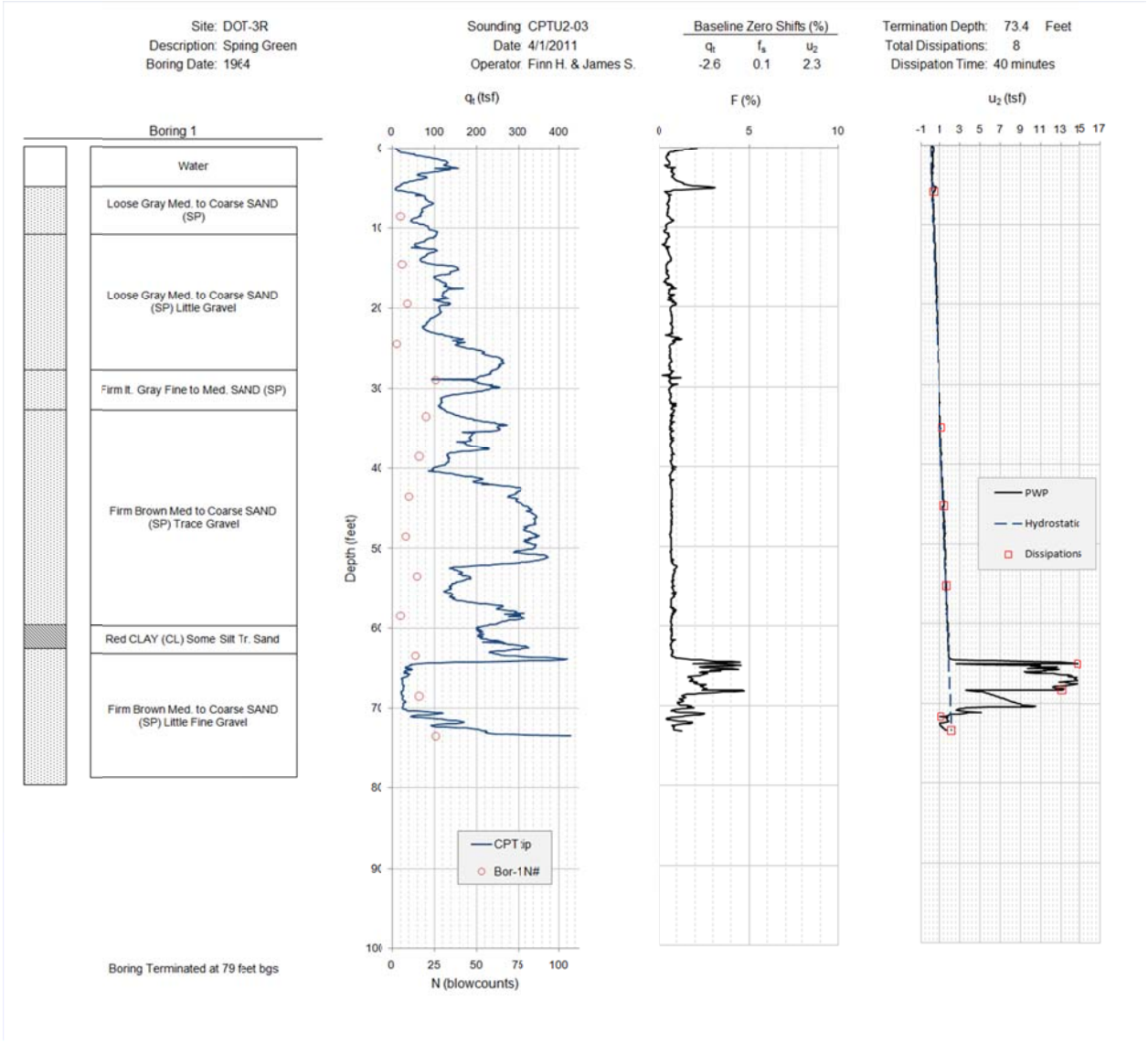

Figure 4.3. Combined boring log and CPT from DOT-3R

To aid in understanding CPT measurements, data collected in this study are plotted adjacent to boring logs (Appendix 2). SPT N-value is plotted on the CPT q_t profile, with a ratio of $(q_t/p_{ref})/N$ equal to a typical value for sandy soils of 4. Figure 4.3 shows an example from the DOT-3R site, adjacent to the Wisconsin River in Spring Green. In agreement with the boring, CPT data indicate a predominantly sand profile, with high tip resistance and low friction ratios. The clay layer at depth, indicated in the CPT profile by increases in friction ratio and pore pressure, is slightly offset in the CPT as compared to the boring due to spatial variability.

When generating cross sections, a single vertical axis at a test location is needed. Cone tip resistance data are typically plotted with the positive x-axis to the right, and friction ratio or pore pressure data are inverted with the positive axis to the left.

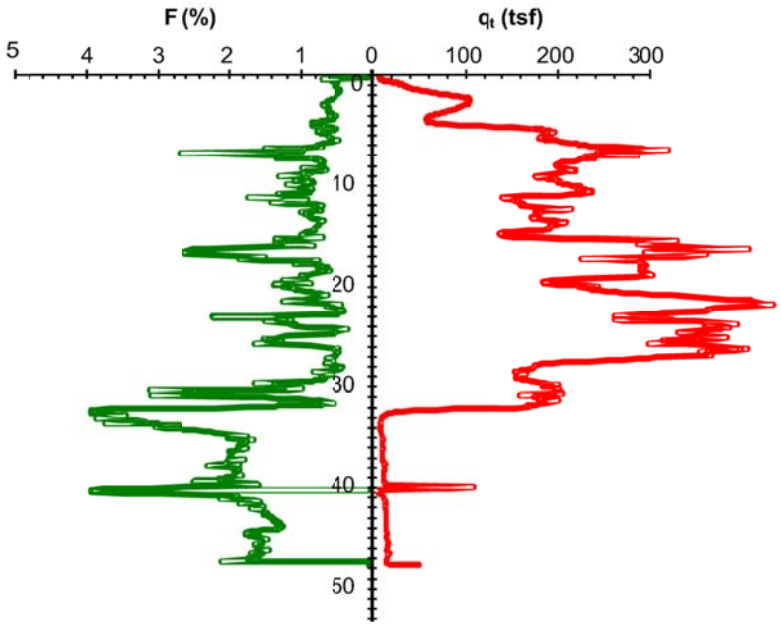

Figure 4.4. Single vertical axis plotting for cross section development based on q_t and F (Mn/DOT 8823-01)

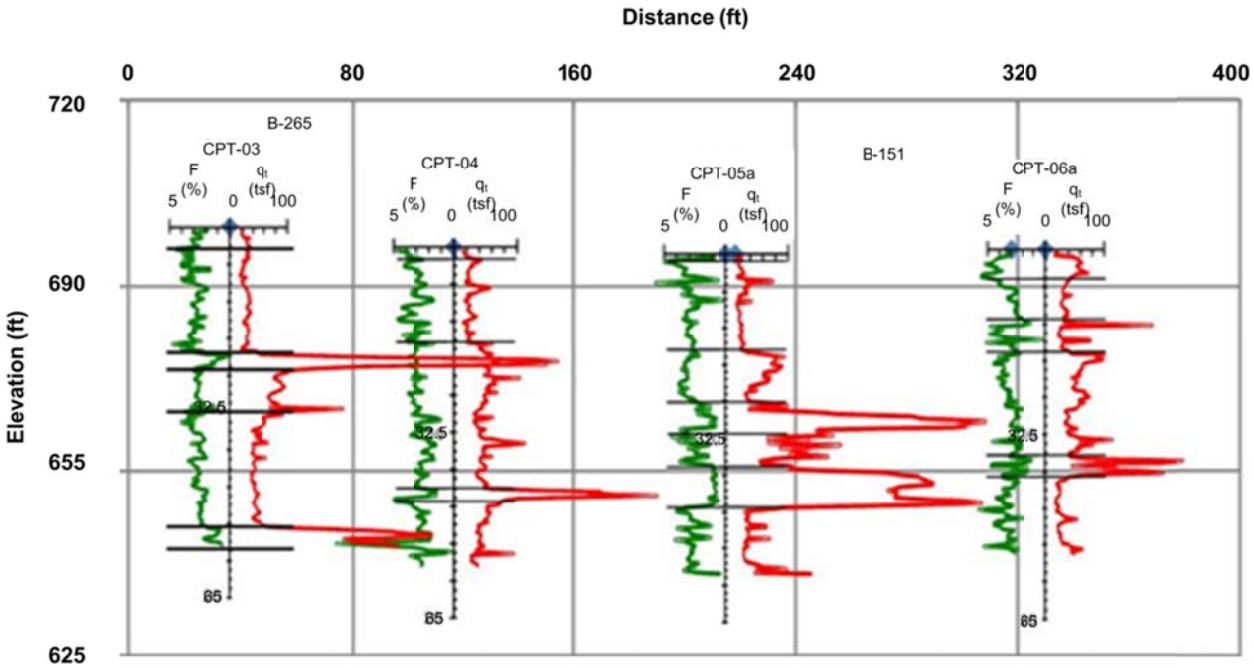

Figure 4.5. Partial cross section for Mitchell Interchange project based on q_t and F

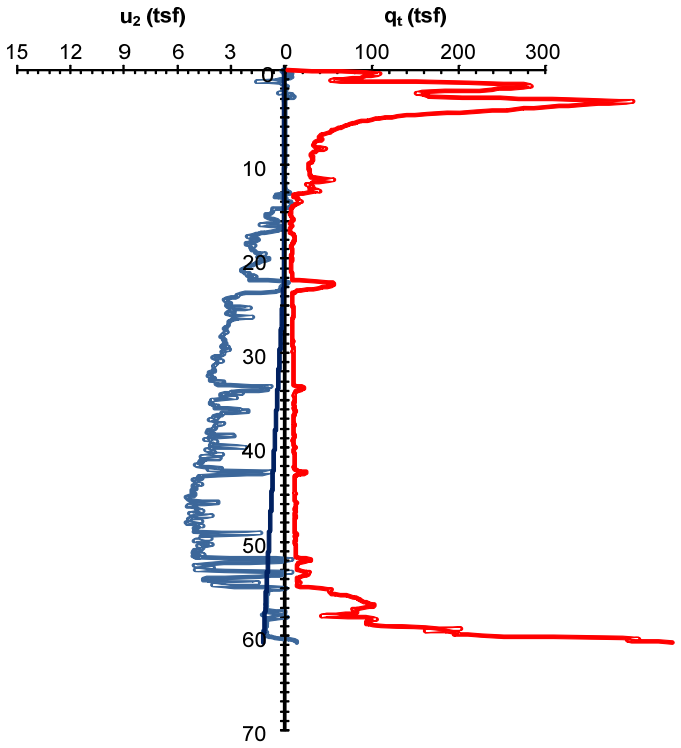

Figure 4.6. Single vertical axis plotting for cross section development based on q_t and u_2 (Marquette Interchange)

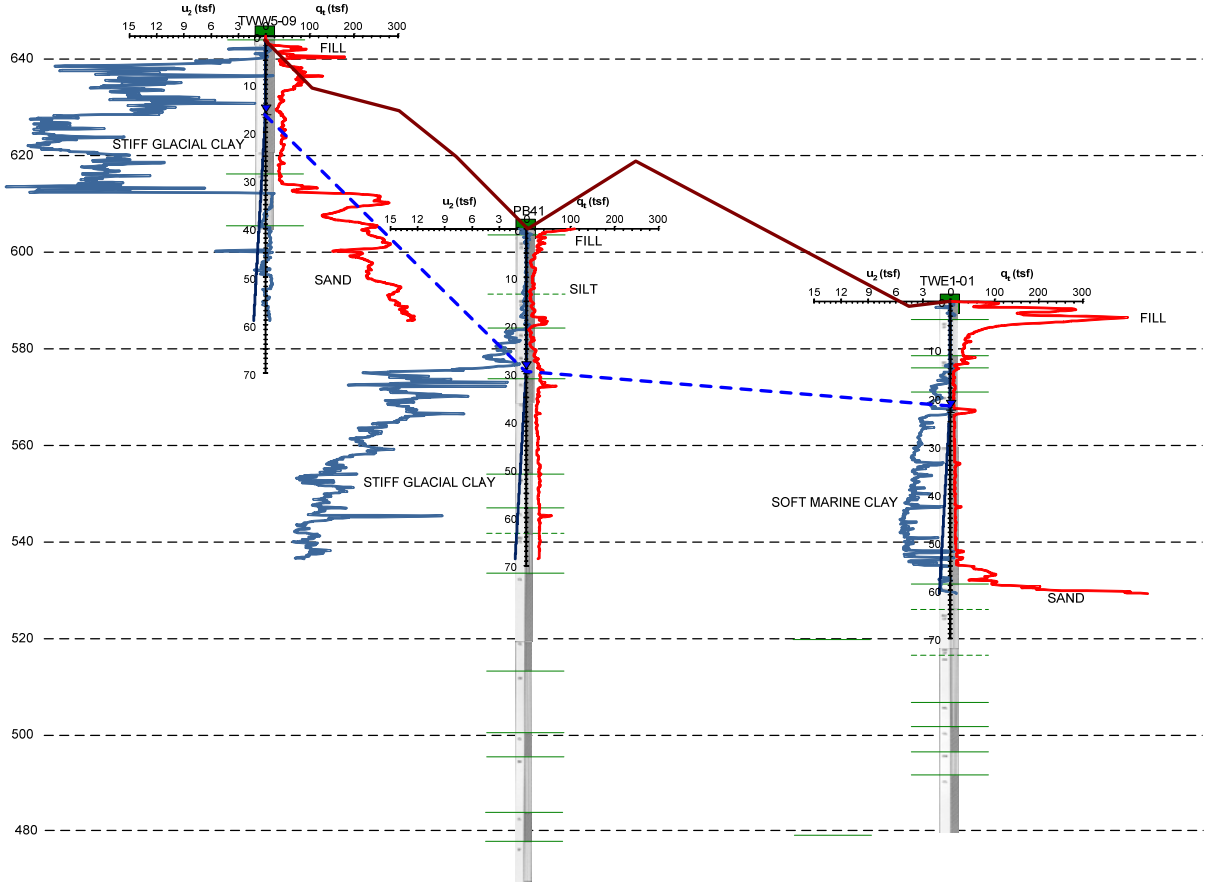

Figure 4.7. West-East partial cross section at the Marquette Interchange based on q_t and u_2

Figures 4.4 and 4.5 illustrate an individual sounding and a partial cross section for plotting based on q_t and F. Figures 4.6 and 4.7 illustrate an individual sounding and a partial cross section for plotting based on q_t and u_2. Sand seams in CPT-05a for Figure 4.5 are readily apparent, primarily based on the high cone tip resistance. Stiff clays are evident near the surface in TWW5-09 (far left) and at depth in PB-41 (center), for Figure 4.7. The clays are identified primarily by their high pore pressures. The lower layer in TWE1-01 (far right) also shows elevated pore pressures. The lower magnitude of these pore pressures, and the tip resistance, indicate penetration in softer lake clays as compared to the stiff tills of TWW5-09 and PB-41. Multiple data types and large range of magnitude for measurements result in cross sections based on CPT data that can provide more visual information than those based on boring logs.

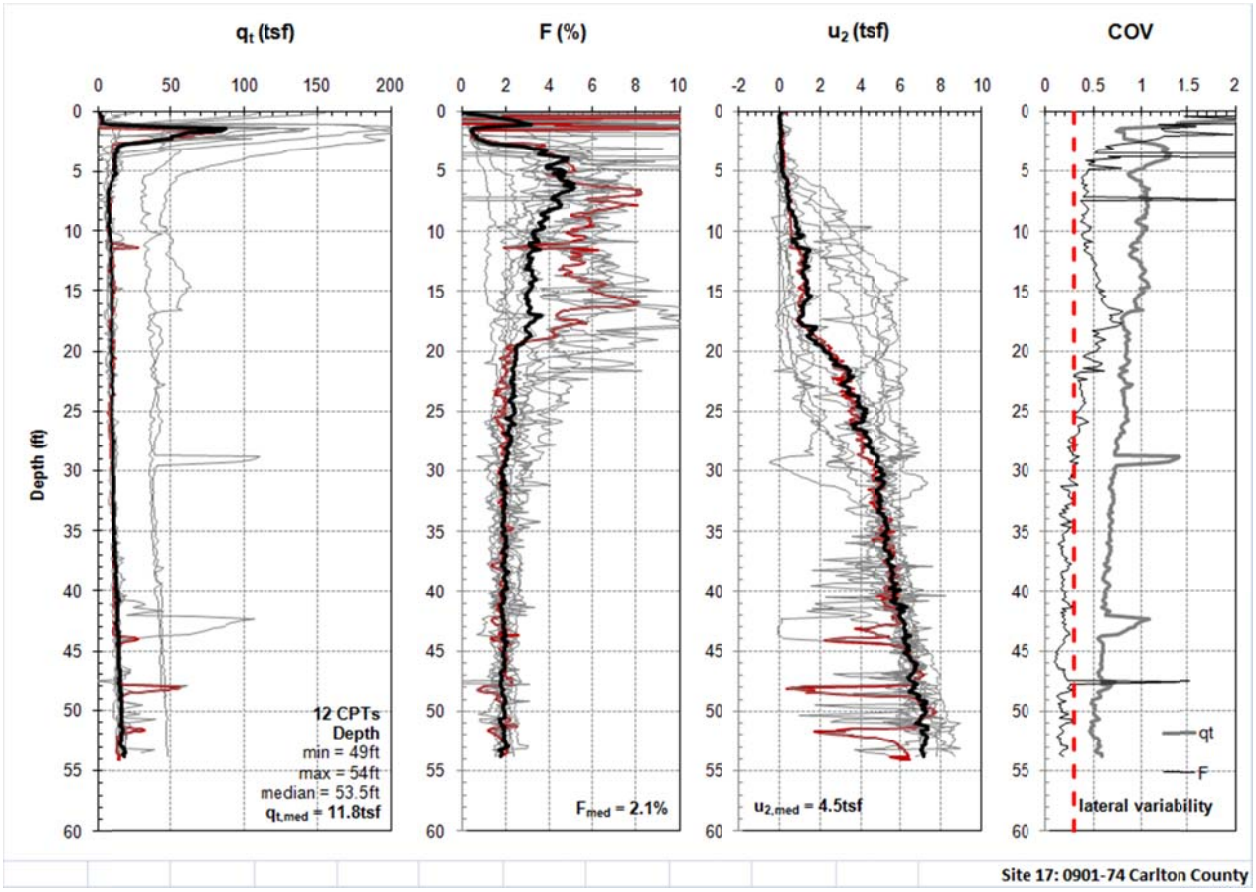

Figure 4.8. Site summary for lake clays at Mn/DOT site 17 in Carlton County

Individual profiles of all CPT soundings analyzed are not contained in this report but are available digitally in the GIS database. Appendix 3 contains site summaries which overlay each

sounding from a given site, or grouping, as well as median values and lateral coefficient of variation for tip resistance and friction ratio. An example profile for Mn/DOT site 17 is shown in Figure 4.8. This is a relatively uniform site, in that 10 of the CPTs overlie each other with q_t equal to the median. There is more variability in friction ratio and pore pressure, with some of these effects attributed to the location of the water table. It is interesting that 2 of the CPT soundings have high cone tip resistance as compared to the others. As the pore pressure response is similar for these two soundings, the high cone tip resistance is likely due to drift or error in assessment of zero readings, and should be confirmed. Multiple measurements within a piezocone test allow for more rational quality control checks of data than single source SPT blowcounts.

Many of the CPT profiles did not have data collected at uniform depths. These occurrences may have resulted from frequency of data recording, different depths of prebore/dummy push, or other factors. To create site summary plots and assessment of lateral coefficient of variation, data for each CPT profile needed to be interpolated to consistent depth readings. This procedure was checked by overlaying a non-processed sounding over the processed sounding (red line in Figure 4.8). Levels of quality control are needed when CPT data are mass processed.

4.1.2 Contractor Documents

CPT data are still typically used by geotechnical engineers, rather than contractors. In Minnesota, consulting engineers and DOT staff have used CPT data for sizing foundations, selecting embedment depths of piles, delineating soft soils, etc.. Use of data by contractors was initially limited, but has grown over time due to increased familiarity with the testing results. No specialized courses were given nor was a CPT contractor manual prepared by Mn/DOT.

Figure 4.9 gives an example of how CPT data has been included in Mn/DOT contract documents. The location of the CPTs is given along with a table of the maximum depth of penetration. Cross sections, in this case, are still based on borings and the contractor would need to request the geotechnical report to actually have the CPT information. As previously shown in Figures 4.5 and 4.7, cross sections can be modified to include CPT results.

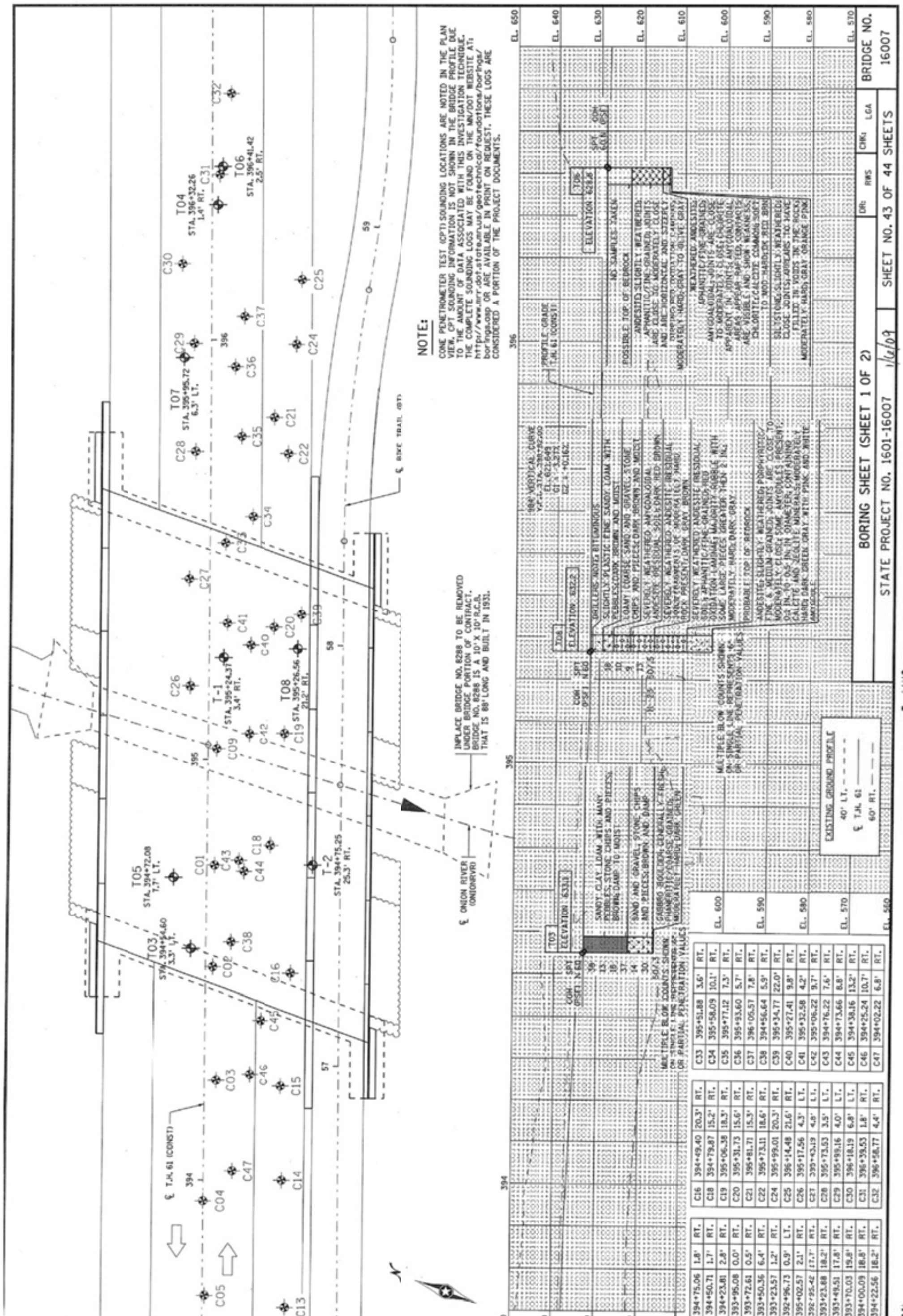

Figure 4.9. Mn/DOT plans including CPT information

4.1.3 Geographic Information System

Data was organized within a Geographic Information System using ArcMap v. 9.3. This allowed for overlaying of aerial photographs, topographic maps, surface geologic maps, with the location of the soundings. Dynamic links to boring logs and excel files of CPT data resulted in efficient organization of data which can be rapidly reviewed, particularly when performing desktop studies related to new projects (e.g., Dasenbrock 2008).

Wisconsin and Minnesota Quaternary geology maps were adapted from data on previously published maps (Goebal et al. 1983, Linebeck et al. 1983 Farrand et al. 1984, Hallberg et al. 1991, Sado et al. 1994, Swinehart et al. 1994, Fullerton et al. 1995, Sado et al. 1995, Fullerton et al. 2000), Aerial photos were obtained through ESRI ArcGIS Online World Imagery, and topographic maps were developed by the USGS available through ESRI. Figure 4.10 through 4.14 illustrate various screenshots from the database, including USGS topographic maps, surface geology, dynamic links to Excel files, and dynamic links pdfs of boring logs / CPT profiles.

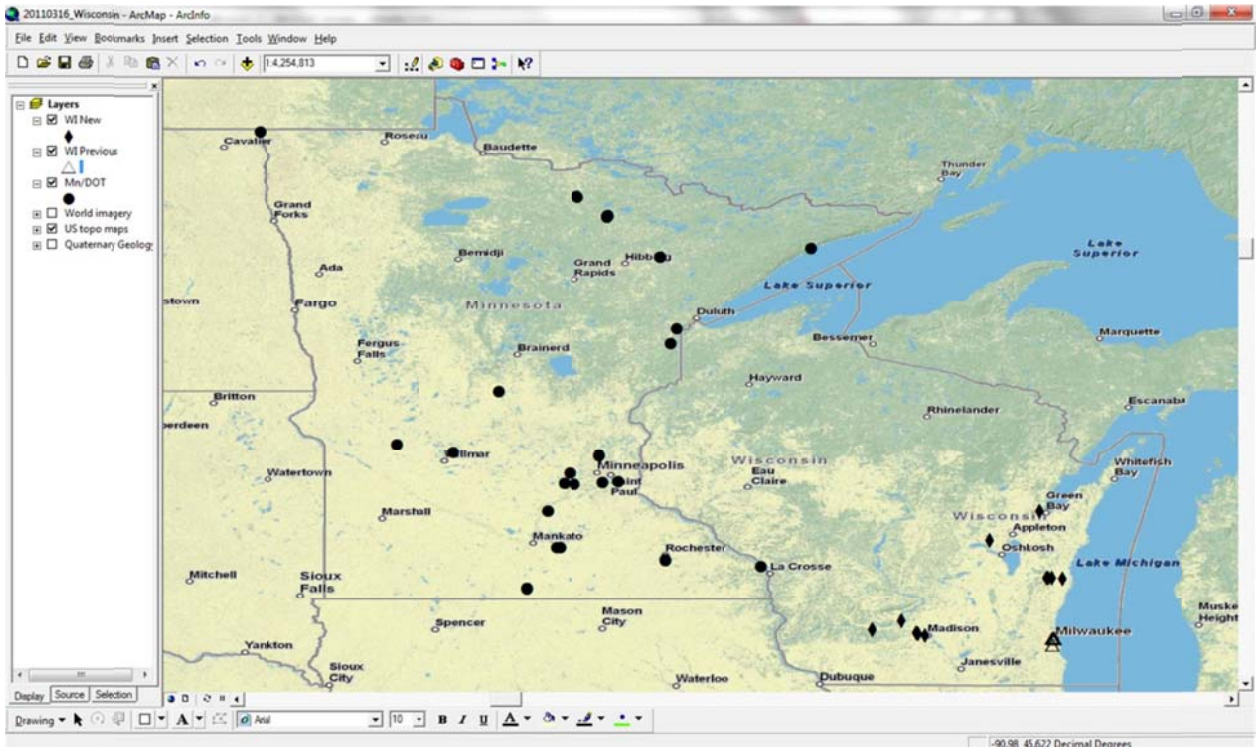

Figure 4.10. Screenshot of GIS database with site locations overlaying USGS topographic

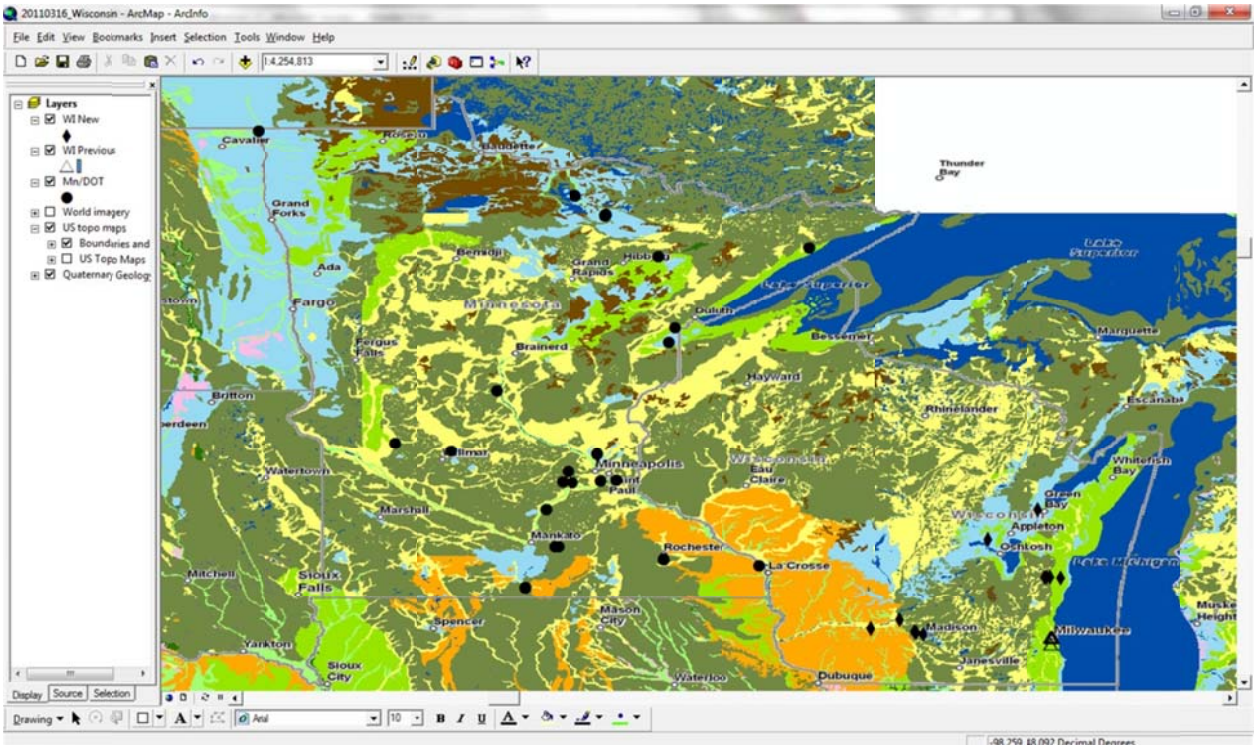

Figure 4.11. Screenshot of GIS database with site locations overlaying simplified surface geology

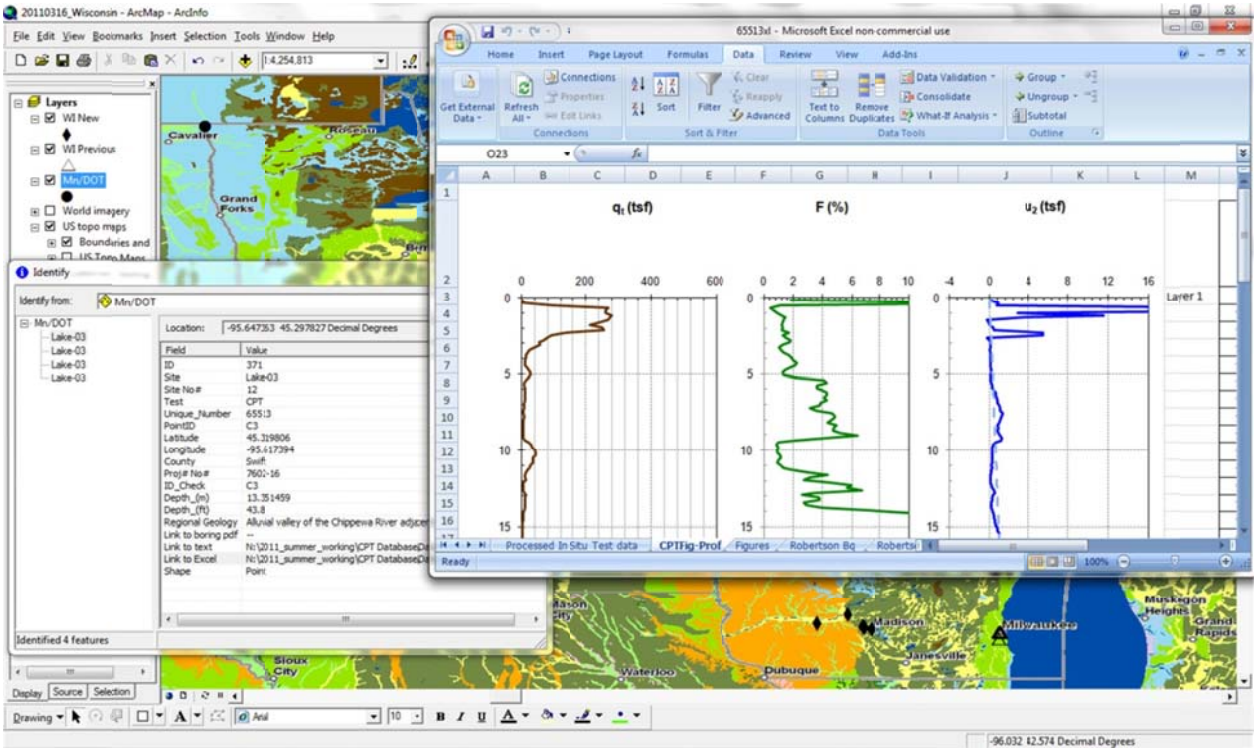

Figure 4.12. Screenshot of GIS database showing link to Excel spreadsheet summary of data (Mn/DOT site)

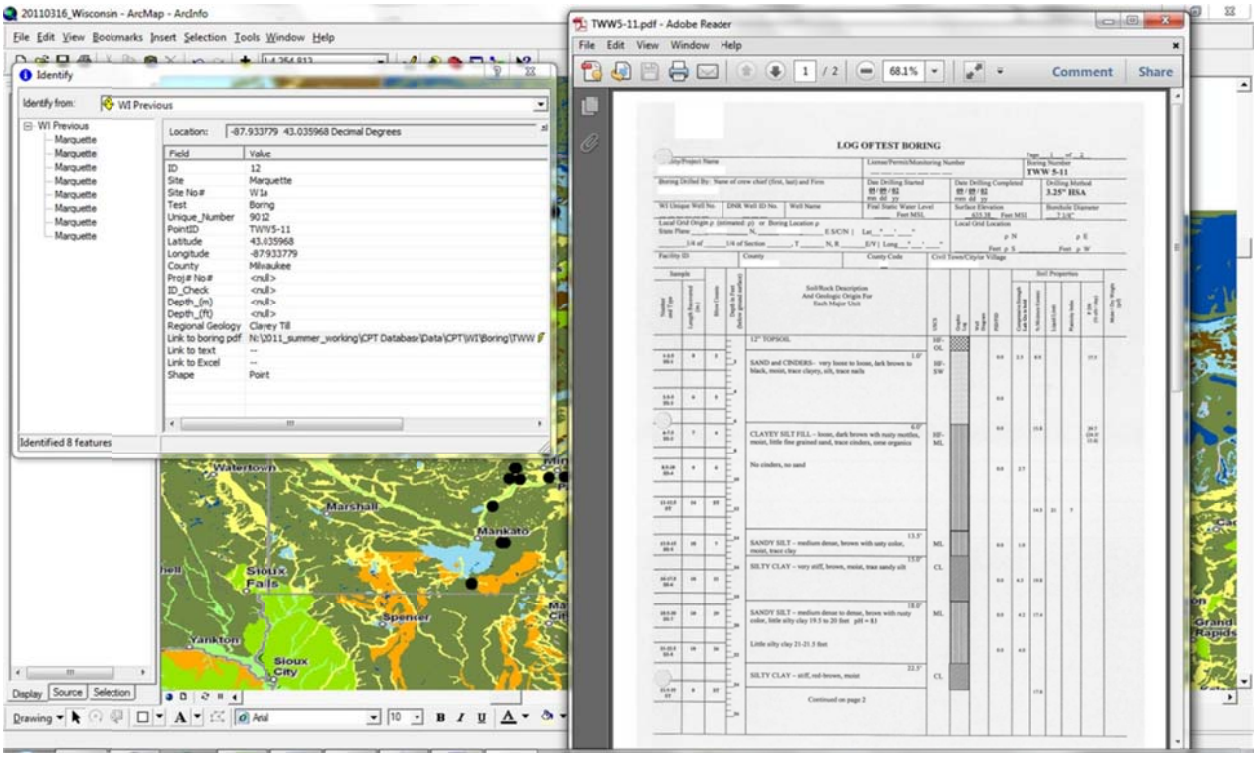

Figure 4.13. Screenshot of GIS database showing link to boring log from Marquette Interchange project

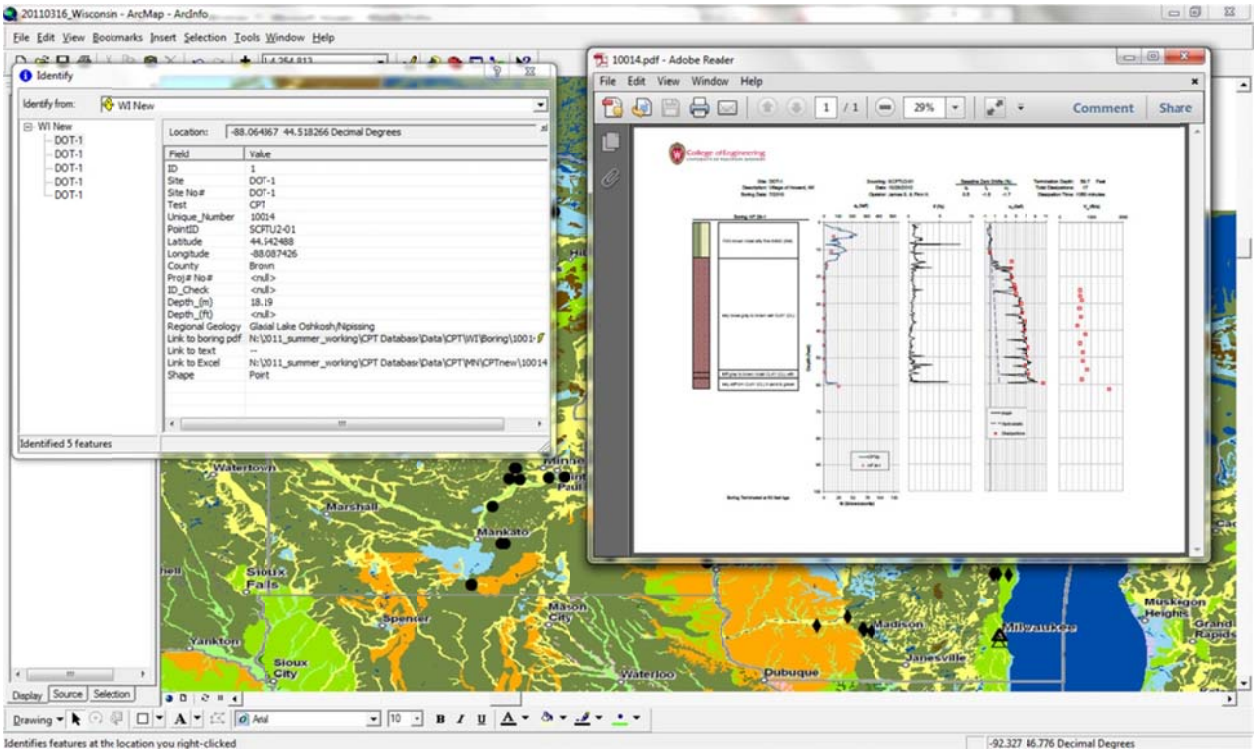

Figure 4.14. Screenshot of GIS database showing link to pdf of combined CPT/boring log for new Wisconsin sites

4.2 Results

A total of 61 soundings at 14 sites were performed for this study, as summarized in Figure 4.15, Table 4.11, Table 4.12, and Appendix 2. Eight of these soundings were probes using the dummy push rod, Figure 4.16, and did not result in tip, sleeve or pore-water pressure measurements. Out of the 53 soundings using the CPT probe, only two did not have saturated pressure transducers, and 15 of the soundings included seismic shear wave velocity measurements. The depths for all soundings combined to a total length of 1848 ft. Appendix 2 provides cone profiles of measured parameters with comparison to WisDOT borings and individual sitemaps.

Dissipation testing was conducted during most soundings. A total of 320 dissipation tests were performed for a cumulative duration of 212 hours. Many of these tests were short duration, less than 5 minutes, tests performed during rod breaks to develop a better indication of drainage conditions.

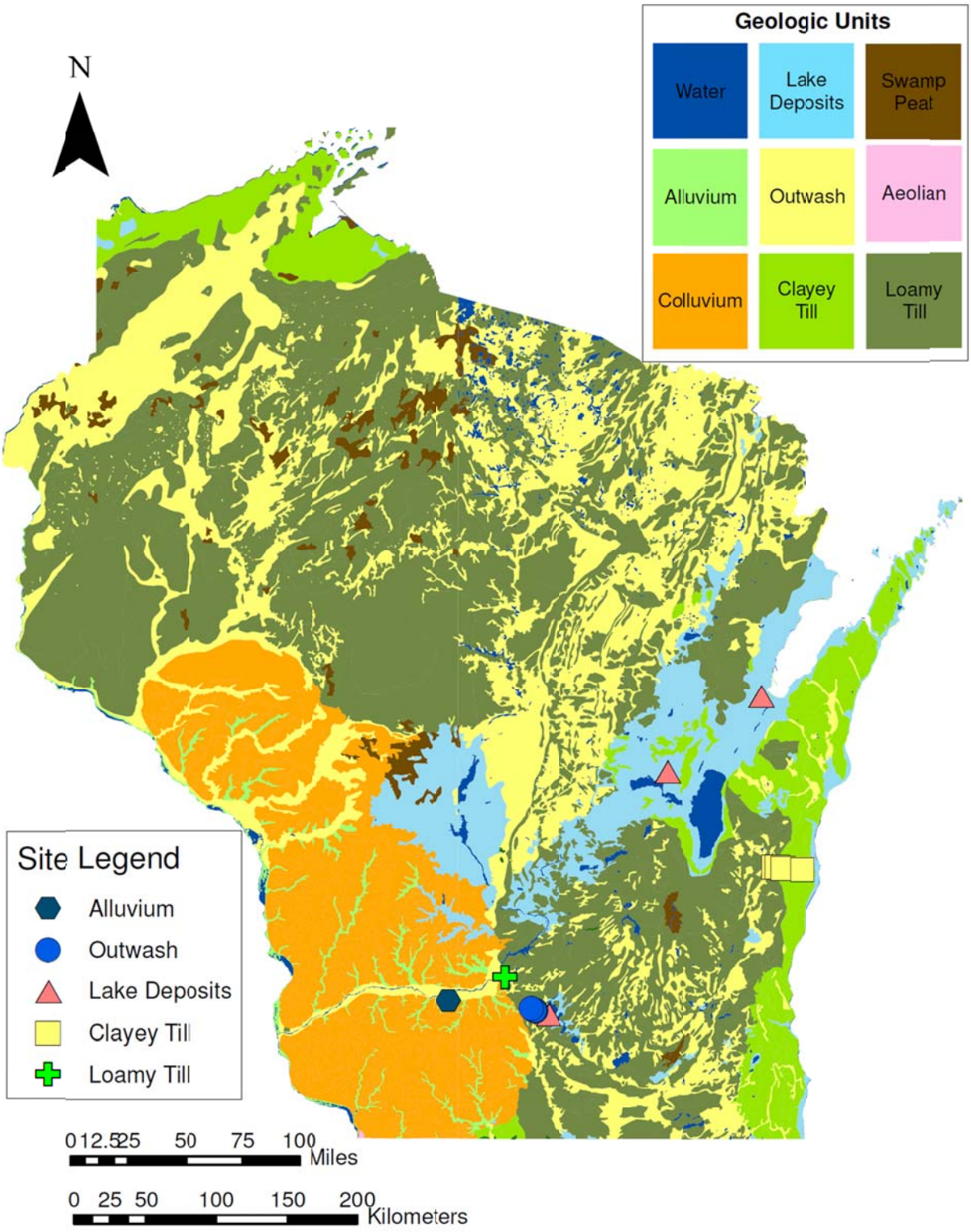

Figure 4.15: CPT test locations shown against surficial geology map.

Figure 4.16. The dummy rod consists of a conical tip welded to a push rod with a 1.75 in outer diameter. The dummy push rod was used to check for near surface refusal and presence of gravel fill. Note white dust on tip from pulverized material.

CPTs were performed following the guidelines of ASTM D 5778 that requires a penetration rate of 0.8 in/s +/- 0.2 in/sec. Variable rate CPT testing was conducted to assess CPT probe advance rate effects at sites UW-1, DOT-10c, and DOT-7. Results are discussed by Hotstream (2011).

Site characteristics and average CPT properties are contained in Tables 4.1 and 4.2. Average CPT properties sorted by estimated surface geology are presented in Tables 4.3. Figure 4.17 characterizes minimum, median, and maximum penetration achieved at each site.

Table 4.1. Summary of regional geology for WisDOT sites tested

UW Site No.	UW Site ID	County	Regional Geology
T01	UW-1	Dane	Lake
T02	Long-10	Dane	Outwash
T03	Long-12	Dane	Outwash
T04	Long-13	Dane	Outwash
T05	DOT-7	Dane	Outwash
T06	Long-11	Dane	Outwash
T07	DOT-1	Brown	Lake / Fill
T08	DOT-16	Winnebago	Clayey Till
T09	DOT-10	Sheboygan	Fill
T10	DOT-10a	Sheboygan	Clayey Till
T11	DOT-10b	Sheboygan	Clayey Till
T12	DOT-10c	Sheboygan	Clayey Till
T13	DOT-3R	Sauk	Alluvium
T14	Long-8	Dane	Alluvium

Table 4.2. Summary of CPT performance for WisDOT sites tested

UW Site No.	UW Site ID	County	# CPTs[1]	Depth (ft)			Median CPTU values			lateral variability[2]
				min	median	max	q_t (tsf)	F (%)	u_2 (tsf)	
T01	UW-1	Dane	4 (5)	13	65	99.6	130	1.0	0.9	low
T02	Long-10	Dane	7	26	26	89	87	1.3	0.3	low-mod
T03	Long-12	Dane	1	-	62.8	-	128	1.4	1.0	-
T04	Long-13	Dane	1	-	56	-	144	1.2	0.5	-
T05	DOT-7	Dane	8	12.5	14.8	42.7	67	0.8	0.4	low
T06	Long-11	Dane	2	23.9	53.2	38.6	177	1.0	0.1	low
T07	DOT-1	Brown	2(5)	3.3	3.3	70	9.7	0.7	5.1	low
T08	DOT-16	Winnebago	4	15	25	35.4	33.8	2.4	2.5	low
T09	DOT-10	Sheboygan	0 (4)	2.5	3.2	3.9	-	-	-	-
T10	DOT-10a	Sheboygan	2 (3)	7.6	7.7	7.9	167	0.7	0.1	mod-high
T11	DOT-10b	Sheboygan	5	5.7	12.8	24	34.4	3.4	0.6	moderate
T12	DOT-10c	Sheboygan	6	19.7	21.9	26.3	29	3.4	1.3	moderate
T13	DOT-3R	Sauk	5	73.4	73.6	78.1	142	0.7	1.1	low
T14	Long-8	Dane	5	2	5.7	9.2	40.7	1.7	0.3	moderate

[1] number in parentheses indicates total number of cones pushed, includes dummy probes that met shallow refusal and erroneous $CPTU_1$ q_c and f_s data from UW-1

[2] for lateral variability, high = a majority of depths with q_t COV > 1, low = a majority of depths with q_t COV ≤ 0.3, moderate = a majority of depths with $0.3 \leq q_t$ COV ≤ 1, dual symbols used for profiles with mixed variability

Table 4.3. Summary of CPT performance for WisDOT sites tested by geology

Regional Geology	# CPTs[1]	Depth (ft)			Median CPTU values			lateral variability[2]
		min	median	max	q_t (tsf)	F (%)	u_2 (tsf)	
Fill	0 (7)	2.5	3.3	3.9	-	-	-	-
Lake	6 (7)	13.1	65.3	99.6	60.1	1.0	1.6	high
Alluvium	10	2	41.3	78.1	141	0.7	1.0	high
Outwash	19	12.5	26.3	88.8	102.6	1.2	0.4	moderate
Clayey Till	17 (18)	5.7	19.4	35.4	32.3	2.9	1.1	low-mod

[1] number in parentheses indicates total number of cones pushed, includes dummy probes that met shallow refusal and erroneous $CPTU_1$ q_c and f_s data from UW-1

[2] for lateral variability, high = a majority of depths with q_t COV > 1, low = a majority of depths with q_t COV ≤ 0.3, moderate = a majority of depths with $0.3 \leq q_t$ COV ≤ 1, dual symbols used for profiles with mixed variability

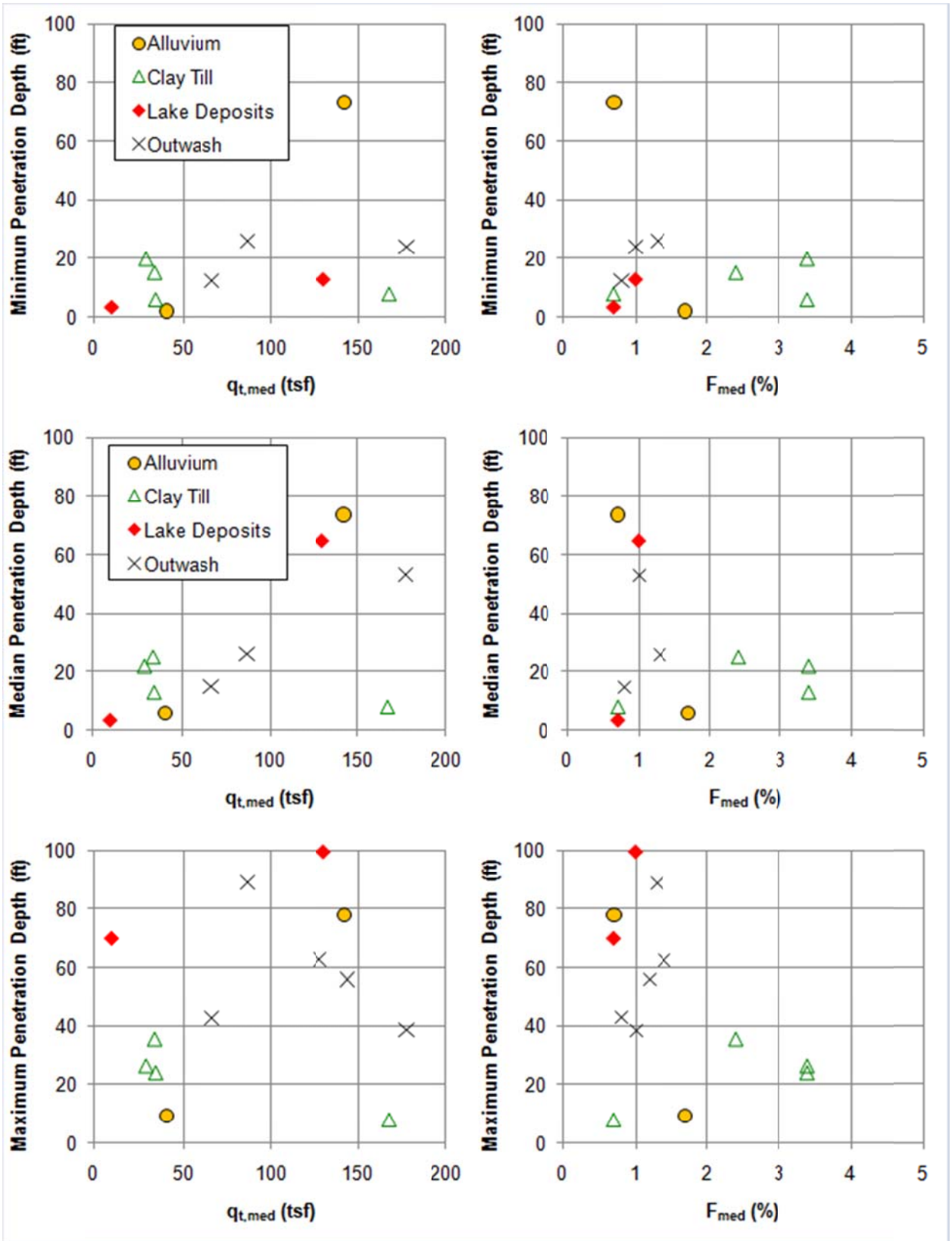

Figure 4.17. Comparison between penetration depth and CPT parameters for geologic conditions tested in Wisconsin

Good success was achieved in Lake, Alluvium, and Outwash conditions, with maximum penetration depths exceeding 75 feet in each geological condition. Data from Long-8 near the Wisconsin river are grouped with the Alluvial deposits from site DOT-3R. Good performance was achieved at site DOT-3R, with a median penetration of 74 feet, but the maximum penetration at site Long-8 was less than 10 feet. The Long-8 site may have had geological conditions more similar to a loamy till than alluvium. The clayey tills of Sheboygan county also resulted in difficult testing conditions, with numerous near surface refusals from cobbles and gravel. Continuing eastward from Plymouth resulted in deeper penetrations, with relatively successful testing at site DOT-10c. The inability to penetrate greater than 4 ft at site DOT-10 is attributed the fill soils that also contain gravel, rather than the natural material. Difficulties were also encountered for the fill soils at site DOT-1 in Green Bay.

On average, penetration depths were lower in this study as compared to data reviewed from Mn/DOT and tests performed by commercial firms in the Milwaukee area. It is noted that median tip resistance values recorded at sites in this study were higher from previous sites in glacial geology reviewed. Both sites in Milwaukee had median tip resistance values less than 50 tsf, and 18/21 Mn/DOT sites had median tip resistance values less than 55 tsf. Only 5/14 sites tested in this study had median tip resistance values less than 55 tsf, and 6/14 had median tip resistance values greater than 125 tsf. This being said, it is not the median tip resistance that results in refusal, it is the local maximum tip resistance or potential to cause sharp changes in inclination. These difficulties arose due to the presence of gravel and cobbles, mostly encountered in the relatively low tip resistance clayey tills.

Commercial testing in the Milwaukee area had greater success when retesting adjacent to a sounding which had met refusal than retesting in this study. If testing in this program met refusal, retesting was performed at an offset of 6 ft. Additional offsets at 30 to 60 feet from a given location were attempted for repeat refusals. Excavation of near surface material aided in some situations, such as DOT-7, but was generally only successful if gravel and cobbles were limited to the upper 1 to 2 feet.

4.3 Equivalent Commercial Costs

The budget for this project was developed based on an estimate of 2 days per site for each of 15 sites, or 30 days total testing. Preliminary estimates from a commercial CPT firm was $3750/day for a 24 ton rig and $4000/day for a 30 ton rig, plus $4/mile round trip mobilization. This would result in a total field testing portion of the project costs that was over twice the total allowable budget of $65,000. A reduced research rate of $700/day was developed for the UW-Madison 24 ton CPT rig, and when combined with a 12 month research assistant salary, tuition, and travel costs, the allowable budget of less than $65,000 could be achieved. The scope of 61 CPTs at 14 sites was completed in 39 days of field work.

Table 4.4. Estimated equivalent commercial costs for testing program undertaken

Item	Unit Cost ($/ea)	Unit (ea)	Cost ($)
Mobilization			
Loop 1 – fall 2010	$4/mi	450 mi	$1,800
Loop 2 – spring 2011	$4/mi	100 mi	$400
Purdue Rig – summer 2011	$4/mi	850 mi	$3,400
Location Setup			
Paved Area / Field	$75/test	61 tests	$4,575
In-situ Testing			
Piezocone testing	$8.50/ft	1848 ft	$15,708
Hole abandonment (grouting)	$4.50/ft	1848 ft	$8,316
Dissipation test	$200/hr	212 hr	$42,400
Seismic Testing	$25/test	163 tests	$4,075
Data Reduction			
Electric Cone Penetrometer Sounding	$75/test	61 tests	$4,575
Out of Town Expenses			
Hotel	$75/day	28 days	$2,100
Meals	$35/crew day	56 crew days	$1,960
		Subtotal without dissipations	$46,909
		Total	$89,309
		Cost / day	$2290/day

Based on the quantity of testing completed, an equivalent value of commercial testing can be estimated. Table 4.4 summarizes estimated costs of the testing program based on typical rates for CPT contractors. The estimated commercial cost of the entire CPT field program was 37% greater than the total allowable project budget of $65,000. That figure would not include costs

associated with compilation of this report, evaluation of CPT data from previous sites, or supplemental borings and laboratory testing performed. The average day rate based on commercial production rates would be on the order of $2,300, however, due to the research nature of this study, productivity in terms of footage was lower than that of a commercial firm. Dissipation testing accounted for 47% of the total estimated commercial budget. Collection and interpretation of dissipation test results was paramount to this study and the understanding of CPT data in Wisconsin, but may not be needed for routine project testing once experience is organized.

5 Evaluation of soil behavior and properties

5.1 CPT and SPT correlations

In areas where use of the CPT is not prevalent, many engineers have developed their experience evaluating soil resistance based on SPT N-value. A first stage in starting to adopt the CPT often involves creating equivalent SPT blowcount profiles from CPT data (e.g., Robertson et al. 1983, Jeffereies & Davies 1993) and then applying SPT based correlation that the engineer is more comfortable with. Now that CPT based correlations to material properties have sufficiently large databases (e.g., Lunne et al. 1997, Mayne 2007), the intermediate step of generating correlations between cone tip resistance and SPT blowcount is unnecessary. However, the large amount of q_t and SPT N-value data that are available in this study makes a review of q_t and N correlations appropriate. Data from Minnesota is presented as energy corrected N_{60} values, while the correction of data from Wisconsin is uncertain and uncorrected N value are used.

Figure 5.1 illustrates correlations between (q_t/p_{ref}) and SPT N-value in relation to CPT normalized cone tip resistance and CPT friction ratio. Detail on the breakdown of the database and specific correlations for different soil types is contained in Tables 5.1 and 5.2. A reference stress (p_{ref}) equal to 1 atmosphere (1.058 tsf) is used to make the correlation nondimensional.

Similar observations are made for each study, which are in general agreement with $(q_t/p_{ref})/N_{60}$ ratios presented by Robertson et al. (1983); (i) $(q_t/p_{ref})/N_{60}$ increases from approximately unity in fine grained soil to approximately 4 in coarse grained soils; (ii) the coefficient of variation is between 50 and 100%. For the new Wisconsin sites (this study), 18 tests in soft clays and organic material had blowcounts of zero, negating the applicability of the N-value or assessment of $(q_t/p_{ref})/N$. The ability to accurately measure resistance in very soft soils is an advantage of the CPT.

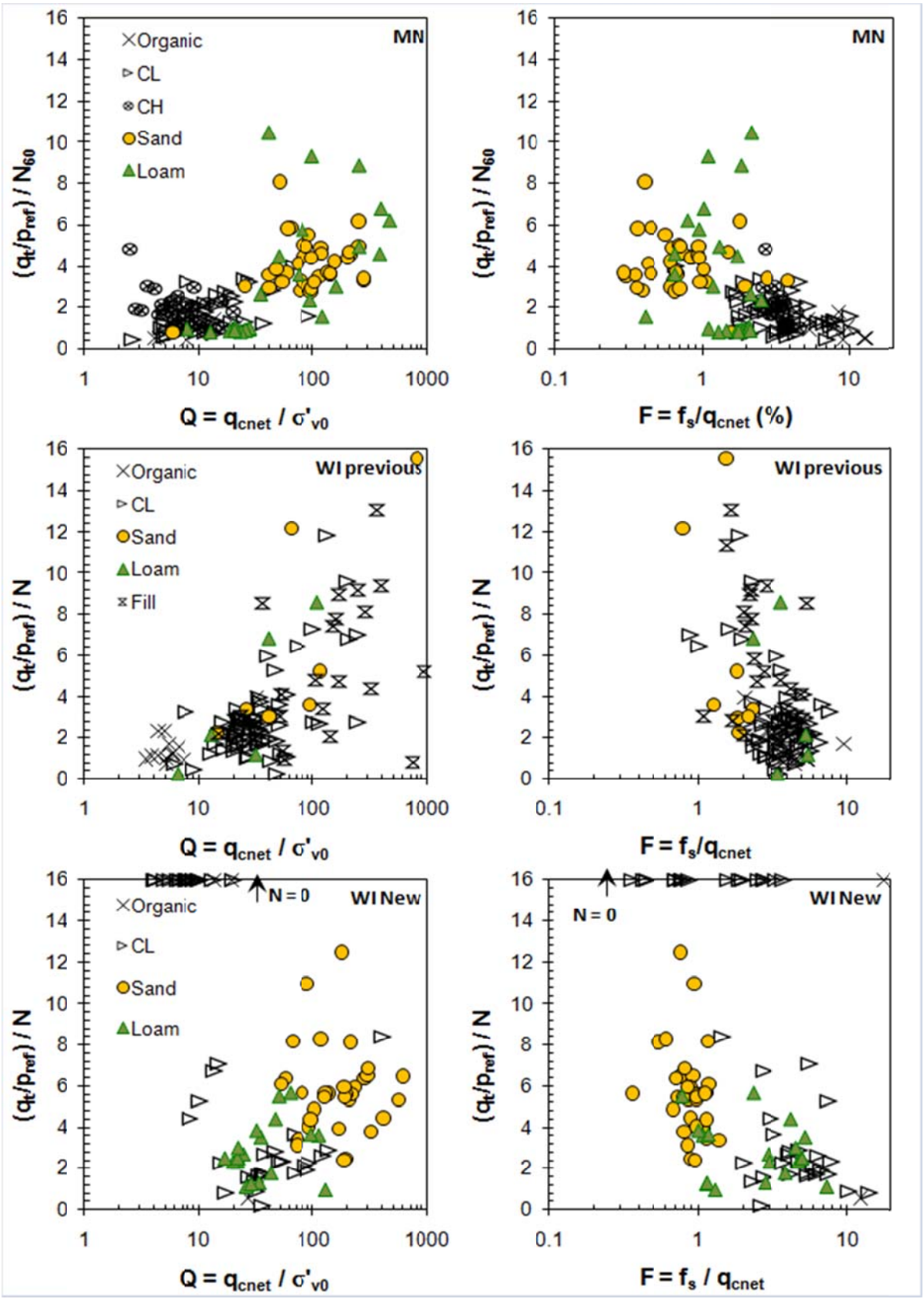

Figure 5.1. Comparison of SPT and CPT penetration resistance

Table 5.1. Comparison of CPT and SPT penetration resistance in organic and clayey soils

Dataset	Organic			Low Plasticity Clay			High Plasticity Clay		
	Median	COV	n	Median	COV	n	Median	COV	n
Minnesota	1.0	0.45	9	1.3	0.53	44	1.9	0.41	28
Wisconsin Marquette / Mitchell	1.2	0.56	13	2.4	0.72	63	-	-	-
Wisconsin UW Study	0.6	-	1[a]	2.3	0.71	26[b]	-	-	-

[a] 2 tests with SPT N-value of 0 (weight of rods or weight of hammer)
[b] 16 tests with SPT N-value of 0 (weight of rods or weight of hammer)

Table 5.2. Comparison of CPT and SPT penetration resistance in sands, sand mixtures, and fill

Dataset	Sand			Loam			Fill		
	Median	COV	n	Median	COV	n	Median	COV	n
Minnesota	3.8	0.31	36	2.5	0.88	24	-	-	-
Wisconsin Marquette / Mitchell	3.5	0.83	8	2.2	0.96	5	4.3	0.82	29
Wisconsin UW Study	5.6	0.46	35	2.5	0.49	20	-	-	-

It is interesting to note, that on average $(q_t/p_{ref})/N$ ratios for Wisconsin sites were 50 to 80% higher than those from Minnesota and the coefficient of variations for the correlations are higher. It is inferred that these differences and higher uncertainties are associated with SPT hammer energy and other correction factors. The higher $(q_t/p_{ref})/N$ ratios for Wisconsin sites indicate lower N-values, which indicate transferred energies greater than 60%. It is recommended that if SPT data is collected at a site, a calibrated hammer is used and data are presented as N_{60} rather than N. This will reduce uncertainty in application, and may lead to less conservative assessment of engineering parameters.

5.2 Assessment of Geotechnical Parameters

This section focuses on correlations between CPT measurements and mechanical parameters. Definitions and a summary of engineering parameters discussed in this section are presented in Section 2.1.2.

5.2.1 Water Flow Characteristics

Within transportation engineering, water flow characteristics are commonly seen as most important to time rate settlement and strength gain for soft ground construction. Of equal concern, particularly in glacial deposits, is whether an in-situ test is performed under drained, undrained or partially drained conditions. These drainage conditions will affect correlations between engineering properties and CPT response. Figure 5.2 illustrates a relationship between water flow characteristics and soil type in relation to drainage conditions during and cone penetration testing. Slightly different boundaries are assessed for coefficient of consolidation (c_h) or hydraulic conductivity (k_h) based assessment of drainage conditions. This section will focus on assessment of the coefficient of consolidation and hydraulic conductivity from in-situ tests.

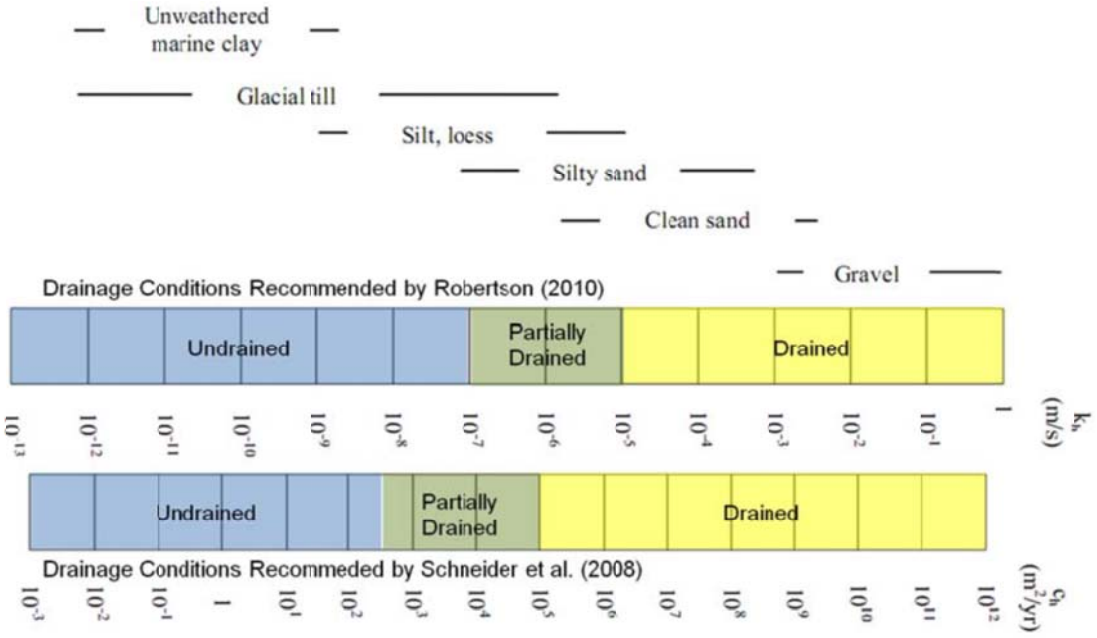

Figure 5.2. Drainage conditions associated with cone penetration testing as compared to soil type

Water flow characteristics cannot be tested in the field using the standard penetration test. Pumping tests would need to be performed after borehole completion. No pumping test data were available for this study. Comparison of water flow characteristics measured in a cone penetration test to laboratory data was performed using results of laboratory oedometer tests provided by WisDOT and performed in the UW-Madison geotechnical laboratory.

Dissipation testing measures the change in pore-water pressure with time during a halt in penetration. This test is analogous to an oedometer test where a load is applied to the soil and reduction in pore pressure (or settlement related to increases in effective stress) is measured with time. Results of CPTU dissipation tests can be used to directly assess the coefficient of consolidation and indirectly assess the hydraulic conductivity.

Results are analyzed in terms of the dimensionless normalized excess pore-water pressure, U:

$$U = \frac{u_t - u_0}{u_i - u_0} = \frac{\Delta u_t}{\Delta u_i} \tag{5.1}$$

u_t is the measured pore pressure at time t, u_0 is the in-situ hydrostatic pore water pressure, and u_i is the measured pore water pressure at the beginning of the dissipation. t_{100} is the time to 100% dissipation of excess pore-water pressures where the measured pore-water pressure is equivalent to the hydrostatic value ($u_m = u_0$). Conventional dissipation curves decrease continually with time. Normalized modified time factors (T*) can be used to analyze the coefficient of consolidation from dissipation tests.

$$c_h = \frac{T^* \cdot r^2 \sqrt{I_r}}{t} \tag{5.2}$$

where r is the cone radius, T* is a modified time factor (Table 5.3) and t is the time to reach that percentage of dissipation or consolidation, for example t_{50} for T^*_{50}. Equation 5.2 is typically applied by determining the initial pore pressure at the beginning of the test, calculating U at each time measurement, and determining the time at 50% dissipation, t_{50}, when U = 0.5. The c_h calculation is typically performed using t_{50}, but may be taken from any point on the dissipation curve. Schnaid et al. (1997) compared the variability of results depending on what percent of consolidation is selected and found that estimates taken at 50% and greater displayed less variability. This is an important point because conducting a dissipation test to hydrostatic values in soils with low hydraulic conductivities may require several days.

Table 5.3. Modified time factors for CPTU dissipations (Teh & Houlsby 1991)

Degree of Consolidation 1-U	T* at the cone shoulder
0.20	0.038
0.30	0.078
0.40	0.142
0.50	0.245
0.60	0.439
0.70	0.804
0.80	1.60

Conventional monotonic dissipation curves may not always be observed in glacial geological conditions. An increase in pore pressure may be measured followed by a decay to the in-situ pore pressure condition, known as a dilatory dissipation. This effect has been contributed to local shear induced pore pressures, as shown for monotonic versus dilatory dissipations in Figure 5.3. A complete hybrid critical state model can be used to quantify dilatory dissipation response, but these solutions are still being refined (Burns & Mayne 1998, Mayne 2007). Analysis of dilatory dissipations in this study used the square root of time method (Figure 5.4) discussed by Sully et al. (1999) to estimate t_{50}, and the Teh & Houlsby (1991) modified time factors. Parametric studies by Hotstream (2011) imply that this method yields c_h values that are within a factor of 1.5 (on the low side), provided that measured penetration pore pressures are positive.

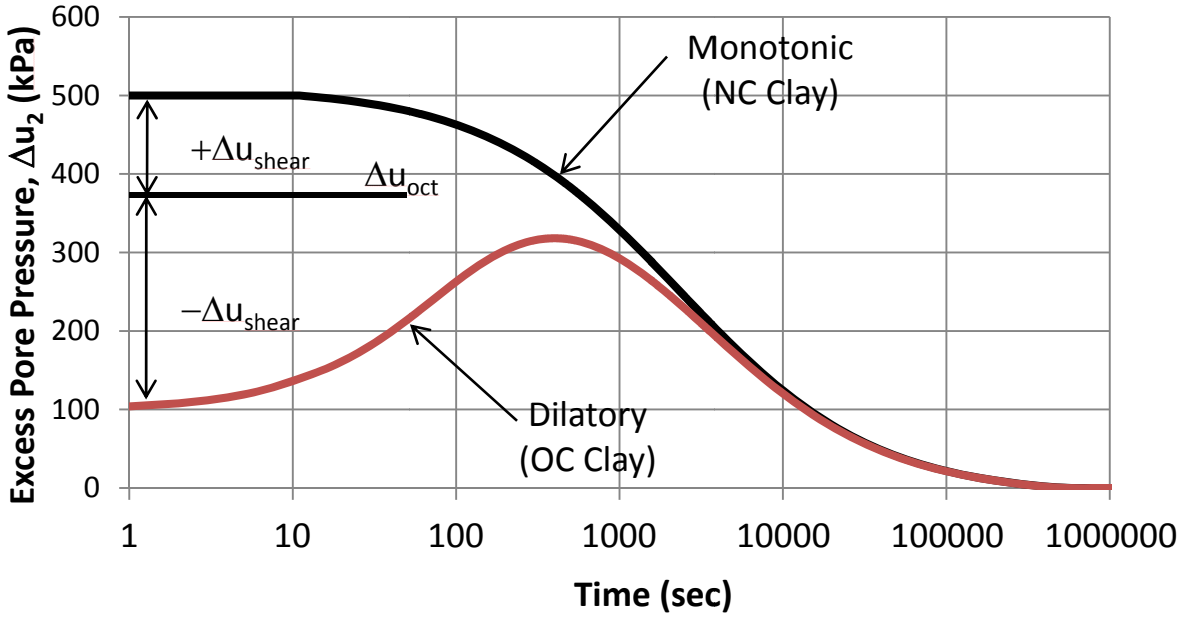

Figure 5.3. Comparison between a monotonic dissipation curve where positive shear pore-water pressures occur during penetration with a dilatory curve where negative pore-water pressures are generated (after Burns and Mayne 1998).

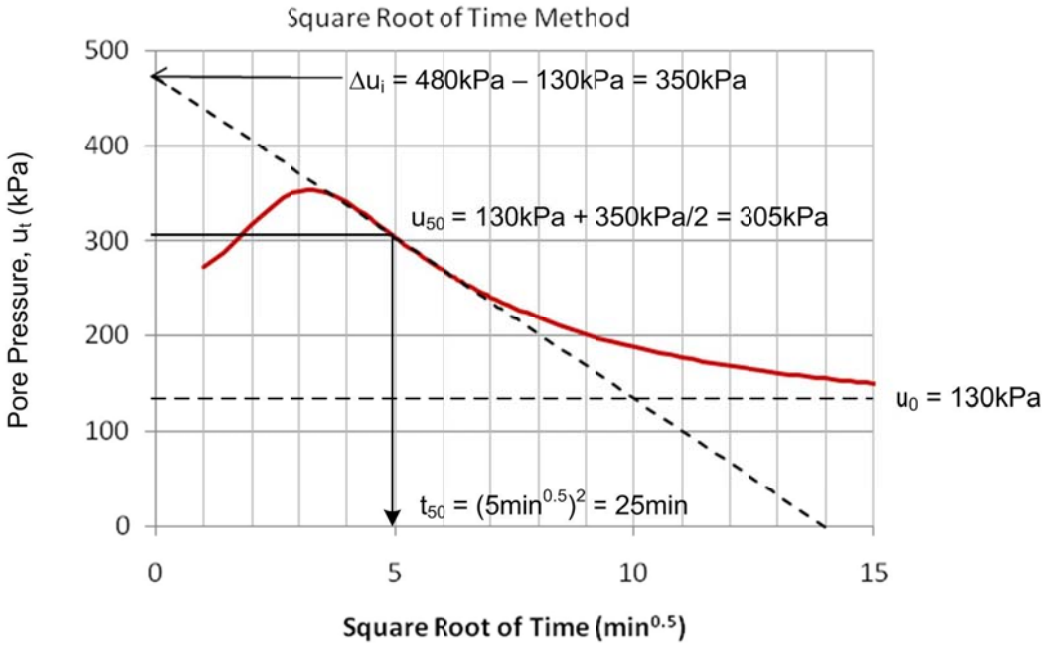

Figure 5.4. Evaluation of dilatory dissipation using square root of time method (after Sully et al. 1999)

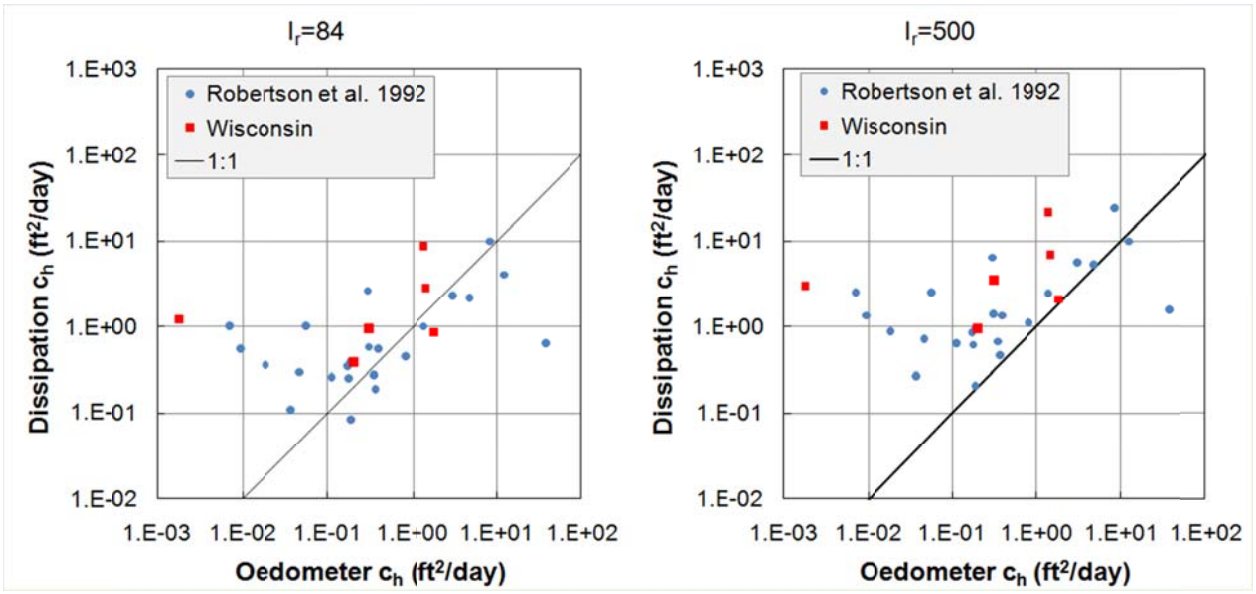

Figure 5.5. Comparison of dissipation data to laboratory oedometer tests

Table 5.4. Summary of laboratory and field coefficient of consolidation data for Wisconsin sites

Site	Local Geology	$t_{50,mean}$ (sec)	mean field c_h (ft^2/day)		mean lab c_v (ft^2/day)
			$I_r = 84$	$I_r = 500$	
DOT-1	Upper Glacial Lake	1791	3.9E-01	9.5E-01	2.0E-01
DOT-1	Lower Glacial Lake	734	9.5E-01	3.5E+00	3.0E-01
DOT-7	Soft Shallow Lake/Palaudal	815	8.5E-01	2.1E+00	1.9E+00
DOT-10c	Upper Till	572	1.2E+00	3.0E+00	1.8E-03
UW-1	Organic	247	2.8E+00	6.9E+00	1.5E+00
UW-1	High Plasticity Silt	79	8.8E+00	2.1E+01	1.4E+00

Assessment of c_h from field dissipation data for assumed rigidity index values of 84 and 500 are compared to laboratory c_v values from oedometer tests in Figure 5.5 and Table 5.4. Multiple c_h and c_v values for a given site were often available, and the geometric mean was used to minimize the influence of spatial variability on assessment of the correlation. A database of field sites with oedometer and dissipation data (Robertson et al. 1992) is included in Figure 5.5. Similar trends are observed for the Wisconsin sites and the global database. Rigidity index values are typically on the order of 100 to 500 in normally consolidated to lightly overconsolidated soils, but may be as low as 5 to 10 in heavily overconsolidated soils (Keaveny & Mitchell 1986). The lower selected rigidity value of 84 tends to result in a slight overprediction of laboratory c_v values from field c_h values. While there is some uncertainty in selection of I_r, much of the difference is likely due to macrofabric and higher horizontal hydraulic conductivity as compared to vertical.

While laboratory data was only available for a limited number of locations where dissipation tests were performed, data in Figure 5.5 give us confidence in the results from the large number of dissipation tests performed in this study.

To evaluate hydraulic conductivity from dissipation tests, the constrained modulus of the soil is needed (Equation 2.1). Constrained modulus can be estimated from CPT data, as discussed in the next section.

5.2.2 Compressibility

Compressibility is the change in volume due to change in effective stress, and is most important for soft clays and organic soils. During cone penetration in soft clays and organic soils, the coefficient of consolidation is low enough that penetration is undrained, and essentially no change in octahedral effective stress occurs. Any estimation of compressibility from CPT parameters is therefore a correlation that has a relatively weak theoretical basis.

A correlation between constrained modulus (1/compressibility) and net cone tip resistance takes the form:

$$D' = \alpha_c' \cdot (q_t - \sigma_{v0}) \tag{5.3}$$

Mayne (2007) highlights that α_c' is site specific and varies from about 1 to 2 in soft high plasticity clays to 10 in cemented clays.

Since D' is an effective stress parameter it may be considered more fundamentally sound to develop correlations between D' and effective cone tip resistance.

$$D' = \alpha_{ce}' \cdot (q_t - u_2) \tag{5.4}$$

Based on deformations below an embankment in a lightly overconsolidated clay and silty clay, Tonni & Gottardi (2011) proposed α_{ce}' of 2.3. Like the correlation to net tip resistance, correlations between D' and effective cone tip resistance appear site specific. The coefficient of

2.3 is on the low end of data from Mayne (2007). Incorporating pore pressures into the correlation between constrained modulus and tip resistance does not improve the correlation. One reason for this less reliable correlation is the influence of the generation of both shear and octahedral pore pressures during penetration, which complicates assessment of soil response.

Table 5.5. Summary of laboratory and field constrained modulus data for Wisconsin sites

Site	Local Geology	Depth (ft)	D' (tsf)	q_{cnet} (tsf)	q_{eff} (tsf)	α'_c	α'_{ce}
DOT-1	Upper Glacial Lake (B810)	16.5	43	6.6	6.3	6.5	6.9
DOT-1	Upper Glacial Lake (B804)	26	14	7.0	7.0	2.0	2.0
DOT-1	Upper Glacial Lake (B810)	31	42	6.5	5.8	6.4	7.2
DOT-1	Lower Glacial Lake (B810)	46	54	5.9	6.6	9.3	8.2
DOT-7	Soft Shallow Lake/Palaudal	7.2	68	11.0	11.3	6.2	6.0
DOT-7	Soft Shallow Lake/Palaudal	11	8.4	4.2	3.0	2.0	2.8
DOT-10c	Upper Till	6.2	94	39.4	38.0	2.4	2.5
UW-1	Organic	12	6.8	3.3	3.5	2.0	2.0
UW-1	High Plasticity Silt	14	12	4.8	4.2	2.5	2.9

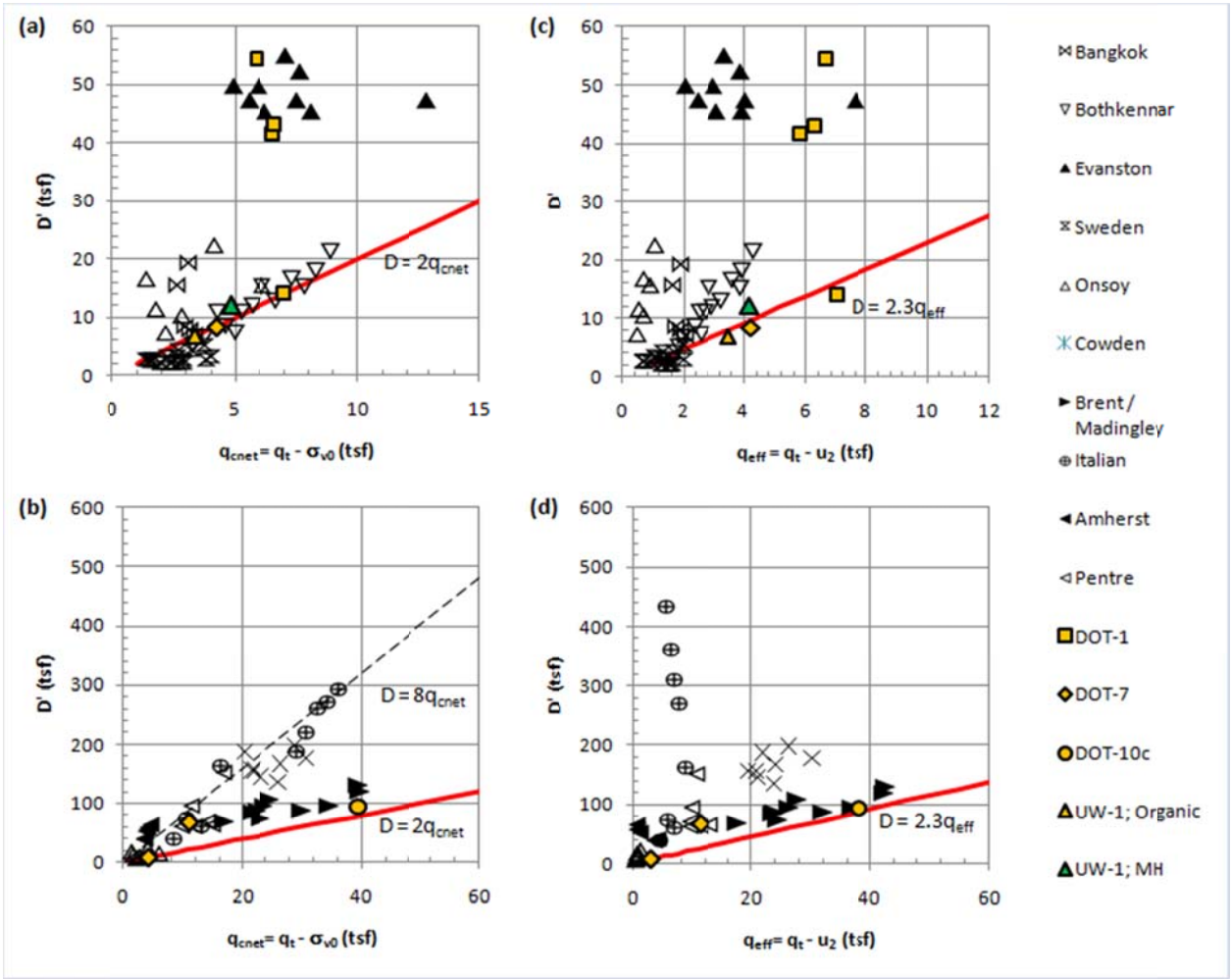

Figure 5.6. Comparison of cone tip resistance to constrained modulus (global data from Mayne 2007)

The Mayne (2007) database is plotted in Figure 5.6 with an overlay of data from Wisconsin. As previously mentioned, there are not unique constrained modulus correlations and the correlation to net tip resistance shows less scatter than the correlation to effective tip resistance. Inclusion of CPT penetration pore pressures does not reduce uncertainty in the correlation, and correlations to q_{cnet} are recommended. Data from Wisconsin tend to follow the lower limit of the correlation with constrained modulus being approximately twice the net cone tip resistance. This was true for very soft low PI soils at DOT-7, as well as very stiff low PI soils at DOT-10c.

Three of the four data points from site DOT-1 (sensitive low plasticity lacustrine clays from Green Bay) tend to plot higher than the average trend, and are similar to lacustrine clays at the Northwestern test site in Evanston. The structured nature of the clay may result in low compressibility (high constrained modulus) as compared to cone tip resistance, however, sample disturbance for the sensitive clays from Green Bay make interpretation of response uncertain, and high quality undisturbed sampling at that site is recommended.

5.2.3 Shear Stiffness

Immediate deformations, whether drained or undrained, occur from applying a shear stress to a soil element. The resistance to distortions caused by shear stresses is the shear stiffness, or shear modulus (G). As previously mentioned, shear stiffness is difficult to evaluate since it increases with effective stress and decreases with increasing strain level (Figure 2.8). Operational stiffness for foundations and retaining walls is much less than that measured in geophysical tests and close to the stiffness measured in pressuremeter unload-reload loops. Depending on the fraction of ultimate capacity to which a wall or foundation is loaded, operational stiffness may be less than that from a pressuremeter unload-reload loop.

Small strain stiffness is covered in Section 7.1 on the seismic cone test, and this section will focus on larger strain measurements of stiffness. No pressuremeter data were available for the field sites tested under this program, and correlations between cone tip resistance and pressuremeter data for Lake Clays and Clayey Tills from the Marquette Interchange and Mitchell Interchange projects are assessed herein. Shear stiffness of sandy soils is addressed in Section 6.1 on the design of shallow foundations.

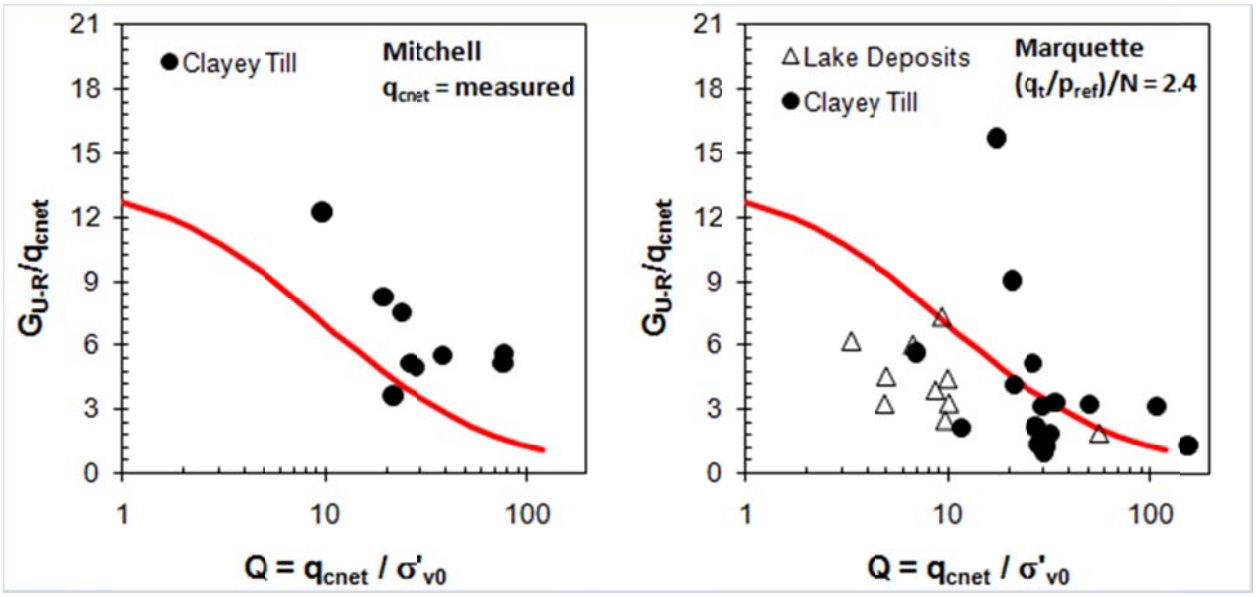

Figure 5.7. Comparison of pressuremeter unload-reload stiffness to cone tip resistance for various values of normalized cone tip resistance

Figure 5.7 compares the unload-reload stiffness from pressuremeter tests to net cone tip resistance. No CPTs were performed adjacent to borings with pressuremeter data for the Marquette Interchange project, and q_t was estimated from SPT N-value using site specific correlations in Table 5.1. The ratio of G_{u-r} to q_{cnet} is analogous to the rigidity index, $I_r = G/s_u$, since net cone tip resistance during undrained penetration is analogous to undrained strength (see next section). I_r has been shown to increase as plasticity index decreases and decrease as OCR increases (e.g., Keaveny & Mitchell 1986). To account for the influence of OCR on I_r in Figure 5.7, G_{u-r}/q_{cnet} is plotted against normalized cone tip resistance, Q. The value Q has been shown to correlate well with OCR (e.g., Mayne 1986, Mayne 2007). The trend line in Figures 5.7a & b roughly shows I_r reducing from 150 to 50 as OCR increases, which is appropriate for a PI=20 clay.

Data from the Mitchell Interchange generally follow the trend in Figure 5.7, however, the data from the Marquette Interchange show lower values of stiffness for the same normalized cone tip resistance. This is not believed to be due to the use of a correlation between SPT and CPT penetration resistance or differences in soil characteristics, but more due to the variability in pressuremeter test methods.

As pressuremeter unload-reload loop depth increases (change in total stress, Δp), the average strain over the loop increases and $G_{u\text{-}r}/G_0$ decreases (i.e., Figure 2.8). When the loop depth (Δp) exceeds twice the undrained strength, the soil is yielding plastically, resulting in lower stiffness values. Average $\Delta p/s_u$ values for pressuremeter tests performed at the Mitchell interchange were 1.5, but were 2.0 for the Marquette Interchange. This greater loop depth during unload-reload loops, as well borehole disturbance and other differences in testing procedures, likely resulted in the differences in correlations between CPT parameters and shear stiffness.

Data generally support the following correlation between intermediate strain level shear stiffness for low plasticity clays from the Milwaukee area:

$$\frac{G_{u-r}}{q_{cnet}} \approx 14\left(1+\frac{Q}{10}\right)^{-1} \tag{5.5}$$

Correlations of this format require additional site specific validation with high quality pressuremeter testing. Additional comparison to results from seismic cone tests may reduce uncertainty in assessment of low-high strain values of shear stiffness.

5.2.4 Resilient Modulus

For design of flexible pavement systems, estimations of the resilient modulus (M_R) are a key design parameter. Resilient modulus is conceptually similar to the unload-reload shear modulus discussed in the previous section, and therefore, it is logical that a state dependent correlation to cone tip resistance could be developed. It is noted that correlations in the previous section were only applicable for low plasticity clays tested at an intermediate strain level, and the empirical coefficients need validation in other soil and loading conditions.

Additional complexities in resilient modulus occur since the resilient modulus is defined at a particular bulk stress level, which will generally differ from the in situ mean effective stress. Schuettpelz et al. (2010) discuss the need to account for void ratio, stress level and strain level in the evaluation of resilient modulus.

While no assessment of resilient modulus from CPT parameters was performed in this study, existing correlations have been discussed by Puppala (2008). The following equation has been used as an estimate of resilient modulus for overburden and traffic conditions based on CPT measurements (Puppala 2008):

$$\frac{M_R}{{\sigma_3}^{0.55}} = \frac{1}{\sigma_1}\left(47q_c + 170.4\frac{f_s}{w}\right) + 1.7\frac{\gamma_d}{\gamma_w} \tag{5.6}$$

Where M_R is the resilient modulus in MPa, q_c is the cone tip resistance in MPa, f_s is the sleeve friction in MPa, σ_1 and σ_3 are the major and minor principal stresses in kPa, w is the water content expressed as a decimal, γ_d is the dry unit weight, and γ_w is the unit weight of water. While it is not recommended to use this dimensionally specific (and inconsistent) empirical correlation that has no link to physical mechanisms, the format highlights that the correlation between strength and stiffness is soil type dependent (i.e., depends on q_c and f_s), varies with void ratio (use of w and γ_d in correlation), as well as mean stress (σ_3). It is recommended to extend the correlation formats discussed by Schuettpelz et al. (2010) in light of sand and clay G/q_{cnet} correlations presented in sections 5.2.3 and 6.1 of this report if attempting to assess resilient modulus from CPT parameters.

5.2.5 Strength

Undrained

A primary application of the cone penetration test is to evaluate undrained strength of clayey soils. The results would be applicable to assess embankment stability, deep foundation axial and lateral resistance, bearing capacity of shallow foundations, among other design issues. The net cone tip resistance is reduced by a cone factor (N_k) to estimate the undrained strength at the time of testing.

$$s_u = \frac{q_{cnet}}{N_k} \tag{5.7}$$

It is often useful to assess data in terms of normalized undrained strength ratio, s_u/σ'_{v0}:

$$\frac{s_u}{\sigma'_{v0}} = \frac{q_{cnet}/\sigma'_{v0}}{N_k} = \frac{Q}{N_k} \tag{5.8}$$

Published values of N_k generally range from 7 to 25 (e.g., Salgado 2008), however, theoretical evaluation of cone factors limit this range to 10 to 15 (e.g., Randolph 2004). Median cone factors for DSS and vane shear (VST) modes of strength are 13.7 (Randolph 2004). The wide range of cone factors published in the literature can largely be attributed to sample disturbance and strength anisotropy. Table 5.6 lists how various issues affect undrained strength, cone tip resistance, and apparent N_k value ($N_{k,app}$).

Table 5.6. Factors influencing apparent cone factor ($N_{k,app}$)

	$s_{u,meas}$↓ $N_{k,app}$↑	$s_{u,meas}$↑ $N_{k,app}$↓	$q_{c,net}$↑ $N_{k,app}$↑
Sample Disturbance	X		
Fissuring	X		
Sensitivity	X		
Spatial Variability	↑/↓	↑/↓	↑/↓
Strength anisotropy	X	X	
Fissured clay	X		
Increase in testing rate (for CPT, viscous)			X
Decrease in testing rate (for CPT, drainage)			X
Increase in testing rate (for reference test, viscous)		X	
Decrease in testing rate (for reference test with uncontrolled drainage conditions, i.e., VST, drainage)		X	
Net area ratio correction for CPT			↑/↓
Drift in CPT baseline			↑/↓

Strength data from this study was available from:

- Soft high plasticity silt at UW-1 (CIUC)
- Soft low plasticity clays at DOT-1 (UU and VST)
- Soft low plasticity clay for the Marquette Interchange Project (UC)
- Stiff low plasticity clay for the Marquette Interchange Project (UC)

Triaxial compression data were available at all sites, however, the test performed included (i) isotropically consolidated undrained compression tests (CIUC); (ii) unconsolidated undrained compression tests (UU); and (iii) unconfined compression (UC) strength tests. Of the 26 triaxial tests, only 1 was a CIUC test. UU and UC compression tests have low reliability and results should be used with caution. Field vane shear tests were also performed at 15 depths at the DOT-1 site. Strength data is compared to CPT net tip resistance in Figure 5.8. Cone factors of 10 and 15 are shown for reference.

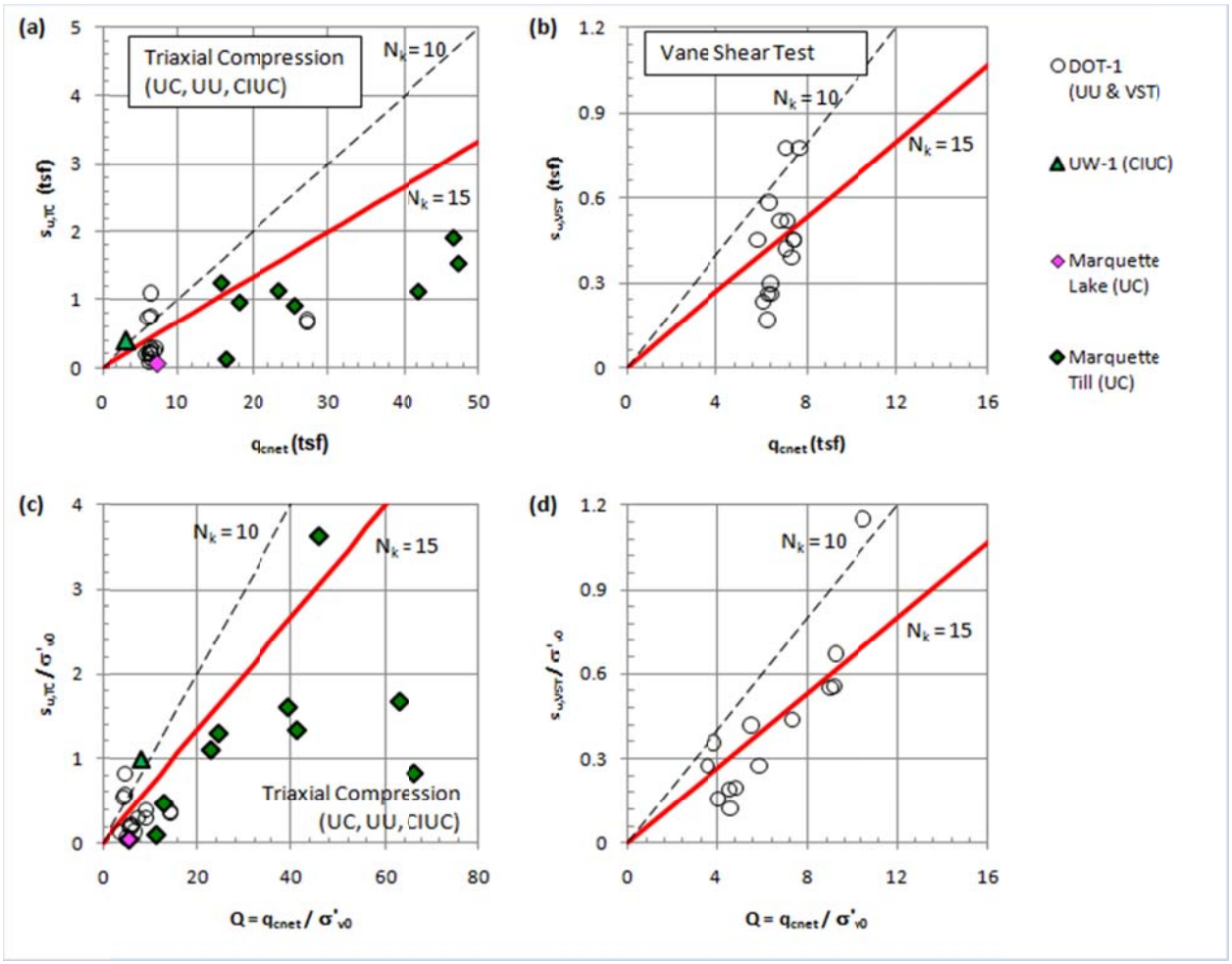

Figure 5.8. Comparison of CPT results to strength data at Wisconsin sites from this study

Poor correlations are observed between laboratory measurements of strength and CPT resistance. This is considered to be predominantly a function of the sampling and laboratory strength testing procedures than variability in the correlation between CPT measurements and strength. Eight of the 25 UU or UC tests had undrained strength ratios less than 0.23. This is below the expected normally consolidated undrained strength ratio, and typical of highly disturbed samples. Better correlations were observed between cone and vane tests, however, the low sensitivity measured by the VST indicate some disturbance during installation and testing, particularly at depth.

Drained

The correlations between CPT parameters and drained strength properties is truly only applicable to drained penetration, which typically occurs in sandy soils. These correlations are difficult to generate in that sampling of sands results in disturbance of density and structure. These changes in void ratio significantly affect measured peak friction angle. Additionally, the mean effective stress level for the zone of soil influencing the tip resistance (p'_f) is typically near $\sqrt{\sigma'_{h0} \cdot q_t}$. This effective stress level is much higher than that in triaxial tests performed to develop correlations between normalized tip resistance and friction angle, which also significantly effects peak friction angle (e.g., Figure 2.10). No drained triaxial data on undisturbed sand samples was available adjacent to CPTs performed in this study. A database of sites where CPTs were performed adjacent to locations where frozen samples of sand were collected and then tested under triaxial conditions (Mayne 2006, 2007) is presented for verification of a correlation between CPT measurements and drained strength (Kulhawy & Mayne 1990):

$$\phi' = 17.6 + 11 \cdot \log\left[\frac{q_t / p_{ref}}{\left(\sigma'_{v0} / p_{ref}\right)^{0.5}}\right] = 17.6 + 11 \cdot \log\left(Q_{t0.5}\right) \qquad (5.9)$$

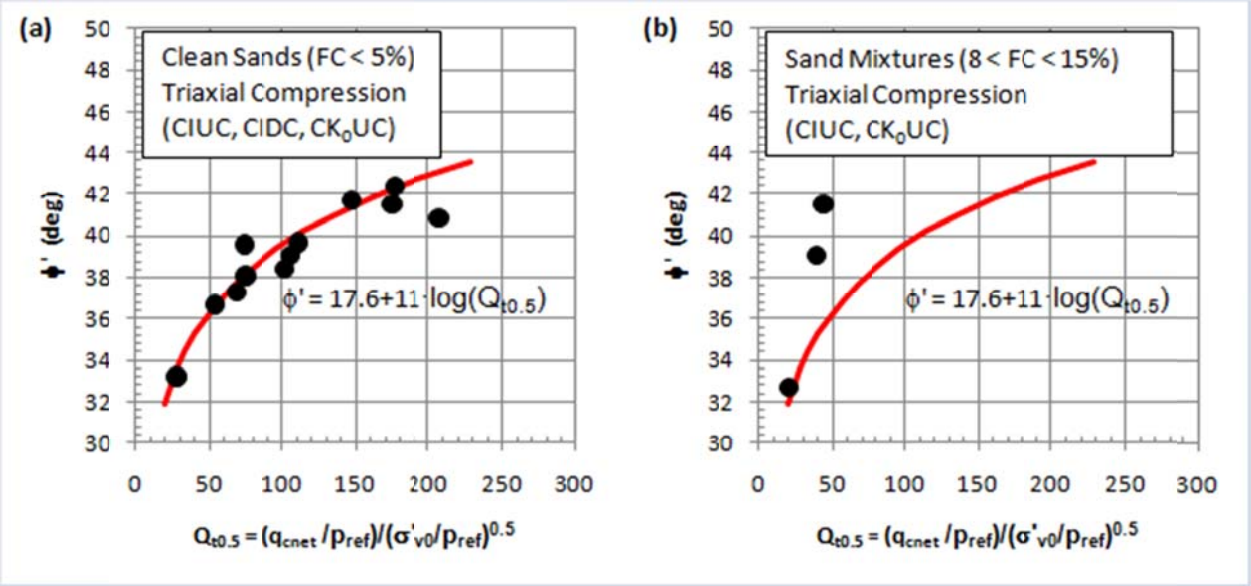

Figure 5.9. Comparison of friction angle measured in triaxial compression tests to normalized cone tip resistance (Mayne 2006, 2007)

The recommended correlation of Kulhawy & Mayne (1990) matches triaxial test results from frozen specimens of clean sands well in Figure 5.9a. Application of the correlation in Figure 5.9b to undrained triaxial tests on clayey tailings with 5 to 15% fines appears slightly conservative. It should be noted that the friction angle for relatively low stress triaxial tests summarized in Figure 5.9 will be too high for application to bearing capacity of shallow foundations in sands. These friction angles should be reduced to account for mean stress at failure (e.g., Equation 2.15).

5.3 Soil Classification

Conventional soil classification for geotechnical engineering is typically performed to the specifications of the USCS (Casagrande 1948, ASTM D 2487 and D 2488) a primarily textural system. The USCS breaks soils into two major divisions: coarse and fine grained soils based on the percentage of fined grained soil particles, nominal diameter < 0.075 mm, passing through the number 200 sieve (#200). Coarse grained soils are sands and gravels defined as having over 50% of the particles with a nominal diameter greater than or retained on the #200. Fine grained soils, silts and clays, have over 50% passing the #200. Further, divisions within these two main groupings are made based on additional factors such as percent fines and plasticity.

Sands and gravels are further grouped based on gradation, or the distribution of particle sizes. A well graded soil exhibits a gradual transition in grain size from coarser gravels and sands to fine sands. A poorly graded soil has a poor distribution of grain sizes and is therefore likely to exhibit a larger void space than a well graded sand or gravel. Fines content, the percentage of particles by mass passing the # 200 sieve, is also considered in the classification of sands and gravels where the fines content greater than 5% changes the classification to indicate the presence of fines. This classification system groups coarse grained soils by void space because the strength and water flow behavior is dependent upon inter-particle interactions and void space.

Silts and clays are classified by consistency limits or the Atterberg limits. These limits represent the water contents at which fine grained soils change behavior. The plastic limit (PL) represents the change in soil behavior from a brittle solid to a plastic material defined as a shear strength of 170 kPa (Wroth & Wood 1978). The liquid limit (LL) represents the threshold between plastic

and viscous liquid behavior and is defined as the shear strength of 1.7 kPa (Wroth & Wood 1978). The difference of these parameters is the Plasticity Index (PI=LL-PL), and is plotted against liquid limit, allowing for classification of fine grained soils in Figure 5.10.

This classification based on Atterberg Limits does not accurately account for grain size differences between silt and clay particles, but rather indexes potential compressibility. Studies have found "silts" classified as clays and "clays" classified as silts (USBR 1998), however; PI is a useful indicator of anticipated soil behavior. The plasticity index has been correlated to the compression index, C_c, (Wroth & Wood 1978, Atkinson 2007):

$$C_c \approx \frac{G_s}{100}\frac{PI}{3.5} \tag{5.10}$$

Estimates of remolded undrained shear strength (s_u) can be estimated using the liquidity index (LI) which is defined as:

$$LI = \frac{w - PL}{PI} \tag{5.11}$$

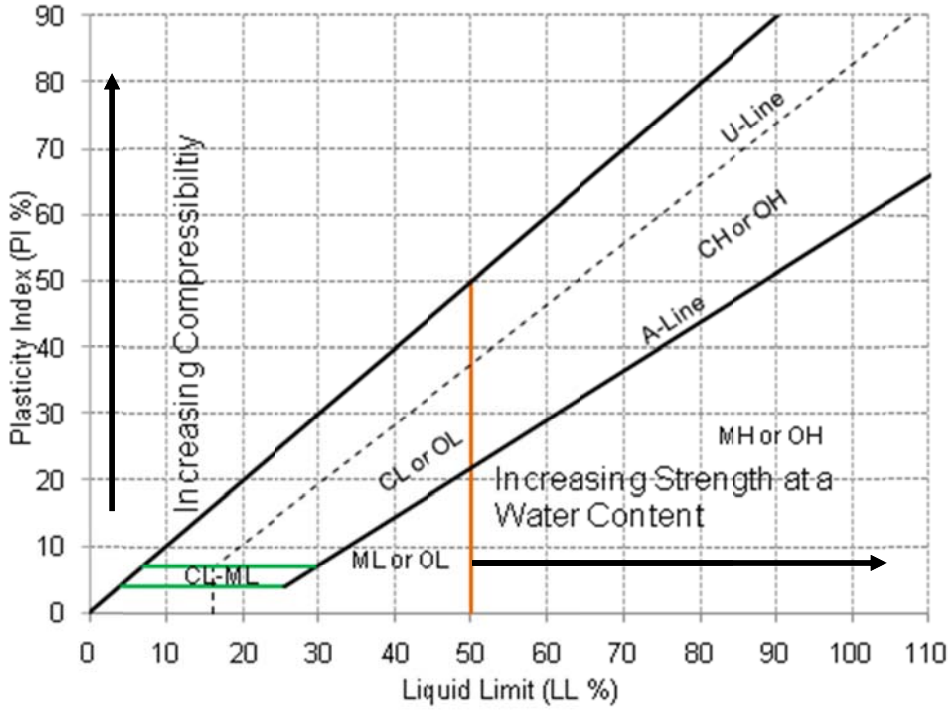

Figure 5.10. USCS plasticity based classification chart for fine grained soils. Note arrows indicating compressibility relationships.

Assuming a power law relationship between strength and water content between the plastic limit, an estimate of the remolded undrained shear strength may be determined for a given LI. Liquidity Index values greater than unity indicate sensitive clays (Bjerrum 1954, Leroueil et al. 1983).

The USCS uses a bimodal system of classifying soils where sands and gravels are grouped predominantly by water flow characteristics, and clays and silts are grouped based on compressibility. Inherent assumptions are made that, under typical rates of loading, fine grained soils will behave in an undrained manner and coarse grained soils behave drained. This assumption works well for end members of the classification, but for soil mixtures of coarse and fine grained particles and borderline soils the system fails in that similar behavior in-situ is observed on both sides of the classification boundary. Douglas and Olsen (1981) make this observation in their comparison of uniformly graded sands where a sample may classify as a silty sand (SM) and another as poorly graded sand (SP) but the expected behavior for typical loading conditions of the two will be similar.

Alternative classification systems include the American Association of State Highway Officials (AASHTO) system and the USDA system. The AASHTO system is similar in methodology to the USCS, except that it groups soils based on their suitability for application for pavement subgrade.

It has been observed that the Robertson (1990, 1991) normalized CPTU soil classification charts may have poor performance in many glacial soils (Ramsey 2002, Schneider et al. 2008). Still, with proper judgment these charts can be applied successfully in practice (e.g., Dasenbrock et al. 2010). To minimize the judgment required for applying normalized CPTU soil classification charts in glacial soil conditions of Wisconsin, the Q-$\Delta u_2/\sigma'_{v0}$ normalized pore pressure charts by Schneider et al. (2008) were used, and new Q-F normalized soil classification charts were developed. Boundary and trend lines for the Q-F chart were developed primarily using clay data from Ramsey (2002), sand and sand mixture data from Moss (2003), and observations of data from glacial soil conditions in Minnesota (from Dasenbrock et al. 2010). Development of the boundaries was performed attempting to construct a similar classification system as that developed in Q-$\Delta u_2/\sigma'_{v0}$ space by Schneider et al. (2008), and charts are shown in Figure 5.11 with zones described and compared to equivalent locations on the Robertson (1990, 1991) charts in Table 5.7. New zones were added when updating the Q-F charts.

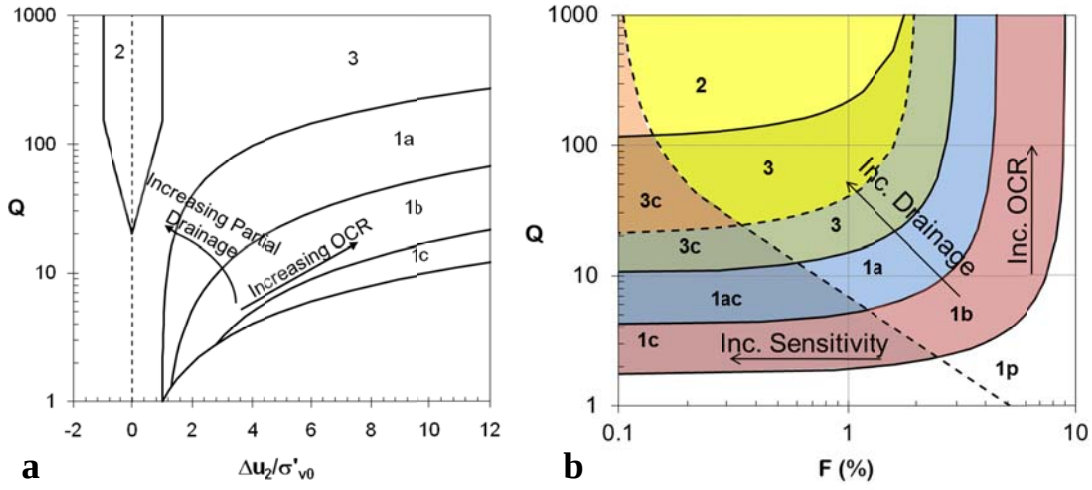

Figure 5.11. SBTn chart in Q- $\Delta u_2/\sigma'_{v0}$ space (Schneider et al. 2008) and Q-F space.

Table 5.7. Soil behavior type number zones and descriptions (after Schneider et al. 2008)

SBTn	Simplified Soil Description	Assessed drainage during cone penetration (this study)	Similar Zone in Robertson (1990) Q-F classification charts	Assessed drainage during cone penetration (Robertson 2010)
1p	Organic soils	Undrained to partially drained	2: Organic Soils – Clay	Undrained
1b	Undrained Clays	Undrained	3: Clay to silty clay	Undrained
1a	Silts and 'Low I_r' Clays	Undrained to partially drained	4: Silt mixtures – Clayey silty to silty clay	Undrained
1c	Sensitive Clays	Undrained	1: Sensitive fine grained	Undrained
1ac	Sensitive silts and sensitive 'Low I_r' clays	Undrained to partially drained	1: Sensitive fine grained	Undrained
3	Transitional soils	Undrained to essentially drained	5: Sand Mixtures – Silty sand to sandy silt	Partially drained
3s	Transitional soils – Sands and sand mixtures	Partially drained to essentially drained	6: Sand	Drained
2	Sands	Essentially drained	7: Dense sand to gravelly sands	Drained

Inferred soil behavior type is quite similar for this system and the Robertson (1990) charts, but tends to become offset by one zone for sands and silty sands and differ significantly for overconsolidated clays. These differences are in agreement with the inferred point at which cone penetration is drained or undrained, as indicated in Figure 5.2. To understand these drainage boundaries and cone penetration testing in Wisconsin, an extensive dissipation testing program was performed. Initial assessment of soil behavior type will be based on drainage conditions during penetration, quantified through dissipation testing.

Cone penetration and drainage conditions are linked through the normalized velocity (V, e.g. Finnie & Randolph 1994).

$$V = \frac{v \cdot d}{c_h} \tag{5.13}$$

Where v is the penetrometer velocity, d is the penetrometer diameter, and c_h is the horizontal coefficient of consolidation. Dissipation times (Section 5.2.1) are typically characterized by the time to 50% consolidation, t_{50}. The normalized velocity (V) is actually equal to t_{50} for standard

cone dimensions (d=1.44 inches) and penetration rates (0.78 in/sec) and an assumed rigidity index of 84 (Figure 5.5a). This relationship is only applicable if penetration is undrained. If penetration is partially drained, normalized time factors tend to increase as compared to the undrained case (Silva et al. 2006, Schneider et al. 2007) and the V-t_{50} relationship needs to be modified. Table 5.8 presents several t_{50} times with anticipated water flow characteristics. The calculated values of V in Table 5.8 agrees well with the suggested ranges for drained penetration with V< 0.1 and undrained penetration occurring at V>30-100 (Randolph 2004).

The location of data in Q-F soil classification charts is shown in Figures 5.12 to 5.16. The sensitivity boundary has been removed such that CPTU soil classification charts should be in better agreement with non state assessment of soil types (i.e., USCS, AASHTO). Table 5.9 provides drainage estimates of several t_{50} values. Hydraulic conductivity was estimated using Equation 2.1 with an assumed D of 100 tsf. This table allows for rough estimation of the water flow properties of the soil.

Table 5.8. Estimates of c_v and V based on different t_{50} times calculated using Teh and Houlsby (1991) solution. Values were corrected based on results by Silva et al. (2006). Calculations based on a cone diameter of 35.6 mm and soil with $I_r = 84$.

v (mm/s)	t_{50} (s)	T_{50}	Apparent c_h (ft^2/day)	Apparent V	$T_{50,pc}/T_{50}$	$T_{50,pc}$	c_h (ft^2/day)	V	Drainage Condition
20	5	0.245	132	5	16	3.9	2119	0.3	Essentially Drained
20	15	0.245	43.7	15	5.6	1.37	247	2.7	Partially Drained
20	30	0.245	18.6	30	2	0.49	44.6	15	Partially Drained
20	100	0.245	6.5	100	1	0.245	6.5	100	Undrained
20	300	0.245	1.9	300	1	0.245	2.2	300	Undrained
20	3000	0.245	0.2	3000	1	0.245	0.2	3000	Undrained

Table 5.9. Legend and range of t_{50} presented in Figures 5.12 to 5.16. Estimated water flow characteristics based on calculations in Table 5.8. Values presented in this table are applicable to a 10 cm^2 cone advanced at the standard steady rate of 20 mm/s.

t_{50} (s)	Symbol	V	c_h (ft^2/day)	k_h (ft/day)	Drainage Condition
0 – 15	●	<2.7	>247	>0.07	Essentially Drained
15-30	○	2.7 – 15	45-247	0.003-0.03	Partially Drained
30-100	◆	15 - 100	6.5-45	0.0003-0.003	Essentially Undrained
100-300	▲	100 – 300	2-6.5	0.0003	Undrained
300-3000	□	300 - 3000	0.2-2	$3x10^{-5}$-$3x10^{-4}$	Undrained

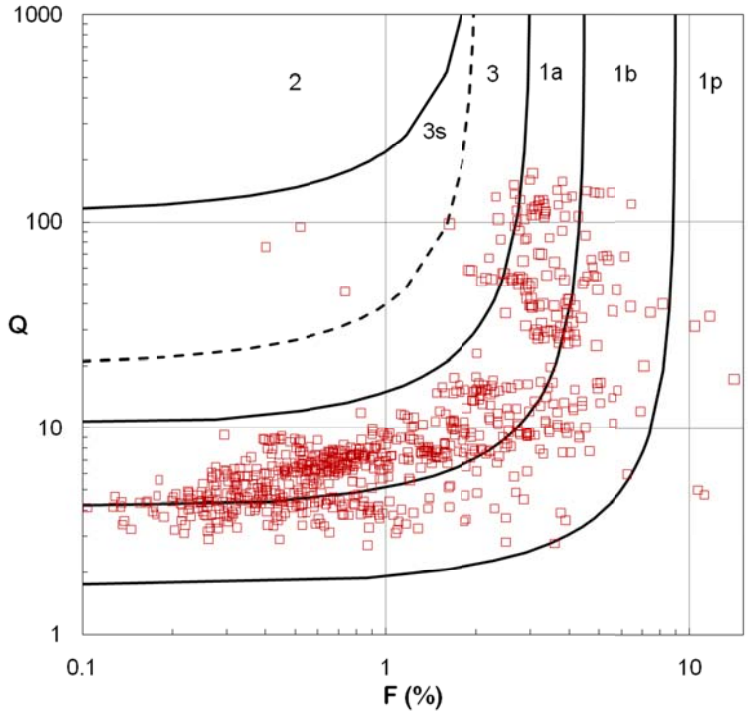

Figure 5.12. Q-F chart with Wisconsin data presented and grouped by dissipation t_{50} times between 300 s to 3000 s. Colors are based on dissipation t_{50} times within a layer, Table 4.1. This is one of 5 figures representing dissipation times and location on the revised Q-F SBTn chart.

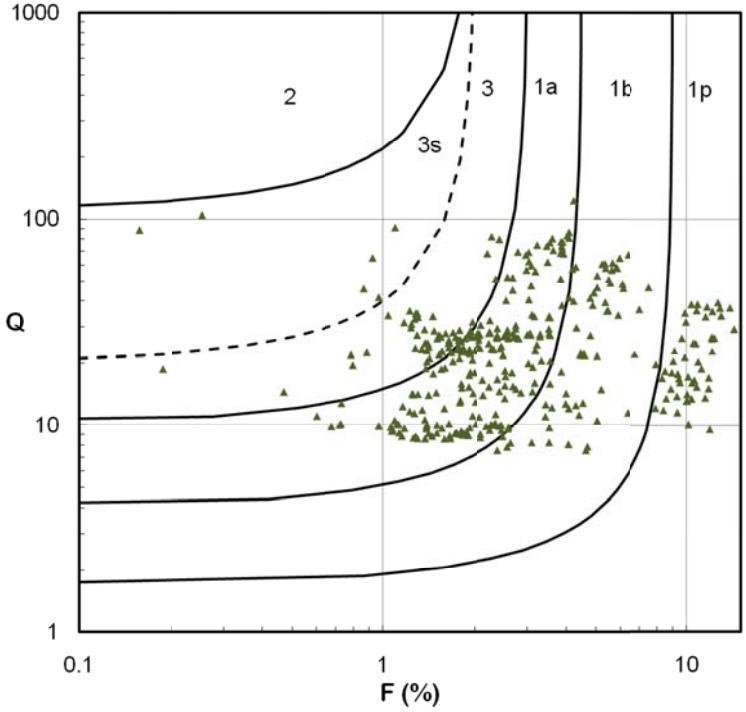

Figure 5.13. Data points in Q-F space for dissipations with t_{50} times of 100 s to 300 s.

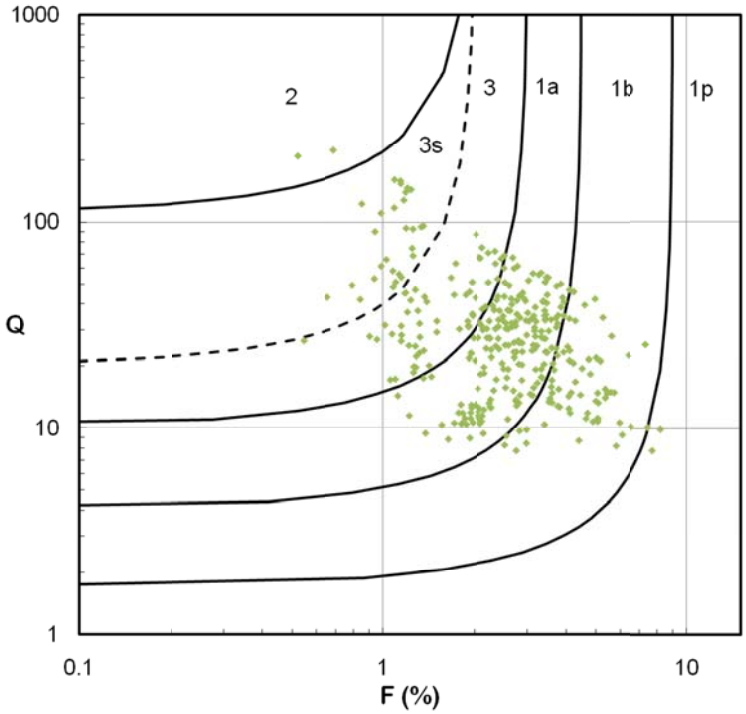

Figure 5.14. Data points in Q-F space for dissipations with t_{50} times of 30 s to 100 s.

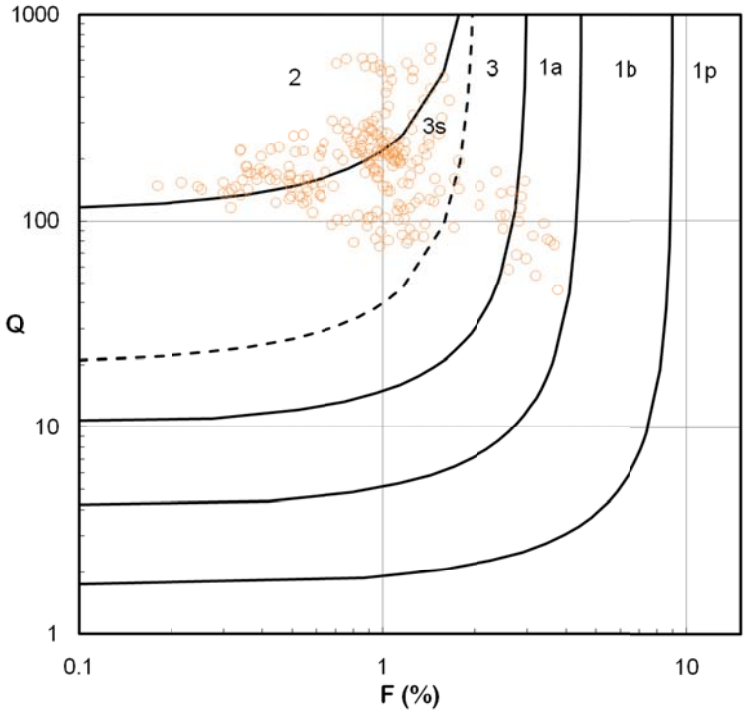

Figure 5.15. Data points in Q-F space for dissipations with t_{50} times of 15 s to 30 s.

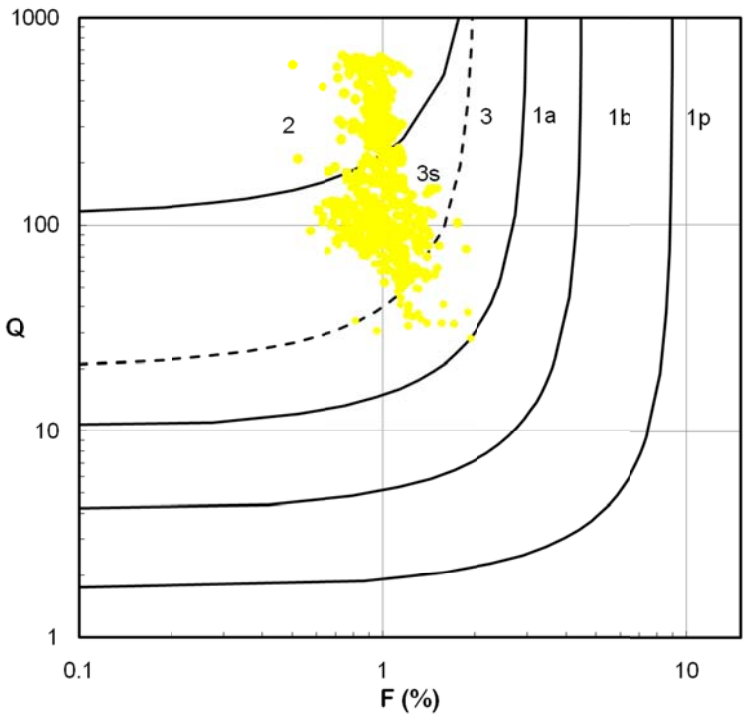

Figure 5.16. Data points in Q-F space for dissipations with t_{50} times of 0 s to 15 s.

Table 5.10. Percentages of points that plot within each soil zone of the revised Q-F SBTn chart for Figures 5.12 to 5.16.

Dissipation t_{50} Times (s)	% Data in 1p	% Data in 1b	% Data in 1a	% Data in 3	% Data in 3s	% Data in 2	Total Points
0 - 15	0	0	0.1	4.2	72.6	23.1	693
15 - 30	0	0	6.1	4.1	45.7	44.1	245
30 - 100	0.6	18.9	55.2	16.6	8.1	0.6	344
100 - 300	9.1	10.3	63	16.4	1.3	0	397
300 - 3000	3	29.5	65.1	1.9	0.4	0	789

Table 5.10 provides the distribution of points that plot within each classification zone for Figures 5.12 to 5.16. The trends of drained layers plotting in zones 3, 3s and 2 are observed with zones 3s and 2 containing the majority of data points for dissipation times of 0 to 30s. The SBTn zones of 1p, 1b, and 1a contain the majority of points with dissipation t_{50} times greater than 100s. In addition to displaying trends in drainage in Q-F space, this series of figures is in agreement with

the shape of the boundaries suggested by the revised Q-F chart of constant F at larger values of Q and variable F values at low Q conditions for soils with similar water flow characteristics.

The next step in evaluating soil classification from CPT data is to provide a link from water flow characteristics to soil type. This was achieved by simplifying data from study CPTU soundings conducted across WI in varying geologic deposits to a number of representative layers. The results of the field work have been summarized in Table 5.11 in 23 representative layers based on visual classification. Many of these layers (13/23) also include laboratory classification. Initial review of the median of the CPTU normalized parameters provides an indication of the relative differences expected between different soil types. Large differences in Q and F are observed between the sand and clay soils as expected. The distribution of these data in soil classification charts is provided in Table 5.12. Layers analyzed in this study are presented in the revised Q-F and Q-$\Delta u_2/\sigma'_{v0}$ space in Figures 5.17 to 5.22.

This large dataset allows a check of the relationships determined for data placement in the revised Q-F classification chart, as well as consistency between Q-F and Q-$\Delta u_2/\sigma'_{v0}$ charts. Firstly, the sand soils, Figure 5.17 and 5.18, typically fall within zones 2 and 3 s as indicated by the dissipation testing performed in this study. The differences in drainage conditions are readily apparent in the pore pressure based charts, where the sand mixtures are showing elevated pore pressures.

Table 5.11. Summary of selected representative soil layers from Wisconsin test locations

Number	Layer	Site	Sounding	Depth Range (meters)	WisDOT Visual Class.	USCS Lab Class.	AASHTO Class.	t_{50} (s)	Number of Points	Number in NC zone rob.	$\sigma'_{vo,avg}$ (kPa)	Median Q	Std. Dev.	Median F (%)	Std. Dev.	Median B_q	Std. Dev.	Median $\Delta u_2/\sigma'_{vo}$	Std. Dev.
1	Lake Sediment	DOT-1	SCPTU2-01	5.7 - 12.1	Silt	CL	A-6	1606	131		101	6.6	0.7	0.7	0.2	0.7	0.1	4.3	0.8
1	Lake Sediment	DOT-1	SCPTU2-02	4.8 - 11.7	Silt some Clay	CL	A-6	1900	139	8	102	6.4	1.4	0.5	0.5	0.6	0.2	3.9	1.3
2	Lake Sediment	DOT-1	SCPTU2-01	12.2 - 18.1	Silt	CL	A-6	823	118		161	4.4	4.5	0.4	0.8	0.8	0.2	3.4	0.7
2	Lake Sediment	DOT-1	SCPTU2-02	11.8 - 17.2	Silt tr. Clay	CL	A-6	874	109	8	166	0.8	0.2	0.6	1.0	0.7	0.3	3.2	1.2
3	Clayey Till	DOT-1	SCPTU2-02	16 - 21.3	Sandy Silt	CL	A-5	3700	105	17	206	12.9	3.2	2.2	1.7	0.4	0.2	5.1	1.8
4	Clayey Till	DOT-10c	SCPTU2-02	1.1 - 3.8	Silt	CL	A-6	572	54	0	32	108.8	29.4	3.4	1.1	0.1	0.0	9.1	3.2
5	Clayey Till	DOT-10c	SCPTU2-02	3.8 - 7.8	Silt	CL	A-6	2205	79	0	63	39.5	20.9	3.3	2.0	0.2	0.1	6.7	5.0
6	Silt	Long-10	CPTU2-03	14.4 - 16	Clayey Silt	-	-	228	33	17	132	24.8	6.0	1.6	0.5	0.4	0.1	10.3	3.7
7	Lake Clay	DOT-7	CPTU2-01	2.2 - 3.6	Fat Clay	CL	A-6	-	28	37	46	7.7	1.1	1.5	0.3	0.3	0.1	2.2	0.6
7	Lake Clay	DOT-7	CPTU2-03	2.1 - 4.0	Fat Clay	CL	A-6	118	39		36	14.2	19.9	1.3	1.2	0.1	0.2	2.5	2.1
7	Lake Clay	DOT-7	CPTU2-04	2.1 - 3.7	Fat Clay	CL	A-6	1512	33		39	7.9	14.8	2.0	0.9	0.1	0.1	0.8	1.0
8	High Plasticity Organic	UW-1	SCPTU2-01	1.8 - 2.9	-	OH	A-8	290	23		21	20.4	20.9	9.2	3.7	0.0	0.1	0.4	0.6
8	High Plasticity Organic	UW-1	SCPTU2-02	1.8 - 2.8	-	OH	A-8	305	21		23	18.2	13.1	10.7	2.7	0.0	0.0	0.5	0.4
8	High Plasticity Organic	UW-1	CPTU2-04	1.9 - 2.9	-	OH	A-8	147	21		19	22.1	15.9	10.8	3.8	0.0	0.0	0.2	0.3
9	Clay	DOT-3R	CPTU2-03	19.7 - 21.5	Clay some Silt, tr Sand	-	-	102	90	61	220	9.9	5.0	2.1	0.9	0.3	0.2	4.1	1.5
9	Clay	DOT-3R	SCPTU2-04	19.5 - 21.3	Clay some Silt, tr Sand	-	-	52	90		220	13.0	5.0	2.3	1.6	0.1	0.1	1.4	1.3
10	Sand Q = 500 - 600	Long-11	CPTU2-02	1.6 - 2.8	M. Dense F. Sand	-	-	-	25	0	44	589.6	41.6	0.9	0.2	0.0	0.0	0.1	0.0
11	Sand Q = 150 - 200	Long-11	CPTU2-02	12.0 - 15.6	M. Dense F. Sand	-	-	10	73	28	189	113.4	26.7	0.8	0.1	0.0	0.0	0.0	0.0
12	Silt	Long-12	SCPTU2-04	8.6 - 11.4	Silt	-	-	183	56	8	141	26.2	3.4	2.2	0.8	0.4	0.1	9.4	3.1
13	Sand (removed silt lenses)	Long-13	SCPTU2-05	9 - 17	M. Dense Sand	-	-	3	106	7	175	102.6	102.6	1.2	1.2	0.0	0.0	0.0	0.0
14	Lake Sediment	DOT-16	SCPTU2-02	3.4 - 4.6	Clay	-	-	156	25	3	50	69.1	10.3	3.6	0.5	0.2	0.1	15.6	3.6
14	Lake Sediment	DOT-16	SCPTU2-04	4.4 - 8.4	Clay	-	-	107	81		69	42.1	7.4	2.6	0.8	0.2	0.1	8.4	4.4
15	Sand/Clay (interbedded)	Long-10	CPTU2-03	0.5 - 3.4	Sandy Silt	SC	A-4/A-6	-	41	0	25	353.1	440.2	2.1	0.5	0.0	0.0	1.1	1.0
16	Clayey Till	DOT-10b	SCPTU2-02	2.0 - 3.4	Silty Clay	-	-	-	29	1	73	50.7	16.9	5.4	2.4	0.0	0.0	0.0	0.7
17	Silty Sand	UW-1	CPTU2-04	0.7 - 1.8	-	SM	A-2-4	19	23	1	14	169.2	151.4	1.2	0.2	0.0	0.0	0.6	0.7
17	Silty Sand	UW-1	SCPTU2-02	0.6 - 1.7	-	SM	A-2-4	24	23		17	112.6	173.1	1.3	0.2	0.0	0.0	0.1	1.0
18	Sand	DOT-7	CPTU2-01	4.6 - 5.7	Fine Sand	-	-	24	74	59	78	154.8	38.8	0.5	0.2	0.0	0.0	0.1	0.0
19	Silt	Long-12	SCPTU2-04	14.7 - 15.5	Silt	-	-	183	17	0	193	27.0	2.6	2.1	0.9	0.3	0.1	7.1	3.4
20	Elastic Silt	UW-1	SCPTU2-01	2.9 - 3.6	-	MH	A-7-6	41	14	4	26	10.4	5.6	2.8	0.9	0.2	0.1	2.9	0.8
20	Elastic Silt	UW-1	SCPTU2-02	2.8 - 3.5	-	MH	A-7-6	81	14		27	29.6	14.5	3.9	1.5	0.1	0.1	1.7	0.9
20	Elastic Silt	UW-1	CPTU2-04	2.9 - 3.5	-	MH	A-7-6	114	12		23	18.1	8.6	2.6	1.9	0.0	0.1	1.0	1.2
21	Poorly Graded Sand	UW-1	SCPTU2-01	3.6 - 10.5	-	SP	A-3	8	139	1	59	228.4	101.1	1.0	0.1	0.0	0.0	0.0	0.1
21	Poorly Graded Sand	UW-1	SCPTU2-02	5.0 - 9.0	-	SP	A-3	18	81		48	227.3	122.0	1.0	0.1	0.0	0.0	0.1	0.1
21	Poorly Graded Sand	UW-1	CPTU2-04	4.0 - 8.0	-	SP	A-3	8	81		48	328.6	131.9	1.0	0.1	0.0	0.0	0.1	0.1
22	Clay w/ Sand (Till?)	UW-1	SCPTU2-01	11.6 - 15.0	-	CL	A-4/A-6	37	68	25	114	30.5	15.2	2.7	1.0	0.0	0.1	0.2	1.4
22	Clay w/ Sand (Till?)	UW-1	SCPTU2-02	11.2 - 16.1	-	CL	A-4/A-6	59	98		117	34.1	14.6	2.4	1.2	0.0	0.0	0.2	0.8
22	Clay w/ Sand (Till?)	UW-1	CPTU2-04	10.9 - 13.0	-	CL	A-4/A-6	40	60		94	41.3	39.6	2.4	0.9	0.0	0.0	-0.3	0.3
23	Poorly Graded Sand	UW-1	SCPTU2-01	15.0 - 20.8	-	SP	A-3	4	116	47	160	75.9	26.6	1.1	0.2	0.0	0.0	0.0	0.1
23	Poorly Graded Sand	UW-1	SCPTU2-02	16.2 - 25.0	-	SP	A-3	8	178		181	102.4	32.0	0.9	0.1	0.0	0.0	0.1	0.0

Table 5.12. Percentage of point plotting in revised Q-F soil classification charts for selected representative layers

Number	Layer	Site	Sounding	Depth Range (meters)	WisDOT Visual Class.	USCS Lab Class.	AASHTO Class.	I_{50} (s)	% Data in 1p	% Data in 1b	% Data in 1a	% Data in 3	% Data in 3s	% Data in 2
1	Lake Sediment	DOT-1	SCPTU2-01	5.7 - 12.1	Silt	CL	A-6	1606	0.0	0.8	99.2	0.0	0.0	0.0
1	Lake Sediment	DOT-1	SCPTU2-02	4.8 - 11.7	Silt some Clay	CL	A-6	1900	0.0	7.9	92.1	0.0	0.0	0.0
2	Lake Sediment	DOT-1	SCPTU2-01	12.2 - 18.1	Silt	CL	A-6	823	0.9	73.4	25.7	0.0	0.0	0.0
2	Lake Sediment	DOT-1	SCPTU2-02	11.8 - 17.2	Silt tr. Clay	CL	A-6	874	0.0	52.5	46.6	0.0	0.8	0.0
3	Clayey Till	DOT-1	SCPTU2-02	16 - 21.3	Sandy Silt	CL	A-5	3700	1.9	31.4	66.7	0.0	0.0	0.0
4	Clayey Till	DOT-10c	SCPTU2-02	1.1 - 3.8	Silt	CL	A-6	572	0.0	29.6	55.6	13.0	1.9	0.0
5	Clayey Till	DOT-10c	SCPTU2-02	3.8 - 7.8	Silt	CL	A-6	2205	3.8	22.8	63.3	10.1	0.0	0.0
6	Silt	Long-10	CPTU2-03	14.4 - 16	Clayey Silt	-	-	228	0.0	0.0	39.4	57.6	3.0	0.0
7	Lake Clay	DOT-7	CPTU2-01	2.2 - 3.6	Fat Clay	CL	A-6	-	0.0	3.6	96.4	0.0	0.0	0.0
7	Lake Clay	DOT-7	CPTU2-03	2.1 - 4.0	Fat Clay	CL	A-6	118	0.0	7.7	71.8	15.4	5.1	0.0
7	Lake Clay	DOT-7	CPTU2-04	2.1 - 3.7	Fat Clay	CL	A-6	1512	0.0	33.3	63.6	0.0	3.0	0.0
8	High Plasticity Organic	UW-1	SCPTU2-01	1.8 - 2.9	-	OH	A-8	290	73.9	17.4	0.0	4.3	4.3	0.0
8	High Plasticity Organic	UW-1	SCPTU2-02	1.8 - 2.8	-	OH	A-8	305	85.7	4.8	9.5	0.0	0.0	0.0
8	High Plasticity Organic	UW-1	CPTU2-04	1.9 - 2.9	-	OH	A-8	147	85.7	9.5	0.0	4.8	0.0	0.0
9	Clay	DOT-3R	CPTU2-03	19.7 - 21.5	Clay some silt, tr sand	-	-	102	0.0	20.0	70.7	2.2	1.1	0.0
9	Clay	DOT-3R	SCPTU2-04	19.5 - 21.3	Clay some Silt, tr Sand	-	-	52	1.1	31.1	62.2	5.6	0.0	0.0
10	Sand Q = 500 - 600	Long-11	CPTU2-02	1.6 - 2.8	M. Dense F. Sand	-	-	-	0.0	0.0	0.0	0.0	0.0	100.0
11	Sand Q = 150 - 200	Long-11	CPTU2-02	12.0 - 15.6	M. Dense F. Sand	-	-	10	0.0	0.0	0.0	0.0	98.6	1.4
12	Silt	Long-12	SCPTU2-04	8.6 - 11.4	Silt	-	-	183	0.0	5.4	67.9	26.8	0.0	0.0
13	Sand (removed silt lenses)	Long-13	SCPTU2-05	9 - 17	M. Dense Sand	-	-	3	0.0	0.0	0.0	7.5	92.5	0.0
14	Lake Sediment	DOT-16	SCPTU2-02	3.4 - 4.6	Clay	-	-	156	0.0	8.0	88.0	4.0	0.0	0.0
14	Lake Sediment	DOT-16	SCPTU2-04	4.4 - 8.4	Clay	-	-	107	0.0	7.4	71.6	21.0	0.0	0.0
15	Sand/Clay (Interbedded)	Long-10	CPTU2-03	0.5 - 3.4	Sandy Silt	SC	A-4/A-6	-	0.0	0.0	7.3	43.9	29.3	19.5
16	Clayey Till	DOT-10b	SCPTU2-02	2.0 - 3.4	Silty Clay	-	-	-	3.4	79.3	10.3	3.4	3.4	0.0
17	Silty Sand	UW-1	CPTU2-04	0.7 - 1.8	-	SM	A-2-4	19	0.0	0.0	4.3	0.0	69.6	26.1
17	Silty Sand	UW-1	SCPTU2-02	0.6 - 1.7	-	SM	A-2-4	24	0.0	0.0	0.0	0.0	91.3	8.7
18	Sand	DOT-7	CPTU2-01	4.6 - 5.7	Fine Sand	-	-	24	0.0	0.0	0.0	0.0	33.8	66.2
19	Silt	Long-12	SCPTU2-04	14.7 - 15.5	Silt	-	-	183	0.0	11.8	70.6	17.6	0.0	0.0
20	Elastic Silt	UW-1	SCPTU2-01	2.9 - 3.6	-	MH	A-7-6	41	0.0	64.3	21.4	7.1	0.0	7.1
20	Elastic Silt	UW-1	SCPTU2-02	2.8 - 3.5	-	MH	A-7-6	81	7.1	64.3	21.4	0.0	0.0	7.1
20	Elastic Silt	UW-1	CPTU2-04	2.9 - 3.5	-	MH	A-7-6	114	8.3	8.3	83.3	0.0	0.0	0.0
21	Poorly Graded Sand	UW-1	SCPTU2-01	3.6 - 10.5	-	SP	A-3	8	0.0	0.0	0.0	0.0	43.9	56.1
21	Poorly Graded Sand	UW-1	SCPTU2-02	5.0 - 9.0	-	SP	A-3	18	0.0	0.0	0.0	0.0	40.7	59.3
21	Poorly Graded Sand	UW-1	CPTU2-04	4.0 - 8.0	-	SP	A-3	8	0.0	0.0	0.0	0.0	0.0	100.0
22	Clay w/ Sand (Till?)	UW-1	SCPTU2-01	11.6 - 15.0	-	CL	A-4/A-6	37	0.0	11.8	70.6	13.2	4.4	0.0
22	Clay w/ Sand (Till?)	UW-1	SCPTU2-02	11.2 - 16.1	-	CL	A-4/A-6	59	0.0	9.2	50.0	31.6	9.2	0.0
22	Clay w/ Sand (Till?)	UW-1	CPTU2-04	10.9 - 13.0	-	CL	A-4/A-6	40	0.0	3.3	51.7	18.3	26.7	0.0
23	Poorly Graded Sand	UW-1	SCPTU2-01	15.0 - 20.8	-	SP	A-3	4	0.0	0.0	0.0	0.0	100.0	0.0
23	Poorly Graded Sand	UW-1	SCPTU2-02	16.2 - 25.0	-	SP	A-3	8	0.0	0.0	0.9	18.1	81.0	0.0
								All Layer Data:	2.4	14	38.7	7.5	25.6	11.7

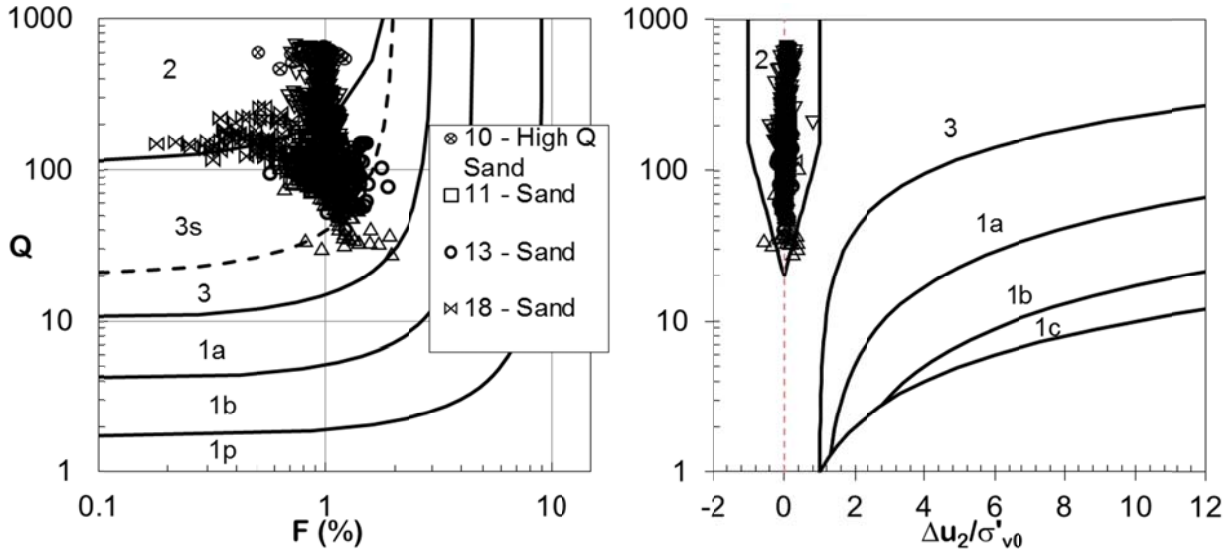

Figure 5.17. Sand layers plotted in Q-F and Q-$\Delta u_2/\sigma'_{v0}$ space.

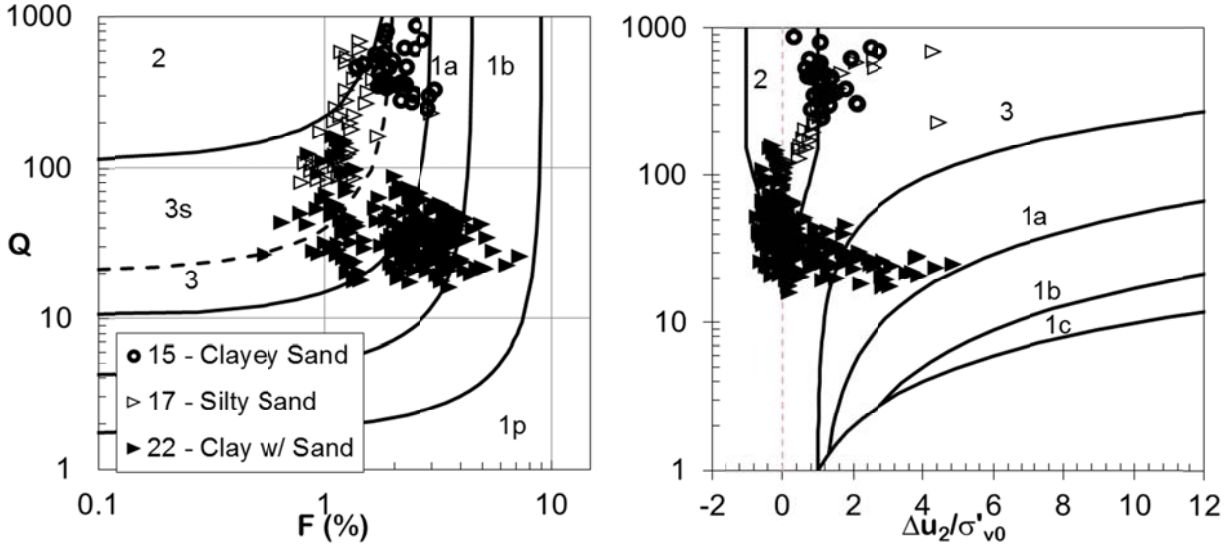

Figure 5.18. Layers of sand mixtures plotted in Q-F and Q-$\Delta u_2/\sigma'_{v0}$ space. Trends in Q-$\Delta u_2/\sigma'_{v0}$ space indicate that these soils behave partially drained to drained during penetration

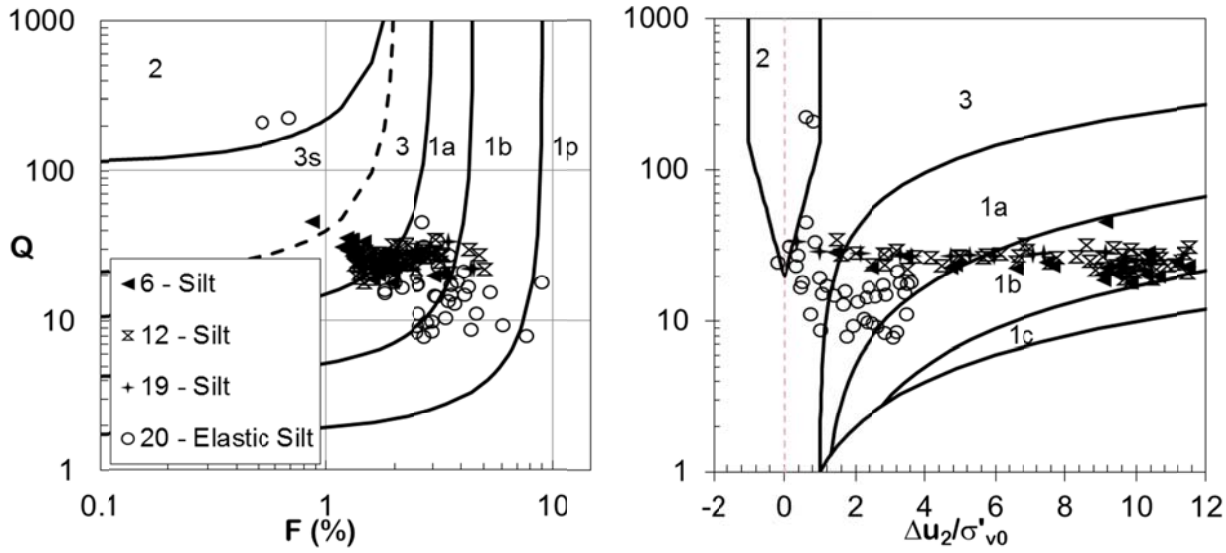

Figure 5.19. Silt layers plotted in Q-F and Q-$\Delta u_2/\sigma'_{v0}$ space. All data suggests variable drainage conditions during penetration

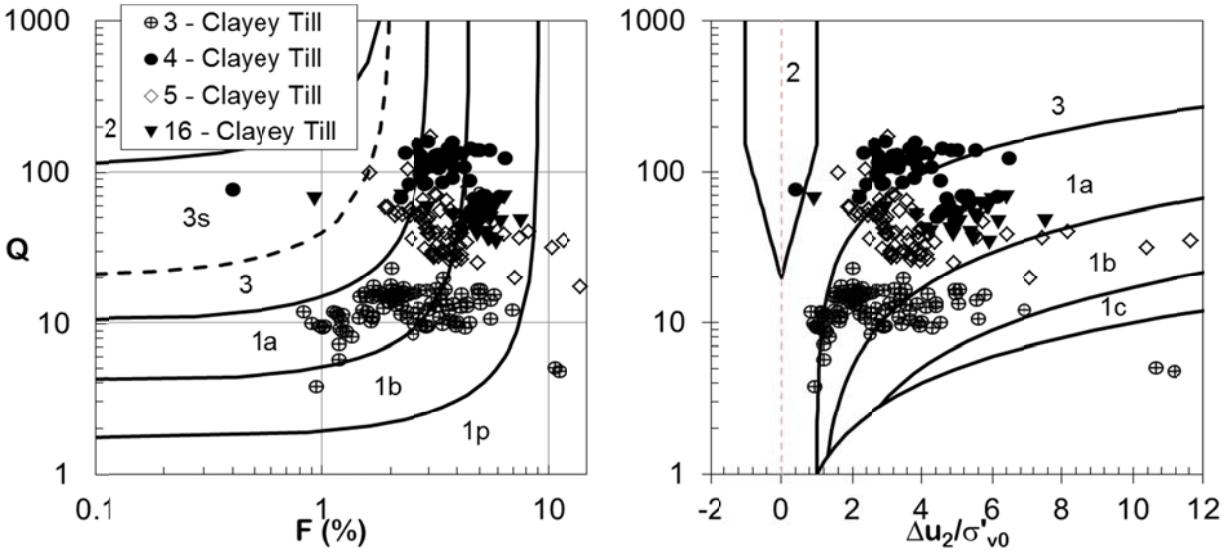

Figure 5.20. Clayey till layers plotted in Q-F and Q-$\Delta u_2/\sigma'_{v0}$ space. The trend of data of increasing Q at constant F with increasing OCR can be observed in Q-F space

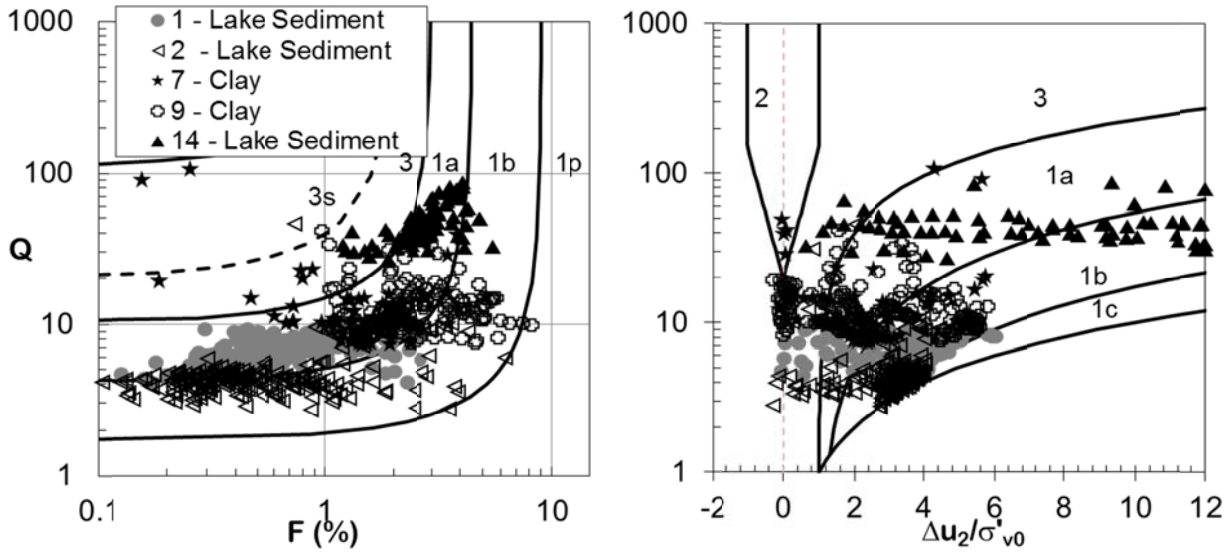

Figure 5.21. Lake deposits plotted in Q-F and Q-$\Delta u_2/\sigma'_{v0}$ space

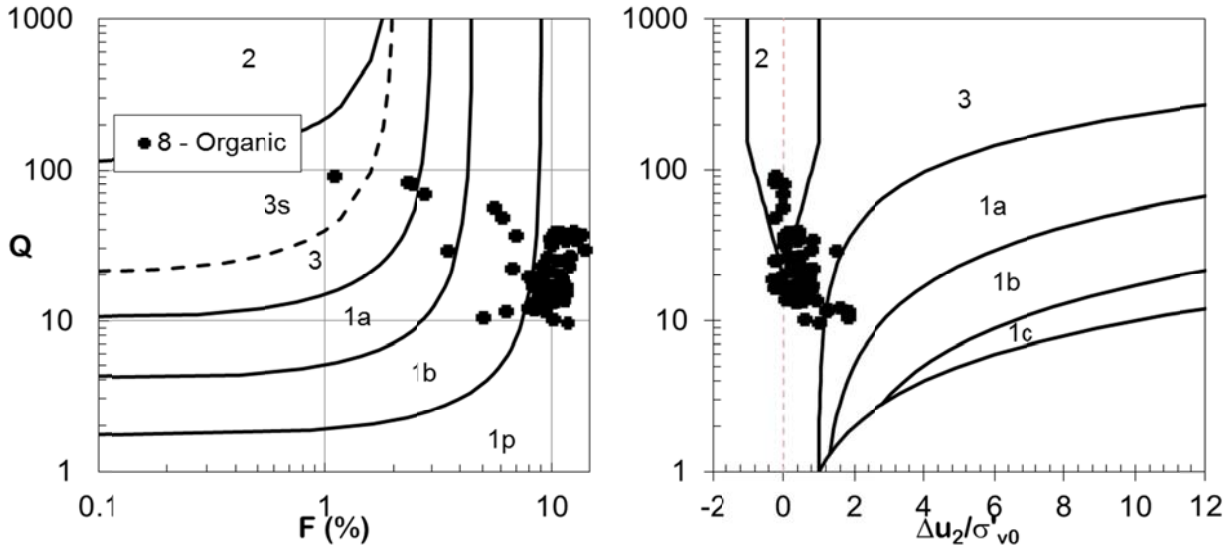

Figure 5.22. Organic layer plotted in Q-F and Q-$\Delta u_2/\sigma'_{v0}$ space.

Several soils are visually identified as "silt" by drillers in Table 5.11, but few of these are accompanied by laboratory data for classification. Review of the dissipation results for these "silt" layers estimates a hydraulic conductivity of 3 to 7 ft/day near the lower end of the suggested range for silts in Figures 2.5 and 5.2. Based on the water flow characteristics and

drillers' visual classifications, these layers are interpreted as silts in the textural sense. These silty soils, however, are likely to have some clay component and additional sampling and classification testing is warranted. Further indication of the partially drained behavior of these soils is observed in $Q\text{-}\Delta u_2/\sigma'_{v0}$ space, with 'movement' of data points between Zones 1b into 3. A small gap in data in these figures occurs in the transitional soils zone (3), with Layer 6 being the only silt soil that plots in the center of that zone in the CPTU classification charts. Many of the silt layers in this study plot on the boundary of zones 3 and 1a. Layer 20 represents a high plasticity silt tested from site UW-1. Index testing resulted in the soil plotting essentially on the A-Line in the Casagrande plasticity chart, showing nearly high plasticity clay behavior. Undrained soil response is anticipated to plot in Zone 1b, and transition through Zone 1b to reach Zone 3 as drainage increases. This trend is observed in the silt data provided in Figure 5.19. Additional CPTU testing in transitional soils or silt deposits may help fill this gap and further develop the boundary shown.

In the clayey soil regions, zones 1a and 1b, the general shape of the zones match the movement of data in classification charts as OCR changes. Variation in OCR and state can be observed when comparing locations of normally consolidated lake clays in Figure 5.21 to the overconsolidated clayey tills in Figure 5.20. The tills typically display larger values of Q and larger values of F.

Organic soils tested at site UW-1 are shown in Figure 5.22. These soils displayed relatively low tip resistances and high friction ratios, with the data points falling within zone 1p. Additionally, low penetration pore pressures and moderate rates of drainage (during dissipation tests) were measured (Figure 5.13). Organic soils and peats are highly variable deposits and the results from one test site do not provide adequate data to fully constrain all organic soils.

Previous discussion of dissipation results highlighted the fact that soils exhibiting different behaviors under typical loading conditions may plot in similar locations in SBTn charts. Figures 5.17 through 5.22 provide some insight into areas of overlapping soil types for typical conditions of Wisconsin to aid in judgment when utilizing cone penetration testing in Wisconsin. Variability is observed, as expected, in the unsorted till data in Figure 5.20. Careful review of the available

data is critical to a correct interpretation of soil type from SBTn charts. Assigning a rigid classification to all data within a certain zone is not recommended; however, incorporating knowledge of the surrounding geology, landscape features, and previous investigations (i.e., soil survey maps and geologic maps) an engineer/geologist may anticipate soils and sequences that will be encountered during an investigation.

A summary of the zones of the soil classification chart in which data plot is provided in Table 5.12. A majority of data plot is zones 1b and 3s, 'Low I_r' clays and silts and sand mixtures. Since the clays tested in this study were predominantly low plasticity index clays, this zone could be considered as low PI clays in Wisconsin. Only one high plasticity inorganic fine grained soil was tested, layer 20. This bias may be due to the relative low occurrence of high plasticity clays and silts in WI or the sites tested.

In relation to soil classification, it is summarized that even when testing in an area with little to no background knowledge, the CPTU is an applicable tool even though it does not provide a soil sample. Sands below the water table are readily identified as plotting in zones 3s and 2 of the revised Q-F SBTn space with no excess pore pressures generated during penetration. Normally to overconsolidated, insensitive clay soils will provide friction ratios greater than 3 and typically positive excess pore pressures. Negative pore pressures are typically associated with highly overconsolidated soils and will therefore coincide with large Q values. Soft layers of concern are readily identified by CPTU testing based on tip resistance, and the extents of these layers can be quickly determined by performing multiple soundings. Pore-water pressures are key in determining drainage characteristics of soils that plot in or near the transition zone. If pore pressures are unavailable (i.e., a low water table) use of Q-F SBTn chart may be done assuming the worst case scenario for a low risk project; for example if a soil plots in zone 3s assume that it is a transitional soil with a significant fines content as suggested by Ramsey (2002). Gradually, as more testing is performed a reliable interpretation of the soils at a site/region can be developed using CPTU.

6 Applications

No field data of foundation or embankment performance was available at the WisDOT CPT test sites, and this section will provide an overview of mechanisms that influence the use of CPT data for design of shallow foundations, axial loading of driven piles, and embankments.

6.1 Shallow Foundations

For shallow foundations to be applicable to transportation structures, the underlying soils typically need to have a high stiffness to minimize deformations. For the most part, if settlements are minimized then a sufficient factor of safety against bearing capacity is achieved (e.g., Mayne & Illingsworth 2010). Bearing capacity calculations still need to be performed, but design decisions related to application of bearing capacity equations are primarily driven by selection of strength parameters, discussed in Section 5.2.4. This section will focus on shear deformations of sands and stiff clays. Consolidation settlements of clay soils would additionally need to be considered for shallow foundation design, but is not specifically addressed herein.

The analysis of settlements caused by shear distortions of the soil beneath shallow foundations can simply be thought of as a stress-strain curve, the stress is the footing load divided by the area (q) and the strain is indicated by the settlement (s) normalized by the footing width (B) or equivalent diameter (D_{eq}).

$$\frac{s}{D_{eq}} = \frac{q}{E} I\left(1-\nu^2\right) = \frac{q}{G}\frac{I}{2}(1-\nu) = \frac{q}{q_t}\left(\frac{G}{q_t}\right)^{-1}\frac{I}{2}(1-\nu) \tag{6.1}$$

where I is an influence factor that is typically defined in terms of elastic modulus. For a rigid footing on an infinitely thick homogeneous elastic half space, I is equal to $\pi/4$. Values of influence factors are affected by a number of issues including:

- Change in shear stiffness with depth
- Footing shape (circle / square, rectangular, strip)

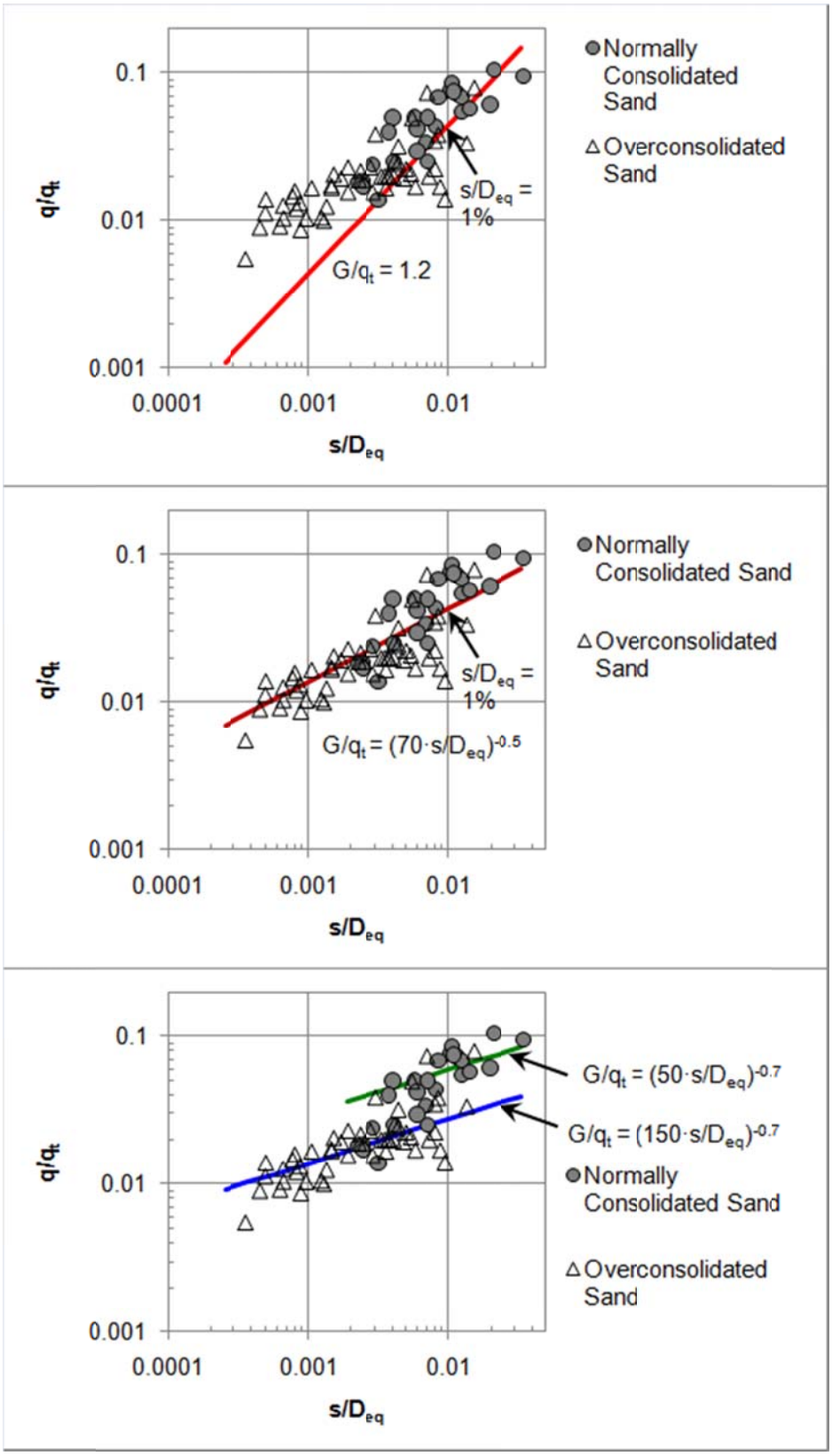

Figure 6.1. Comparison of database of footing tests to empirical correlations between shear modulus and cone tip resistance

- Foundation stiffness
- Foundation embedment
- Presence of shallow bedrock

Various influence factors are discussed by Mayne & Poulos (1999) and Mayne (2007), and this section will focus on the homogeneous case for sandy soils. Selection of shear stiffness for undrained clays is discussed in Section 5.2.3.

Figure 6.1 compares correlations between shear modulus and cone tip resistance in two different formats for assessment of shallow foundation footing settlements.

- Constant ratio of G/q_t (after Schmertmann 1978)
- G/q_t reducing as s/D_{eq} (i.e., strain level) increases

Correlations were selected to provide a good match to data at a normalized settlement of 1% of the footing equivalent diameter. This corresponds to settlement of 1 inch for a 7.5 ft square foundation.

The constant ratio of G/q_t can match the database for a given value of s/D_{eq}, but over predicts settlements for smaller s/D_{eq} and under predicts settlements for larger s/D_{eq}. This is the main difficulty in selection of stiffness for settlement calculations, as illustrated in Figure 2.8. To account for stiffness nonlinearity, a power law function may be used. Mayne & Illingsworth (2010) suggest stiffness reduces as a function of $s/D_{eq}^{0.5}$. The entire database, of both overconsolidated and normally consolidated sands, is fit well using $s/D_{eq}^{0.5}$. Alternatively, Burland & Burbidge (1985) suggest that G/q_t reduces as a function of $s/D_{eq}^{0.7}$. When using this relationship, 'overconsolidated' sands are typically 2 times stiffer than normally consolidated sands, but there is some overlap of the databases.

It should be noted that the stiffness relationships for clayey soils in Section 5.2.3 did not include a reduction in modulus due to strain level. Linking small strain shear modulus from seismic cone

tests to larger strain measurements of stiffness from pressuremeter tests may be a first step (i.e., Lehane & Fahey 2004), but still requires comparison to a database of footing tests.

6.2 Axial loading of Driven Piled Foundations

Design of driven piles is one of the oldest applications of the CPT. The similarity in geometry between a pile and CPT (Figure 6.2) and full displacement method of installation makes analysis of driven displacement piles straight forward. The cone tip resistance, q_t, is analogous to the base resistance for a pile, q_b. The CPT sleeve friction, f_s, is analogous to a pile shaft friction, τ_f. Four main differences between a CPT and pile need to be accounted for:

- The CPT has a much smaller diameter than the pile, and the tip resistance needs to be averaged over the zone of influence related to the pile diameter ($q_{t,avg}$).
- End bearing capacity is typically at a relative settlement, w/D, where the full resistance is not mobilized and $q_{t,avg}$ needs to be reduced.
- CPT sleeve friction is measured near the cone tip. Pile shaft friction tends to reduce with distance behind the pile tip due to a phenomenon known as '*friction fatigue*'.
- CPT sleeve friction is measured immediately after displacement of soil by the cone tip. Pile shaft friction, and CPT sleeve friction, typically increases with time after installation.

Pile end bearing will be discussed, followed by shaft friction.

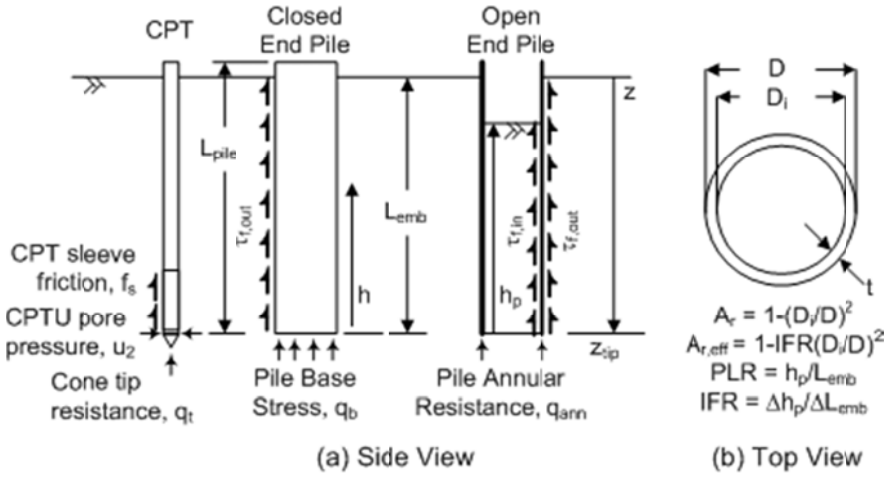

Figure 6.2. Comparison between CPT and pile

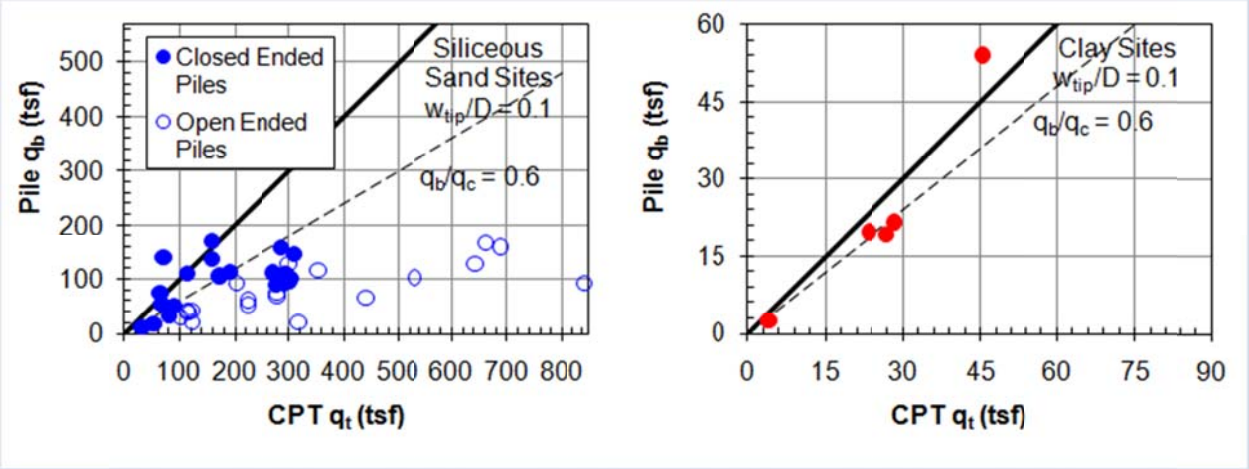

Figure 6.3. Comparison of pile q_b to CPT q_t (data from Xu et al. 2008, Chow 1997)

Figure 6.3 compares CPT q_t to pile q_b in sands and clays for a tip displacement of 0.1D. The pile base stress, q_b is typically less than CPT q_t, and is quantified as:

$$q_b = \alpha_b \cdot q_{t,avg} \tag{6.2}$$

For closed ended piles, α_b is on the order of 0.6 in both sands and clays. This reduction in q_t is typically associated with partial mobilization of base resistance at a tip displacement of 0.1D. Smaller fractions of cone tip resistance would be available for pile base resistance if using the Davisson offset definition of failure.

Lower values of base resistance are mobilized at a tip displacement of 0.1D in sands if a pile is driven open ended and does not plug. The base resistance becomes a function of the degree of displacement of soil during pile installation that is a function of pile plugging and relative area of steel. This degree of displacement can be quantified using the effective area ratio:

$$A_{r,eff} = 1 - IFR\left(\frac{D_i}{D}\right)^2 \tag{6.3}$$

Where IFR is the incremental filling ratio defined as the incremental change in plug height over an increment of pile driving (IFR = $\Delta h_p/\Delta L_{emb}$, Figure 6.2). For the case of a fully plugged pile

(IFR = 0), $A_{r,eff} = 1$ and an open ended pile would be expected to behave in a similar manner to a closed ended pile. The fraction of CPT tip resistance mobilized at a base displacement of 0.1D increases with $A_{r,eff}$ (Xu et al. 2008):

$$\alpha_b = \frac{q_b}{q_{t,avg}} = 0.15 + 0.45A_{r,eff} \tag{6.4}$$

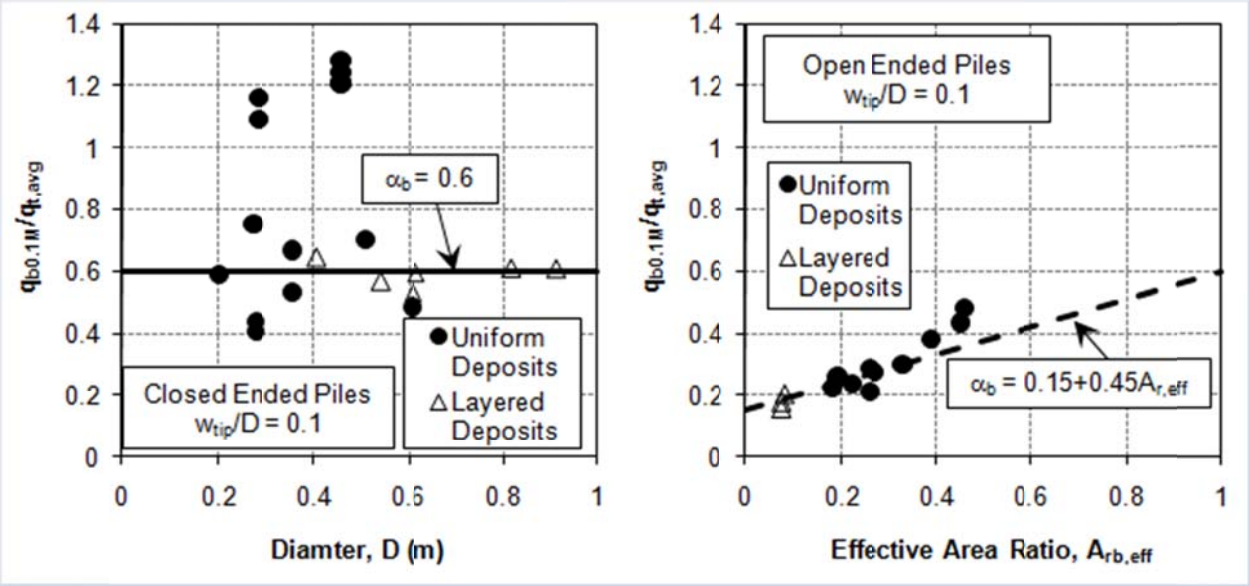

Figure 6.4. Pile end bearing in siliceous sands (after Xu et al. 2008)

Figure 6.4 compares pile load test data to average CPT end bearing resistance. A good agreement with design correlations is observed, provided that the cone tip resistance is properly averaged to account for differences between CPT diameter and pile diameter, as well as differences between open and closed ended piles.

The Dutch (Schmertmann) averaging technique that incorporates a minimum path rule from 8 pile diameters above the cone tip to up to 4 pile diameters below the cone tip has been the most effective CPT averaging technique reviewed (Xu & Lehane 2005, Xu et al. 2008). This averaging technique is illustrated in Figure 6.5.

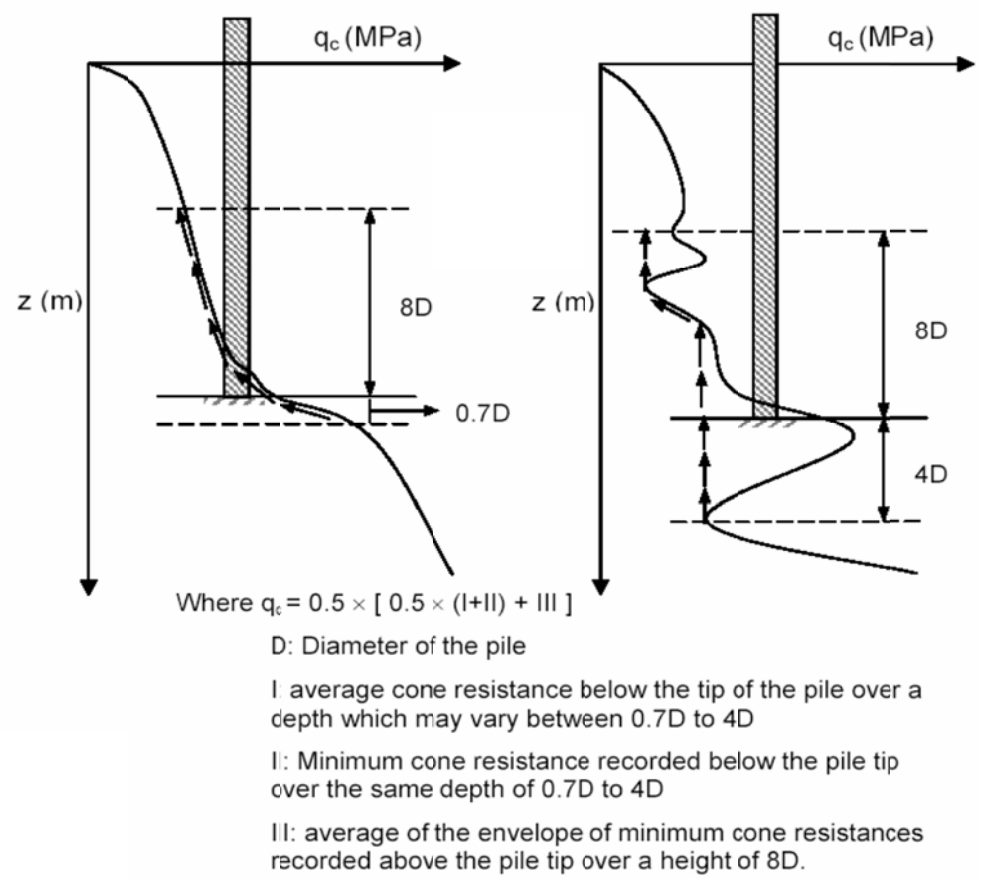

Figure 6.5. CPT averaging based on the Dutch method (after Schmertmann 1978)

The shaft friction of piles in sand is a function of the radial effective stress at failure (σ'_{rf}) on the side of a pile and the soil-pile interface friction angle (δ_f):

$$\tau_f = \sigma'_{rf} \tan\delta_f = \left(\sigma'_{rc} + \Delta\sigma'_{rd}\right)\tan\delta_f \qquad (6.5)$$

The radial effective stress at failure can be separated as the radial effective stress after installation and consolidation/equalization (σ'_{rc}) and the change in radial stress during loading ($\Delta\sigma'_{rd}$) (e.g., Lehane et al. 1993). Due to the difficulties in estimating radial effective stress, σ'_{rf} historically has been taken as a function of the vertical effective stress through an earth pressure coefficient ($\sigma'_{rf} = K_f \cdot \sigma'_{v0}$; e.g. API 2000). The 'earth pressure coefficient' in sandy soils has been shown to change with pile embedment and soil density (e.g., Lehane et al. 1993, Jardine et al.

2005), and also be influenced by the relative level of soil displacement during pile installation (e.g., Gavin & Lehane 2003). Pile shaft friction correlations between τ_f based on CPT q_t are still considered more reliable than correlations to CPT f_s.

A multi variable expression relating τ_f to q_t has been developed based on mechanisms influencing pile shaft friction and the assumed (relative density independent) correlation between radial effective stress after installation and equalization and q_t (Lehane & Jardine 1994, Gavin & Lehane 2003, Lehane et al. 2005):

$$\tau_f = \frac{f_t}{f_c}\left[\frac{q_t \cdot A_{rs,eff}}{a}\max\left(\frac{h}{D},\nu\right)^{-c} + \Delta\sigma'_{rd}\right]\tan\delta_f \qquad (6.6)$$

Terms within Equation 6.6 are illustrated in Figure 6.2, where f_t/f_c is the ratio of friction in tension to that in compression (taken as unity in compression), $A_{rs,eff}$ is the effective area ratio of the pile toe during installation and 'h' is the height above the pile tip. $A_{rs,eff}$ is affected by plugging at various stages during installation, which is best assessed using the IFR that may vary with depth during driving. With the above expression, fitting parameters are related to various mechanisms that affect the correlation between q_t and τ_f:

- a = parameter to account for the reduction in radial stress behind the pile tip
- b = parameter to account for differences between open and closed ended piles
- c = exponent to account for 'friction fatigue'
- ν = parameter to account for and upper limit on $(h/D)^{-c}$ near the pile tip

It is noted that friction fatigue is the reduction in local friction, which occurs as a pile tip is driven deeper into the soil (e.g., White & Lehane, 2004). Within the UWA-05 method for siliceous sands, the parameters a, b, c, and ν have been calibrated for piles in compression to equal 33, 0.3, 0.5, and 2 (Lehane et al. 2005, 2008). For clays, 'a' is dependent on OCR and sensitivity, while 'b', 'c', and 'ν' have been preliminarily estimated as 0.1, 0.2, and 2, respectively (Schneider et al. 2010).

If the effects of friction fatigue, area ratio, ratio of tension to compression shaft capacity, change in radial effective stress during loading, and interface friction angle are ignored, the parameters c, b, $\Delta\sigma'_{rd}$, $\tan\delta_f$ and f_t/f_c in Equation 6.6 become equal to 0, 0, 0, 1, and 1, respectively. Equation 6.6 therefore simplifies to:

$$\tau_f = \frac{q_t}{\alpha_s} \tag{6.7}$$

Equation 6.7 is commonly referred to as a CPT 'alpha' method. Eslami & Fellenius (1997) recommend using α_s equal to 250 for clean siliceous sands, and it is common to take α_s as 40 in clays. An intermediate value of α_s equal to 100 is often used in sandy silts and clayey silts. It is recommended to use α_s of 40 in heavily over consolidated clayey and loamy tills, if cone penetration is undrained. The parameter α_s is related to the parameter 'a' from Equation 5, but has a higher value since the effects of friction fatigue, area ratio, ratio of tension to compression shaft capacity, change in radial effective stress during loading, and interface friction angle are ignored. Use of simplified α_s values calibrated to empirical databases clearly induces bias when applied to conditions outside of the database used to calibrate the method.

It is logical, and tempting, to try to use CPT f_s to estimate pile shaft friction (e.g., Begemann 1965). A comparison between average CPT f_s and average pile τ_f for databases of pile load tests in clays is shown in Figure 6.6. Two regimes of dominant behavior are identified from Figure 6.6; (i) setup, where $\tau_{f,avg}/f_{s,avg}$ is greater than unity; and (ii) friction fatigue, where $\tau_{f,avg}/f_{s,avg}$ is less than unity.

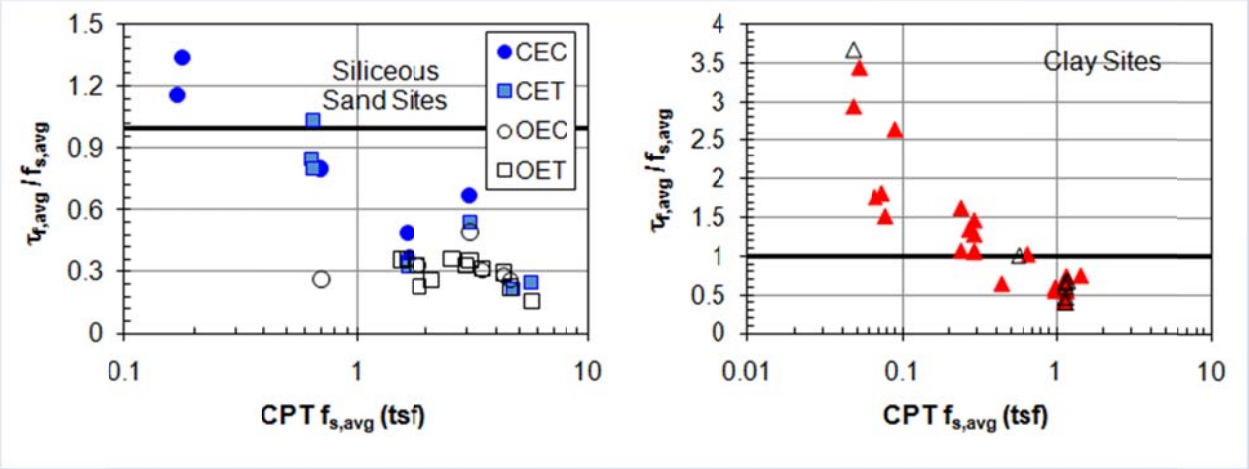

Figure 6.6. Comparison of CPT $f_{s,avg}$ and pile $\tau_{f,avg}$

Most cases of piles in sand are dominated by the friction fatigue mechanism, with $\tau_{favg}/f_{s,avg}$ (much) less than unity. Open ended piles tend to have $\tau_{favg}/f_{s,avg}$ on the order of 0.3, with values of 0.4 to 0.6 for closed ended piles.

It is well known that pile shaft friction in clays increases with time due to radial consolidation and increases in effective stress at the pile wall. For low values of CPT sleeve friction (i.e., soft clays), this setup mechanism tends to dominate response. For stiffer clays with higher values of f_s, reduction in radial stress behind the pile tip during installation tends to lead to $\tau_{f,avg}/f_{s,avg}$ less than unity.

Increases in CPT sleeve friction with consolidation time for the DOT-1 site in Green Bay are shown in Figure 6.7. The site consists of 2 layers of soft sensitive lacustrine clays, the upper lake deposits between a depth of 15 and 35 ft and the lower lake deposits between a depth of 35 and 50 ft. The upper and lower layers are inferred to have similar strengths (on the order of 0.4 to 0.5 tsf), however, the lower layer appears to have a higher sensitivity and a higher coefficient of consolidation, likely due to thinly spaced varves. The relatively uniform nature of the clay layers allowed for direct comparison of sleeve friction setup tests at multiple depths. Dissipation tests were performed in two soundings at 3.3 ft intervals through the layers, each to a difference degree of consolidation. The difference between sleeve friction at the end of installation prior to

the dissipation test and the sleeve friction measured immediately after the dissipation test is indicative of the increase in friction due to consolidation.

Sleeve friction was relatively constant with time until normalized time factors (T) exceeded 3 and 70% of pore pressures had dissipated. These observations are in general agreement with previous studies by Lehane & Jardine (1994) and Karlsrud et al. (1993) in that while pore pressures are reducing after pile or cone installation, total stresses are also reducing. This results in a relatively constant (to decreasing) effective stress, and therefore constant to decreasing shaft friction, until a large fraction of the pore pressures are dissipated.

Based on Figure 6.6, response of clays with a sleeve friction on the order of 0.3 to 0.5 tsf would be dominated by setup, and previous pile loads tests showed increases of 3 to 3.5 times. CPT sleeve frictions increased from as low as 0.01 tsf to 0.23 tsf, or an increase of 25 times. On average, the upper layer increased by a factor of five from 0.04 tsf to 0.2 tsf, while the lower layer increased by a factor of 10 from 0.02 to 0.2 tsf. These setup ratios are higher than those typically observed, and this may be a function of the location of the friction sleeve close to the cone tip. Additional study into assessing pile setup from CPT is warranted.

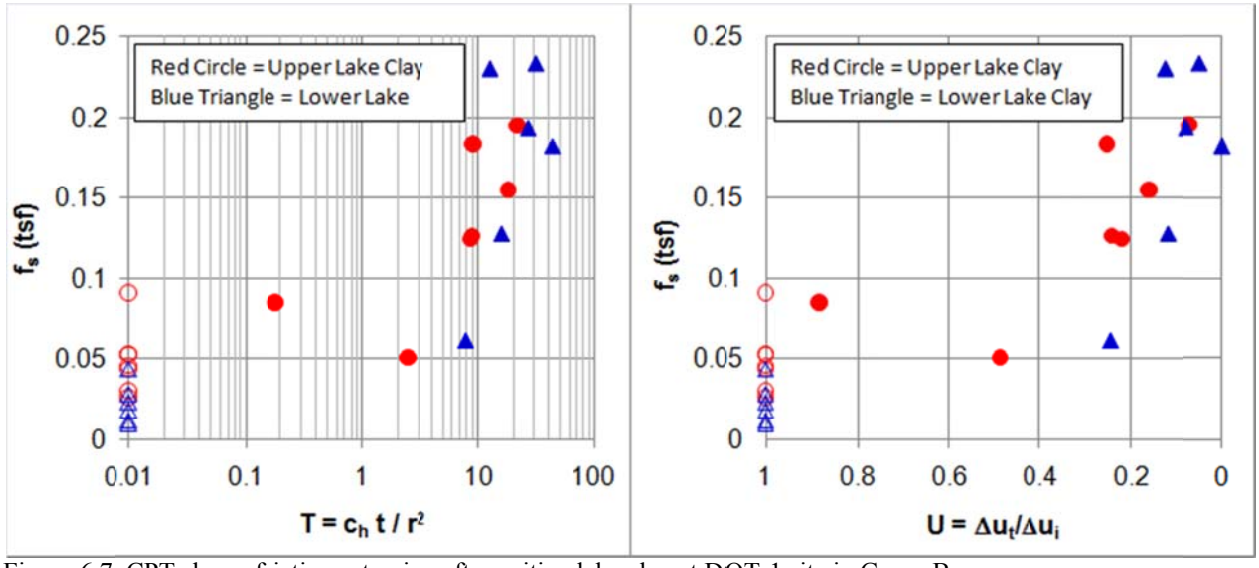

Figure 6.7. CPT sleeve friction setup in soft sensitive lake clay at DOT-1 site in Green Bay

6.3 Embankments on Soft Soils

Embankments on soft soils involve three major design issues:

- Stability, evaluated through the undrained strength
- Magnitude of settlements
- Time for settlements and strength increase to occur

The cone penetration test is ideal to assess undrained strength and time dependent properties, and has some application to assessment of the magnitude of settlements.

Cone penetration testing can reliably be used to evaluate soil strength at the time of testing through the cone factor N_k, as discussed in Section 5.2.4. To assess changes in strength with time under an embankment, both the change in in-situ effective stress and change in state (OCR) need to be quantified (i.e., Ladd 1991). Increases in effective stress due to consolidation under an embankment increase strength, but increases in effective stress reduce OCR that reduces the undrained strength ratio:

$$\frac{s_u}{\sigma'_{v0}} = \left(\frac{s_u}{\sigma'_{v0}}\right)_{NC} OCR^{(1-C_r/C_c)} \approx \frac{\sin\phi}{2} OCR^{0.8} \approx 0.23 \cdot OCR^{0.8} \qquad (6.8)$$

To be able to understand changes in strength with time, the OCR and normalized undrained strength ratio need to be quantified. Mayne (2007) provides a thorough discussion of estimating OCR and/or preconsolidation stress from CPTU data. OCR correlations were not assessed in this study as no high quality preconsolidation stress data were available.

Magnitude of settlements can be quantified by constrained modulus estimated from CPT (Section 5.2.2). The constrained modulus is relatively constant prior to the preconsolidation stress, but drops significantly for normally consolidated soils. In normally consolidated soils, constrained modulus will increase with increasing effective stress, and appropriate stress ranges must be used for assessment of compressibility.

Dissipation data can be very useful for evaluating time dependent behavior. For application to embankments, the dissipation results are directly applicable to radial drainage when using prefabricated vertical drains. Due to anisotropy in hydraulic conductivity and coefficient of consolidation, c_h from dissipation tests may overestimate c_v by up to an order of magnitude in varved clays.

7 Specialized Equipment and Non Standard Procedures

7.1 Seismic Piezocone Penetration Test

Methods for performing a seismic piezocone cone test (SCPTU) are highlighted in Chapter 3. The purpose of a SCPTU is to measure a fourth independent parameter, small strain shear stiffness ($G_0=\rho V_s^2$). Small strain stiffness needs to be reduced to operation values applicable to design, such as those discusses in Chapter 5. Methods for modulus reduction are discussed by Mayne (2007).

The geophone in the SCPTU probe allows for the measurement of the seismic shear wave arrival time of the soils tested. There are two basic setups for seismic measurements. In a true interval system there are two geophones which measure shear wave arrival times over a set distance. The alternative configuration known as the pseudo interval uses one geophone and the measurements are averaged over two readings. Incremental shear wave velocity, whether true interval or pseudo interval, is the change in distance traveled divided by the difference in arrival times for two successive shear waves, $V_s = \Delta d/\Delta t$. Comparisons between the two configurations indicate that the pseudo interval provides similar results to the true interval SCPTU (Robertson et al. 1986). Stiffness data from seismic cone can be compared to cone tip resistance, which is useful for identifying aged and cemented layers. Figure 7.1 shows shear waves collected at UW-1, and Figure 7.2 shows the process seismic cone profile. Additional seismic cone data is included in Appendix 2.

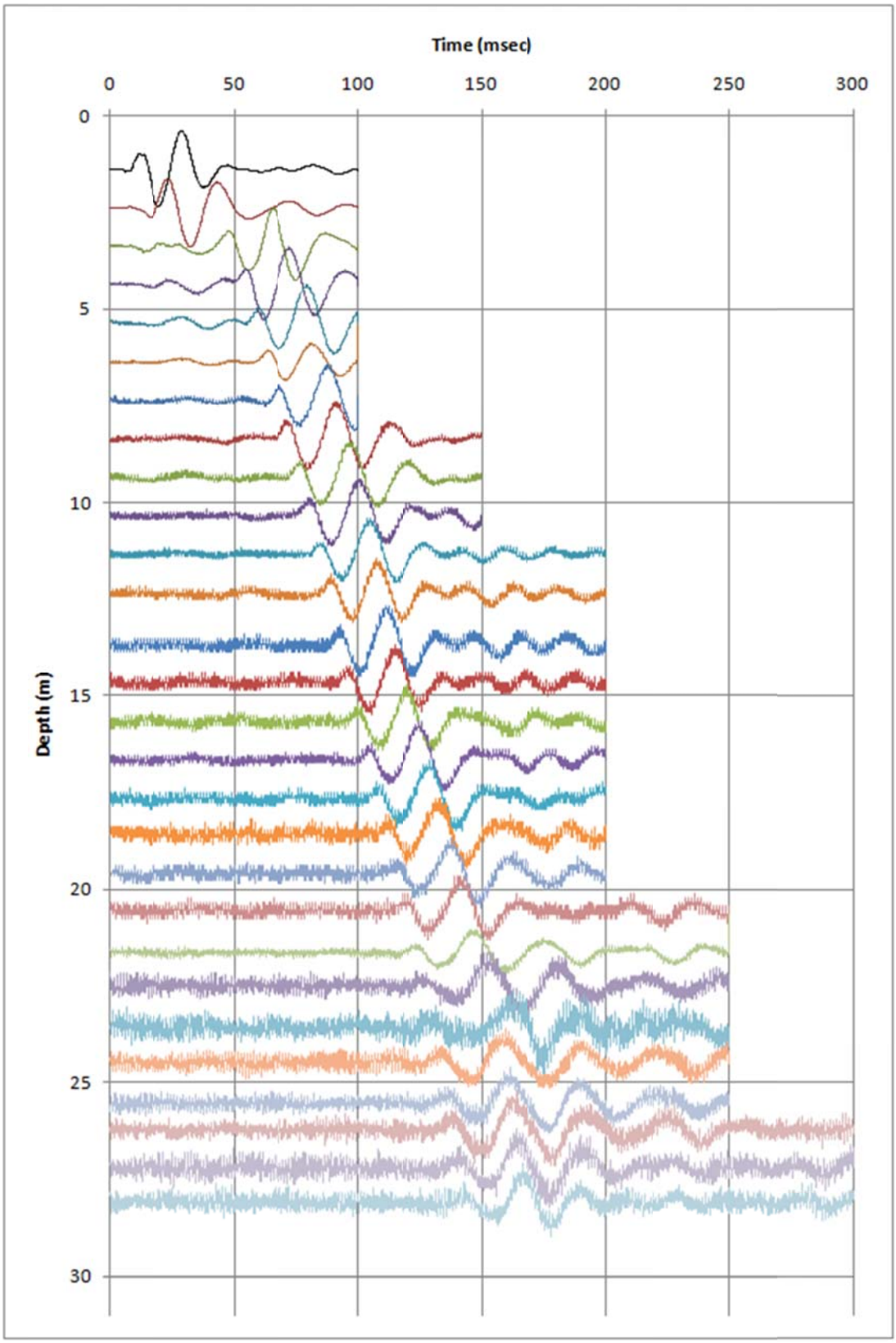

Figure 7.1. Recorded shear wave velocity data for SCPTU2-01 at site UW-1

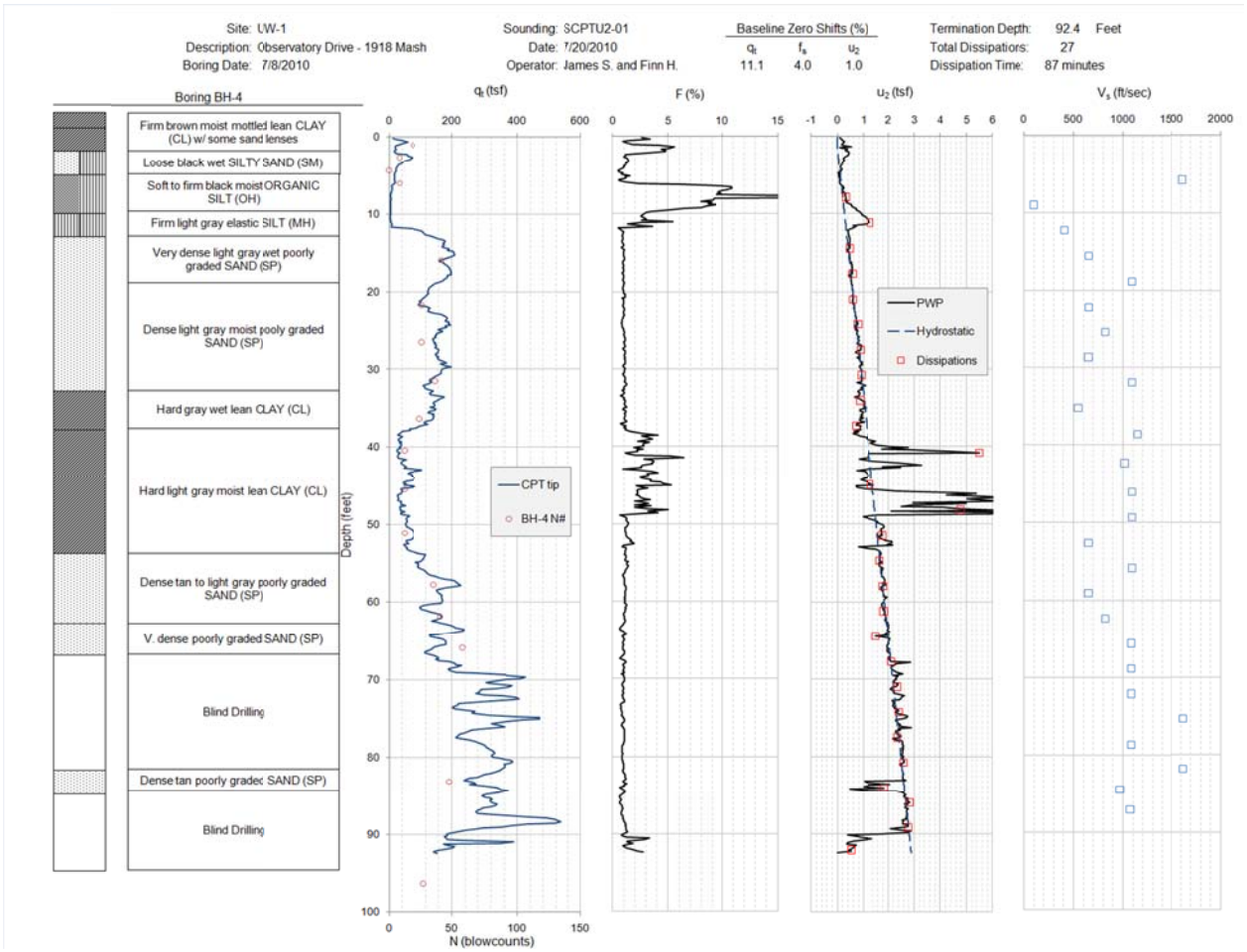

Figure 7.2. Processed results for seismic cone at site UW-1

7.2 Hard Ground Conditions

Despite the UW-Madison CPT rig having a reaction weight of 24 tons, premature refusal was met at a number of sites due to near surface gravel and cobbles or compacted fill with gravel. Increasing the rig weight may increase penetration, however, increased rig weight may also lead to more frequent damage to cones. Pre-pushing a dummy rod or pre-excavating the upper 1 to 2 feet of soil aided in achieving desired penetration depths, but in many cases this also led to excessive inclination of the cone and premature refusal due to that parameter.

Peuchen (1998) and Mayne (2007) provide excellent summaries of testing equipment and techniques for hard ground conditions, and this section will highlight a few options. Table 7.1 (from Mayne 2007) summarizes techniques for cone penetration testing in hard geomaterials.

Offshore cone penetration testing has relied on the use of wireline techniques and alternating drilling and in-situ testing since the early 70s (Figure 7.3, Zuidberg 1974, Fugro 2001, 2002), but, use of these same technologies have only been advancing for onshore applications over the past 20 years. Figure 7.4 illustrates results from an onshore investigation where CPT and drilling were combined. Penetration was successful to tip resistance values of 1200 tsf, however, this required reducing the cone size to 5 cm^2 (1 inch diameter) (Kolk et al. 2005).

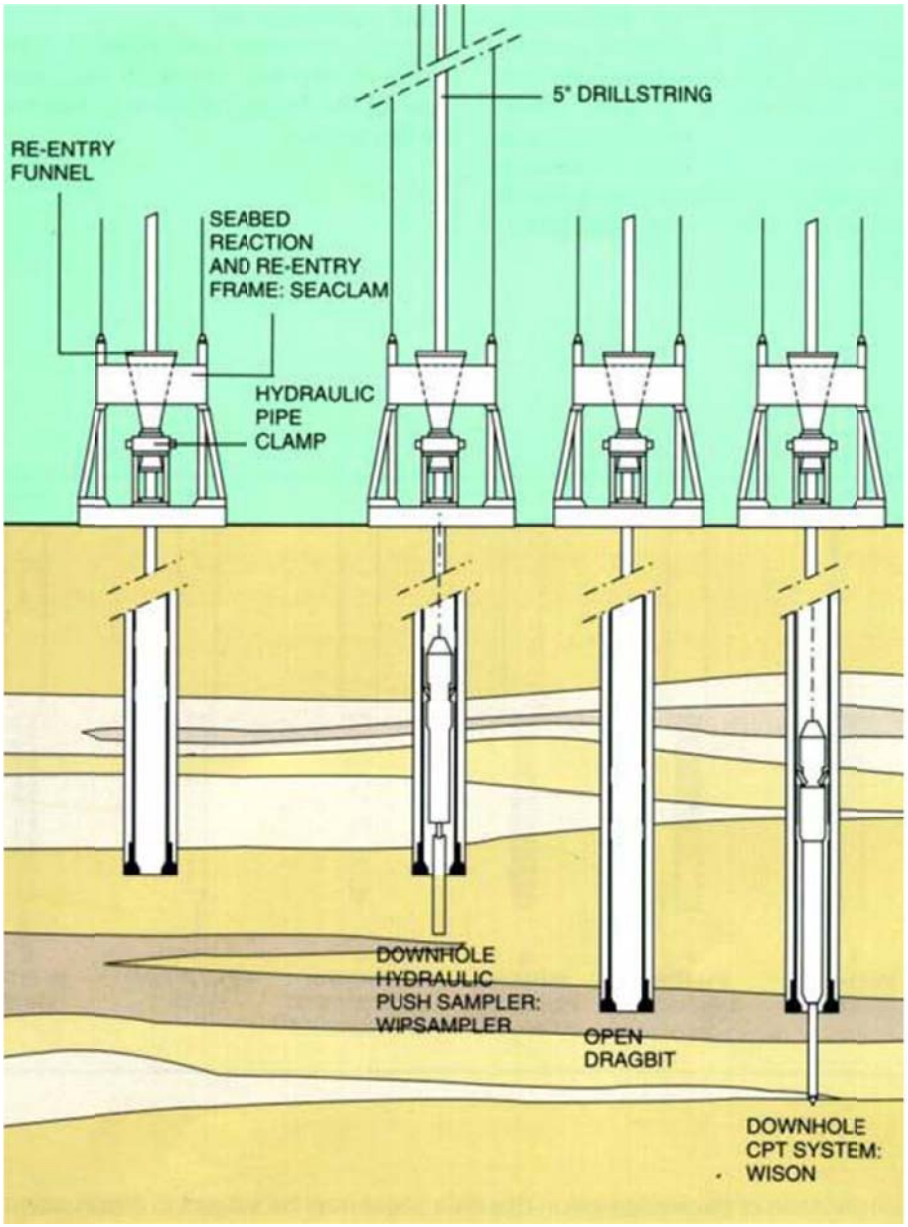

Figure 7.3. Schematic of Fugro's wireline CPT and sampling system (Wison) (Fugro 2001)

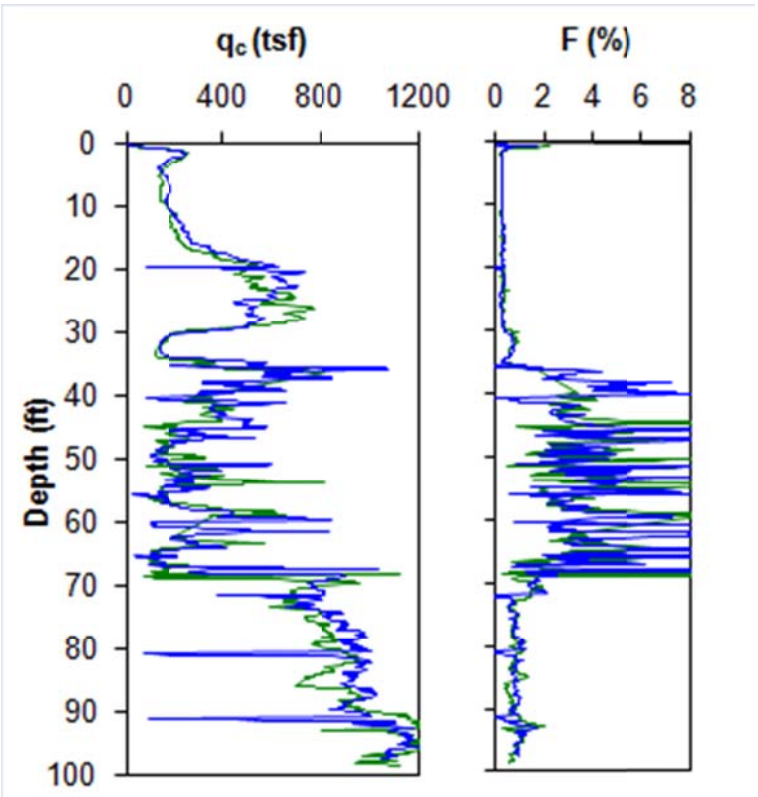

Figure 7.4. Combined drilling and cone penetration testing in very dense sand and cemented clay at Ras Tanajib site, Saudi Arabia (Kolk et al. 2005)

Figure 7.5. CPT rig with drilling capabilities (Mayne 2007)

Table 7.1. Special techniques for increased success of cone penetration in hard geomaterials (after Mayne 2007)

Advancing Technique	**Comments / Remarks**	**Reference**
Downhole thrust system	Single push stroke generally limited to 2 to 3m. Push to depths greater than 500ft below the seabed are common by alternating push with drilling.	Zuidberg (1974)
Friction reducer	Common to use on all soundings. Can have a variety of geometries, through tot be soil type specific. Less successful in very dense sands	van de Graaf and Schenk (1988)
Penetrometer that is a larger diameter than rods (i.e., 1.73 inch cone with 1.44 inch rods)	Similar concept to friction reducer	van de Graaf and Schenk (1988)
Guide casing: Double set of rods, standard 1.44 inch rods supported inside larger 44mm rods to prevent buckling	Works well for soft soils with dense soils at depth	Peuchen (1988)
Earth anchors	Increases capacity for reaction. Difficult to use in construction fill. Purdue rig used with and without anchors during this project	
Heavy 20 ton deadweight CPT trucks and track rigs with central push	Increased weight of reaction over standard drill rig	Mayne et al. (1995)
Mud injection	Needs pump and line system for bentonitic slurry	van Staveren (1995)
ROTAP – Outer coring bit	Special drilling cases through cemented zones	Sterkx and van Calster (1995)
Static – Dynamic penetrometer	Switches from static mode to dynamic mode when needed	Sanglerat et al. (1995)
Cycling rods (up and down)	May break through locally hard thin zones of soil	Shinn (1995)
Drill out (downhole CPTs)	Alternate between drilling and pushing	NNI (1996)
Very heavy 30 and 40 ton rigs	Mass may be added to 20 ton rig after it arrives at site or included on truck, depending on road weight restrictions. Mn/DOT operates one 30 ton rig.	Bratton (2000)
Sonic CPT	Use of vibrator to facilitate penetration through gravels and hard zones	Bratton (2000)
EAPS	Wireline system for enhanced access penetrometer systems	Farrington (2000); Shinn and Haas (2004); Farrington and Shinn (2006)
CPTWD	Cone penetration test while drilling	Sacchetto et al. (2004)

Figure 7.6 CPTWD wireline cone penetration system (Sacchetto et al. 2004)

CPT rigs are available that have drilling capabilities (Figure 7.5), however, this technique is generally only time effective for drilling through near surface impediments. Many of the difficulties with ground conditions encountered during this project were related to near surface impediments. While these may not have resulted in refusal, they often caused problems with cone inclination. To penetrate through hard or cemented layers at depth, a combined drilling and cone testing system is needed.

Wireline techniques show the most promise for achieving penetration in hard and cemented materials at depth in a rapid and cost effective manner. Two systems were highlighted by Mayne (2007):

- CPTWD – cone penetration while drilling (Figure 7.6, Sacchetto et al. 2004)

- EAPS – Enhanced access penetrometer system (Figure 7.7, Farrington 2000, Shinn & Haas 2004, Farrington & Shinn 2006)

These systems have reached penetrations in excess of 100 ft and show comparable measurements to standard CPT systems. It is noted that Mn/DOT has not required the use of wireline techniques, but has chosen to go with a heavier 30 ton rig to achieve 100 ft of penetration at their bridge sites.

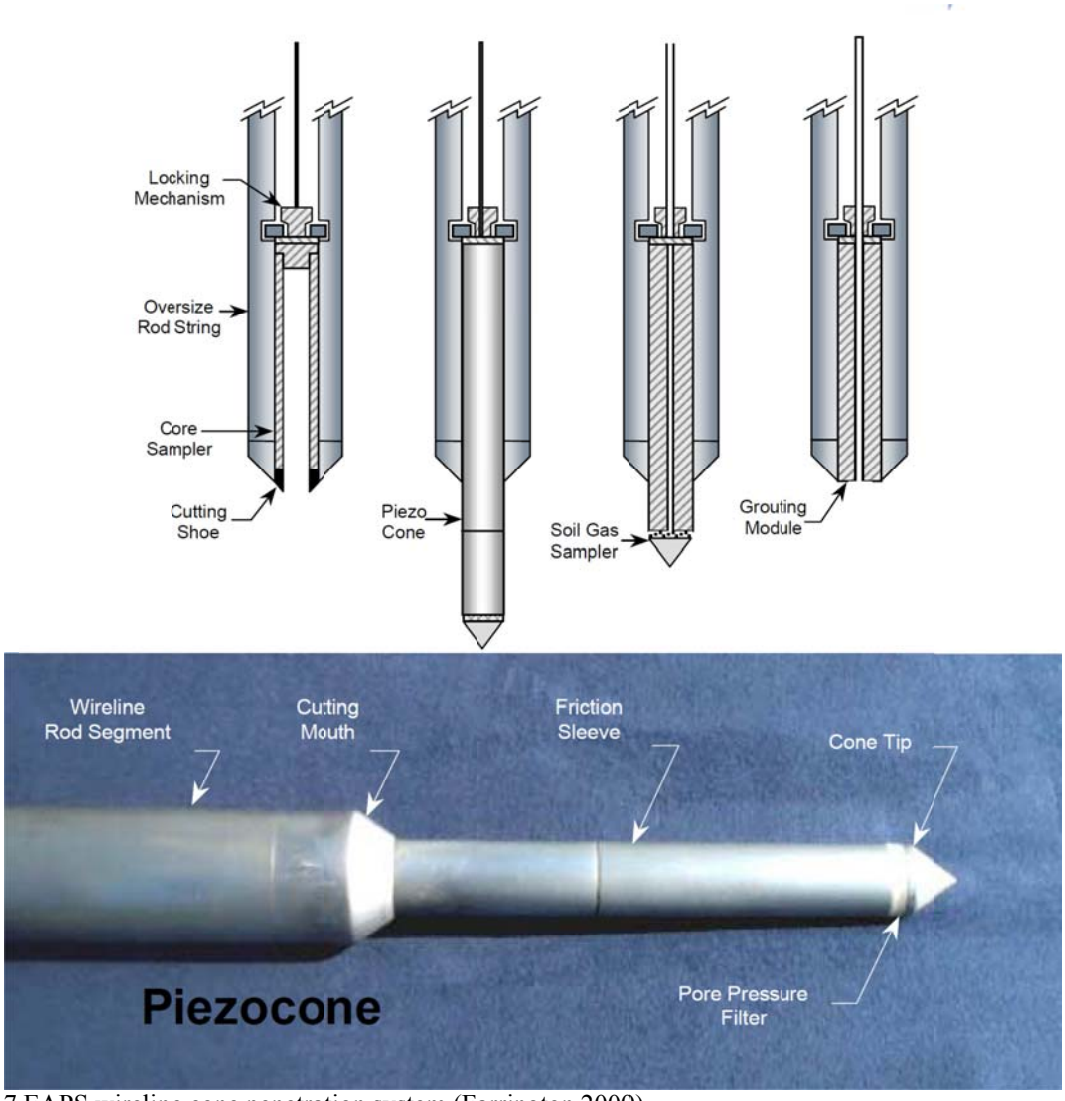

Figure 7.7 EAPS wireline cone penetration system (Farrington 2000)

8 Conclusions and Recommendations

The objectives of this research were to evaluate the potential use of CPT technology for Wisconsin DOT projects. Tests were performed at sites in different geological conditions around the state and CPT results were compared to available data. This report was written to aid in understanding CPT data and how it relates to geologic history and engineering parameters. Analysis of the data compiled in the GIS will give the user more experience and familiarity with CPT results.

Conclusions and recommendations will address the specific objectives of the project.

Departmental subsurface investigative methods (generally soil borings) and cone penetrometer findings will be compared at a number of sites with differing soils and geology.

Cone penetration in excess of 75 feet was achieved at sites in alluvium, outwash, and lake deposits. Difficulties were encountered in clay tills that had a significant amount of gravel and cobbles, as well as fill soils with gravel and cobbles. Commercial firms that performed testing for the Marquette Interchange and Mitchell Interchange project had slightly better success in Clay tills, reaching a maximum penetration depth of 92 feet for the Marquette interchange.

While the databases for evaluating soil engineering parameters from CPT data does not need the intermediate step of CPT-SPT correlations, some interesting observations occurred from comparing those parameters. The correlations between SPT N-value and CPT tip resistance at WisDOT sites indicated higher ratios and more scatter compared to data from Mn/DOT. Mn/DOT uses corrected blowcounts with calibrated hammer energies. Correction of SPT blowcount for energy and other factors would be expected to result in more reliable site investigation than current practice.

Evaluation of design parameters will be compared.

Comparison between CPT data and engineering parameters was available for:

- Coefficient of consolidation
- Constrained modulus
- Shear stiffness of undrained clays
- Undrained strength, and
- Soil type

Good correlation was achieved for coefficient of consolidation and soil type (using soil behavior type charts updated for this project). The small amount of data and questionable quality for constrained modulus, preconsolidation stress (not discussed), shear stiffness, and undrained strength did not allow for conclusions to be drawn.

Although no data from Wisconsin were available, global databases were used to provide discussion of:

- drained friction angle in sands
- shear stiffness of sands (shallow foundation settlements in sands)
- axial pile capacity; and
- embankment performance

Discuss advantages and limitations of CPT equipment, operations and interpretation will be presented.

Testing in Wisconsin and comparison to existing data reinforced existing experience related to the CPT:

<u>Advantages</u>

- CPT data are of higher quality than SPT or laboratory samples collected using current practice
- CPT results are available quicker than drilling, sampling, and lab testing

- The high volume of CPT data gives confidence in the ability to assess uncertainties and variability in soil conditions at a given site.

Disadvantages

- CPT may meet refusal due to changes in inclination if gravel or cobbles are present
- CPTs in excess of 100 ft were not achieved in this study

These disadvantages have been overcome by Mn/DOT and local CPT contractors in that area. Commercial CPT contractors are expected to have more success in achieving deep penetration than achieved in this research project, mainly due to the available capital to handle damage to CPT equipment.

Detailed suggestions for the application of this technology on WisDOT projects will be presented.

It has taken some time for Mn/DOT to use the CPT on a wide range of projects. WisDOT should not expect immediate success and cost savings from use of the CPT. They will need to constantly evaluate and update their site investigation experience. The electronic GIS provided with this project provides a framework where experience can be collected and rapidly reviewed. However, for the use of the CPT to be successful on a high percentage of Wisconsin DOT projects, an in house champion is needed to promote use of the technology and guide its application.

For future projects, it is recommended to perform more CPTs than borings, and to start the CPT program a week or two before the drilling program. This will still require mobilization of two rigs, but if the CPT is not successful, the scope of the drillers can be expanded. Perform targeted sampling of critical and representative layers, not sampling on standard intervals. Borings should be performed adjacent to CPTs and the drillers need to take high quality samples. The sample quality and results of strength testing (i.e., UU and UC) observed in this study does not produce reliable results, making it difficult to assess uncertainty, reliability, and levels of conservatism in

design. High quality sampling proposed for the DOT-1 site should be a good first step to improving practice and understanding the inherent assumptions behind successful designs.

Ideally, each of the 23 representative layers evaluated in detail in this report would have high quality sampling and laboratory testing performed at some time in the future. Only with consistent evaluations from laboratory and in-situ test data can practice move forward and cost savings be realized.

9 References

Acomb, L. J., Mickelson, D. M., & Evenson, E. B. (1982). "Till Stratigraphy and Late Glacial Events in the Lake Michigan Lobe of Eastern Wisconsin." Geological Society of America Bulletin , 93, 289-296.

Almeida, M., Danziger, F., and Lunne, T. (1996). "The use of the piezocone test to predict the axial capacity of driven and jacked piles." *Canadian Geotechnical Journal*, 33(1), 23-41.

Amundsen, T., Lunne, T., and Christophersen, H.P. (1985). "Advanced deep-water soil investigation at the Troll East field." Advances in Underwater Technology, Offshore Site Investigation, 3, Grahan & Trotman, London, 165 – 186.

API (2000). "Recommended Practice for Planning, Designing, and Constructing Fixed Offshore Platforms – Working Stress Design," API RP2A, 21st Edition, American Petroleum Institute, Washington, D.C.

ASTM (American Society for Testing and Materials) (2000). "Standard test method for performing electronic friction cone and piezocone penetration testing of soils." D5778-95, ASTM Book of Standards, Vol. 04-09.

ASTM (2004) "Standard Test Method for Consolidated Undrained Triaxial Compression Test for Cohesive Soils" D4767, ASTM Book of Standards.

ASTM (2004) "Standard Test Methods for One-Dimensional Consolidation Properties of Soils Using Incremental Loading" D2435, ASTM Book of Standards.

ASTM (2005) "Standard Test Methods for Laboratory Determnation of Water (Moisture) Content of Soil and Rock by Mass" D2216, ASTM Book of Standards.

ASTM (2007) "Standard Test Method for Particle-Size Analysis of Soils" D422, ASTM Book of Standards.

ASTM (2007) "Standard Test Method for Unconsolidated-Undrained Triaxial Compression Test on Cohesive Soils" D2850, ASTM Book of Standards.

ASTM (2009) "Standard Practice for Description and Identification of Soils (Visual-Manual Procedure)" D2488, ASTM Book of Standards.

ASTM (2009) "Standard Test Methods for Particle-Size Distribution (Gradation) of Soils Using Sieve Analysis" D6913, ASTM Book of Standards.

ASTM (2010) "Standard Test Methods for Liquid Limit, Plastic Limit, and Plasticity Index of Soils" D4318, ASTM Book of Standards.

ASTM (2010) "Standard Practice for Classification of Soils for Engineering Purposes (Unified Soil Classification System)" D2487, ASTM Book of Standards.

Atkinson, J. (2007). The Mechanics of Soils and Foundations. New York: Taylor & Francis.

Attig, J. A., & Knox, J. C. (2008). "Catastrophic Flooding from Glacial Lake Wisconsin." *Geomorphology*, 93, 384-397.

Attig, J. W., Clayton, L., & Mickelson, D. M. (1985). "Correlation of Late Wisconsin Glacial Phases in Western Great Lakes Area." Geological Society of America Bulletin , 96, 1585-1593.

Begemann, H. K. (1965). "The Friction Jacket Cone as an Aid in Determining the Soil Profile." Proceedings of the 6th International Conference on Soil Mechanics and Foundation Engineering, 1, pp. 17-20. Montreal.

Bjerrum, L. (1954). "Geotechnical Properties of Norwegian Marine Clays." *Géotechnique*, 4 (2), 49-69.

Bolton, M.D. (1986). "The Strength and Dilatancy of Sands." *Géotechnique*, 36(1), 65-78.

Burland, J. B., & Burbidge, M. C. (1985). "Settlement of Foundations on Sand and Gravel." *In Proceedings fo the Institution of Civil Engineering, Part I, 78 (6)*, pp. 1325-1381.

Burns, S. E., & Mayne, P. W. (1998a). "Monotonic and Dilatory Pore-Pressure Decay During Piezocone Test in Clay." *Canadian Geotechnical Journal*, 35, 1063-1073.

Campanella, R.G., Robertson, P.K. & Gillespie, D. (1986). "Seismic cone penetration test." Use of In Situ tests in Geotechnical Engineering, GSP 6, Blacksburg, VA, ASCE, 116-130.

Casagrande, A. (1948). "Classification and Identification of Soils." Transactions. 113, pp. 901-930. ASCE.

Chow, F. C. (1997). "Investigations into the behaviour of displacement piles for offshore foundations." PhD Thesis, Imperial College, London.

Clark, P. U., Dyke, A. S., Shakun, J. D., Carlson, A. E., Clark, J., Wohlfarth, B., et al. (2009). "The Last Glacial Maximum." *Science , 325*, 710-714.

Clayton, J. A., & Knox, J. C. (2008). "Catastrophic Flooding from Glacial Lake Wisconsin." *Geomorphology*, 93, 384-397.

Clayton, L., & Moran, S. R. (1982). "Chronology of Late Wisconsinan Glaciation in Middle North America." *Quaternary Science Reviews*, 1, 55-82.

Clayton, L., Attig, J. W., Mickelson, D. M., Johnson, M. D., & Syverson, K. M. (2006). "Glaciation of Wisconsin." Madison, WI: Wisconsin Geologic and Natural History Survey.

Coop, M.R. (2005). "On the Mechanics of Reconstituted and Natural Sands." Deformation Characteristics of Geomaterials, Lyon, Taylor & Francis, 29-58.

Dasenbrock, D.D. 2008." Geotechnical Data Sharing and Electronic Data Exchange at Minnesota DOT." GeoCongress 2008: Characterization, Monitoring, and Modeling of GeoSystems (GSP 179), ASCE, Reston, VA.

Dasenbrock, D. D., Schneider, J. A., & Mergen, E. M. (2010). "CPT Experience in Glacial Geological Conditions of Minnesota, USA." Proceedings of CPT 2010. Huntington Beach, CA.

Delft Laboratory of Soil Mechanics (Delft) (1936). "The predetermination of the required length and the prediction of the toe resistance of piles." Proc. 1st Int. Conf. on Soil Mech. and Foundation Eng., Cambridge, 181-184.

De Groot, D. J., & Lutenegger, A. J. (2003). "Geology and Engineering Properties of the Conneticut Valley Varved Clay." *Characterization and Engineering Properties of Natural Soils* (pp. 695-724). Lisse, The Netherlands: Swets and Zeitlinger.

Douglas, B.J., and Olsen, R.S. (1981). "Soil classification using the electric cone penetrometer test." Cone Penetration Testing and Experience, ASCE, 209-227.

Edil, T. B., & Mickelson, D. M. (1995). "Overconsolidated Glacial Tills in Eastern Wisconsin." Transportation Research Record, 1479, 99-106.

Eslami, A., and Fellenius, B. (1997). "Pile capacity by direct CPT and CPTu methods applied to 102 case histories." *Canadian Geotech. J.*, 34, 886-904.

ESRI ArcGIS Online, World Imagery [Aerial Photographs]. Visual Scale. http://www.arcgis.com/home/group.html?owner=esri&title=ESRI%20Maps%20and%20Data.

ESRI ArcGIS Online, US Topo Maps [Topographic Maps]. Visual Scale. http://www.arcgis.com/home/group.html?owner=esri&title=ESRI%20Maps%20and%20Data.

Farrand, W. R., Mickelson, D. M., Cowan, R. W., & Geobel, J. E. (1984). "Quaternary Geologic Map of the Lake Superior 4° x 6° Quadrangle, United States." Map I-1420 (NL-16) . United States Geological Survey.

Farrington, S. P. (2000). "Development of a Wirline CPT System for Multiple Tool Usage." *Proceedings, Industry Partnerships for Environmental Science and Technology*, (p. 40).

Farrington, S. P., & Shinn, J. D. (2006). "Hybrid Penetration for Geotechnical Site Investigation." *Proceedings, Geo-Congress 2006*, (p. 5 pp). Atlanta, GA.

Finnie, I. M., & Randolph, M. F. (1994). "Punch-through and Liquefaction Induced Failure of Shallow Foundations on Calcareous Sediments." Proceedings of the International Conference on Behavior of Offshore Structures, (pp. 217-230). Boston.

Fugro (2001). "Geophysical and Geotechncial Techniques for the Investigation of Near-Seabed Soils and Rocks," Fugro NV, Leidschendam, NL, 51 p.

Fugro (2002). "Down to Earth and Up-to-Date," Fugro NV, Leidschendam, NL, 304 p.

Fullerton, D. S., Ringrose, S. M., Clayton, L., Schreiner, B. T., & Goebel, J. E. (2000). Quaternary Geologic Map of the Winnepeg 4°x6° Quadrangle, United States and Canada. *I-1420 (NM-14)* . USGS.

Gavin, K., and Lehane, B.M. (2007). "Base load-displacement response of piles in sand." *Canadian Geotechnical Journal*, 44(9), 1053-1063.

Goebel, J. E., Mickelson, D. M., Farrand, W. R., Clayton, L., Knox, J. C., Cahow, A., et al. (1983). "Quaternary Geologic Map of the Minneapolis 4° x 6° Quadrangle, United States." Map I-1420 (NL-15). United States Geologic Survey.

Hallberg, G. R., Lineback, J. A., Mickelson, D. M., Knox, J. C., Geobel, J. F., Hobbs, H. C., et al. (1991). "Quaternary Geologic Map of the Des Moines 4° x 6° Quadrangle, United States." Map I-1420 (NK-15). United States Geological Survey.

Hooyer, T. S. (2007). “Late-Glacial History of East-Central Wisconsin.” Madison, WI: Wisconsin Geological and Natural History Survey.

Hotstream, J. N. (2011).” Classification of Wisconsin glacial soils using the cone penetration test.” M.S. Thesis, University of Wisconsin – Madison.

Houlsby, G.T., and Hitchman, R. (1988). “Calibration chamber tests of a cone penetrometer in sand.” *Géotechnique*, 38(1), 39-44.

Hvorslev, M.J. (1953). “Cone penetrometer operated by rotary drilling rig.” Proc. 3rd Int. Conf. on Soil Mech. and Foundation Engineering, Vol. 1, 236.

International Commission on Stratigraphy. (2010). *International Stratigraphic Chart.* http://www.stratigraphy.org/ics%20chart/09_2010/StratChart2010.jpg.

Jamiolkowski, M. B., Lo Presti, D. F. C., and Manassero, M. 2003. “Evaluation of Relative Density and Shear Strength of Sands from Cone Penetration Test.” Soil Behaviour and Soft Ground Construction, (GSP 119), ASCE, Reston, VA, 201-238.

Janbu, N., 1985. “Soil Models in Offshore Engineering (25th Rankine Lecture).” *Géotechnique*, 35:243-281.

Jardine, R. J., Chow, F. C., Overy, R. F., Standing, J. R. (2005). *ICP design methods for driven piles in sands and clays*. Thomas Telford, London, 97.

Jefferies, M. G., & Been, K. (2006). *Soil Liquefaction: A Critical State Approach.* London and New York: Taylor and Francis.

Jefferies, M. G., & Davies, M. P. (1993). “Use of CPTu to Estimate Equivalent SPT N60.” *Geotechnical Testing Journal*, 16 (4), 458-468.

Karlsrud, K., Hansen, S.B., Dyvic, R., and Kalsnes, B. (1993). “NGI’s pile tests at Tilbrook and Pentre – review of testing procedures and results.” Large-scale pile tests in clay, Thomas Telford, London, 405-429.

Keaveny, J. M., & Mitchell, J. K. (1986). “Strength of Fine-Grained Soils Using the Piezocone.” Use of In-Situ Tests in Geotechnical Engineering (pp. 668-699). Reston: ASCE.

Kolk, H. J., Baaijens, A. E., & Senders, M. (2005). “Design Criteria for Pipe Piles in Silica Sands.” *Frontiers in Offshore Geotechnics (Proc. ISFOG, Perth, Australia)* (pp. 711-716). London, United Kingdom: Taylor and Francis Group.

Kulhawy, F. H., & Mayne, P. W. (1990). “Manual on Estimating Soil Properties for Foundation Design.” Palo Alto, CA: Electric Power Research Institute.

Ladd, C.C. (1991). “Stability Evaluation During Staged Construction.” *ASCE Journal of Geotechnical Engineering*, 117(4), 540-615.

Ladd, C.C., and DeGroot, D.J. 2003. Recommended Practice for Soft Ground Site Characterization. Arthur Casagrande Lecture. In Soil and Rock America 2003: Proceedings of the 12th Panamerican Conference on Soil Mechanics and Geotechnical Engineering, Cambridge, Mass., 22–26 June 2003. VGE Verlag Glückauf, 2003. Vol. 1, pp. 3–57.

Lambeck, K., & Chappell, J. (2001). “Sea Level Change Through the Last Glacial Cycle.” *Nature , 292*, 679-686.

Lehane, B.M. and Fahey, M. (2004). “Using SCPT and DMT Data for Settlement Prediction in Sand.” Proc. 2nd International Conf. on Site Characterisation, Porto, Portugal, Vol. 2, 1673–1680, Millpress, Rotterdam.

Lehane, B.M. and Jardine R.J. (1994). :Displacement-Pile Behavior in a Soft Marine Clay.” *Canadian Geotechnical Journal.* 31, 181-191.

Lehane, B.M., Jardine, R.J., Bond, A.J., and Frank, R. (1993). “Mechanisms of Shaft Friction in Sand from Instrumented Pile Tests.” *J. Geotech. Eng.*, 119 (1), 19-35.

Lehane, B.M., Schneider, J.A., and Xu, X. (2005). “CPT based design of driven piles in sand for offshore structures.” Report GEO 05345, The University of Western Australia.

Lehane, B.M., Schneider, J.A., and Xu, X. 2008. “Design of Displacement Piles in Siliceous Sands Using the CPT.” *Australian Geomechanics*, 43(2), 21-40.

Leroueil, S., Tavenas, F., Samson, L., & Morin, P. (1983). “Preconsolidation Pressure of Champlain Clays. Part 2 Laboratory Determination.” *Canadian Geotechnical Journal*, 20, 803-816.

Liao, T., Bell, K. R., & Senapathy, H. (2010). “CPT in Glacial Soils After Deep Excavation.” *Proceedings of CPT 2010*, (p. 8). Huntington Beach, CA.

Lineback, J. A., Bleuer, N. K., Mickelson, D. M., Farrand, W. R., & Goldthwait, R. P. (1983). “Quaternary Geologic Map of the Chicago 4° x 6° Quadrangle, United States.” Map I-420 (NK-16). United States Geological Survey.

Lisiecki, L. E., & Raymo, M. E. (2005). “A Plio-Pleistocene Stack of 57 Globally Distributed Benthic d18O Records.” *Paleoceanography , 20*, 1003.

Lunne, T., Eidsmoen, T., Gillespie, D., and Howland, J.D. (1986). “Laboratory and field evaluation of cone penetrometers.” Use of In Situ Tests in Geotechnical Engineering, GSP 6, ASCE, 714-729.

Lunne, T. M., Robertson, P. K., & Powell, J. M. (1997). *Cone Penetration Testing in Geotechnical Practice.* New York, NY: Blackie Academic, EF Spon/Routledge Publishers.

Mayne, P.W. (1980). "Cam-Clay Predictions of Undrained Shear Strength", *Journal of the Geotechnical Engineering Division*, ASCE, Vol. 106 (GT11), 1219-1242.

Mayne, P.W. (1986). "CPT Indexing of In-Situ OCR in Clays", Use of In-Situ Tests in Geotechnical Engineering (GSP 6), ASCE, New York, NY, pp. 780-793.

Mayne, P. W. (2001). “Stress-Strain-Strength-Flow Parameters from Enhanced In-Situ Tests.” Proceedings, International Conference on In-Situ Measurement of Soil Properties and Case Histories, (pp. 27-48). Bali, Indonesia.

Mayne, P. W. (2006). “The 2nd James K. Mitchell Lecture: Undisturbed Sand Strength from Seismic Cone Tests.” *Geomechanics and Geoengineering , 1* (4), 239-247.

Mayne, P. W. (2007). “Cone Penetration Testing: A Synthesis of Highway Practice.” Washington, D. C.: Transportation Research Board.

Mayne, P. W., & Illingworth, F. (2010). “Direct CPT Method for Footing Response in Sands Using a Database Approach.” *Proceedings of CPT 2010*, (p. 8). Huntington Beach, CA.

Mayne, P. W., & Poulos, H. G. (1999). "Approximate Displacement Influence Factors for Elastic Shallow Foundations." *Jounal of Geotechnical and Geoenvironmental Engineering , 125* (6), 453-460.

Meyerhof, G.G. (1956). "Penetration tests and bearing capacity of cohesionless soils." *J. Soil Mech. and Foundation Div.*, 82(SM1), Paper 886, 19.

Mickelson, D. M., Acomb, L. J., & Edil, T. B. (1978). "The Origin of Preconsolidated and Normally Consolidated Tills in Eastern Wisconsin, USA." Moraines and Varves: Origin, Genesis and Classification (pp. 179-187). Zurich: Balkema.

Moss, R. E. (2003). "CPT-Based Probalistic Assessment of Seismic Soil Liquefaction Initiation." PhD. Dissertation University of California, Berkeley.

Moss, R. E., Seed, R. B., & Olsen, R. S. (2006). "Normalizing the CPT for Overburden Stress." *Journal of Geotechnical and Geoenvironmental Engineering*, 132 (3), 378-387.

Olsen, R.S., Mitchell, J.K. (1995). "CPT stress normalization and prediction of soil classification." Proc., Int. Symp. on Cone Penetration Testing, CPT'95, Linköping, 2, Geotechnical Society. SGF Report 3:95, 257 – 262.

Peuchen, J. (1998). Commercial CPT Profiling in Soft Rocks and Hard Soils. *Geotechnical Site Characterization. 2*, pp. 1131-1137. Rotterdam, The Netherlands: Balkema.

Puppula, A. J. (2008). "Estimating Stiffness of Subgrade and Unbound Materials for Pavement Design: A Synthesis of Highway Practice." Washington, D. C.: Transportation Research Board.

Ramsey, N. (2002). "A Calibrated Model for the Interpretation of Cone Penetration Tests in North Sea Quaternary Soils." Offshore Site Investigation and Geotechnics: Diversity and Sustainability, (pp. 341-356). London.

Randolph, M. F. (2004). "Characterization of Soft Sediments for Offshore Applications." 2nd Int. Conf. on Site Characterization (Proc. ISC'2, Porto). I, pp. 209-232. Rotterdam, the Netherlands: Millpress.

Robertson, P. K. (1990). "Soil Classification Using the Cone Penetration Test." *Canadian Geotechnical Journal*, 27, 151-158.

Robertson, P. K. (1991). "Soil Classification Using the Cone Penetration Test: Reply." *Canadian Geotechnical Journal*, 28, 176-178.

Robertson, P. K. (2010). Estimating in-situ soil permeability from CPT & CPTu. *2nd International Symposium on Cone Penetration Testing*, *II.* Huntington Beach, CA.

Robertson, P. K., & Wride, C. E. (1998). "Evaluating cyclic liquefaction potential using the cone penetration test." *Canadian Geotechnical Journal*, 35, 442-459.

Robertson, P. K., Campanella, R. G., & Wightman, A. (1983). "SPT-CPT Correlations." *Journal of the Geotechnical Engineering Division , 108* (No. GT 11), 1449-1459.

Robertson, P. K., Campanella, R. G., Gillespie, D., & Rice, A. (1986). "Seismic CPT to Measure In Situ Shear Wave Velocity." *Journal of Geotechnical Engineering*, 112 (8), 791-803.

Robertson, P. K., Sully, J. P., Woeller, D. J., Lunne, T., Powell, J. J., & Gillespie, D. G. (1992). "Estimating Coefficient of Consolidation from Piezocone Tests." *Canadian Geotechnical Journal*, 29, 539-550.

Sacchetto, M. A., Trevisan, A., Elmgren, K., & Melander, K. (2004). "Cone Penetration Test While Drilling." *Geotechnical and Geophysical Site Characterization. 1*, pp. 787-794. Rotterdam, The Netherlands: Millpress.

Sado, E. V., Fullerton, D. S., & Farrand, W. R. (1994). Quaternary Geologic Map of the Lake Nipigon 4°x6° Quadrangle, United States and Canada. I-1420 (NM-16) . USGS.

Sado, E. V., Fullerton, D. S., Goebal, J. E., & Ringrose, S. M. (1995). Quaternary Geologic Map of the Lake of the Woods 4°x6° Quadrangle, United States and Canada. *I-1420 (NM-15)* . USGS.

Salgado, R. (2008) *The Engineering of Foundations*, McGraw Hill.

Salgado, R., Mitchell, J. K., & Jamiolkowski, M. (1997). "Cavity Expansion and Penetration Resistance in Sands." *Journal of Geotechnical and Geoenvironmental Engineering.* 123, 334-354.

Santamarina, J.C., Klein, K.A., and Fam, M.A. 2001. *Soils and Waves*. John Wiley & Sons, New York.

Schmertmann, J. H. (1975). Measurement of In Situ Shear Strength. Proceedings of the Conference on In Situ Measurement of Soil Properties (pp. 57-138). Raleigh, NC: ASCE.

Schmertmann, J. H. (1978). Guidelines for Cone Test, Performance, and Design (No. FHWATS-78209): U.S. Federal Highway Administration.

Schmertmann, J.H. (1995). "CPT'63(+) – A history in the USA from a University of Florida viewpoint." Proc. Int. Symp. On Cone Penetration Testing, Vol. 3, 269-275.

Schneider, J. A., Lehane, B. A., & Schnaid, F. (2007). "Velocity Effects on Piezocone Measurements in Normally and Overconsolidated Clays." *International Journal of Physical Modeling in Geotechnics*, 2, 23-34.

Schneider, J. A., Randolph, M. F., Mayne, P. W., & Ramsey, N. R. (2008). "Analysis of Factors Influencing Soil Classification Using Normalized Piezocone Tip Resistance and Pore Pressure Parameters." *Journal of Geotechnical and Geoenvironmental Engineering*, 134 (11), 1569-1586.

Schneider, J. A., Xu, X., & Lehane, B. M. (2010). End Bearing Formulation for CPT Based Driven Pile Design Methods in Siliceous Sands. *Proceedings of CPT 2010*, (p.7). Huntington Beach, CA.

Schofield, A., & Wroth, P. (1968). *Critical State Soil Mechanics.*

Schuettpelz, C.C., Fratta, D., and Edil, T. (2010). "Mechanistic corrections for determining the resilient modulus of base course materials based on elastic wave measurements." *Journal of Geotechnical and Geoenvironmental Engineering*, 136(8), 1086-1094.

Shinn, J. K., & Haas, J. W. (2004). "Enhanced Access Penetration System: A Direct Push System for Difficult Site Conditions." *Geotechnical and Geophysical Site Characterization. 1*, pp. 795-800. Rotterdam, The Netherlands: Millpress.

Shockley, W.G., Cunny, R.W., and Strohm, W.E., Jr. (1961). "Investigations with rotary cone penetrometer," Proc. 5th Int. Conf. on Soil Mech. and Foundation Eng., Vol. 1, 523.

Silva, M. F., White, D. J., & Bolton, M. D. (2006). "An Analytical Study of the Effect of Penetration Rate on Piezocone Tests in Clay." *International Journal of Numerical Analytical Methods in Geomechanics*, 30, 501-527.

Stratigraphics (2003a). "Piezometric cone penetration testing with soil electrical conductivity measurements: Marquette Interchange West Leg Core, Milwaukee, Wisconsin." Prepared for Soils and Engineering Services, Inc., Report 03-110-190, December.

Stratigraphics (2003b). "Piezometric cone penetration testing with soil electrical conductivity measurements: Marquette Interchange, Milwaukee, Wisconsin." Prepared for Maxim Technologies, Report 03-120-050, April.

Sully, J. P., Robertson, P. K., Campanella, R. G., & Woeller, D. J. (1999). "An approach to evaluation of field CPTU dissipation data in overconsolidated fine-grained soils." *Canadian Geotechnical Journal*, 36, 369-381.

Teh, C. I., & Houlsby, G. T. (1991). An analytical study of the cone penetration test in clay. *Géotechnique*, 41 (1), 17-34.

Tonni, L., & Gottardi, G. (2011). "Analysis and Interpretation of Peizocone Data on the Silty Soil of the Venetian Lagoon (Treporti Test Site)." *Canadian Geotechnical Journal , 48* (4), 616-633.

Torstensson, B. A. (1975). "Pore Pressure Sounding Instrument." Proceedings of the Conference on In Situ Measurement of Soil Properties. 2, pp. 48-55. Raleigh, NC: ASCE.

Transporation Research Center-LTAP. (1999). Work Zone Safety. Madison, WI: University of Wisconsin-Madison.

U.S. Bureau of Reclamation - U.S. Department of the Interior. (1998). Earth Manual - Part 1. Denver: US Government Printing Office.

Viggiani, G., & Atkinson, J. H. (1995). Stiffness of Fine-Grained Soil at Small Strains. *Géotechnique , 45* (2), 249-265.

White, D. J., & Lehane, B. M. (2004). Friction Fatigue on Displacement Piles in Sand. *Géotechnique , 54* (10), 645-658.

Wisconsin Geological and Natural History Survey (WGNHS). (1983). Thickness of Unconsolidated Material in Wisconsin. Madison, Wisconsin: University of Wisconsin-Extension.

Wissa, A.E.Z., Martin, R.T., and Garlanger, J.E. (1975). "The piezometer probe." Proc. ASCE Specialty Conference on In Situ Measurement of Soil Properties, Vol. 1, Raleigh, NC,536-545.

Wroth, C. P. (1984). Interpretation of In Situ Soil Tests. Géotechnique , 34 (4), 449-489.

Wroth, C. P. (1988). Penetration Testing - A More Rigorous Approach to Interpretation. In J. De Ruiter (Ed.), Penetration Testing 1988 (pp. 303-311). Orlando: Balkema.

Wroth, C.P., and Houlsby, G.T. (1985). “Soil mechanics: property characterization & analysis procedures.” Proc., 11th Int. Conf. on Soil Mech. and Foundation Eng., ICSMFE, Vol. 1, San Francisco, 1-56.

Wroth, C. P., & Wood, D. M. (1978). The Correlation of Index Properties with Some Basic Engineering Properties of Soil. *Canadian Geotechnical Journal*, 137-145.

Xu, X., and Lehane, B. M. (2005). “Evaluation of end-bearing capacity of closed-ended pile in sand from cone penetration data.” Proceedings of the First International Symposium on Frontiers in Offshore Geotechnics, Perth, 733-739.

Xu, X., Schneider, J. A., & Lehane, B. M. (2008). Cone Penetration Test Methods for End-Bearing Assessment of Open-and Close-Ended Driven Piles in Siliceous Sand. *Canadian Geotechnical Journal, 45*, 1130-1141.

Zuidberg, H. (1974). Use of Static Cone Penetrometer Testing in the North Sea. *Porceedings of the European Symposium on Penetration Testing (ESOPT)*, *2.2*, pp. 433-436. Stockholm, Sweden.

Appendix 1

Location of cone penetration tests reviewed from previous investigations

State Location

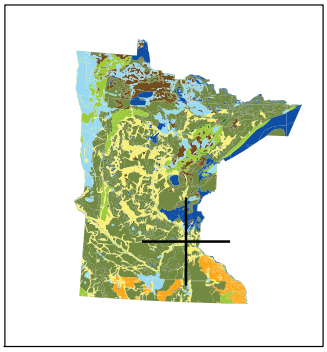

City Location

ESRI Aerial Photo - Scale 1:24,000

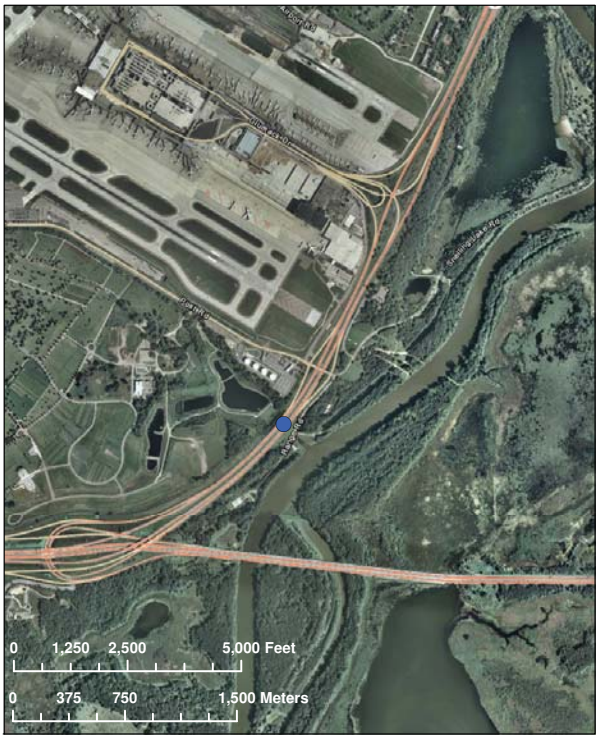

ESRI Aerial Photo - Scale 1:1,500

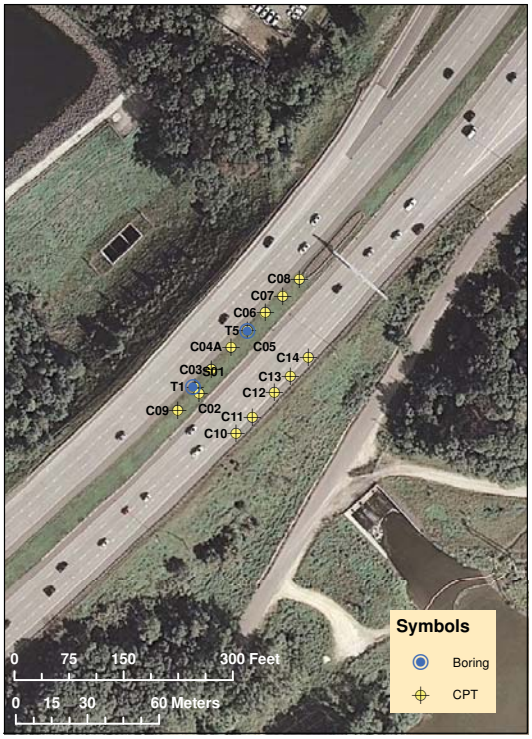

Description:

The intent of this map is to provide information on the site location and layout of the investigation. Several sources of data were compiled to generate these maps of varying scales. The map scale decreases, area shown decreases, from left to right. Site location is shown from a state level, to city level, to aerial photo and finally a detailed site aerial photo with locations of specific borings conducted for the bridge design.

Source Maps:

DeLorme. Delorme World Basemap [Computer Map]. 1:288,000. [Online Database]. 2009.
ESRI ArcGIS Online, World Imagery [Aerial Photographs]. Visual Scale. http://www.arcgis.com/home/group.html?owner=esri&title=ESRI%20Maps%20and%20Data. (June 22, 2011)
Minnesota Dept. of Natural Resources. "Minnesota State Outline." [ESRI Shapefile]. Created by Minnesota DNR - MIS Bureau, 2007.

Site Location Maps
Minnesota Site 1
STH 5 along Minnesota River
Hennepin County, MN

Project No: 0092-10-10
Map Scale: Varies
Date: June 22, 2011
Map By: JNH
Reviewed By: JAS

State Location

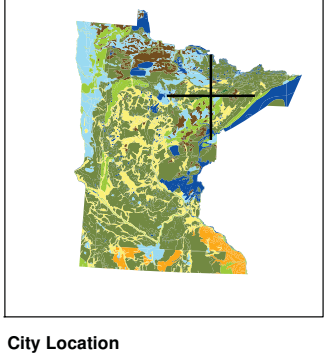

City Location

ESRI Aerial Photo - Scale 1:24,000

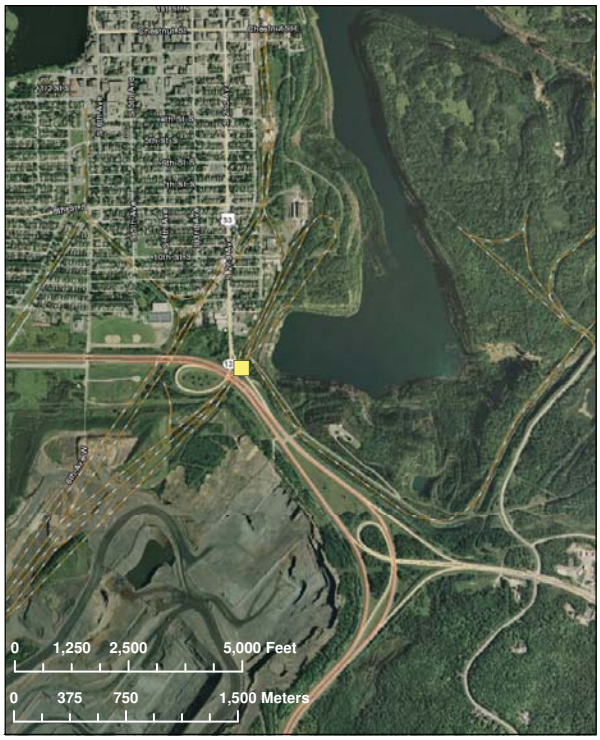

ESRI Aerial Photo - Scale 1:2,000

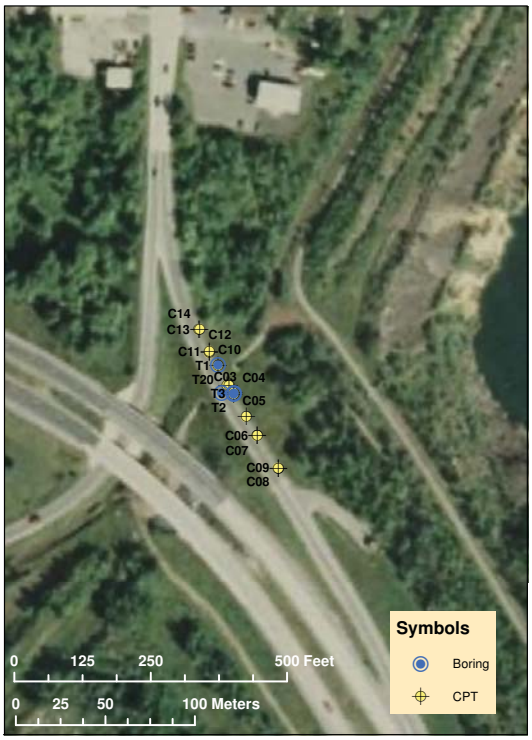

Description:

The intent of this map is to provide information on the site location and layout of the investigation. Several sources of data were compiled to generate these maps of varying scales. The map scale decreases, area shown decreases, from left to right. Site location is shown from a state level, to city level, to aerial photo and finally a detailed site aerial photo with locations of specific borings conducted for the bridge design.

Source Maps:

DeLorme. Delorme World Basemap [Computer Map]. 1:288,000. [Online Database]. 2009.
ESRI ArcGIS Online, World Imagery [Aerial Photographs]. Visual Scale. http://www.arcgis.com/home/group.html?owner=esri&title=ESRI%20Maps%20and%20Data. (June 25, 2011)
Minnesota Dept. of Natural Resources. "Minnesota State Outline." [ESRI Shapefile]. Created by Minnesota DNR - MIS Bureau, 2007.

Site Location Maps
Minnesota Site 2
USH-53 in Virginia
St. Louis County, MN

Project No: 0092-10-10
Map Scale: Varies
Date: June 25, 2011
Map By: JNH
Reviewed By: JAS

State Location

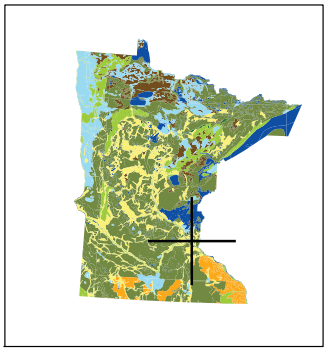

City Location

ESRI Aerial Photo - Scale 1:24,000

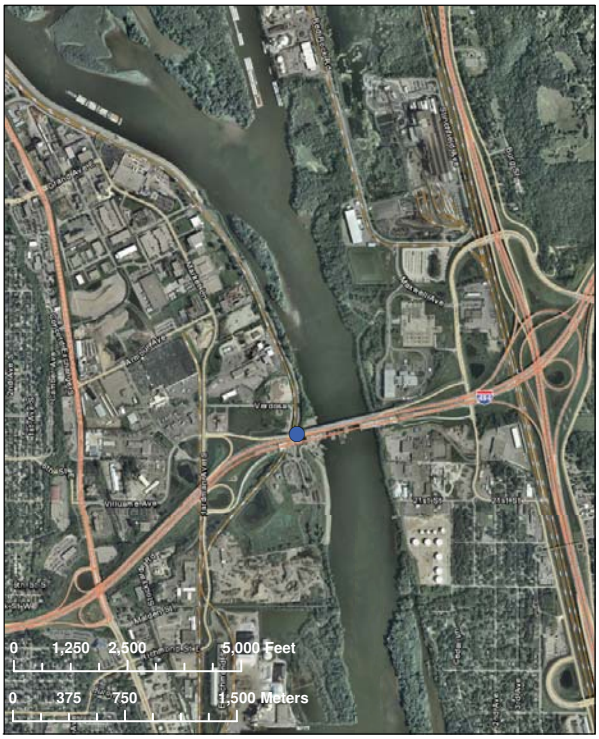

ESRI Aerial Photo - Scale 1:2,500

Description:

The intent of this map is to provide information on the site location and layout of the investigation. Several sources of data were compiled to generate these maps of varying scales. The map scale decreases, area shown decreases, from left to right. Site location is shown from a state level, to city level, to aerial photo and finally a detailed site aerial photo with locations of specific borings conducted for the bridge design.

Source Maps:

DeLorme. Delorme World Basemap [Computer Map]. 1:288,000. [Online Database]. 2009.
ESRI ArcGIS Online, World Imagery [Aerial Photographs]. Visual Scale. http://www.arcgis.com/home/group.html?owner=esri&title=ESRI%20Maps%20and%20Data. (June 25, 2011)
Minnesota Dept. of Natural Resources. "Minnesota State Outline." [ESRI Shapefile]. Created by Minnesota DNR - MIS Bureau, 2007.

Site Location Maps
Minnesota Site 3
I-494 over Mississippi River
Washington County, MN

Project No: 0092-10-10
Map Scale: Varies
Date: June 25, 2011
Map By: JNH
Reviewed By: JAS

State Location

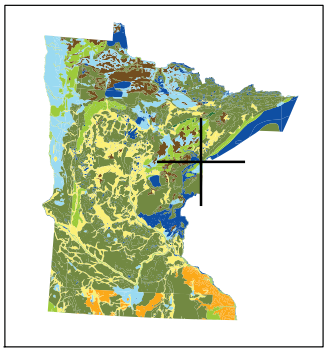

City Location

ESRI Aerial Photo - Scale 1:24,000

ESRI Aerial Photo - Scale 1:2,000

Description:

The intent of this map is to provide information on the site location and layout of the investigation. Several sources of data were compiled to generate these maps of varying scales. The map scale decreases, area shown decreases, from left to right. Site location is shown from a state level, to city level, to aerial photo and finally a detailed site aerial photo with locations of specific borings conducted for the bridge design.

Source Maps:

DeLorme. Delorme World Basemap [Computer Map]. 1:288,000. [Online Database]. 2009.
ESRI ArcGIS Online, World Imagery [Aerial Photographs]. Visual Scale. http://www.arcgis.com/home/group.html?owner=esri&title=ESRI%20Maps%20and%20Data. (June 30, 2011)
Minnesota Dept. of Natural Resources. "Minnesota State Outline." [ESRI Shapefile]. Created by Minnesota DNR - MIS Bureau, 2007.

Site Location Maps
Minnesota Site 4
STH 210 near St. Louis River
Carlton County, MN

Project No: 0092-10-10
Map Scale: Varies
Date: June 30, 2011
Map By: JNH
Reviewed By: JAS

State Location

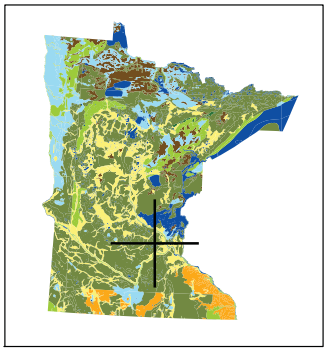

City Location

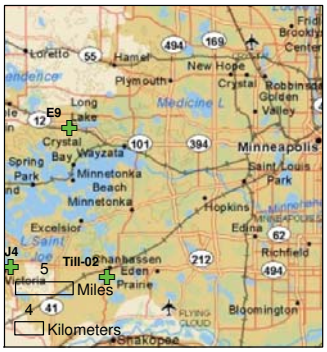

ESRI Aerial Photo - Scale 1:24,000

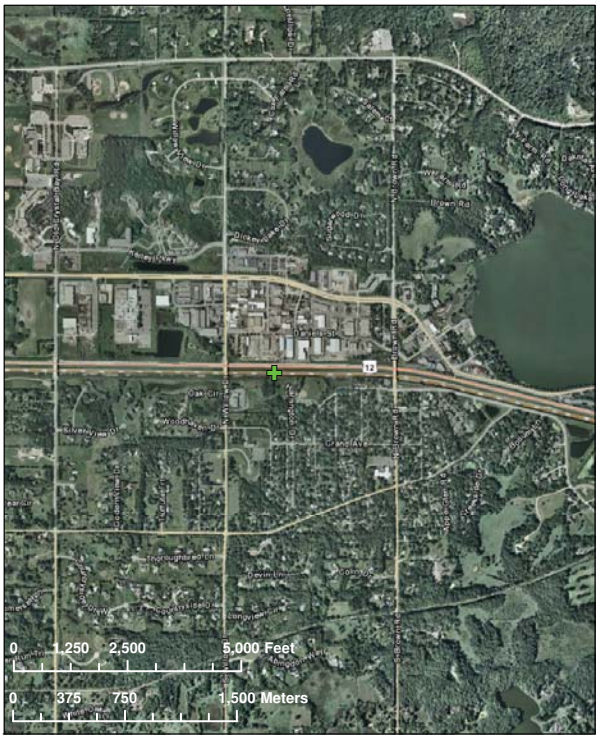

ESRI Aerial Photo - Scale 1:3,000

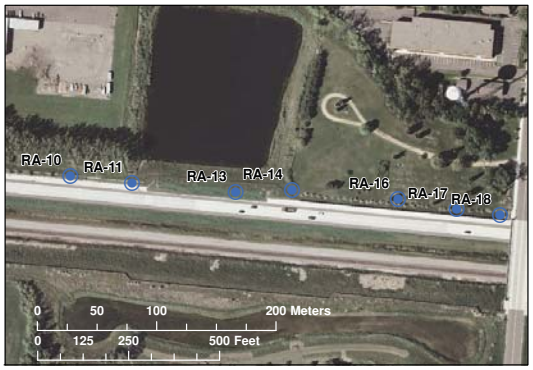

ESRI Aerial Photo - Scale 1:2,000

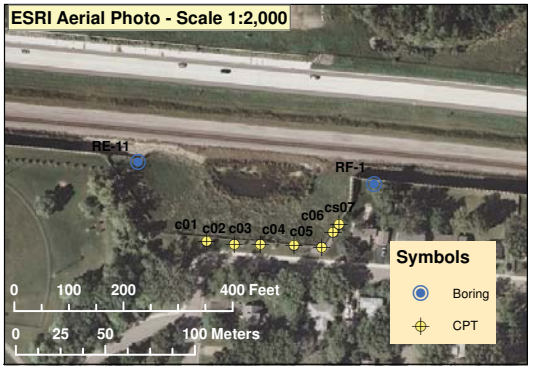

Description:

The intent of this map is to provide information on the site location and layout of the investigation. Several sources of data were compiled to generate these maps of varying scales. The map scale decreases, area shown decreases, from left to right. Site location is shown from a state level, to city level, to aerial photo and finally a detailed site aerial photo with locations of specific borings conducted for the bridge design.

Source Maps:

DeLorme. Delorme World Basemap [Computer Map]. 1:288,000. [Online Database]. 2009.
ESRI ArcGIS Online, World Imagery [Aerial Photographs]. Visual Scale. http://www.arcgis.com/home/group.html?owner=esri&title=ESRI%20Maps%20and%20Data. (June 30, 2011)
Minnesota Dept. of Natural Resources. "Minnesota State Outline." [ESRI Shapefile]. Created by Minnesota DNR - MIS Bureau, 2007.

Site Location Maps
Minnesota Site 5
I-12 Sound Barrier
Hennepin County, MN

Project No: 0092-10-10
Map Scale: Varies
Date: June 30, 2011
Map By: JNH
Reviewed By: JAS

State Location

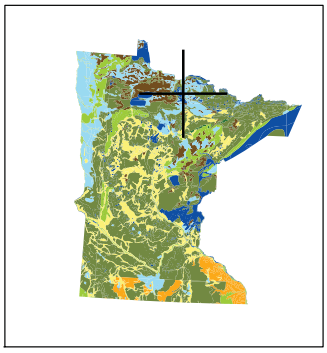

City Location

ESRI Aerial Photo - Scale 1:24,000

ESRI Aerial Photo - Scale 1:2,000

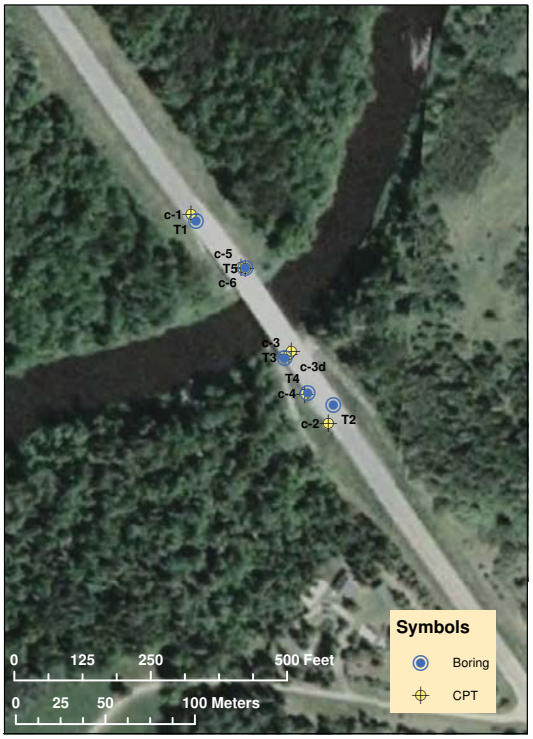

Description:

The intent of this map is to provide information on the site location and layout of the investigation. Several sources of data were compiled to generate these maps of varying scales. The map scale decreases, area shown decreases, from left to right. Site location is shown from a state level, to city level, to aerial photo and finally a detailed site aerial photo with locations of specific borings conducted for the bridge design.

Source Maps:

DeLorme. Delorme World Basemap [Computer Map]. 1:288,000. [Online Database]. 2009.
ESRI ArcGIS Online, World Imagery [Aerial Photographs]. Visual Scale. http://www.arcgis.com/home/group.html?owner=esri&title=ESRI%20Maps%20and%20Data. (June 22, 2011)
Minnesota Dept. of Natural Resources. "Minnesota State Outline." [ESRI Shapefile]. Created by Minnesota DNR - MIS Bureau, 2007.

Site Location Maps
Minnesota Site 6
STH 65 and Little Fork River
Koochiching County, MN

Project No: 0092-10-10
Map Scale: Varies
Date: June 22, 2011
Map By: JNH
Reviewed By: JAS

State Location

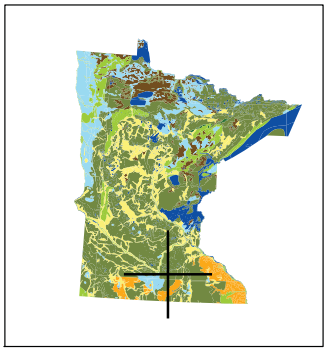

City Location

ESRI Aerial Photo - Scale 1:35,000

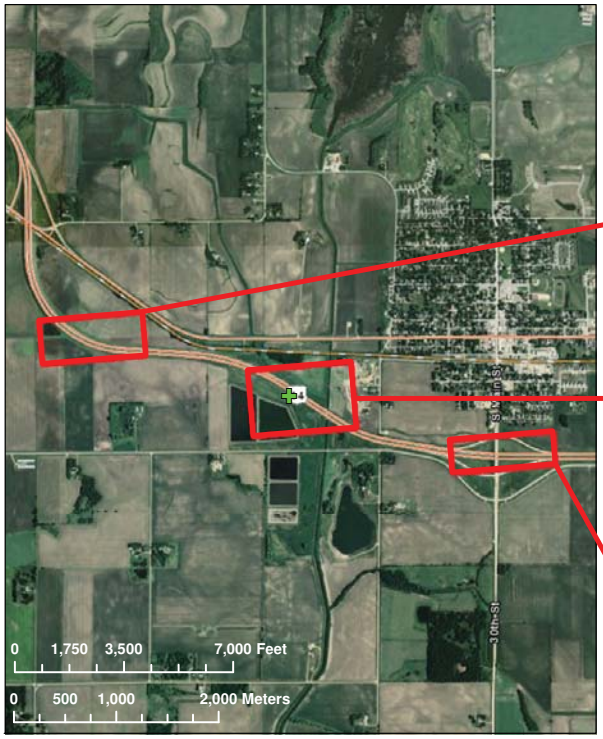

ESRI Aerial Photo - Scale 1:2,000

Description:

The intent of this map is to provide information on the site location and layout of the investigation. Several sources of data were compiled to generate these maps of varying scales. The map scale decreases, area shown decreases, from left to right. Site location is shown from a state level, to city level, to aerial photo and finally a detailed site aerial photo with locations of specific borings conducted for the bridge design.

Source Maps:

DeLorme. Delorme World Basemap [Computer Map]. 1:288,000. [Online Database]. 2009.
ESRI ArcGIS Online, World Imagery [Aerial Photographs]. Visual Scale. http://www.arcgis.com/home/group.html?owner=esri&title=ESRI%20Maps%20and%20Data. (June 25, 2011)
Minnesota Dept. of Natural Resources. "Minnesota State Outline." [ESRI Shapefile]. Created by Minnesota DNR - MIS Bureau, 2007.

Site Location Maps
Minnesota Site 7
USH-14 near Janesville
Waseca County, MN

Project No: 0092-10-10
Map Scale: Varies
Date: June 25, 2011
Map By: JNH
Reviewed By: JAS

State Location

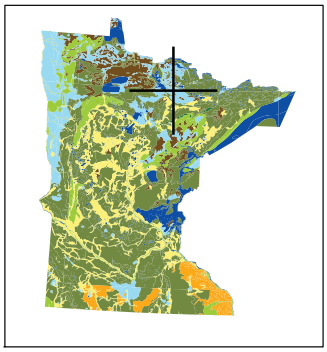

City Location

ESRI Aerial Photo - Scale 1:24,000

ESRI Aerial Photo - Scale 1:8,000

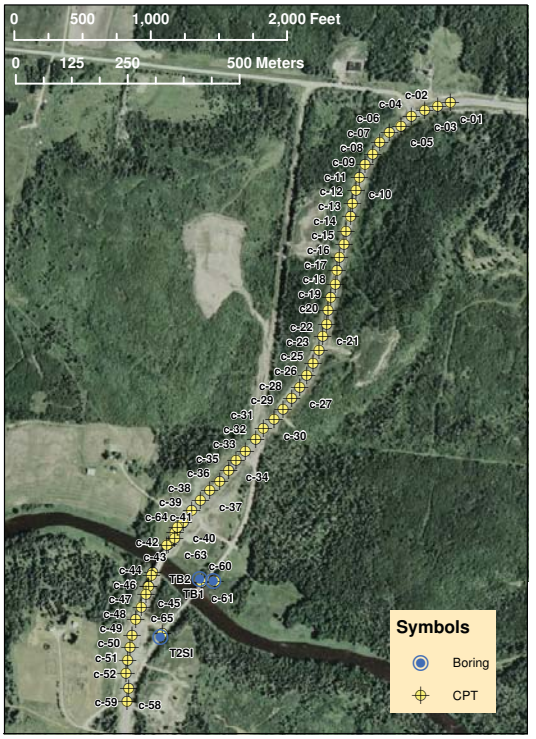

Description:

The intent of this map is to provide information on the site location and layout of the investigation. Several sources of data were compiled to generate these maps of varying scales. The map scale decreases, area shown decreases, from left to right. Site location is shown from a state level, to city level, to aerial photo and finally a detailed site aerial photo with locations of specific borings conducted for the bridge design.

Source Maps:

DeLorme. Delorme World Basemap [Computer Map]. 1:288,000. [Online Database]. 2009.
ESRI ArcGIS Online, World Imagery [Aerial Photographs]. Visual Scale. http://www.arcgis.com/home/group.html?owner=esri&title=ESRI%20Maps%20and%20Data. (July 11, 2011)
Minnesota Dept. of Natural Resources. "Minnesota State Outline." [ESRI Shapefile]. Created by Minnesota DNR - MIS Bureau, 2007.

Site Location Maps
Minnesota Site 8
STH-65 over Little Fork River
Koochiching County, MN

Project No: 0092-10-10
Map Scale: Varies
Date: July 11, 2011
Map By: JNH
Reviewed By: JAS

State Location

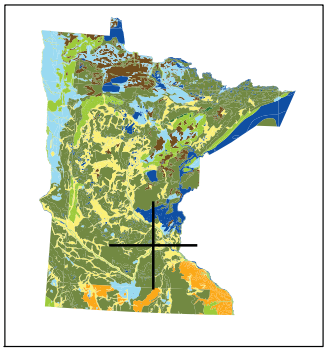

City Location

ESRI Aerial Photo - Scale 1:24,000

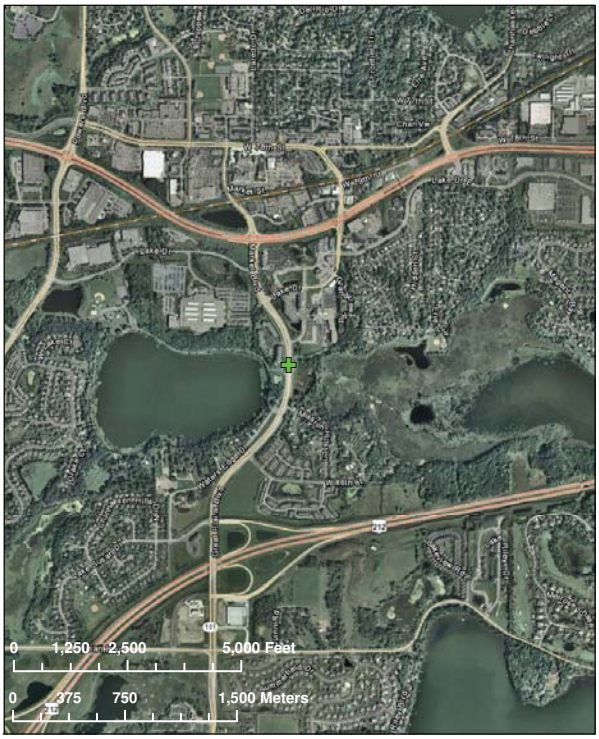

ESRI Aerial Photo - Scale 1:3,000

Description:

The intent of this map is to provide information on the site location and layout of the investigation. Several sources of data were compiled to generate these maps of varying scales. The map scale decreases, area shown decreases, from left to right. Site location is shown from a state level, to city level, to aerial photo and finally a detailed site aerial photo with locations of specific borings conducted for the bridge design.

Source Maps:

DeLorme. Delorme World Basemap [Computer Map]. 1:288,000. [Online Database]. 2009.
ESRI ArcGIS Online, World Imagery [Aerial Photographs]. Visual Scale. http://www.arcgis.com/home/group.html?owner=esri&title=ESRI%20Maps%20and%20Data. (July 11, 2011)
Minnesota Dept. of Natural Resources. "Minnesota State Outline." [ESRI Shapefile]. Created by Minnesota DNR - MIS Bureau, 2007.

Site Location Maps
Minnesota Site 9
STH-101 near Lake Susan
Carver County, MN

Project No: 0092-10-10
Map Scale: Varies
Date: July 11, 2011
Map By: JNH
Reviewed By: JAS

State Location

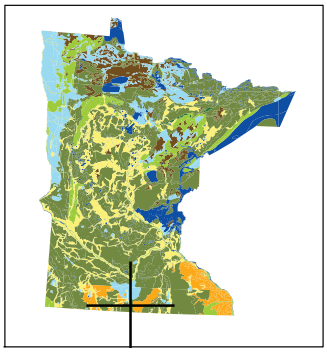

City Location

ESRI Aerial Photo - Scale 1:24,000

ESRI Aerial Photo - Scale 1:2,500

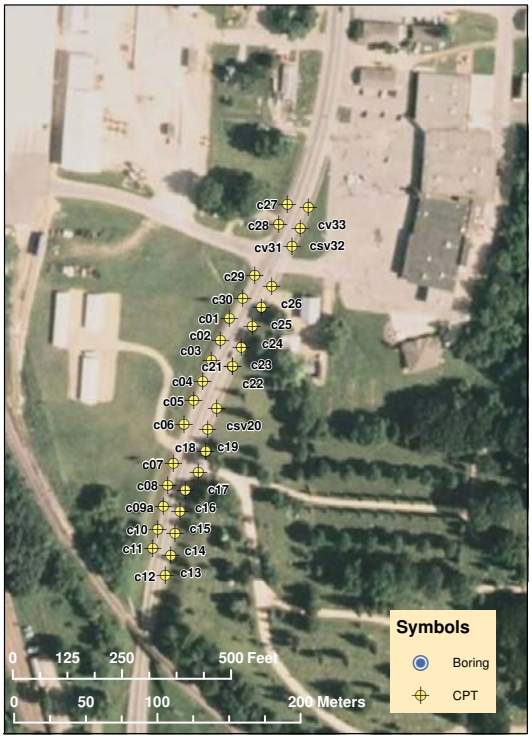

Description:

The intent of this map is to provide information on the site location and layout of the investigation. Several sources of data were compiled to generate these maps of varying scales. The map scale decreases, area shown decreases, from left to right. Site location is shown from a state level, to city level, to aerial photo and finally a detailed site aerial photo with locations of specific borings conducted for the bridge design.

Source Maps:

DeLorme. Delorme World Basemap [Computer Map]. 1:288,000. [Online Database]. 2009.
ESRI ArcGIS Online, World Imagery [Aerial Photographs]. Visual Scale. http://www.arcgis.com/home/group.html?owner=esri&title=ESRI%20Maps%20and%20Data. (July 11, 2011)
Minnesota Dept. of Natural Resources. "Minnesota State Outline." [ESRI Shapefile]. Created by Minnesota DNR - MIS Bureau, 2007.

Site Location Maps
Minnesota Site 10
USH-169 in Blue Earth City
Faribault County, MN

Project No: 0092-10-10
Map Scale: Varies
Date: July 11, 2011
Map By: JNH
Reviewed By: JAS

State Location

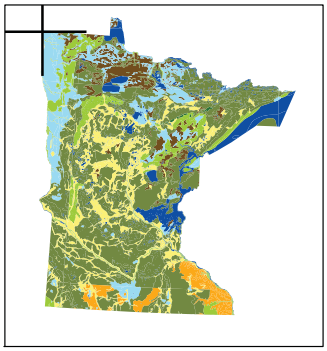

City Location

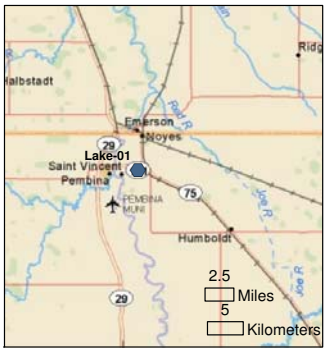

ESRI Aerial Photo - Scale 1:24,000

ESRI Aerial Photo - Scale 1:2,000

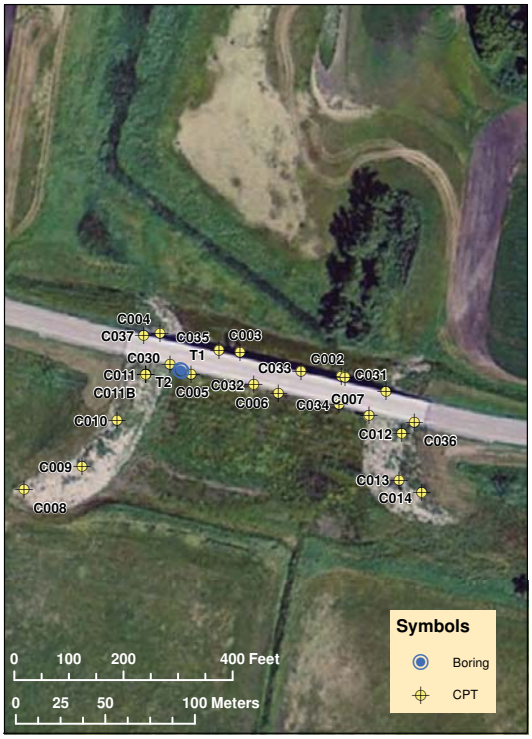

Description:

The intent of this map is to provide information on the site location and layout of the investigation. Several sources of data were compiled to generate these maps of varying scales. The map scale decreases, area shown decreases, from left to right. Site location is shown from a state level, to city level, to aerial photo and finally a detailed site aerial photo with locations of specific borings conducted for the bridge design.

Source Maps:

DeLorme. Delorme World Basemap [Computer Map]. 1:288,000. [Online Database]. 2009.
ESRI ArcGIS Online, World Imagery [Aerial Photographs]. Visual Scale. http://www.arcgis.com/home/group.html?owner=esri&title=ESRI%20Maps%20and%20Data. (July 7, 2011)
Minnesota Dept. of Natural Resources. "Minnesota State Outline." [ESRI Shapefile]. Created by Minnesota DNR - MIS Bureau, 2007.

Site Location Maps
Minnesota Site 11
STH 171 near the Red River
Kittson County, MN

Project No: 0092-10-10
Map Scale: Varies
Date: July 7, 2011
Map By: JNH
Reviewed By: JAS

State Location

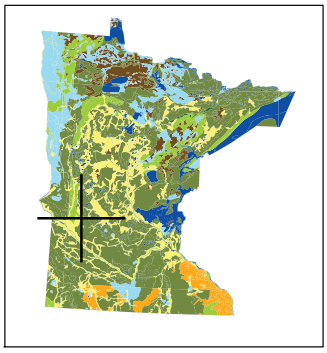

City Location

ESRI Aerial Photo - Scale 1:24,000

ESRI Aerial Photo - Scale 1:2,000

Description:

The intent of this map is to provide information on the site location and layout of the investigation. Several sources of data were compiled to generate these maps of varying scales. The map scale decreases, area shown decreases, from left to right. Site location is shown from a state level, to city level, to aerial photo and finally a detailed site aerial photo with locations of specific borings conducted for the bridge design.

Source Maps:

DeLorme. Delorme World Basemap [Computer Map]. 1:288,000. [Online Database]. 2009.
ESRI ArcGIS Online, World Imagery [Aerial Photographs]. Visual Scale. http://www.arcgis.com/home/group.html?owner=esri&title=ESRI%20Maps%20and%20Data. (July 7, 2011)
Minnesota Dept. of Natural Resources. "Minnesota State Outline." [ESRI Shapefile]. Created by Minnesota DNR - MIS Bureau, 2007.

Site Location Maps
Minnesota Site 12
STH-9 on Chippewa River
Swift County, MN

Project No: 0092-10-10
Map Scale: Varies
Date: July 7, 2011
Map By: JNH
Reviewed By: JAS

State Location

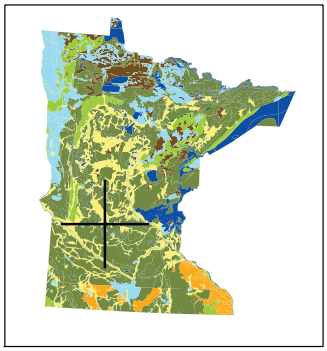

City Location

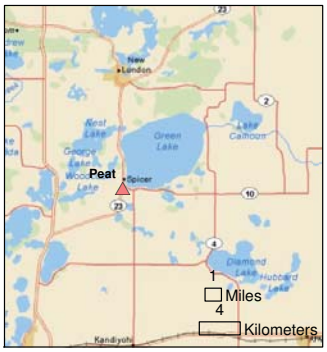

ESRI Aerial Photo - Scale 1:24,000

ESRI Aerial Photo - Scale 1:2,500

Description:

The intent of this map is to provide information on the site location and layout of the investigation. Several sources of data were compiled to generate these maps of varying scales. The map scale decreases, area shown decreases, from left to right. Site location is shown from a state level, to city level, to aerial photo and finally a detailed site aerial photo with locations of specific borings conducted for the bridge design.

Source Maps:

DeLorme. Delorme World Basemap [Computer Map]. 1:288,000. [Online Database]. 2009.
ESRI ArcGIS Online, World Imagery [Aerial Photographs]. Visual Scale. http://www.arcgis.com/home/group.html?owner=esri&title=ESRI%20Maps%20and%20Data. (July 11, 2011)
Minnesota Dept. of Natural Resources. "Minnesota State Outline." [ESRI Shapefile]. Created by Minnesota DNR - MIS Bureau, 2007.

Site Location Maps
Minnesota Site 13
STH-23 Near Spicer
Kandiyohi County, MN

Project No: 0092-10-10
Map Scale: Varies
Date: July 11, 2011
Map By: JNH
Reviewed By: JAS

State Location

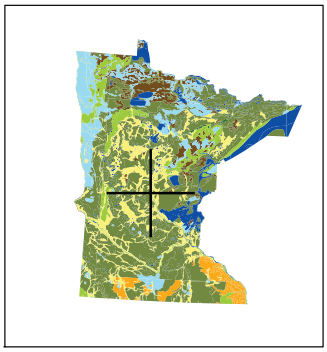

City Location

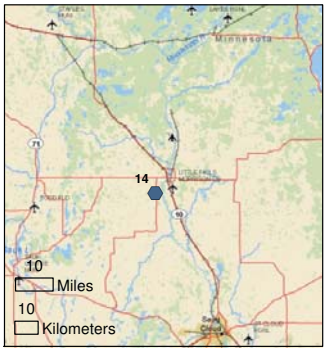

ESRI Aerial Photo - Scale 1:24,000

ESRI Aerial Photo - Scale 1:2,000

Description:

The intent of this map is to provide information on the site location and layout of the investigation. Several sources of data were compiled to generate these maps of varying scales. The map scale decreases, area shown decreases, from left to right. Site location is shown from a state level, to city level, to aerial photo and finally a detailed site aerial photo with locations of specific borings conducted for the bridge design.

Source Maps:

DeLorme. Delorme World Basemap [Computer Map]. 1:288,000. [Online Database]. 2009.
ESRI ArcGIS Online, World Imagery [Aerial Photographs]. Visual Scale. http://www.arcgis.com/home/group.html?owner=esri&title=ESRI%20Maps%20and%20Data. (June 22, 2011)
Minnesota Dept. of Natural Resources. "Minnesota State Outline." [ESRI Shapefile]. Created by Minnesota DNR - MIS Bureau, 2007.

Site Location Maps
Minnesota Site 14
Swan River and STH 238
Morrison County, MN

Project No: 0092-10-10
Map Scale: Varies
Date: June 22, 2011
Map By: JNH
Reviewed By: JAS

State Location

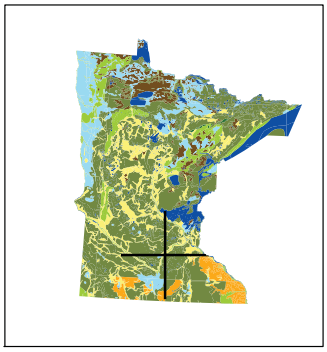

City Location

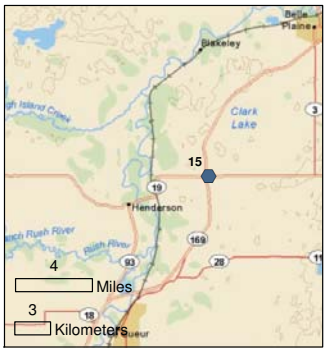

ESRI Aerial Photo - Scale 1:24,000

ESRI Aerial Photo - Scale 1:2,000

Description:

The intent of this map is to provide information on the site location and layout of the investigation. Several sources of data were compiled to generate these maps of varying scales. The map scale decreases, area shown decreases, from left to right. Site location is shown from a state level, to city level, to aerial photo and finally a detailed site aerial photo with locations of specific borings conducted for the bridge design.

Source Maps:

DeLorme. Delorme World Basemap [Computer Map]. 1:288,000. [Online Database]. 2009.
ESRI ArcGIS Online, World Imagery [Aerial Photographs]. Visual Scale. http://www.arcgis.com/home/group.html?owner=esri&title=ESRI%20Maps%20and%20Data. (June 22, 2011)
Minnesota Dept. of Natural Resources. "Minnesota State Outline." [ESRI Shapefile]. Created by Minnesota DNR - MIS Bureau, 2007.

Site Location Maps
Minnesota Site 15
USH 169 & STH 19
LeSueur County, MN

Project No: 0092-10-10
Map Scale: Varies
Date: June 22, 2011
Map By: JNH
Reviewed By: JAS

State Location

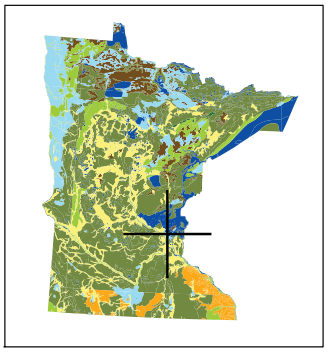

City Location

ESRI Aerial Photo - Scale 1:24,000

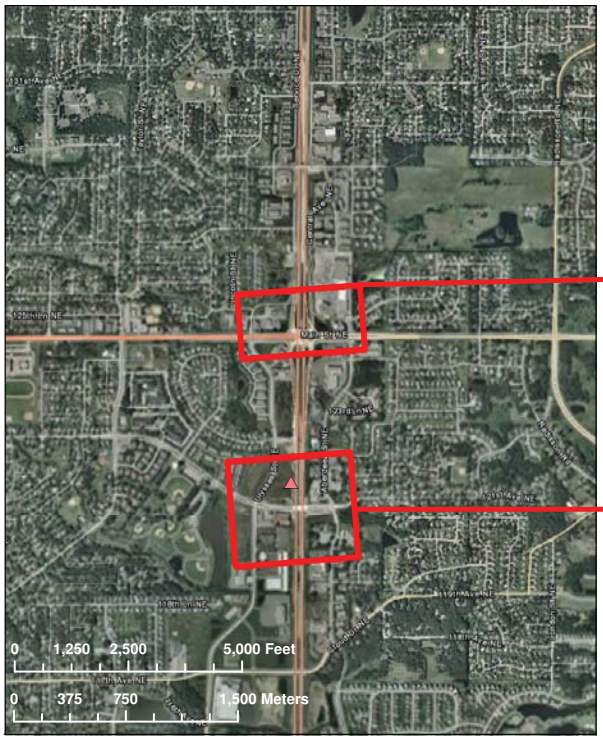

ESRI Aerial Photo - Scale 1:4,000

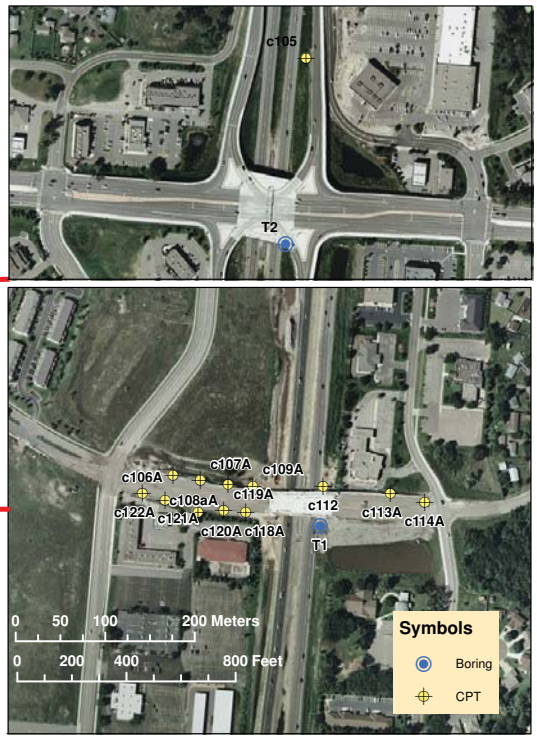

Description:

The intent of this map is to provide information on the site location and layout of the investigation. Several sources of data were compiled to generate these maps of varying scales. The map scale decreases, area shown decreases, from left to right. Site location is shown from a state level, to city level, to aerial photo and finally a detailed site aerial photo with locations of specific borings conducted for the bridge design.

Source Maps:

DeLorme. Delorme World Basemap [Computer Map]. 1:288,000. [Online Database]. 2009.
ESRI ArcGIS Online, World Imagery [Aerial Photographs]. Visual Scale. http://www.arcgis.com/home/group.html?owner=esri&title=ESRI%20Maps%20and%20Data. (June 30, 2011)
Minnesota Dept. of Natural Resources. "Minnesota State Outline." [ESRI Shapefile]. Created by Minnesota DNR - MIS Bureau, 2007.

Site Location Maps
Minnesota Site 16
STH 65 at Johnsville
Anoka County, MN

Project No: 0092-10-10
Map Scale: Varies
Date: June 30, 2011
Map By: JNH
Reviewed By: JAS

State Location

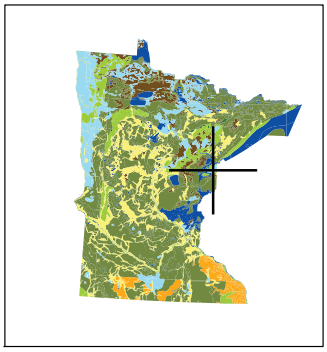

City Location

ESRI Aerial Photo - Scale 1:24,000

ESRI Aerial Photo - Scale 1:2,500

Description:

The intent of this map is to provide information on the site location and layout of the investigation. Several sources of data were compiled to generate these maps of varying scales. The map scale decreases, area shown decreases, from left to right. Site location is shown from a state level, to city level, to aerial photo and finally a detailed site aerial photo with locations of specific borings conducted for the bridge design.

Source Maps:

DeLorme. Delorme World Basemap [Computer Map]. 1:288,000. [Online Database]. 2009.
ESRI ArcGIS Online, World Imagery [Aerial Photographs]. Visual Scale. http://www.arcgis.com/home/group.html?owner=esri&title=ESRI%20Maps%20and%20Data. (July 7, 2011)
Minnesota Dept. of Natural Resources. "Minnesota State Outline." [ESRI Shapefile]. Created by Minnesota DNR - MIS Bureau, 2007.

Site Location Maps
Minnesota Site 17
STH 23 & S. Fork Nemadji River
Carlton County, MN

Project No: 0092-10-10
Map Scale: Varies
Date: July 7, 2011
Map By: JNH
Reviewed By: JAS

State Location

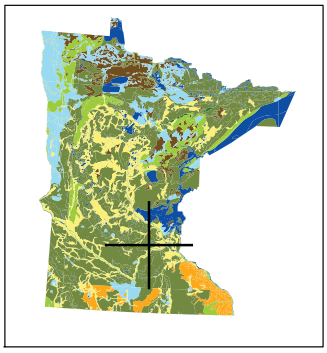

City Location

ESRI Aerial Photo - Scale 1:24,000

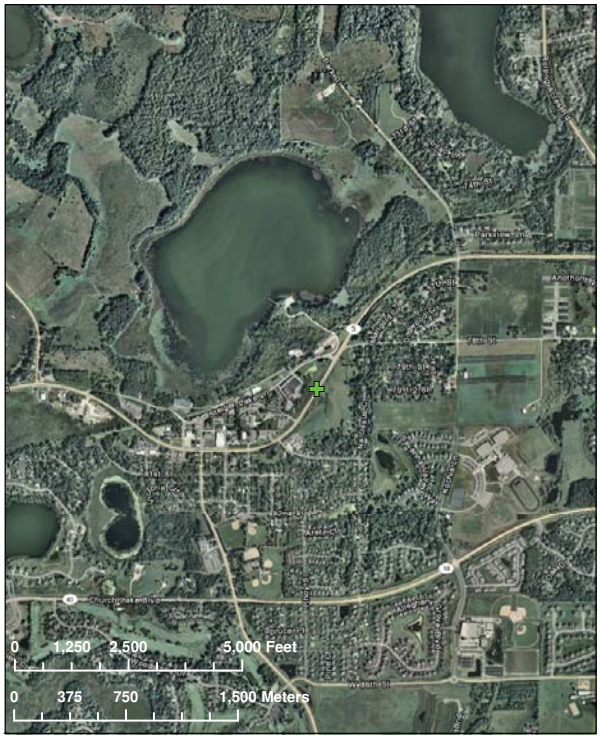

ESRI Aerial Photo - Scale 1:2,500

Description:

The intent of this map is to provide information on the site location and layout of the investigation. Several sources of data were compiled to generate these maps of varying scales. The map scale decreases, area shown decreases, from left to right. Site location is shown from a state level, to city level, to aerial photo and finally a detailed site aerial photo with locations of specific borings conducted for the bridge design.

Source Maps:

DeLorme. Delorme World Basemap [Computer Map]. 1:288,000. [Online Database]. 2009.
ESRI ArcGIS Online, World Imagery [Aerial Photographs]. Visual Scale. http://www.arcgis.com/home/group.html?owner=esri&title=ESRI%20Maps%20and%20Data. (July 7, 2011)
Minnesota Dept. of Natural Resources. "Minnesota State Outline." [ESRI Shapefile]. Created by Minnesota DNR - MIS Bureau, 2007.

Site Location Maps
Minnesota Site 18
STH 5 in Victoria
Carver County, MN

Project No: 0092-10-10
Map Scale: Varies
Date: July 7, 2011
Map By: JNH
Reviewed By: JAS

State Location

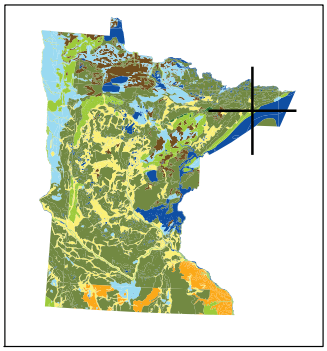

City Location

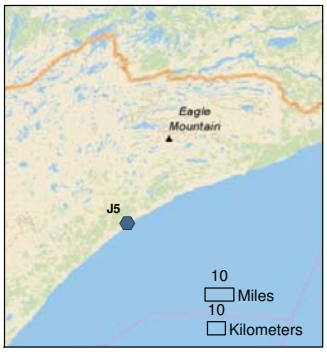

ESRI Aerial Photo - Scale 1:24,000

ESRI Aerial Photo - Scale 1:700

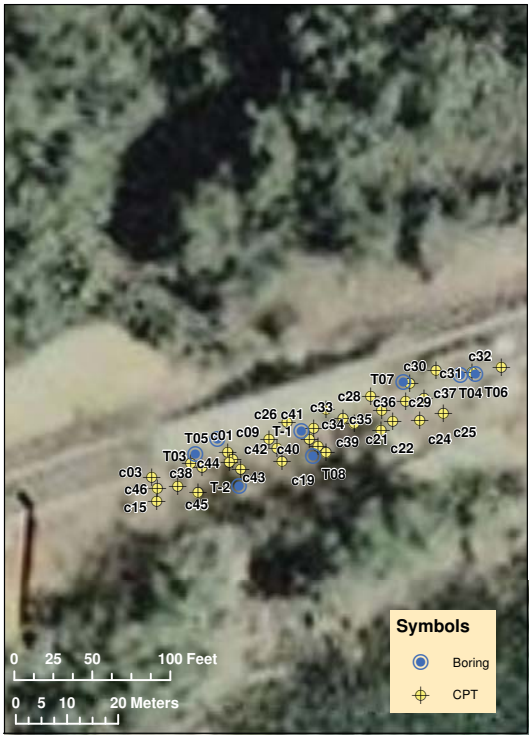

Description:

The intent of this map is to provide information on the site location and layout of the investigation. Several sources of data were compiled to generate these maps of varying scales. The map scale decreases, area shown decreases, from left to right. Site location is shown from a state level, to city level, to aerial photo and finally a detailed site aerial photo with locations of specific borings conducted for the bridge design.

Source Maps:

DeLorme. Delorme World Basemap [Computer Map]. 1:288,000. [Online Database]. 2009.
ESRI ArcGIS Online, World Imagery [Aerial Photographs]. Visual Scale. http://www.arcgis.com/home/group.html?owner=esri&title=ESRI%20Maps%20and%20Data. (July 7, 2011)
Minnesota Dept. of Natural Resources. "Minnesota State Outline." [ESRI Shapefile]. Created by Minnesota DNR - MIS Bureau, 2007.

Site Location Maps
Minnesota Site 19
USH 61 & Onion River
Cook County, MN

Project No: 0092-10-10
Map Scale: Varies
Date: July 7, 2011
Map By: JNH
Reviewed By: JAS

State Location

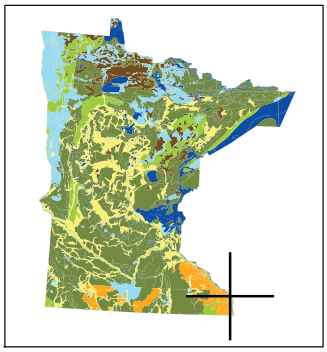

City Location

ESRI Aerial Photo - Scale 1:24,000

ESRI Aerial Photo - Scale 1:3,000

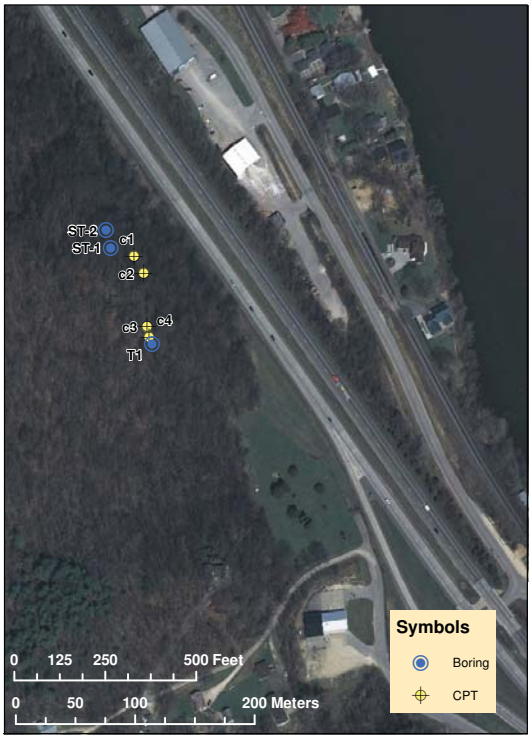

Description:

The intent of this map is to provide information on the site location and layout of the investigation. Several sources of data were compiled to generate these maps of varying scales. The map scale decreases, area shown decreases, from left to right. Site location is shown from a state level, to city level, to aerial photo and finally a detailed site aerial photo with locations of specific borings conducted for the bridge design.

Source Maps:

DeLorme. Delorme World Basemap [Computer Map]. 1:288,000. [Online Database]. 2009.
ESRI ArcGIS Online, World Imagery [Aerial Photographs]. Visual Scale. http://www.arcgis.com/home/group.html?owner=esri&title=ESRI%20Maps%20and%20Data. (July 7, 2011)
Minnesota Dept. of Natural Resources. "Minnesota State Outline." [ESRI Shapefile]. Created by Minnesota DNR - MIS Bureau, 2007.

Site Location Maps
Minnesota Site 20
IH-90 near Dakota
Winona County, MN

Project No: 0092-10-10
Map Scale: Varies
Date: July 7, 2011
Map By: JNH
Reviewed By: JAS

State Location

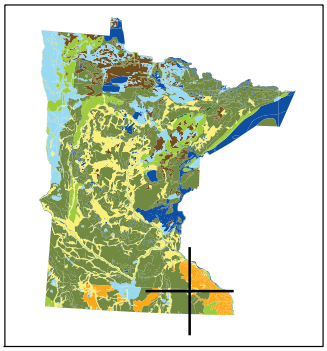

City Location

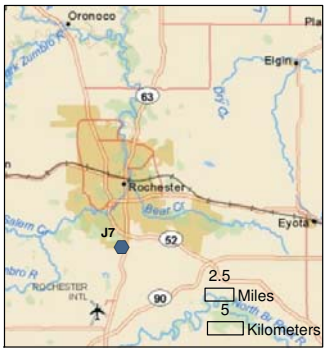

ESRI Aerial Photo - Scale 1:24,000

ESRI Aerial Photo - Scale 1:5,000

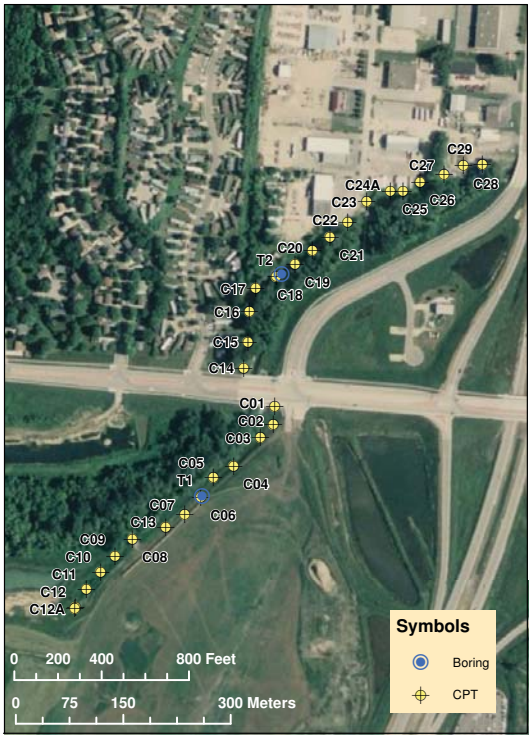

Description:

The intent of this map is to provide information on the site location and layout of the investigation. Several sources of data were compiled to generate these maps of varying scales. The map scale decreases, area shown decreases, from left to right. Site location is shown from a state level, to city level, to aerial photo and finally a detailed site aerial photo with locations of specific borings conducted for the bridge design.

Source Maps:

DeLorme. Delorme World Basemap [Computer Map]. 1:288,000. [Online Database]. 2009.
ESRI ArcGIS Online, World Imagery [Aerial Photographs]. Visual Scale. http://www.arcgis.com/home/group.html?owner=esri&title=ESRI%20Maps%20and%20Data. (July 7, 2011)
Minnesota Dept. of Natural Resources. "Minnesota State Outline." [ESRI Shapefile]. Created by Minnesota DNR - MIS Bureau, 2007.

Site Location Maps
Minnesota Site 21
USH 63 near Rochester
Olmsted County, MN

Project No: 0092-10-10
Map Scale: Varies
Date: July 7, 2011
Map By: JNH
Reviewed By: JAS

State Location

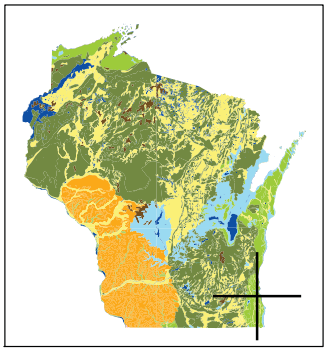

City Location

ESRI Aerial Photo - Scale 1:24,000

ESRI Aerial Photo - Scale 1:15,000

Description:

The intent of this map is to provide information on the site location and layout of the investigation. Several sources of data were compiled to generate these maps of varying scales. The map scale decreases, area shown decreases, from left to right. Site location is shown from a state level, to city level, to aerial photo and finally a detailed site aerial photo with locations of specific borings conducted for the site investigation.

Source Maps:

DeLorme. Delorme World Basemap [Computer Map]. 1:288,000. [Online Database]. 2009.
ESRI ArcGIS Online, World Imagery [Aerial Photographs]. Visual Scale. http://www.arcgis.com/home/group.html?owner=esri&title=ESRI%20Maps%20and%20Data. (August 9, 2011)
United States Geological Survey. "April 2007 Color Orthoimagery – Madison, WI" [aerial photographs]. USGS, 2007. Accessed online http://seamless.usgs.gov/ (August 9, 2011).
Wisconsin Dept. of Natural Resources. "Wisconsin State Outline." [ESRI Shapefile]. Created by U. S. Census Bureau, 2008.

Site Location Maps
Mitchell Interchange
Milwaukee County

Project No: 0092-10-10
Map Scale: Varies
Date: August 9, 2011
Map By: JNH
Reviewed By: JAS

State Location

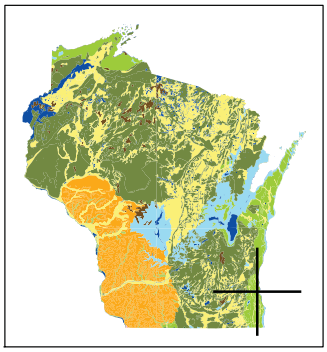

City Location

ESRI Aerial Photo - Scale 1:30,000

ESRI Aerial Photo - Scale 1:15,000

Description:

The intent of this map is to provide information on the site location and layout of the investigation. Several sources of data were compiled to generate these maps of varying scales. The map scale decreases, area shown decreases, from left to right. Site location is shown from a state level, to city level, to aerial photo and finally a detailed site aerial photo with locations of specific borings conducted for the site investigation.

Source Maps:

DeLorme. Delorme World Basemap [Computer Map]. 1:288,000. [Online Database]. 2009.
ESRI ArcGIS Online, World Imagery [Aerial Photographs]. Visual Scale. http://www.arcgis.com/home/group.html?owner=esri&title=ESRI%20Maps%20and%20Data. (August 9, 2011)
United States Geological Survey. "April 2007 Color Orthoimagery – Madison, WI" [aerial photographs]. USGS, 2007. Accessed online http://seamless.usgs.gov/ (August 9, 2011).
Wisconsin Dept. of Natural Resources. "Wisconsin State Outline." [ESRI Shapefile]. Created by U. S. Census Bureau, 2008.

Site Location Maps
Marquette Interchange
Milwaukee County

Project No: 0092-10-10
Map Scale: Varies
Date: August 9, 2011
Map By: JNH
Reviewed By: JAS

Appendix 2

Cone penetration tests completed during this study

State Location

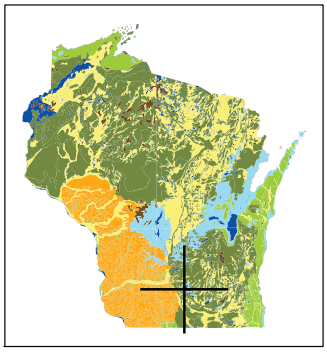

City Location

ESRI Aerial Photo - Scale 1:24,000

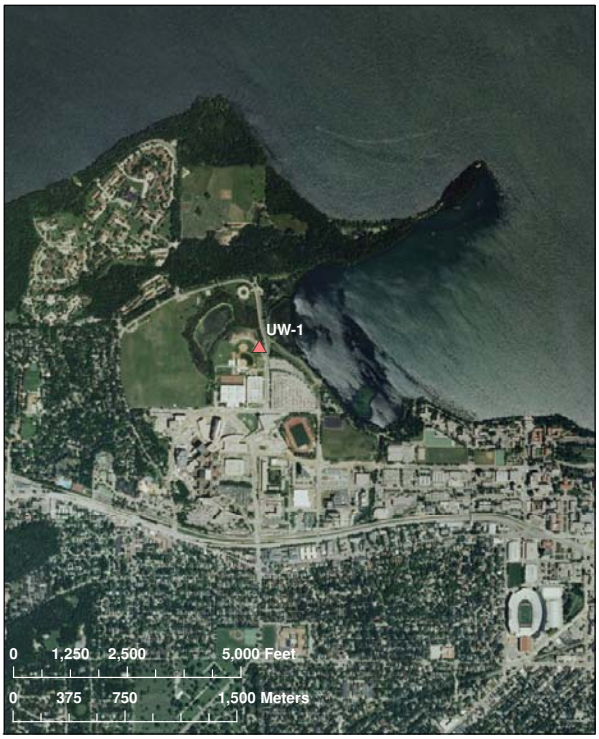

Madison Orthoimagery (April 2007) - Scale 1:1,000

Description:

The intent of this map is to provide information on the site location and layout of the investigation. Several sources of data were compiled to generate these maps of varying scales. The map scale decreases, area shown decreases, from left to right. Site location is shown from a state level, to city level, to aerial photo and finally a detailed site aerial photo with locations of specific borings conducted for the site investigation.

Source Maps:

DeLorme. Delorme World Basemap [Computer Map]. 1:288,000. [Online Database]. 2009.
ESRI ArcGIS Online, World Imagery [Aerial Photographs]. Visual Scale. http://www.arcgis.com/home/group.html?owner=esri&title=ESRI%20Maps%20and%20Data. (August 25, 2010)
United States Geological Survey. "April 2007 Color Orthoimagery – Madison, WI" [aerial photographs]. USGS, 2007. Accessed online http://seamless.usgs.gov/ (August 25, 2010).
Wisconsin Dept. of Natural Resources. "Wisconsin State Outline." [ESRI Shapefile]. Created by U. S. Census Bureau, 2008.

Site Location Maps
WHRP Site UW-1
Madison, Dane County

Project No: 0092-10-10
Map Scale: Varies
Date: August 25, 2010
Map By: JNH
Reviewed By: JAS

College of Engineering
UNIVERSITY OF WISCONSIN-MADISON

Site: UW-1
Description: Observatory Drive - 1918 Marsh
Boring Date: 7/8/2010

Sounding: SCPTU2-01
Date: 7/20/2010
Operator: James S. and Finn H.

Baseline Zero Shifts (%)

q_t	f_s	u_2
11.1	4.0	1.0

Termination Depth: 92.4 Feet
Total Dissipations: 27
Dissipation Time: 87 minutes

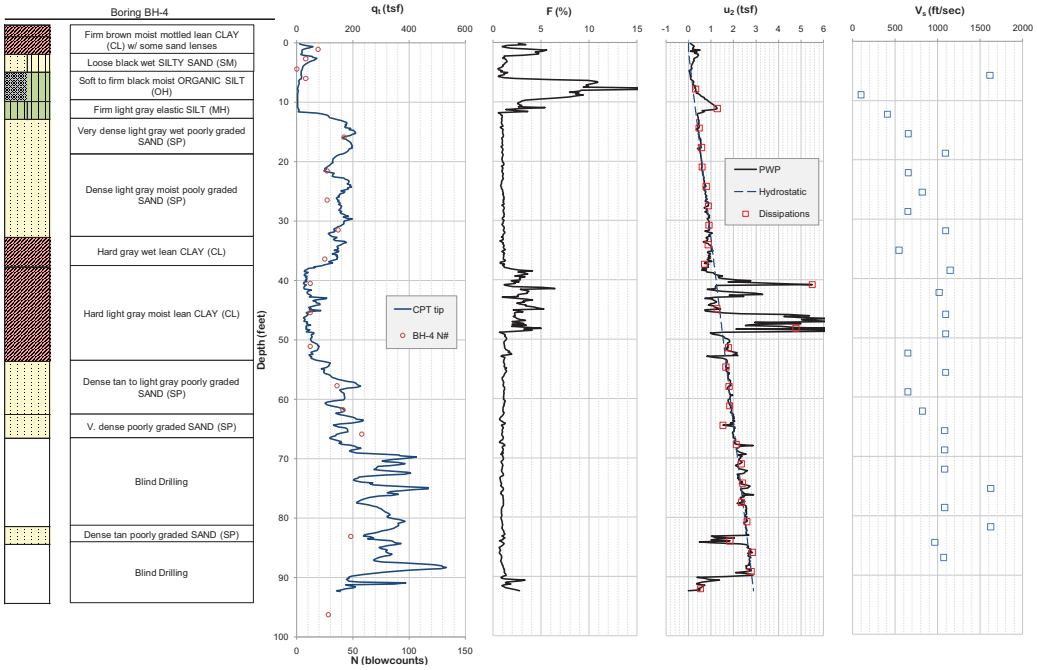

College of Engineering
UNIVERSITY OF WISCONSIN-MADISON

Site: UW-1
Description: Observatory Drive - 1918 Marsh
Boring Date: 7/8/2010

Sounding: SCPTU2-02
Date: 7/21/2010
Operator: James S.

Baseline Zero Shifts (%)

q_t	f_s	u_2
0.0	3.2	3.9

Termination Depth: 90.6 Feet
Total Dissipations: 27
Dissipation Time: 87 minutes

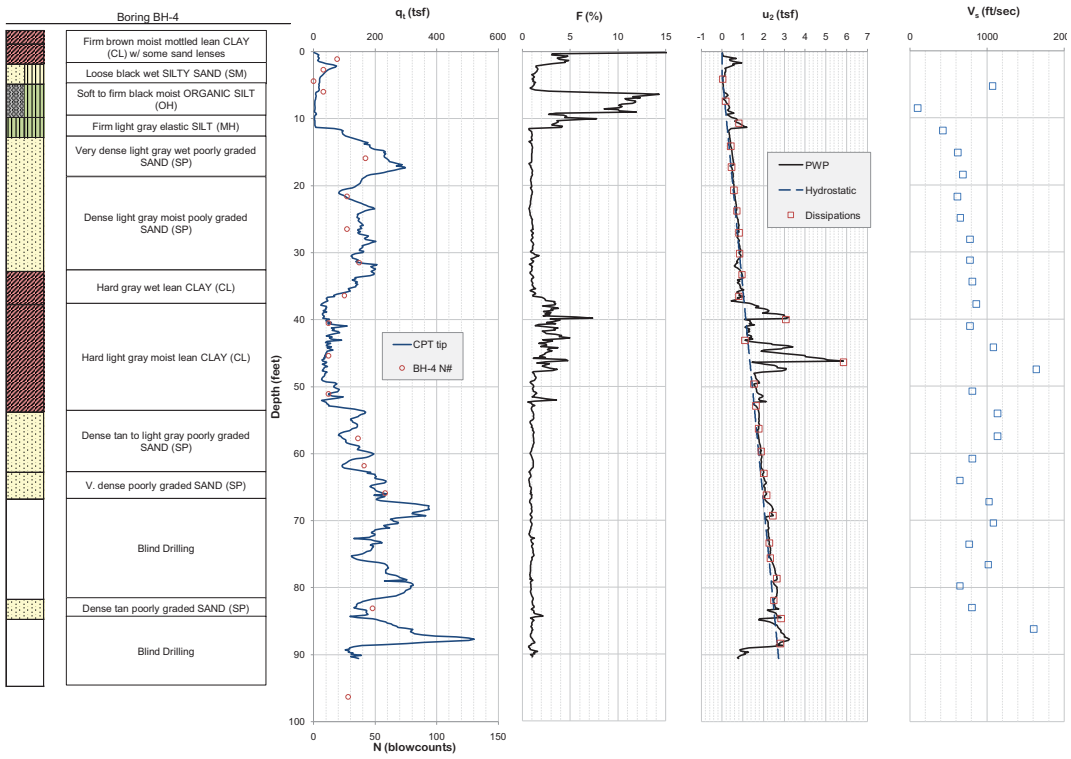

College of Engineering
UNIVERSITY OF WISCONSIN-MADISON

Site: UW-1
Description: Observatory Drive - 1918 Marsh
Boring Date: 7/8/2010

Sounding: CPTU2-03
Date: 7/21/2010
Operator: James S.

Baseline Zero Shifts (%)

q_t	f_s	u_2
17.9	1.9	3.4

Advance Rate: 100 mm/s

Termination Depth: 51.6 Feet
Total Dissipations: 18
Dissipation Time: 76 Minutes

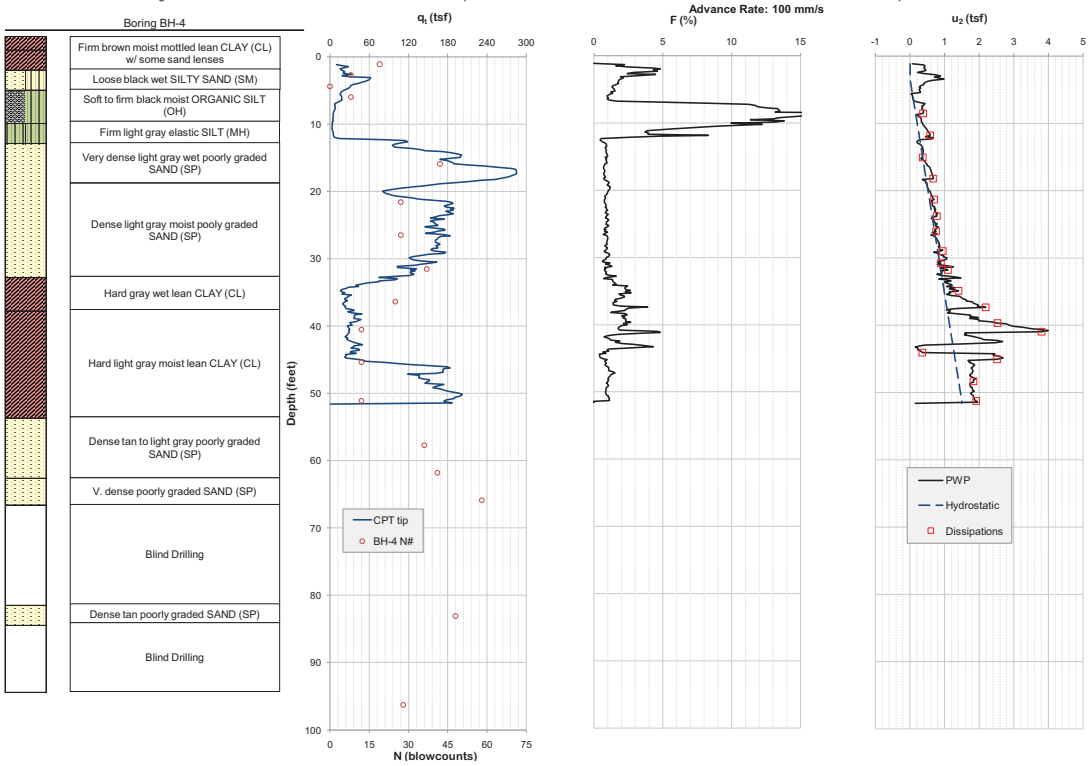

College of Engineering
UNIVERSITY OF WISCONSIN-MADISON

Site: UW-1
Description: Observatory Drive - 1918 Marsh
Boring Date: 7/8/2010

Sounding: CPTU2-04
Date: 7/25/2010
Operator: James S.

Baseline Zero Shifts (%)

q_t	f_s	u_2
-5.0	1.3	3.0

Termination Depth: 43.7 Feet
Total Dissipations: 14
Dissipation Time: 441 minutes

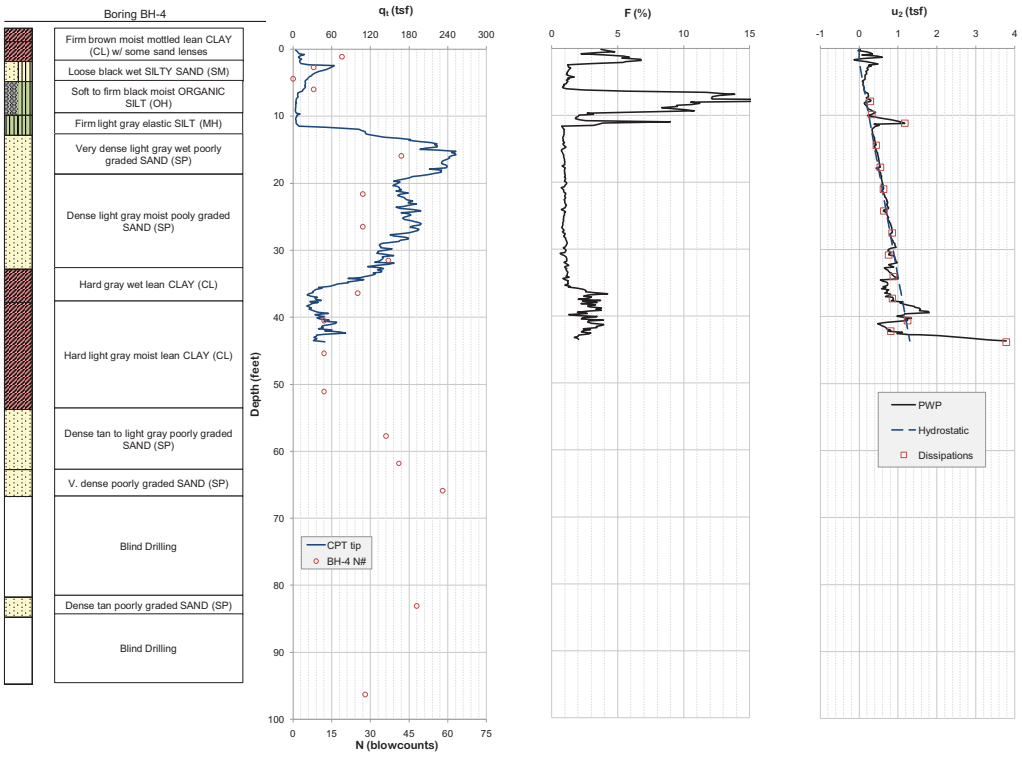

College of Engineering
UNIVERSITY OF WISCONSIN-MADISON

Site: UW-1
Description: Observatory Drive - 1918 Marsh
Boring Date: 7/8/2010

Sounding: CPTU1-05
Date: 7/26/2010
Operator: Finn H.

Baseline Zero Shifts (%)

q_t	f_s	u_2
-10.6	-6.0	-1.3

Termination Depth: 13.1 Feet
Total Dissipations: 5
Dissipation Time: 188 minutes

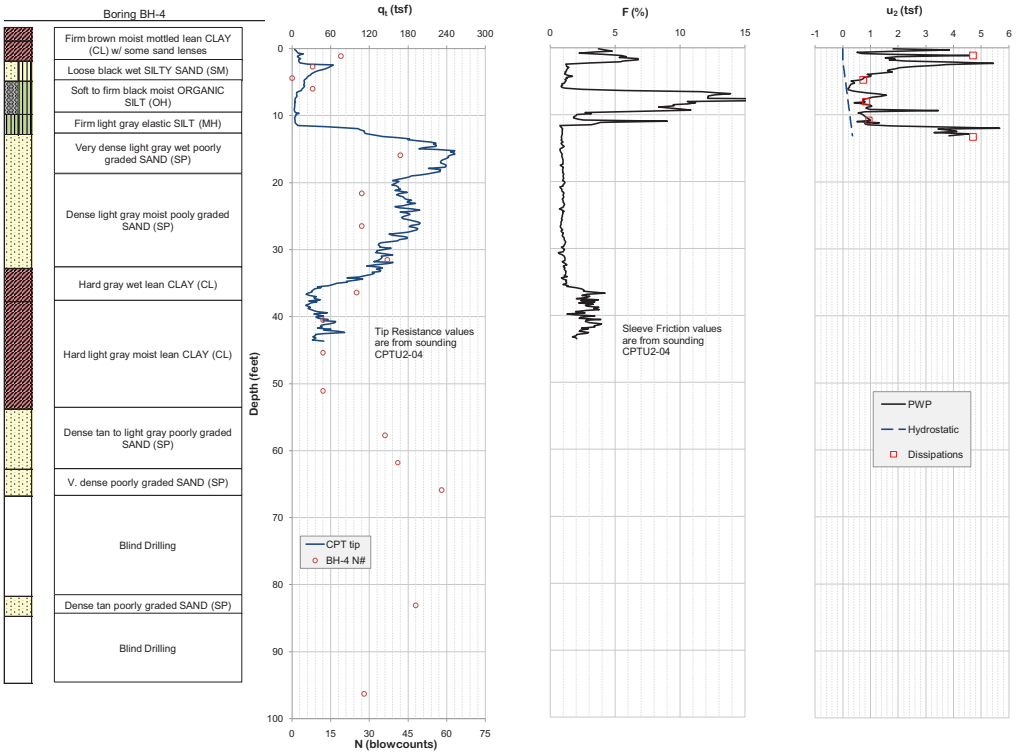

State Location

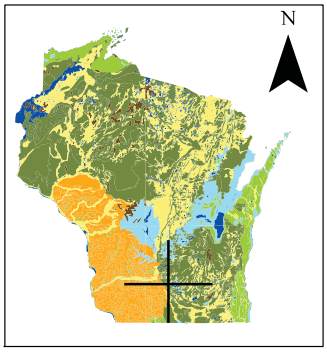

City Location

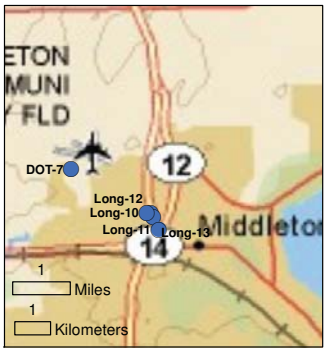

ESRI Aerial Photo - Scale 1:24,000

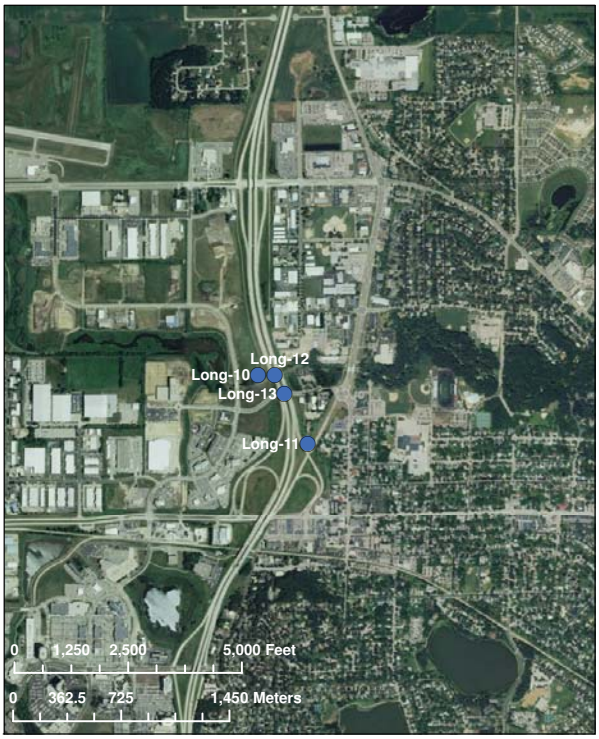

Madison Orthoimagery (July 2005) - Scale 1:700

Description:

The intent of this map is to provide information on the site location and layout of the investigation. Several sources of data were compiled to generate these maps of varying scales. The map scale decreases, area shown decreases, from left to right. Site location is shown from a state level, to city level, to aerial photo and finally a detailed site aerial photo with locations of specific borings conducted for the bridge design.

Source Maps:

DeLorme. Delorme World Basemap [Computer Map]. 1:288,000. [Online Database]. 2009.
ESRI ArcGIS Online, World Imagery [Aerial Photographs]. Visual Scale. http://www.arcgis.com/home/group.html?owner=esri&title=ESRI%20Maps%20and%20Data. (August 17, 2010)
United States Geological Survey. "July 2007 Color Orthoimagery – Madison, WI" [aerial photographs]. USGS, 2007. Accessed online http://seamless.usgs.gov/ [8/17/2010].
Wisconsin Dept. of Natural Resources. "Wisconsin State Outline." [ESRI Shapefile]. Created by U. S. Census Bureau, 2008.

Site Location Maps
WHRP Site Long-10
Middleton, Dane County

Project No: 5300-03-78
Map Scale: Varies
Date: June 10, 2011
Map By: EMM
Reviewed By: JAS

College of Engineering
UNIVERSITY OF WISCONSIN-MADISON

Site: Long-10
Description: Pedestrian Bridge & Pheasant Branch Crk.
Boring Date: Feb. - Mar. 2000

Sounding: CPTU2-03
Date: 10/5/2010
Operator: Finn H., Elliott M. & James S.

Baseline Zero Shifts (%)

q_t	f_s	u_2
17.9	1.9	3.4

Termination Depth: 88.7 Feet
Total Dissipations: 23
Dissipation Time: 130 Minutes

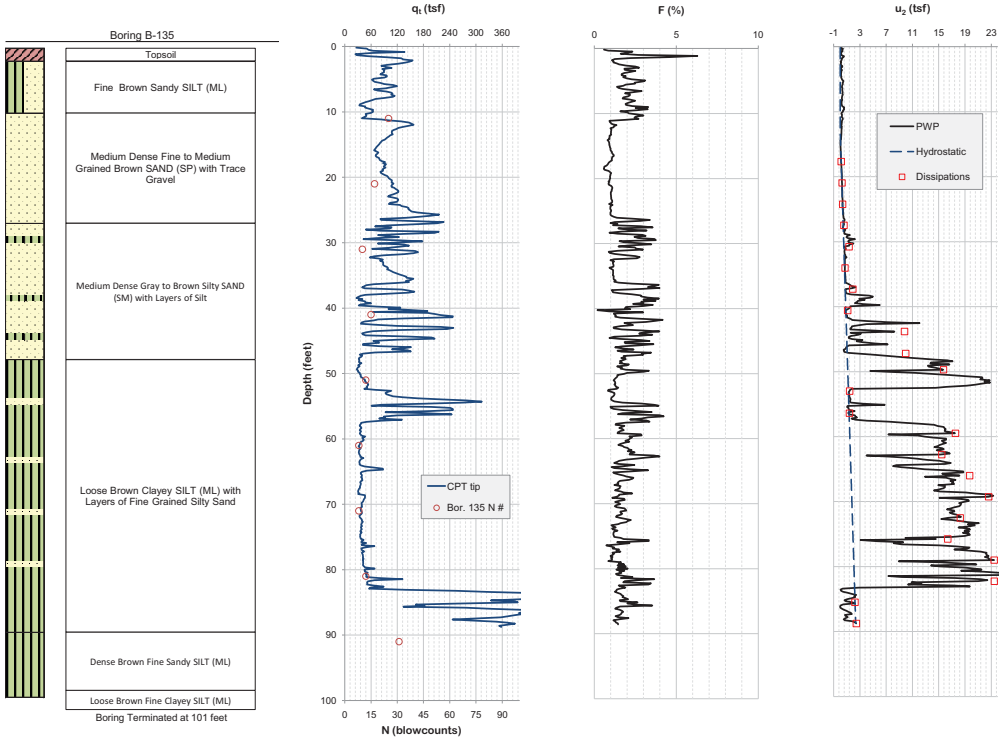

College of Engineering
UNIVERSITY OF WISCONSIN-MADISON

Site: Long-10
Description: Pedestrian Bridge & Pheasant Branch Crk.
Boring Date: Feb. - Mar. 2000

Sounding: CPTU2-04
Date: 6/7/2011
Operator: Seth S. & Finn H.

Baseline Zero Shifts (%)

q_t	f_s	u_2
N/A	N/A	N/A

Termination Depth: 26.5 Feet
Total Dissipations: 0
Dissipation Time: 0

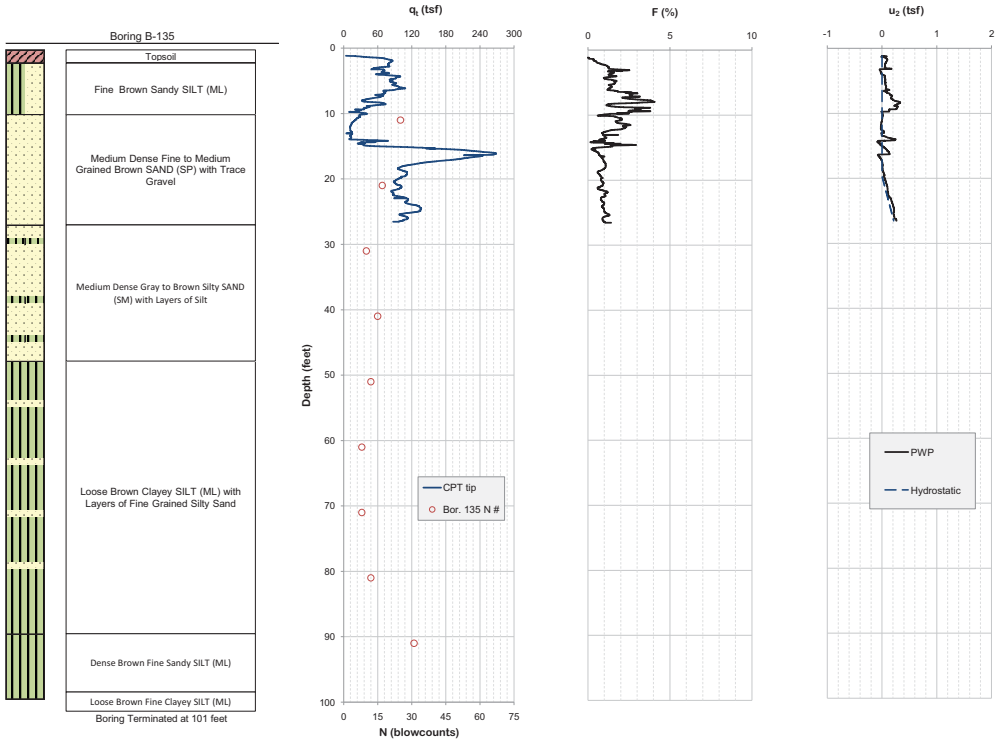

College of Engineering
UNIVERSITY OF WISCONSIN-MADISON

Site: Long-10
Description: Pedestrian Bridge & Pheasant Branch Crk.
Boring Date: Feb. - Mar. 2000

Sounding: CPTU2-05
Date: 6/7/2011
Operator: Seth S. & Finn H.

Baseline Zero Shifts (%)

q_t	f_s	u_2
N/A	N/A	N/A

Termination Depth: 26.5 Feet
Total Dissipations: 0
Dissipation Time: 0

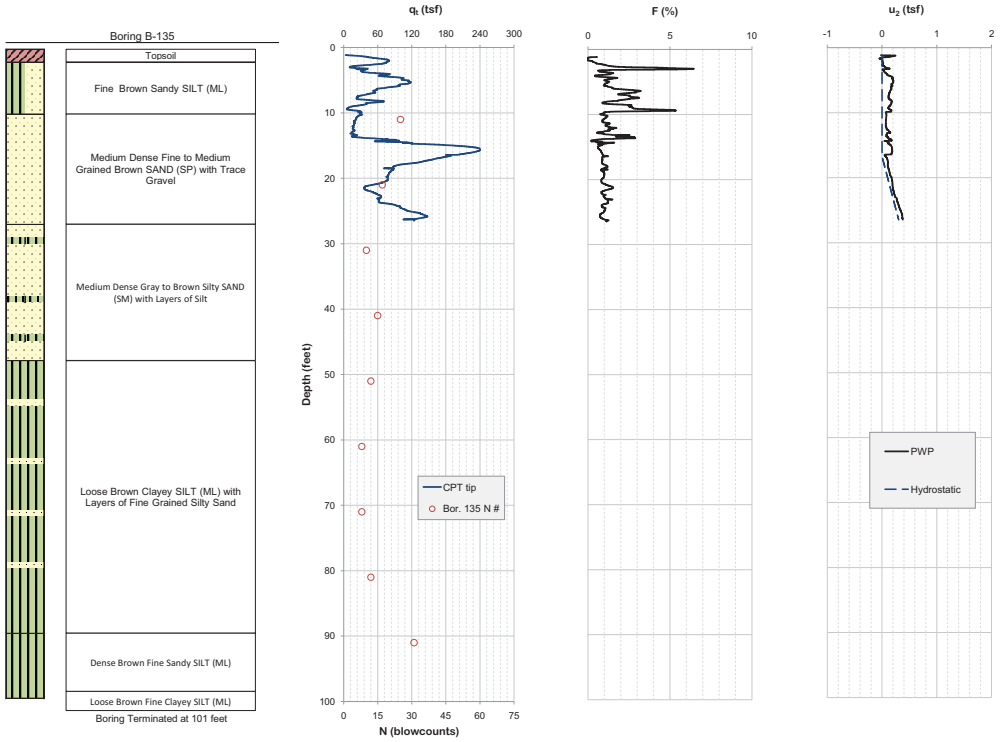

College of Engineering
UNIVERSITY OF WISCONSIN-MADISON

Site: Long-10
Description: Pedestrian Bridge & Pheasant Branch Crk.
Boring Date: Feb. - Mar. 2000

Sounding: CPTU2-06
Date: 6/8/2011
Operator: Finn H. & Seth S.

Baseline Zero Shifts (%)

q_t	f_s	u_2
6.9	4.2	3.4

Termination Depth: 26.0 Feet
Total Dissipations: 0
Dissipation Time: 0

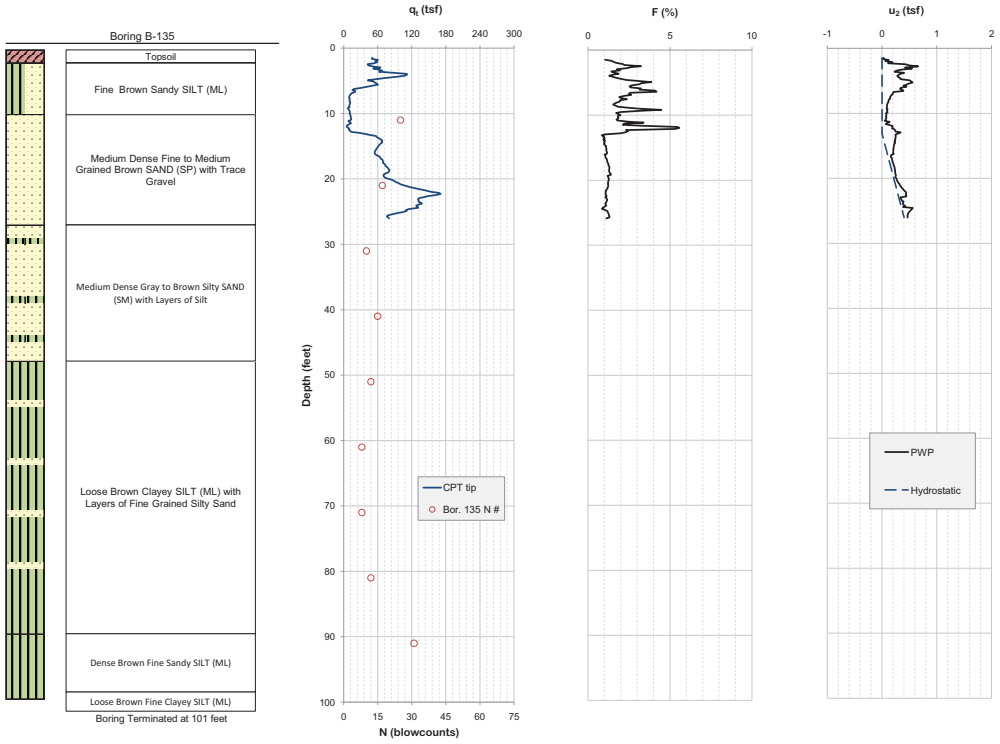

College of Engineering
UNIVERSITY OF WISCONSIN-MADISON

Site: Long-10
Description: Pedestrian Bridge & Pheasant Branch Crk
Boring Date: Feb. - Mar. 2000

Sounding: CPTU2-07
Date: 6/8/2011
Operator: Finn H. & Seth S.

Baseline Zero Shifts (%)

q_t	f_s	u_2
20.2	3.1	0.7

Termination Depth: 42.5 Feet
Total Dissipations: 2
Dissipation Time: 3 Minutes

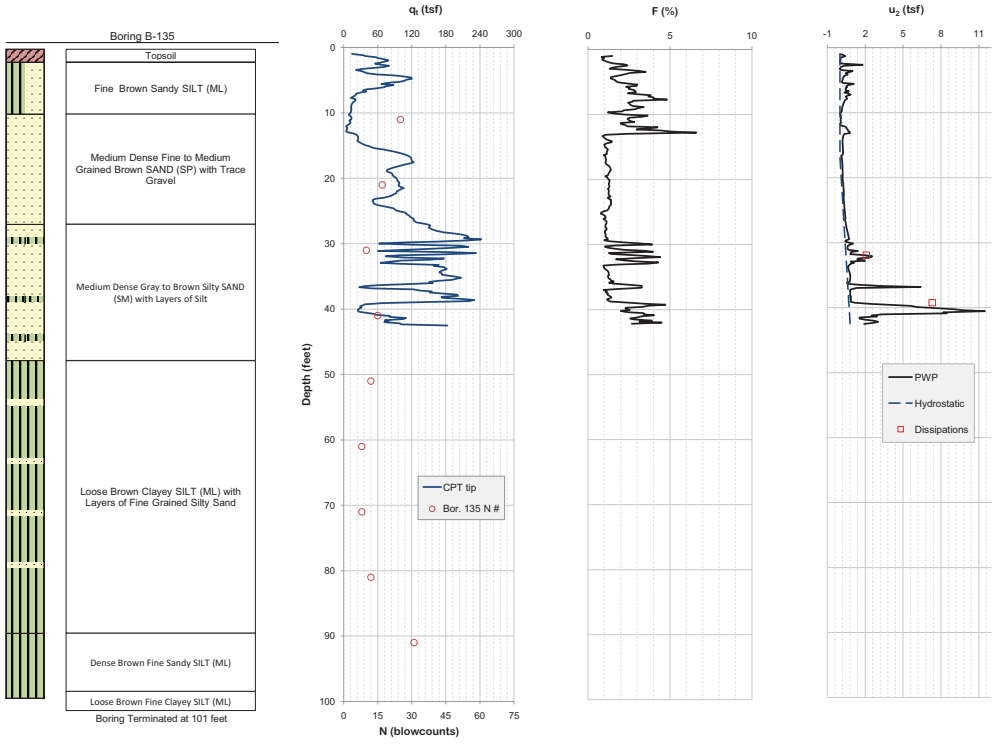

College of Engineering
UNIVERSITY OF WISCONSIN-MADISON

Site: Long-10
Description: Pedestrian Bridge & Pheasant Branch Crk.
Boring Date: Feb. - Mar. 2000

Sounding: CPTU2-08
Date: 6/9/2011
Operator: Finn H. & Seth S.

Baseline Zero Shifts (%)

q_t	f_s	u_2
2.3	-2.7	6.6

Termination Depth: 45.1 Feet
Total Dissipations: 2
Dissipation Time: 7 Minutes

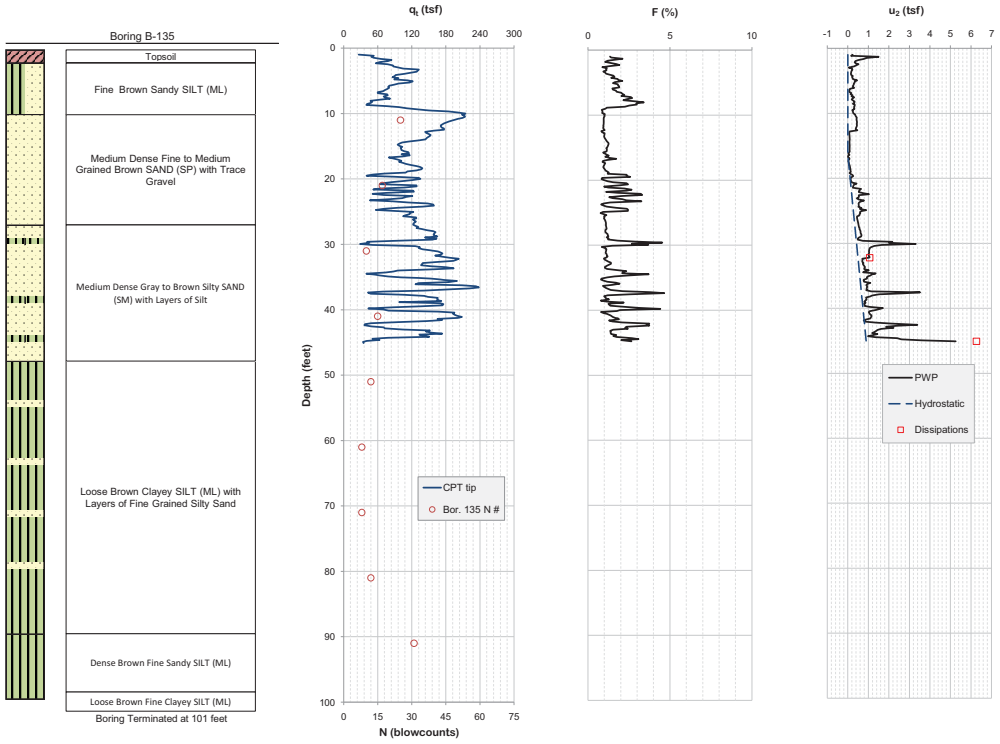

College of Engineering
UNIVERSITY OF WISCONSIN-MADISON

Site: Long-10
Description: Pedestrian Bridge & Pheasant Branch Crk.
Boring Date: Feb. - Mar. 2000

Sounding: CPTU2-09
Date: 6/8/2011
Operator: Seth S. & Finn H.

Baseline Zero Shifts (%)

q_t	f_s	u_2
N/A	N/A	N/A

Termination Depth: 22.8 Feet
Total Dissipations: 0
Dissipation Time: 0

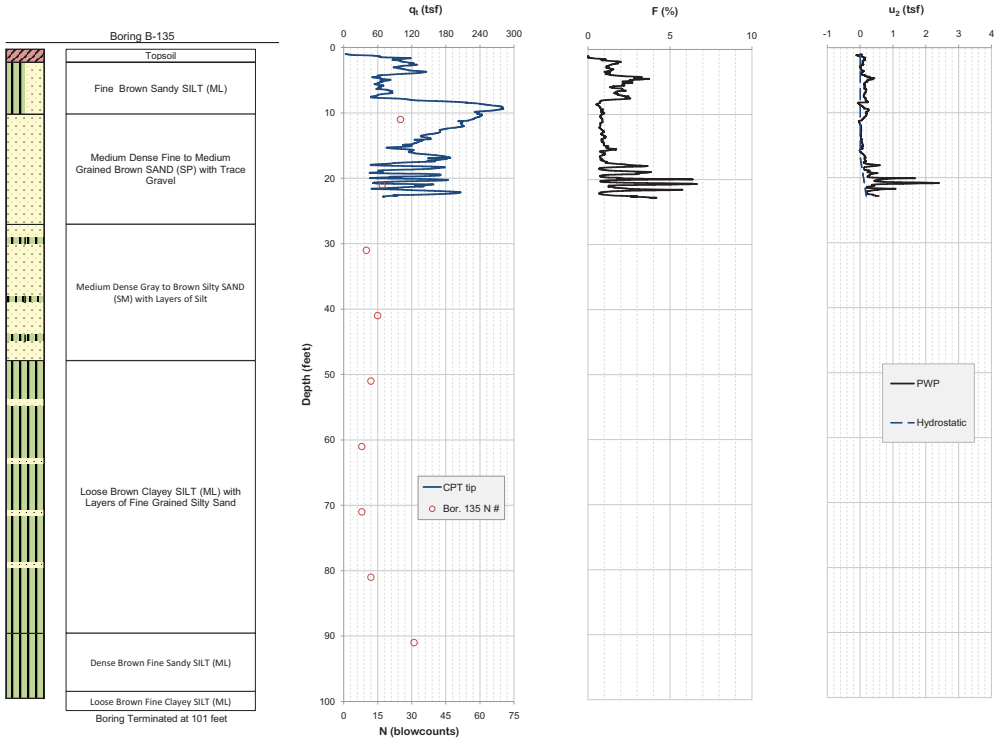

State Location

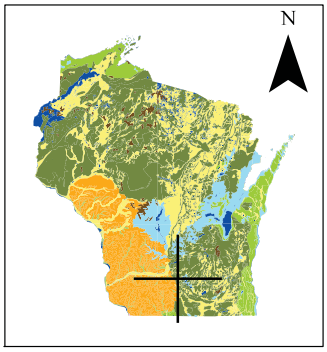

City Location

ESRI Aerial Photo - Scale 1:24,000

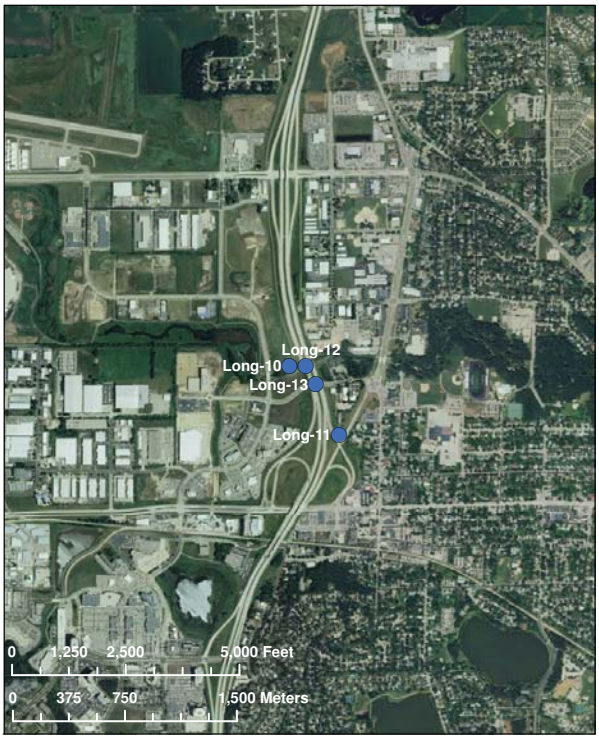

Madison Orthoimagery (April 2007) - Scale 1:1,000

Description:

The intent of this map is to provide information on the site location and layout of the investigation. Several sources of data were compiled to generate these maps of varying scales. The map scale decreases, area shown decreases, from left to right. Site location is shown from a state level, to city level, to aerial photo and finally a detailed site aerial photo with locations of specific borings conducted for the bridge design.

Source Maps:

DeLorme. Delorme World Basemap [Computer Map]. 1:288,000. [Online Database]. 2009.
ESRI ArcGIS Online, World Imagery [Aerial Photographs]. Visual Scale. http://www.arcgis.com/home/group.html?owner=esri&title=ESRI%20Maps%20and%20Data. (August 17, 2010)
United States Geological Survey. "April 2007 Color Orthoimagery – Madison, WI" [aerial photographs]. USGS, 2007. Accessed online http://seamless.usgs.gov/ [8/17/2010].
Wisconsin Dept. of Natural Resources. "Wisconsin State Outline." [ESRI Shapefile]. Created by U. S. Census Bureau, 2008.

Site Location Maps
WHRP Site Long-12
Middleton, Dane County, WI

Project No: 0092-10-10
Map Projection: NAD 1983
Map Scale: Varies
Date: October 12, 2010
Map By: EMM
Reviewed By: JAS

College of Engineering
UNIVERSITY OF WISCONSIN-MADISON

Site: Long-12
Description: USH-12 Middleton, WI
Boring Date: 2/22/2000

Sounding: SCPTU2-04
Date: 10/10/2010
Operator: Finn H.

Baseline Zero Shifts (%)

q_t	f_s	u_2
0.5	1.1	1.0

Termination Depth: 62.8 Feet
Total Dissipations: 3
Dissipation Time: 55 minutes

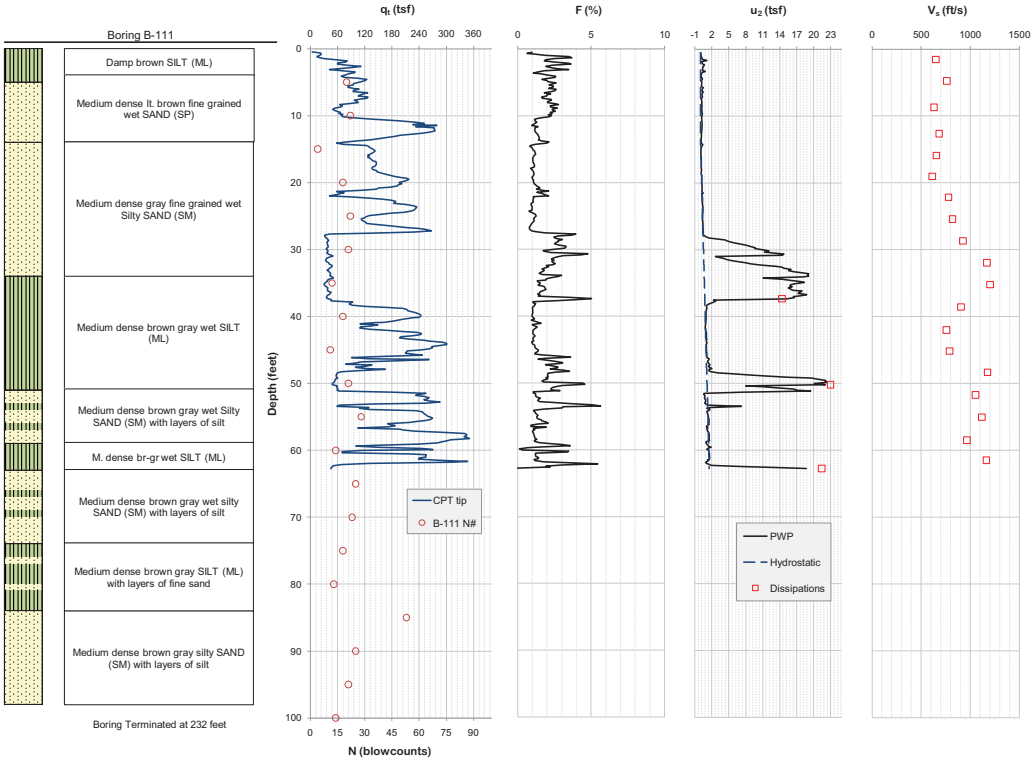

State Location

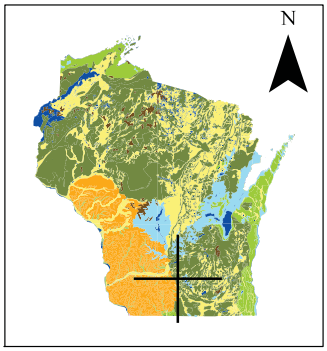

City Location

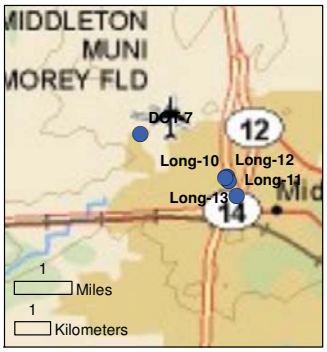

ESRI Aerial Photo - Scale 1:24,000

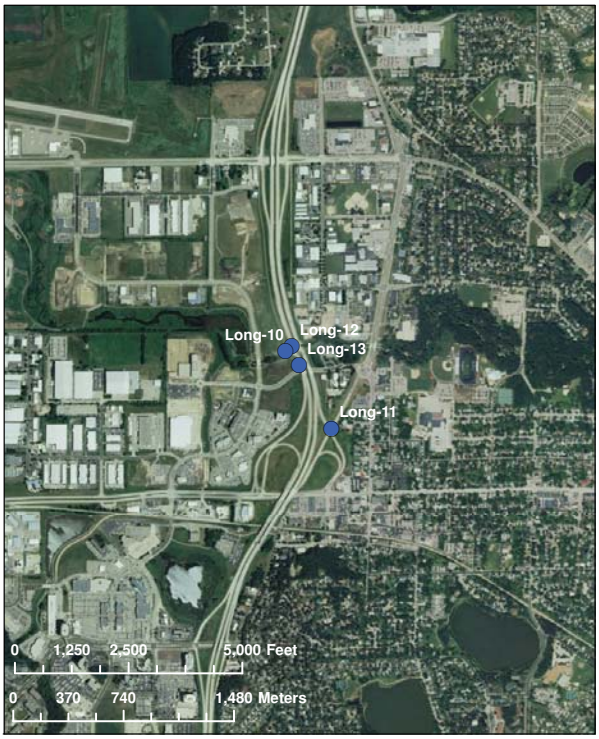

Madison Orthoimagery (April 2007) - Scale 1:1,000

Description:

The intent of this map is to provide information on the site location and layout of the investigation. Several sources of data were compiled to generate these maps of varying scales. The map scale decreases, area shown decreases, from left to right. Site location is shown from a state level, to city level, to aerial photo and finally a detailed site aerial photo with locations of specific borings conducted for the bridge design.

Source Maps:

DeLorme. Delorme World Basemap [Computer Map]. 1:288,000. [Online Database]. 2009.
ESRI ArcGIS Online, World Imagery [Aerial Photographs]. Visual Scale. http://www.arcgis.com/home/group.html?owner=esri&title=ESRI%20Maps%20and%20Data. (August 17, 2010)
United States Geological Survey. "April 2007 Color Orthoimagery – Madison, WI" [aerial photographs]. USGS, 2007. Accessed online http://seamless.usgs.gov/ [8/17/2010].
Wisconsin Dept. of Natural Resources. "Wisconsin State Outline." [ESRI Shapefile]. Created by U. S. Census Bureau, 2008.

Site Location Maps
WHRP Site Long-13
Middleton, Dane County, WI

Project No: 5300-03-78
Map Projection: NAD 1983
Map Scale: Varies
Date: August 25, 2010
Map By: EMM
Reviewed By: JAS

College of Engineering
UNIVERSITY OF WISCONSIN-MADISON

Site: Long-13
Description: US-12 over Murphy Road, Middleton
Boring Date: 2/22/2000

Sounding: CPTU2-05
Date: 10/13/2010
Operator: Finn H. & Elliott M.

Baseline Zero Shifts (%)

q_t	f_s	u_2
3.9	-0.6	0.2

Termination Depth: 56.2 Feet
Total Dissipations: 2
Dissipation Time: 15 minutes

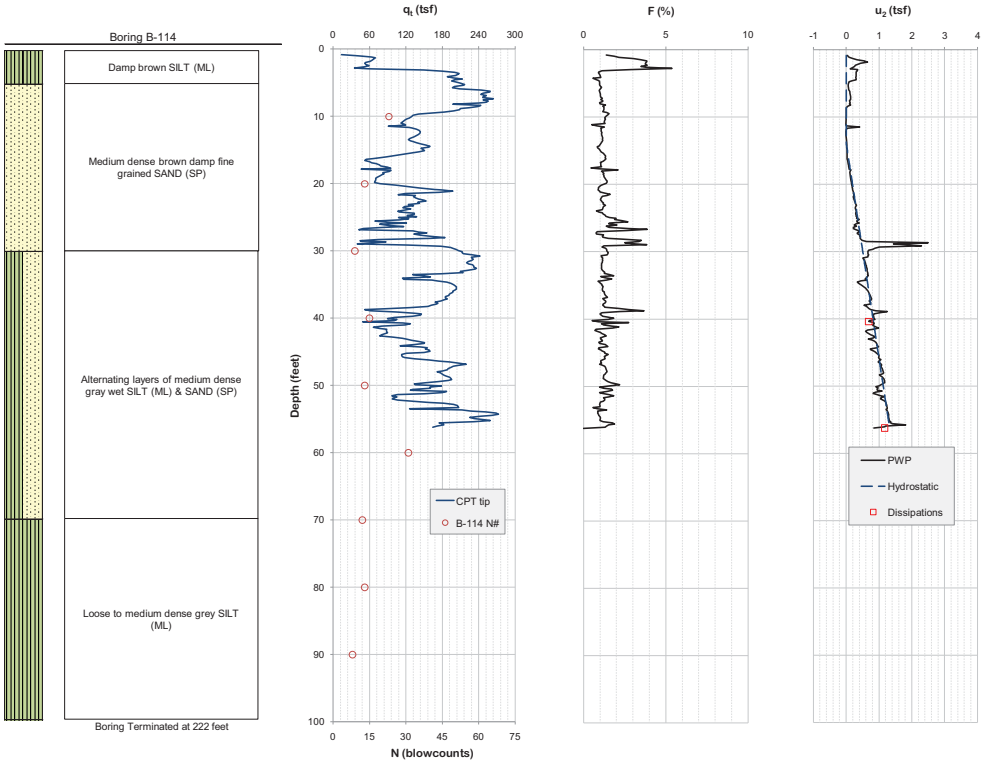

State Location

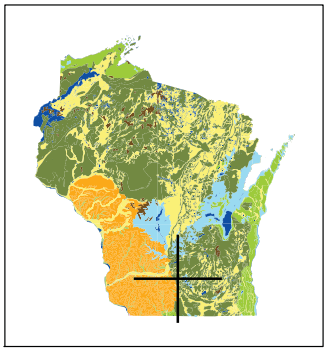

City Location

ESRI Aerial Photo - Scale 1:24,000

Madison Orthoimagery (April 2007) - Scale 1:500

Description:

The intent of this map is to provide information on the site location and layout of the investigation. Several sources of data were compiled to generate these maps of varying scales. The map scale decreases, area shown decreases, from left to right. Site location is shown from a state level, to city level, to aerial photo and finally a detailed site aerial photo with locations of specific borings conducted for the bridge design.

Source Maps:

DeLorme. Delorme World Basemap [Computer Map]. 1:288,000. [Online Database]. 2009.
ESRI ArcGIS Online, World Imagery [Aerial Photographs]. Visual Scale. http://www.arcgis.com/home/group.html?owner=esri&title=ESRI%20Maps%20and%20Data. (August 17, 2010)
United States Geological Survey. "April 2007 Color Orthoimagery – Madison, WI" [aerial photographs]. USGS, 2007. Accessed online http://seamless.usgs.gov/ [8/17/2010].
Wisconsin Dept. of Natural Resources. "Wisconsin State Outline." [ESRI Shapefile]. Created by U. S. Census Bureau, 2008.

Site Location Maps
WHRP Site DOT-7
Middleton, Dane County, WI

Project No: 0092-10-10
Map Projection: NAD 1983
Map Scale: Varies
Date: August 16, 2010
Map By: JNH
Reviewed By: JAS

College of Engineering
UNIVERSITY OF WISCONSIN-MADISON

Site: DOT-7
Description: Middleton, WI
Boring Date: 3/20/2001

Sounding: CPTU2-01
Date: 10/14/2010
Operator: James S. & Finn H.

Baseline Zero Shifts (%)

q_t	f_s	u_2
4.2	1.7	0.2

Termination Depth: 33.7 Feet
Total Dissipations: 7
Dissipation Time: 61 minutes

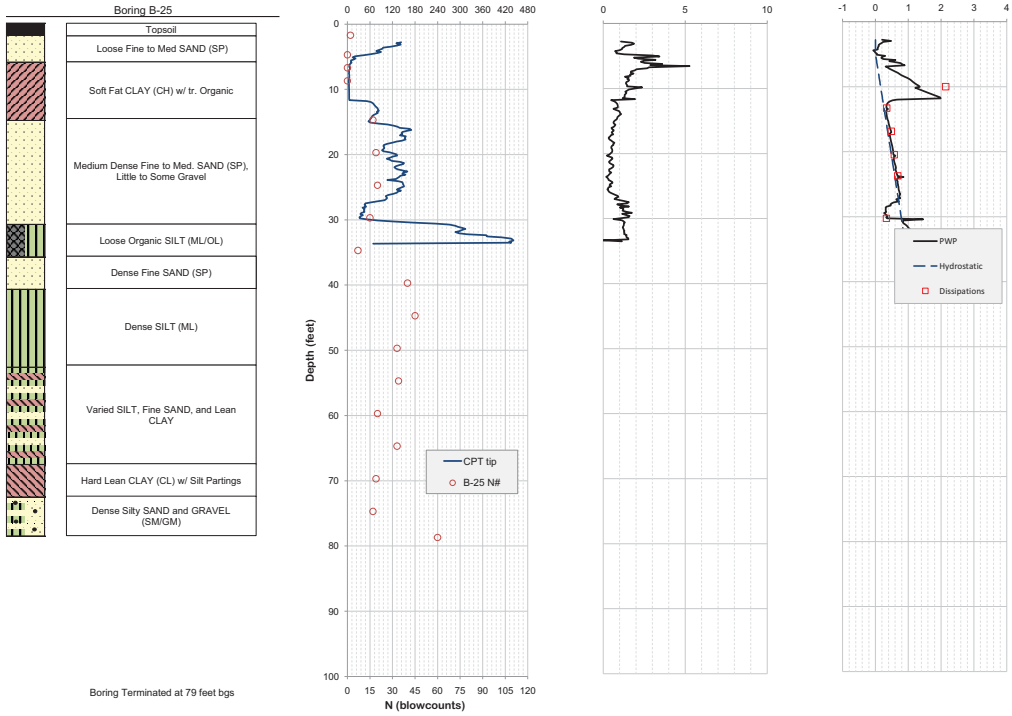

College of Engineering
UNIVERSITY OF WISCONSIN-MADISON

Site: DOT-7
Description: Middleton, WI
Boring Date: 3/20/2001

Sounding: CPTU2-02
Date: 10/14/2010
Operator: James S. & Finn H.

Baseline Zero Shifts (%)

q_t	f_s	u_2
9.9	1.8	0.3

Termination Depth: 14.1 Feet
Total Dissipations: 5
Dissipation Time: 1107 minutes

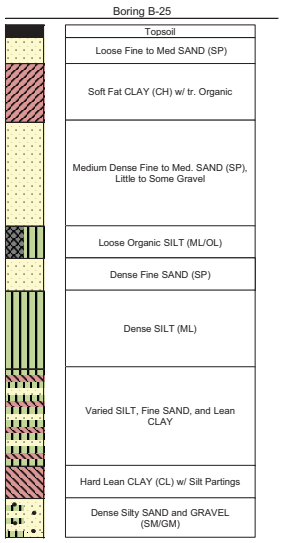

Boring Terminated at 79 feet bgs

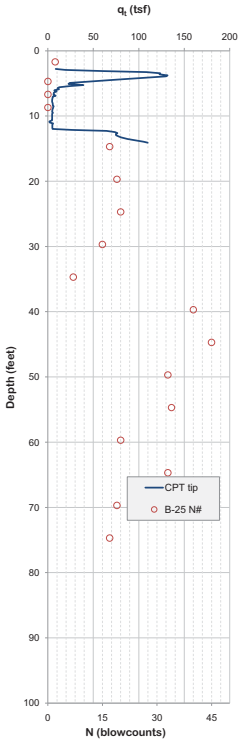

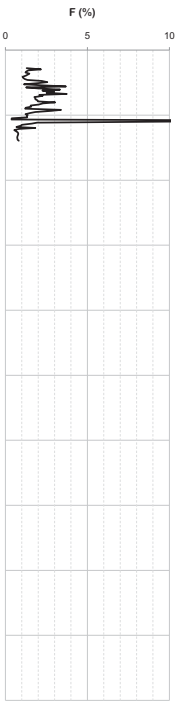

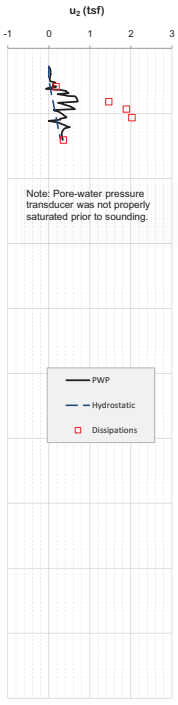

College of Engineering
UNIVERSITY OF WISCONSIN-MADISON

Site: DOT-7
Description: Middleton, WI
Boring Date: 3/20/2001

Sounding: CPTU2-03/03a
Date: 10/16/2010
Operator: James S. & Finn H.

Baseline Zero Shifts (%)

q_t	f_s	u_2
-1.1	-0.5	0.3

Termination Depth: 42.6 Feet
Total Dissipations: 5
Dissipation Time: 534 minutes

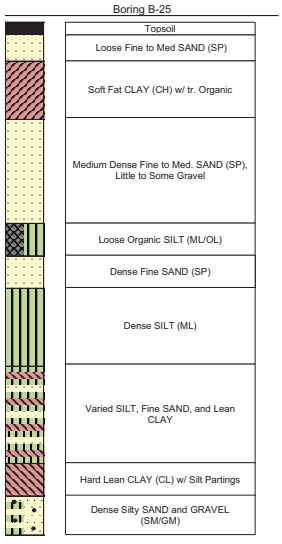

Boring Terminated at 79 feet bgs

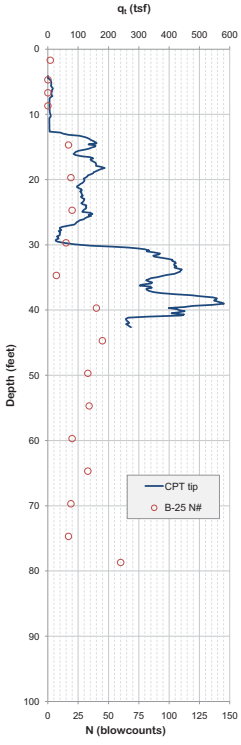

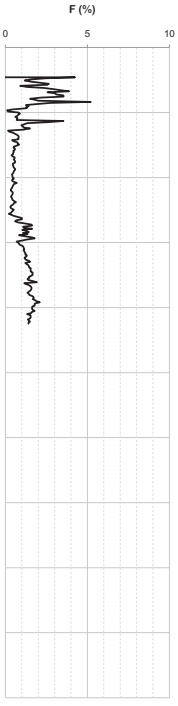

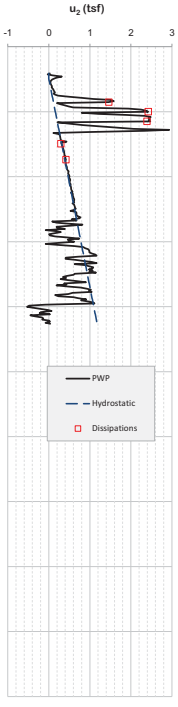

College of Engineering
UNIVERSITY OF WISCONSIN-MADISON

Site: DOT-7
Description: Airport Road, Middleton, WI
Boring Date: 2002

Sounding: CPTU2-04
Date: 6/1/2011
Operator: James S., Finn H., Seth S.

Baseline Zero Shifts (%)

q_t	f_s	u_2
-4.3	1.9	2.3

Termination Depth: 14.9 Feet
Total Dissipations: 5
Dissipation Time: 317 minutes

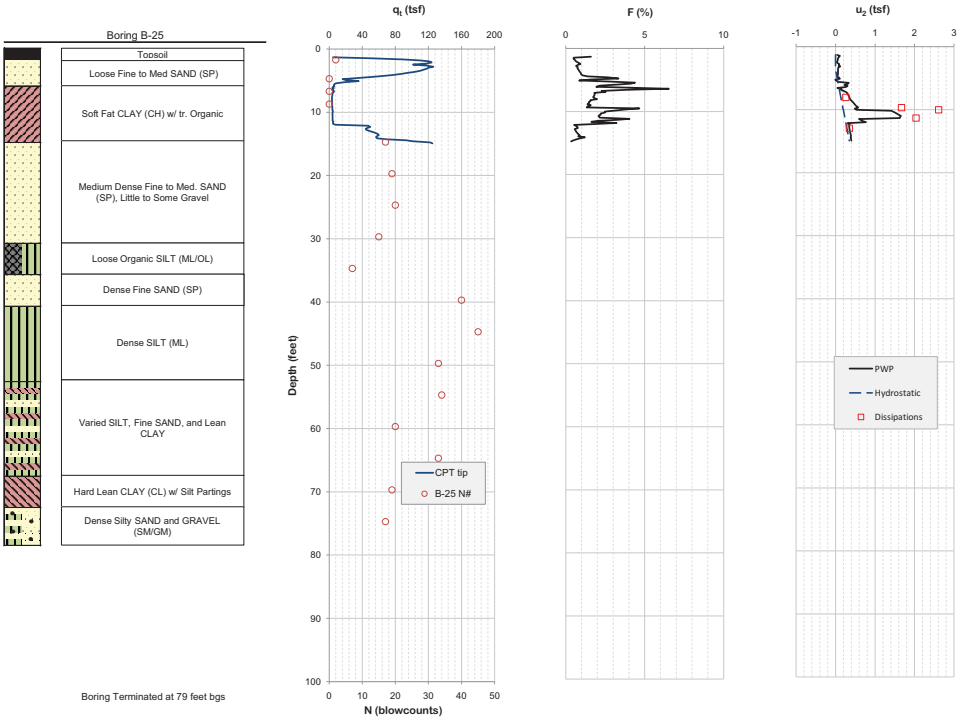

Boring Terminated at 79 feet bgs

College of Engineering
UNIVERSITY OF WISCONSIN-MADISON

Site: DOT-7
Description: Airport Road, Middleton, WI
Boring Date: 2002

Sounding: CPTU2-05
Date: 6/1/2011
Operator: James S., Finn H., Seth S.

Baseline Zero Shifts (%)

q_t	f_s	u_2
-1.7	-5.1	0.7

Advance Rate: 0.01 mm/s

Termination Depth: 12.3 Feet
Total Dissipations: 4
Dissipation Time: 483 minutes

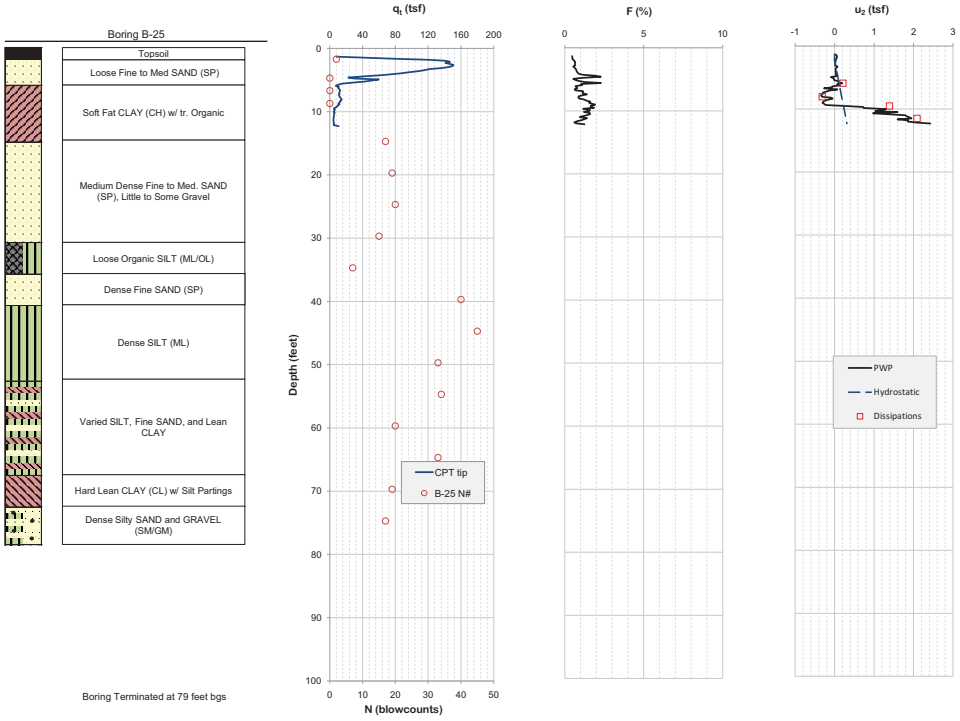

Boring Terminated at 79 feet bgs

College of Engineering
UNIVERSITY OF WISCONSIN-MADISON

Site: DOT-7
Description: Airport Road, Middleton, WI
Boring Date: 2002

Sounding: CPTU2-06
Date: 6/2/2011
Operator: Finn H. & Seth S.

Baseline Zero Shifts (%)

q_t	f_s	u_2
-10.3	-2.2	2.6

Advance Rate: 1.6 mm/s

Termination Depth: 13.0 Feet
Total Dissipations: 4
Dissipation Time: 257 minutes

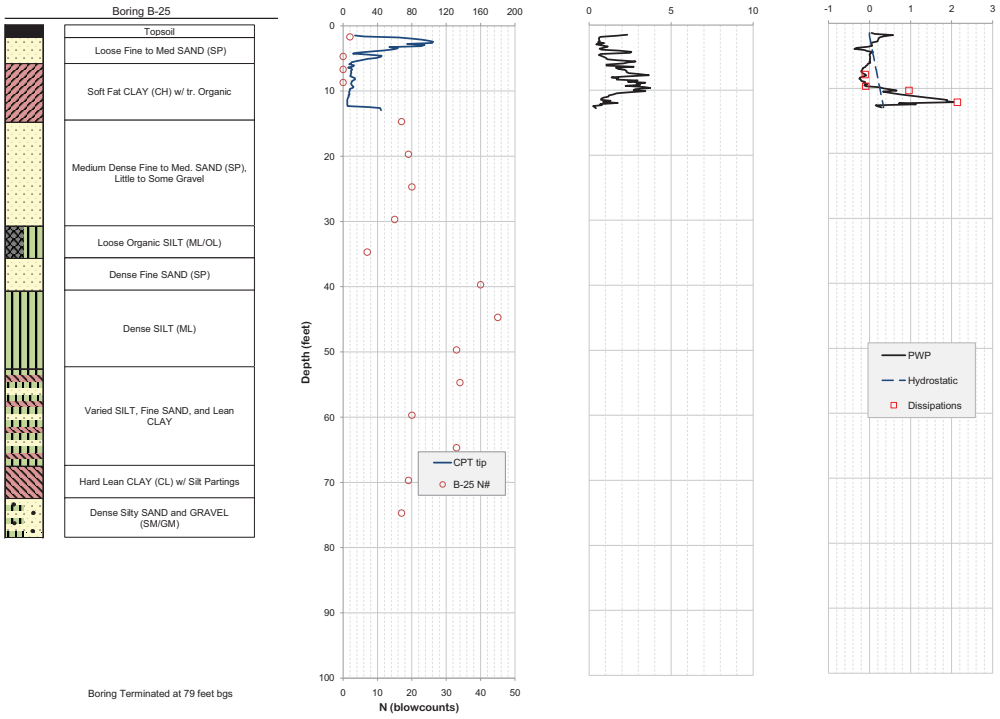

Boring Terminated at 79 feet bgs

College of Engineering
UNIVERSITY OF WISCONSIN-MADISON

Site: DOT-7
Description: Airport Road, Middleton
Boring Date: 2002

Sounding: CPTU2-07
Date: 6/3/2011
Operator: James S. & Seth S.

Baseline Zero Shifts (%)

q_t	f_s	u_2
-1.7	1.6	0.9

Advance Rate: 50 mm/s

Termination Depth: 12.8 Feet
Total Dissipations: 4
Dissipation Time: 213 minutes

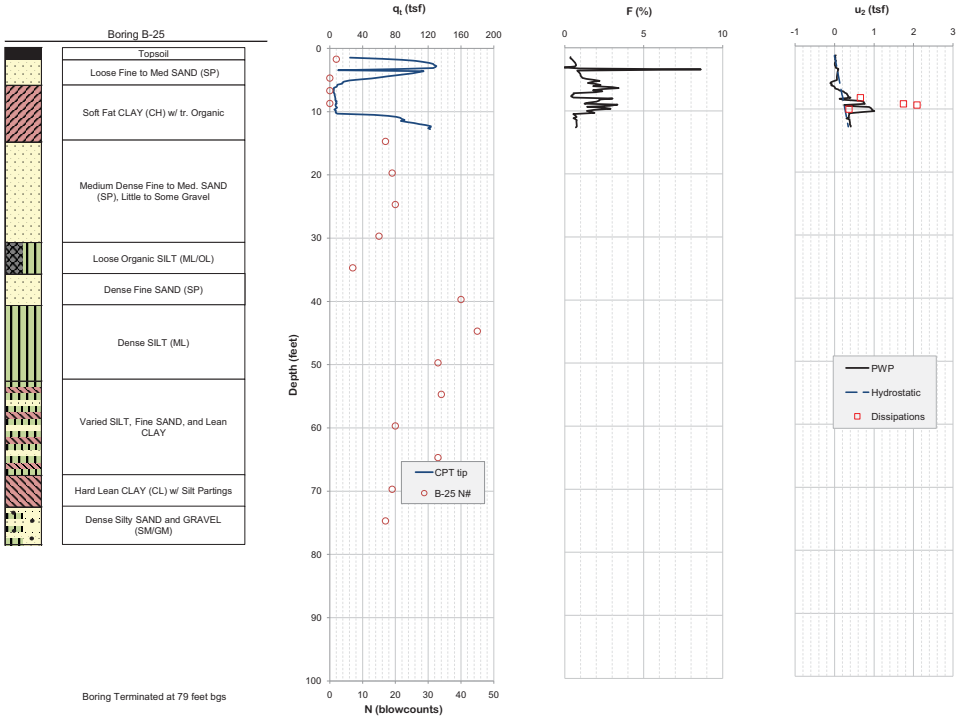

Boring Terminated at 79 feet bgs

College of Engineering
UNIVERSITY OF WISCONSIN-MADISON

Site: DOT-7
Description: Airport Road, Middleton
Boring Date: 2002

Sounding: CPTU2-08
Date: 6/3/2011
Operator: Seth S. and Finn H.

Baseline Zero Shifts (%)

q_t	f_s	u_2
N/A	N/A	N/A

Termination Depth: 25.9 Feet
Total Dissipations: 0
Dissipation Time: 0

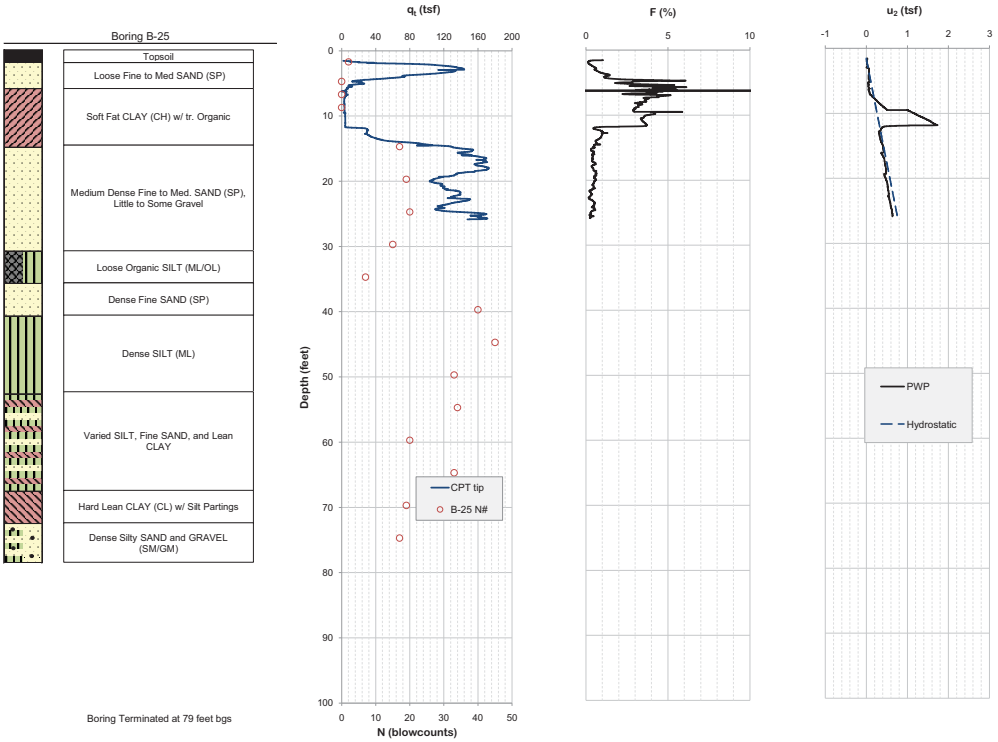

State Location

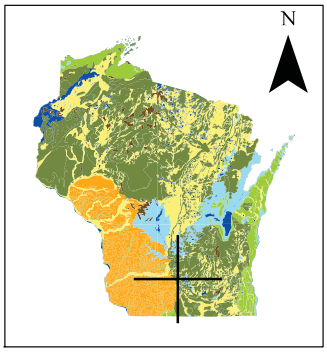

City Location

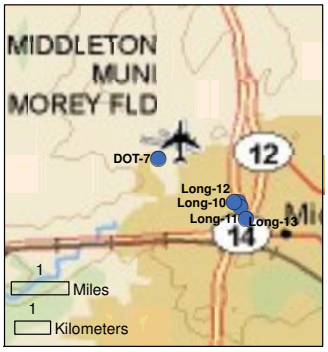

ESRI Aerial Photo - Scale 1:24,000

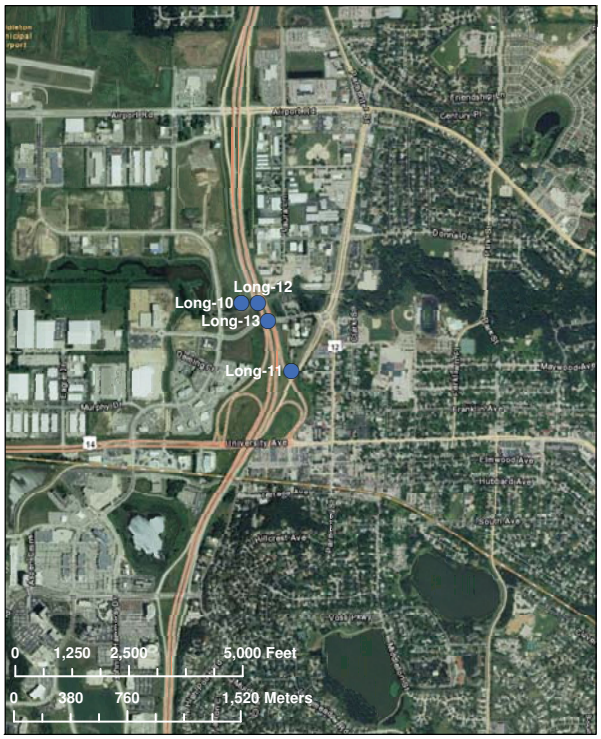

Madison Orthoimagery (April 2007) - Scale 1:1,000

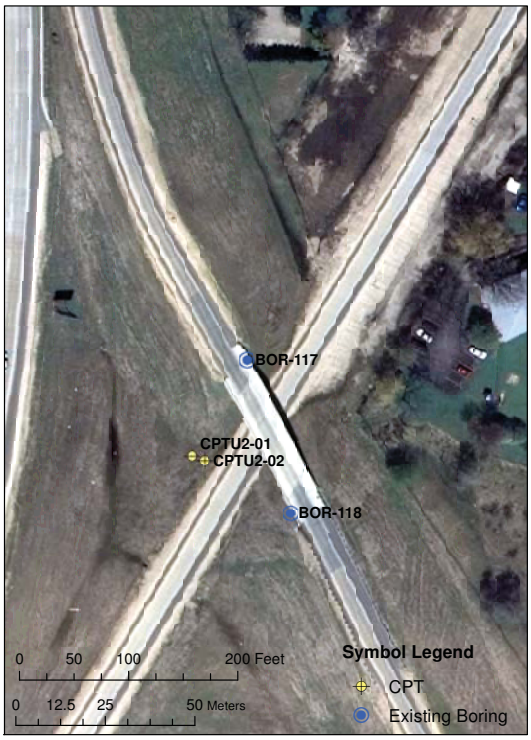

Description:

The intent of this map is to provide information on the site location and layout of the investigation. Several sources of data were compiled to generate these maps of varying scales. The map scale decreases, area shown decreases, from left to right. Site location is shown from a state level, to city level, to aerial photo and finally a detailed site aerial photo with locations of specific borings conducted for the bridge design.

Source Maps:

DeLorme. Delorme World Basemap [Computer Map]. 1:288,000. [Online Database]. 2009.
ESRI ArcGIS Online, World Imagery [Aerial Photographs]. Visual Scale. http://www.arcgis.com/home/group.html?owner=esri&title=ESRI%20Maps%20and%20Data. (August 17, 2010)
United States Geological Survey. "April 2007 Color Orthoimagery – Madison, WI" [aerial photographs]. USGS, 2007. Accessed online http://seamless.usgs.gov/ [8/17/2010].
Wisconsin Dept. of Natural Resources. "Wisconsin State Outline." [ESRI Shapefile]. Created by U. S. Census Bureau, 2008.

Site Location Maps
WHRP Site Long-11
Middleton, Dane County, WI

Project No: 0092-10-10
Map Projection: NAD 1983
Map Scale: Varies
Date: August 30, 2010
Map By: EMM
Reviewed By: JNH

College of Engineering
UNIVERSITY OF WISCONSIN-MADISON

Site: Long-11
Description: USH-12 Middleton, WI
Boring Date: Feb. - Mar. 2000

Sounding: CPTU2-01
Date: 10/18/2010
Operator: Finn H. & Skyler N.

Baseline Zero Shifts (%)

q_t	f_s	u_2
4.9	-1.6	-2.1

Termination Depth: 23.9 Feet
Total Dissipations: 1
Dissipation Time: 6 minutes

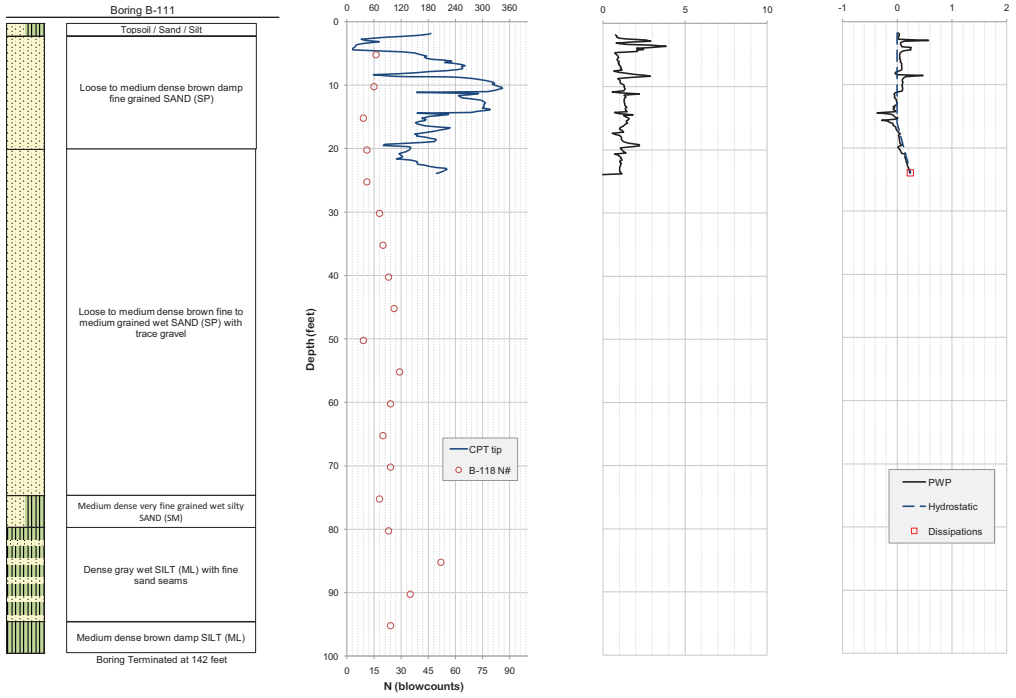

College of Engineering
UNIVERSITY OF WISCONSIN-MADISON

Site: Long-11
Description: Middleton, WI
Boring Date: Feb. - Mar. 2000

Sounding: CPTU2-02
Date: 10/18/2010
Operator: Finn H., Elliott M. & James S.

Baseline Zero Shifts (%)

q_t	f_s	u_2
4.1	1.3	1.8

Termination Depth: 53.2 Feet
Total Dissipations: 7
Dissipation Time: 44 minutes

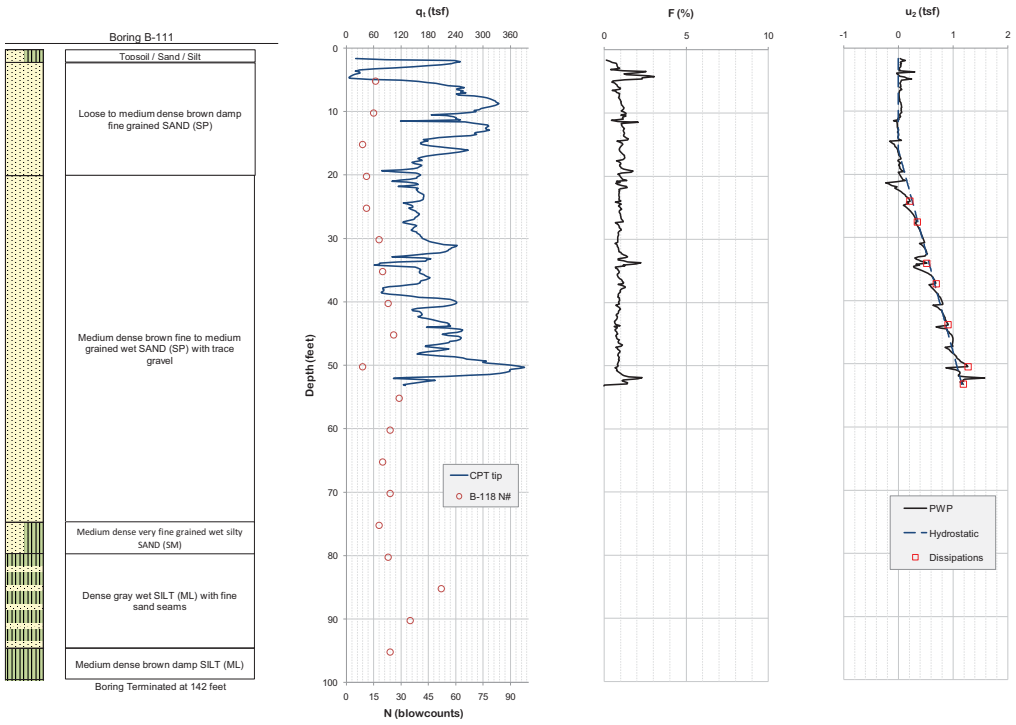

State Location

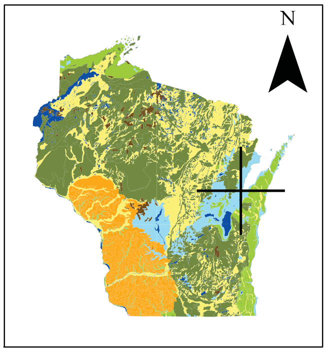

City Location

ESRI Aerial Photo - Scale 1:24,000

Green Bay Orthoimagery (July 2005) - Scale 1:3,000

Description:

The intent of this map is to provide information on the site location and layout of the investigation. Several sources of data were compiled to generate these maps of varying scales. The map scale decreases, area shown decreases, from left to right. Site location is shown from a state level, to city level, to aerial photo and finally a detailed site aerial photo with locations of specific borings conducted for the roadway design.

Source Maps:

DeLorme. Delorme World Basemap [Computer Map]. 1:288,000. [Online Database]. 2009.
ESRI ArcGIS Online, World Imagery [Aerial Photographs]. Visual Scale. http://www.arcgis.com/home/group.html?owner=esri&title=ESRI%20Maps%20and%20Data. (August 24, 2010)
United States Geological Survey. "July 2007 Color Orthoimagery – Green Bay / Appleton / Oshkosh, WI" [aerial photographs]. USGS, 2007. Accessed online http://seamless.usgs.gov/ [8/24/2010].
Wisconsin Dept. of Natural Resources. "Wisconsin State Outline." [ESRI Shapefile]. Created by U. S. Census Bureau, 2008.

Plate 1: Site Location Map
WHRP Site DOT-1
Howard, Brown County

Project No: 0092-10-10
Map Scale: Varies
Date: January 28, 2011
Map By: JNH
Reviewed By: JAS

College of Engineering
UNIVERSITY OF WISCONSIN-MADISON

Site: DOT-1
Description: Village of Howard, WI
Boring Date: 7/2010

Sounding: SCPTU2-01
Date: 10/28/2010
Operator: James S. & Finn H.

Baseline Zero Shifts (%)		
q_t	f_s	u_2
0.5	-1.6	-1.7

Termination Depth: 59.7 Feet
Total Dissipations: 17
Dissipation Time: 1050 minutes

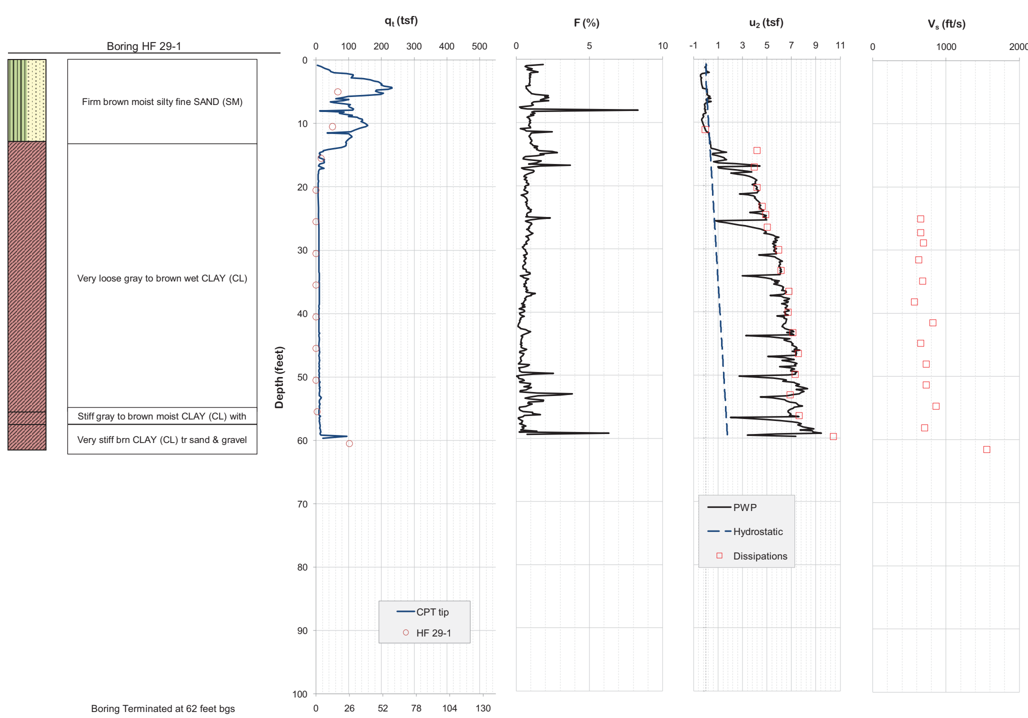

College of Engineering
UNIVERSITY OF WISCONSIN-MADISON

Site: DOT-1
Description: Howard, WI
Boring Date: 7/2010

Sounding: CPTU2-02
Date: 10/29/2010
Operator: James S. & Finn H.

Baseline Zero Shifts (%)

q_t	f_s	u_2
6.5	-1.0	-2.6

Termination Depth: 69.9 Feet
Total Dissipations: 19
Dissipation Time: 2191 minutes

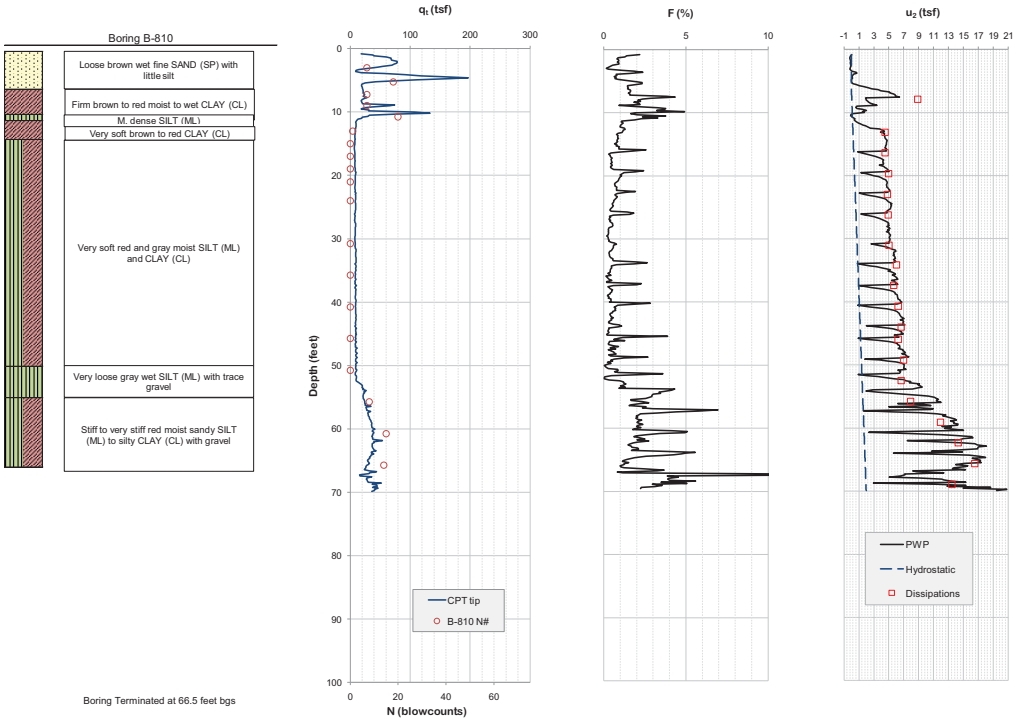

Boring Terminated at 66.5 feet bgs

College of Engineering
UNIVERSITY OF WISCONSIN-MADISON

Site: DOT-1
Description: Howard, WI
Boring Date: 7/2010

Sounding: C-3
Date: 1/30/1900
Operator: Finn H. & Elliott M.

Baseline Zero Shifts (%)

q_t	f_s	u_2

Termination Depth: 3.3 Feet
Total Dissipations:
Dissipation Time:

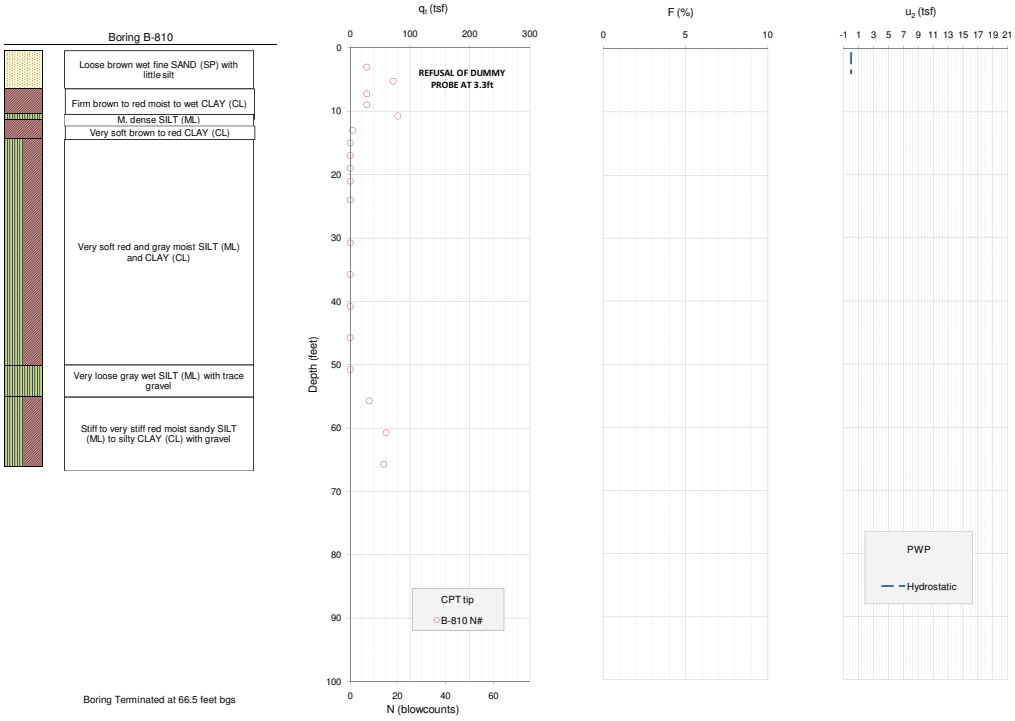

Boring Terminated at 66.5 feet bgs

College of Engineering
UNIVERSITY OF WISCONSIN MADISON

Site: DOT-1
Description: Howard, WI
Boring Date: 7/2010

Sounding: C-4
Date: 1/30/1900
Operator: Finn H. & Elliott M.

Baseline Zero Shifts (%)
q_t f_s u_2

Termination Depth: 3.3 Feet
Total Dissipations:
Dissipation Time:

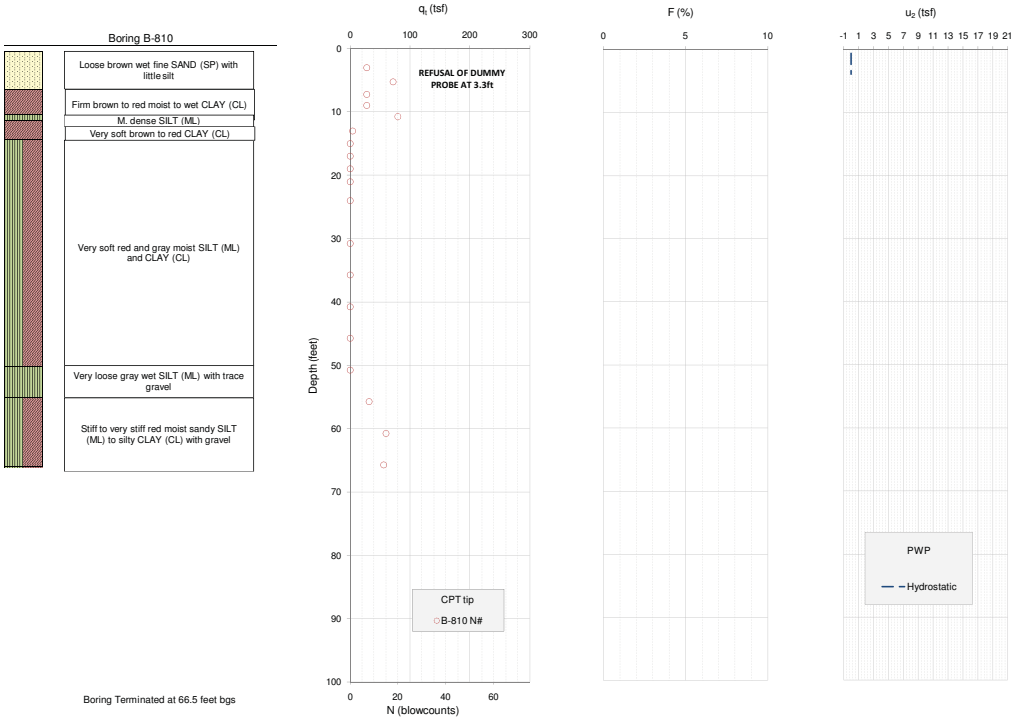

Boring Terminated at 66.5 feet bgs

College of Engineering
UNIVERSITY OF WISCONSIN MADISON

Site: DOT-1
Description: Howard, WI
Boring Date: 7/2010

Sounding: C-5
Date: 1/30/1900
Operator: Finn H. & Elliott M.

Baseline Zero Shifts (%)
q_t f_s u_2

Termination Depth: 3.3 Feet
Total Dissipations:
Dissipation Time:

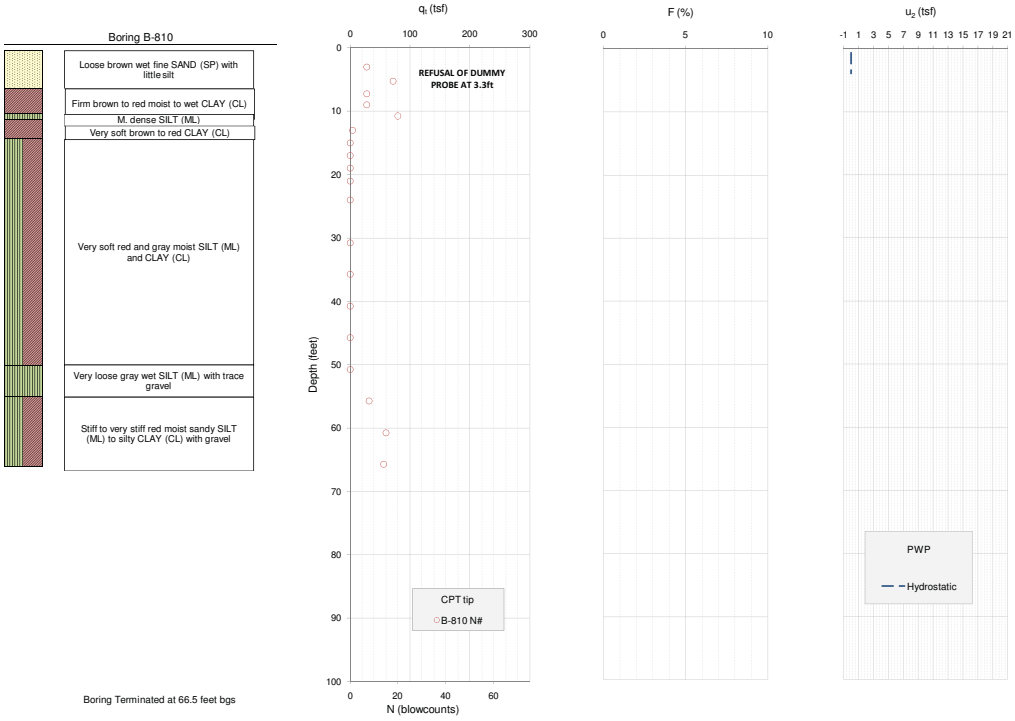

Boring Terminated at 66.5 feet bgs

State Location

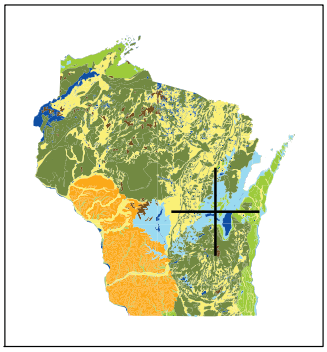

City Location

ESRI Aerial Photo - Scale 1:24,000

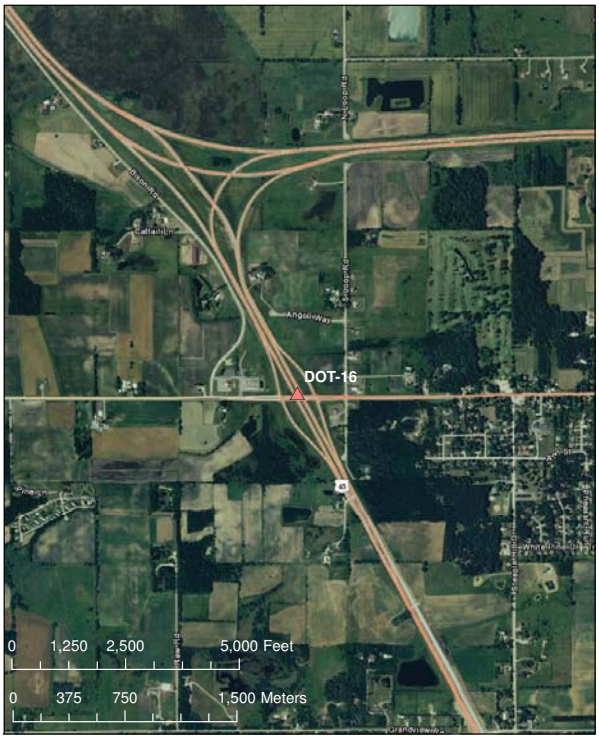

Appleton Orthoimagery (July 2005) - Scale 1:1,500

Description:

The intent of this map is to provide information on the site location and layout of the investigation. Several sources of data were compiled to generate these maps of varying scales. The map scale decreases, area shown decreases, from left to right. Site location is shown from a state level, to city level, to aerial photo and finally a detailed site aerial photo with locations of specific borings conducted for the bridge design.

Source Maps:

DeLorme. Delorme World Basemap [Computer Map]. 1:288,000. [Online Database]. 2009.
ESRI ArcGIS Online, World Imagery [Aerial Photographs]. Visual Scale. http://www.arcgis.com/home/group.html?owner=esri&title=ESRI%20Maps%20and%20Data. (August 17, 2010)
United States Geological Survey. "July 2007 Color Orthoimagery – Green Bay / Appleton / Oshkosh, WI" [aerial photographs]. USGS, 2007. Accessed online http://seamless.usgs.gov/ [8/17/2010].
Wisconsin Dept. of Natural Resources. "Wisconsin State Outline." [ESRI Shapefile]. Created by U. S. Census Bureau, 2008.

Site Location Maps
WHRP Site DOT-16
Winchester, Winnebago County

Project No: 0092-10-10
Map Scale: Varies
Date: August 16, 2010
Map By: JNH
Reviewed By: JAS

College of Engineering
UNIVERSITY OF WISCONSIN-MADISON

Site: DOT-16
Description: Winchester, WI
Boring Date: 3/20/2001

Sounding: SCPTU2-01a
Date: 11/6/2010
Operator: Finn H. & Skyler N.

Baseline Zero Shifts (%)

q_t	f_s	u_2
9.7	-2.4	3.7

Termination Depth: 90.6 Feet
Total Dissipations: 8
Dissipation Time: 37 minutes

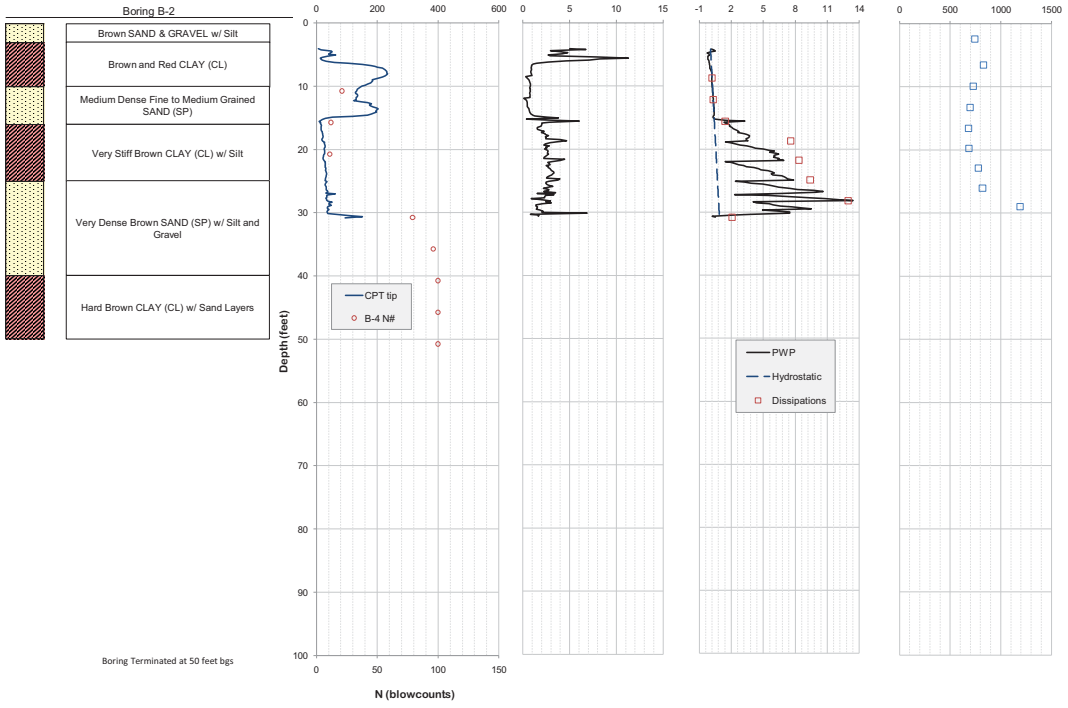

College of Engineering
UNIVERSITY OF WISCONSIN-MADISON

Site: DOT-16
Description: Winchester, WI
Boring Date: 3/21/2001

Sounding: SCPTU2-02/02a
Date: 11/6/2010
Operator: Finn H. & Skyler N.

Baseline Zero Shifts (%)

q_t	f_s	u_2
1.2	0.0	-2.2

Termination Depth: 90.6 Feet
Total Dissipations: 4
Dissipation Time: 16 minutes

Boring B-3

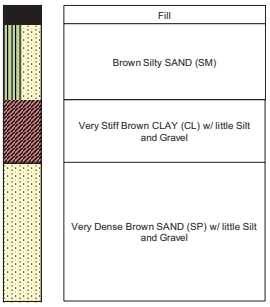

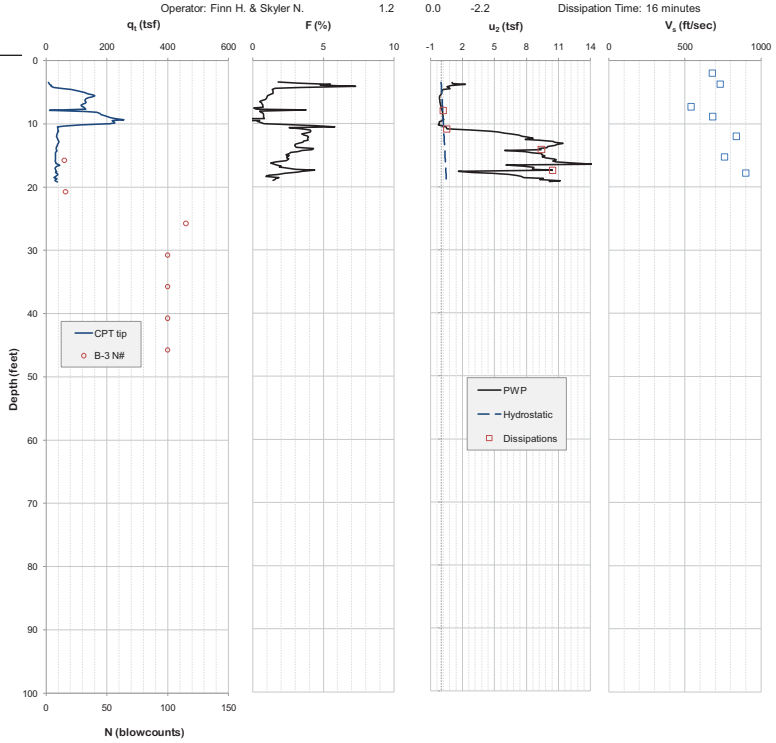

Boring Terminated at 47 feet bgs

College of Engineering
UNIVERSITY OF WISCONSIN-MADISON

Site: DOT-16
Description: Winchester, WI
Boring Date: 3/20/2001

Sounding: CPTU2-03
Date: 11/7/2010
Operator: Finn H. & Skyler N.

Baseline Zero Shifts (%)

q_t	f_s	u_2
18.0	0.7	-1.4

Termination Depth: 90.6 Feet
Total Dissipations: 4
Dissipation Time: 28 minutes

Boring B-1

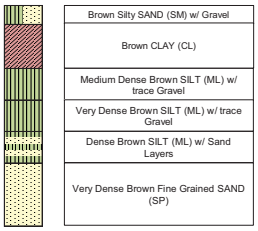

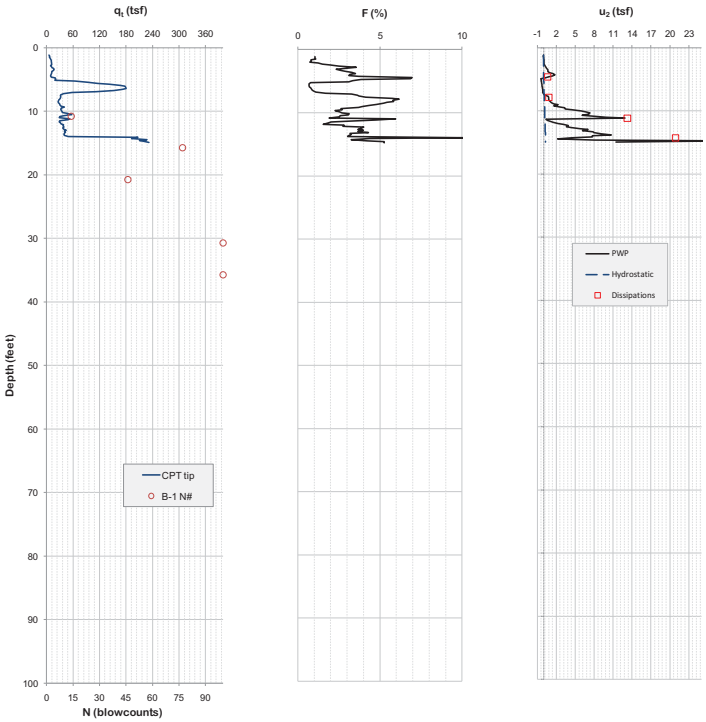

Boring Terminated at 35 feet BGS

College of Engineering
UNIVERSITY OF WISCONSIN-MADISON

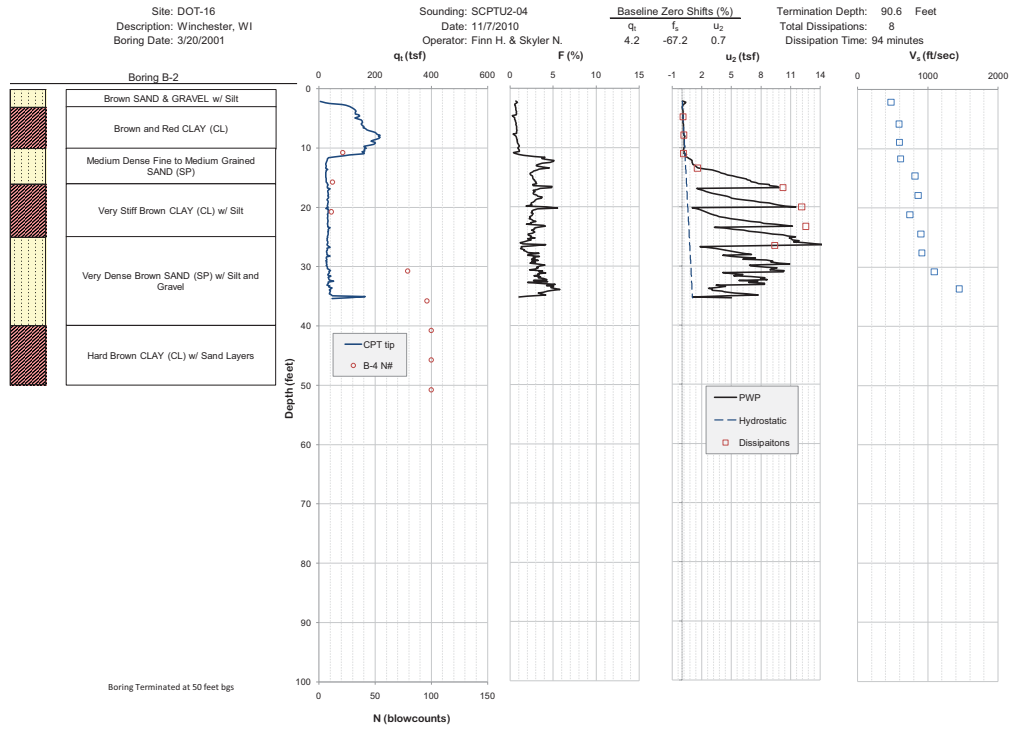

State Location

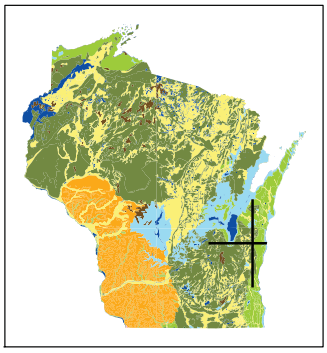

City Location

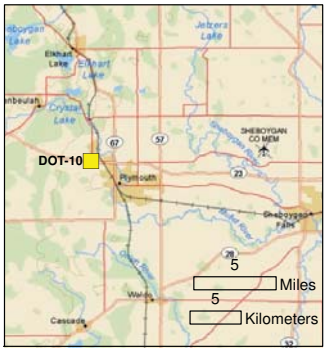

ESRI Aerial Photo - Scale 1:24,000

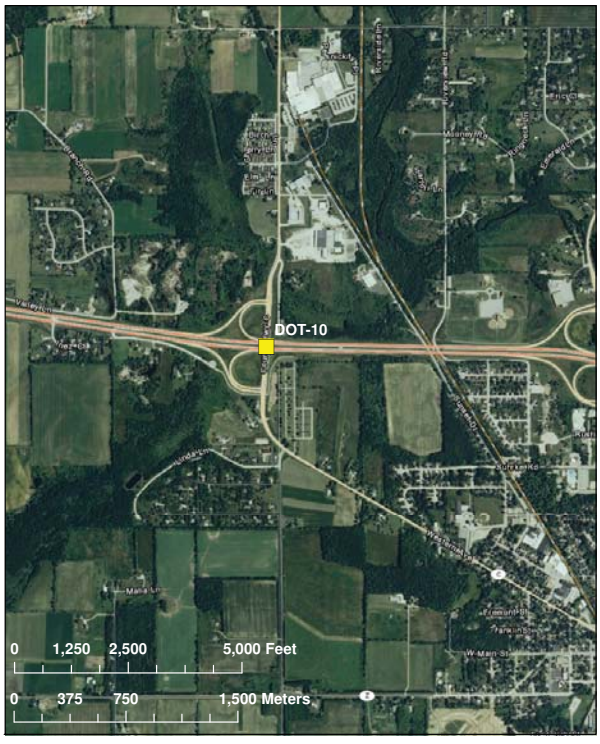

ESRI Aerial Photo - Scale 1:2,000

Description:

The intent of this map is to provide information on the site location and layout of the investigation. Several sources of data were compiled to generate these maps of varying scales. The map scale decreases, area shown decreases, from left to right. Site location is shown from a state level, to city level, to aerial photo and finally a detailed site aerial photo with locations of specific borings conducted for the bridge design.

Source Maps:

DeLorme. Delorme World Basemap [Computer Map]. 1:288,000. [Online Database]. 2009.
ESRI ArcGIS Online, World Imagery [Aerial Photographs]. Visual Scale. http://www.arcgis.com/home/group.html?owner=esri&title=ESRI%20Maps%20and%20Data. (August 25, 2010)
Wisconsin Dept. of Natural Resources. "Wisconsin State Outline." [ESRI Shapefile]. Created by U. S. Census Bureau, 2008.

Site Location Maps
WHRP Site DOT-10
Plymouth, Sheboygan County

Project No: 0092-10-10
Map Scale: Varies
Date: August 25, 2010
Map By: JNH
Reviewed By: JAS

State Location

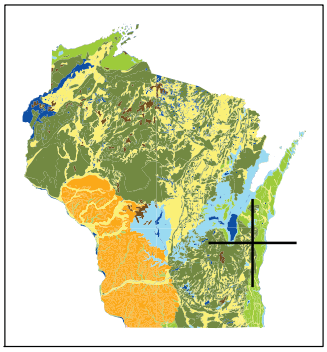

City Location

ESRI Aerial Photo - Scale 1:24,000

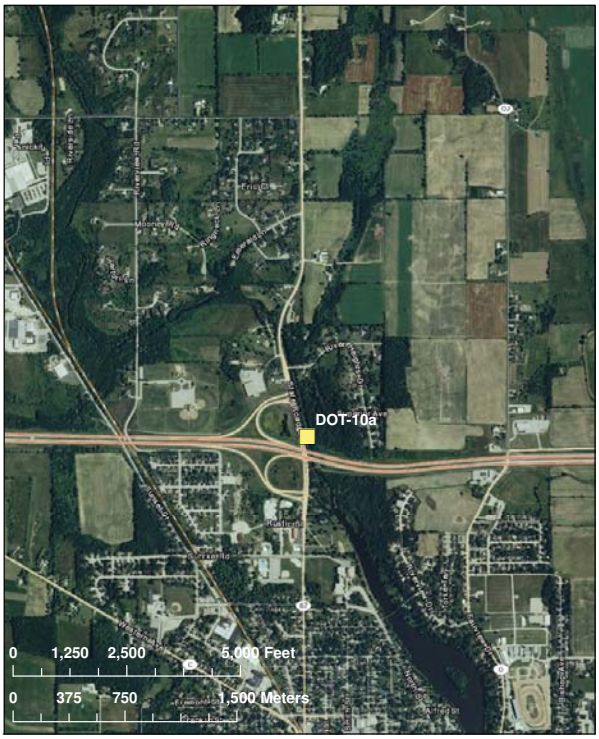

ESRI Aerial Photo - Scale 1:2,000

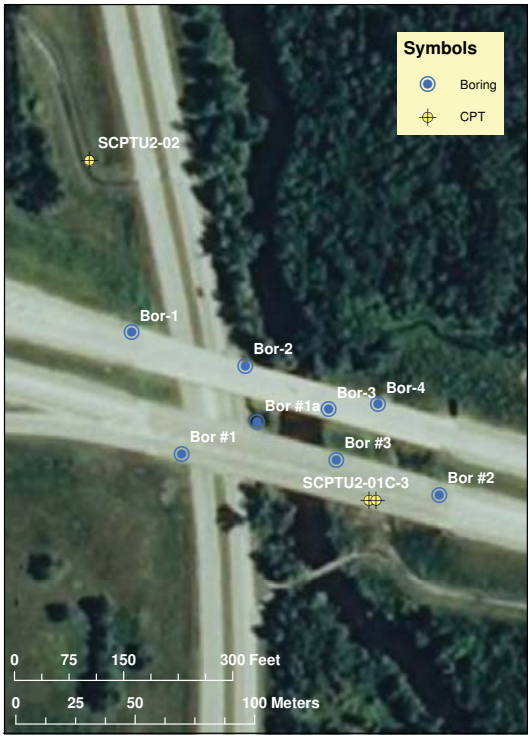

Description:

The intent of this map is to provide information on the site location and layout of the investigation. Several sources of data were compiled to generate these maps of varying scales. The map scale decreases, area shown decreases, from left to right. Site location is shown from a state level, to city level, to aerial photo and finally a detailed site aerial photo with locations of specific borings conducted for the bridge design.

Source Maps:

DeLorme. Delorme World Basemap [Computer Map]. 1:288,000. [Online Database]. 2009.
ESRI ArcGIS Online, World Imagery [Aerial Photographs]. Visual Scale. http://www.arcgis.com/home/group.html?owner=esri&title=ESRI%20Maps%20and%20Data. (August 25, 2010)
Wisconsin Dept. of Natural Resources. "Wisconsin State Outline." [ESRI Shapefile]. Created by U. S. Census Bureau, 2008.

Site Location Maps
WHRP Site DOT-10a
Plymouth, Sheboygan County

Project No: 0092-10-10
Map Scale: Varies
Date: August 25, 2010
Map By: JNH
Reviewed By: JAS

College of Engineering
UNIVERSITY OF WISCONSIN-MADISON

Site: DOT-10a
Description: Plymouth, WI
Boring Date: 2004

Sounding: CPTU2-01
Date: 11/15/2010
Operator: Elliott M. & James S.

Baseline Zero Shifts (%)

q_t	f_s	u_2
-4.2	-0.8	6.2

Termination Depth: 5.6 Feet
Total Dissipations: 1
Dissipation Time: 6 minutes

Boring Bor-3

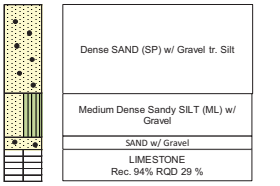

Boring Terminated at 28 feet

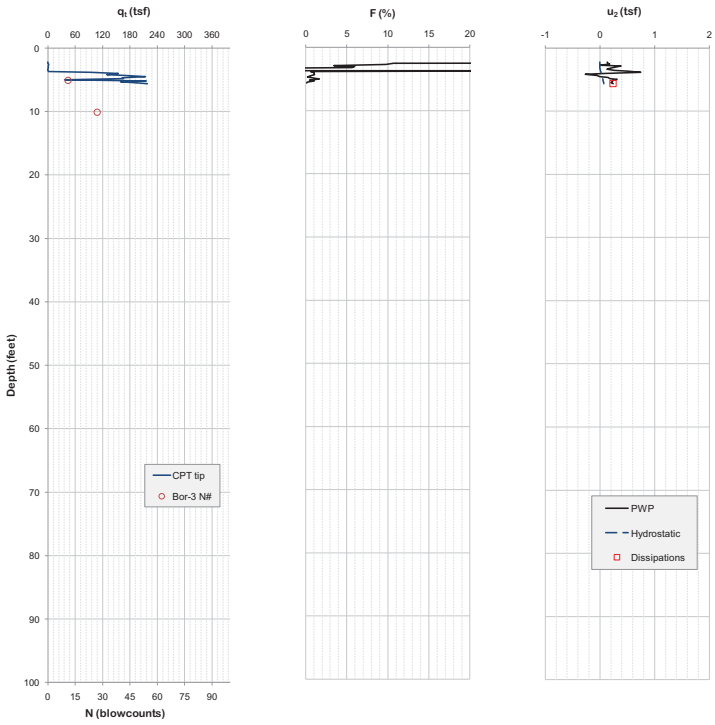

College of Engineering
UNIVERSITY OF WISCONSIN MADISON

Site: DOT-10a
Description: Plymouth, WI
Boring Date: 2004

Sounding: C-3
Date: 11/16/2010
Operator: Elliott M. & James S.

Baseline Zero Shifts (%)

q_t	f_s	u_2

Termination Depth: 8.0 Feet
Total Dissipations:
Dissipation Time:

Boring Bor-3

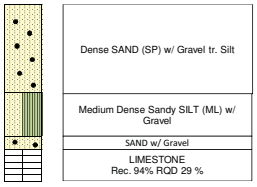

Boring Terminated at 28 feet

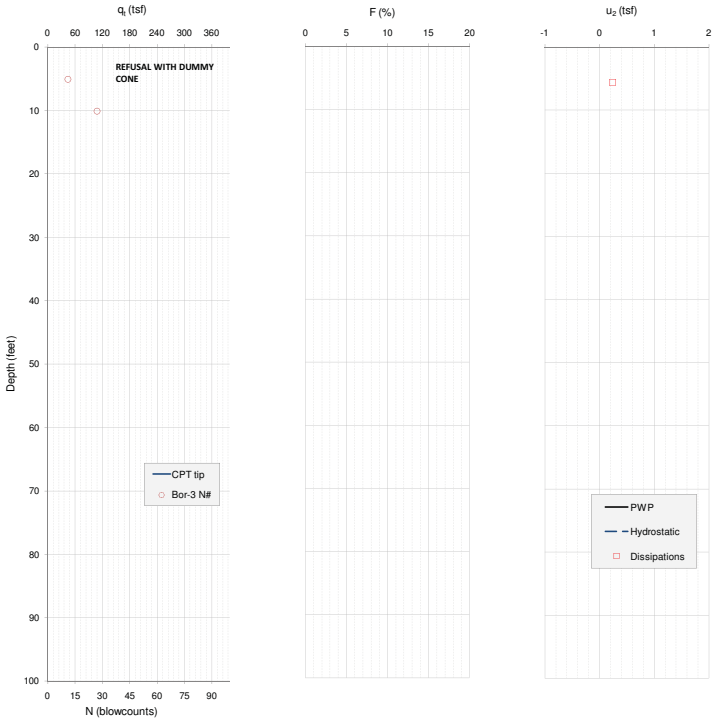

College of Engineering
UNIVERSITY OF WISCONSIN-MADISON

Site: DOT-10a
Description: Plymouth, WI
Boring Date: 2004

Sounding: CPTU2-02
Date: 11/18/2010
Operator: Finn H. & Elliott M.

Baseline Zero Shifts (%)

q_t	f_s	u_2
3.0	-0.6	-0.7

Termination Depth: 7.5 Feet
Total Dissipations: 1
Dissipation Time: 1 minute

Boring Bor-1

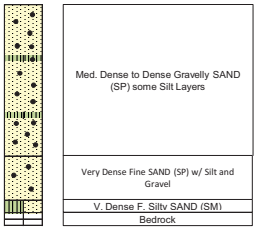

Boring Terminated at 35 feet

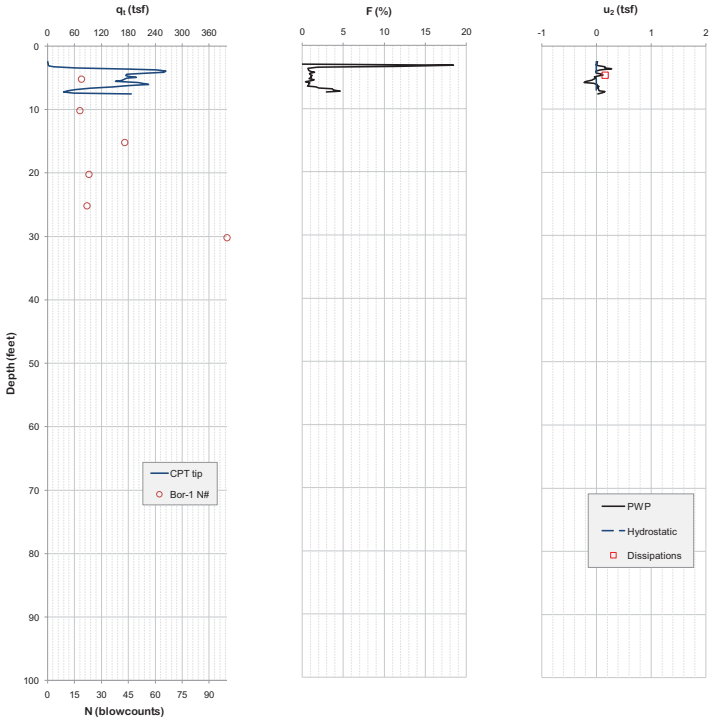

State Location

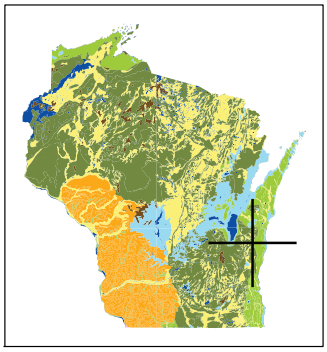

City Location

ESRI Aerial Photo - Scale 1:24,000

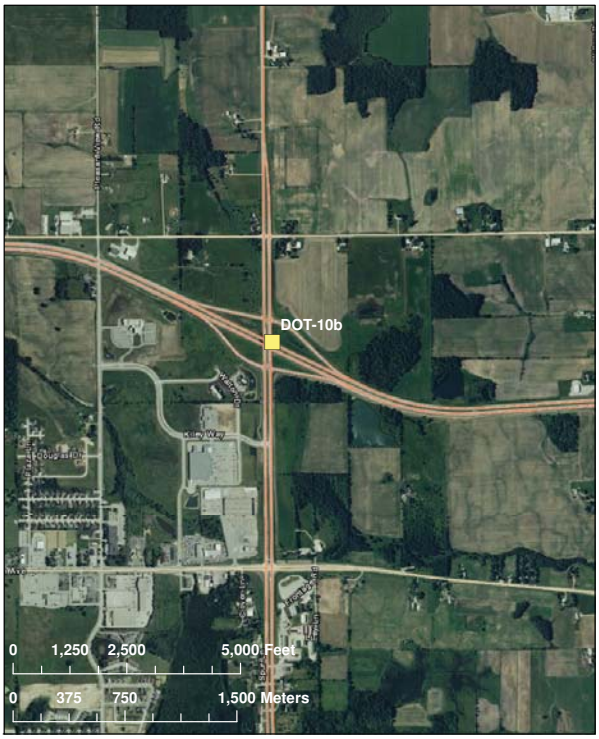

ESRI Aerial Photo - Scale 1:2,000

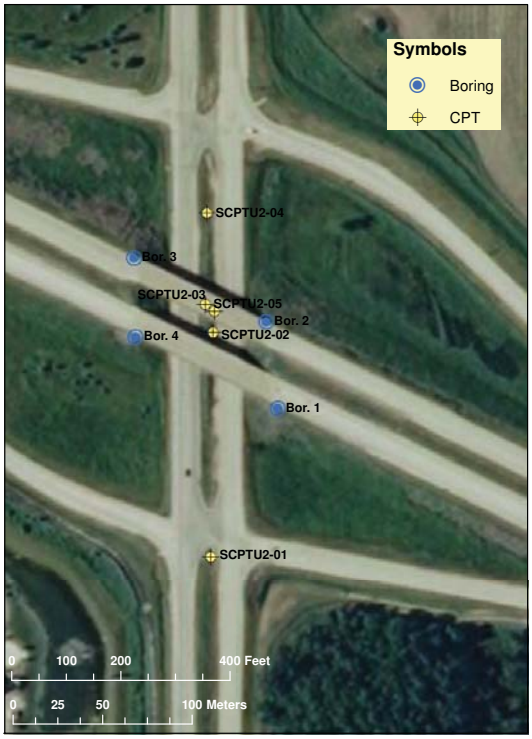

Description:

The intent of this map is to provide information on the site location and layout of the investigation. Several sources of data were compiled to generate these maps of varying scales. The map scale decreases, area shown decreases, from left to right. Site location is shown from a state level, to city level, to aerial photo and finally a detailed site aerial photo with locations of specific borings conducted for the bridge design.

Source Maps:

DeLorme. Delorme World Basemap [Computer Map]. 1:288,000. [Online Database]. 2009.
ESRI ArcGIS Online, World Imagery [Aerial Photographs]. Visual Scale. http://www.arcgis.com/home/group.html?owner=esri&title=ESRI%20Maps%20and%20Data. (August 25, 2010)
Wisconsin Dept. of Natural Resources. "Wisconsin State Outline." [ESRI Shapefile]. Created by U. S. Census Bureau, 2008.

Site Location Maps
WHRP DOT-10b
Plymouth, Sheboygan County

Project No: 0092-10-10
Map Scale: Varies
Date: August 25, 2010
Map By: JNH
Reviewed By: JAS

College of Engineering
UNIVERSITY OF WISCONSIN-MADISON

Site: DOT-10b
Description: Plymouth, WI
Boring Date: 1981

Sounding: SCPTU2-02
Date: 11/19/2010
Operator: Finn H. & James S.

Baseline Zero Shifts (%)

q_t	f_s	u_2
6.1	-0.5	0.5

Termination Depth: 18.0 Feet
Total Dissipations: 5
Dissipation Time: 67 minutes

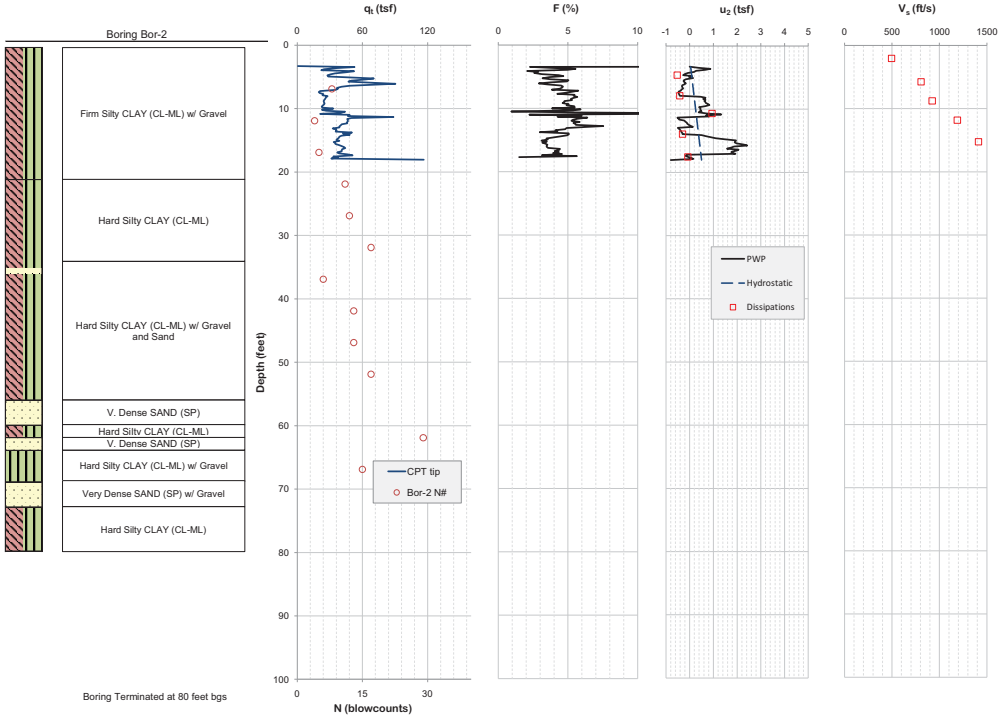

College of Engineering
UNIVERSITY OF WISCONSIN-MADISON

Site: DOT-10b
Description: Plymouth, WI
Boring Date: 1981

Sounding: SCPTU2-01
Date: 11/19/2010
Operator: Finn H. & Elliott M.

Baseline Zero Shifts (%)

q_t	f_s	u_2
8.0	-1.4	2.1

Termination Depth: 12.0 Feet
Total Dissipations: 4
Dissipation Time: 84 minutes

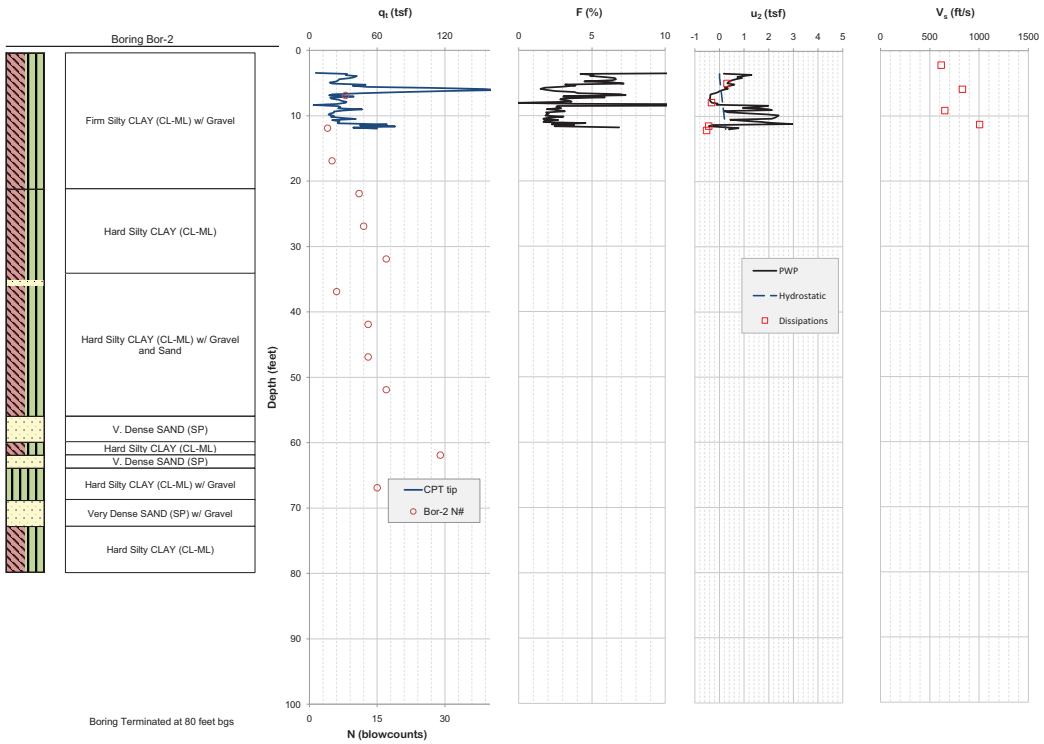

Boring Terminated at 80 feet bgs

College of Engineering
UNIVERSITY OF WISCONSIN-MADISON

Site: DOT-10b
Description: Plymouth, WI
Boring Date: 1981

Sounding: SCPTU2-03
Date: 11/20/2010
Operator: Finn H. & James S.

Baseline Zero Shifts (%)

q_t	f_s	u_2
-1.3	0.5	3.5

Termination Depth: 0.0 Feet
Total Dissipations: 2
Dissipation Time: 48 minutes

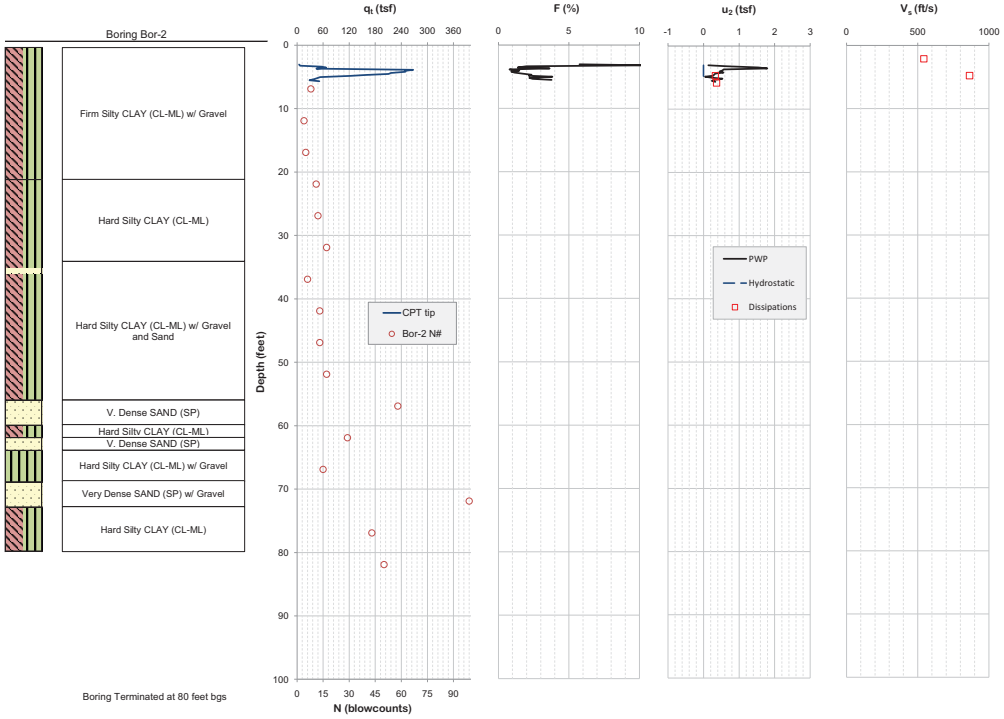

Boring Terminated at 80 feet bgs

College of Engineering
UNIVERSITY OF WISCONSIN-MADISON

Site: DOT-10b
Description: Plymouth, WI
Boring Date: 1981

Sounding: SCPTU2-04/04a
Date: 11/20/2010
Operator: Finn H. & James S.

Baseline Zero Shifts (%)

q_t	f_s	u_2
5.9	9.0	10.5

Termination Depth: 23.7 Feet
Total Dissipations: 6
Dissipation Time: 185 minutes

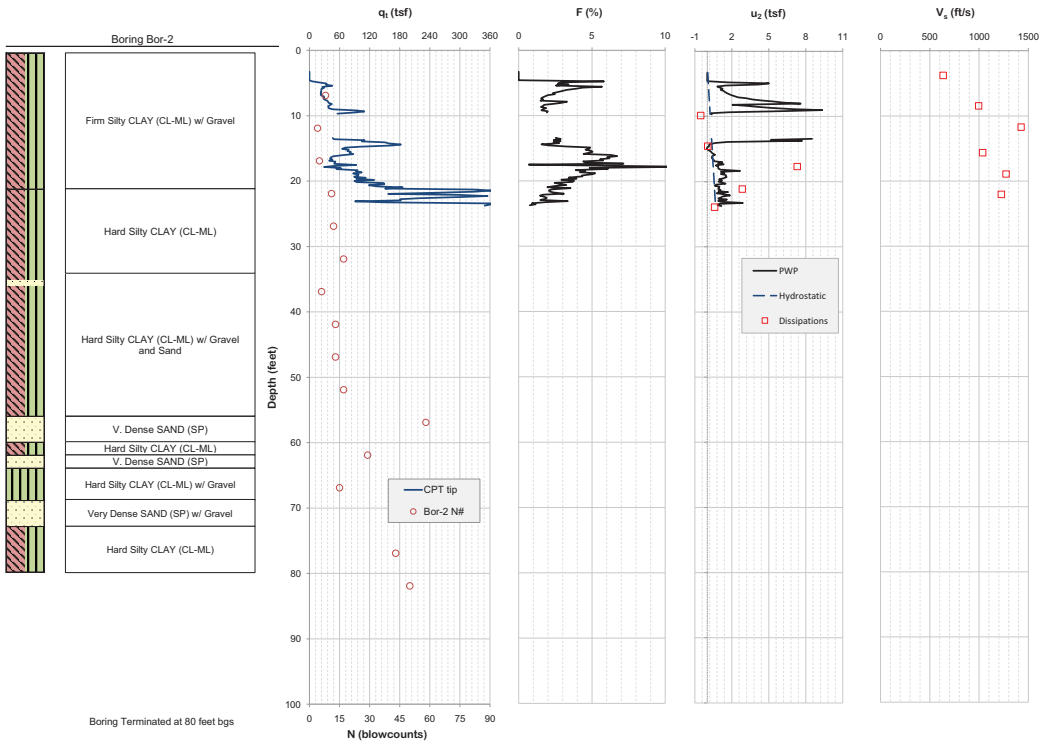

Boring Terminated at 80 feet bgs

College of Engineering
UNIVERSITY OF WISCONSIN-MADISON

Site: DOT-10b
Description: Plymouth, WI
Boring Date: 1981

Sounding: SCPTU2-05
Date: 11/20/2010
Operator: Finn H. & James S.

Baseline Zero Shifts (%)

q_t	f_s	u_2
-2.7	-2.2	-3.0

Termination Depth: 12.5 Feet
Total Dissipations: 2
Dissipation Time: 41 minutes

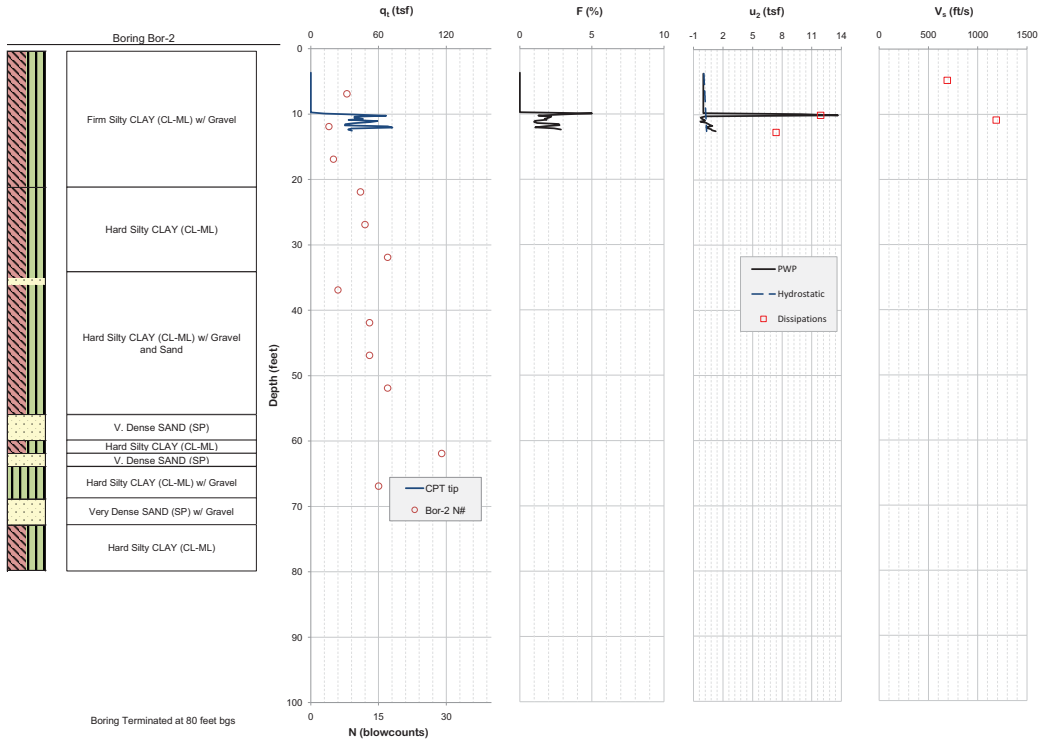

Boring Terminated at 80 feet bgs

State Location

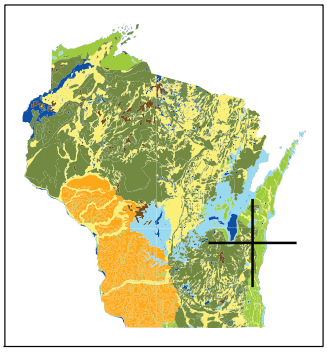

City Location

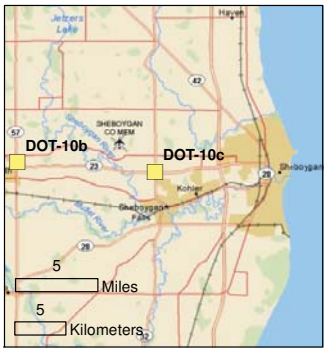

ESRI Aerial Photo - Scale 1:24,000

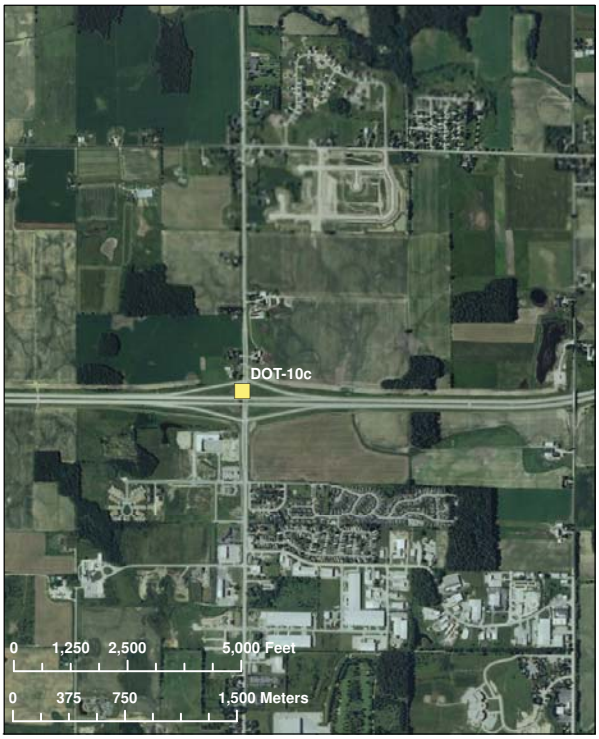

ESRI Aerial Photo - Scale 1:2,000

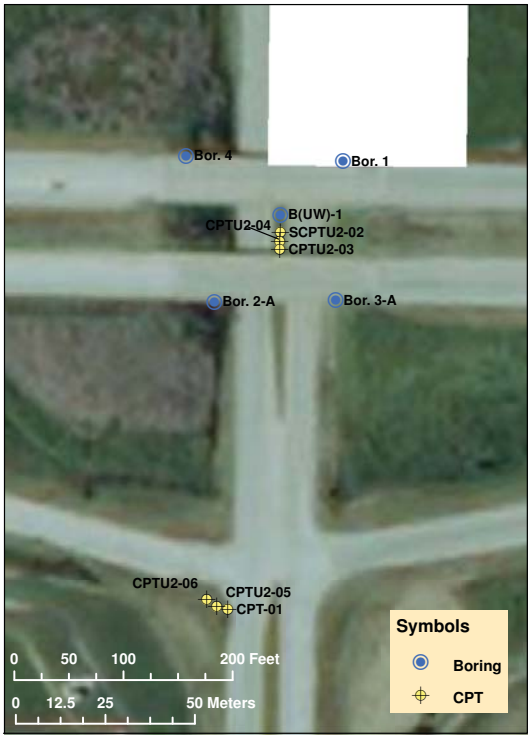

Description:

The intent of this map is to provide information on the site location and layout of the investigation. Several sources of data were compiled to generate these maps of varying scales. The map scale decreases, area shown decreases, from left to right. Site location is shown from a state level, to city level, to aerial photo and finally a detailed site aerial photo with locations of specific borings conducted for the bridge design.

Source Maps:

DeLorme. Delorme World Basemap [Computer Map]. 1:288,000. [Online Database]. 2009.
ESRI ArcGIS Online, World Imagery [Aerial Photographs]. Visual Scale. http://www.arcgis.com/home/group.html?owner=esri&title=ESRI%20Maps%20and%20Data. (August 25, 2010)
Wisconsin Dept. of Natural Resources. "Wisconsin State Outline." [ESRI Shapefile]. Created by U. S. Census Bureau, 2008.

Site Location Maps
WHRP Site DOT-10c
Sheboygan Falls, Sheboygan County

Project No: 0092-10-10
Map Scale: Varies
Date: August 25, 2010
Map By: JNH
Reviewed By: JAS

College of Engineering
UNIVERSITY OF WISCONSIN-MADISON

Site: DOT-10c
Description: Sheboygan Falls, WI
Boring Date: 3/20/2001

Sounding: CPT-01
Date: 11/22/2010
Operator: Finn H. & James S.

Baseline Zero Shifts (%)

q_t	f_s	u_2
3.8	-1.4	-1.9

Termination Depth: 19.4 Feet
Total Dissipations: 0
Dissipation Time: 0

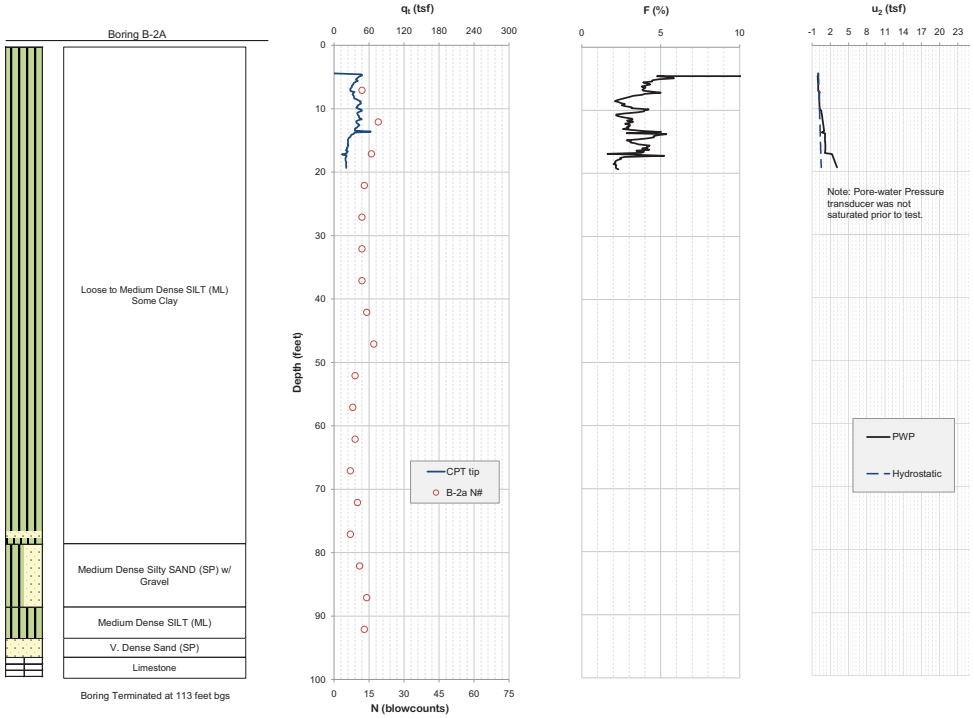

College of Engineering
UNIVERSITY OF WISCONSIN-MADISON

Site: DOT-10c
Description: STH 23 & STH 32, Sheboygan Falls, WI
Boring Date: 3/20/2001

Sounding: SCPTU2-02
Date: 11/28/2010
Operator: Finn H., James S., Elliott M.

Baseline Zero Shifts (%)

q_t	f_s	u_2
7.3	0.0	3.1

Termination Depth: 25.6 Feet
Total Dissipations: 8
Dissipation Time: 2887 minutes

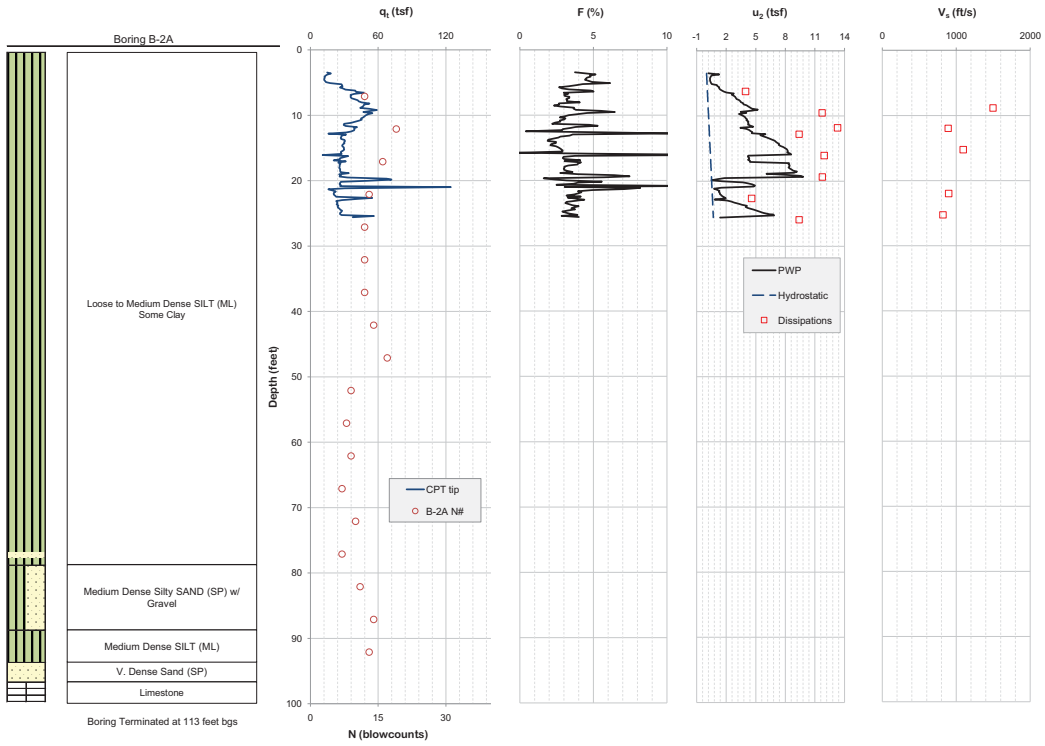

College of Engineering
UNIVERSITY OF WISCONSIN-MADISON

Site: DOT-10c
Description: STH 23 & STH 32, Sheboygan Falls, WI
Boring Date: 3/20/2001

Sounding: CPTU2-03
Date: 6/4/2011
Operator: James S., Finn H., Seth S.

Baseline Zero Shifts (%)

q_t	f_s	u_2
-3.9	0.6	2.7

Advance Rate: 0.1 mm/sec

Termination Depth: 19.5 Feet
Total Dissipations: 4
Dissipation Time: 640 minutes

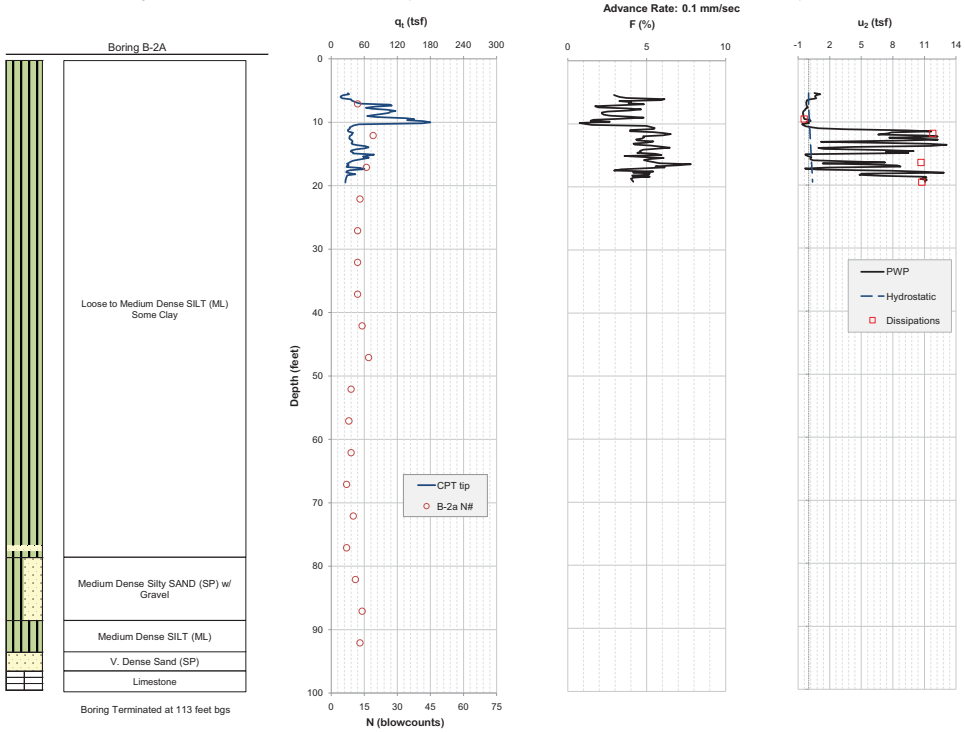

College of Engineering
UNIVERSITY OF WISCONSIN-MADISON

Site: DOT-10c
Description: STH 23 & STH 32, Sheboygan Falls, WI
Boring Date: 3/20/2001

Sounding: CPTU2-04
Date: 6/5/2011
Operator: Finn H., Seth S.

Baseline Zero Shifts (%)

q_t	f_s	u_2
0.2	-4.6	9.1

Advance Rate: 1.6 mm/sec

Termination Depth: 22.5 Feet
Total Dissipations: 6
Dissipation Time: 700 minutes

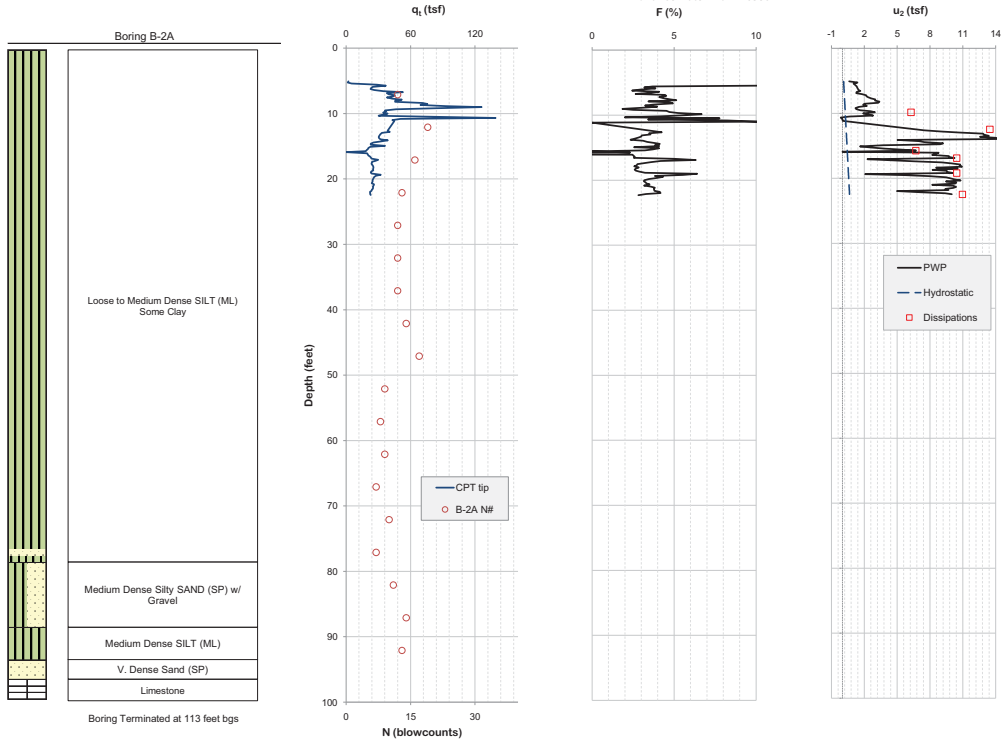

College of Engineering
UNIVERSITY OF WISCONSIN-MADISON

Site: DOT-10c
Description: STH 23 & STH 32, Sheboygan Falls, WI
Boring Date: 3/20/2001

Sounding: CPTU2-05
Date: 6/6/2011
Operator: Finn H., Seth S.

Baseline Zero Shifts (%)

q_t	f_s	u_2
-6.2	1.0	-8.2

Termination Depth: 21.2 Feet
Total Dissipations: 2
Dissipation Time: 10 minutes

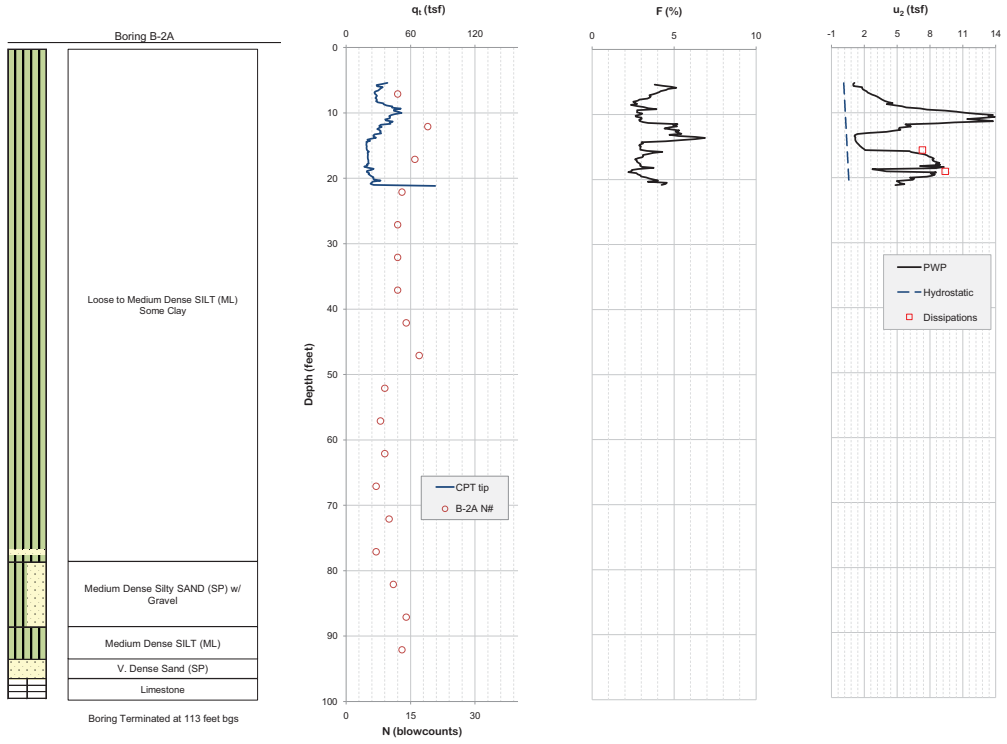

College of Engineering
UNIVERSITY OF WISCONSIN-MADISON

Site: DOT-10c
Description: STH 23 & STH 32, Sheboygan Falls, WI
Boring Date: 3/20/2001

Sounding: CPTU2-06
Date: 6/7/2011
Operator: Seth S. & Finn H.

Baseline Zero Shifts (%)

q_t	f_s	u_2
N/A	N/A	N/A

Termination Depth: 20.0 Feet
Total Dissipations: 0
Dissipation Time: 0

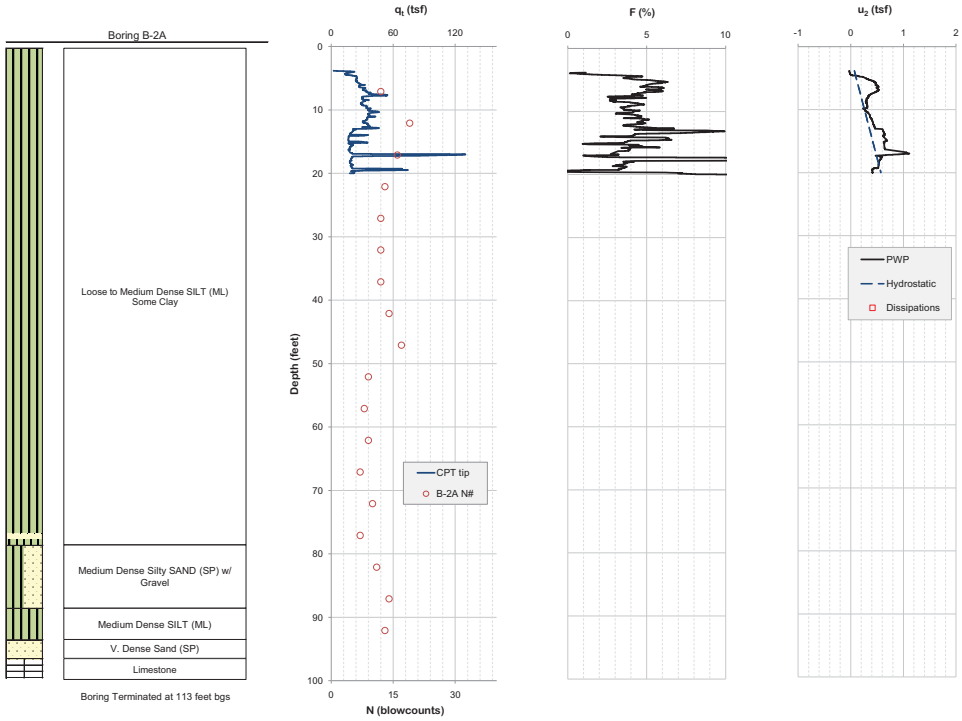

State Location

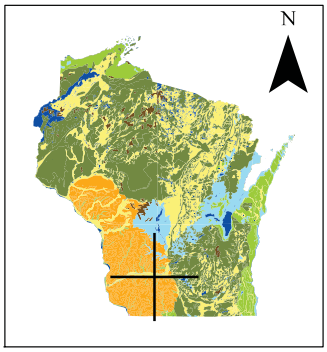

City Location

ESRI Aerial Photo - Scale 1:24,000

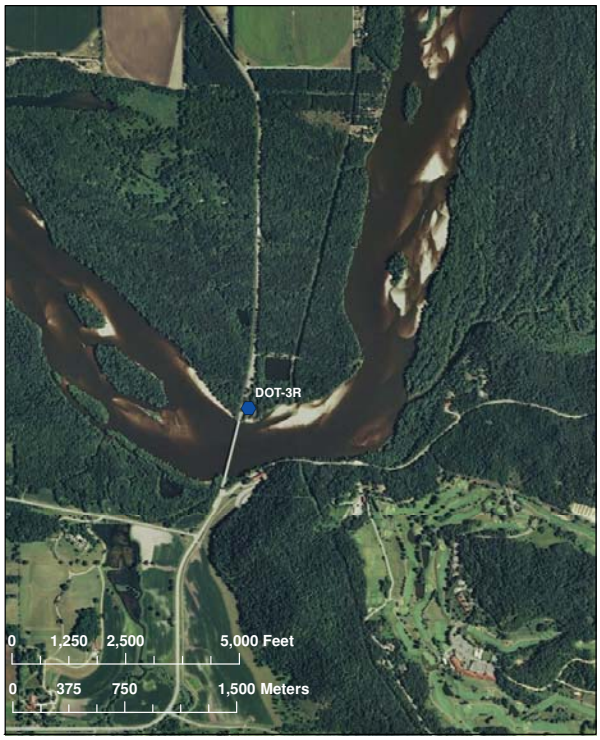

ESRI Aerial Photo - Scale 1:3,000

Description:

The intent of this map is to provide information on the site location and layout of the investigation. Several sources of data were compiled to generate these maps of varying scales. The map scale decreases, area shown decreases, from left to right. Site location is shown from a state level, to city level, to aerial photo and finally a detailed site aerial photo with locations of specific borings conducted for the bridge design.

Source Maps:

DeLorme. Delorme World Basemap [Computer Map]. 1:288,000. [Online Database]. 2009.
ESRI ArcGIS Online, World Imagery [Aerial Photographs]. Visual Scale. http://www.arcgis.com/home/group.html?owner=esri&title=ESRI%20Maps%20and%20Data. (August 24, 2010)
Wisconsin Dept. of Natural Resources. "Wisconsin State Outline." [ESRI Shapefile]. Created by U. S. Census Bureau, 2008.

Site Location Maps
WHRP Site DOT-3R
STH-23 & Wisconsin River
Sauk County

Project No: 0092-10-10
Map Scale: Varies
Date: April 5,2011
Map By: JNH
Reviewed By: JAS

College of Engineering
UNIVERSITY OF WISCONSIN-MADISON

Site: DOT-3R
Description: Spring Green, WI
Boring Date: 1964

Sounding: CPTU2-01
Date: 3/31/2011
Operator: Finn H. & James S.

Baseline Zero Shifts (%)

q_t	f_s	u_2
-2.6	1.3	3.0

Termination Depth: 74.5 Feet
Total Dissipations: 0
Dissipation Time: 0

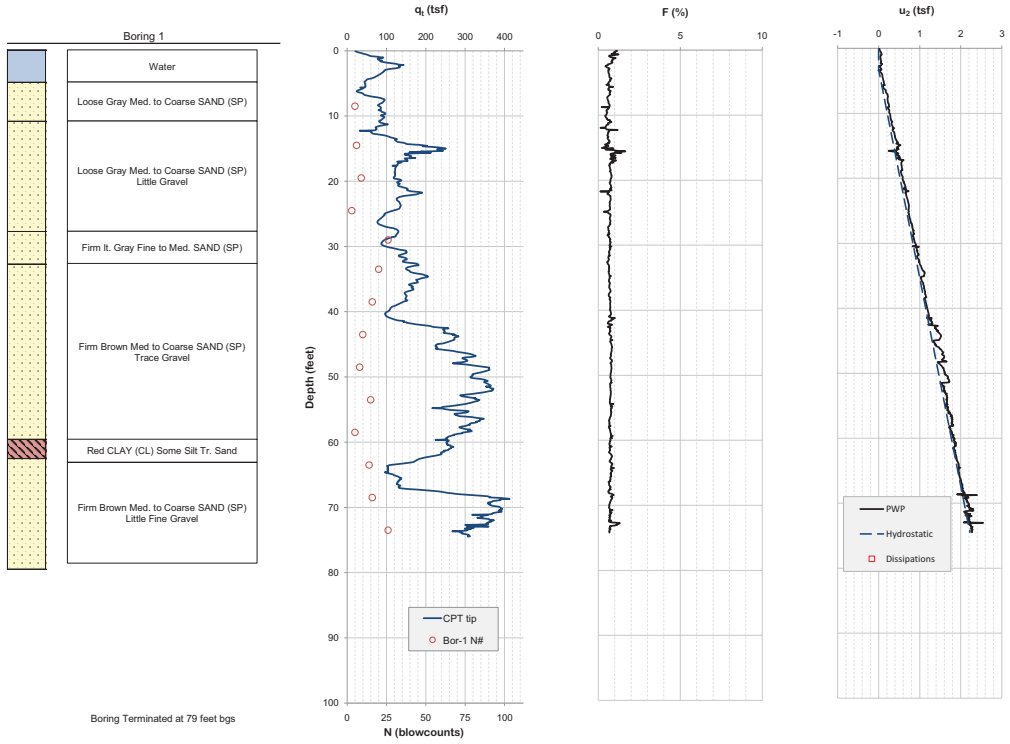

Boring Terminated at 79 feet bgs

College of Engineering
UNIVERSITY OF WISCONSIN-MADISON

Site: DOT-3R
Description: Spring Green, WI
Boring Date: 1964

Sounding: SCPTU2-01
Date: 4/1/2011
Operator: Finn & James

Baseline Zero Shifts (%)

q_t	f_s	u_2
3.0	0.6	-3.7

Termination Depth: 78.0 Feet
Total Dissipations: 24
Dissipation Time: 172 minutes

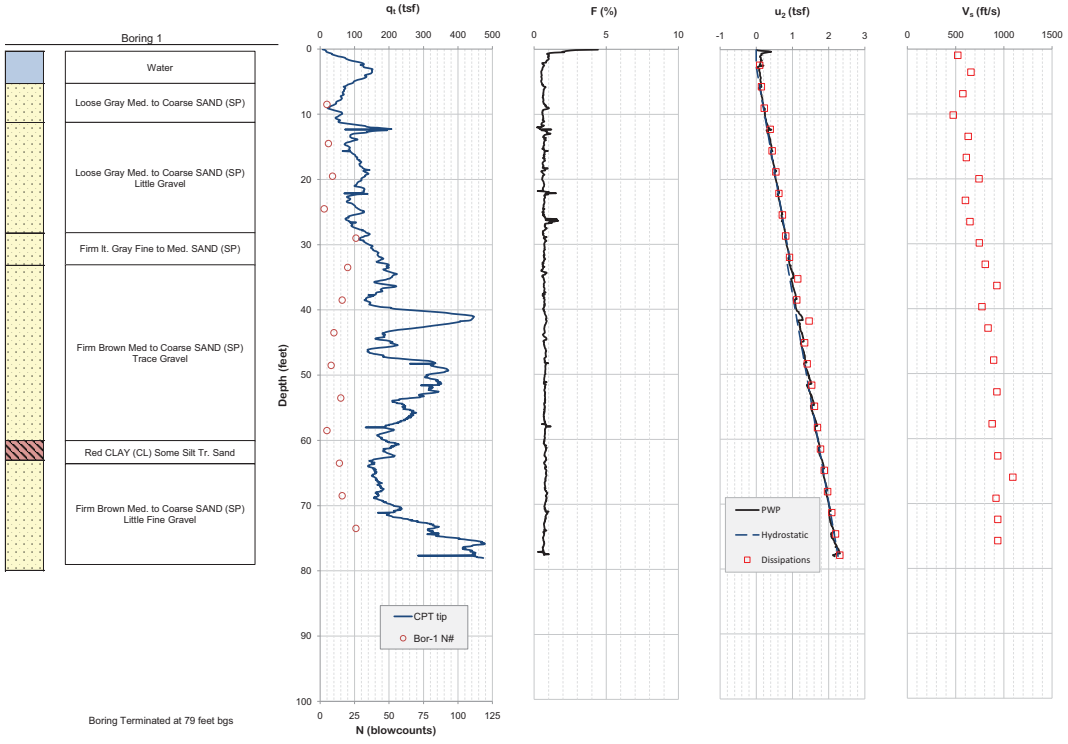

Boring Terminated at 79 feet bgs

College of Engineering
UNIVERSITY OF WISCONSIN-MADISON

Site: DOT-3R
Description: Spring Green
Boring Date: 1964

Sounding: CPTU2-03
Date: 4/1/2011
Operator: Finn H. & James S.

Baseline Zero Shifts (%)		
q_t	f_s	u_2
-2.6	0.1	2.3

Termination Depth: 73.4 Feet
Total Dissipations: 8
Dissipation Time: 40 minutes

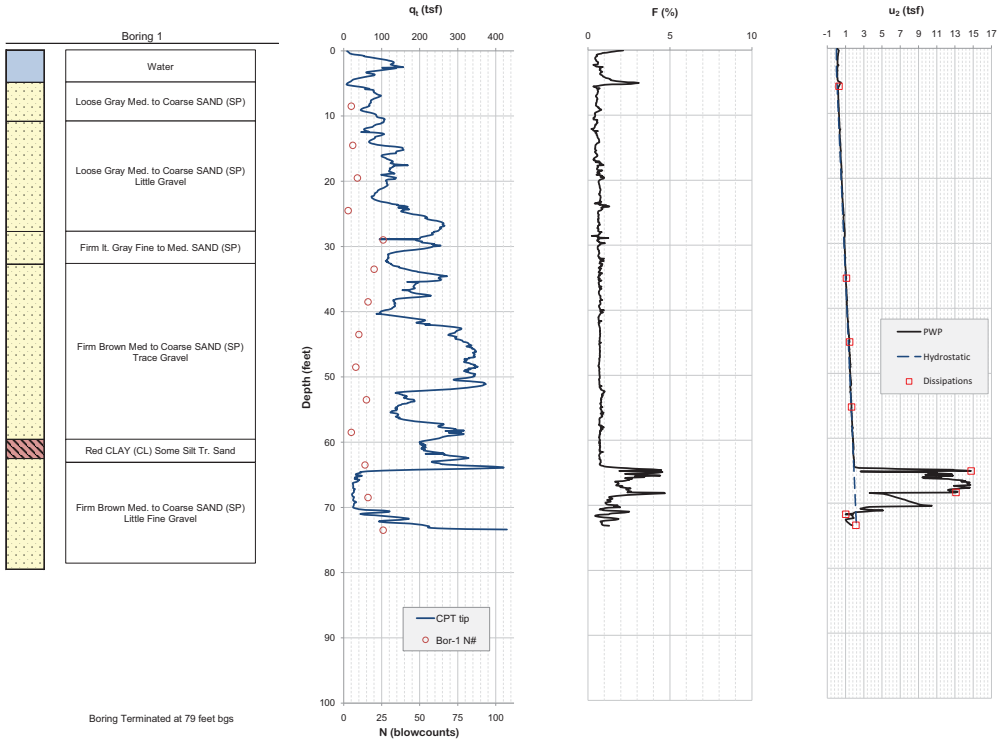

Boring Terminated at 79 feet bgs

College of Engineering
UNIVERSITY OF WISCONSIN-MADISON

Site: DOT-3R
Description: Spring Green, WI
Boring Date: 1964

Sounding: CPTU2-04
Date: 4/1/2011 - 4/2/2011
Operator: Finn H. & James S.

Baseline Zero Shifts (%)		
q_t	f_s	u_2
3.0	-1.6	0.8

Termination Depth: 73.5 Feet
Total Dissipations: 15
Dissipation Time: 339 minutes

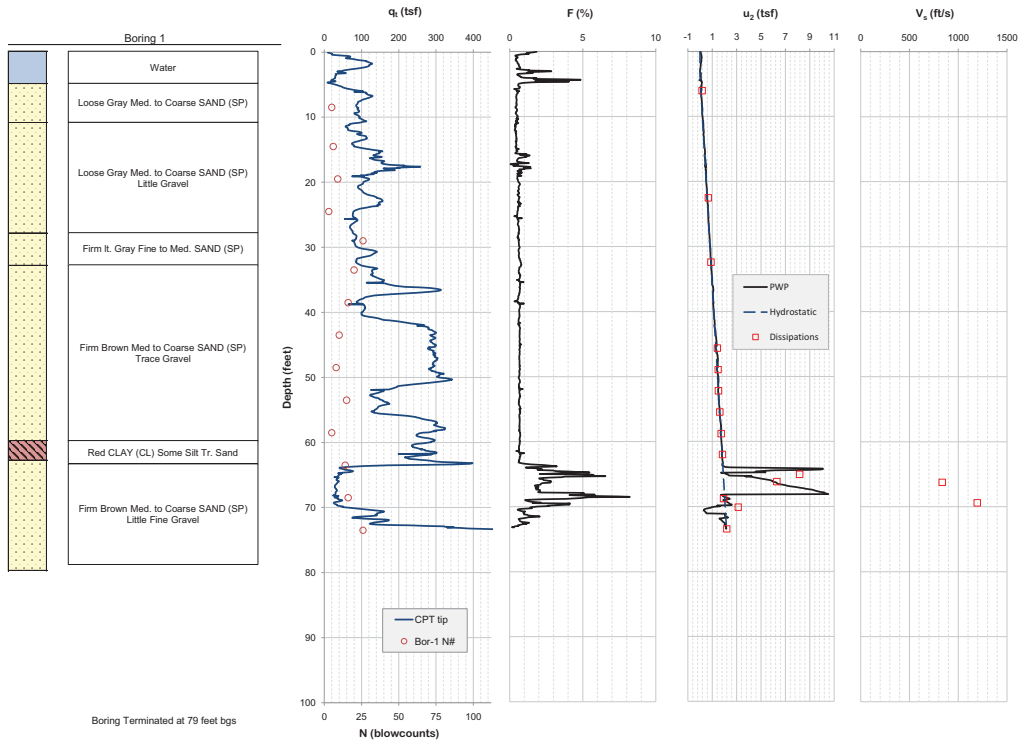

Boring Terminated at 79 feet bgs

College of Engineering
UNIVERSITY OF WISCONSIN-MADISON

Site: DOT-3R
Description: Spring Green, WI
Boring Date: 1964

Sounding: CPTU2-05
Date: 4/2/2011
Operator: Finn H. & James S.

Baseline Zero Shifts (%)

q_t	f_s	u_2
-8.6	-2.8	4.9

Termination Depth: 73.6 Feet
Total Dissipations: 5
Dissipation Time: 15 minutes

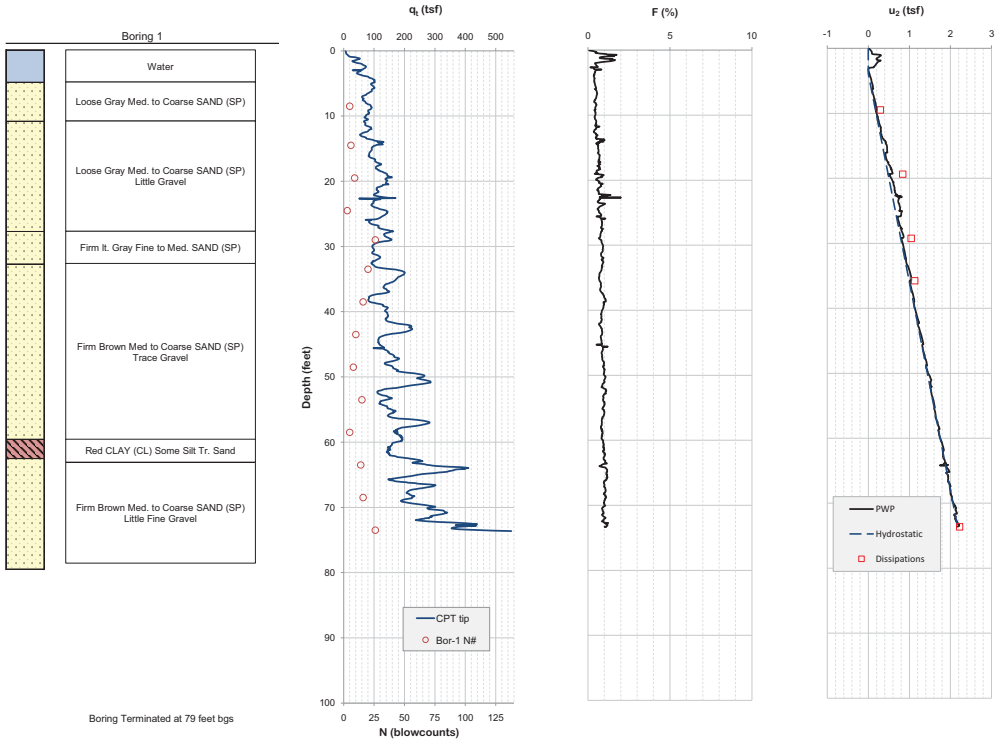

State Location

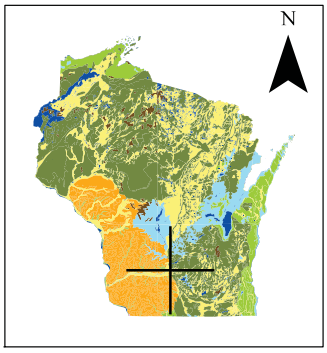

City Location

ESRI Aerial Photo - Scale 1:24,000

ESRI Aerial Photo - Scale 1:2,000

Description:

The intent of this map is to provide information on the site location and layout of the investigation. Several sources of data were compiled to generate these maps of varying scales. The map scale decreases, area shown decreases, from left to right. Site location is shown from a state level, to city level, to aerial photo and finally a detailed site aerial photo with locations of specific borings conducted for the bridge design.

Source Maps:

DeLorme. Delorme World Basemap [Computer Map]. 1:288,000. [Online Database]. 2009.
ESRI ArcGIS Online, World Imagery [Aerial Photographs]. Visual Scale. http://www.arcgis.com/home/group.html?owner=esri&title=ESRI%20Maps%20and%20Data. (August 24, 2010)
Wisconsin Dept. of Natural Resources. "Wisconsin State Outline." [ESRI Shapefile]. Created by U. S. Census Bureau, 2008.

Site Location Maps
WHRP Site Long-8
US-12, Dane County

Project No: 0092-10-10
Map Scale: Varies
Date: April 13, 2011
Map By: JNH
Reviewed By: JAS

College of Engineering
UNIVERSITY OF WISCONSIN-MADISON

Site: Long-8
Description: Roxbury, WI
Boring Date: 4/11/2001

Sounding: CPTU2-01
Date: 4/3/2011
Operator: Finn H. & James S.

Baseline Zero Shifts (%)		
q_t	f_s	u_2
6.9	-1.9	-1.5

Termination Depth: 9.5 Feet
Total Dissipations: 0
Dissipation Time: 0

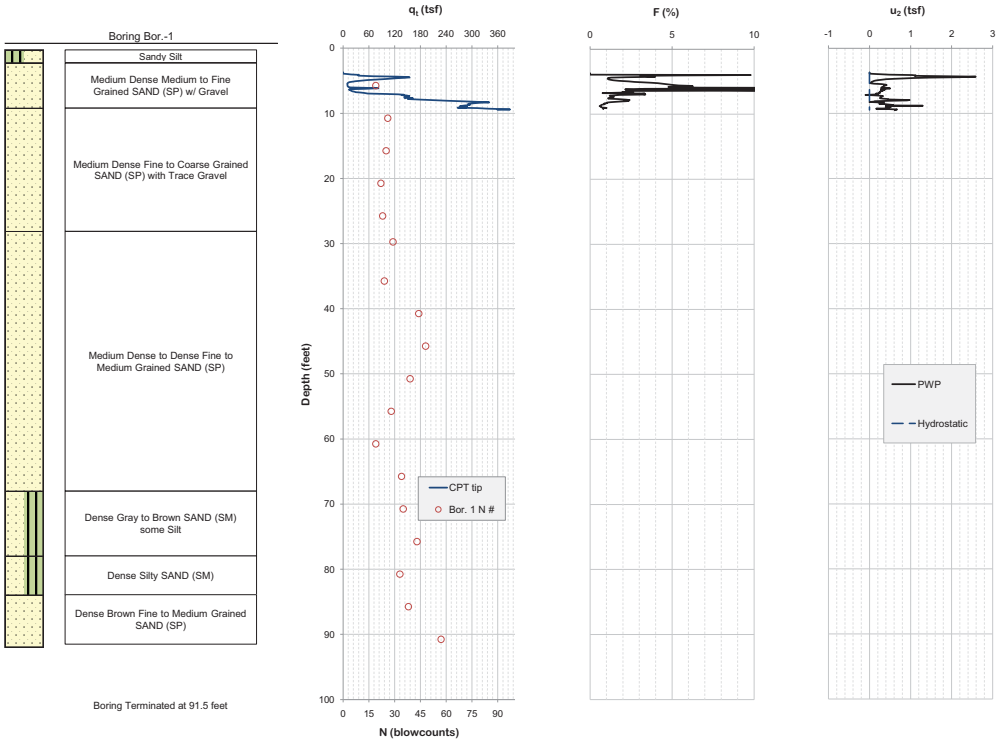

College of Engineering
UNIVERSITY OF WISCONSIN-MADISON

Site: Long-8
Description: Roxbury, WI
Boring Date: 4/11/2001

Sounding: CPTU2-02/02a
Date: 4/3/2011
Operator: Finn H. & James S.

Baseline Zero Shifts (%)		
q_t	f_s	u_2
1.9	-2.1	1.5

Termination Depth: 6.8 Feet
Total Dissipations: 0
Dissipation Time: 0

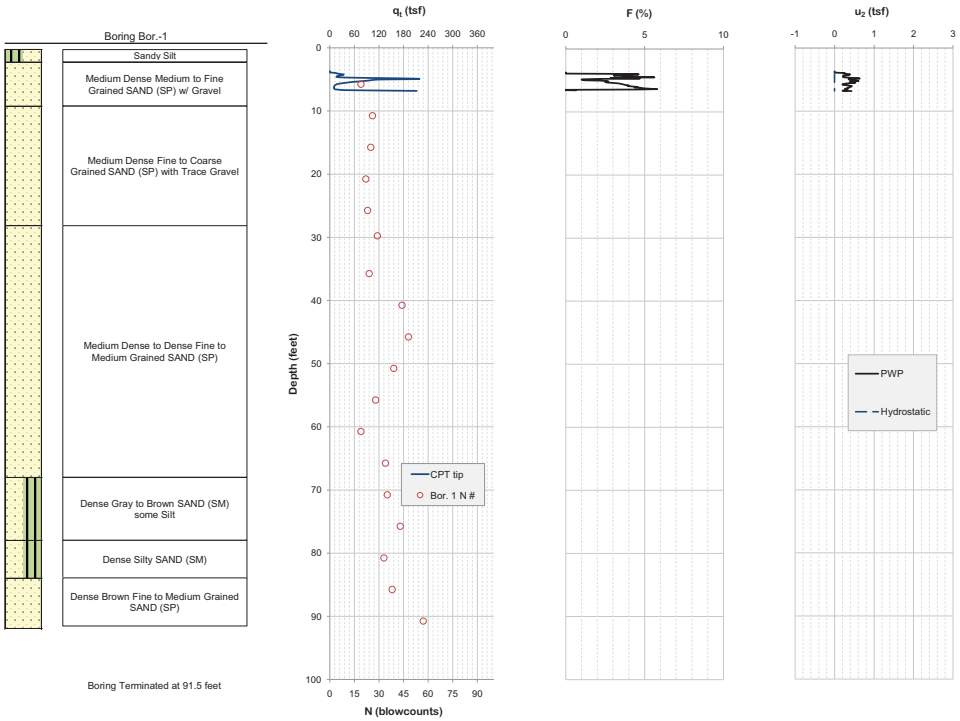

College of Engineering
UNIVERSITY OF WISCONSIN-MADISON

Site: Long-8
Description: Roxbury, WI
Boring Date: 4/11/2001

Sounding: SCPTU2-03
Date: 4/3/2011
Operator: Finn H. & James S.

Baseline Zero Shifts (%)		
q_t	f_s	u_2
2.1	31.8	-0.1

Termination Depth: 3.2 Feet
Total Dissipations: 0
Dissipation Time: 0

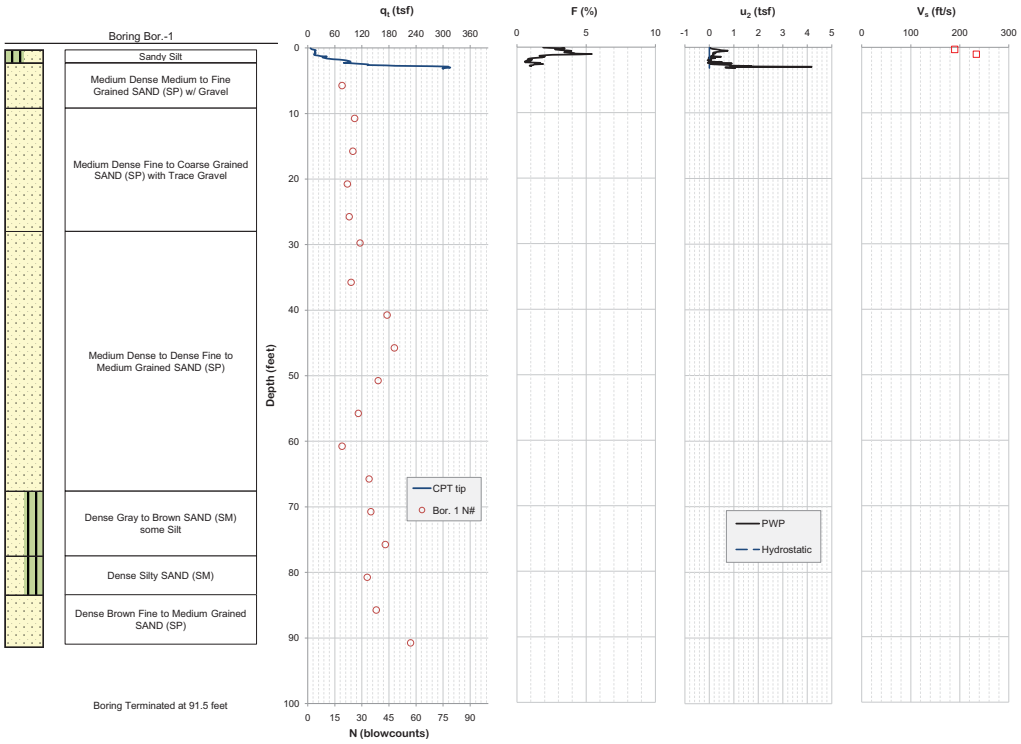

College of Engineering
UNIVERSITY OF WISCONSIN-MADISON

Site: Long-8
Description: Roxbury, WI
Boring Date: 4/11/2001

Sounding: SCPTU2-04
Date: 4/3/2011
Operator: Finn H. & James S.

Baseline Zero Shifts (%)		
q_t	f_s	u_2
2.8	-0.3	-0.2

Termination Depth: 3.2 Feet
Total Dissipations: 0
Dissipation Time: 0

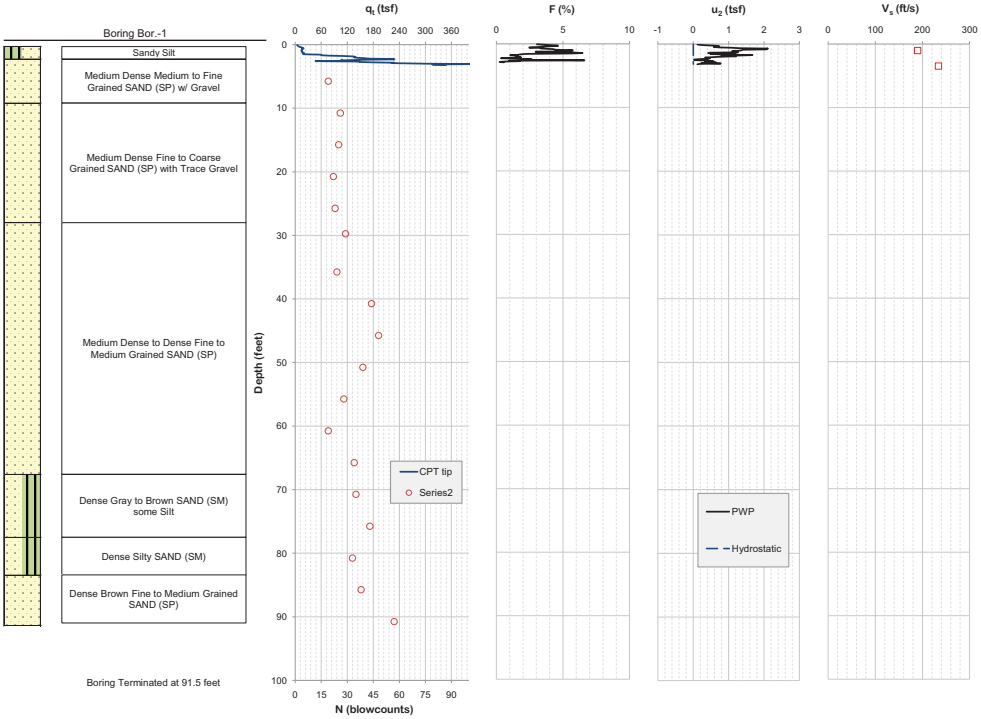

College of Engineering
UNIVERSITY OF WISCONSIN-MADISON

Site: Long-8
Description: Roxbury, WI
Boring Date: 4/11/2001

Sounding: CPTU2-05
Date: 4/4/2011
Operator: Finn H. & James S.

Baseline Zero Shifts (%)

q_t	f_s	u_2
-2.0	-0.6	-0.8

Termination Depth: 1.9 Feet
Total Dissipations: 0
Dissipation Time: 0

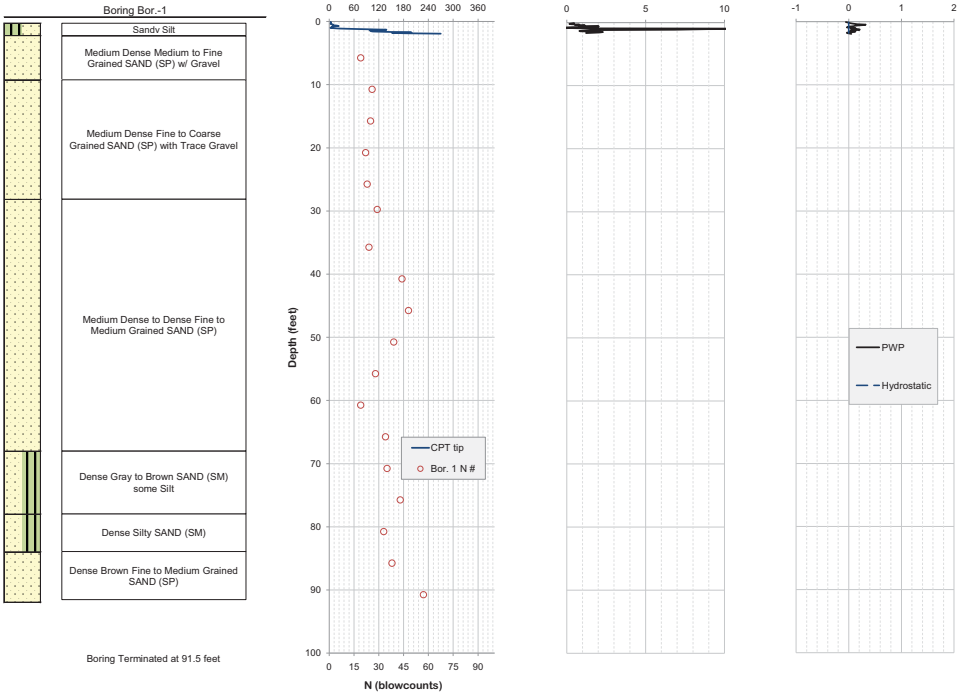

Appendix 3

Cone penetration test site summaries

Previous investigations in Minnesota

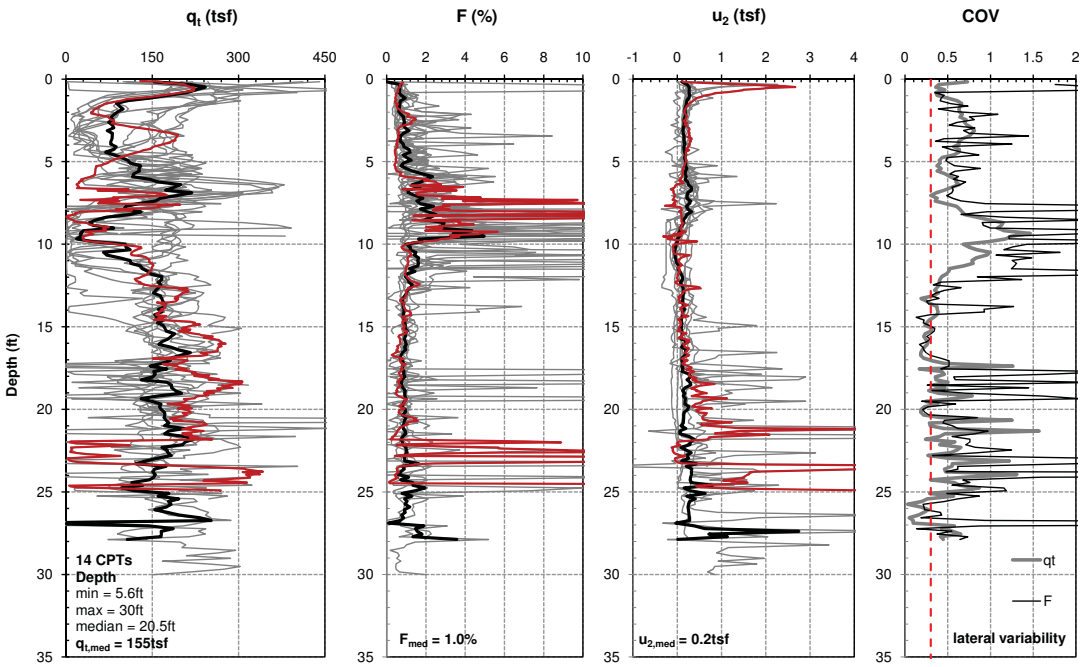

Site 1: MAC Hennepin County

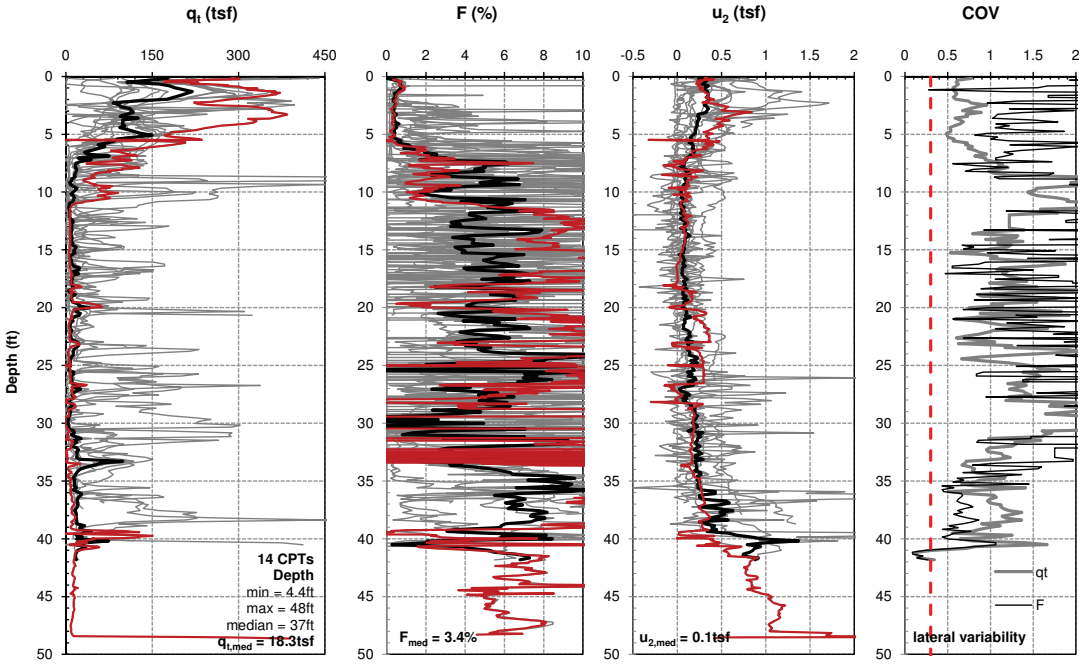

Site 2: 6918-69 St. Louis County

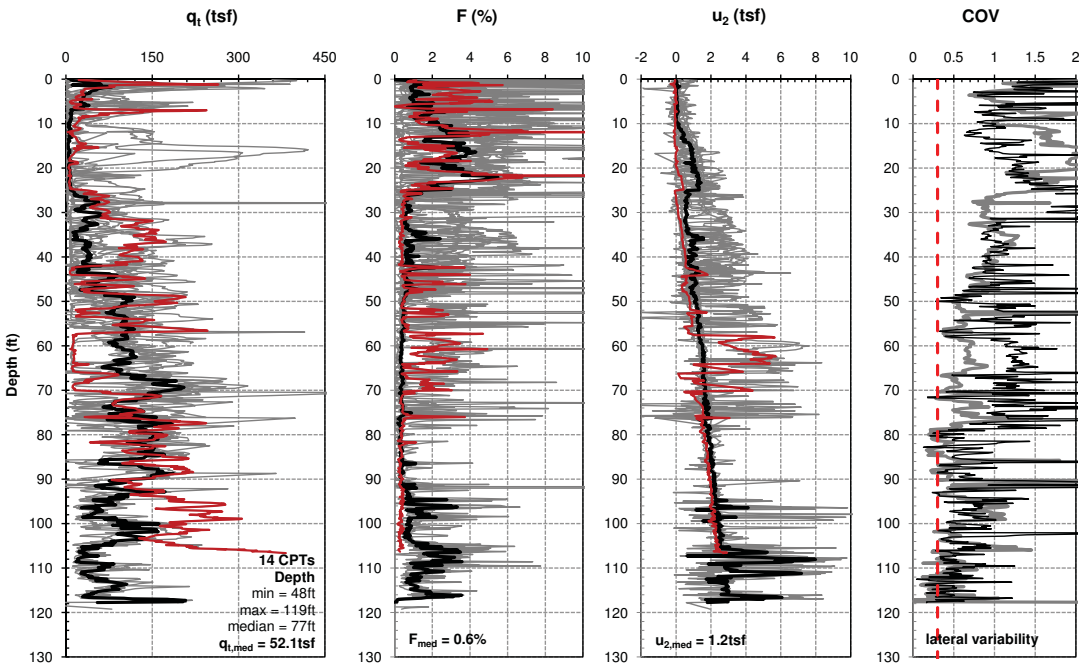

Site 3: 8285-80 Washington County (Wakota Bridge)

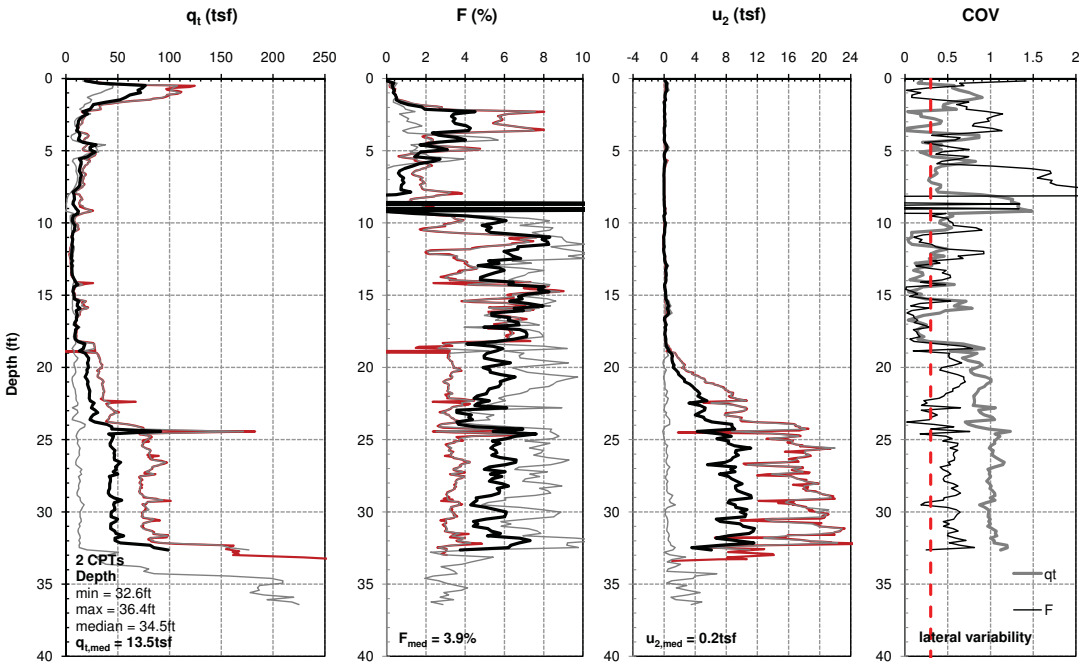

Site 4: 0916-16 Carlton County

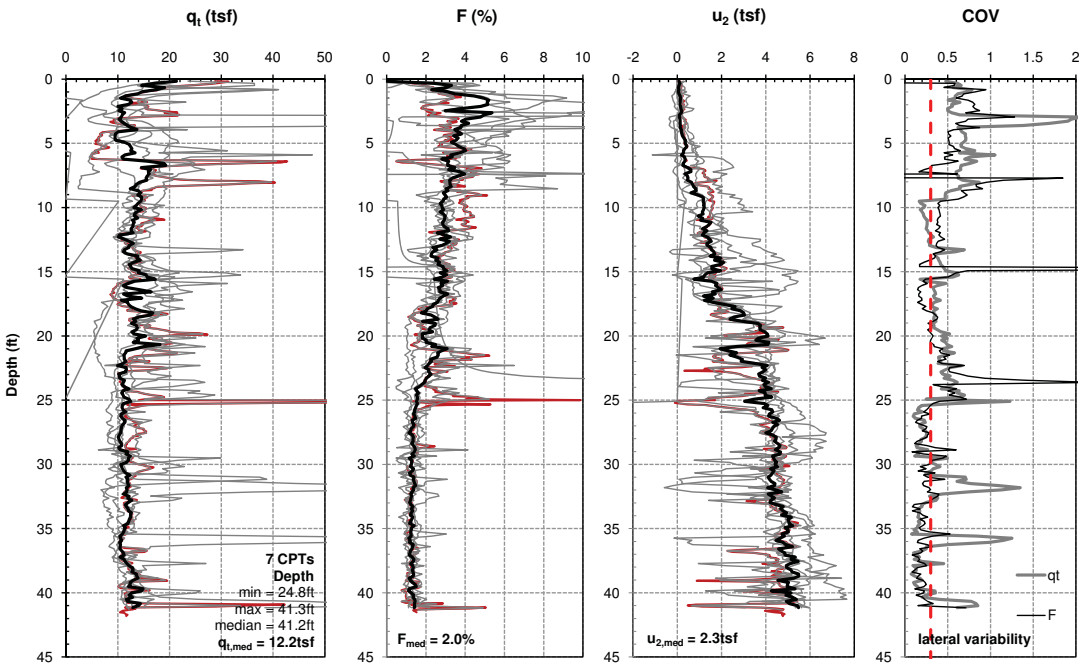

Site 5: 2713-75 Hennepin County

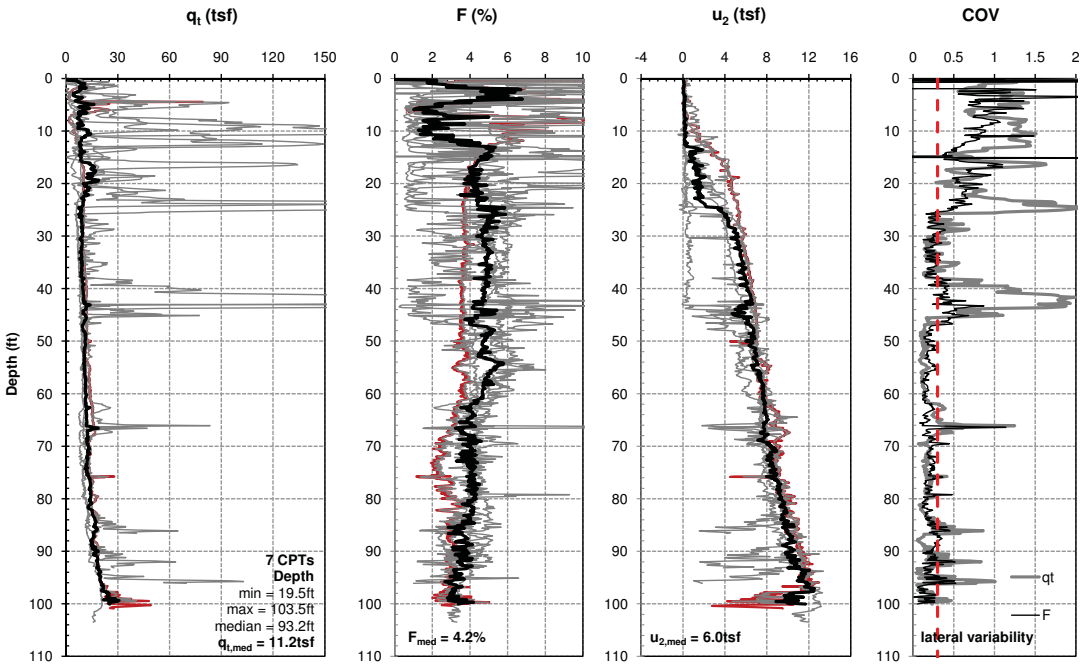

Site 6: 3609-30 Koochiching County

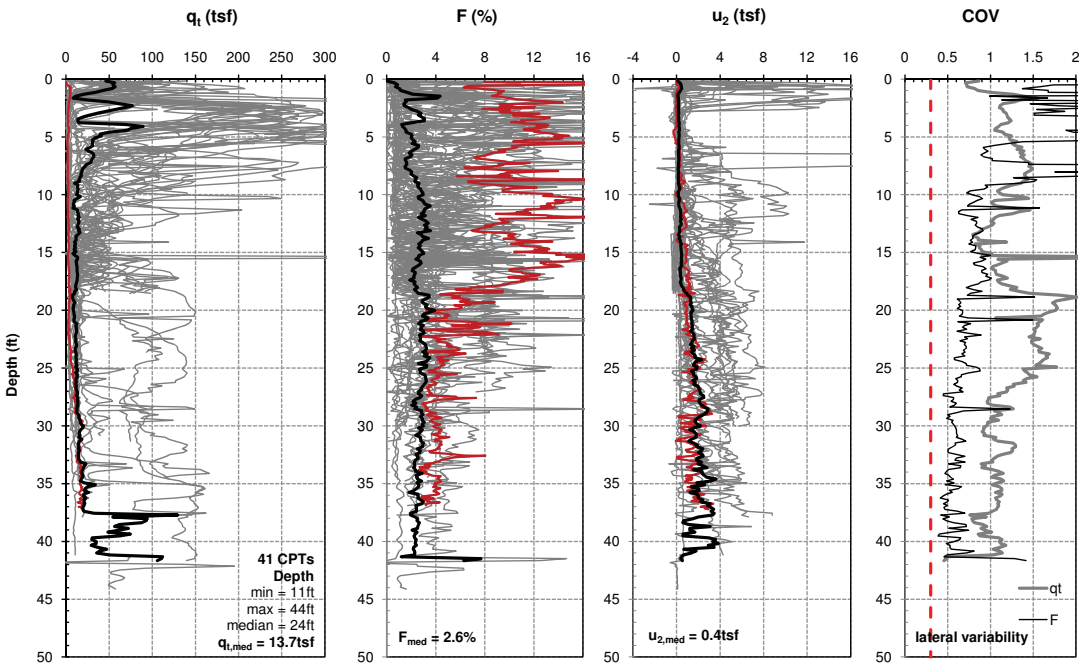

Site 7: 8103-47 Waseca County

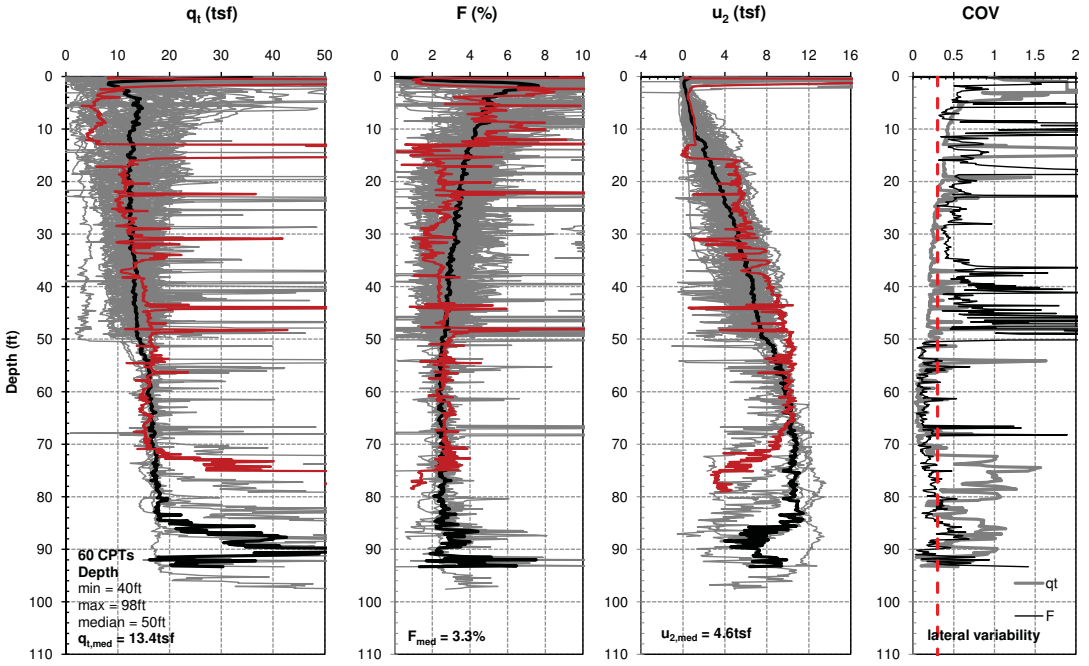

Site 8: 3609-25 Koochiching County

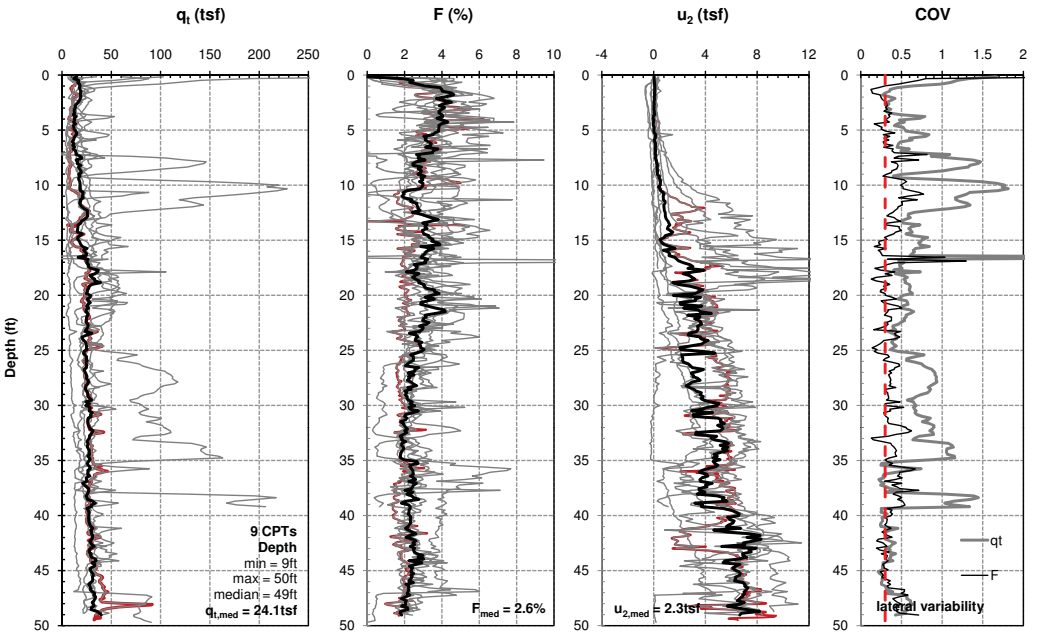

Site 9: 1009-16 Carver County

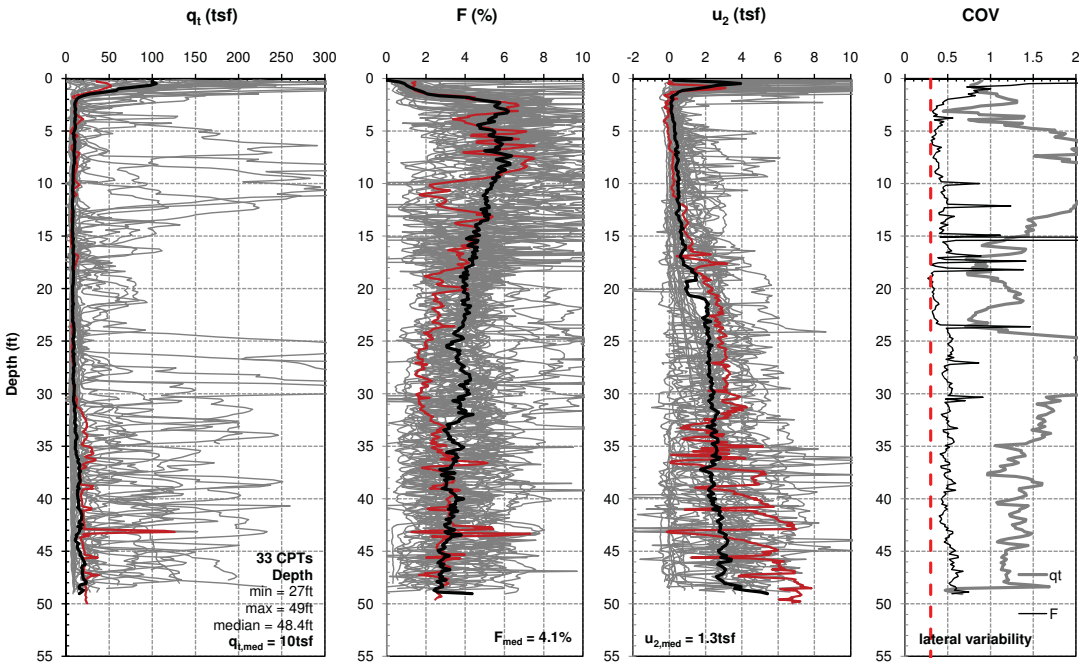

Site 10: 2207-32 Faribault County

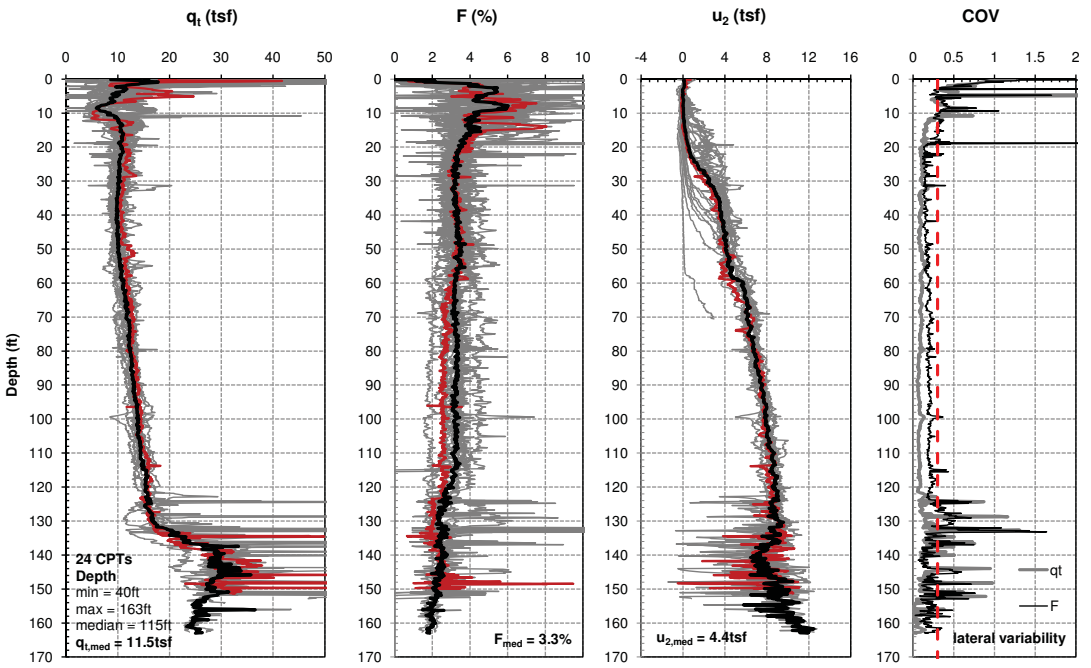

Site 11: 3507-12 Kittson County

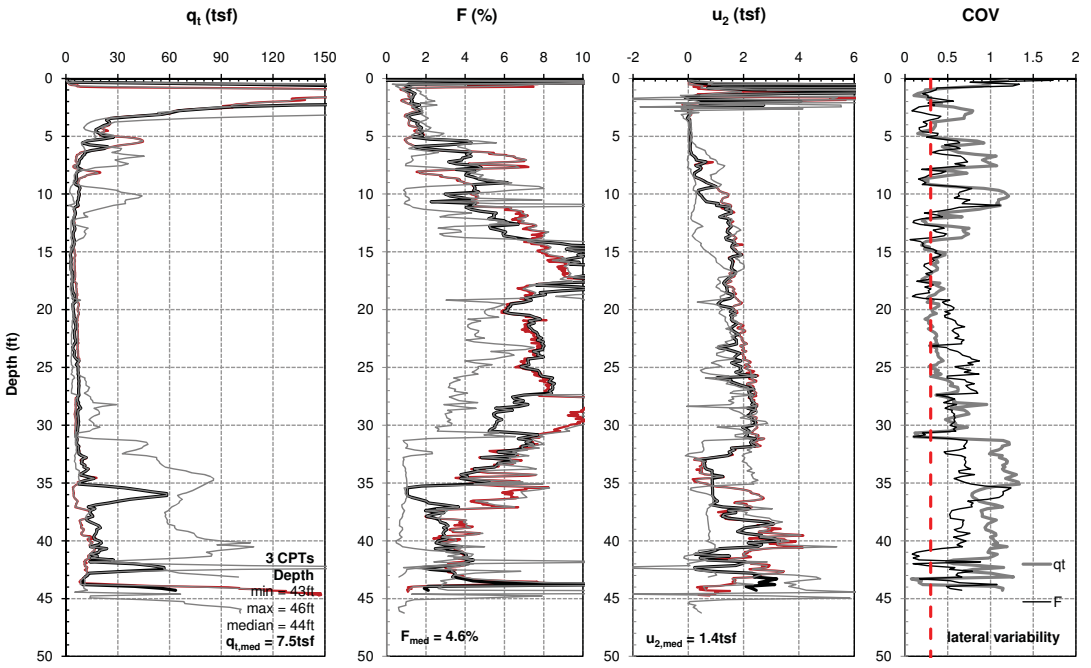

Site 12: 7602-16 Swift County

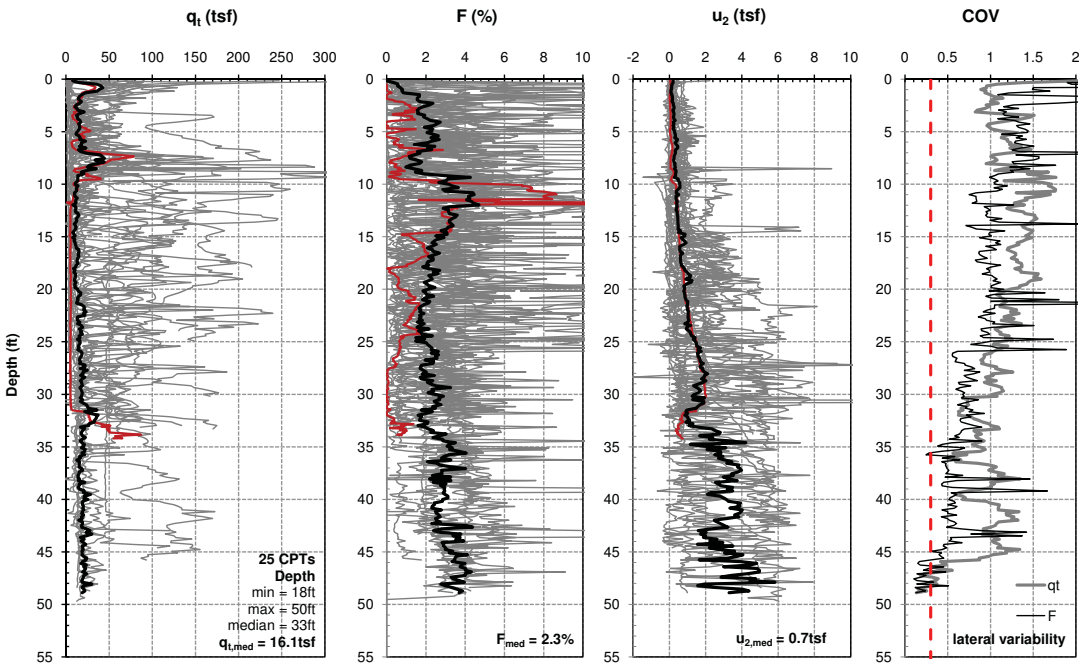

Site 13: 3413-22 Kandiyohi County

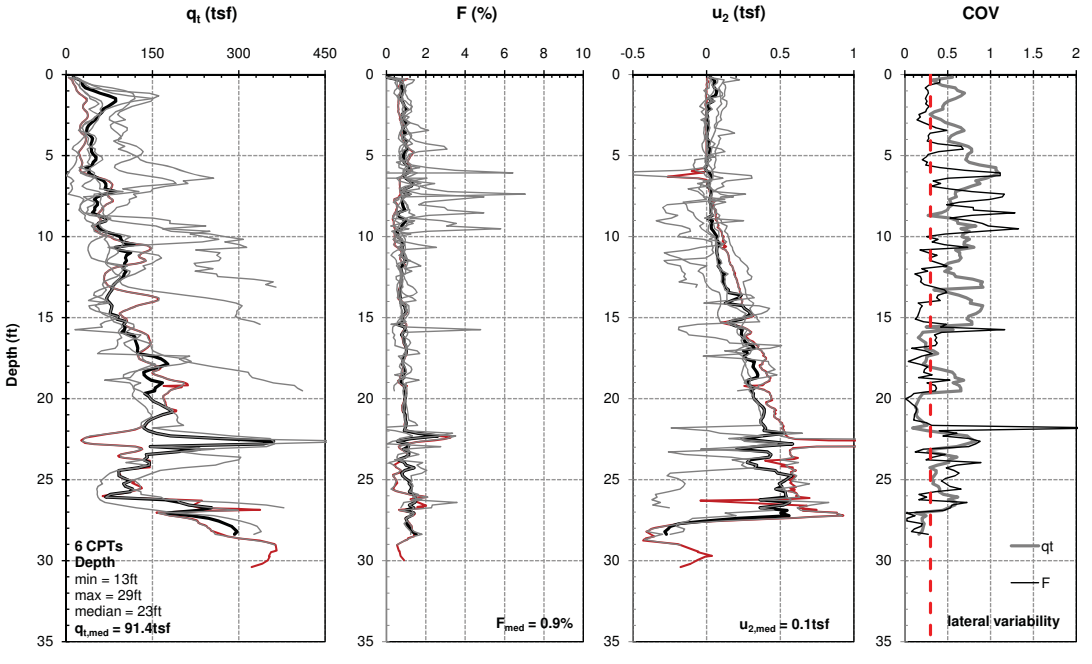

Site 14: 4913-21 Morrison County

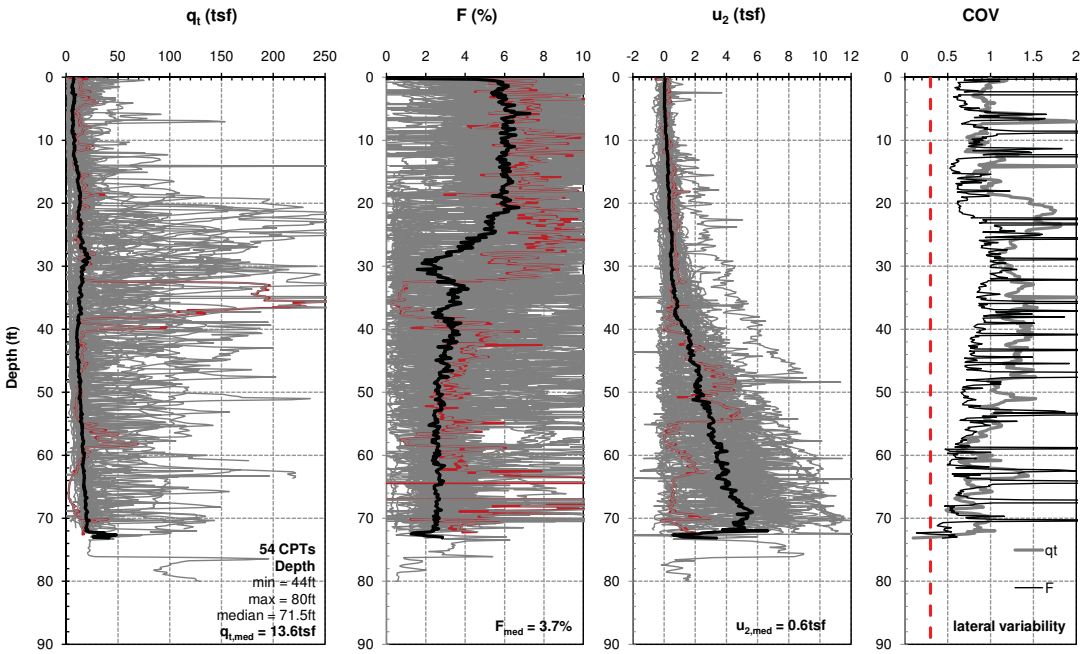

Site 15: 4013-43 LeSueur County

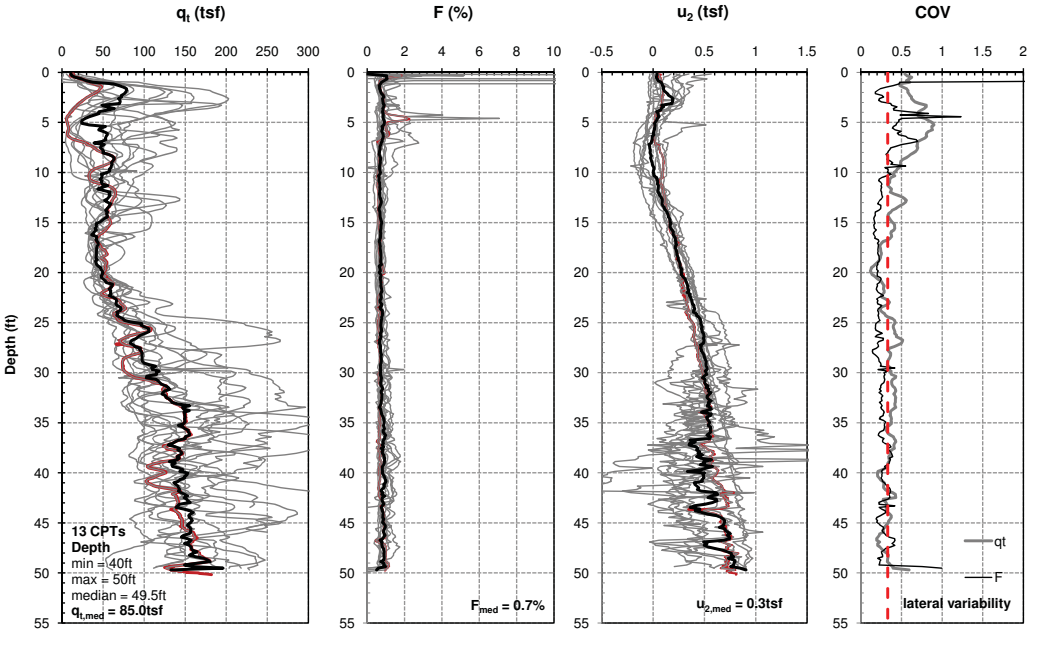

Site 16: 0208-123 Anoka

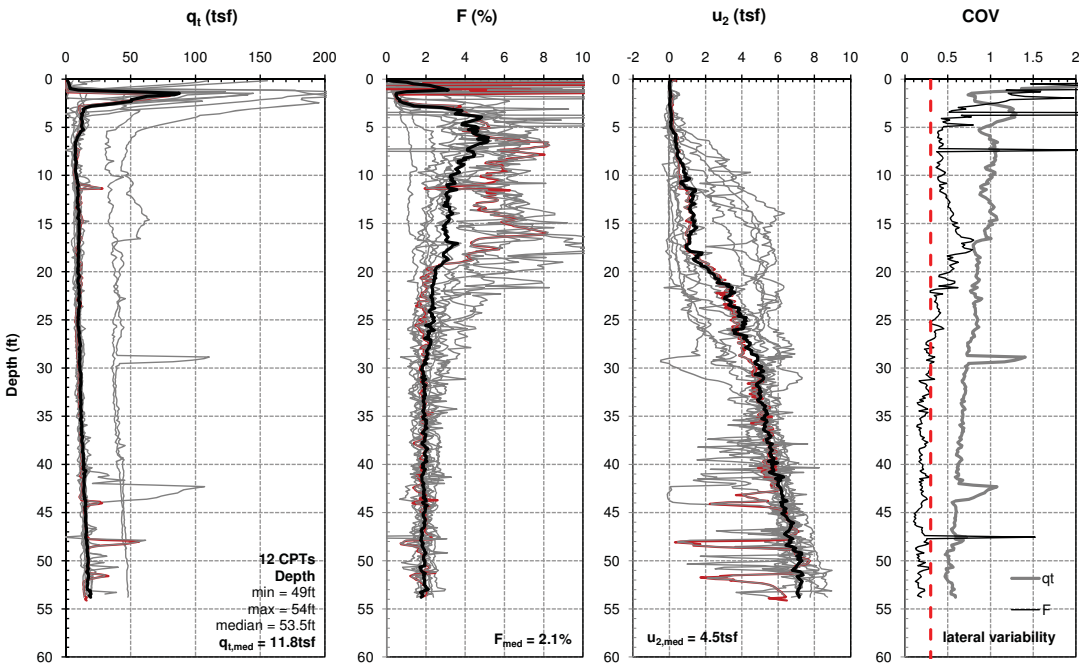

Site 17: 0901-74 Carlton County

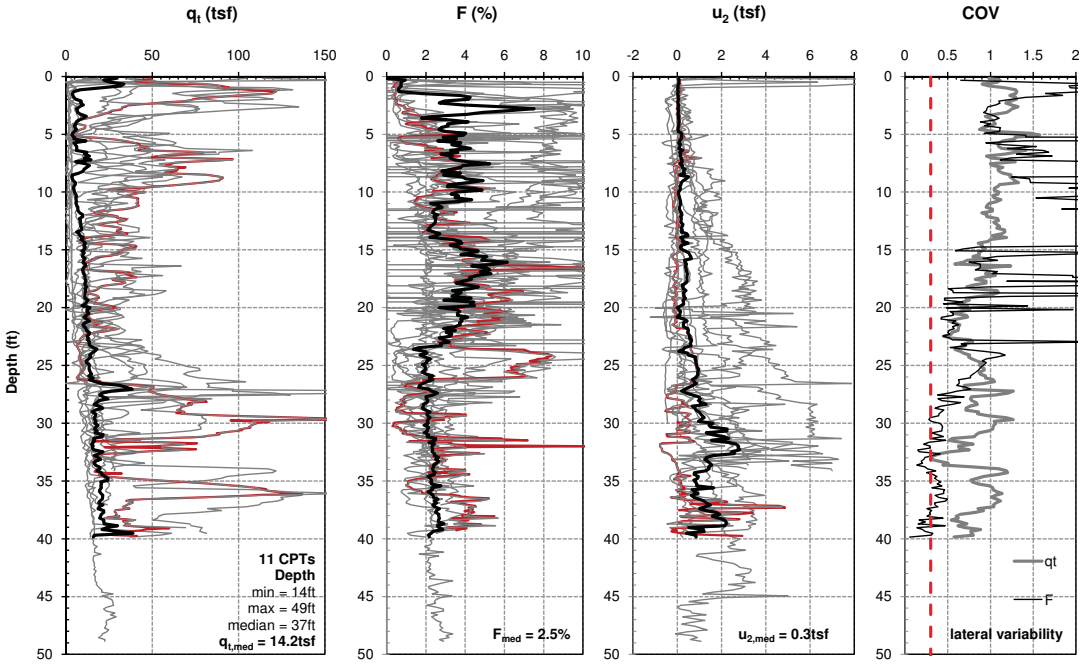

Site 18: 1002-79 Carver County

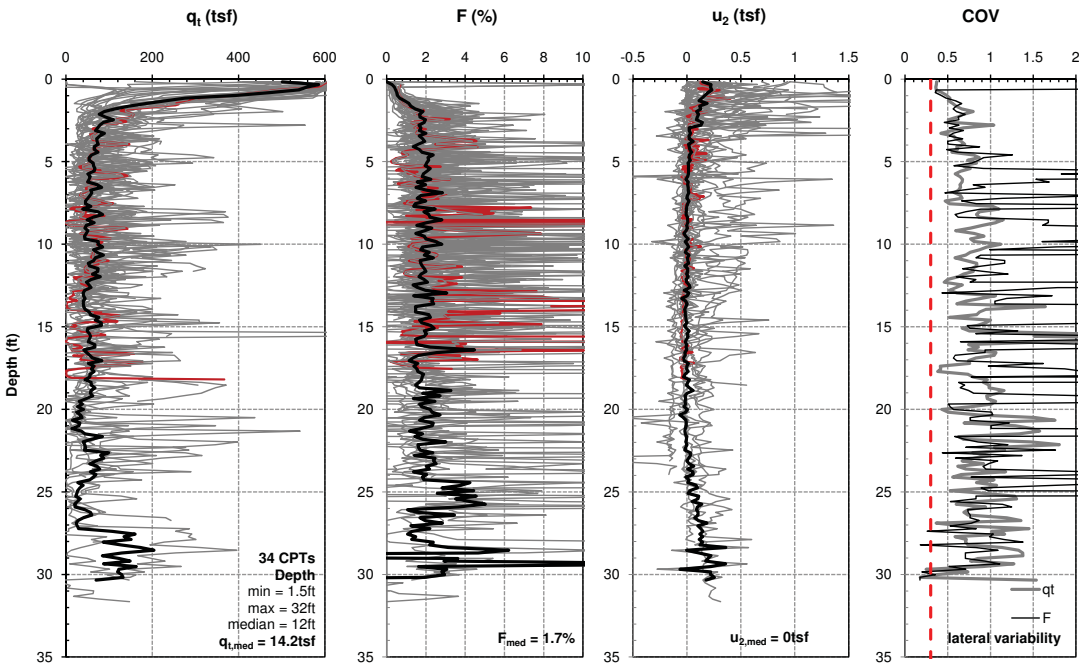

Site 19: 1601-48 Cook County

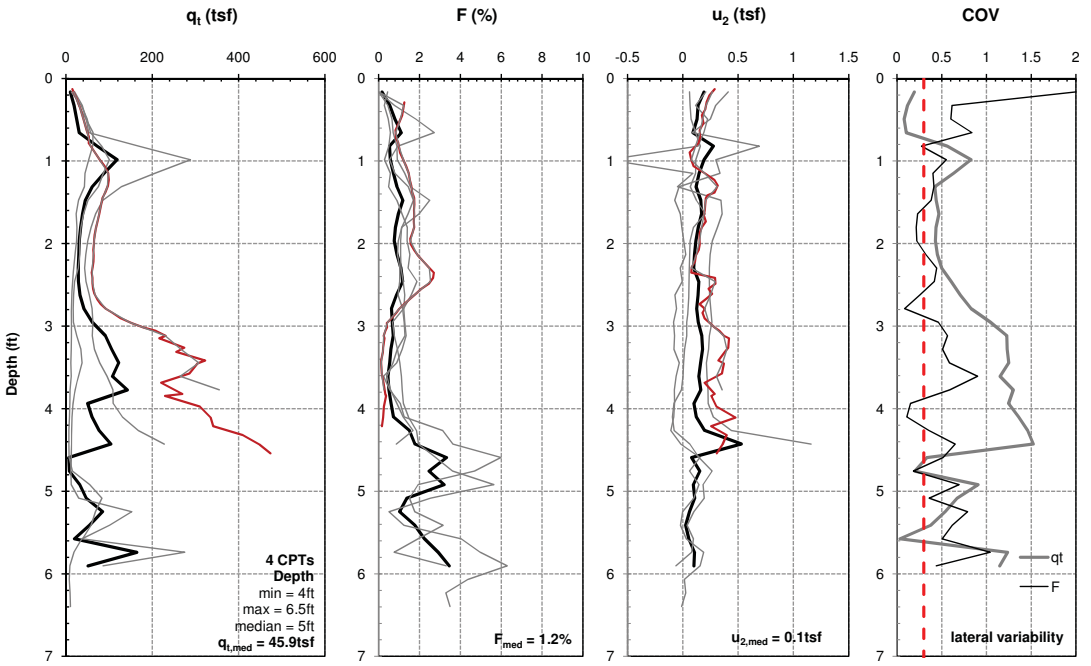

Site 20: 8580-149 Winona County

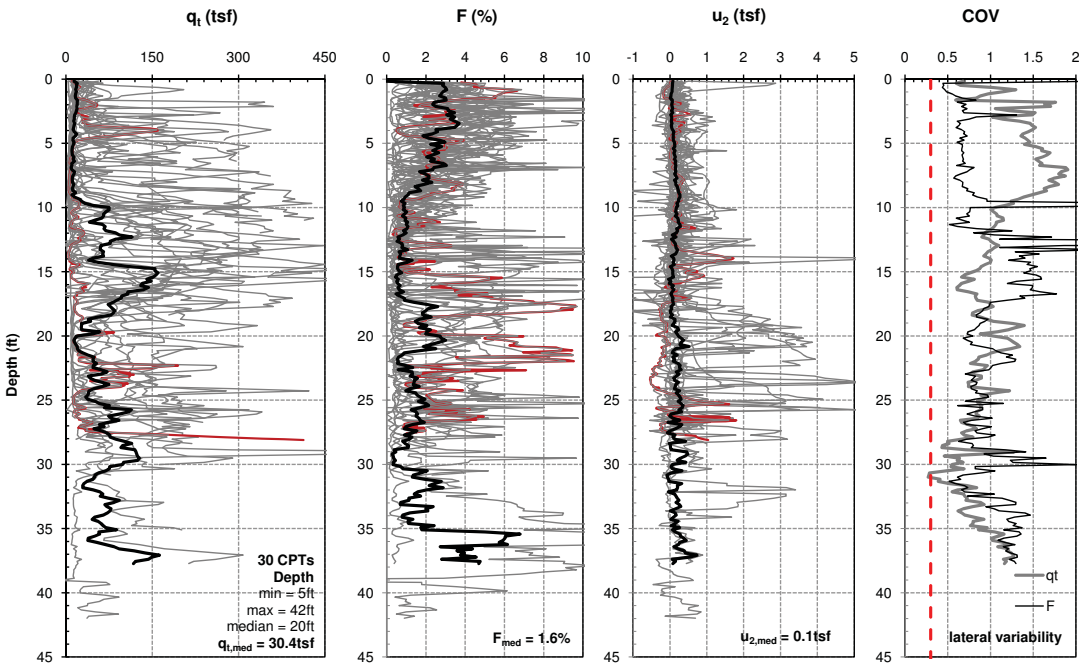

Site 21: 5509-63 Olmsted County

Previous investigations in Milwaukee county

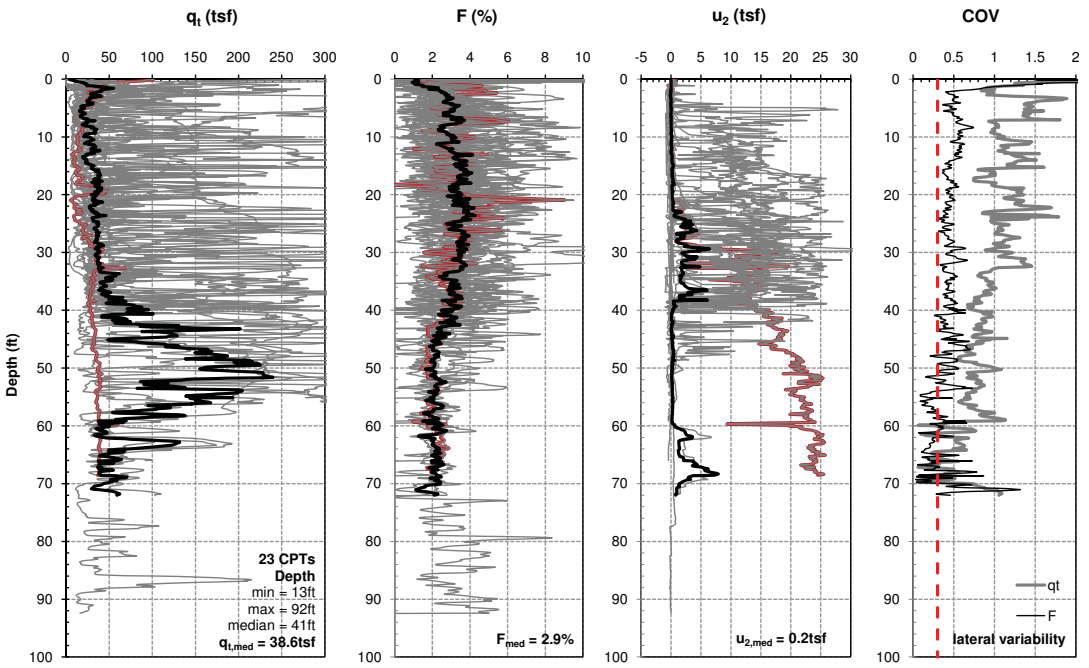

Site W1a: Marquette Till Milwaukee County (Clay Compare PB41)

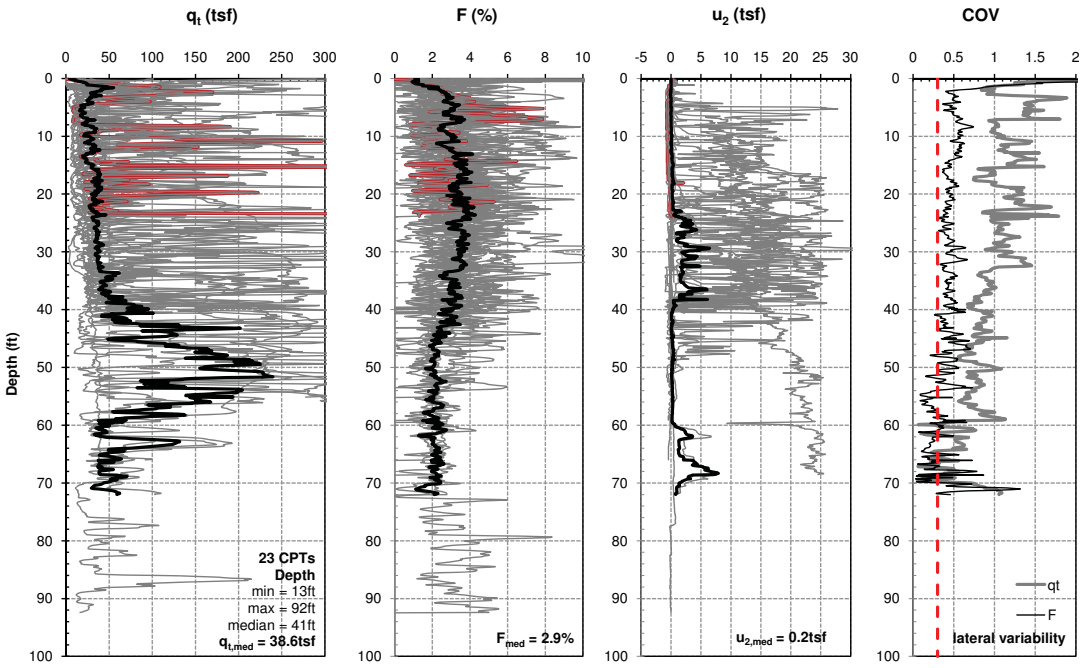

Site W1a: Marquette Till Milwaukee County (Fill Compare TWE3-1)

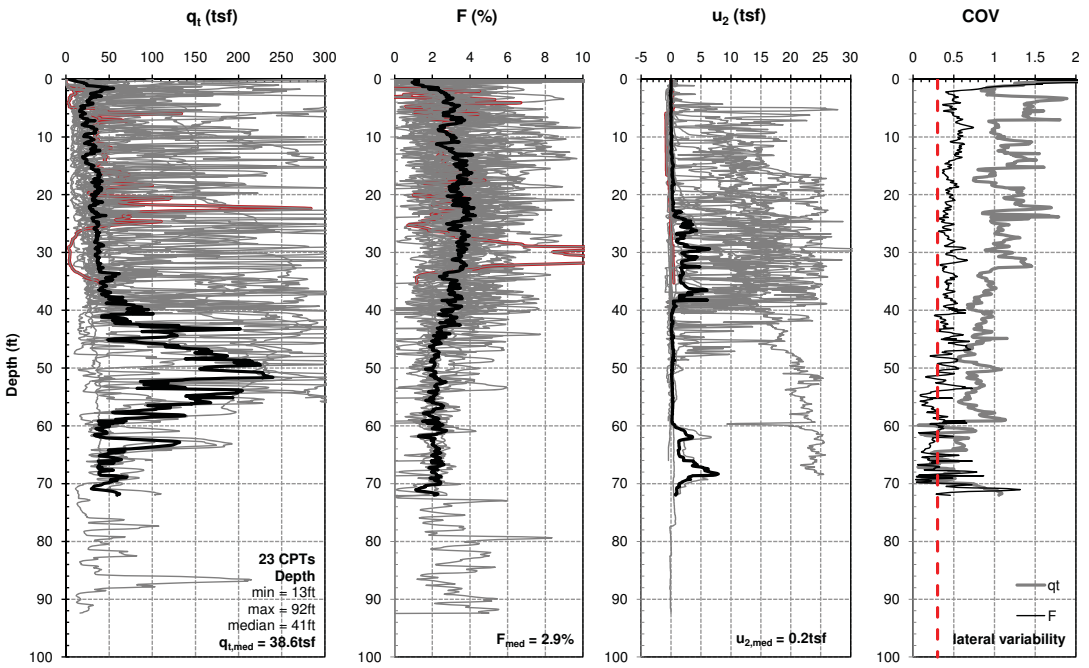

Site W1a: Marquette Till Milwaukee County (Clay/Sand Compare TWW5-09)

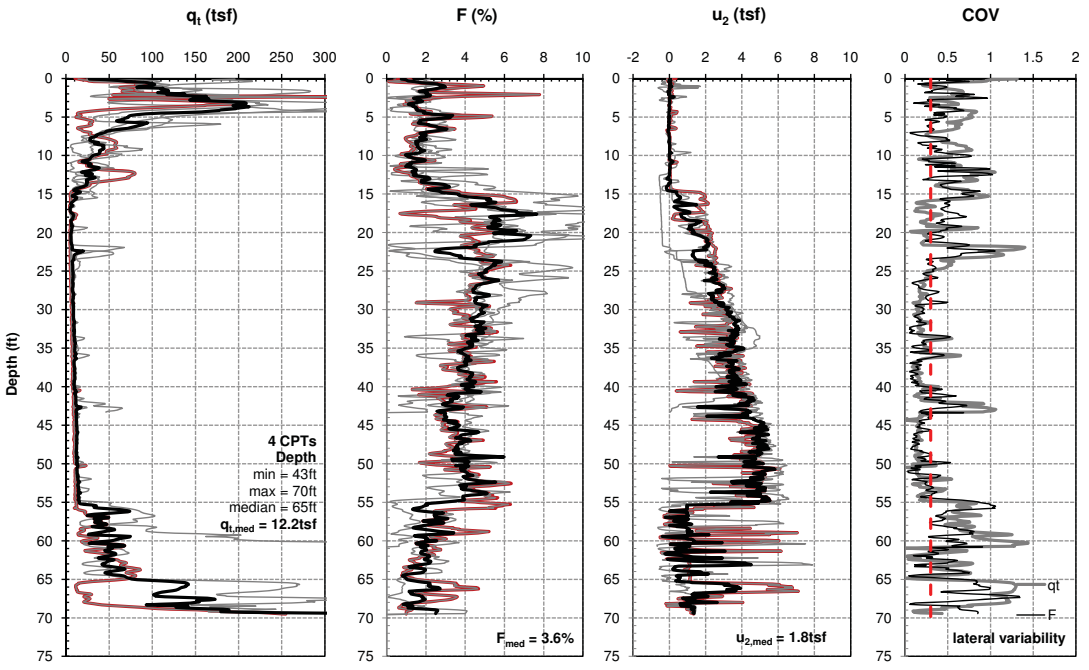

Site W1b: Marquette Lake Milwaukee County

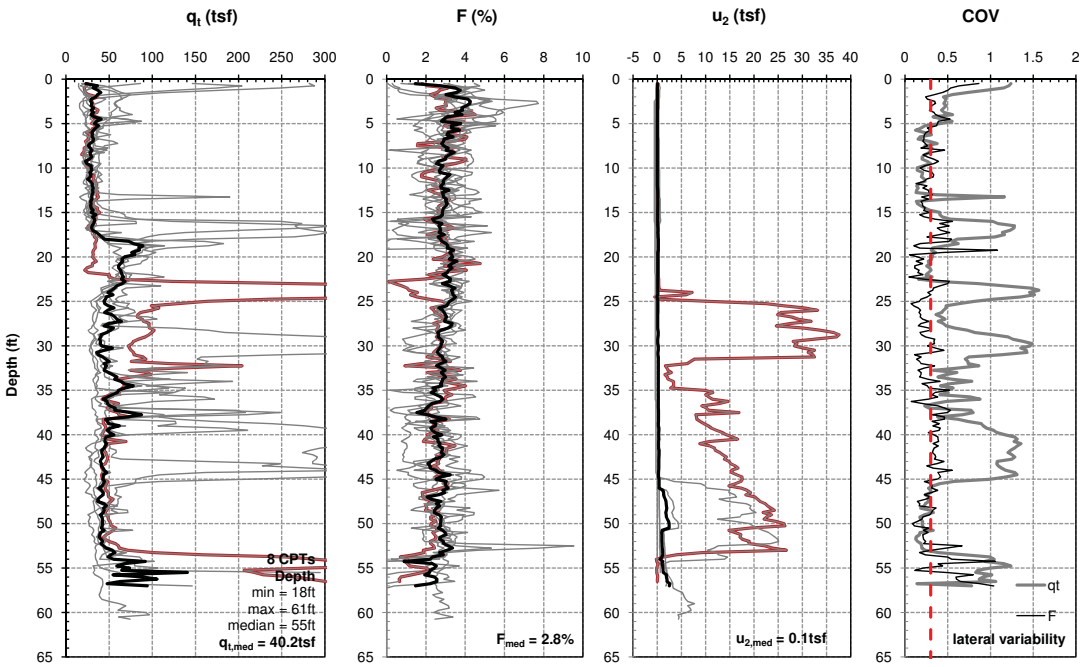

Site W2: Mitchell Milwaukee County

Testing from this study – sorted by site

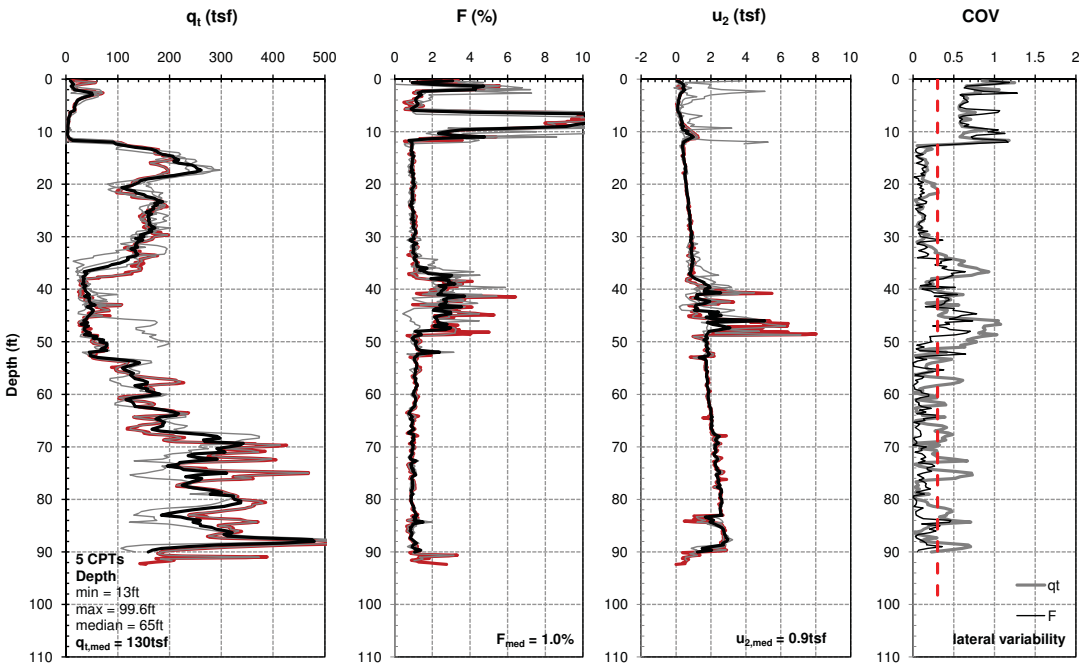

Site UW-1: Dane County

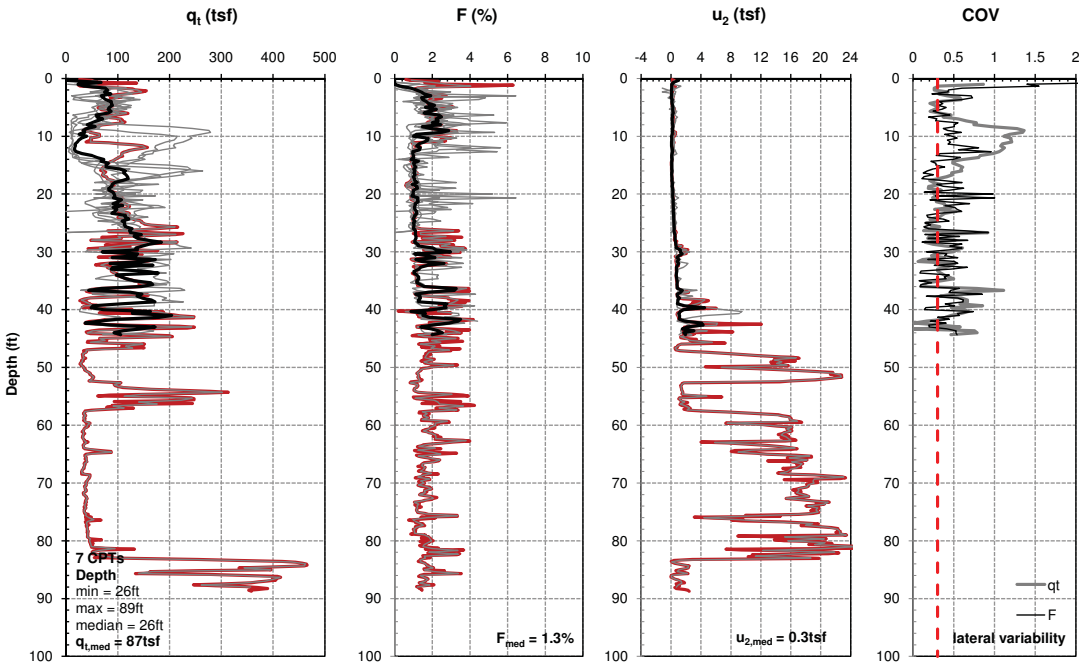

Site Long-10: Dane County

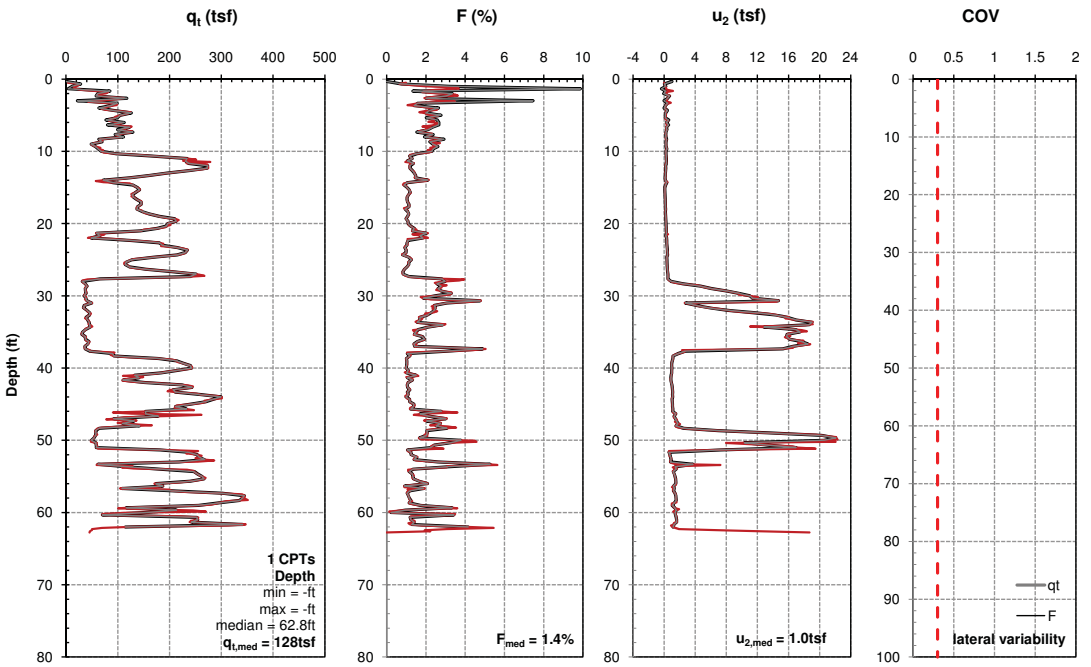

Site Long-12: Dane County

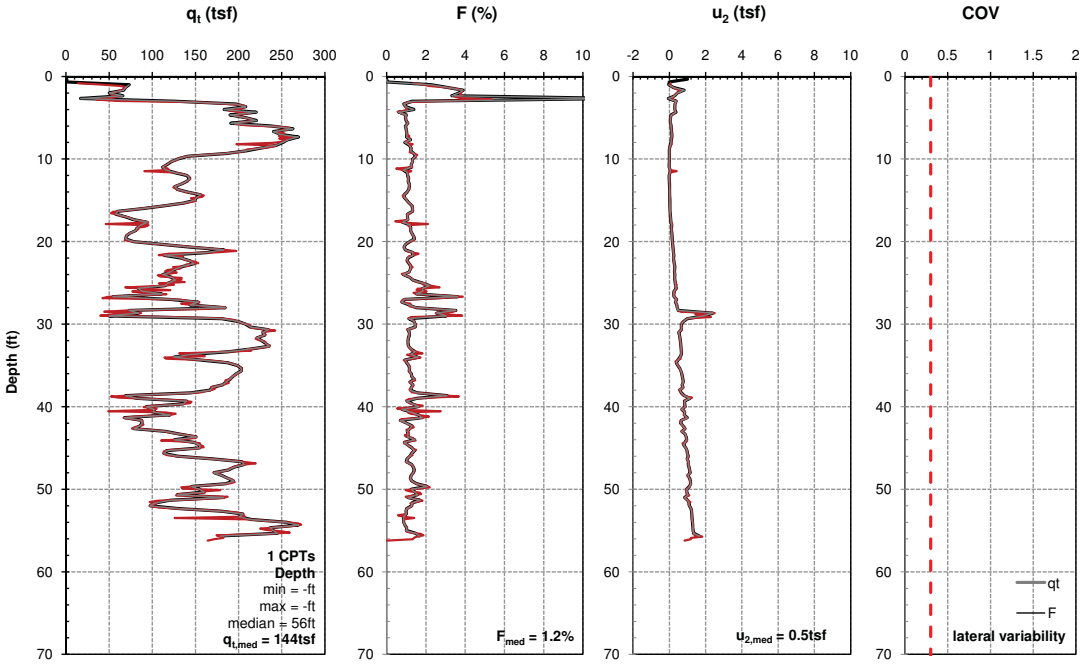

Site Long-13: Dane County

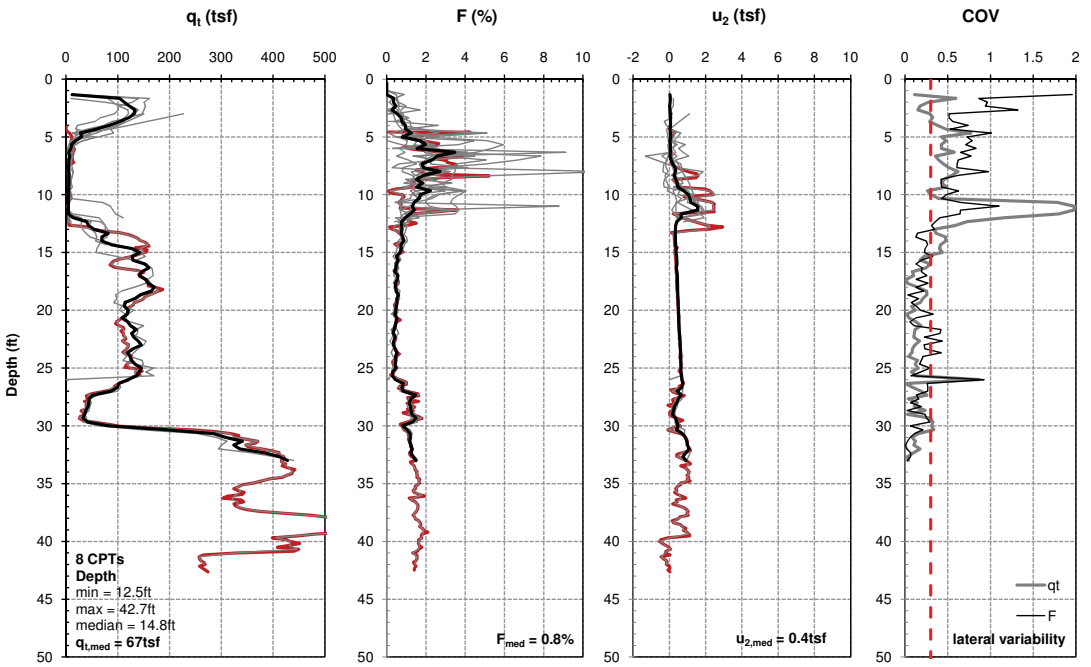

Site DOT-7: Dane County

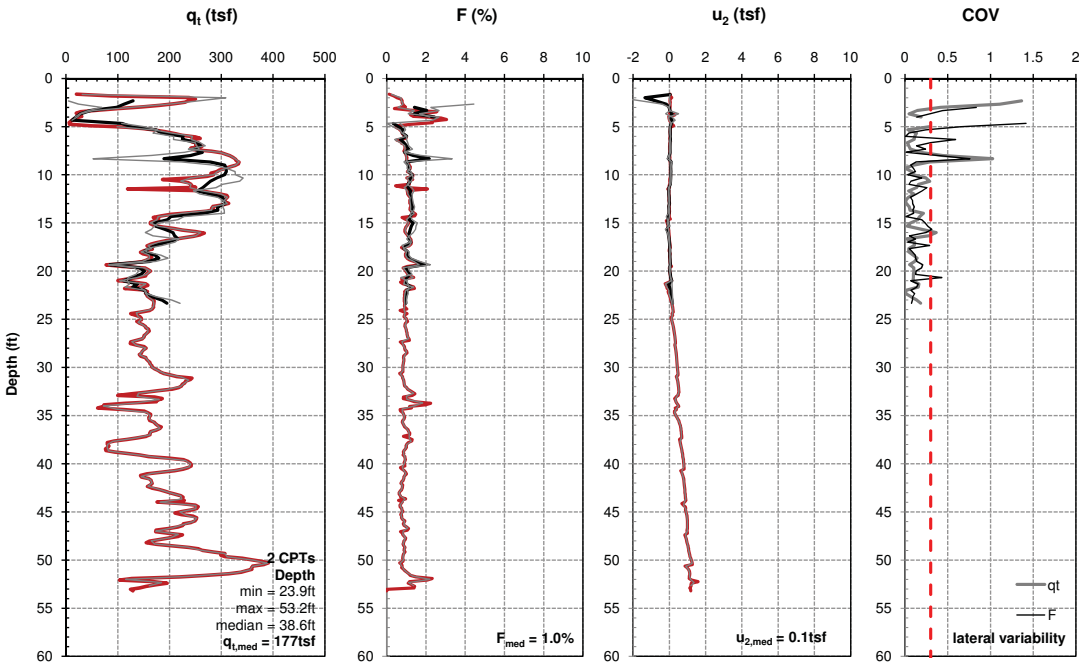

Site Long-11: Dane County

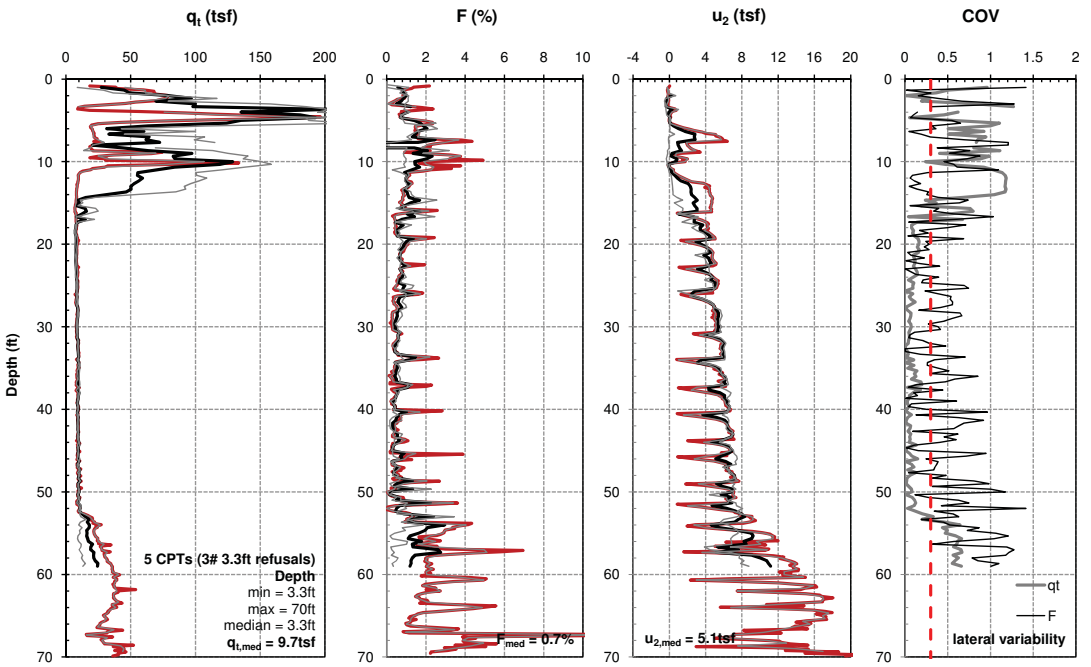

Site DOT-1: Brown County

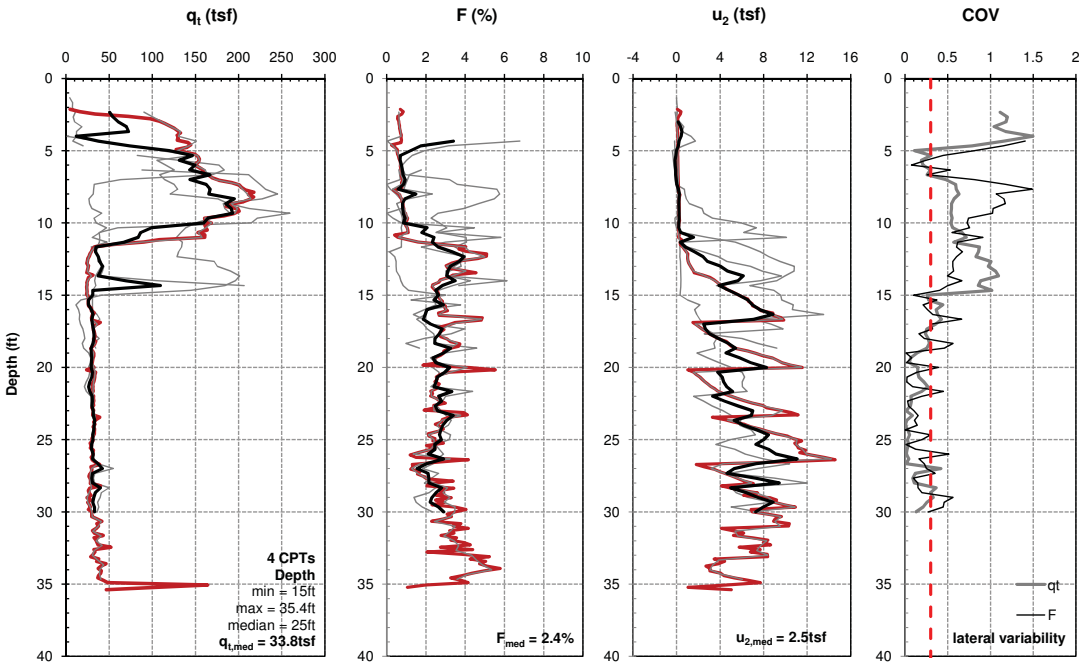

Site DOT-16: Winnebago County

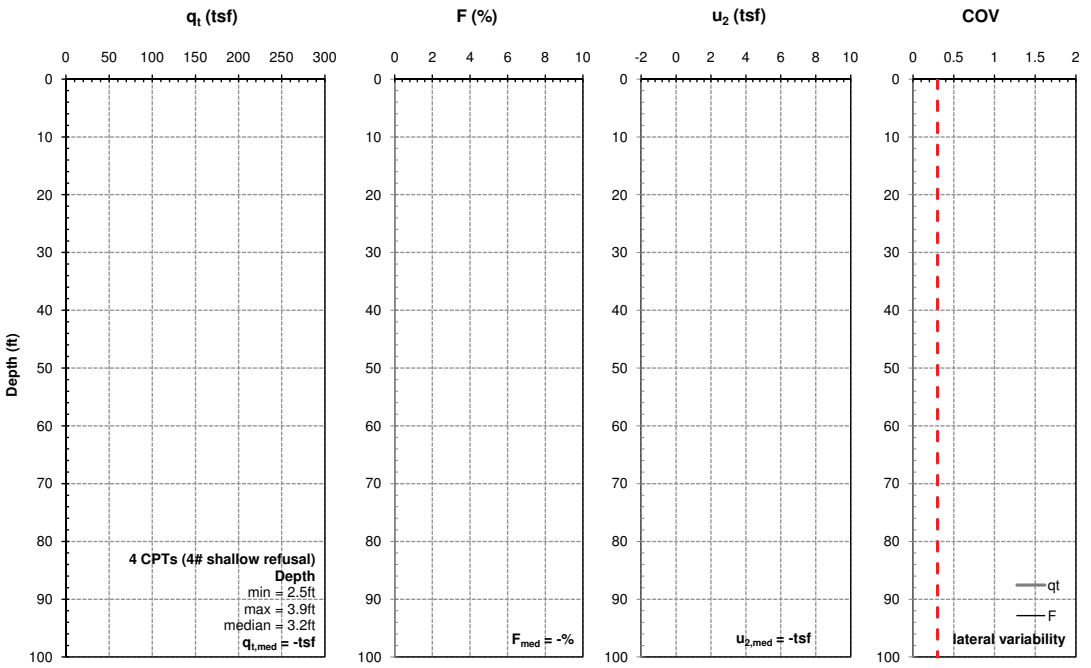

Site DOT-10: Sheboygan County

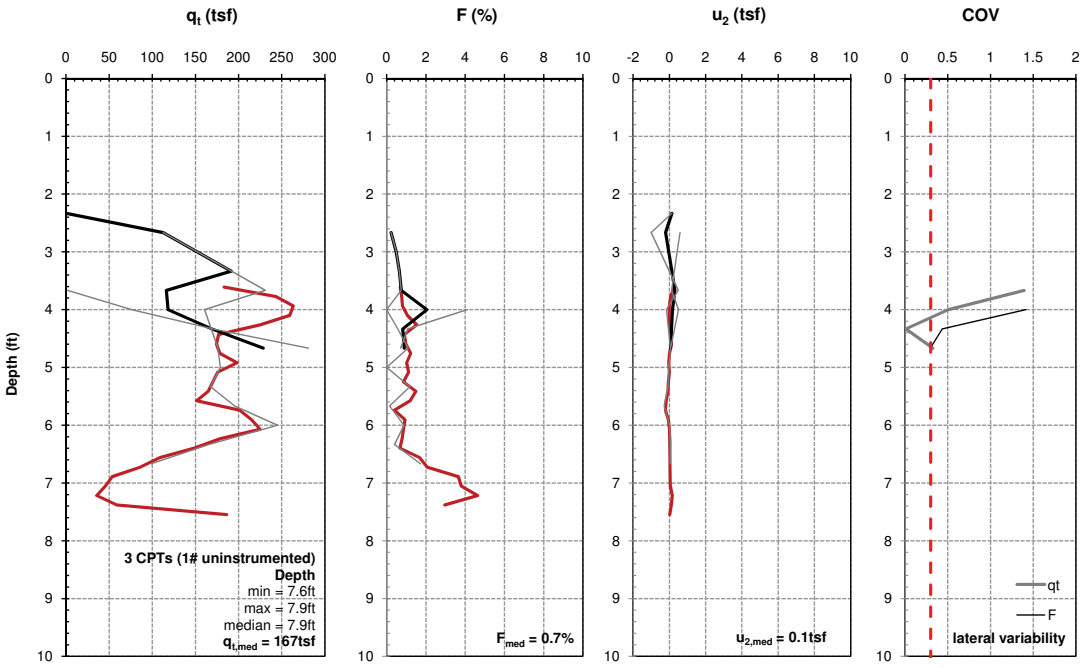

Site DOT-10a: Sheboygan County

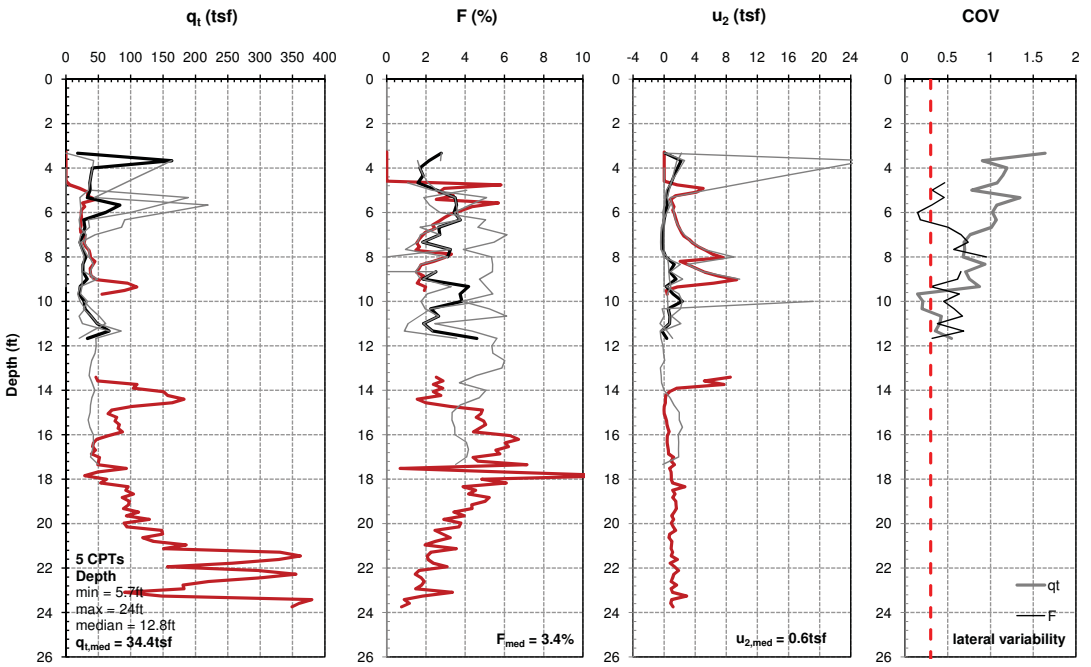

Site DOT-10b: Sheboygan County

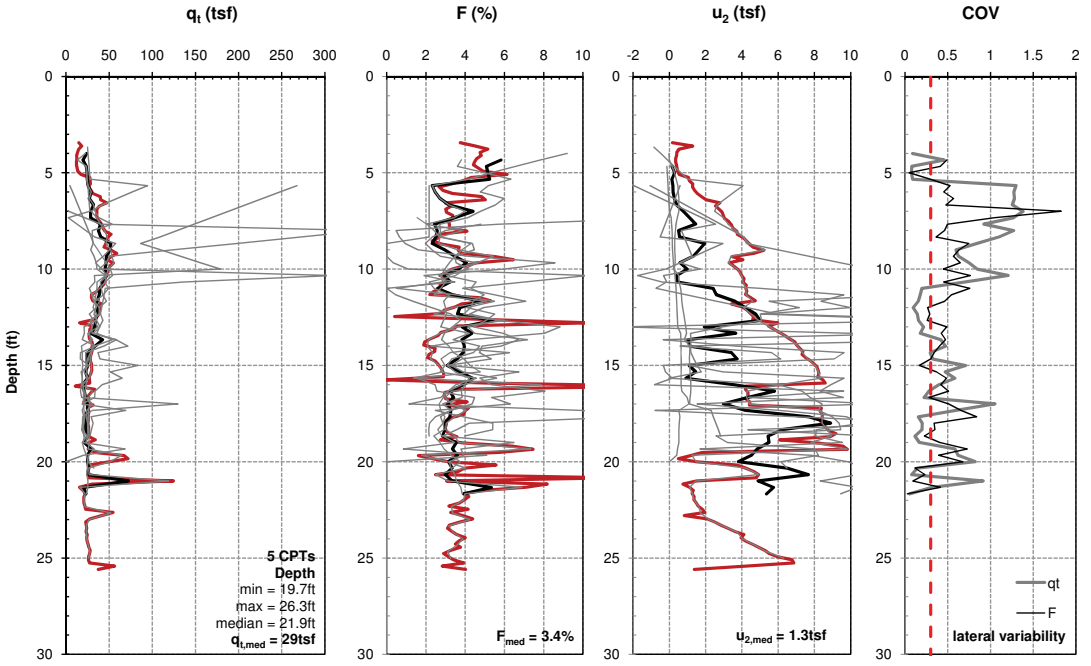

Site DOT-10c: Sheboygan County

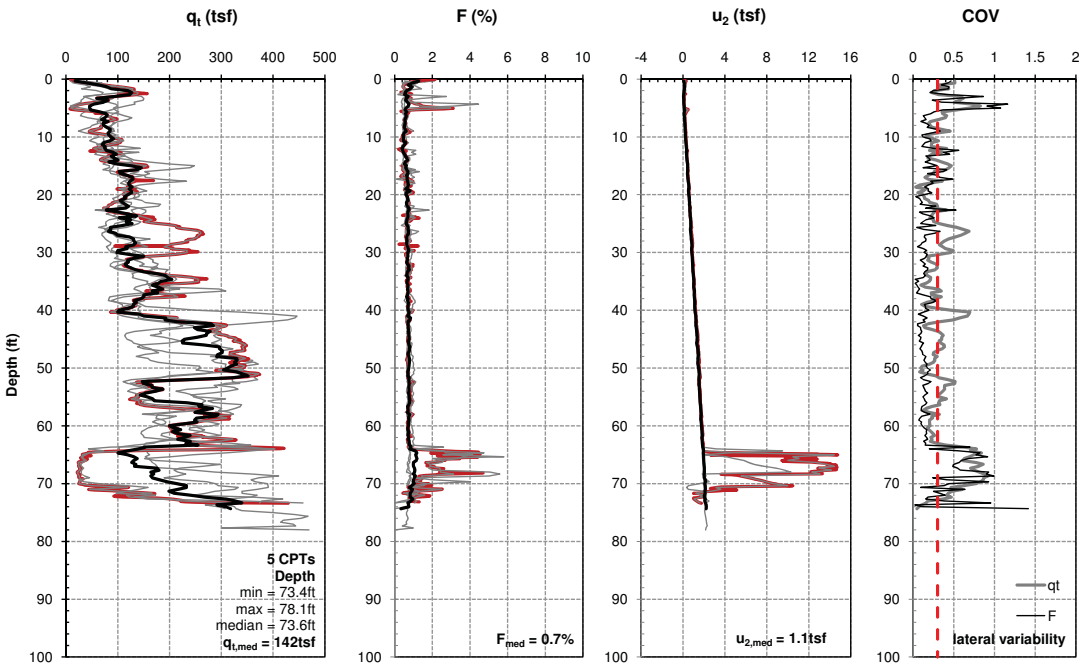

Site DOT-3R: Sauk County

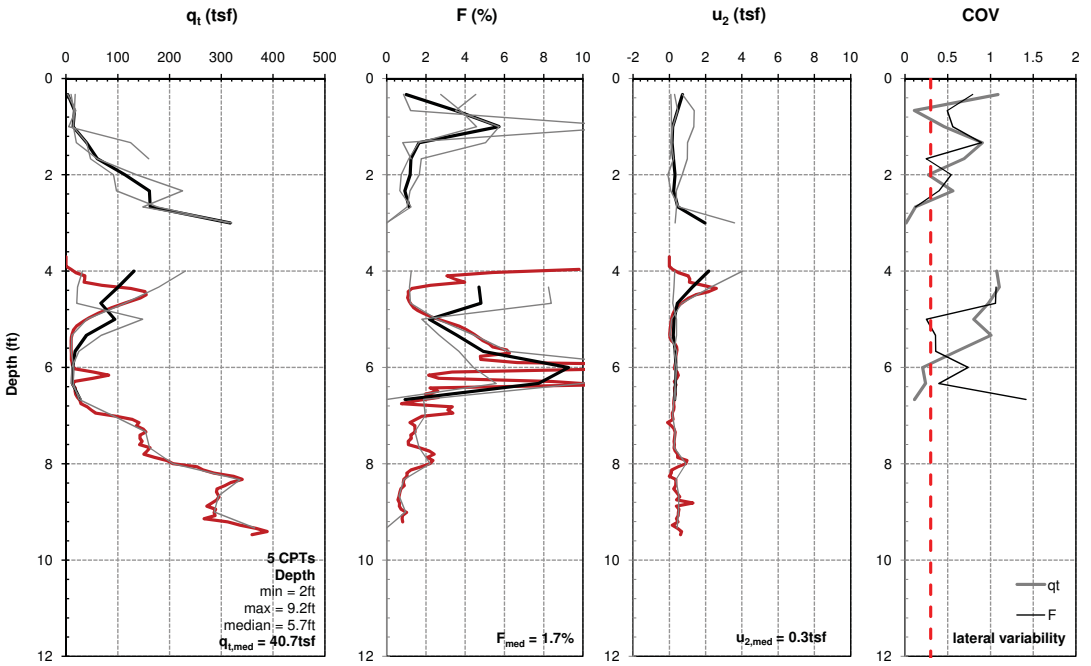

Site Long-8: Dane County

Testing from this study – sorted by inferred predominant geologic origin

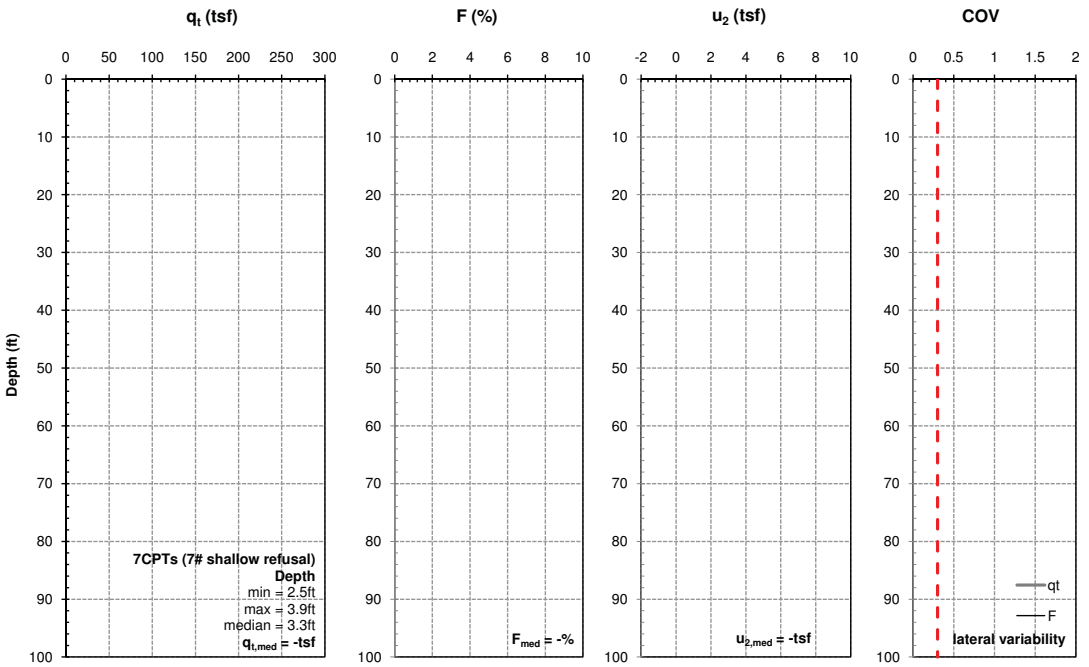

DOT-1, DOT-10: Fill

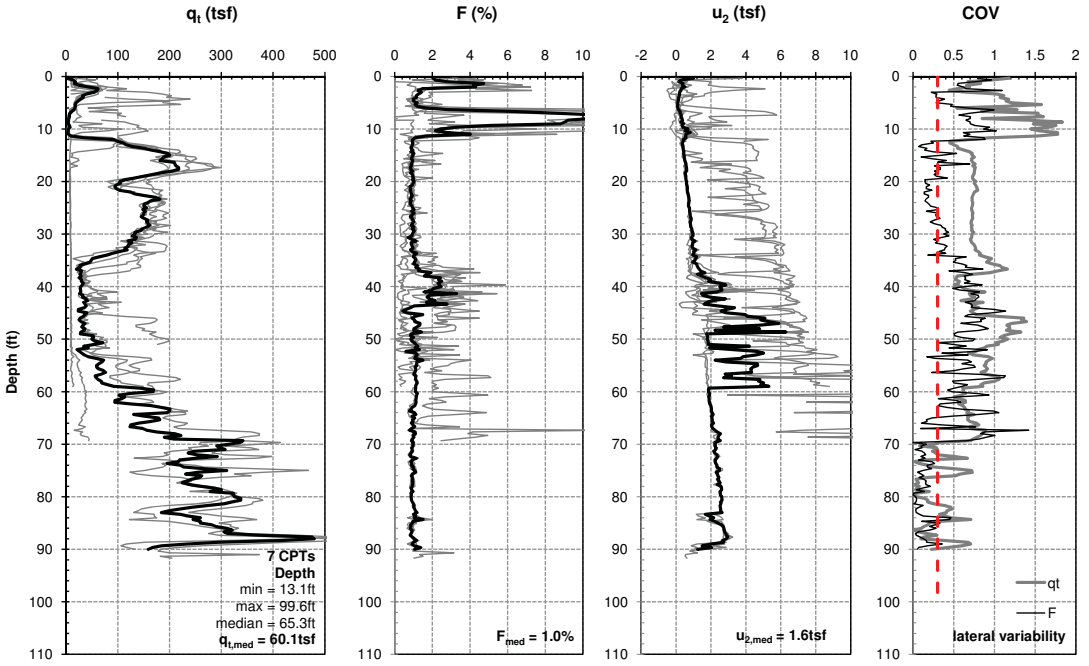

UW-1, DOT-1: Lake

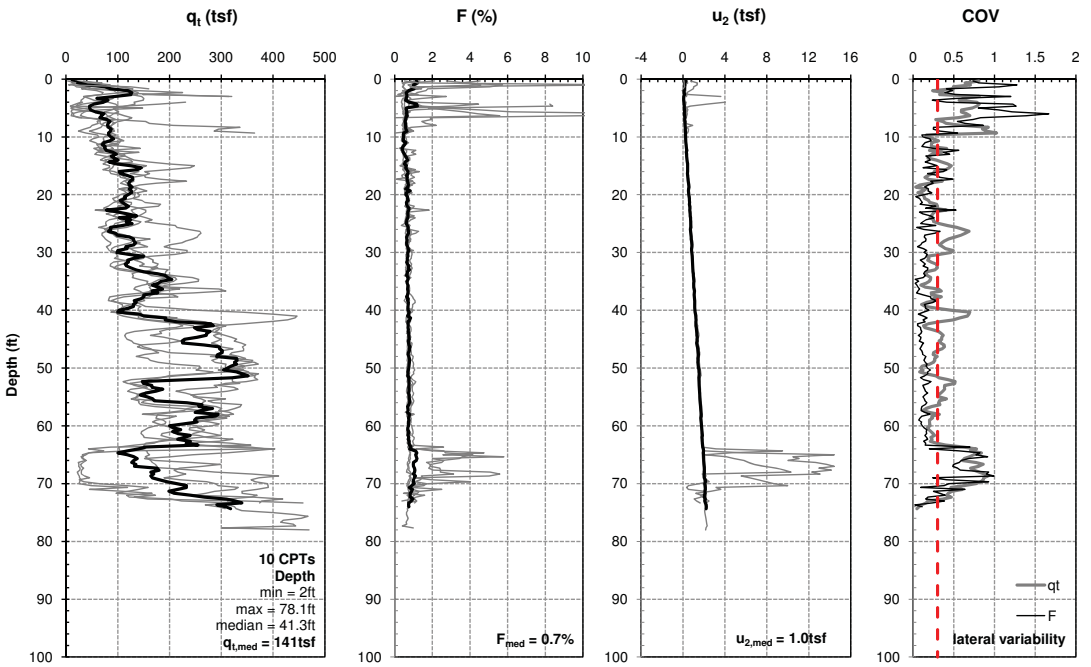

DOT-3R, Long-9: Alluvium

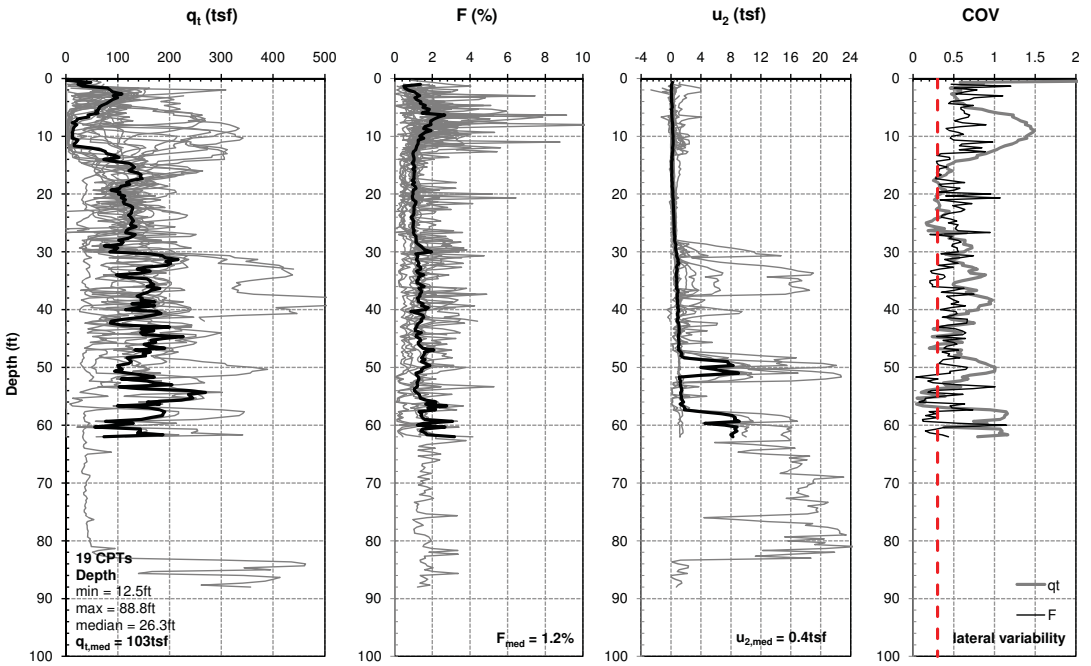

Long-10, Long-11, Long-12, Long-13, DOT-7: Outwash

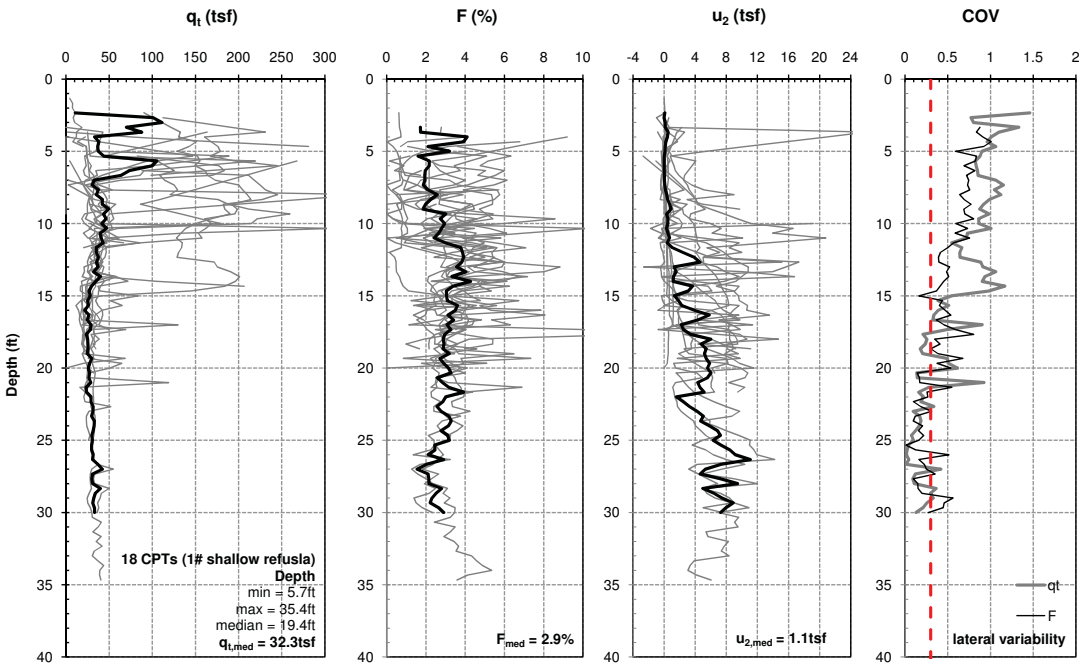

DOT-10a, DOT-10b, DOT-10c, Dot-16: Clayey Till

Appendix 4

Supplemental soil borings and laboratory data performed for this study

Long-10

- Auger Boring with Classification and Grain Size Summary
- Grain Size Analysis Curves

Sample	Midpoint Depth (meters)	Descripton (Visual)	USCS	m_c (%)	Fines (%)	D_{10} (mm)	D_{30} (mm)	D_{50} (mm)	D_{60} (mm)	C_c	C_u	Notes:
0	0.05	Topsoil - Dark Brown Mottled SILTY CLAY (ML-CL)			-	-	-	-	-			
B-01	0.20	Dark Brown Moist CLAY w/ Silt and Rootlets			-	-	-	-	-			
B-02	0.40	Fill - Crushed Limestone GRAVEL with a Brown to Black CLAY w/ Silt Matrix			-	-	-	-	-			
B-03	0.55	Dark Gray Moist Mottled CLAY w/ Silt and Fe Staining			-	-	-	-	-			
B-04	0.70	Brown Fine Grained Poorly Graded SAND (SP) w/ Trace Silt and Some Clay	SP-SC	6.8	10.3	< 0.075	0.16	0.22	0.26	1.3	3.5	
B-05	0.78	Interbedded SAND (SP) and CLAY (CL)	CL	14.5	55.2	< 0.075	< 0.075	< 0.075	0.11	N/A	N/A	
B-06	0.87	Tan Fine Poorly Graded SAND (SP) w/ Silt and Gray Clay	SC	8.2	22.8	< 0.075	0.10	0.16	0.19	0.7	2.5	
B-07	0.98	Tan Fine Grained Poorly Graded SAND (SP) w/ Clay Interbeds	SC	8.6	20.6	< 0.075	0.11	0.16	0.19	0.9	2.6	
B-08	1.08	Brown Fine Grained Poorly Graded SAND (SP) w/ Gray Clay Interbeds	SC	13.3	42.1	< 0.075	< 0.075	0.11	0.15	0.5	1.9	
B-09	1.13	Interbedded Brown Fine Grained Poorly Graded SAND (SP) and Gray CLAY (CL)	SC	14.6	46.8	< 0.075	< 0.075	0.09	0.14	0.5	1.9	
B-10	1.29	Brown Fine Poorly Graded SAND (SP) and Gray CLAY (CL)	SC	13.3	36.4	< 0.075	< 0.075	0.13	0.16	0.5	2.2	
B-11	1.39	Brown Fine Grained Poorly Graded SAND (SP) w/ Gray Clay Interbeds	SC	14.0	40.1	< 0.075	< 0.075	0.13	0.17	0.4	2.3	
B-12	1.49	Brown Fine Poorly Graded SAND (SP) and Gray CLAY (CL)	SC	13.3	34.3	< 0.075	< 0.075	0.16	0.19	0.4	2.6	
B-13	1.60	Brown Fine to Medium Grained Poorly Graded SAND (SP) w/ Gray CLAY Interbeds	SC	9.8	26.3	< 0.075	0.10	0.18	0.22	0.6	2.9	
B-14	1.72	Brown Fine Grained Poorly Graded SAND (SP) w/ Gray Clay Interbeds	SC	11.0	33.2	< 0.075	< 0.075	0.16	0.19	0.4	2.6	
B-15	1.83	Brown Fine Grained Poorly Graded SAND (SP) w/ Trace Fines Intermixed Gray CLAY		13.6								Data recording error
B-16	1.57	Brown Fine Grained Poorly Graded SAND (SP) and Gray Clay w/ Some Silt	SC	12.3	34.8	< 0.075	< 0.075	0.15	0.19	0.4	2.5	
B-17	1.68	Brown Fine Grained Poorly Graded SAND (SP) w/ Gray CLAY layers and Trace Organics (Wood Particles)	SC	11.3	25.7	< 0.075	0.10	0.17	0.21	0.7	2.8	
B-18	1.79	Brown Fine Grained Poorly Graded SAND (SP) w/ Gray Clay Interbeds	SC	10.8	33.1	< 0.075	< 0.075	0.15	0.19	0.4	2.5	
B-19	1.90	Brown Gray CLAY w/ Brown Fine Grained Poorly Graded SAND (SP) Interbeds	CL	16.0	53.7	< 0.075	< 0.075	< 0.075	0.13	N/A	N/A	
B-20	2.02	Interbedded Brown Fine Grained SAND (SP) and Gray Lean CLAY (CL) w/ Silt	SC	16.9	44.1	< 0.075	< 0.075	0.10	0.15	0.5	1.9	
B-21	2.16	Tan Fine Grained Poorly Graded SAND (SC) w/ Gray CLAY lenses	SC	6.0	23.9	< 0.075	0.09	0.14	0.15	0.7	2.0	
B-22	2.29	Tan Fine Grained Poorly Graded SAND (SP) w/ Some Silt	SP-SM	9.8	4.0	0.083	0.11	0.14	0.15	1.1	1.8	
B-23	2.39	Tan Fine Grained Poorly Graded SAND (SP)	SP	5.2	0.7	0.13	0.16	0.20	0.22	1.0	1.7	
B-24	2.49	Tan Fine Grained Poorly Graded SAND (SP)	SP	4.2	0.3	0.13	0.14	0.14	0.15	1.0	1.2	
B-25	2.60	Tan Fine Grained Poorly Graded SAND (SP)	SP	4.6	0.5	0.13	0.14	0.18	0.25	1.0	3.4	
B-26	2.73	Tan Fine Grained Poorly Graded SAND(SP) w/ Fe Staining and Trace Fines	SP	5.2	1.0	0.089	0.13	0.19	0.23	0.8	2.6	
B-27	2.86	Tan Fine Grained Poorly Graded SAND (SP)	SP	5.7	0.6	0.14	0.18	0.23	0.26	0.9	1.9	
B-28	2.98	Tan Fine Grained Poorly Graded SAND (SP) w/ Trace Silt and Fe Staining	SP	4.6	1.1	0.14	0.18	0.23	0.25	0.9	1.9	
B-29	3.11	Tan Fine Grained Poorly Graded SAND (SP) w/ Trace Clay	SP	4.5	1.8	0.14	0.19	0.25	0.27	1.0	2.0	
B-30	3.23	Tan Fine Grained Poorly Graded SAND (SP)	SP	4.4	0.9	0.14	0.20	0.27	0.29	1.0	2.2	Not Accurate mc - some s
B-31	3.34	Tan to Brown Fine to Medium Grained Poorly Graded SAND (SP) w/ Trace Silt	SP	4.7	1.5	0.12	0.19	0.27	0.31	1.0	2.5	
B-32	3.45	Tan Fine Grained Poorly Graded SAND (SP)	SP	6.1	1.1	0.13	0.18	0.23	0.26	0.9	2.0	
B-33	3.58	Tan Wet Fine to Medium Grained Poorly Graded SAND (SP)	SP	7.3	0.8	0.14	0.20	0.27	0.30	1.0	2.1	
B-34	3.72	Tan Fine to Medium Grained Poorly Graded SAND (SP) w/ Trace Fines	SP	11.3	1.0	0.13	0.19	0.26	0.28	0.9	2.2	
B-35	3.85	Tan Fine to Medium Grained Poorly Graded SAND (SP)	SP	18.4	1.0	0.13	0.19	0.27	0.30	1.0	2.3	
B-36	3.96	Tan Wet Medium to Fine Grained Poorly Graded SAND (SP) w/ Some Fine Gravel	SP	20.2	0.6	0.16	0.25	0.31	0.35	1.2	2.1	
B-37	4.06	Tan to Orange Wet Medium to Fine Grained Poorly Graded SAND (SP) some pebbles	SP	20.3	0.5	0.16	0.23	0.29	0.32	1.0	1.9	
B-38	4.15	Brown Wet Fine to Medium Grained Poorly Graded SAND (SP)	SP	24.0	0.5	0.16	0.23	0.29	0.33	1.0	2.0	
B-39	4.18	Tan to Orange Wet Medium to Fine Grained Poorly Graded SAND (SP)	SP	18.9	0.9	0.16	0.23	0.29	0.32	1.0	2.0	

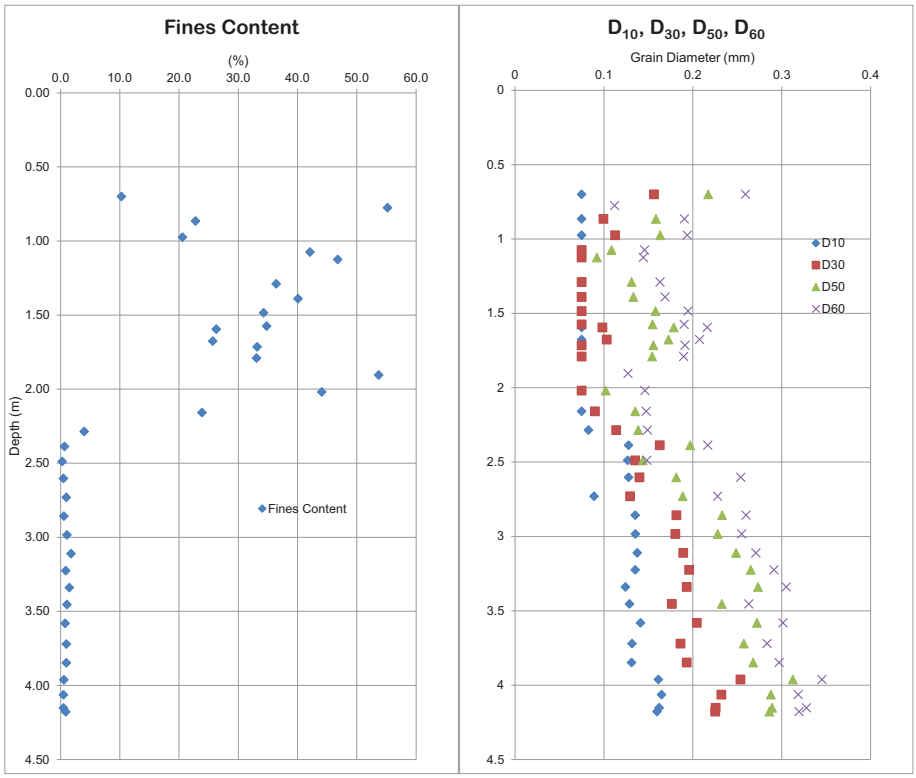

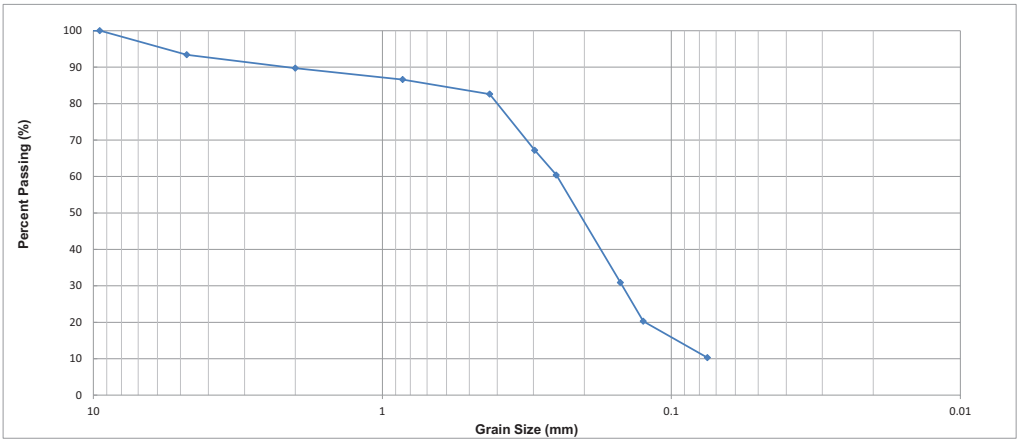

Boring: B(UW)-1 Sample: B-4 Description: Brown Fine Grained Poorly Graded SAND (SP) w/ Trace Silt and Some Clay

D_{10} < 0.075 mm
D_{30} 0.16 mm
D_{50} 0.22 mm
D_{60} 0.26 mm

C_c 1.3 C_u 3.5

USCS Grain Size Percentages

Gravel		Sand			Fines
Coarse	Fine	Coarse	Medium	Fine	
0	0	0	7.1	72.2	10.3

Performed by: JNH Checked by:

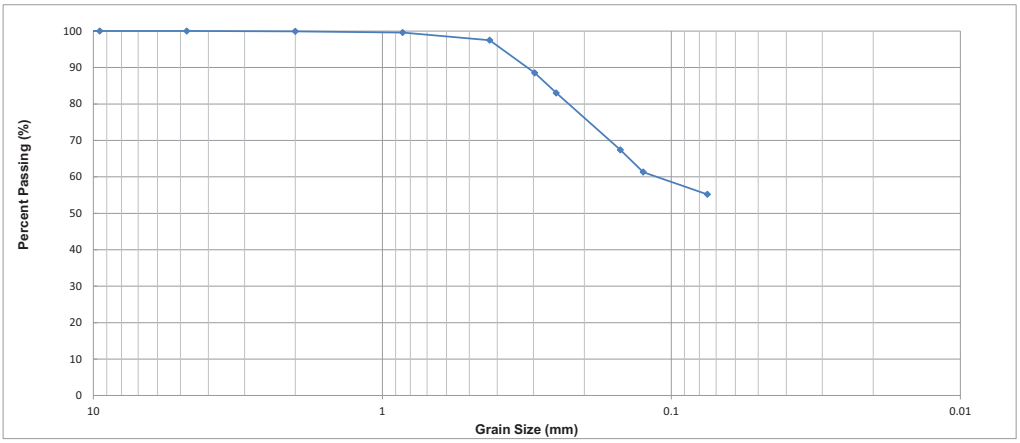

Boring: B(UW)-1 Sample: B-5 Description: Interbedded SAND (SP) and CLAY (CL)

D_{10} < 0.075 mm
D_{30} < 0.075 mm
D_{50} < 0.075 mm
D_{60} 0.11 mm

C_c N/A C_u N/A

USCS Grain Size Percentages

Gravel		Sand			Fines
Coarse	Fine	Coarse	Medium	Fine	
0	0	0.1	2.4	42.4	55.2

Performed by: JNH Checked by:

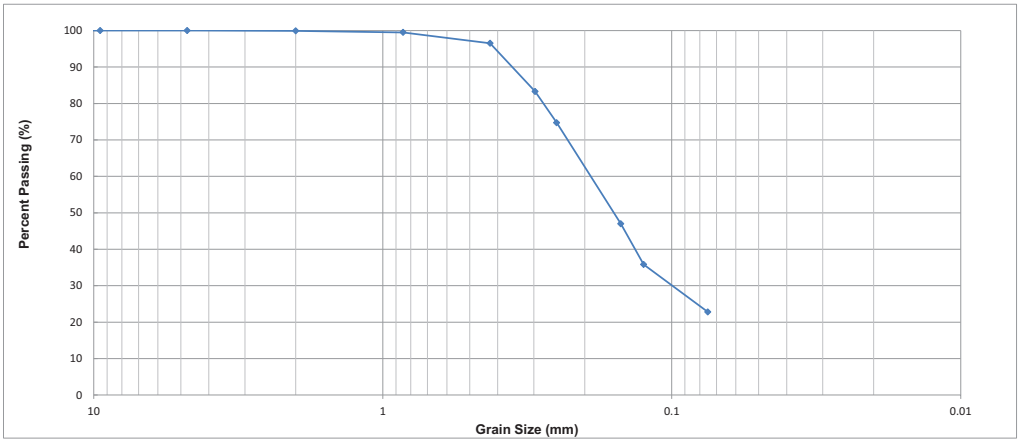

Boring: B(UW)-1 Sample: B-6 Description: Tan Fine Poorly Graded SAND (SP) w/ Silt and Gray Clay

D_{10}	< 0.075	mm
D_{30}	0.10	mm
D_{50}	0.16	mm
D_{60}	0.19	mm

C_c 0.7 C_u 2.5

USCS Grain Size Percentages

Gravel		Sand			Fines
Coarse	Fine	Coarse	Medium	Fine	
0	0	0.1	3.4	73.6	22.8

Performed by: JNH Checked by:

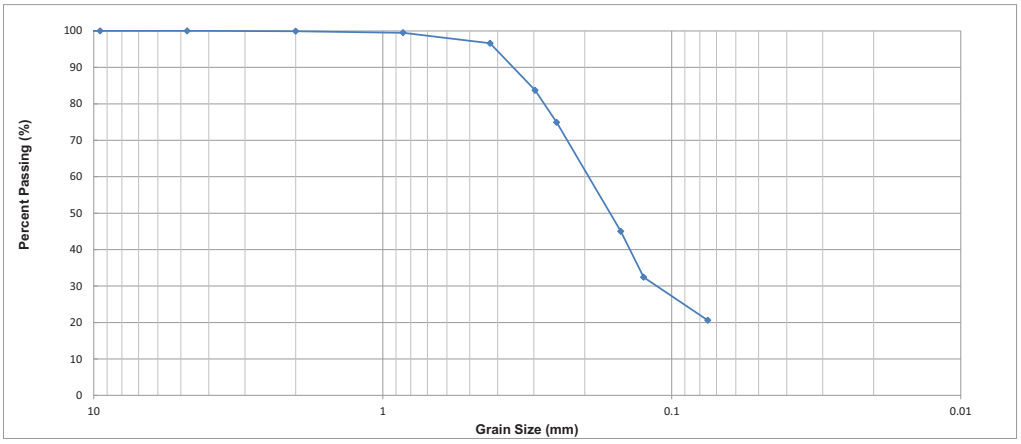

Boring: B(UW)-1 Sample: B-7 Description: Tan Fine Grained Poorly Graded SAND (SP) w/ Clay Interbeds

D_{10}	< 0.075	mm
D_{30}	0.11	mm
D_{50}	0.16	mm
D_{60}	0.19	mm

C_c 0.9 C_u 2.6

USCS Grain Size Percentages

Gravel		Sand			Fines
Coarse	Fine	Coarse	Medium	Fine	
0	0	0.1	3.3	75.9	20.6

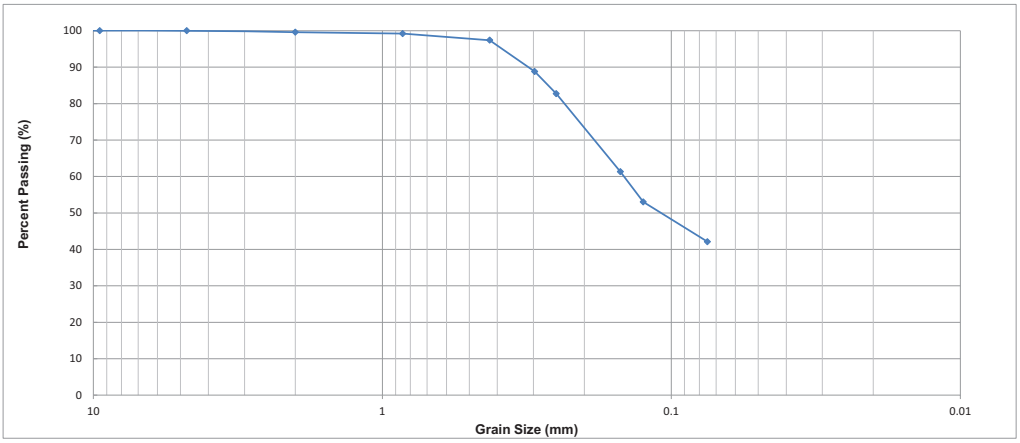

Boring: B(UW)-1 Sample: B-8 Description: Brown Fine Grained Poorly Graded SAND (SP) w/ Gray Clay Interbeds

D_{10} < 0.075 mm
D_{30} < 0.075 mm
D_{50} 0.11 mm
D_{60} 0.15 mm

C_c 0.5 C_u 1.9

USCS Grain Size Percentages

Gravel		Sand			Fines
Coarse	Fine	Coarse	Medium	Fine	
0	0	0.4	2.2	55.2	42.1

Performed by: JNH Checked by:

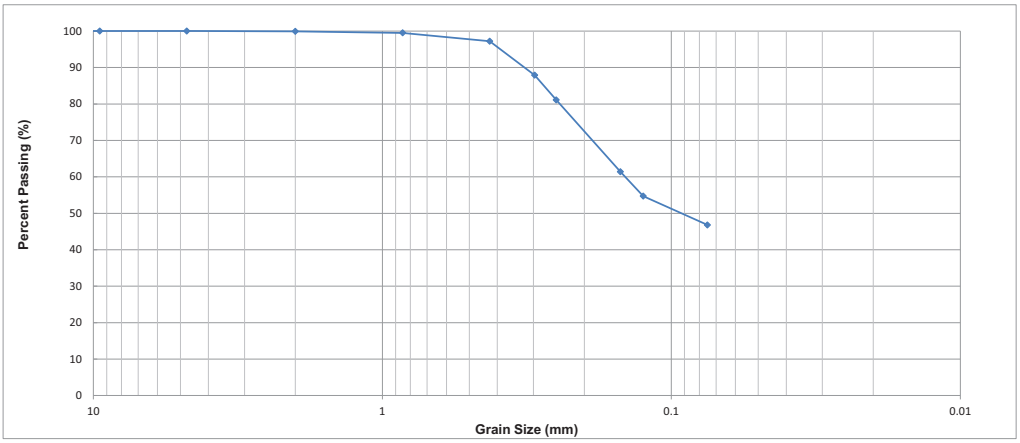

Boring: B(UW)-1 Sample: B-9 Description: Interbedded Brown Fine Grained Poorly Graded SAND (SP) and Gray CLAY (CL)

D_{10} < 0.075 mm
D_{30} < 0.075 mm
D_{50} 0.092 mm
D_{60} 0.14 mm

C_c 0.5 C_u 1.9

USCS Grain Size Percentages

Gravel		Sand			Fines
Coarse	Fine	Coarse	Medium	Fine	
0	0	0.1	2.7	50.4	46.8

Performed by: JNH Checked by:

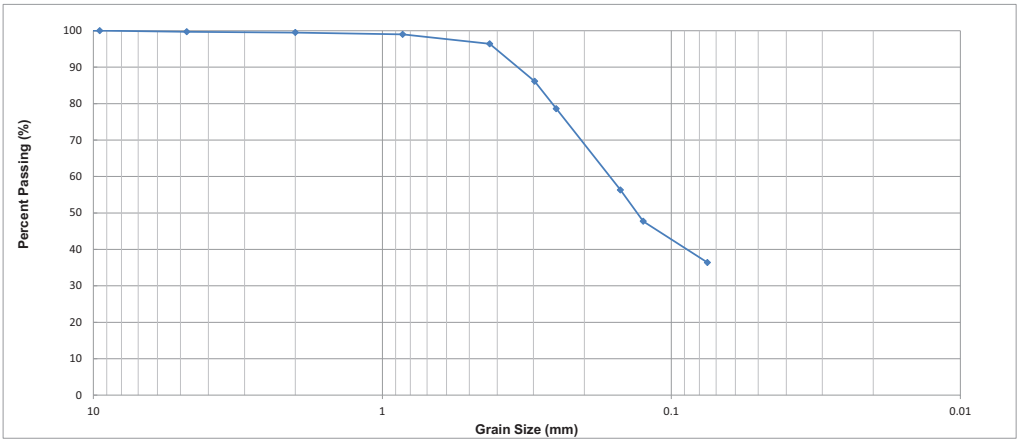

Boring: B(UW)-1 Sample: B-10 Description: Brown Fine Poorly Graded SAND (SP) and Gray CLAY (CL)

D_{10}	< 0.075	mm
D_{30}	< 0.075	mm
D_{50}	0.13	mm
D_{60}	0.16	mm

C_c 0.5 C_u 2.2

USCS Grain Size Percentages

Gravel		Sand			Fines
Coarse	Fine	Coarse	Medium	Fine	
0	0.3	0.2	3.1	60	36.4

Performed by: JNH Checked by:

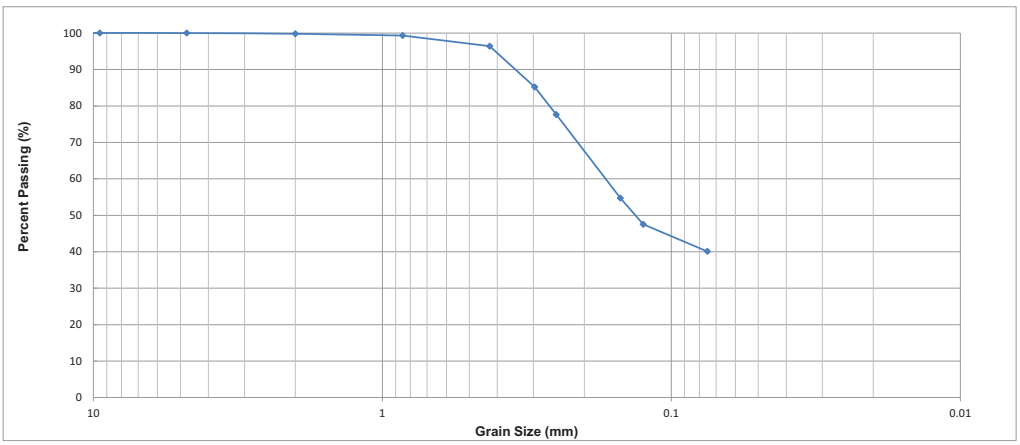

Boring: B(UW)-1 Sample: B-11 Description: Brown Fine Grained Poorly Graded SAND (SP) w/ Gray Clay Interbeds

D_{10}	< 0.075	mm
D_{30}	< 0.075	mm
D_{50}	0.13	mm
D_{60}	0.17	mm

C_c 0.4 C_u 2.3

USCS Grain Size Percentages

Gravel		Sand			Fines
Coarse	Fine	Coarse	Medium	Fine	
0	0	0.2	3.4	56.3	40.1

Performed by: JNH Checked by:

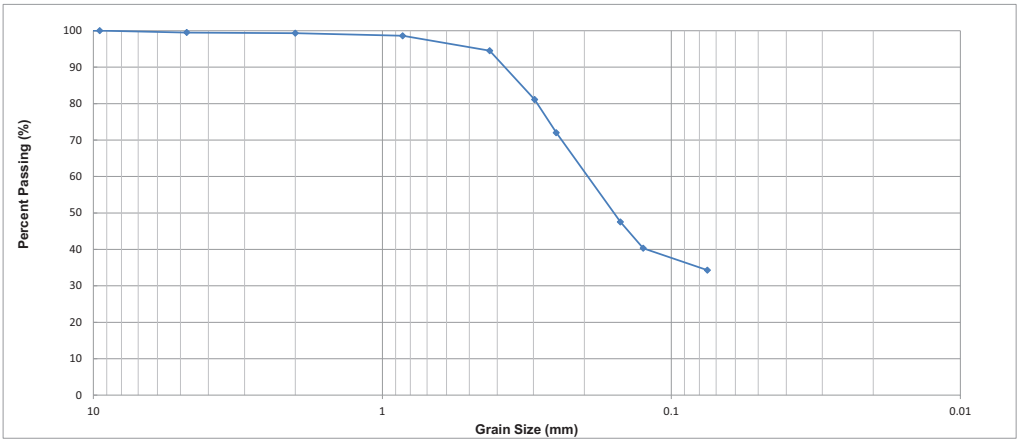

Boring: B(UW)-1 Sample: B-12 Description: Brown Fine Poorly Graded SAND (SP) and Gray CLAY (CL)

D_{10}	< 0.075	mm
D_{30}	< 0.075	mm
D_{50}	0.16	mm
D_{60}	0.19	mm

C_c 0.4 C_u 2.6

USCS Grain Size Percentages

Gravel		Sand			Fines
Coarse	Fine	Coarse	Medium	Fine	
0	0.5	0.3	4.8	60.1	34.3

Performed by: JNH Checked by:

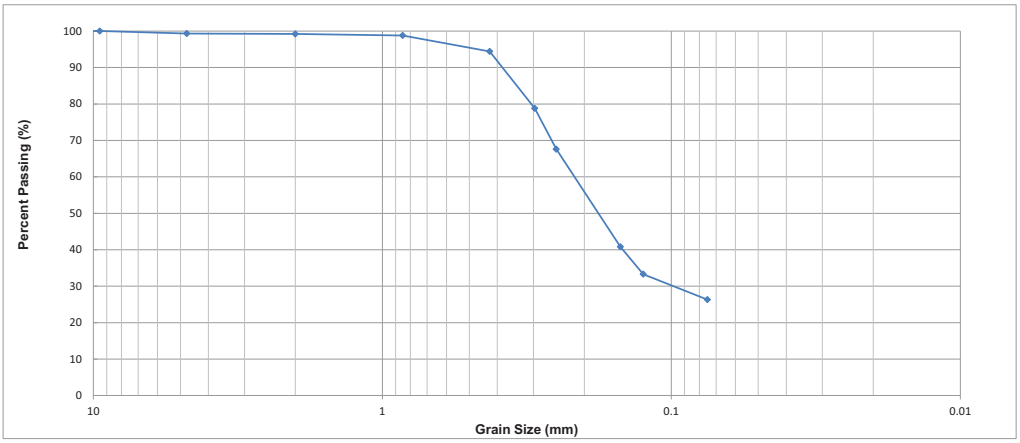

Boring: B(UW)-1 Sample: B-13 Description: Brown Fine to Medium Grained Poorly Graded SAND (SP) w/ Gray CLAY Interbeds

D_{10}	< 0.075	mm
D_{30}	0.098	mm
D_{50}	0.18	mm
D_{60}	0.22	mm

C_c 0.6 C_u 2.9

USCS Grain Size Percentages

Gravel		Sand			Fines
Coarse	Fine	Coarse	Medium	Fine	
0	0.7	0.2	4.8	68.2	26.3

Performed by: JNH Checked by:

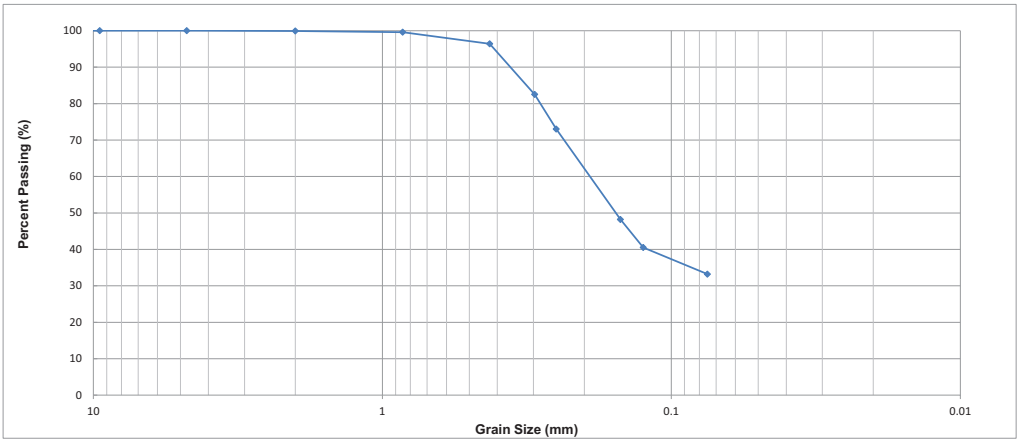

Boring: B(UW)-1 Sample: B-14 Description: Brown Fine Grained Poorly Graded SAND (SP) w/ Gray Clay Interbeds

D_{10}	< 0.075	mm
D_{30}	< 0.075	mm
D_{50}	0.16	mm
D_{60}	0.19	mm

C_c 0.4 C_u 2.6

USCS Grain Size Percentages

Gravel		Sand			Fines
Coarse	Fine	Coarse	Medium	Fine	
0	0	0.1	3.4	63.2	33.2

Performed by: JNH Checked by:

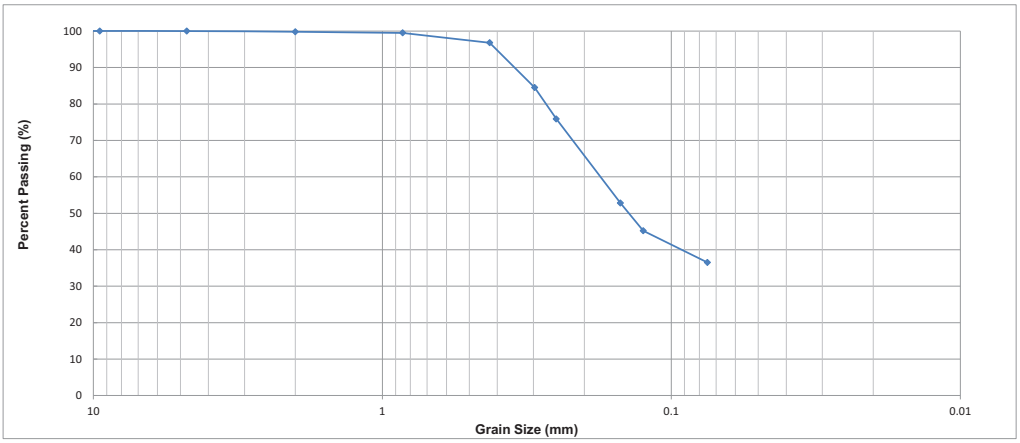

Boring: B(UW)-1 Sample: B-15 Description: Brown Fine Grained Poorly Graded SAND (SP) w/ Trace Fines Intermixed Gray CLAY

D_{10}	< 0.075	mm
D_{30}	< 0.075	mm
D_{50}	0.14	mm
D_{60}	0.18	mm

C_c 0.4 C_u 2.3

USCS Grain Size Percentages

Gravel		Sand			Fines
Coarse	Fine	Coarse	Medium	Fine	
0	0	0.2	3.1	60.4	36.5

Performed by: JNH Checked by:

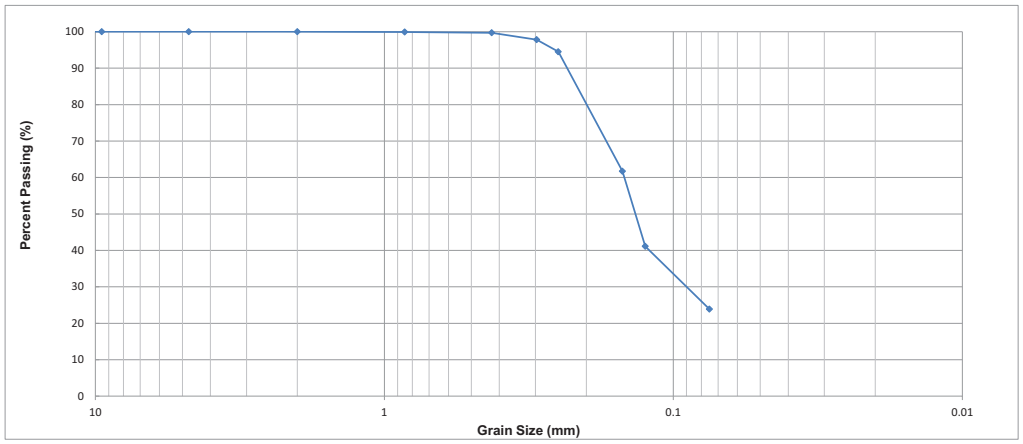

Boring: B(UW)-1 Sample: B-21 Description: Tan Fine Grained Poorly Graded SAND (SC) w/ Gray CLAY lenses

D_{10}	< 0.075	mm
D_{30}	0.090	mm
D_{50}	0.14	mm
D_{60}	0.15	mm

C_c 0.7 C_u 2.0

USCS Grain Size Percentages

Gravel		Sand			Fines
Coarse	Fine	Coarse	Medium	Fine	
0	0	0	0.4	75.7	23.9

Performed by: JNH Checked by:

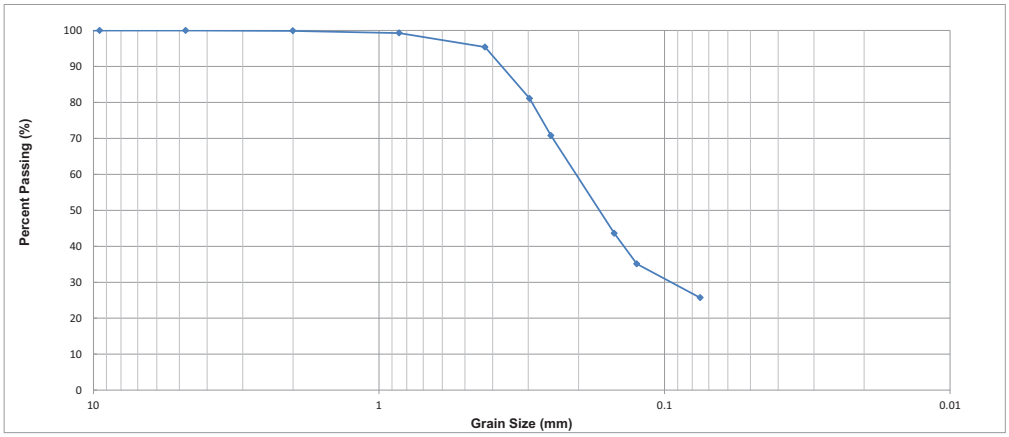

Boring: B(UW)-1 Sample: B-17 Description: Brown Fine Grained Poorly Graded SAND (SP) w/ Gray CLAY layers and Trace Organi

D_{10}	< 0.075	mm
D_{30}	0.10	mm
D_{50}	0.17	mm
D_{60}	0.21	mm

C_c 0.7 C_u 2.8

USCS Grain Size Percentages

Gravel		Sand			Fines
Coarse	Fine	Coarse	Medium	Fine	
0	0	0.1	4.4	69.7	25.7

Performed by: JNH Checked by:

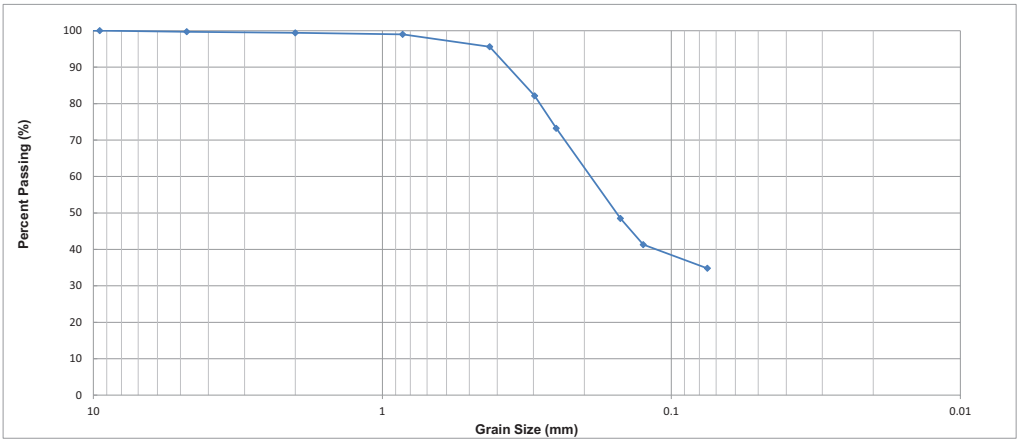

Boring: B(UW)-1 Sample: B-16 Description: Brown Fine Grained Poorly Graded SAND (SP) and Gray Clay w/ Some Silt

D_{10}	< 0.075	mm
D_{30}	< 0.075	mm
D_{50}	0.15	mm
D_{60}	0.19	mm

C_c 0.4 C_u 2.5

USCS Grain Size Percentages

Gravel		Sand			Fines
Coarse	Fine	Coarse	Medium	Fine	
0	0.3	0.3	3.8	60.7	34.8

Performed by: JNH Checked by:

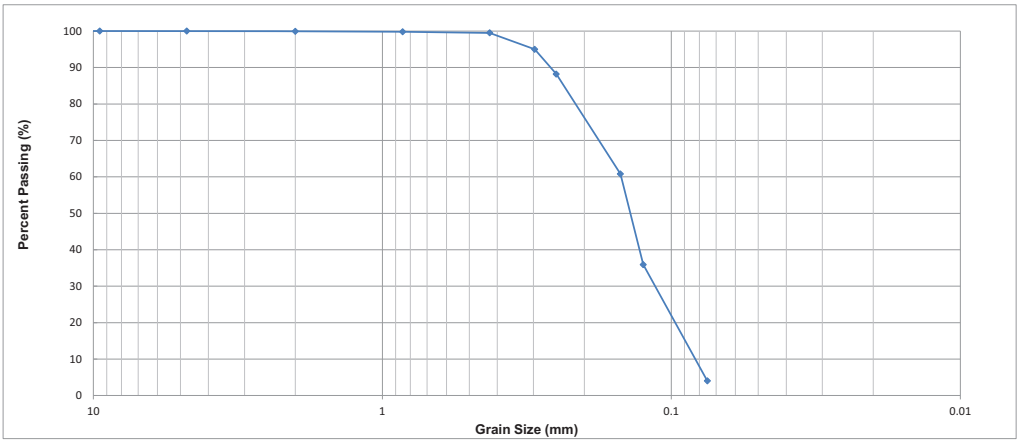

Boring: B(UW)-1 Sample: B-22 Description: Tan Fine Grained Poorly Graded SAND (SP) w/ Some Silt

D_{10}	0.083	mm
D_{30}	0.114	mm
D_{50}	0.14	mm
D_{60}	0.15	mm

C_c 1.1 C_u 1.8

USCS Grain Size Percentages

Gravel		Sand			Fines
Coarse	Fine	Coarse	Medium	Fine	
0	0	0.1	0.4	95.5	4

Performed by: JNH Checked by:

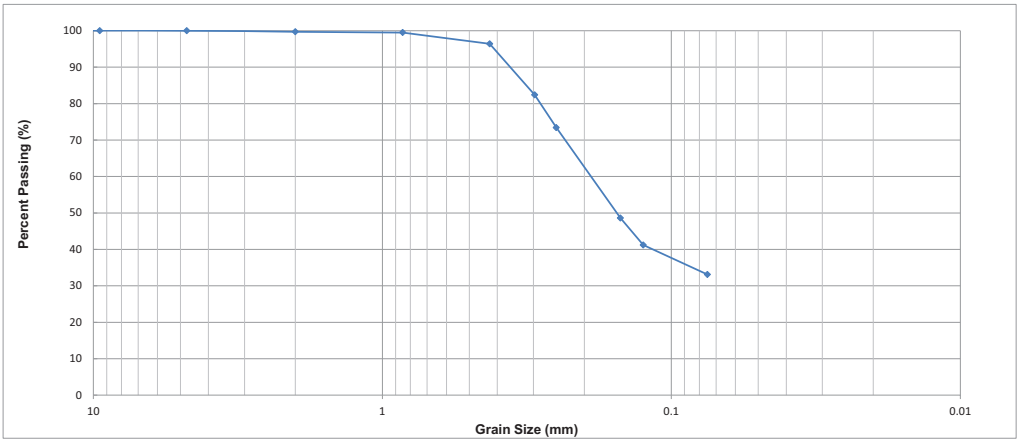

Boring: B(UW)-1 Sample: B-18 Description: Brown Fine Grained Poorly Graded SAND (SP) w/ Gray Clay Interbeds

D_{10} < 0.075 mm
D_{30} < 0.075 mm
D_{50} 0.15 mm
D_{60} 0.19 mm

C_c 0.4 C_u 2.5

USCS Grain Size Percentages

Gravel		Sand			Fines
Coarse	Fine	Coarse	Medium	Fine	
0	0	0.3	3.4	63.4	33.1

Performed by: JNH Checked by:

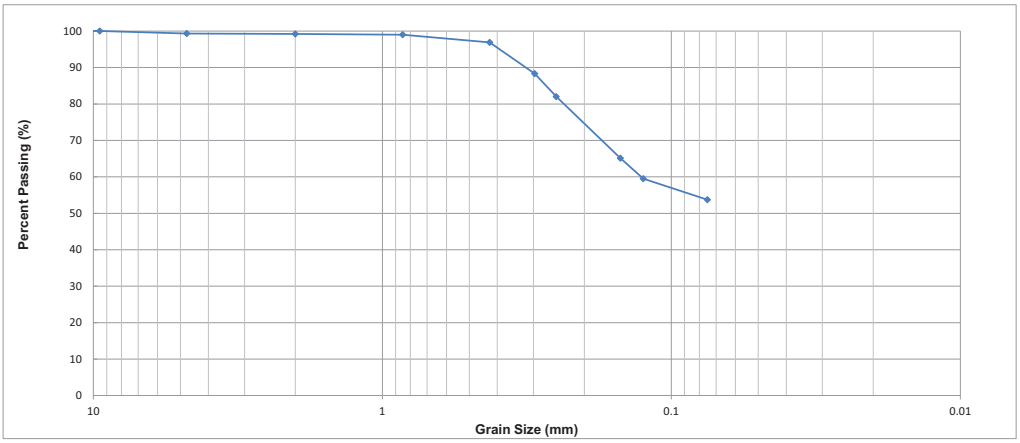

Boring: B(UW)-1 Sample: B-19 Description: Brown Gray CLAY w/ Brown Fine Grained Poorly Graded SAND (SP) Interbeds

D_{10} < 0.075 mm
D_{30} < 0.075 mm
D_{50} < 0.075 mm
D_{60} 0.13 mm

C_c N/A C_u N/A

USCS Grain Size Percentages

Gravel		Sand			Fines
Coarse	Fine	Coarse	Medium	Fine	
0	0.7	0.1	2.3	43.2	53.7

Performed by: JNH Checked by:

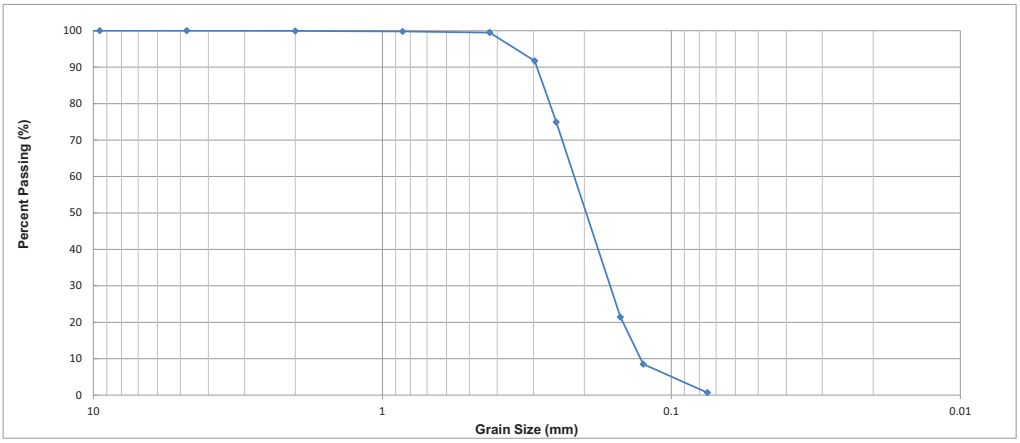

Boring: B(UW)-1 Sample: B-23 Description: Tan Fine Grained Poorly Graded SAND (SP)

D_{10}	0.13	mm
D_{30}	0.16	mm
D_{50}	0.20	mm
D_{60}	0.22	mm

C_c 1.0 C_u 1.7

USCS Grain Size Percentages

Gravel		Sand			Fines
Coarse	Fine	Coarse	Medium	Fine	
0	0	0.1	0.4	98.9	0.7

Performed by: JNH Checked by:

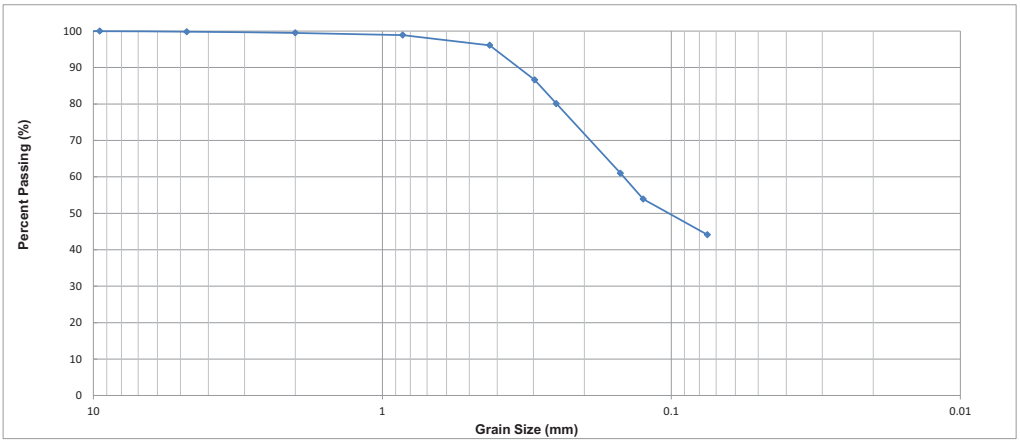

Boring: B(UW)-1 Sample: B-20 Description: Interbedded Brown Fine Grained SAND (SP) and Gray Lean CLAY (CL) w/ Silt

D_{10}	< 0.075	mm
D_{30}	< 0.075	mm
D_{50}	0.10	mm
D_{60}	0.15	mm

C_c 0.5 C_u 1.9

USCS Grain Size Percentages

Gravel		Sand			Fines
Coarse	Fine	Coarse	Medium	Fine	
0	0.2	0.3	3.4	52.1	44.1

Performed by: JNH Checked by:

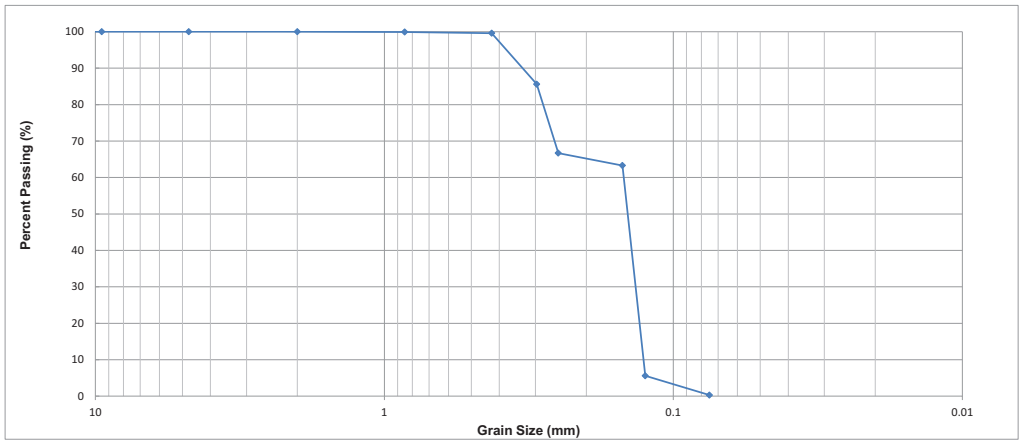

Boring: B(UW)-1 Sample: B-24 Description: Tan Fine Grained Poorly Graded SAND (SP)

D_{10}	0.13	mm
D_{30}	0.14	mm
D_{50}	0.14	mm
D_{60}	0.15	mm

C_c 1.0 C_u 1.2

USCS Grain Size Percentages

Gravel		Sand			Fines
Coarse	Fine	Coarse	Medium	Fine	
0	0	0	0.5	99.3	0.3

Performed by: JNH Checked by:

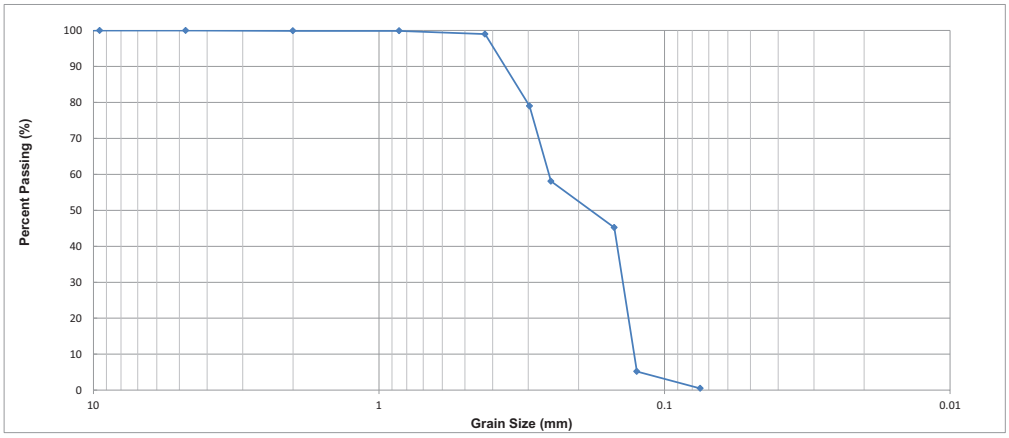

Boring: B(UW)-1 Sample: B-25 Description: Tan Fine Grained Poorly Graded SAND (SP)

D_{10}	0.13	mm
D_{30}	0.14	mm
D_{50}	0.18	mm
D_{60}	0.25	mm

C_c 1.0 C_u 3.4

USCS Grain Size Percentages

Gravel		Sand			Fines
Coarse	Fine	Coarse	Medium	Fine	
0	0	0	0.9	98.5	0.5

Performed by: JNH Checked by:

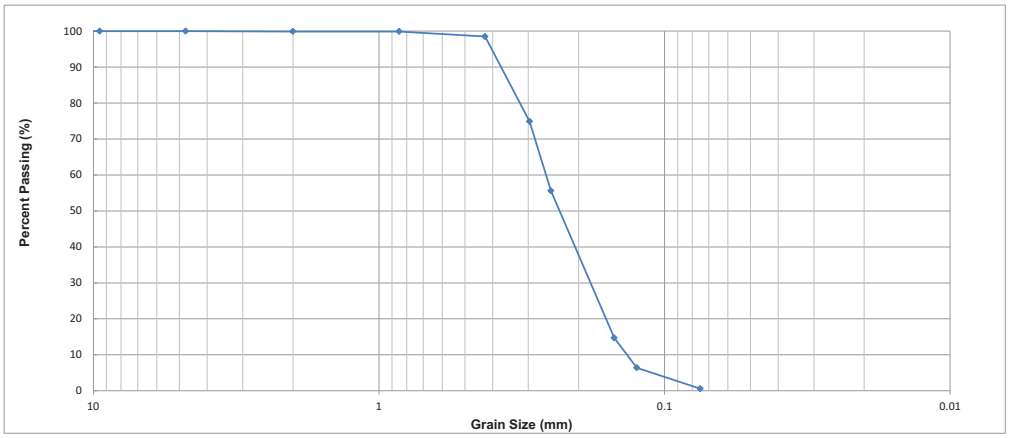

Boring: B(UW)-1 Sample: B-27 Description: Tan Fine Grained Poorly Graded SAND (SP)

D_{10}	0.14	mm
D_{30}	0.18	mm
D_{50}	0.23	mm
D_{60}	0.26	mm

C_c 0.9 C_u 1.9

USCS Grain Size Percentages

Gravel		Sand			Fines
Coarse	Fine	Coarse	Medium	Fine	
0	0	0.1	1.4	97.9	0.6

Performed by: JNH Checked by:

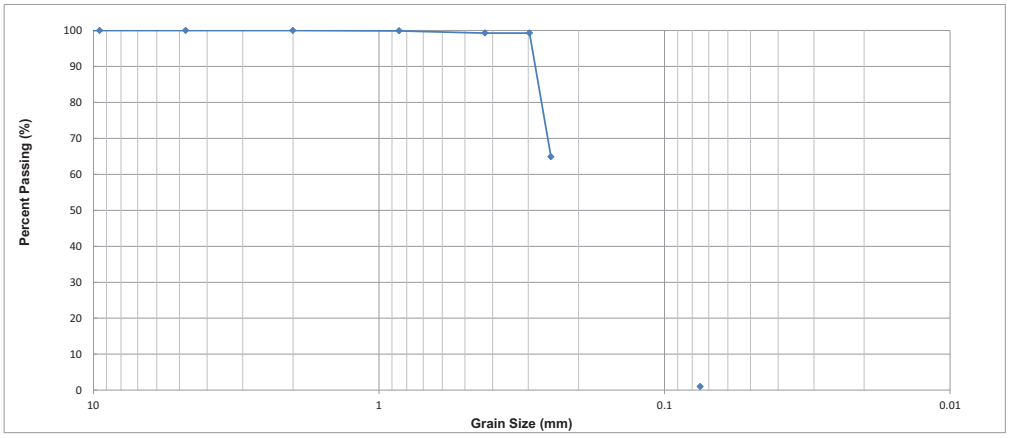

Boring: B(UW)-1 Sample: B-26 Description: Tan Fine Grained Poorly Graded SAND(SP) w/ Fe Staining and Trace Fines

D_{10}	0.089	mm
D_{30}	0.13	mm
D_{50}	0.19	mm
D_{60}	0.23	mm

C_c 0.8 C_u 2.6

USCS Grain Size Percentages

Gravel		Sand			Fines
Coarse	Fine	Coarse	Medium	Fine	
0	0	0	0.7	98.3	1

Performed by: JNH Checked by:

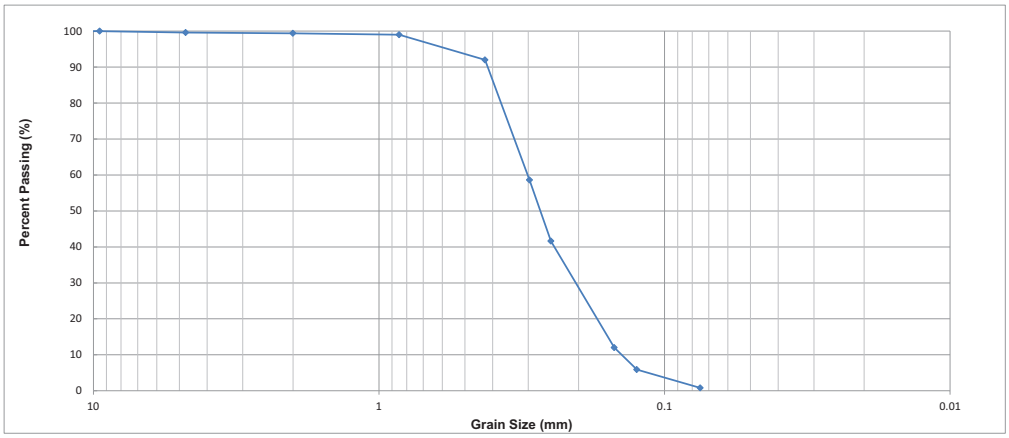

Boring: B(UW)-1 Sample: B-33 Description: Tan Wet Fine to Medium Grained Poorly Graded SAND (SP)

D_{10}	0.14	mm
D_{30}	0.20	mm
D_{50}	0.27	mm
D_{60}	0.30	mm

C_c 1.0 C_u 2.1

USCS Grain Size Percentages

Gravel		Sand			Fines
Coarse	Fine	Coarse	Medium	Fine	
0	0.4	0.3	7.4	91.2	0.8

Performed by: JNH Checked by:

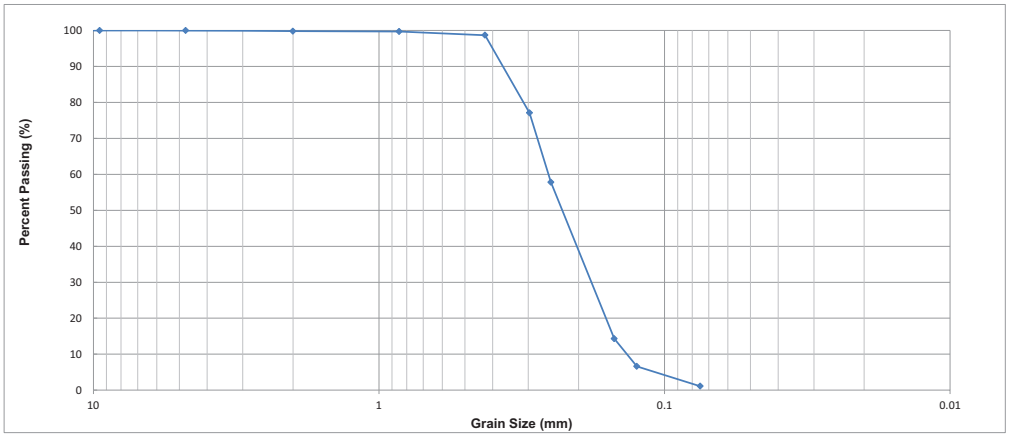

Boring: B(UW)-1 Sample: B-28 Description: Tan Fine Grained Poorly Graded SAND (SP) w/ Trace Silt and Fe Staining

D_{10}	0.14	mm
D_{30}	0.18	mm
D_{50}	0.23	mm
D_{60}	0.25	mm

C_c 0.9 C_u 1.9

USCS Grain Size Percentages

Gravel		Sand			Fines
Coarse	Fine	Coarse	Medium	Fine	
0	0	0.2	1.1	97.6	1.1

Performed by: JNH Checked by:

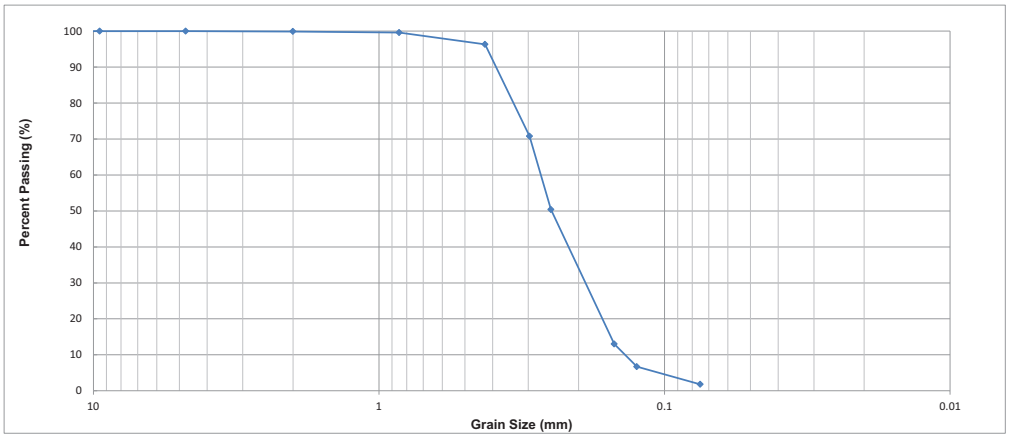

Boring: B(UW)-1 Sample: B-29 Description: Tan Fine Grained Poorly Graded SAND (SP) w/ Trace Clay

D_{10}	0.14	mm
D_{30}	0.19	mm
D_{50}	0.25	mm
D_{60}	0.27	mm

C_c 1.0 C_u 2.0

USCS Grain Size Percentages

Gravel		Sand			Fines
Coarse	Fine	Coarse	Medium	Fine	
0	0	0.1	3.5	94.5	1.8

Performed by: JNH Checked by:

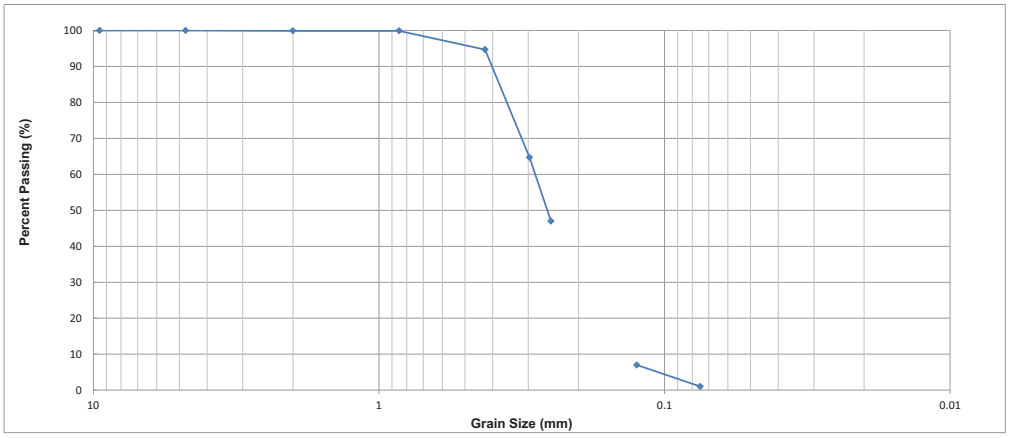

Boring: B(UW)-1 Sample: B-34 Description: Tan Fine to Medium Grained Poorly Graded SAND (SP) w/ Trace Fines

D_{10}	0.13	mm
D_{30}	0.19	mm
D_{50}	0.26	mm
D_{60}	0.28	mm

C_c 0.9 C_u 2.2

USCS Grain Size Percentages

Gravel		Sand			Fines
Coarse	Fine	Coarse	Medium	Fine	
0	0	0.1	5.3	93.6	1

Performed by: JNH Checked by:

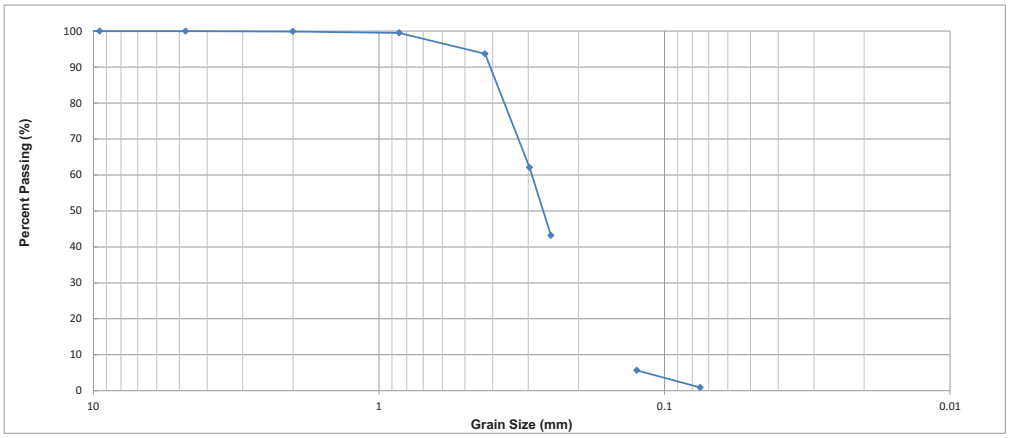

Boring: B(UW)-1 Sample: B-30 Description: Tan Fine Grained Poorly Graded SAND (SP)

D_{10}	0.14	mm
D_{30}	0.20	mm
D_{50}	0.27	mm
D_{60}	0.29	mm

C_c 1.0 C_u 2.2

USCS Grain Size Percentages

Gravel		Sand			Fines
Coarse	Fine	Coarse	Medium	Fine	
0	0	0.1	6.2	92.9	0.9

Performed by: JNH Checked by:

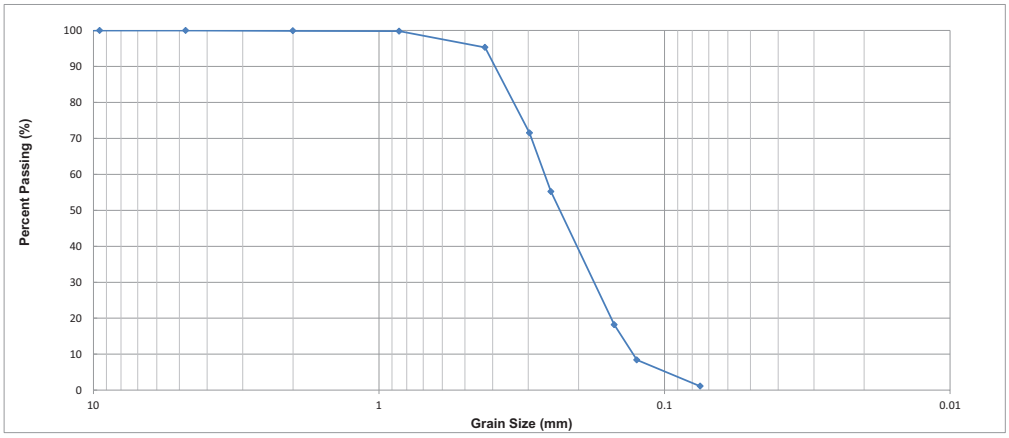

Boring: B(UW)-1 Sample: B-32 Description: Tan Fine Grained Poorly Graded SAND (SP)

D_{10}	0.13	mm
D_{30}	0.18	mm
D_{50}	0.23	mm
D_{60}	0.26	mm

C_c 0.9 C_u 2.0

USCS Grain Size Percentages

Gravel		Sand			Fines
Coarse	Fine	Coarse	Medium	Fine	
0	0	0.1	4.6	94.1	1.1

Performed by: JNH Checked by:

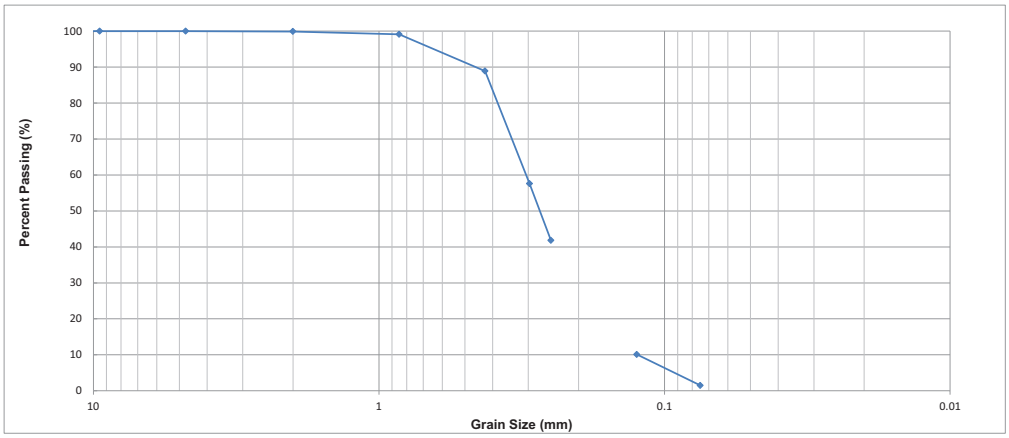

Boring: B(UW)-1 Sample: B-31 Description: Tan to Brown Fine to Medium Grained Poorly Graded SAND (SP) w/ Trace Silt

D_{10} 0.12 mm
D_{30} 0.19 mm
D_{50} 0.27 mm
D_{60} 0.31 mm

C_c 1.0 C_u 2.5

USCS Grain Size Percentages

Gravel		Sand			Fines
Coarse	Fine	Coarse	Medium	Fine	
0	0	0.1	10.9	87.4	1.5

Performed by: JNH Checked by:

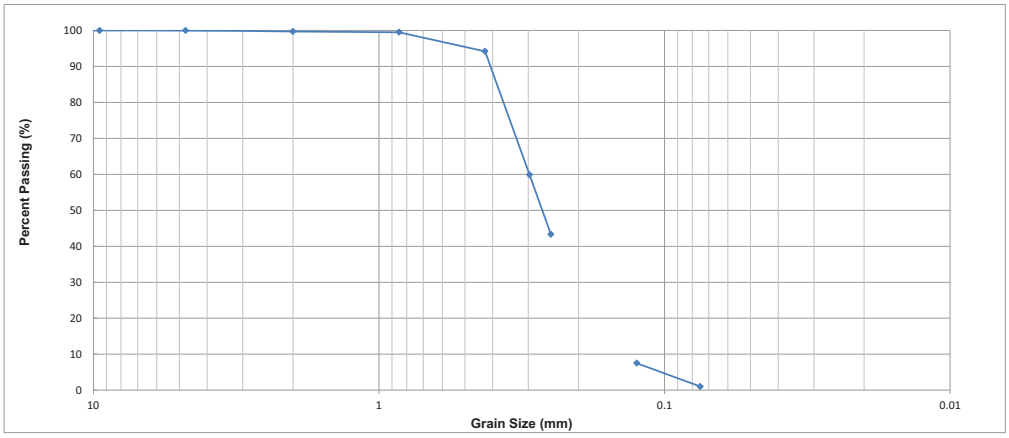

Boring: B(UW)-1 Sample: B-35 Description: Tan Fine to Medium Grained Poorly Graded SAND (SP)

D_{10} 0.13 mm
D_{30} 0.19 mm
D_{50} 0.27 mm
D_{60} 0.30 mm

C_c 1.0 C_u 2.3

USCS Grain Size Percentages

Gravel		Sand			Fines
Coarse	Fine	Coarse	Medium	Fine	
0	0	0.3	5.4	93.2	1

Performed by: JNH Checked by:

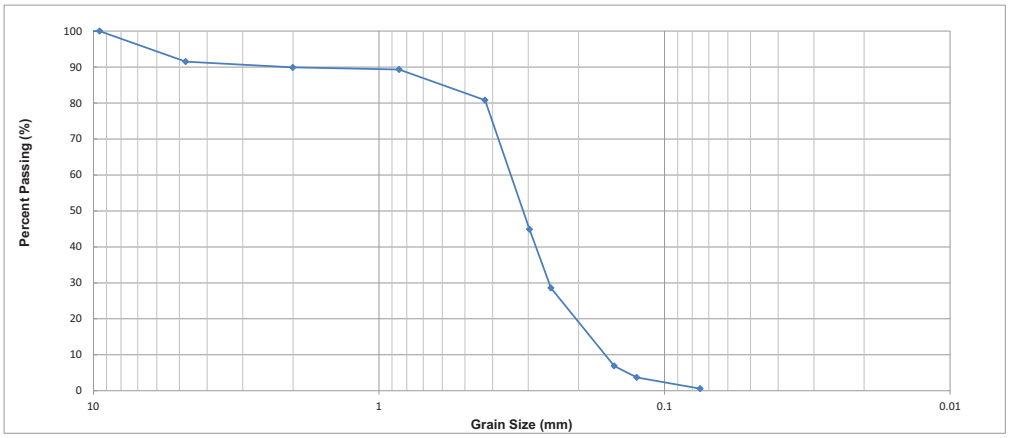

Boring: B(UW)-1 Sample: B-36 Description: Tan Wet Medium to Fine Grained Poorly Graded SAND (SP) w/ Some Fine Gravel

D_{10}	0.16	mm
D_{30}	0.25	mm
D_{50}	0.31	mm
D_{60}	0.35	mm

C_c 1.2 C_u 2.1

USCS Grain Size Percentages

Gravel		Sand			Fines
Coarse	Fine	Coarse	Medium	Fine	
0	8.5	1.6	9.1	80.2	0.6

Performed by: JNH Checked by:

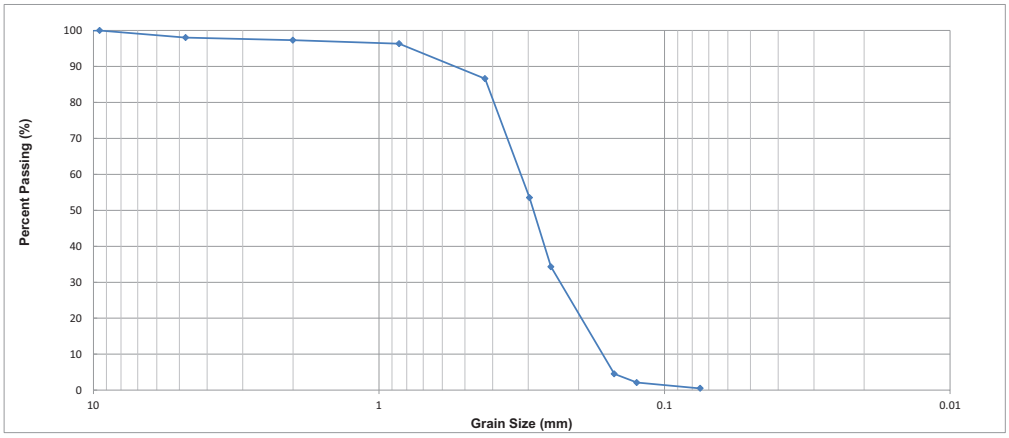

Boring: B(UW)-1 Sample: B-37 Description: Tan to Orange Wet Medium to Fine Grained Poorly Graded SAND (SP) some pebbles

D_{10}	0.16	mm
D_{30}	0.23	mm
D_{50}	0.29	mm
D_{60}	0.32	mm

C_c 1.0 C_u 1.9

USCS Grain Size Percentages

Gravel		Sand			Fines
Coarse	Fine	Coarse	Medium	Fine	
0	2	0.7	10.6	86.1	0.5

Performed by: JNH Checked by:

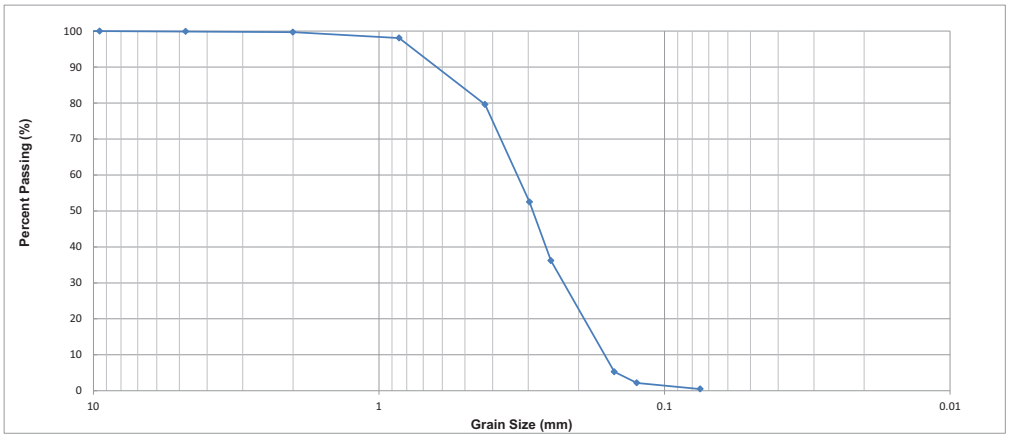

Boring: B(UW)-1 Sample: B-38 Description: Brown Wet Fine to Medium Grained Poorly Graded SAND (SP)

D_{10}	0.16	mm
D_{30}	0.23	mm
D_{50}	0.29	mm
D_{60}	0.33	mm

C_c 1.0 C_u 2.0

USCS Grain Size Percentages

Gravel		Sand			Fines
Coarse	Fine	Coarse	Medium	Fine	
0	0.1	0.2	20.1	79	0.5

Performed by: JNH Checked by:

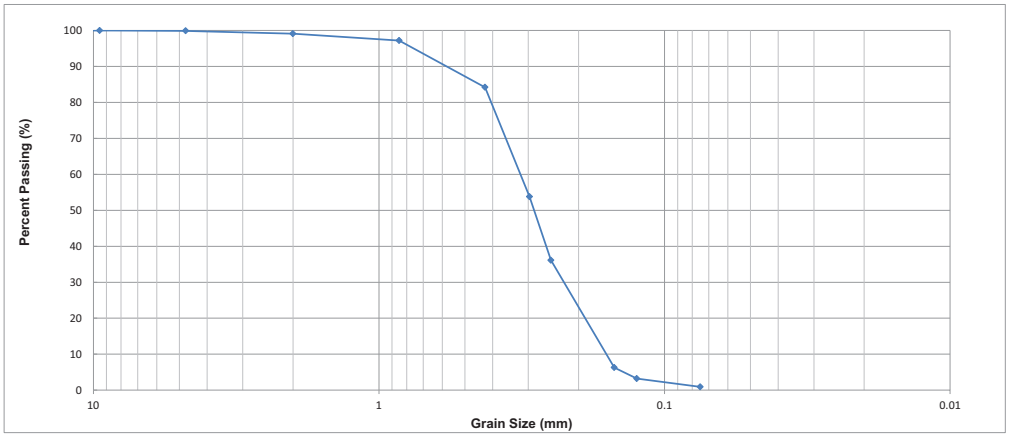

Boring: B(UW)-1 Sample: B-39 Description: Tan to Orange Wet Medium to Fine Grained Poorly Graded SAND (SP)

D_{10}	0.16	mm
D_{30}	0.23	mm
D_{50}	0.29	mm
D_{60}	0.32	mm

C_c 1.0 C_u 2.0

USCS Grain Size Percentages

Gravel		Sand			Fines
Coarse	Fine	Coarse	Medium	Fine	
0	0.1	0.8	14.9	83.3	0.9

Performed by: JNH Checked by:

UW-1

- Boring Log
- Laboratory Test Summary Table
- Atterberg Limits Results
- Grain Size Analysis Curves
- Oedometer Testing Results

COLLEGE OF ENGINEERING
UNIVERSITY OF WISCONSIN-MADISON
Geological Engineering Program

LOG OF TEST BORING

Facility / Project Name CEE 476 Test Site	Date (mm/dd/yy) Started 7/8/2010	Boring Number BH-4
Boring Drilled by: Crew Chief & Firm Alex (Driller) Kevin (Helper); Badger State Drilling	Date (mm/dd/yy) Finished 7/8/2010	Drilling Method H.S.A to 4.6 m Rotary Wash to termination
Final Static Water Level 1.4m	Surface Elevation ` 400 feet NAVD 1929	Borehole Diameter 159 mm HSA 150 mm RW
State Wisconsin	County Dane	Civil Town / City / Village Madison	Drill Rig D 120

Sample Number and Type	Recovery (cm)	Blow Counts	Depth (m)	Soil / Rock Description and Geologic Origin for Each Major Unit	USCS	Graphic Log	Well Diagram	s_u (kPa) / ϕ'	water content	Liquid Limit	Plasticity Index	Fines Content	Unit Weight	σ'_{vy}	C_C
			0.5												
S-1	27.9	2-2-2		Firm dark brown moist mottled lean CLAY (CL) with some sand lenses	CL				16	37	18				
			1.0												
N/A	0	7-5-14		-No Recovery											
S-2			1.5	-Fine sand lense	CL				21	30	15				
S-3	45.7	7-4-4			SM				53			23			
			2.0	Very loose to loose black wet SILTY SAND (SM)											
S-4	45.7	WOH			SM				74			32			
S-5			2.5		SM				74			19			
S-6	38.1	2-4-4			OH				187	212	NP				
			3.0	Soft to Firm black moist ORGANIC SILT (OH)					217						
Tube 7	38.1				OH				458	483	182				
			3.5												
Tube 8	33								161						
			4.0						123				11.8	55	0.93
Tube 9	61				MH			38	74				14.5	58	0.43
			4.5	Firm light gray moist elastic SILT (MH) with sand sized shell fragments				45º	75	85	46		16.5		
			5.0												
				-Setup Rotary Wash Drilling											
			5.5												
S-7	34.3	10-17-25		Very dense light gray wet poorly graded SAND (SP)	SP				18			2			
			6.0												
			6.5												
			7.0												
S-8	27.9	7-11-16	7.5	Dense light gray moist poorly graded SAND with silt (SP-SM)	SP-SM				18			7			
			8.0												
			8.5												
S-9	35.6	12-13-14	9.0	Dense light gray moist poorly graded SAND (SP)	SP				18			8			
			9.5	-1cm thick clay lense											
			10.0												

Sample Number and Type	Recovery (cm)	Blow Counts	Depth (m)	Soil / Rock Description and Geologic Origin for Each Major Unit	USCS	Graphic Log	Well Diagram	s_u (kPa) / ϕ'	water content	Liquid Limit	Plasticity Index	Fines Content	Unit Weight	σ'_{vy}	C_C / C_S
S-10	22.9	13-18-19	10.5	Dense light gray moist poorly graded SAND (SP)	SP				22						
			11.0												
			11.5												
S-11	35.6	10-12-13	12.0	Hard gray wet lean CLAY (CL) with sand	CL				20	35	18	54			
			12.5												
			13.0	Hard light gray moist lean CLAY (CL)											
S-12	45	3-5-7			CL				22	24	8	82			
			13.5												
			14.0												
			14.5												
S-13	45	5-5-7			CL				20	25	9	98			
			15.0												
			15.5												
			16.0												
S-14	45	7-4-8	16.5		CL										
			17.0												
			17.5												
			18.0												
S-15	20.32	18-20-16	18.5	Dense tan to light gray poorly graded SAND (SP)	SP				19						
			19.0												
			19.5												
S-16	27.9	13-19-22		-becoming very dense	SP				19			4			
			20.0												
			20.5												
S-17	30.5	19-27-31	21.0	Very dense tan to light gray poorly graded SAND (SP) with silt	SP-SM				18			6			
			21.5	Blind Drilling 21.3 m to 25.9 m											
			22.0												

Facility / Project Name: GLE 476 Test Site

Boring Number: BH-4

Sample Number and Type	Sample Recovery (cm)	Blow Counts	Depth (m)	Soil / Rock Description and Geologic Origin for Each Major Unit	USCS	Graphic Log	Well Diagram	s_u (kPa) / ϕ'	water content	Liquid Limit	Plasticity Index	Fines Content	Unit Weight	σ'_{vy}	C_C / C_S
			22.5	Blind Drilling 21.3 m to 25.9 m											
			23.0												
			23.5												
			24.0												
			24.5												
			25.0												
			25.5												
			26.0												
S-18	25.4	18-22-26		Dense tan to light gray poorly graded SAND (SP)	SP				18			7			
			26.5												
			27.0	Blind Drilling 26.4 m to 30 m											
			27.5												
			28.0												
			28.5												
			29.0												
			29.5												
			30.0												
	0	9-9-19		-No Recovery											
			30.5												
				Boring Terminated at 30.5 m Below Ground											
			31.0	Surface											
			31.5												
				Well Details:											
			32.0	Well Schedule 40 PVC Inner Diameter 50mm											
				Screen Slot Size: 0.25 mm											
			32.5	Annular Space: Boring diameter 150 mm											
				Bentonite seal from surface to 27.7 m											
			33.0	Fine sand (Ohio #40 -60) from 27.7 m to 28 m											
				Filter Pack (Ohio #5) from 28 m to 30.2 m											
			33.5												
			34.0												

Laboratory Test Summary, Site UW-1, Boring BH-4

ID	Top Depth (m)	Bottom Depth (m)	Approx. σ'_{vo} (kPa)	Boring Desc.	Field Log USCS	Moisture Content (%)	Unit Weight (kN/m^3)	D_{50} (mm)	D_{10} (mm)	% Fines	LL	PI	Organic Content	ϕ' (deg)	s_u (kPa)	C_C	C_S	e_o to σ'_{vo} (%)	σ'_{vy} (kPa)
S-1	0.46	0.91	12	Clay	CH	16					37	18							
S-2	1.37	1.52	25	Clay	CH	21					30	15							
S-3	1.52	1.83	28	Sand	SP	53		0.27	0.04	23									
S-4	1.83	2.29	35	Sand	SP	74		0.17	0.02	32									
S-5	2.29	2.44	40	Sand	SP	74		0.37	0.05	19									
S-6	2.44	2.74	43	Organic (some sand, remove)	ML/OL	187					212		59						
Tube7	2.74	3.35	46	Organic	ML/OL	217							65						
Tube7	3.35	3.35	48	Organic	ML/OL	458					483	182							
Tube8	3.35	3.96	51	Organic	ML/OL	161							41						
Tube8	3.35	3.96	51	Organic	ML/OL	123	11.8									0.93	0.11	5.3	$=s'_{vo}$
Tube9	3.96	4.57	55	Silt	MH	74	14.5									0.43	0.06	7.2	$=s'_{vo}$
Tube9	3.96	4.57	55	Silt	MH	75	16.5				85	46		45	38				
S-7	5.64	6.1	66	Sand (silty)	SP	18		0.28	0.14	2									
S-8	7.16	7.62	77	Sand	SP	18		0.26	0.09	7									
S-9	8.69	9.14	87	Sand	SP	18				8									
S-10	10.21	10.67	98	Sand	SP	22													
S-11	11.73	12.19	109	Silt	SC	20				54	35	18							
S-12	13.26	13.72	119	Silt	ML-CL	22				82	24	8							
S-13	14.78	15.24	130	Silt	ML	20				98	25	9							
S-14	16.31	16.76	141	Silt	ML	22				84	NP	NP							
S-15	18.29	18.75	155	Sand	SP	19													
S-16	19.35	19.81	162	Sand	SP	19		0.27	0.13	4									
S-17	20.88	21.34	173	Sand	SP	18		0.22	0.09	6									
S-18	25.91	26.37	208	Sand	SP	18		0.28	0.14	7									

Atterberg Limits, Site UW-1, Boring BH-4

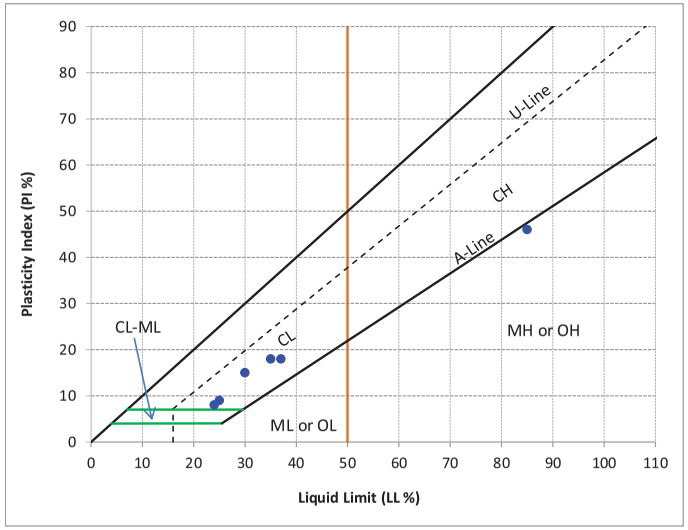

Boring	Sample	w (%)	LL	PL	PI	LI	USCS
BH-4	S-1	16	37	19	18	-0.2	CL
BH-4	S-2	21	30	15	15	0.4	CL
BH-4	Tube7	217	483	301	182	-0.5	OH
BH-4	Tube9	75	85	39	46	0.8	MH
BH-4	S-11	20	35	17	18	0.2	CL
BH-4	S-12	22	24	16	8	0.7	CL
BH-4	S-13	20	25	16	9	0.4	CL

Grain Size Analysis, Site UW-1, Boring BH-4

Sieve	Diamter (mm)	Sample S-3 % Pass	Sample S-4 % Pass	Sample S-5 % Pass	Sample S-7 % Pass	Sample S-8 % Pass	Sample S-9 % Pass	Sample S-16 % Pass	Sample S-17 % Pass	Sample S-18 % Pass
4	4.75	90.0	95.6	88.3	99.8	100.0	99.6	99.8	99.5	99.6
10	2	80.0	86.8	76.9	97.7	99.7	98.5	99.0	99.1	96.7
20	0.85	68.2	76.9	65.4	95.4	98.0	96.9	97.6	97.9	93.5
40	0.425	57.1	66.6	52.5	82.3	75.9	87.4	90.0	88.2	83.3
60	0.25	48.0	57.8	42.6	42.5	47.5	54.1	42.8	59	41.1
100	0.152	36.6	47.2	31.1	11.4	18.3	18.4	11.8	26.9	12.2
200	0.075	22.7	32.4	18.6	1.7	7.1	4.0	4.1	5.7	3.5
	USCS	SM	SM	SM	SP	SP-SM	SP	SP	SP-SM	SP

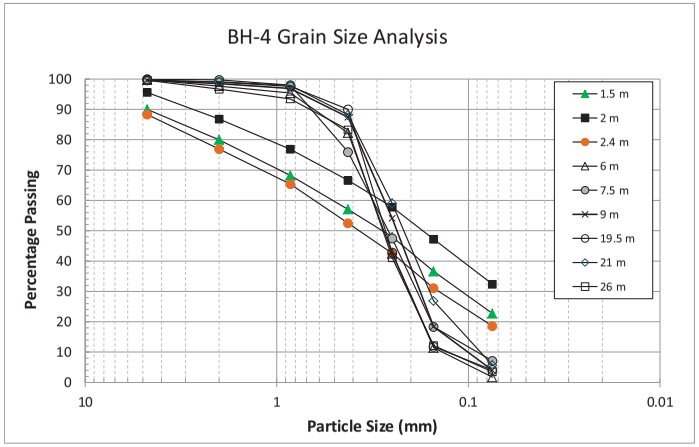

Oedometer Test Results
Tube 8; BH-4

Boring: BH-4 3.7 m
Sample: Tube 8
Description: Soft to firm black moist ORGANIC SILT (OH)

OCR 1 Normally Consolidated

C_C 0.93

C_S 0.11

P_c' 55 kPa

s'v0 38 kPa

Step	Load	Δy_0	Δy_{12}	D	Stress	H_0	ΔH	ε_a	e_0	Δe	e	c_v	Data
	(kN)	(mm)	(mm)	(mm)	(kPa)	(mm)	(mm)					cm^2/s	Rating
1	0.025	2.0883	2.0728	63.50	8	25.40	-0.015	-0.001	3.72	-0.003	3.724		
2	0.135	3.0507	3.436	63.50	43	25.40	1.348	0.053	3.72	0.250	3.471		
3	0.218	3.5783	4.1198	63.50	69	25.40	2.032	0.080	3.72	0.378	3.344	0.059263	Good
4	0.343	4.2653	4.8656	63.50	108	25.40	2.777	0.109	3.72	0.516	3.205	0.017597	Good
5	0.59	5.1503	6.0477	63.50	186	25.40	3.959	0.156	3.72	0.736	2.985	0.021252	Good
6	1.09	6.3479	7.3133	63.50	344	25.40	5.225	0.206	3.72	0.971	2.750	0.016418	Good
7	0.591	7.2901	7.3133	63.50	187	25.40	5.225	0.206	3.72	0.971	2.750	0.042789	Fair
8	0.342	7.1756	7.0828	63.50	108	25.40	4.995	0.197	3.72	0.928	2.793	0.028657	Fair
9	0.217	7.0519	6.9714	63.50	69	25.40	4.883	0.192	3.72	0.908	2.813	0.009817	Poor
10	0.156	6.9606	6.9157	63.50	49	25.40	4.827	0.190	3.72	0.897	2.824	0.055783	Poor
11	0.218	6.942	6.9513	63.50	69	25.40	4.863	0.191	3.72	0.904	2.817		Bad
12	0.344	6.976	7.0132	63.50	109	25.40	4.925	0.194	3.72	0.915	2.806	0.09914	Fair
13	0.593	7.055	7.1493	63.50	187	25.40	5.061	0.199	3.72	0.941	2.780	0.07218	Fair
14	1.091	7.2437	7.4851	63.50	344	25.40	5.397	0.212	3.72	1.003	2.718	0.015425	Fair
15	2.088	7.7852	8.8126	63.50	659	25.40	6.724	0.265	3.72	1.250	2.471	0.016343	Good
16	4.084	9.2304	10.25	63.50	1290	25.40	8.162	0.321	3.72	1.517	2.204	0.012356	Good
17	8.074	10.4248	11.8344	63.50	2549	25.40	9.746	0.384	3.72	1.812	1.910	0.011709	Good
18	4.087	11.8235	11.6379	63.50	1291	25.40	9.550	0.376	3.72	1.775	1.946		
19	2.09	11.5946	11.4986	63.50	660	25.40	9.410	0.370	3.72	1.749	1.972	Virgin	Recomp.
20	1.091	11.463	11.3888	63.50	344	25.40	9.301	0.366	3.72	1.729	1.992	c_v	c_v
21	0.545	11.3439	11.2047	63.50	172	25.40	9.116	0.359	3.72	1.694	2.027	cm^2/s	cm^2/s
22	0.341	11.1969	11.084	63.50	108	25.40	8.996	0.354	3.72	1.672	2.049	0.015946	0.07137
23	0.219	11.0669	10.9463	63.50	69	25.40	8.858	0.349	3.72	1.646	2.075		
24	0.158	10.9478	10.8426	63.50	50	25.40	8.754	0.345	3.72	1.627	2.094		
25	0.001	10.8859	9.6342	63.50	0.3	25.40	7.546	0.297	3.72	1.403	2.319	a_v	-0.00724
												m_v	0.001533
												D	652.142

70 kPa Load Step - Taylor Method

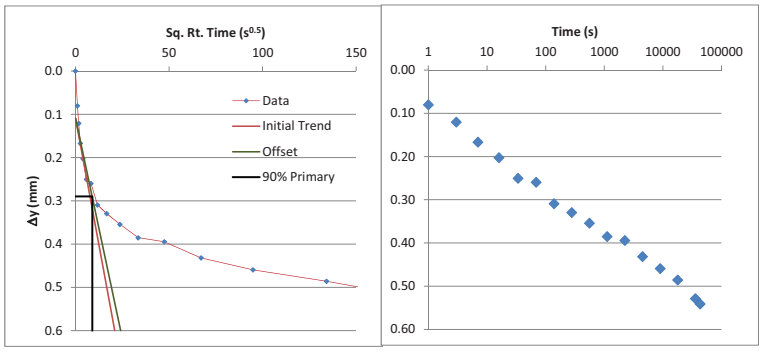

Initial Trend

x	y
0	0.11
21	0.6

t90 (s) 81

Offset

x	y
0	0.11
24.15	0.6

Hdr (m) 0.02

cv (m^2/s) 5.926E-06

90% Primary

x	y
0	0.29
9	0.29
9	0.6

cv (cm^2/s) 0.0592633

110 kPa Load Step - Taylor Method

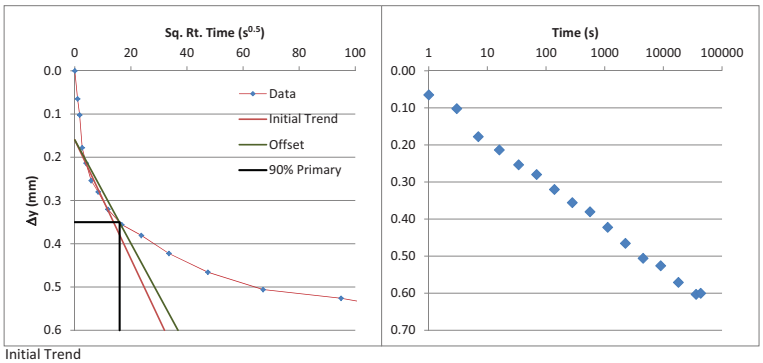

Initial Trend

x	y
0	0.16
32	0.6

t90 (s) 256

Offset

x	y
0	0.16
36.8	0.6

Hdr (m) 0.0230

cv (m^2/s) 1.76E-06

90% Primary

x	y
0	0.35
16	0.35
16	0.6

cv (cm^2/s) 0.0175967

189 kPa Load Step - Taylor Method

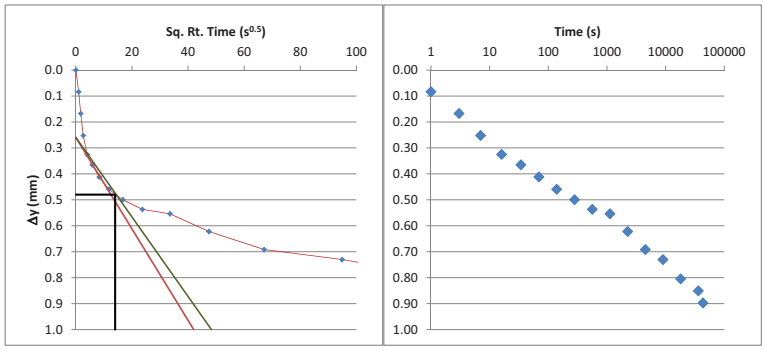

Initial Trend

x	y
0	0.26
42	1

t90 (s) 196

Offset

x	y
0	0.26
48.3	1

Hdr (m) 0.0222

cv (m^2/s) 2.125E-06

90% Primary

x	y
0	0.48
14	0.48
14	1

cv (cm^2/s) 0.0212522

350 kPa Load Step - Taylor Method

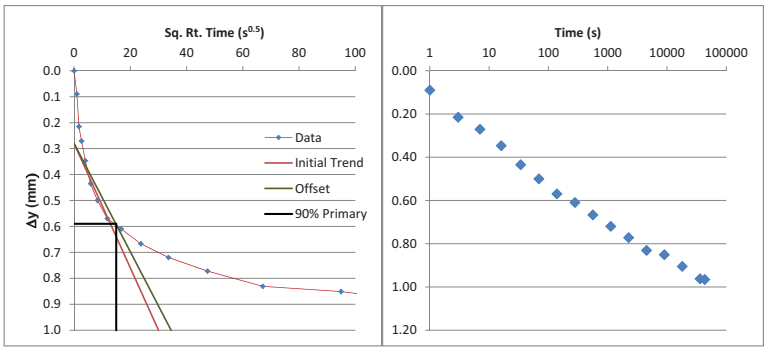

Initial Trend

x	y
0	0.28
30	1

t90 (s) 225

Offset

x	y
0	0.28
34.5	1

Hdr (m) 0.0209

90% Primary

x	y
0	0.59
15	0.59
15	1

cv (m^2/s) 1.642E-06

cv (cm^2/s) 0.0164176

190 kPa Load Step - Taylor Method

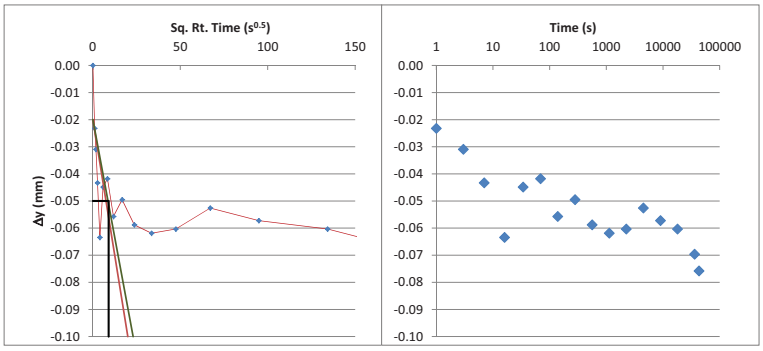

Initial Trend

x	y
0	-0.02
20	-0.1

t90 (s) 81

Offset

x	y
0	-0.02
23	-0.1

Hdr (m) 0.0202

90% Primary

x	y
0	-0.05
9	-0.05
9	-0.1

cv (m^2/s) 4.279E-06

cv (cm^2/s) 0.0427892

110 kPa Reload Step - Taylor Method

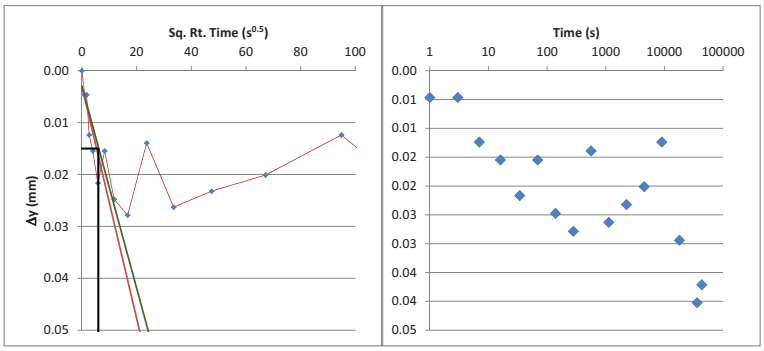

Initial Trend

x	y
0	0.003
30	0.07

t90 (s) 36

Offset

x	y
0	0.003
34.5	0.07

Hdr (m) 0.0205

cv (m^2/s) 9.914E-06

90% Primary

x	y
0	0.015
6	0.015
6	0.07

cv (cm^2/s) 0.0991404

190 kPa Reload Step - Taylor Method

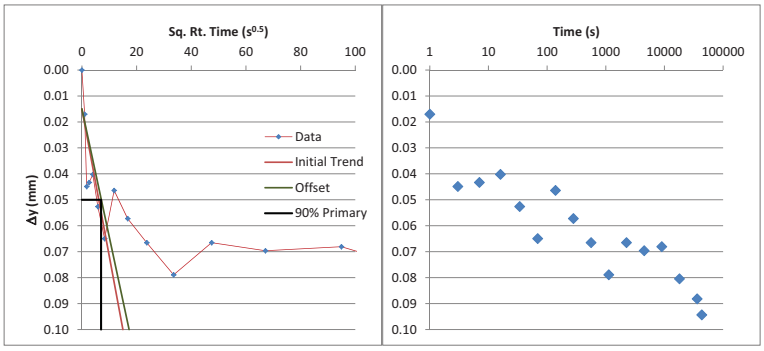

Initial Trend

x	y
0	0.015
15	0.1

t90 (s) 49

Offset

x	y
0	0.015
17.25	0.1

Hdr (m) 0.0204

cv (m^2/s) 7.218E-06

90% Primary

x	y
0	0.05
7	0.05
7	0.1

cv (cm^2/s) 0.0721801

350 kPa Load Step - Taylor Method

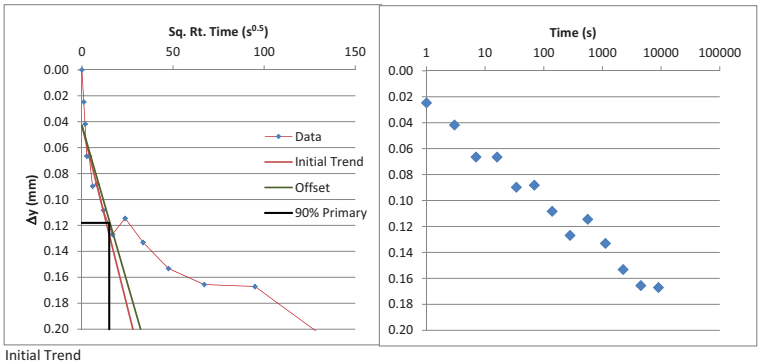

Initial Trend

x	y
0	0.043
28	0.2

Offset

x	y
0	0.043
32.2	0.2

90% Primary

x	y
0	0.118
15	0.118
15	0.2

t90 (s) 225

Hdr (m) 0.0202

cv (m^2/s) 1.543E-06

cv (cm^2/s) 0.0154253

670 kPa Load Step - Taylor Method

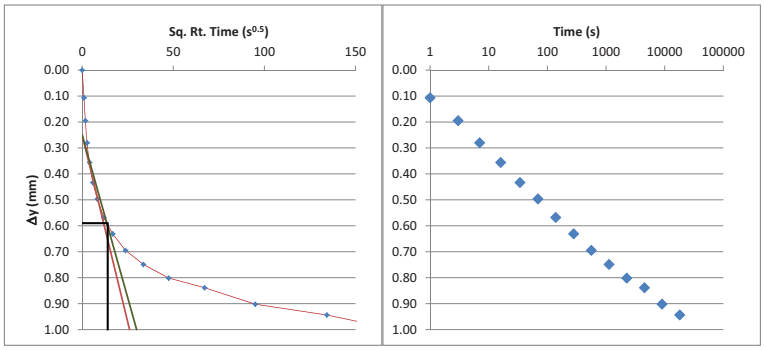

Initial Trend

x	y
0	0.25
26	1

Offset

x	y
0	0.25
29.9	1

90% Primary

x	y
0	0.59
14	0.59
14	1

t90 (s) 196

Hdr (m) 0.0194

cv (m^2/s) 1.634E-06

cv (cm^2/s) 0.0163427

1310 kPa Load Step - Taylor Method

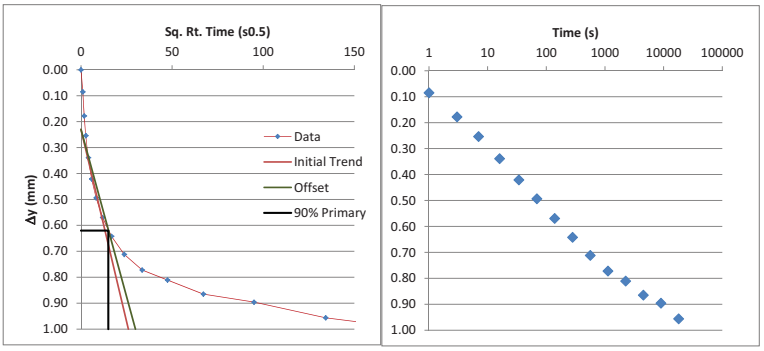

Initial Trend

x	y
0	0.23
26	1

t90 (s) 225

Offset

x	y
0	0.23
29.9	1

Hdr (m) 0.0181

90% Primary

x	y
0	0.62
15	0.62
15	1

cv (m^2/s) 1.236E-06

cv (cm^2/s) 0.0123559

2590 kPa Load Step - Taylor Method

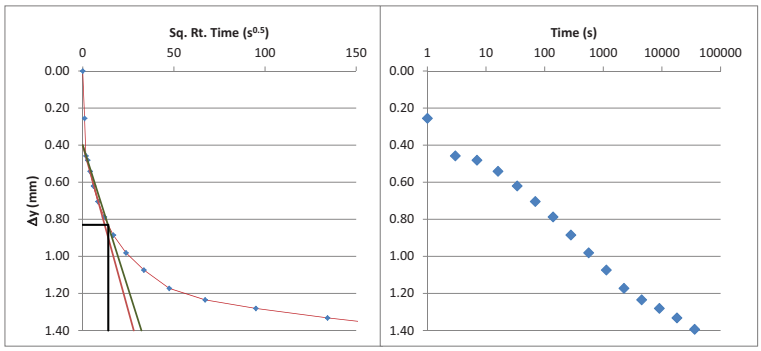

Initial Trend

x	y
0	0.4
28	1.4

t90 (s) 196

Offset

x	y
0	0.4
32.2	1.4

Hdr (m) 0.0165

90% Primary

x	y
0	0.83
14	0.83
14	1.4

cv (m^2/s) 1.171E-06

cv (cm^2/s) 0.0117088

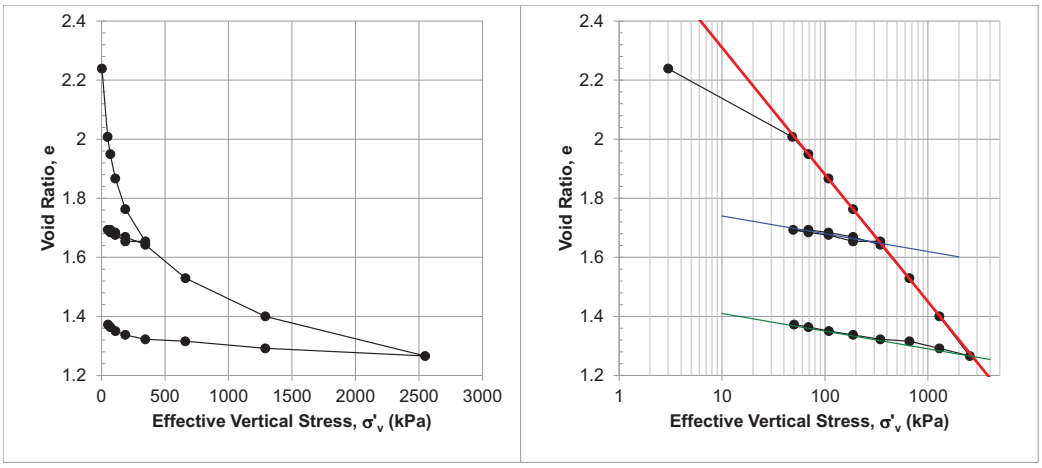

Boring: BH-4
Sample: Tube 9
Description: Firm light gray moist elastic SILT (MH) with sand sized shell fragments

OCR 1 Normally Consolidated

C_c 0.43
C_s 0.06
P_c' 58 kPa

Step	Load	$\Delta\gamma_0$	$\Delta\gamma_{12}$	D	Stress	H_0	ΔH	ε_a	e_0	Δe	e	c_v	Curve
	(kN)	(mm)	(mm)	(mm)	(kPa)	(mm)	(mm)					cm^2/s	Fitting
1	0.011	0.1272	0.1469	63.50	3	25.40	0.020	0.001	2.24	0.003	2.239		
2	0.153	0.1378	1.9562	63.50	48	25.40	1.829	0.072	2.24	0.233	2.008	0.011273	Good
3	0.218	1.9821	2.4154	63.50	69	25.40	2.288	0.090	2.24	0.292	1.949	0.002755	Fair
4	0.342	2.4382	3.0585	63.50	108	25.40	2.931	0.115	2.24	0.374	1.867	0.005612	Good
5	0.592	3.1117	3.875	63.50	187	25.40	3.748	0.148	2.24	0.478	1.763	0.012749	Good
6	1.091	3.9328	4.7295	63.50	344	25.40	4.602	0.181	2.24	0.587	1.654	0.014968	Good
7	0.592	4.699	4.7295	63.50	187	25.40	4.602	0.181	2.24	0.587	1.654	0.919946	Poor
8	0.342	4.62	4.5592	63.50	108	25.40	4.432	0.174	2.24	0.566	1.676	0.075185	Fair
9	0.218	4.5455	4.4923	63.50	69	25.40	4.365	0.172	2.24	0.557	1.684	0.103819	Fair
10	0.155	4.4755	4.4238	63.50	49	25.40	4.297	0.169	2.24	0.548	1.693	0.417867	Poor
11	0.217	4.4238	4.4238	63.50	69	25.40	4.297	0.169	2.24	0.548	1.693		Bad
12	0.343	4.4588	4.4938	63.50	108	25.40	4.367	0.172	2.24	0.557	1.684		Bad
13	0.592	4.5455	4.6124	63.50	187	25.40	4.485	0.177	2.24	0.572	1.669	0.03092	Poor
14	1.09	4.6717	4.8176	63.50	344	25.40	4.690	0.185	2.24	0.599	1.643	0.102411	Fair
15	2.089	4.921	5.7056	63.50	660	25.40	5.578	0.220	2.24	0.712	1.530	0.01786	Good
16	4.084	5.8196	6.7197	63.50	1290	25.40	6.593	0.260	2.24	0.841	1.400	0.021843	Good
17	8.074	6.8428	7.7703	63.50	2549	25.40	7.643	0.301	2.24	0.975	1.266	0.012487	Good
18	4.086	7.7308	7.5665	63.50	1290	25.40	7.439	0.293	2.24	0.949	1.292		
19	2.088	7.5392	7.3795	63.50	659	25.40	7.252	0.286	2.24	0.925	1.316		
20	1.09	7.3826	7.3263	63.50	344	25.40	7.199	0.283	2.24	0.919	1.323		
21	0.592	7.2716	7.2093	63.50	187	25.40	7.082	0.279	2.24	0.904	1.338		
22	0.344	7.1864	7.1089	63.50	109	25.40	6.982	0.275	2.24	0.891	1.350		
23	0.218	7.0755	7.0025	63.50	69	25.40	6.875	0.271	2.24	0.877	1.364		
24	0.157	6.9949	6.9371	63.50	50	25.40	6.810	0.268	2.24	0.869	1.372		
25	-0.001	6.8003	5.926	63.50	-0.3	25.40	5.799	0.228	2.24	0.740	1.501		

Averaged	
Virgin c_v	Recomp. c_v
cm^2/s	cm^2/s
0.015197	0.093805

50 kPa Load Increment - Taylor and Casagrande Methods

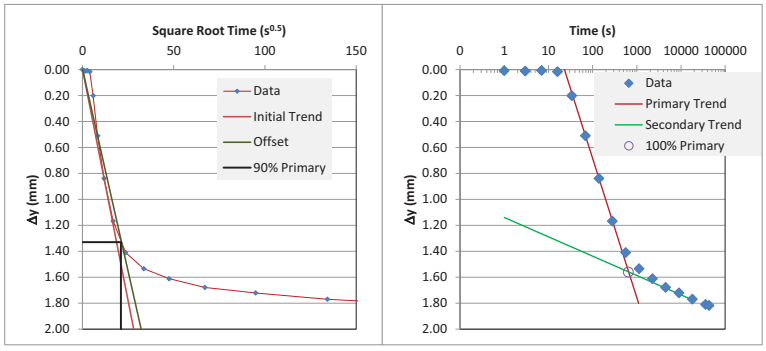

Initial Trend

x	y	
0	0	t90 (s)
28	2	441

Offset

x	y	Hdr (m)
0	0	0.024213
32.2	2	
		cv (m^2/s)

90% Primary

x	y	cv (cm^2/s)
0	1.33	0.011273
21	1.33	
21	2	

Secondary Trend

x	y	
1	1.14	t50 (s)
20000	1.78	100

Primary Trend

x	y	Hdr (m)
23	0	0.024869
1100	1.8	
		cv (m^2/s)
		1.22E-06

100% Primary

x	y	cv (cm^2/s)
640	1.56	0.012184

69 kPa Load Increment - Taylor Method

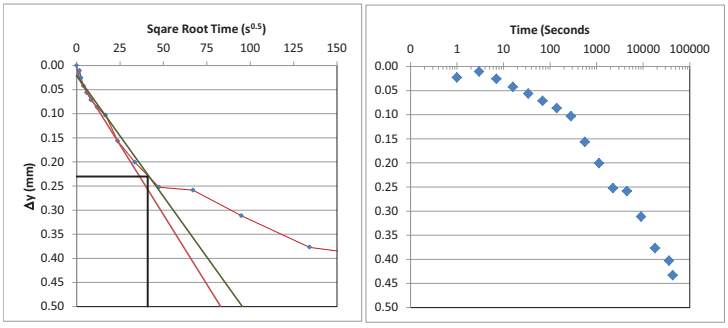

Initial Trend

x	y	
0	0.02	t90 (s)
83	0.5	1681

Offset

x	y	Hdr (m)
0	0.02	0.023370
95.45	0.5	
		cv (m^2/s)

90% Primary

x	y	cv (cm^2/s)
0	0.23	2.755E-07
41	0.23	
41	0.5	

110 kPa Load Increment - Taylor Method

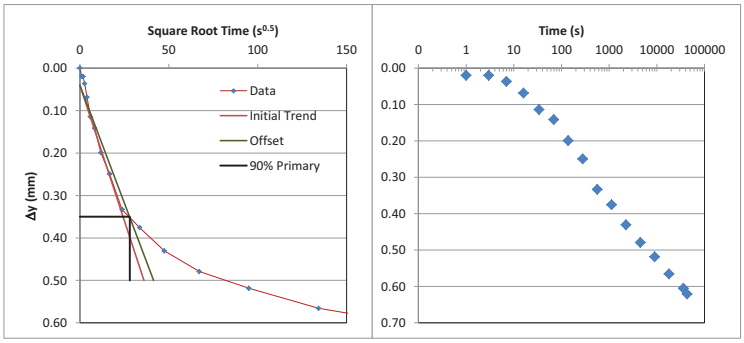

Initial Trend

x	y
0	0.04
36	0.5

Offset

x	y
0	0.04
41.4	0.5

90% Primary

x	y
0	0.35
28	0.35
28	0.5

t90 (s) 784

Hdr (m) 0.022779

cv (m^2/s) 5.612E-07

cv (cm^2/s) 0.0056123

190 kPa Load Increment - Taylor and Casagrande Method

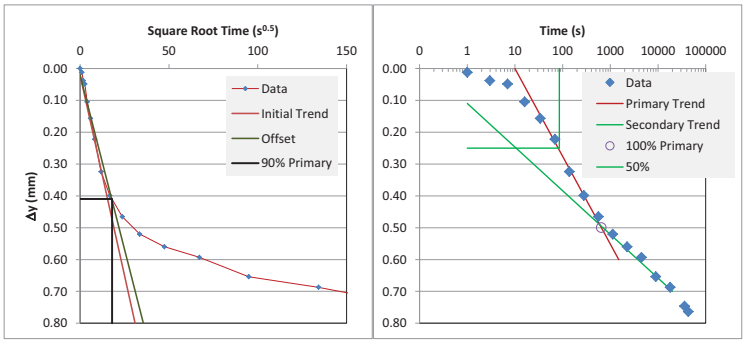

Initial Trend

x	y
0	0.02
31	0.8

Offset

x	y
0	0.02
35.65	0.8

90% Primary

x	y
0	0.41
18	0.41
18	0.8

t90 (s) 324

Hdr (m) 0.022070

cv (m^2/s) 1.275E-06

cv (cm^2/s) 0.0127488

Secondary Trend

x	y
1	0.11
20000	0.7

Primary Trend

x	y
10	0
1500	0.6

100% Primary

x	y
650	0.5

t50 (s) 85

Hdr (m) 0.022247

cv (m^2/s) 1.15E-06

cv (cm^2/s) 0.01147

350 kPa Load Increment - Taylor and Casagrande

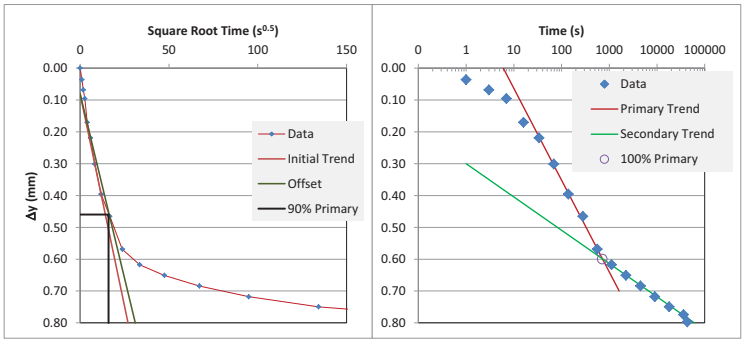

Initial Trend

x	y	
0	0.08	t90 (s)
27	0.8	256

Offset

x	y	Hdr (m)
0	0.08	0.021257
31.05	0.8	
		cv (m^2/s)

90% Primary

x	y	
0	0.46	cv (cm^2/s)
16	0.46	0.0149677
16	0.8	

Secondary Trend

x	y	
1	0.3	t50 (s)
60000	0.8	69

Primary Trend

x	y	Hdr (m)
6	0	0.021351
1600	0.7	
		cv (m^2/s)
		1.3E-06

100% Primary

x	y	cv (cm^2/s)
720	0.6	0.013015

190 kPa Unload Step - Taylor Method

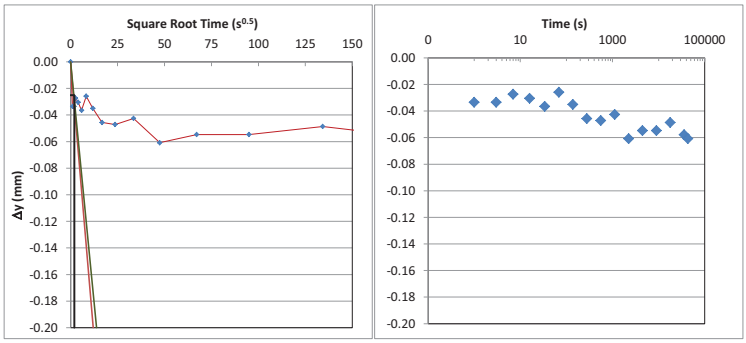

Initial Trend

x	y	
0	0	t90 (s)
12	-0.2	4

Offset

x	y	Hdr (m)
0	0	0.020831
13.8	-0.2	
		cv (m^2/s)

90% Primary

x	y	
0	-0.025	cv (cm^2/s)
2	-0.025	0.9199459
2	-0.2	

110 kPa Unload Step - Taylor Method

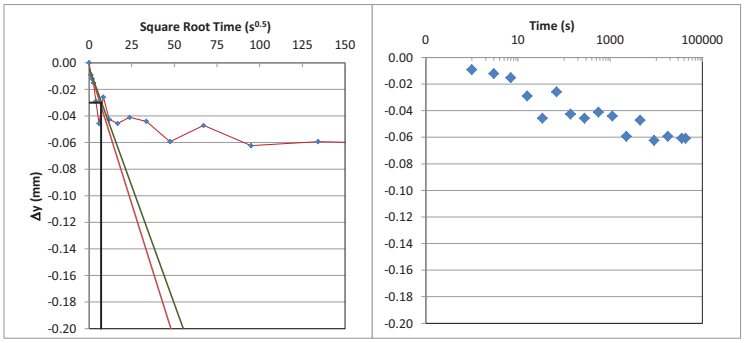

Initial Trend

x	y	
0	-0.004	t90 (s)
48	-0.2	49

Offset		Hdr (m)
x	y	0.020843
0	-0.004	
55.2	-0.2	
		cv (m^2/s)
90% Primary		7.519E-06
x	y	
0	-0.03	cv (cm^2/s)
7	-0.03	0.0751854
7	-0.2	

70 kPa Unload Step - Taylor Method

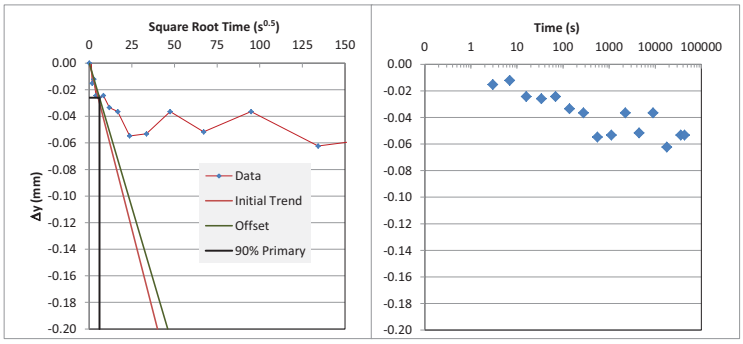

Initial Trend

x	y	
0	0	t90 (s)
40	-0.2	36

Offset		Hdr (m)
x	y	0.020994
0	0	
46	-0.2	
		cv (m^2/s)
90% Primary		1.038E-05
x	y	
0	-0.026	cv (cm^2/s)
6	-0.026	0.1038191
6	-0.2	

50 kPa Unload Step - Taylor

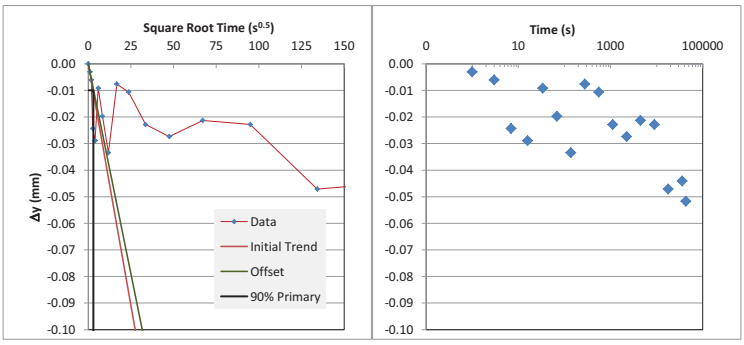

Initial Trend

x	y	
0	0	t90 (s)
55	-0.2	9

Offset		Hdr (m)
x	y	0.021059
0	0	
63.25	-0.2	
		cv (m^2/s)
90% Primary		4.179E-05
x	y	
0	-0.01	cv (cm^2/s)
3	-0.01	0.4178671
3	-0.2	

190 kPa Reload Step - Taylor Method

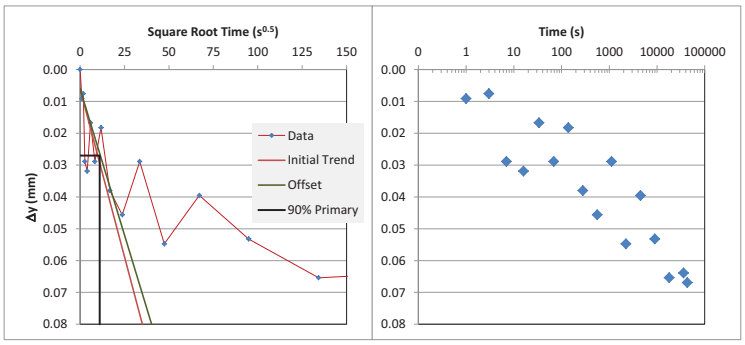

Initial Trend

x	y	
0	0.006	t90 (s)
35	0.08	121

Offset		Hdr (m)
x	y	0.021005
0	0.006	
40.25	0.08	
		cv (m^2/s)
90% Primary		3.092E-06
x	y	
0	0.027	cv (cm^2/s)
11	0.027	0.0309197
11	0.08	

350 kPa Reload Step - Taylor Method

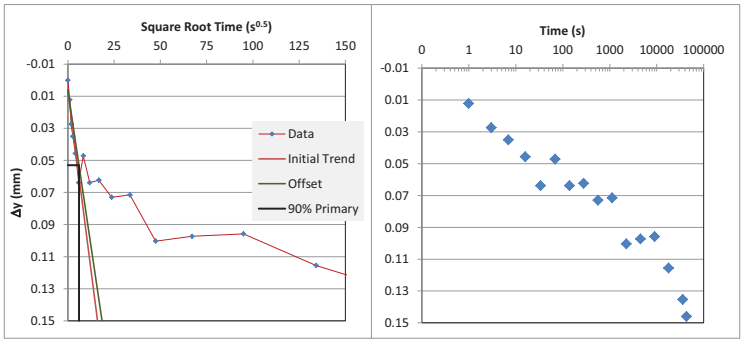

Initial Trend

x	y	
0	0.006	t90 (s)
16	0.15	36

Offset		Hdr (m)
x	y	0.020851
0	0.006	
18.4	0.15	
		cv (m^2/s)
90% Primary		1.024E-05
x	y	
0	0.053	cv (cm^2/s)
6	0.053	0.1024106
6	0.15	

670 kPa Load Step - Taylor Method

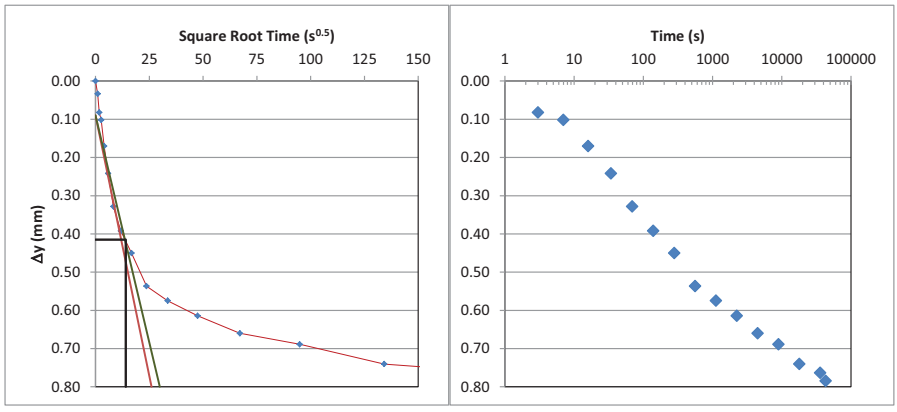

Initial Trend

x	y	
0	0.09	t90 (s)
26	0.8	196

Offset		Hdr (m)
x	y	0.020317
0	0.09	
29.9	0.8	

1310 kPa Load Step - Taylor and Casagrande Methods

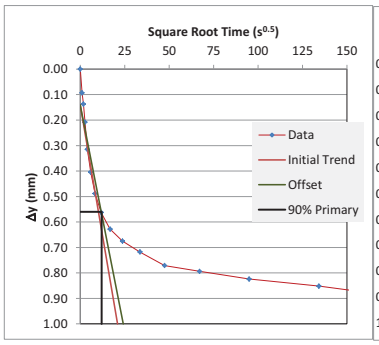

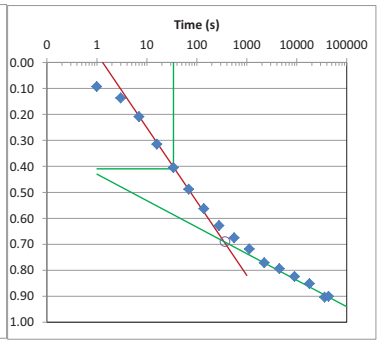

Initial Trend

x	y	
0	0.14	t90 (s)
21	1	144

Offset

x	y	Hdr (m)
0	0.14	0.019259
24.15	1	

	cv (m^2/s)
90% Primary	2.184E-06

x	y	cv (cm^2/s)
0	0.56	0.0218425
12	0.56	
12	1	

Secondary Trend

x	y	
1	0.43	t50 (s)
100000	0.94	34

Primary Trend

x	y	Hdr (m)
1.3	0	0.019417
1000	0.82	

	cv (m^2/s)
	2.18E-06

100% Primary

x	y	cv (cm^2/s)
370	0.69	0.021845

2590 kPa Load Step - Taylor and Casagrande Methods

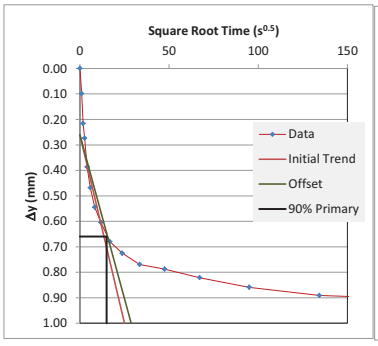

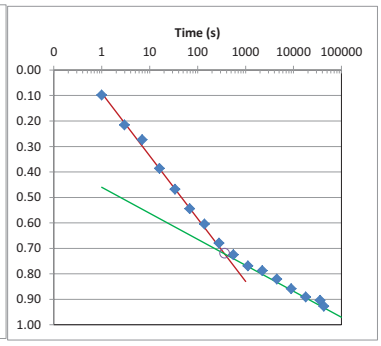

Initial Trend

x	y	
0	0.26	t90 (s)
25	1	225

Offset

x	y	Hdr (m)
0	0.26	0.018202
28.75	1	

	cv (m^2/s)
90% Primary	1.249E-06

x	y	cv (cm^2/s)
0	0.66	0.0124873
15	0.66	
15	1	

Secondary Trend

x	y	
1	0.46	t50 (s)
100000	0.97	12

Primary Trend

x	y	Hdr (m)
1	0.09	0.018534
1000	0.83	

	cv (m^2/s)
	5.64E-06

100% Primary

x	y	cv (cm^2/s)
370	0.72	0.056392

DOT-7

- Boring Log
- Laboratory Test Summary Table
- Atterberg Limits Results
- Grain Size Analysis Curves
- Oedometer Testing Results

College of Engineering
UNIVERSITY OF WISCONSIN-MADISON
Geological Engineering Program

Facility / Project Name DOT-7 WHRP 0092-10-10 CPT Project	Date (mm/dd/yy) Started 5/20/2011	Boring Number B(UW)-1
Boring Drilled by: Crew Chief & Firm Finn Hotstream & Dave Bohnoff	Date (mm/dd/yy) Finished 5/20/2011	Drilling Method Auger Boring
Final Static Water Level 1.27 m	Surface Elevation ` 925 feet NAVD 1929	Borehole Diameter 230 mm
State Wisconsin	County Dane	Civil Town / City / Village Middleton
		Drill Rig Gehl Skid Steer

Sample Number and Type	Sample Recovery (cm)	Sample Type	Depth (m)	Soil / Rock Description and Geologic Origin for Each Major Unit	USCS	Graphic Log	s_u (kPa) / ϕ'	water content	Liquid Limit	Plasticity Index	Fines Content	Dry Unit Weight	σ'_{vy} (kPa)	C_C
				Top Soil										
			0.25											
			0.50	Tan Moist Fine Grained Poorly Graded SAND (SP)										
			0.75											
AU-1	N/A	Auger	1.00					11.1			1.6			
			1.25	Reddish Tan to Gray Wet Sandy CLAY (CL)										
			1.50											
AU-2	N/A	Auger						23.8	30	15				
			1.75											
T-1	32	Tube		Dark Gray Firm Wet Lean CLAY (CL) with										
			2.00	Silt and Fine Sand Trace Roots				34.6	37	19	70			0.18
AU-3		Auger		- 0.02 m Gray Fine SAND (SP) lense				36.2			2.7			
T-2	0	Tube	2.25					23	39	21				
			2.50											
				- Hole Collapase										
T-3	16	Tube	2.75	Dark Gray Soft Wet Lean CLAY (CL) with										
				Silt and Some Fine Sand, Laminated Structure										
T-4	27	Tube	3.00						40	23				
			3.25					35.1						
								33.3	39	21	90	13.3	30	0.23
			3.50											
				Boring Terminated at 3.47 m depth										

ID	Depth (m)	Approx. σ'_{v0} (kPa)	Boring Desc.	USCS	Moisture Content (%)	Unit Weight (kN/m^3)	D_{50} (mm)	D_{10} (mm)	% Sand	% Fines	% Silt	% Clay	LL	PI	C_C	C_S	ε_a to σ'_{v0} (%)	σ'_{vy} (kPa)
AU-1	1	19.0	Tan SAND	SP	11		0.27	0.092	98.3	1.6	-	-						
AU-2	1.5	35.0	Rd/Br Sa. CLAY	CL	23.8													
AU-3	2.4	46.0	Grey CLAY	CL	34.6													
T-1	2.1	44.4	Fine SAND	SP	36.2		0.11	0.08	97.3	2.7			30	15				
T-1	2.2	44.9	Grey CLAY	CL	38.8	13.76	0.041	0.0047	29.8	70.3	59.9	10.4	37	19	0.19	0.02	4.6	130
T-1	2.3	45.5	Grey CLAY	CL	23								39	21				
T-3	3.15	50.0	Grey CLAY	CL									40	23				
T-4	3.4	51.4	Grey CLAY	CL	35.1	13.33	0.018	< 0.0013	10.4	89.6	65.8	23.8			0.22	0.01	1.3	43
T-4	3.45	51.6	Grey CLAY	CL	33.3								39	21				

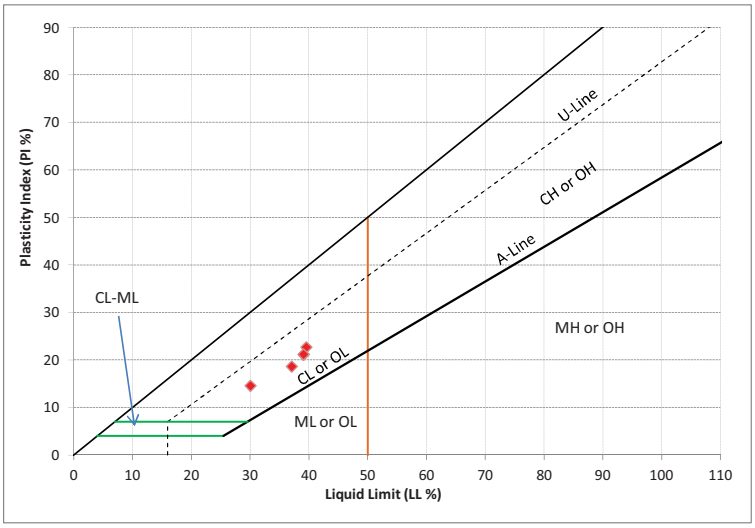

Boring	Sample	Depth	USCS	PL	LL	PI
B(UW)-1	AU-3	1	CL	16	30	15
B(UW)-1	T-1	2	CL	19	37	19
B(UW)-1	T-1	2.3	CL	18	39	21
B(UW)-1	T-3	3.15	CL	17	40	23
B(UW)-1	T-4	3.45	CL	18	39	21

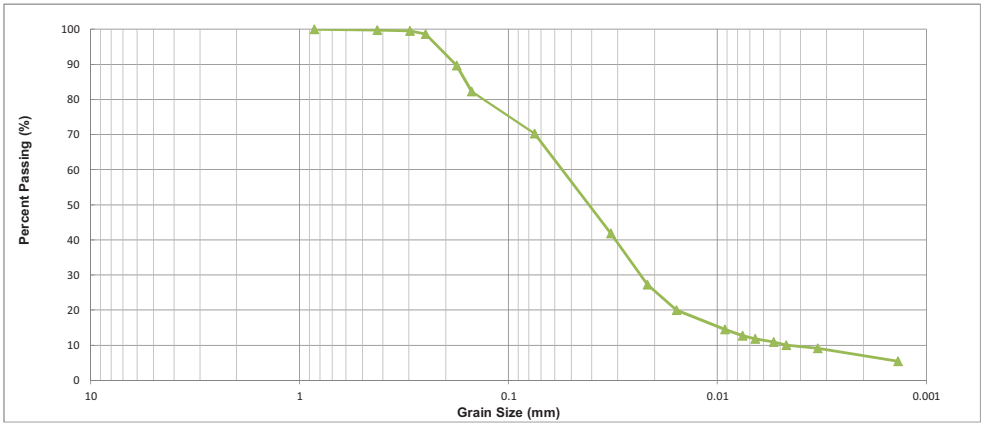

Boring: B(UW)-1 Sample: 2.2 m Description: Dark Gray Firm Moist Lean CLAY (CL) with Fine Sand and Silt Trace Rootlets

D_{10}	0.0047	mm
D_{30}	0.023	mm
D_{50}	0.041	mm
D_{60}	0.055	mm

C_c 7.0 C_u 39.5

USCS Grain Size Percentages

Gravel		Sand			Fines	70.3
Coarse	Fine	Coarse	Medium	Fine	Silt	Clay
0	0	0	0.2	29.6	59.9	10.4

Performed by: JNH Checked by:

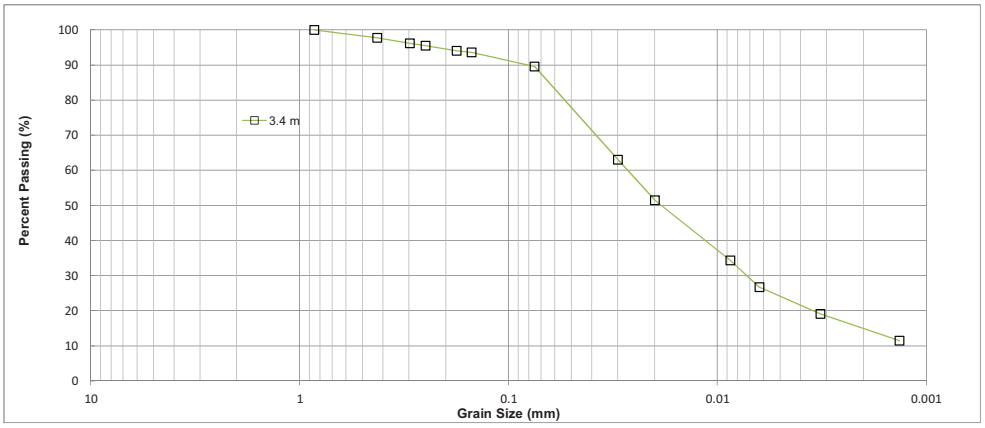

Boring: B(UW)-1 Sample: 3.42 m Description: Dark Gray Soft Moist Lean CLAY (CL) with Fine Sand and Silt Laminations

D_{10}	< 0.0013	mm
D_{30}	0.0075	mm
D_{50}	0.018	mm
D_{60}	0.027	mm

C_c 1.6 C_u 20.7

USCS Grain Size Percentages

Gravel		Sand			Fines	89.6
Coarse	Fine	Coarse	Medium	Fine	Silt	Clay
0	0	0	2.3	8.2	65.8	23.8

Performed by: JNH Checked by:

DOT-7 Oedometer Summary

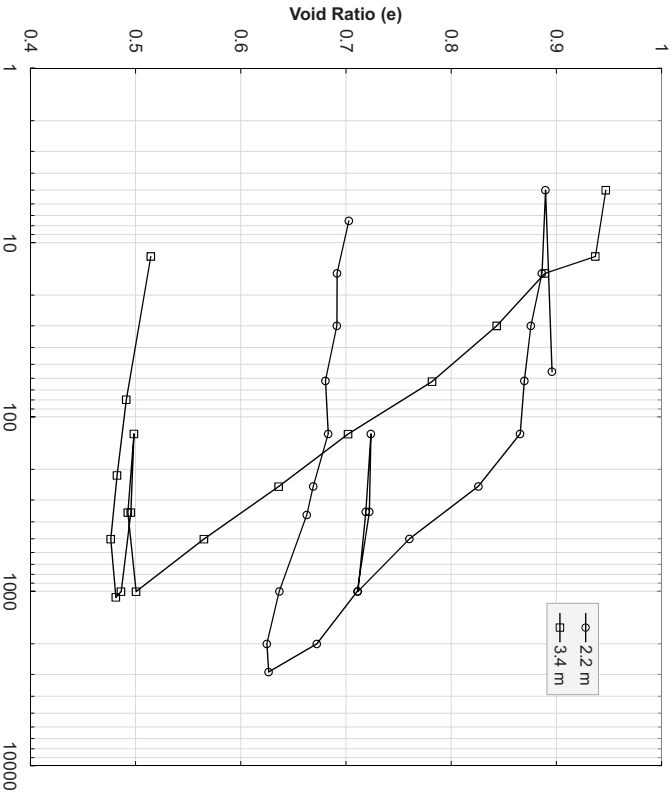

Depth: 2.2 m Tube-1
Firm Gray Lean CLAY (CL)

e_0	0.889		
σ'_{vo} (kPa)	33	σ_y' (kPa)	130
m_c (%)	38.8	C_c	0.19
γ_{dry} (kN/m^3)	13.76	C_r	0.02
Virgin Line c_v (cm^2/s)	0.05	OCR	3.9
Rebound c_v (cm^2/s)	0.76		

LL	37	% Sand	29.8
PL	19	% Silt	59.9
PI	18	% Clay	10.4

Depth: 3.4 m Tube-3
Soft Wet Lean CLAY (CL)

e_0	0.950		
σ'_{vo} (kPa)	43	σ_y' (kPa)	43
m_c (%)	35.1	C_c	0.22
γ_{dry} (kN/m^3)	13.33	C_r	0.01
Virgin Line c_v (cm^2/s)	0.002	OCR	1
Rebound c_v (cm^2/s)	0.010		

LL	39	% Sand	10.5
PL	18	% Silt	65.8
PI	21	% Clay	23.8

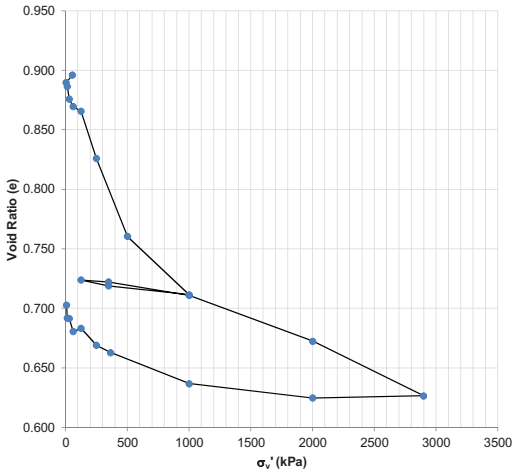

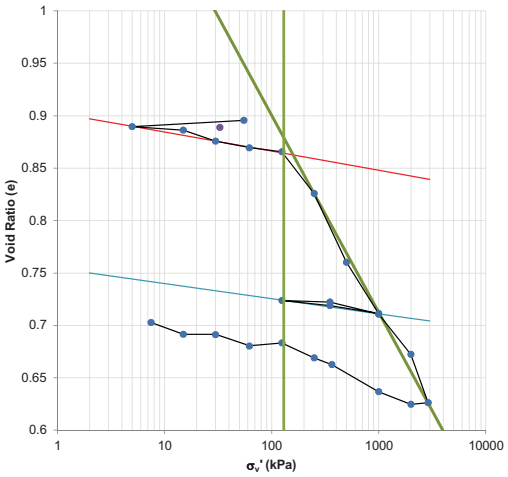

Site: DOT-7 Middleton Airport Road
Boring: B(UW)-1
Depth: 2.2 m

Description: Soft Dark Gray Moist Clay (CL) with silt and fine sand

LL:	37	PL:	19	PI:	18		
m_c	38.8	%		% Sand	29.8		
γ_{dry}	13.76	kN/m^3		% Silt	59.9		
σ_{vo}'	33	kPa		% Clay	10.4		
e_o	0.889						

σ_y'	130	kPa
C_c	0.188	
C_s	0.0163	

Step	Pressure (kPa)	H_o (m)	H_{100} (m)	H_f (m)	ΔH (m)	ε_a	e_0	e_{100}	e_f	Taylor c_v (cm^2/sec)	Casagrande c_v (cm^2/sec)	Quality on cv determination
1	55	0.025385	0.025476	0.02548	-9.1E-05	-0.35986606	0.889	0.896	0.896	-	-	
2	5	0.025385	0.025393	0.02539	-8.3E-06	-0.03271617	0.889	0.890	0.890			
3	15	0.025385	0.025349	0.02535	3.58E-05	0.140925744	0.889	0.886	0.886			
4	30	0.025385	0.025207	0.02521	0.000178	0.699598188	0.889	0.876	0.876			
5	62	0.025385	0.025124	0.02512	0.000261	1.029261375	0.889	0.870	0.870			
6	125	0.025385	0.025069	0.02492	0.000469	1.847134134	0.889	0.866	0.854	7.33E-02	1.04E+00	Poor
7	250	0.025385	0.024536	0.02422	0.001163	4.582588143	0.889	0.826	0.802	1.06E-01	9.24E-02	Good
8	500	0.025385	0.023657	0.02356	0.001827	7.197238527	0.889	0.760	0.753	5.57E-02	3.13E-02	Good
9	1000	0.025385	0.022998	0.02288	0.002509	9.882339965	0.889	0.711	0.702	3.37E-02	1.77E-02	Good
10	350	0.025385	0.023098	0.02310	0.00229	9.019184558	0.889	0.719	0.719	1.21E+00	6.99E-01	Poor
11	125	0.025385	0.023163	0.02323	0.002156	8.493236163	0.889	0.724	0.729	3.04E-01	6.20E-01	Poor
12	350	0.025385	0.023143	0.02314	0.002245	8.843029348	0.889	0.722	0.722	3.03E-03	9.62E-02	Poor
13	1000	0.025385	0.022991	0.02296	0.002428	9.565262951	0.889	0.711	0.708	4.67E-03	5.66E-02	Fair
14	2000	0.025385	0.022474	0.02231	0.003078	12.12704353	0.889	0.672	0.660	2.22E-02	2.41E-02	Good
15	2900	0.025385	0.021857	0.02180	0.003586	14.12512507	0.889	0.626	0.622	2.96E-03	2.39E-03	Fair
16	2000	0.025385	0.021834	0.02183	0.003551	13.9892338	0.889	0.625	0.625			
17	1000	0.025385	0.021994	0.02199	0.003391	13.35759701	0.889	0.637	0.637			
18	365	0.025385	0.022345	0.02234	0.00304	11.97604885	0.889	0.663	0.663			
19	250	0.555972	0.022429	0.02243	0.533544	95.96588407	0.889	0.669	0.669			
20	125	0.556377	0.022619	0.02262	0.533758	95.93460618	0.889	0.683	0.683			
21	62	0.557188	0.022583	0.02258	0.534604	95.94693761	0.889	0.680	0.680			
22	30	0.558819	0.022729	0.02273	0.53609	95.9325959	0.889	0.691	0.691			
23	15	0.562083	0.022732	0.02273	0.539351	95.95575964	0.889	0.692	0.692			
24	7.5	0.5686	0.022882	0.02288	0.545717	95.97570513	0.889	0.703	0.703			

Virgin Line cv (cm2/s)	Rebound cv (cm2/s)
0.048	0.757

Taylor - 1000 kPa Reload

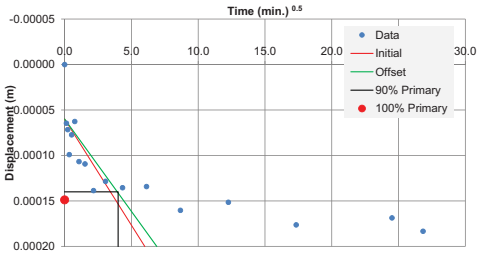

Taylor Construction

Initial						x	y
0	0.00006		Offset		90%	0	0.00014
6	0.0002		0	0.00006		4	0.00014
			6.9	0.0002		4	0.0002

ΔH_{90} (m)	0.023		
t_{90} (sec)	960		
	y	x	
ΔH_{100}	0.000149	0	
H_{100} (m)	0.022991		
c_v (m^2/s)	4.67E-07		
c_v (cm^2/s)	4.67E-03		

Casagrande - 1000 kPa Reload

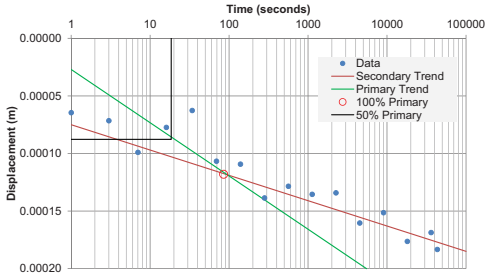

Casagrande Construction

							100% Consolidation		
Secondary Trend			Primary Trend			time	85	seconds
1	0.000075		1	0.000027		DH	0.000118	meters
100000	0.000185		5500	0.0002		Height	0.02302	
						e	0.713	

ΔH_0	1	0.00006	50% Line	
	3	0.00007	19	0
difference		0.00001	19	0.00009
ΔH_o		0.00006	0.001	0.00009
H_o		0.02308		
ΔH_{50}		0.00009		
t_{50} (sec)		19		
c_v (m^2/s)		5.66E-06		
c_v (cm^2/s)		5.66E-02		

Taylor - 1000 kPa

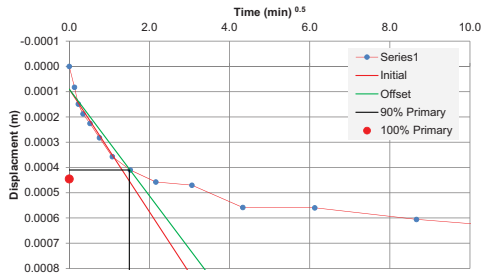

Taylor Construction

Initial						x	y
0	0.00009		Offset		90%	0	0.00041
3.75	0.001		0	0.00009		1.5	0.00041
			4.3125	0.001		1.5	0.001

ΔH_{90} (m)	0.023148		
t_{90} (sec)	135		
	y	x	
ΔH_{100}	0.000446	0	
H_{100} (m)	0.023112		
c_v (m^2/s)	3.37E-06		
c_v (cm^2/s)	3.37E-02		

Casagrande - 1000 kPa

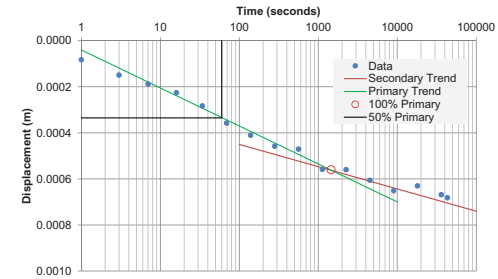

Casagrande Construction

							100% Consolidation		
Secondary Trend			Primary Trend			time	1450	seconds	
100	0.00045		1	0.00004		DH	0.00056	meters	
100000	0.00074		10000	0.0007		Height	0.02300		
						e	0.711		

ΔH_0	3	0.00015	50% Line	
	7	0.00019	60	0
difference		0.00004	60	0.00033
ΔH_o		0.00011	0.1	0.00033
H_o		0.02345		
ΔH_{50}		0.00033		
t_{50} (sec)		60		
c_v (m^2/s)		1.77E-06		
c_v (cm^2/s)		1.77E-02		

Taylor - 500 kPa

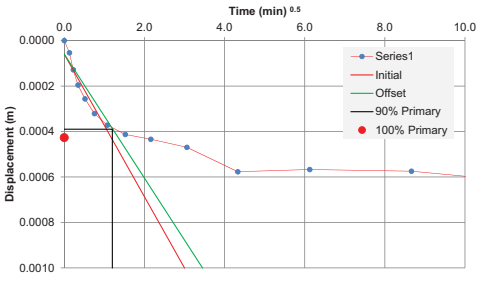

Taylor Construction

0	0.00006		0	0.00006	
3	0.001		3.45	0.001	
	x	y		ΔH_{90} (m)	0.023832
90%	0	0.00039		t_{90} (sec)	86.4
	1.2	0.00039		y	x
	1.2	0.001		ΔH_{100}	0.000427 0
				H_{100} (m)	0.023795

Casagrande - 500 kPa

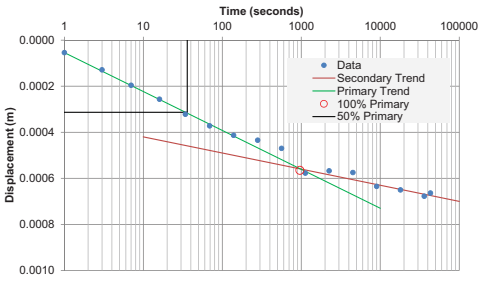

Casagrande Construction

Secondary Trend			Primary Trend		100% Consolidation		
10	0.00042		1	0.000054	time	960	seconds
100000	0.0007		10000	0.00073	DH	0.000565	meters
					Height	0.02366	
					e	0.760	
ΔH_0	3	0.00013			50% Line		
	7	0.00020			36	0	
	difference	0.00007			36	0.00031	
	ΔH_o	0.00006			0.1	0.00031	
	H_o	0.02416					
	ΔH_{50}	0.00031					
	t_{50} (sec)	36					
	c_v (m^2/s)	3.13E-06					
	c_v (cm^2/s)	3.13E-02					

Taylor - 250 kPa

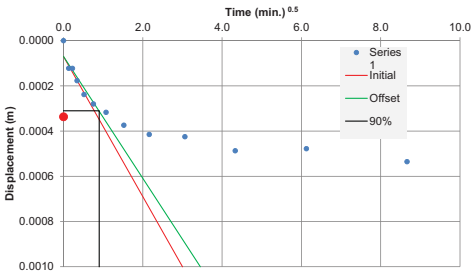

Taylor Construction

			Offset		
0	0.00007		0	0.00007	
3	0.001		3.45	0.001	
	x	y			
90%	0	0.00031		H_{100} (m)	0.024579
	0.9	0.00031			
	0.9	0.001		c_v (m^2/s)	1.06E-05
ΔH_{90} (m)	0.024606			c_v (cm^2/s)	1.06E-01
t_{90} (sec)	48.6				
	y	x			
ΔH_{100}	0.000337	0			

Casagrande - 250 kPa

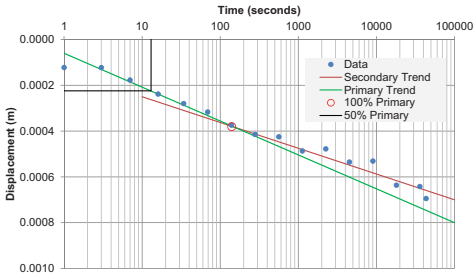

Casagrande Construction

Secondary Trend			Primary Trend		ΔH_0	3	0.00012
10	0.00025		1	0.00006		7	0.00018
100000	0.0007		100000	0.0008		difference	0.00005
						ΔH_o	0.00007
100% Consolidation						H_o	0.02485
time	140	seconds				ΔH_{50}	0.00022
DH	0.00038	meters				t_{50} (sec)	13
Height	0.02454				50% Line		
e	0.826				13	0	
					13	0.00022	
					0.1	0.00022	

	c_v (m^2/s)	9.24E-06
	c_v (cm^2/s)	9.24E-02

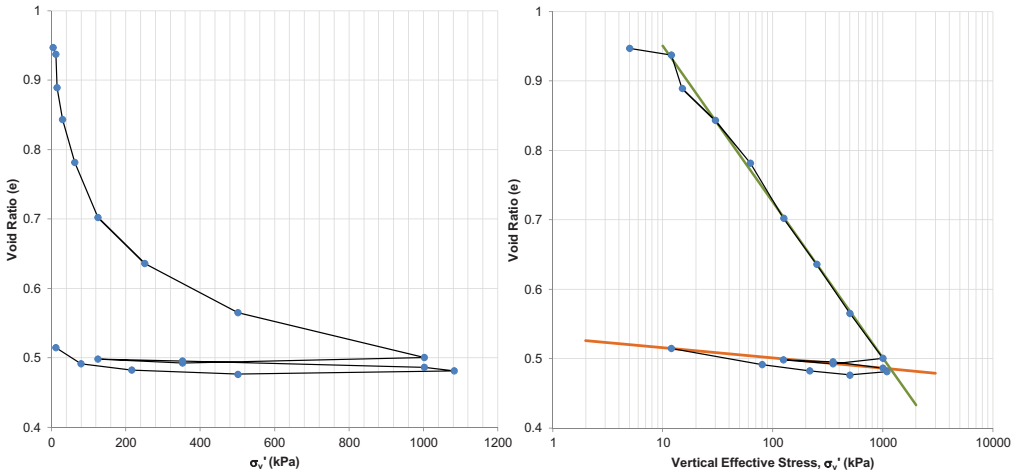

Site: DOT-7 Middleton Airport Road
Boring: B(UW)-1
Depth: 3.4 m

Description: Soft Dark Gray Moist Clay (CL) with silt and some fine sand / Laminations

LL: 39 PL: 18 PI: 21

σ_y' 37 kPa

m_c 35.1 %

γ_{dry} 13.33 kN/m^3

σ_{vo}' 43 kPa

e_o 0.950

% Sand 10.5
% Silt 65.8
% Clay 23.8

C_c 0.225

C_s 0.0147

Step	Pressure (kPa)	H_o (m)	H_{100} (m)	H_f (m)	ΔH (m)	ε_a	e_0	e_{100}	e_f	Taylor c_v (cm^2/sec)	Casagrande c_v (cm^2/sec)	Quality of cv
1	5	0.02538		0.02533	4.57E-05	0.180141844	0.950	0.947	0.947	-	-	
2	12	0.02538	0.025213	0.02505	0.000333	1.311032309	0.950	0.937	0.924	3.23E+01	-	Fair
3	15	0.02538	0.024588	0.02446	0.000925	3.6428684	0.950	0.889	0.879	2.18E+06	1.08E+06	Good
4	30	0.02538	0.02399	0.02387	0.001506	5.934672971	0.950	0.843	0.834	3.12E+04	1.12E+04	Good
5	62.7	0.02538	0.023189	0.02295	0.002428	9.567533491	0.950	0.782	0.763	1.09E-03	1.03E-03	Good
6	125.4	0.02538	0.022152	0.02199	0.003386	13.34050433	0.950	0.702	0.690	1.35E-03	8.48E-04	Good
7	250.8	0.02538	0.021294	0.02110	0.004285	16.88329393	0.950	0.636	0.621	1.53E-03	1.36E-03	Good
8	501.5	0.02538	0.020368	0.02017	0.005215	20.54617809	0.950	0.565	0.549	2.10E-03	1.62E-03	Good
9	1003	0.02538	0.01953	0.01936	0.006017	23.70866824	0.950	0.501	0.488	5.50E-03	1.76E-03	Good
10	353	0.02538	0.019427	0.01943	0.005949	23.43845548	0.950	0.493	0.493	8.96E-03	8.84E-03	Good
11	125	0.02538	0.019502	0.01954	0.005842	23.01812451	0.950	0.498	0.501	7.26E-03	8.12E-03	Good
12	353	0.02538	0.019465	0.01945	0.005926	23.34838455	0.950	0.496	0.495	1.15E-02	1.17E-02	Good
13	1003	0.02538	0.019343	0.01928	0.006096	24.01891253	0.950	0.486	0.482	1.15E-02	1.23E-02	Good
14	1082.8	0.02538	0.019279	0.01917	0.006205	24.44925138	0.950	0.481	0.473	1.62E-02	2.03E-02	Poor
15	501.5	0.02538	0.019216	0.01922	0.006159	24.26910954	0.950	0.476	0.477	1.89E-02	1.14E-02	Fair
16	216.6	0.02538	0.019294	0.01930	0.006078	23.94885737	0.950	0.482	0.483	8.97E-03	1.02E-02	Good
17	79.7	0.02538	0.019409	0.01943	0.005949	23.43845548	0.950	0.491	0.493	4.60E-03	4.62E-03	Fair
18	12	0.02538	0.019711	0.01993	0.005451	21.47691095	0.950	0.514	0.531	1.01E-03	3.25E-03	Fair

Virgin Line avg. c_v (cm^2/s)	Rebound avg. c_v (cm^2/s)
1.82E-03	9.81E-03

Taylor - 353 kPa Reload

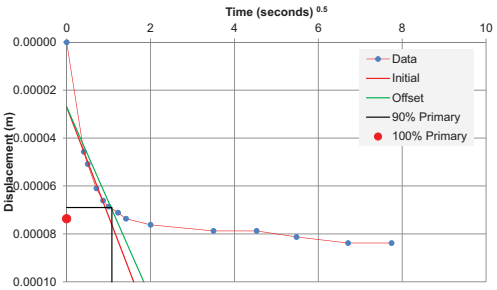

Taylor Construction

Initial		ΔH_{90} (m)	0.019469
0	0.000027	t_{90} (sec)	69.984
1.6	0.0001	y	x
		ΔH_{100}	7.367E-05	0
		H_{100} (m)	0.0194643
Offset			
0	0.000027	c_v (m^2/s)	1.15E-06
1.84	0.0001	c_v (cm^2/s)	1.15E-02

	x	y
90%	0	0.000069
	1.08	0.000069
	1.08	0.0001

Casagrande - 353 kPa Reload

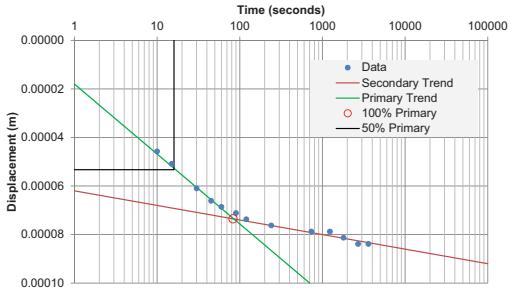

Casagrande Construction

Secondary Trend	
1	0.000062
100000	0.000092
Primary Trend	
1	1.8E-05
700	0.0001

100% Consolidation		
time	83	seconds
DH	7.35E-05	meters
Height	0.01946	
e	0.496	

50% Line

16	0
16	0.00005
0.001	0.00005
ΔH_0	15	0.00005
	60	0.00007
difference		0.00002
ΔH_o		0.00003
H_o		0.01950
ΔH_{50}		0.00005
t_{50} (sec)		16
c_v (m^2/s)		1.17E-06
c_v (cm^2/s)		1.17E-02

Taylor - 125.4 kPa

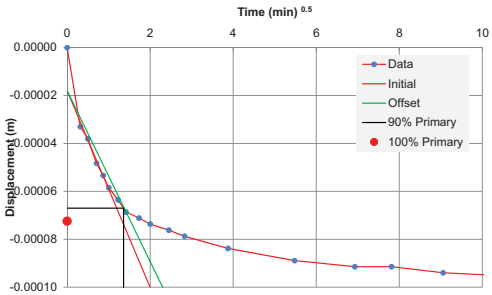

Taylor Construction

Initial		ΔH_{90} (m)	0.01949832
0	-1.8E-05	t_{90} (sec)	110.976
2	-0.0001	y	x
		ΔH_{100}	-7.244E-05	0
		H_{100} (m)	0.01950376
Offset			
0	-1.8E-05		
2.3	-0.0001	c_v (m^2/s)	7.26E-07
		c_v (cm^2/s)	7.26E-03

	x	y
90%	0	-6.7E-05
	1.36	-6.7E-05
	1.36	-0.0001

Casagrande - 125.4 kPa

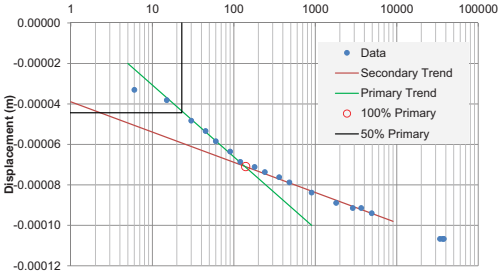

Casagrande Construction

Secondary Trend	
1	-3.9E-05
9000	-9.8E-05
Primary Trend	
5	-0.00002
900	-0.0001

100% Consolidation		
time	140	seconds
DH	-7.1E-05	meters
Height	0.01950	
e	0.498	

50% Line

23	0
23	-0.00004
0.1	-0.00004
ΔH_0	15	-0.00004
	60	-0.00006
difference		-0.00002
ΔH_o		-0.00002
H_o		0.01945
ΔH_{50}		-0.00004
t_{50} (sec)		23
c_v (m^2/s)		8.12E-07
c_v (cm^2/s)		8.12E-03

Taylor - 353 kPa

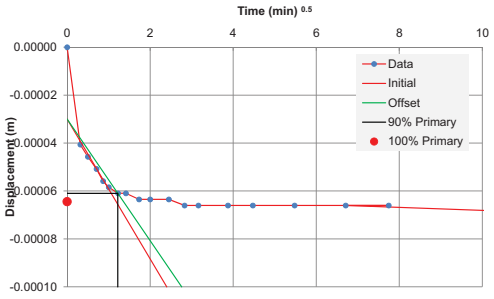

Taylor Construction

Initial

0	-0.00003
2.4	-0.0001

Offset

0	-0.00003
2.76	-0.0001

	x	y
90%	0	-6.1E-05
	1.22	-6.1E-05
	1.22	-0.0001

ΔH_{90} (m) 0.01942374

t_{90} (sec) 89.304

	y	x
ΔH_{100}	-6.444E-05	0

H_{100} (m) 0.01942718

c_v (m^2/s) 8.96E-07

c_v (cm^2/s) 8.96E-03

Casagrande - 353 kPa

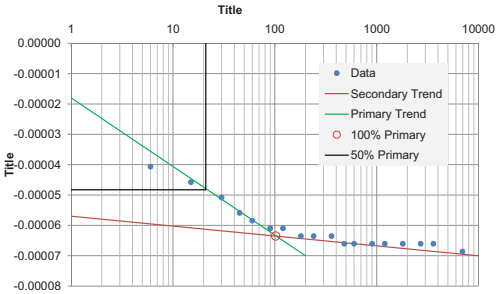

Casagrande Construction

Secondary Trend

1	-5.7E-05
10000	-0.00007

Primary Trend

1	-1.8E-05
200	-0.00007

100% Consolidation

time	102	seconds
DH	-6.4E-05	meters
Height	0.01943	
e	0.493	

50% Line

21	0
21	-0.00005
0.1	-0.00005

ΔH_0	15	-0.00005
	60	-0.00006
	difference	-0.00001
	ΔH_o	-0.00003
	H_o	0.01940
	ΔH_{50}	-0.00005
	t_{50} (sec)	21

c_v (m^2/s) 8.84E-07

c_v (cm^2/s) 8.84E-03

Taylor - 501.5 kPa

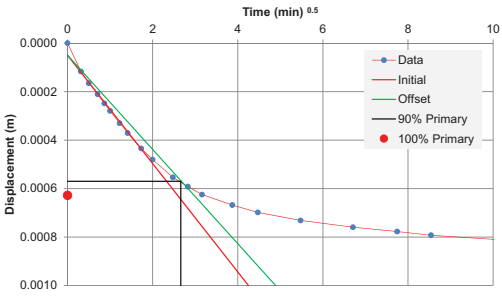

Taylor Construction

0	0.00005
4.25	0.001
0	0.00005
4.8875	0.001

	x	y
90%	0	0.00057
	2.66	0.00057
	2.66	0.001

ΔH_{90} (m) 0.020525

t_{90} (sec) 424.536

	y	x
ΔH_{100}	0.000628	0

H_{100} (m) 0.020467

c_v (m^2/s) 2.10E-07

c_v (cm^2/s) 2.10E-03

Casagrande - 501.5 kPa

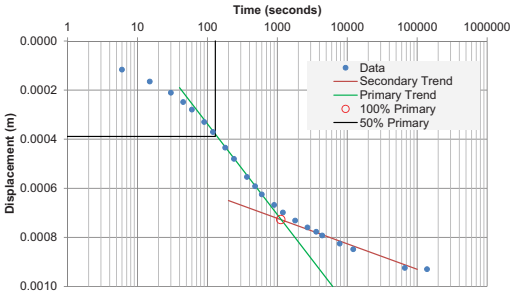

Casagrande Construction

Secondary Trend

200	0.00065
100000	0.00093

Primary Trend

40	0.00019
6200	0.001

100% Consolidation

time	1120	seconds
DH	0.000727	meters
Height	0.02037	
e	0.565	

50% Line

130	0
130	0.00039
0.1	0.00039

ΔH_0	15	0.00017
	60	0.00028
	difference	0.00011
	ΔH_o	0.00005
	H_o	0.02104
	ΔH_{50}	0.00039
	t_{50} (sec)	130

7042.254

c_v (m^2/s) 1.62E-07

c_v (cm^2/s) 1.62E-03

Taylor - 250.8 kPa

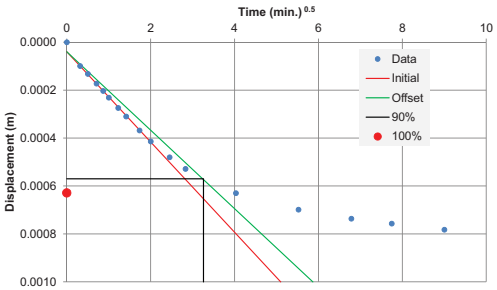

Taylor Construction

		ΔH_{90} (m)	0.021424	
0	0.00004	t_{90} (sec)	637.656	
5.1	0.001		y	x
		ΔH_{100}	0.000629	0
Offset		H_{100} (m)	0.021365	
0	0.00004			
5.865	0.001	c_v (m^2/s)		1.53E-07
		c_v (cm^2/s)		1.53E-03
	x	y		
90%	0	0.00057		
	3.26	0.00057		
	3.26	0.001		

Casagrande - 250.8 kPa

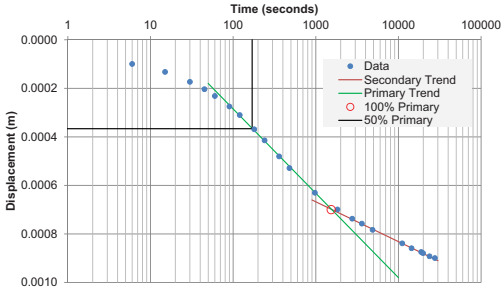

Casagrande Construction

Secondary Trend					
900	0.00066				
30000	0.00091				
Primary Trend					
50	0.00018				
10000	0.00098				
100% Consolidation					
time	1540	seconds			
DH	0.0007	meters			
Height	0.02129		7042.254		
e	0.636				

50% Line

0	0		
0	0.00000		
0.1	0.00000		
ΔH_0	15	0.00013	
	60	0.00023	
	difference	0.00010	
	ΔH_o	0.00003	
	H_o	0.02196	
	ΔH_{50}	0.00037	
	t_{50} (sec)	170	
	c_v (m^2/s)	1.36E-07	
	c_v (cm^2/s)	1.36E-03	

Taylor - 125.4 kPa

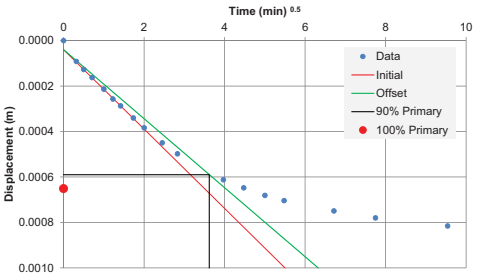

Taylor Construction

Initial				
0	0.00004	ΔH_{90} (m)	0.022362	
5.5	0.001	t_{90} (sec)	786.264	
		ΔH_{100}	0.000651	0
Offset				
0	0.00004	H_{100} (m)	0.022301	
6.325	0.001			
		c_v (m^2/s)		1.35E-07
		c_v (cm^2/s)		1.35E-03
90%	0	0.00059		
	3.62	0.00059		
	3.62	0.001		

Casagrande - 125.4 kPa

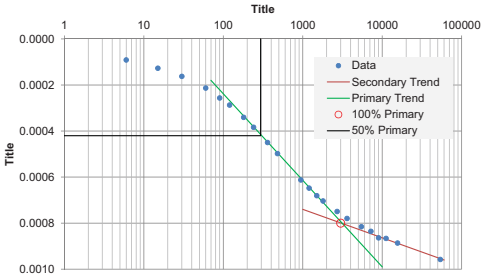

Casagrande Construction

Secondary Trend					
1000	0.00074				
60000	0.00096				
Primary Trend					
70	0.00018				
10000	0.00099				
100% Consolidation					
time	3000	seconds			
DH	0.0008	meters			
Height	0.02215				
e	0.702				

50% Line

295	0		
295	0.00042		
0.1	0.00042		
ΔH_0	15	0.00013	
	60	0.00021	
	difference	0.00009	
	ΔH_o	0.00004	
	H_o	0.02291	
	ΔH_{50}	0.00042	
	t_{50} (sec)	295	
	c_v (m^2/s)	8.48E-08	
	c_v (cm^2/s)	8.48E-04	

DOT-10c

- Boring Log
- Laboratory Test Summary Table
- Atterberg Limits Results
- Grain Size Analysis Curves
- Oedometer Testing Results

College of Engineering
UNIVERSITY OF WISCONSIN-MADISON
Geological Engineering Program

Facility / Project Name DOT-10c WHRP 0092-10-10 CPT Project	Date (mm/dd/yy) Started 5/24/2011	Boring Number B(UW)-1
Boring Drilled by: Crew Chief & Firm Finn Hotstream & Dave Bohnoff	Date (mm/dd/yy) Finished 5/24/2011	Drilling Method Auger Boring
Final Static Water Level 2.3 m	Surface Elevation `715 feet NGVD 1929	Borehole Diameter 230 mm
State Wisconsin	County Sheboygan	Civil Town / City / Village Sheboygan Falls
		Drill Rig Gehl Skid Steer

Sample Number and Type	Sample Recovery (cm)	Sample Type	Depth (m)	Soil / Rock Description and Geologic Origin for Each Major Unit	USCS	Graphic Log	s_u (kPa) / ϕ'	water content	Liquid Limit	Plasticity Index	Fines Content	Dry Unit Weight	σ'_{vy} (kPa)	C_C
				Topsoil										
B-1	N/A	AUGER	0.25	Red Tan and Gray Moist Fissured										
			0.50	Lean CLAY (CL) w/ Silt and Fine Sand										
			0.75											
			1.00											
B-2	N/A	AUGER	1.25											
T-3	30	TUBE			CL									
			1.50											
			1.75											
T-1	8	TUBE		- Gravel	CL									
B-3	N/A	AUGER	2.00					18.1	28	15	92.6	17.3		
			2.25											
				- Hole Collapse										
T-2	13	TUBE	2.50		CL			14.5	25	13	76			
			2.75	Terminated Boring at 2.54 m										
			3.00	Notes: Offset boring 1 m and augered down to 1.1 m to sample T-3										

ID	Depth (m)	Approx. σ'_{v0} (kPa)	Boring Desc.	USCS	Moisture Content (%)	Unit Weight (kN/m^3)	D_{50} (mm)	D_{10} (mm)	% Sands	% Fines	% Silt	% Clay	LL	PI	C_C	C_S	ε_S to σ'_{v0} (%)	σ'_{vy} (kPa)
B-1	0.25	5	Red/Tan CLAY	CL														
B-2	1.25	25	Red/Tan CLAY	CL														
T-3	1.3	26	Red/Tan CLAY	CL														
T-1	1.9	38	Red/Tan CLAY	CL	18.1	17.25	0.014	<0.0013	7.4	92.6	57.1	35.5	28	15	0.38	0.06	10.2	2150
T-1	2	40	Red/Tan CLAY	CL									32	15				
B-3	2.1	42	Red/Tan CLAY	CL			0.019	<0.0013	23.9	76	44.6	31.4						
T-2	2.3	46	Red/Tan CLAY	CL	14.5								25	13				

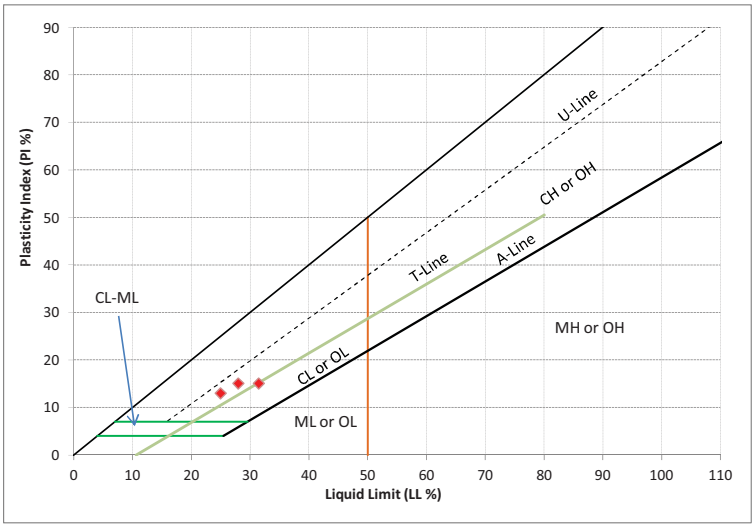

Boring	Sample	Depth	USCS	PL	LL	PI
B(UW)-1	Tube-2	2.29	CL	12	25	13
B(UW)-1	Tube-1	1.9	CL	13	28	15
Fall Cone	Tube-1	1.9	CL	17	32	15

*T-Line from Boulton and Paul (1976)

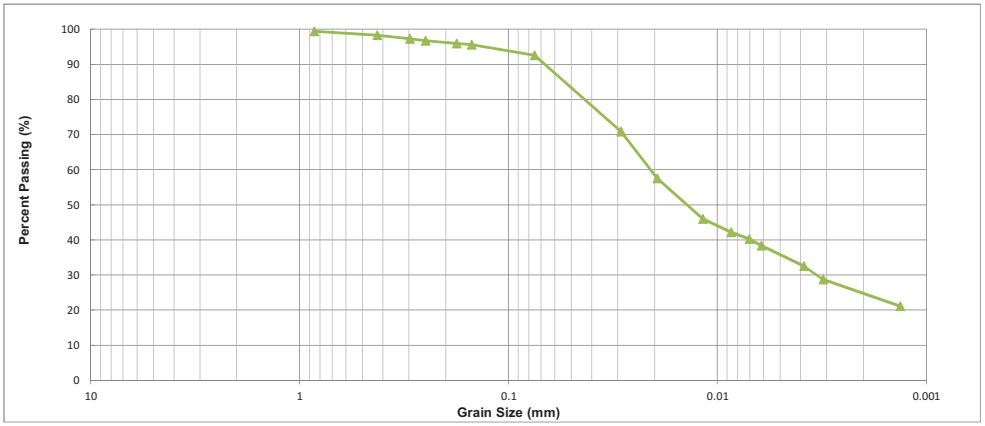

Boring: B(UW)-1 Sample: 1.8 m Description: Reddish Tan to Gray Very Stiff Slightly Moist Lean CLAY (CL) with Silt tr. F. Sand

D_{10}	< 0.0013	mm
D_{30}	0.0033	mm
D_{50}	0.014	mm
D_{60}	0.021	mm

C_c 0.4 C_u 16.1

USCS Grain Size Percentages

Gravel		Sand			Fines	92.6
Coarse	Fine	Coarse	Medium	Fine	Silt	Clay
0	0	0	1.7	5.7	57.1	35.5

7.4

Performed by: JNH Checked by:

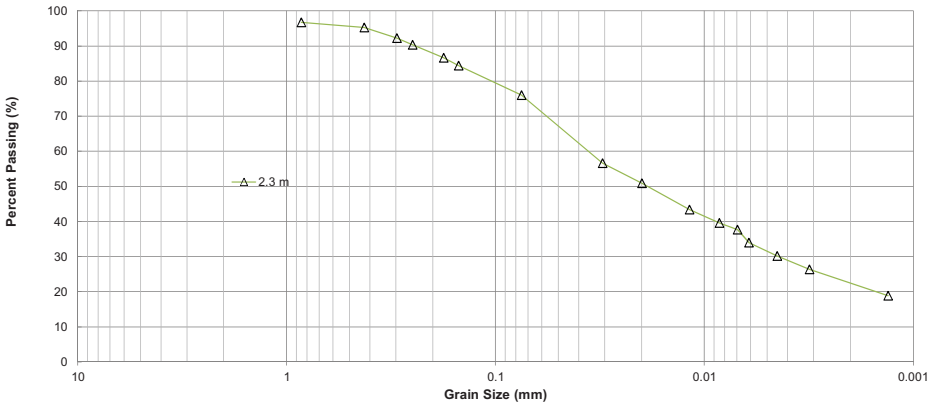

Boring: B(UW)-1 Sample: 2.3 m Description: Reddish Tan to Gray Very Stiff Slightly Moist Lean CLAY (CL) with Silt tr. F. Sand

D_{10}	< 0.0013	mm
D_{30}	0.0044	mm
D_{50}	0.019	mm
D_{60}	0.036	mm

C_c 0.4 C_u 27.6

USCS Grain Size Percentages

Gravel		Sand			Fines	76
Coarse	Fine	Coarse	Medium	Fine	Silt	Clay
0	0	1.9	2.8	19.2	44.6	31.4
			23.9			

Performed by: JNH Checked by:

Step	Pressure (kPa)	H_o (m)	H_{100} (m)	H_f (m)	DH (m)	e_a	e_0	e_{100}	e_f	Taylor c_v (cm^2/sec)	Casagrande c_v (cm^2/sec)	Quality
1	25	0.02672		0.02691957	-0.00020	-0.7	0.507	-1.00E+00	0.518			
2	25	0.02694	0.026938	0.02693757	0.00000	0.0	0.507	0.519	0.519			
3	60	0.02694	0.0268	0.02688278	0.00005	0.2	0.507	0.512	0.516			
4	125	0.02694	0.026849	0.02662364	0.00031	1.2	0.507	0.514	0.502	0.1898	0.0050	Poor
5	250	0.02694	0.026424	0.02612479	0.00081	3.0	0.507	0.490	0.473	0.0000	0.0049	Poor
6	500	0.02694	0.02581	0.02571079	0.00123	4.6	0.507	0.456	0.450	0.0047	0.0027	Good
7	1000	0.02694	0.025195	0.02496423	0.00197	7.3	0.507	0.421	0.408	0.0539	0.0109	Fair
8	2000	0.02694	0.024221	0.02418012	0.00276	10.2	0.507	0.366	0.364	0.0000	0.0236	Good
9	4000	0.02694	0.023246	0.02309937	0.00384	14.2	0.507	0.311	0.303	0.0059	0.0101	Good
10	1000	0.02694	0.02335	0.02338005	0.00356	13.2	0.507	0.317	0.319			
11	250	0.02694	0.023744	0.02375528	0.00318	11.8	0.507	0.339	0.340	8.24E-03	0.013114362	Fair
12	1	0.02694	0.02575	0.02818728	-0.00125	-4.6	0.507	0.452	0.590	1.83E-03		Bad
13	250	0.02694	0.023952	0.02387478	0.00306	11.4	0.507	0.351	0.347	3.60E-03	0.00332001	Poor
14	1000	0.02694	0.023083	0.02309055	0.00385	14.3	0.507	0.302	0.302	6.15E-06	0.006846673	Good
15	4000	0.02694	0.021999	0.02186045	0.00508	18.8	0.507	0.241	0.233	2.32E-05	0.015743017	Good
16	8000	0.02694	0.020843	0.02074574	0.00619	23.0	0.507	0.176	0.170	2.83E-05	0.012205062	Good
17	12000	0.02694	0.020017	0.02002824	0.00691	25.6	0.507	0.129	0.130	5.26E-06	0.00089663	Fair
18	8000	0.02694	0.02033	0.02033474	0.00660	24.5	0.507	0.147	0.147			
19	4000	0.02694	0.02065	0.02066474	0.00627	23.3	0.507	0.165	0.165			
20	1000	0.02694	0.02108	0.02121924	0.00572	21.2	0.507	0.189	0.197			
21	250	0.02694	0.02141	0.02172174	0.00522	19.4	0.507	0.208	0.225			
22	1	0.02694	0.0277	0.02846224	-0.00152	-5.7	0.507	0.562	0.605			
										Virgin Line Avg. c_v (cm^2/s)	Rebound Avg. c_v (cm^2/s)	
										1.92E-05	3.60E-03	

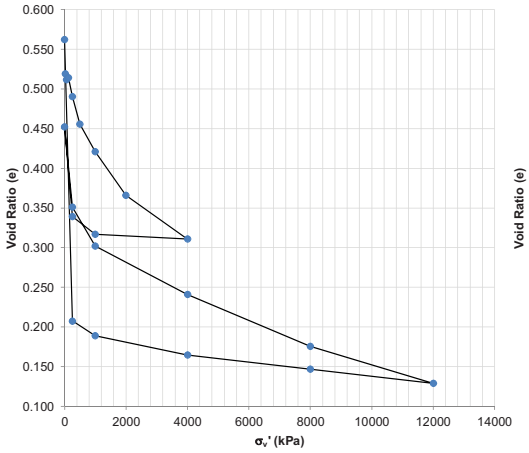

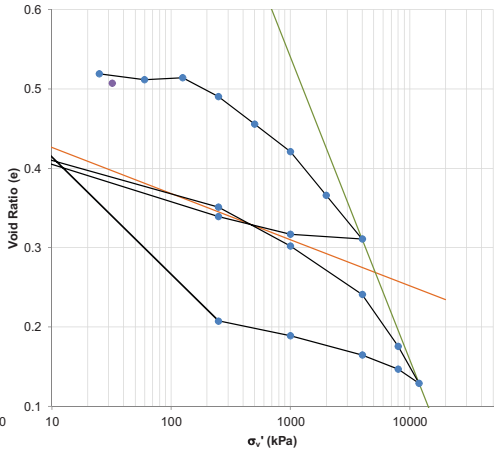

Site: DOT-10c STH-23 & STH-32 Sheboygan Falls, WI
Boring: B(UW)-1
Depth: 1.9

Description:

LL:	28	PL:	13	PI:	15

σ_y' 2150 kPa

m_c	18.1	%	% Sand
γ_{dry}	17.25	kN/m^3	% Silt
σ_{vo}'	32	kPa	% Clay
e_o	0.507		

C_c 0.381

C_s 0.0581

OCR 67

8000 kPa Load Step - Taylor and Casagrande Methods

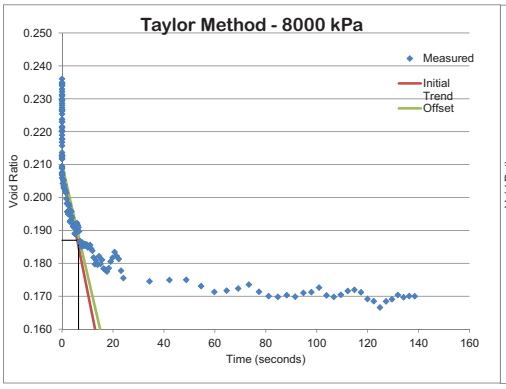

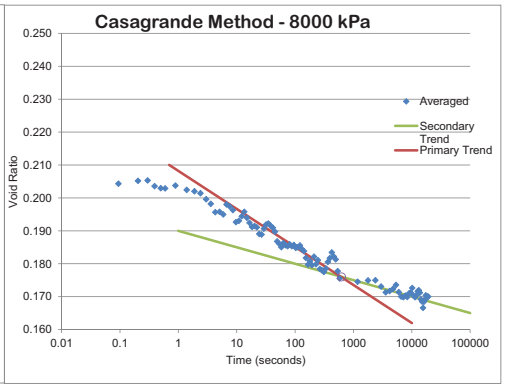

Initial Trend		Offset		t_{90} and e_{90}		c_v	Secondary Trend		Primary Trend		t_{100} (sec)	625	
0	0.21	0	0.21	0	0.187	2.83E-05	Time (sec)	e	Time (sec)	e	e_{100}	0.176	c_v
13	0.16	14.95	0.16	6.5	0.187	cm^2/sec	1	0.19	0.7	0.21	e_o	0.207	0.0122
				6.5	0.16		100000	0.165	10000	0.162	e_{50}	0.1915	cm^2/sec
											t_{50} (sec)	18	

4000 kPa Reload Step - Taylor and Casagrande Methods

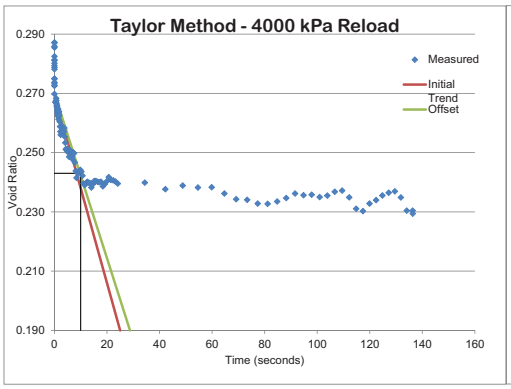

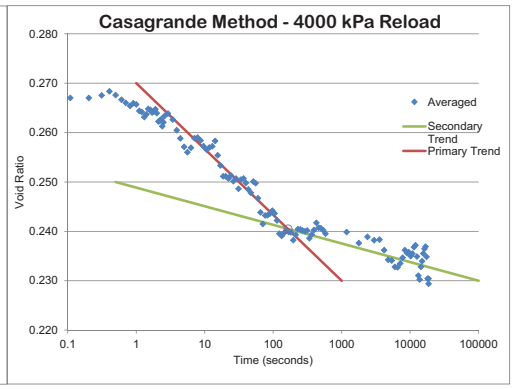

Initial Trend		Offset		t_{90} and e_{90}		c_v	Secondary Trend		Primary Trend		t_{100} (sec)	165	
0	0.27	0	0.27	0	0.243	2.32E-05	Time (sec)	e	Time (sec)	e	e_{100}	0.2405	c_v
25	0.19	28.75	0.19	10	0.243	cm^2/sec	0.5	0.25	1	0.27	e_o	0.273	0.0157
				10	0.19		100000	0.23	1000	0.23	e_{50}	0.25675	cm^2/sec
											t_{50} (sec)	15.5	

1000 kPa Reload Step - Taylor and Casagrande Methods

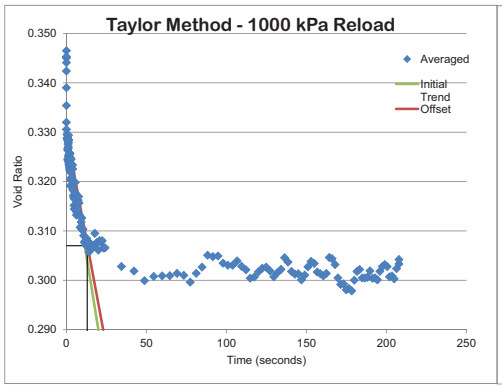

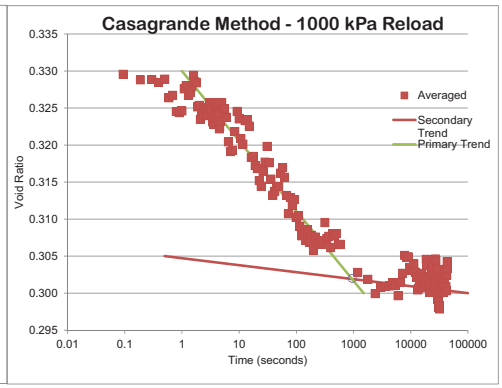

Initial Trend		Offset		t_{90} and e_{90}		c_v	Secondary Trend		Primary Trend		t_{100} (sec)	950	
0	0.33	0	0.33	0	0.307	6.15E-06	Time (sec)	e	Time (sec)	e	e_{100}	0.302	c_v
20	0.29	23	0.29	13	0.307	cm^2/sec	0.5	0.305	1	0.33	e_o	0.324	0.0068
				13	0.25		100000	0.3	1500	0.3	e_{50}	0.313	cm^2/sec
											t_{50} (sec)	39	

250 kPa Reload Step - Taylor and Casagrande Methods

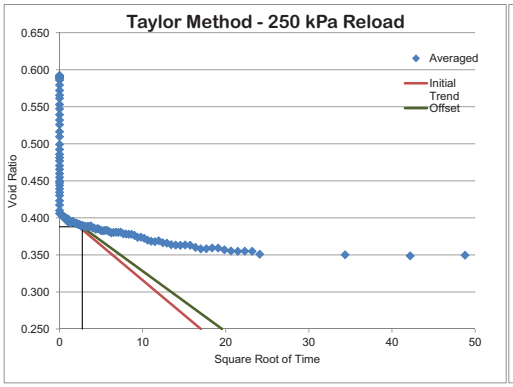

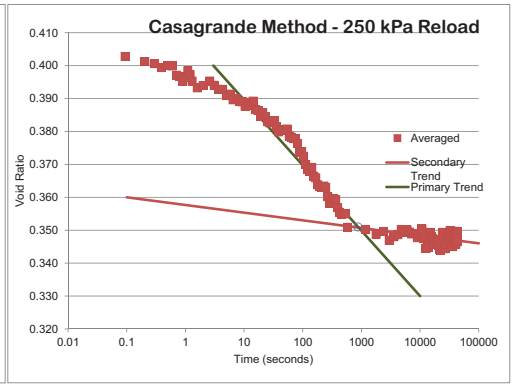

Initial Trend		Offset		t_{90} and e_{90}		c_v	Secondary Trend		Primary Trend		t_{100} (sec)	870	
0	0.41	0	0.41	0	0.388	3.60E-03	Time (sec)	e	Time (sec)	e	e_{100}	0.351	c_v
17	0.25	19.55	0.25	2.75	0.388	cm^2/sec	0.1	0.36	3	0.4	e_o	0.399	0.0033
				2.75	0.25		100000	0.346	10000	0.33	e_{50}	0.375	cm^2/sec
											t_{50} (sec)	88	

250 kPa Unload Step - Taylor and Casagrande Methods

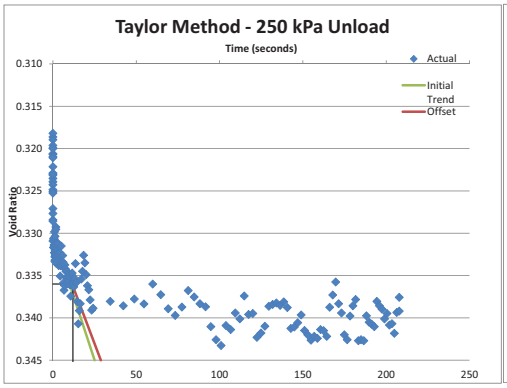

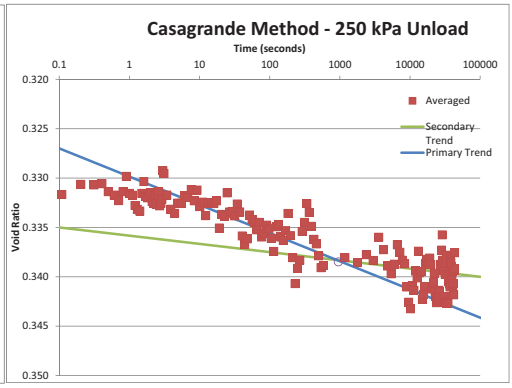

Initial Trend		Offset		t_{90} and e_{90}		c_v	Secondary Trend		Primary Trend		t_{100} (sec)	950	
0	0.33	0	0.33	0	0.336	8.24E-03	Time (sec)	e	Time (sec)	e	e_{100}	0.3385	c_v
25	0.345	28.75	0.345	12	0.336	cm^2/sec	0.1	0.335	0.1	0.327	e_o	0.33	0.0131
				12	0.35		100000	0.34	200000	0.345	e_{50}	0.33425	cm^2/sec
											t_{50} (sec)	21	

4000 kPa Load Step - Taylor and Casagrande Methods

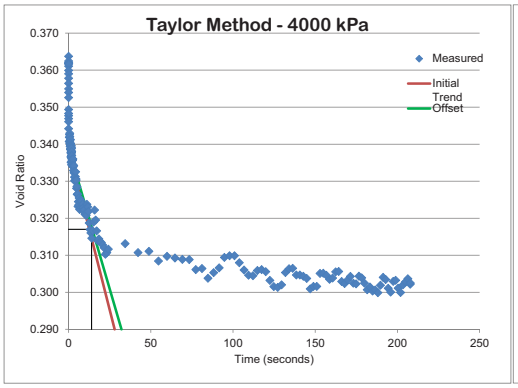

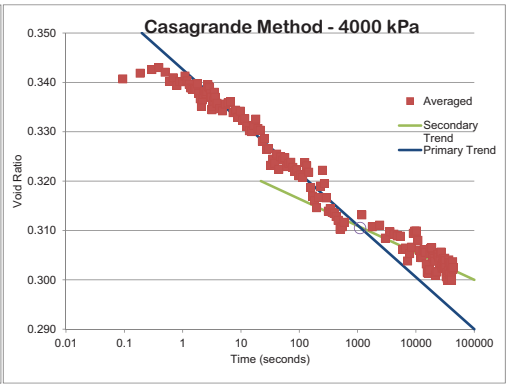

Initial Trend		Offset		t_{90} and e_{90}		c_v	Secondary Trend		Primary Trend		t_{100} (sec)	1100	
0	0.339	0	0.339	0	0.317	0.00588	Time (sec)	e	Time (sec)	e	e_{100}	0.3105	c_v
28	0.29	32.2	0.29	14	0.317	cm^2/sec	22	0.32	0.2	0.35	e_o	0.343	0.0101
				14	0.29		100000	0.3	100000	0.29	e_{50}	0.32675	cm^2/sec
											t_{50} (sec)	27	

2000 kPa Load Step - Taylor and Casagrande Methods

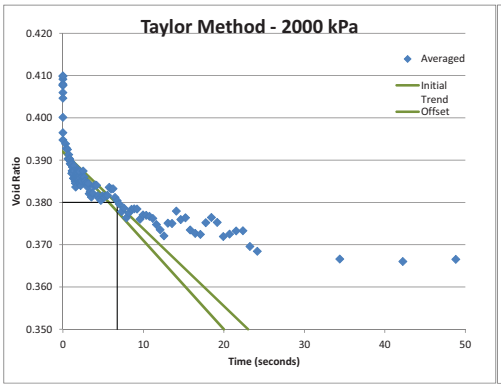

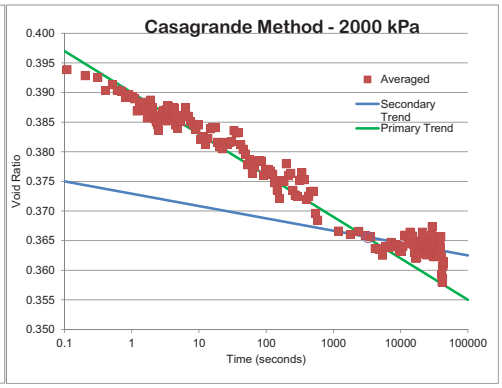

Initial Trend		Offset		t_{90} and e_{90}		c_v	Secondary		Primary		t_{100} (sec)	3300	
0	0.392	0	0.392	0	0.38	0.00001	Time (sec)	e	Time (sec)	e	e_{100}	0.3655	c_v
20	0.35	23	0.35	6.75	0.38	cm^2/sec	0.1	0.375	0.1	0.397	e_o	0.396	0.0236
				6.75	0.35		100000	0.3625	100000	0.355	e_{50}	0.38075	cm^2/sec
											t_{50} (sec)	12.5	

1000 kPa Load Step - Taylor Method

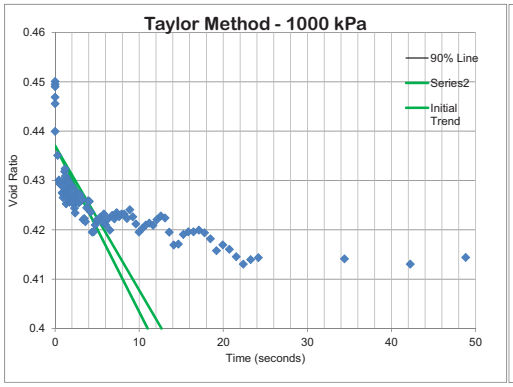

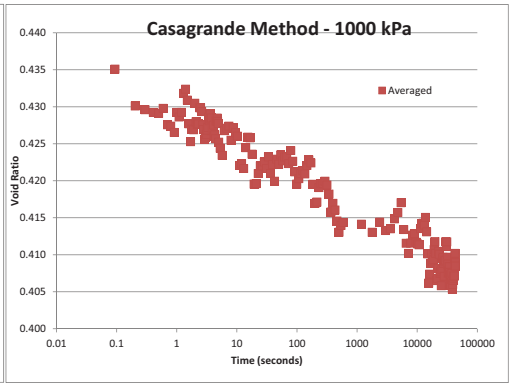

Initial Trend		90% Line		t_{90} and e_{90}		c_v
0	0.437	0	0.437	0	0.423	0.05395
11	0.4	12.65	0.4	5	0.423	cm^2/sec

500 kPa Load Step - Taylor and Casagrande Methods

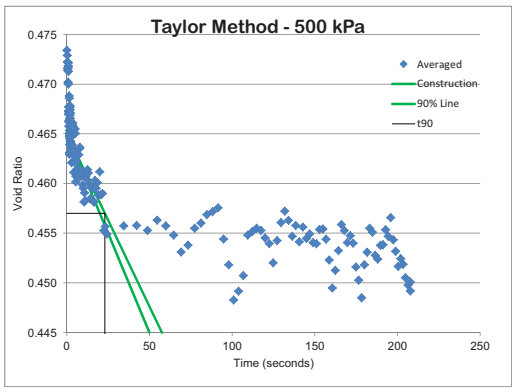

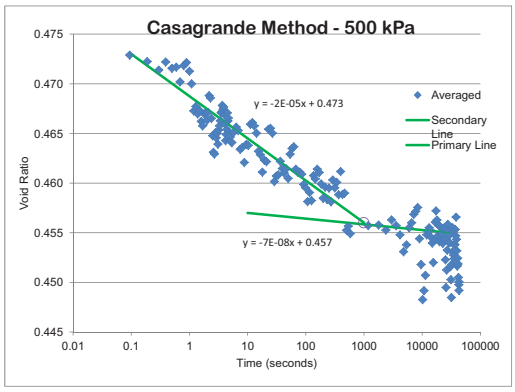

Initial		Offset		t_{90} (sec)			Secondary		Primary		t_{100} (sec)	1000	
0	0.465	0	0.465	0	0.457	c_v	Time (sec)	e	Time (sec)	e	e_{100}	0.456	c_v
50	0.445	57.5	0.445	23	0.457	0.0027	30000	0.455	1000	0.456	e_o	0.468	0.0047
				23	0	cm^2/sec	10	0.457	0.1	0.473	e_{50}	0.462	cm^2/sec
											t_{50} (sec)	70	

Appendix 5

CPT calibration and pre-post test zero readings

VERTEK

250 Beanville Road
Randolph, Vt. 05060
802-728-4588
800-639-6315

Digital Cone Penetrometer Calibration

Cone Serial Number	DSG0440	
Customer	UNIV. OF WISCONSIN-M	
Reference Load Cell	INTERFACE 1120AF-25K S/N	127965A
Reference Press. Gauge	DRESSER D XD 1000PSIG S/N	3432

TIP

Full range V	1.7849
Baseline V	0.00794
Full Scale Force	100000 KPA
Output Units	KPA
Unit Conv. Factor	1

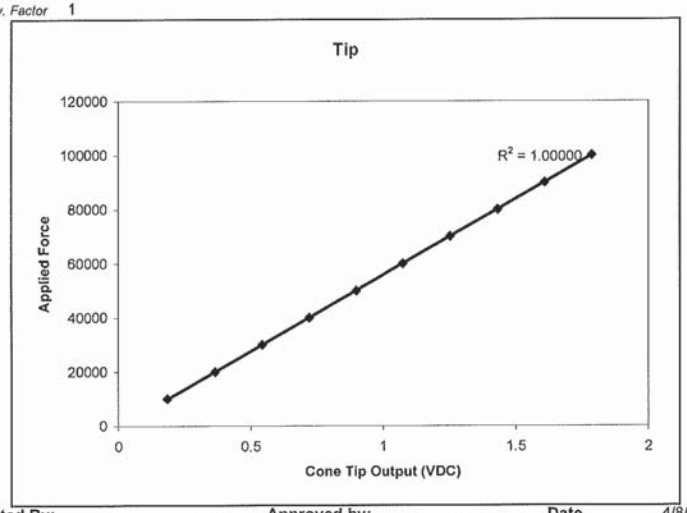

Calibrated By: PCB Signed: Paul C. Birdsong **Approved by:** R HULL Signed: Ron Hull **Date** 4/8/2010

VERTEK

250 Beanville Road
Randolph, Vt. 05060
802-728-4588
800-639-6315

Digital Cone Penetrometer Calibration

Cone Serial Number	DSG0440	
Customer	UNIV. OF WISCONSIN-M	
Reference Load Cell	INTERFACE 1120AF-25K S/N	127965A
Reference Press. Gauge	DRESSER D XD 1000PSIG S/N	3432

FRICTION

Full range V	2.6536
Baseline V	-0.3114
Full Scale Force	1000 KPA
Output Units	KPA
Unit Conv. Factor	1

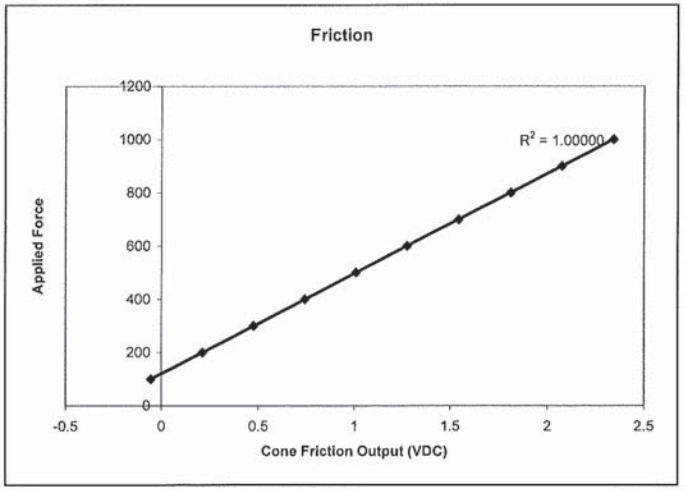

Calibrated By: PCB Signed: Paul Birdsong **Approved by:** R HULL Signed: Ron Hull **Date** 4/8/2010

					Output			Units			Percent Shift		
Site	Sounding	Date	Operator	Baseline	TIP	FRICTION	u_2	TIP (MPa)	FRICTION (kPa)	u_2 (kPa)	TIP	FRICTION	u_2
10-002	SCPTU2-01	7/20/2010	James S.	Initial	0.00648	-0.32189	-0.12335	0.363	-121.303	-207.439	11.07	4.02	0.96
				Final	0.0058	-0.30919	-0.12217	0.325	-116.517	-205.454			
10-002	SCPTU2-02	7/21/2010	James S.	Initial	0.00675	-0.32148	-0.12486	0.378	-121.149	-209.978	0.00	3.23	3.94
				Final	0.00675	-0.31127	-0.12004	0.378	-117.301	-201.872			
10-002	CPTU2-03	7/21/2010	James S.	Initial	0.00695	-0.32118	-0.12473	0.389	-121.036	-209.759	26.38	4.27	7.18
				Final	0.00533	-0.30775	-0.11608	0.299	-115.975	-195.213			
10-002	CPTU2-04	7/25/2010	James S.	Initial	0.00906	-0.31375	-0.12556	0.508	-118.236	-211.155	-4.95	1.30	2.96
				Final	0.00952	-0.30971	-0.1219	0.533	-116.713	-205.000			
10-002	CPTU1-05	7/25/2010	Finn H.	Initial	0.00843	-0.29433	-0.12527	0.472	-110.917	-210.667	-10.56	-6.01	-1.34
				Final	0.00937	-0.31258	-0.12696	0.525	-117.795	-213.510			
10-003	CPTU2-03	10/5/2010	Finn H.	Initial	0.00857	-0.31136	-0.12433	0.480	-117.335	-209.087	17.93	1.95	3.39
				Final	0.00716	-0.30535	-0.12018	0.401	-115.070	-202.108			
10-004	SCPTU2-04	10/10/2010	Finn H.	Initial	0.0092	-0.30856	-0.12538	0.515	-116.280	-210.852	0.54	1.09	1.04
				Final	0.00915	-0.30521	-0.12408	0.513	-115.017	-208.666			
10-005	SCPTU2-05	10/13/2010	Finn H.	Initial	0.009	-0.30425	-0.12466	0.504	-114.656	-209.642	3.85	-0.56	0.18
				Final	0.00866	-0.30596	-0.12444	0.485	-115.300	-209.272			
10-006	CPTU2-01	10/14/2010	James S.	Initial	0.00923	-0.3083	-0.12451	0.517	-116.182	-209.389	4.20	1.68	0.18
				Final	0.00885	-0.30317	-0.12428	0.496	-114.249	-209.003			
10-006	CPTU2-02	10/15/2010	James S.	Initial	0.00908	-0.30465	-0.1247	0.509	-114.806	-209.709	9.94	1.76	0.33
				Final	0.00822	-0.29933	-0.12429	0.461	-112.801	-209.019			
10-006	CPTU2-03	10/16/2010	Finn H. & James S.	Initial	0.00906	-0.29796	-0.12405	0.508	-112.285	-208.616	-1.10	-0.50	0.34
				Final	0.00916	-0.29946	-0.12363	0.513	-112.850	-207.909			
10-006	CPTU2-03a	10/16/2010	Finn H. & James S.	Initial	0.0089	-0.29709	-0.12337	0.499	-111.957	-207.472	-2.22	-0.14	0.74
				Final	0.0091	-0.29751	-0.12246	0.510	-112.116	-205.942			
10-007	CPTU2-01	10/18/2010	Finn H. & James S.	Initial	0.00984	-0.29329	-0.12441	0.551	-110.525	-209.221	4.89	-1.64	-2.12
				Final	0.00937	-0.29814	-0.12707	0.525	-112.353	-213.695			
10-007	CPTU2-02	10/18/2010	Finn H. & James S.	Initial	0.00925	-0.30045	-0.12612	0.518	-113.224	-212.097	4.08	1.30	1.81
				Final	0.00888	-0.29657	-0.12386	0.498	-111.761	-208.296			
10-008	SCPTU2-01	10/28/2010	Finn H.	Initial	0.01239	-0.29614	-0.12456	0.694	-111.599	-209.473	0.49	-1.61	-1.67
				Final	0.01233	-0.30096	-0.12666	0.691	-113.416	-213.005			
10-008	SCPTU2-02	10/29/2010	James S. & Finn H.	Initial	0.01251	-0.29891	-0.12442	0.701	-112.643	-209.238	6.95	-0.25	-1.37
				Final	0.01167	-0.29966	-0.12614	0.654	-112.926	-212.131			
10-008	SCPTU2-02a	10/29/2010	Finn H. & James S.	Initial	0.01228	-0.30023	-0.12458	0.688	-113.141	-209.507	6.47	-1.03	-2.64
				Final	0.01151	-0.30335	-0.12791	0.645	-114.316	-215.107			
10-009	SCPTU2-01A	11/6/2010	Finn H. & Skyler N.	Initial	0.01341	-0.29747	-0.13083	0.751	-112.101	-220.018	9.70	-2.44	3.70
				Final	0.01217	-0.30481	-0.12608	0.682	-114.867	-212.030			
10-009	SCPTU2-02	11/6/2010	Finn H. & Skyler N.	Initial	0.01313	-0.30042	-0.12443	0.736	-113.212	-209.255	-190.03	936.45	14.34
				Final	0.51357	0.19468	-0.10778	28.773	73.364	-181.254			
10-009	SCPTU2-02a	11/6/2010	Finn H. & Skyler N.	Initial	0.01287	-0.29885	-0.12364	0.721	-112.621	-207.926	1.17	-0.05	-2.20
				Final	0.01272	-0.29899	-0.12639	0.713	-112.673	-212.551			

* CPTU performed using Purdue equiment where baselines were not obtained

					Output			Units			Percent Shift		
Site	Sounding	Date	Operator	Baseline	TIP	FRICTION	u_2	TIP (MPa)	FRICTION (kPa)	u_2 (kPa)	TIP	FRICTION	u_2
10-009	SCPTU2-03	11/7/2010	Finn H. & Skyler N.	Initial	0.01371	-0.29926	-0.12575	0.768	-112.775	-211.475	17.97	0.65	-1.38
				Final	0.01145	-0.29732	-0.1275	0.641	-112.044	-214.418			
10-009	SCPTU2-04	11/7/2010	Finn H. & Skyler N.	Initial	0.0135	-0.29708	-0.12447	0.756	-111.954	-209.322	4.24	-67.22	0.69
				Final	0.01294	-0.5979	-0.12362	0.725	-225.317	-207.893			
10-010a	SCPTU2-01	11/15/2010	Elliott M. & James S.	Initial	0.01313	-0.58338	-0.13367	0.736	-219.845	-224.794	-4.18	-0.80	6.19
				Final	0.01369	-0.58804	-0.12565	0.767	-221.601	-211.307			
10-010a	SCPTU2-02	11/18/2010	Elliott M. & James S.	Initial	0.01369	-0.58162	-0.12554	0.767	-219.181	-211.122	3.04	-0.56	-0.74
				Final	0.01328	-0.58488	-0.12647	0.744	-220.410	-212.686			
10-010b	SCPTU2-01	11/19/2010	Finn H. & Elliott M.	Initial	0.01347	-0.58007	-0.1295	0.755	-218.597	-217.781	7.95	-1.39	2.07
				Final	0.01244	-0.58819	-0.12685	0.697	-221.657	-213.325			
10-010b	SCPTU2-02	11/19/2010	Finn H. & James S.	Initial	0.01327	-0.58573	-0.12558	0.743	-220.730	-211.189	6.14	-0.48	0.49
				Final	0.01248	-0.58852	-0.12497	0.699	-221.782	-210.163			
10-010b	SCPTU2-03	11/20/2010	Finn H. & James S.	Initial	0.01203	-0.58296	-0.13092	0.674	-219.686	-220.169	-1.32	0.51	3.51
				Final	0.01219	-0.57998	-0.12641	0.683	-218.563	-212.585			
10-010b	SCPTU2-04	11/20/2010	Finn H. & James S.	Initial	0.01234	-0.57322	-0.13677	0.691	-216.016	-230.007	5.92	8.99	10.50
				Final	0.01163	-0.52393	-0.12313	0.652	-197.441	-207.069			
10-010b	SCPTU2-04a	11/20/2010	Finn H. & James S.	Initial	0.01205	-0.51521	-0.1287	0.675	-194.155	-216.436	-	-	-
				Final	-	-	-	-	-	-			
10-010b	SCPTU2-05	11/20/2010	Finn H. & James S.	Initial	0.01177	-0.51357	-0.12259	0.659	-193.537	-206.161	-2.68	-2.23	-3.00
				Final	0.01209	-0.52515	-0.12632	0.677	-197.901	-212.433			
10-010c	CPTU2-01	11/22/2010	Finn H. & James S.	Initial	0.01166	-0.52103	-0.1252	0.653	-196.348	-210.550	3.76	-1.39	-1.93
				Final	0.01123	-0.52831	-0.12764	0.629	-199.092	-214.653			
10-010c	SCPTU2-02	11/28/2010	Finn H. & James S.	Initial	0.012	-0.5193	-0.13153	0.672	-195.696	-221.195	7.34	0.03	3.11
				Final	0.01115	-0.51914	-0.1275	0.625	-195.636	-214.418			
11-001	CPTU2-01	3/31/2011	Finn H. & James S.	Initial	0.01484	-0.5183	-0.12493	0.831	-195.320	-210.096	-2.59	1.33	2.98
				Final	0.01523	-0.51145	-0.12126	0.853	-192.738	-203.924			
11-001	SCPTU2-02	4/1/2011	Finn H. & James S.	Initial	0.01545	-0.51439	-0.12434	0.866	-193.846	-209.103	3.02	0.62	-3.73
				Final	0.01499	-0.5112	-0.12907	0.840	-192.644	-217.058			
11-001	CPTU2-03	4/1/2011	Finn H. & James S.	Initial	0.01515	-0.50641	-0.13034	0.849	-190.839	-219.194	-2.61	0.09	2.29
				Final	0.01555	-0.50596	-0.12739	0.871	-190.669	-214.233			
11-001	CPTU2-04	4/1/2011	Finn H. & James S.	Initial	0.01515	-0.50181	-0.12616	0.849	-189.105	-212.164	3.02	-1.57	0.82
				Final	0.0147	-0.50973	-0.12513	0.824	-192.090	-210.432			
11-001	CPTU2-05	4/2/2011	Finn H. & James S.	Initial	0.01443	-0.49566	-0.12607	0.808	-186.788	-212.013	-8.56	-2.80	4.88
				Final	0.01572	-0.50972	-0.12007	0.881	-192.086	-201.923			
11-002	CPTU2-01	4/3/2011	Finn H. & James S.	Initial	0.01568	-0.49628	-0.12466	0.878	-187.021	-209.642	6.93	-1.90	-1.47
				Final	0.01463	-0.50581	-0.1265	0.820	-190.613	-212.736			
11-002	CPTU2-02	4/3/2011	Finn H. & James S.	Initial	0.01452	-0.50299	-0.12746	0.813	-189.550	-214.350	1.95	-2.13	1.45
				Final	0.01424	-0.51381	-0.12562	0.798	-193.628	-211.256			
11-002	CPTU2-02a	4/3/2011	Finn H. & James S.	Initial	0.01425	-0.51304	-0.12592	0.798	-193.337	-211.761	-2.97	-0.29	-0.06
				Final	0.01468	-0.51452	-0.126	0.822	-193.895	-211.895			

* CPTU performed using Purdue equiment where baselines were not obtained

					Output			Units			Percent Shift		
Site	Sounding	Date	Operator	Baseline	TIP	FRICTION	u_2	TIP (MPa)	FRICTION (kPa)	u_2 (kPa)	TIP	FRICTION	u_2
11-002	SCPTU2-03	4/3/2011	Finn H. & James S.	Initial	0.0151	-0.49982	-0.12521	0.846	-188.355	-210.567	2.07	31.80	-0.11
				Final	0.01479	-0.36268	-0.12535	0.829	-136.675	-210.802			
11-002	SCPTU2-04	4/3/2011	Finn H. & James S.	Initial	0.01469	-0.35253	-0.12626	0.823	-132.850	-212.332	2.83	-0.32	-0.21
				Final	0.01428	-0.35367	-0.12653	0.800	-133.279	-212.786			
11-002	CPTU2-05	4/4/2011	Finn H. & James S.	Initial	0.01481	-0.35453	-0.12538	0.830	-133.603	-210.852	-2.01	-0.62	-0.79
				Final	0.01511	-0.35672	-0.12637	0.847	-134.429	-212.517			
11-003	CPTU2-04	6/1/2011	Finn H., James S., & Seth S.	Initial	0.01293	-0.34863	-0.12799	0.724	-131.380	-215.242	-4.31	1.86	2.33
				Final	0.0135	-0.34219	-0.12504	0.756	-128.953	-210.281			
11-003	CPTU2-05	6/1/2011	Finn H., James S., & Seth S.	Initial	0.01314	-0.32479	-0.12626	0.736	-122.396	-212.332	-1.66	-5.14	0.72
				Final	0.01336	-0.34191	-0.12536	0.749	-128.848	-210.819			
11-003	CPTU2-06	6/2/2011	Finn H., James S., & Seth S.	Initial	0.01314	-0.341	-0.12823	0.736	-128.505	-215.645	-10.25	-2.19	2.58
				Final	0.01456	-0.34855	-0.12497	0.816	-131.350	-210.163			
11-003	CPTU2-07	6/3/2011	James S., & Seth S.	Initial	0.01274	-0.35354	-0.12664	0.714	-133.230	-212.971	-1.71	1.65	0.86
				Final	0.01296	-0.34777	-0.12556	0.726	-131.056	-211.155			
11-003	CPTU2-08	6/3/2011	Seth S. & Finn H.	Initial	-	-	-	-	-	-	*	*	*
				Final	-	-	-	-	-	-			
11-004	CPTU2-03	6/4/2011	Finn H., James S., & Seth	Initial	0.01246	-0.34923	-0.12547	0.698	-131.606	-211.004	-3.86	0.62	2.68
				Final	0.01295	-0.34707	-0.12215	0.726	-130.792	-205.421			
11-004	CPTU2-04	6/5/2011	Finn H., James S., & Seth	Initial	0.01265	-0.34061	-0.13393	0.709	-128.358	-225.231	0.24	-4.56	9.09
				Final	0.01262	-0.3565	-0.12229	0.707	-134.346	-205.656			
11-004	CPTU2-04a	6/5/2011	Finn H., James S., & Seth S.	Initial	0.01242	-0.35963	-0.12579	0.696	-135.525	-211.542	0.24	0.18	3.15
				Final	0.01239	-0.35897	-0.12189	0.694	-135.277	-204.983			
11-004	CPTU2-05	6/6/2011	Finn H. & Seth S.	Initial	0.01259	-0.36194	-0.12425	0.705	-136.396	-208.952	-6.23	1.00	-8.16
				Final	0.0134	-0.35833	-0.13482	0.751	-135.035	-226.728			
11-004	CPTU2-06	6/6/2011	Seth S. & Finn H.	Initial	-	-	-	0.647	-44.511	-247.116	*	*	*
				Final	-	-	-	-	-	-			
11-005	CPTU2-04	6/7/2011	Seth S. & Finn H.	Initial	-	-	-	0.171	11.919	165.407	*	*	*
				Final	-	-	-	-	-	-			
11-005	CPTU2-05	6/7/2011	Seth S. & Finn H.	Initial	-	-	-	-0.710	-45.655	-250.817	*	*	*
				Final	-	-	-	-	-	-			
11-005	CPTU2-06	6/8/2011	Finn H. & Seth S.	Initial	0.01348	-0.37318	-0.12392	0.755	-140.632	-208.397	6.91	4.18	3.37
				Final	0.01258	-0.35791	-0.11981	0.705	-134.877	-201.485			
11-005	CPTU2-07	6/8/2011	Finn H. & Seth S.	Initial	0.01573	-0.36628	-0.12282	0.881	-138.031	-206.547	20.23	3.14	0.72
				Final	0.01284	-0.35496	-0.12194	0.719	-133.765	-205.067			
11-005	CPTU2-08	6/9/2011	Finn H. & Seth S.	Initial	0.01345	-0.34841	-0.12487	0.754	-131.297	-209.995	2.26	-2.66	6.62
				Final	0.01315	-0.35782	-0.11687	0.737	-134.843	-196.541			
11-005	CPTU2-09	6/9/2011	Seth S. & Finn H.	Initial	-	-	-	0.248	-7.109	-171.340	*	*	*
				Final	-	-	-	-	-	-			

* CPTU performed using Purdue equiment where baselines were not obtained

Wisconsin Highway Research Program
University of Wisconsin-Madison
1415 Engineering Drive
Madison, WI 53706
608/265-4481
http://wisdotresearch.wi.gov/whrp

CFIRE

University of Wisconsin-Madison
Department of Civil and Environmental Engineering
1410 Engineering Drive, Room 270
Madison, WI 53706
Phone: 608-263-3175
Fax: 608-263-2512
cfire.wistrans.org